Preface to the Third Edition

At the time when the second edition of this book was published the study of the liquid state was a rapidly expanding field of research. In the twenty years since then, the subject has matured both theoretically and experimentally to a point where a real understanding exists of the behaviour of "simple" liquids at the microscopic level. Although there has been a shift in emphasis towards more complex systems, there remains in our view a place for a book that deals with the principles of liquid-state theory, covering both statics and dynamics. Thus, in preparing a third edition, we have resisted the temptation to broaden too far the scope of the book, and the focus remains firmly on simple systems, though many of the methods we describe continue to find a wider range of application. Nonetheless, some reorganisation of the book has been required in order to give proper weight to more recent developments. The most obvious change is in the space devoted to the theory of inhomogeneous fluids, an area in which considerable progress has been made since 1986. Other major additions are sections on the properties of supercooled liquids, which include a discussion of the mode-coupling theory of the kinetic glass transition, on theories of condensation and freezing and on the electric double layer. To make way for this and other new material, some sections from the second edition have either been reduced in length or omitted altogether. In particular, we no longer see a need to include a complete chapter on molecular simulation, the publication of several excellent texts on the subject having filled what was previously a serious gap in the literature. Our aim has been to emphasise what seems to us to be work of lasting interest. Such judgements are inevitably somewhat subjective and, as before, the choice of topics is coloured by our own experience and tastes. We make no attempt to provide an exhaustive list of references, limiting ourselves to what we consider to be the fundamental papers in different areas, along with selected applications.

We are grateful to a number of colleagues who have helped us in different ways: Dor Ben-Amotz, Teresa Head-Gordon, David Heyes, David Grier, Bill Jorgensen, Gerhard Kahl, Peter Monson, Anna Oleksy, Albert Reiner, Phil Salmon, Ilja Siepmann, Alan Soper, George Stell and Jens-Boie Suck. Bob Evans made many helpful suggestions concerning the much revised chapter on ionic liquids, George Jackson acted as our guide to the literature on the theory of associating liquids, Alberto Parola provided a valuable set of notes on hierarchical reference theory, and Jean-Jacques Weis undertook on our behalf new Monte Carlo calculations of the dielectric constant of dipolar hard spheres. Our task could not have been completed without the support, encouragement and advice of these and other colleagues, to all of whom we give our thanks. Finally, we thank the respective publishers for permission to reproduce figures from Journal of Chemical Physics, Journal of Non-Crystalline Solids, Physical Review and Physical Review Letters.

November 2005

J.P. HANSEN
I.R. MCDONALD

Preface to the Second Edition

The first edition of this book was written in the wake of an unprecedented advance in our understanding of the microscopic structure and dynamics of simple liquids. The rapid progress made in a number of different experimental and theoretical areas had led to a rather clear and complete picture of the properties of simple atomic liquids. In the ten years that have passed since then, interest in the liquid state has remained very active, and the methods described in our book have been successfully generalised and applied to a variety of more complicated systems. Important developments have therefore been seen in the theory of ionic, molecular and polar liquids, of liquid metals, and of the liquid surface, while the quantitative reliability of theories of atomic fluids has also improved.

In an attempt to give a balanced account both of the basic theory and of the advances of the past decade, this new edition has been rearranged and considerably expanded relative to the earlier one. Every chapter has been completely rewritten, and three new chapters have been added, devoted to ionic, metallic and molecular liquids, together with substantial new sections on the theory of inhomogeneous fluids. The material contained in Chapter 10 of the first edition, which dealt with phase transitions, has been omitted, since it proved impossible to do justice to such a large field in the limited space available. Although many excellent review articles and monographs have appeared in recent years, a comprehensive and up-to-date treatment of the theory of "simple" liquids appears to be lacking, and we hope that the new edition of our book will fill this gap. The choice of material again reflects our own tastes, but we have aimed at presenting the main ideas of modern liquid-state theory in a way that is both pedagogical and, so far as possible, self-contained. The book should be accessible to graduate students and research workers, both experimentalists and theorists, who have a good background in elementary statistical mechanics. We are well aware, however, that certain sections, notably in Chapters 4, 6, 9 and 12 require more concentration from the reader than others. Although the book is not intended to be exhaustive, we give many references to material that is not covered in depth in the text. Even at this level, it is impossible to include all the relevant work. Omissions may reflect our ignorance or a lack of good judgement, but we consider that our goal will have been achieved if the book serves as an introduction and guide to a continuously growing field.

While preparing the new edition, we have benefited from the advice, criticism and help of many colleagues. We give our sincere thanks to all. There are, alas, too many names to list individually, but we wish to acknowledge our particular debt to Marc Baus, David Chandler, Giovanni Ciccotti, Bob Evans, Paul Madden and Dominic Tildesley, who have read large parts of the manuscript; to Susan O'Gorman, for her help with Chapter 4; and to Eduardo Waisman, who wrote the first (and almost final) version of Appendix B. We

are also grateful to those colleagues who have supplied references, preprints, and material for figures and tables, and to authors and publishers for permission to reproduce diagrams from published papers. The last stages of the work were carried out at the Institut Laue-Langevin in Grenoble, and we thank Philippe Nozières for the invitations that made our visits possible. Finally, we are greatly indebted to Martine Hansen, Christiane Lanceron, Rehda Mazighi and Susan O'Gorman for their help and patience in the preparation of the manuscript and figures.

May 1986

J.P. HANSEN
I.R. MCDONALD

Preface to the First Edition

The past ten years or so have seen a remarkable growth in our understanding of the statistical mechanics of simple liquids. Many of these advances have not yet been treated fully in any book and the present work is aimed at filling this gap at a level similar to that of Egelstaff's "The Liquid State", though with a greater emphasis on theoretical developments. We discuss both static and dynamic properties, but no attempt is made at completeness and the choice of topics naturally reflects our own interests. The emphasis throughout is placed on theories which have been brought to a stage at which numerical comparison with experiment can be made. We have attempted to make the book as self-contained as possible, assuming only a knowledge of statistical mechanics at a final-year undergraduate level. We have also included a large number of references to work which lack of space has prevented us from discussing in detail. Our hope is that the book will prove useful to all those interested in the physics and chemistry of liquids.

Our thanks go to many friends for their help and encouragement. We wish, in particular, to express our gratitude to Loup Verlet for allowing us to make unlimited use of his unpublished lecture notes on the theory of liquids. He, together with Dominique Levesque, Konrad Singer and George Stell, have read several parts of the manuscript and made suggestions for its improvement. We are also greatly indebted to Jean-Jacques Weis for his help with the section on molecular liquids. The work was completed during a summer spent as visitors to the Chemistry Division of the National Research Council of Canada; it is a pleasure to have this opportunity to thank Mike Klein for his hospitality at that time and for making the visit possible. Thanks go finally to Susan O'Gorman for her help with mathematical problems and for checking the references; to John Copley, Jan Sengers and Sidney Yip for sending us useful material; and to Mrs K.L. Hales for so patiently typing the many drafts.

A number of figures and tables have been reproduced, with permission, from The Physical Review, Journal of Chemical Physics, Molecular Physics and Physica; detailed acknowledgements are made at appropriate points in the text.

June 1976

J.P. HANSEN
I.R. MCDONALD

CHAPTER 1

Introduction

1.1 THE LIQUID STATE

The liquid state of matter is intuitively perceived as being intermediate in nature between a gas and a solid. Thus a natural starting point for discussion of the properties of any given substance is the relationship between pressure P, number density ρ and temperature T in the different phases, summarised in the equation of state $f(P, \rho, T) = 0$. The phase diagram in the ρ–T plane typical of a simple, one-component system is sketched in Figure 1.1. The region of existence of the liquid phase is bounded above by the critical point (subscript c) and below by the triple point (subscript t). Above the critical point there is only a single fluid phase, so a continuous path exists from liquid to fluid to vapour; this is not true of the transition from liquid to solid, because the solid–fluid coexistence line, or melting curve, does not terminate at a critical point. In many respects the properties of the dense, supercritical fluid are not very different from those of the liquid, and much of the theory we develop in later chapters applies equally well to the two cases.

We shall be concerned in this book almost exclusively with classical liquids. For atomic systems a simple test of the classical hypothesis is provided by the value of the de Broglie thermal wavelength Λ, defined as

$$\Lambda = \left(\frac{2\pi\beta\hbar^2}{m} \right)^{1/2} \tag{1.1.1}$$

where m is the mass of an atom and $\beta = 1/k_{\mathrm{B}}T$. To justify a classical treatment of static properties it is necessary that Λ be much less than a, where $a \approx \rho^{-1/3}$ is the mean nearest-neighbour separation. In the case of molecules we require, in addition, that $\Theta_{\mathrm{rot}} \ll T$, where $\Theta_{\mathrm{rot}} = \hbar^2/2Ik_{\mathrm{B}}$ is a characteristic rotational temperature (I is the molecular moment of inertia). Some typical results are shown in Table 1.1, from which we see that quantum effects should be small for all the systems listed, with the exceptions of hydrogen and neon.

Use of the classical approximation leads to an important simplification, namely that the contributions to thermodynamic properties which arise from thermal motion can be separated from those due to interactions between particles. The separation of kinetic and potential terms suggests a simple means of characterising the liquid state. Let V_N be the total potential energy of a system, where N is the number of particles, and let K_N be the total

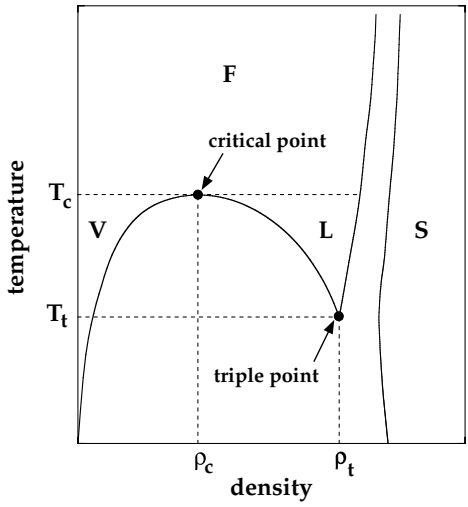

FIG. 1.1. Schematic phase diagram of a typical monatomic substance, showing the boundaries between solid (S), liquid (L) and vapour (V) or fluid (F) phases.

TABLE 1.1. *Test of the classical hypothesis*

Liquid	T_t/K	Λ/Å	Λ/a	Θ_{rot}/T_t
H_2	14.1	3.3	0.97	6.1
Ne	24.5	0.78	0.26	
CH_4	91	0.46	0.12	0.083
N_2	63	0.42	0.11	0.046
Li	454	0.31	0.11	
Ar	84	0.30	0.083	
HCl	159	0.23	0.063	0.094
Na	371	0.19	0.054	
Kr	116	0.18	0.046	
CCl_4	250	0.09	0.017	0.001

Λ is the de Broglie thermal wavelength at $T = T_t$ and $a = (V/N)^{1/3}$.

kinetic energy. Then in the liquid state we find that $K_N/|V_N| \approx 1$, whereas $K_N/|V_N| \gg 1$ corresponds to the dilute gas and $K_N/|V_N| \ll 1$ to the low-temperature solid. Alternatively, if we characterise a given system by a length σ and an energy ε, corresponding roughly to the range and strength of the intermolecular forces, we find that in the liquid region of the phase diagram the reduced number density $\rho^* = N\sigma^3/V$ and reduced temperature $T^* = k_B T/\varepsilon$ are both of order unity. Liquids and dense fluids are also distinguished from dilute gases by the greater importance of collisional processes and short-range, positional correlations, and from solids by the lack of long-range order; their structure is in many

TABLE 1.2. *Selected properties of typical simple liquids*

Property	Ar	Na	N_2
T_t/K	84	371	63
T_b/K ($P = 1$ atm)	87	1155	77
T_c/K	151	2600	126
T_c/T_t	1.8	7.0	2.0
ρ_t/nm^{-3}	21	24	19
C_P/C_V	2.2	1.1	1.6
L_{vap}/kJ mol^{-1}	6.5	99	5.6
$\chi_T/10^{-12}$ cm^2 dyn^{-1}	200	19	180
c/m s^{-1}	863	2250	995
γ/dyn cm^{-1}	13	191	12
$D/10^{-5}$ cm^2 s^{-1}	1.6	4.3	1.0
η/mg cm^{-1} s^{-1}	2.8	7.0	3.8
λ/mW cm^{-1} K^{-1}	1.3	8800	1.6
$(k_B T/2\pi D\eta)$/Å	4.1	2.7	3.6

χ_T = isothermal compressibility, c = speed of sound, γ = surface tension, D = self-diffusion coefficient, η = shear viscosity and λ = thermal conductivity, all at $T = T_t$; L_{vap} = heat of vaporisation at $T = T_b$.

cases dominated by the "excluded-volume" effect associated with the packing together of particles with hard cores.

Selected properties of a simple monatomic liquid (argon), a simple molecular liquid (nitrogen) and a simple liquid metal (sodium) are listed in Table 1.2. Not unexpectedly, the properties of the liquid metal are in certain respects very different from those of the other systems, notably in the values of the thermal conductivity, isothermal compressibility, surface tension, heat of vaporisation and the ratio of critical to triple-point temperatures; the source of these differences should become clear in Chapter 10. The quantity $k_B T/2\pi D\eta$ in the table provides a Stokes-law estimate of the particle diameter.

1.2 INTERMOLECULAR FORCES AND MODEL POTENTIALS

The most important feature of the pair potential between atoms or molecules is the harsh repulsion that appears at short range and has its origin in the overlap of the outer electron shells. The effect of these strongly repulsive forces is to create the short-range order that is characteristic of the liquid state. The attractive forces, which act at long range, vary much more smoothly with the distance between particles and play only a minor role in determining the structure of the liquid. They provide, instead, an essentially uniform, attractive background and give rise to the cohesive energy that is required to stabilise the liquid. This separation of the effects of repulsive and attractive forces is a very old-established concept. It lies at the heart of the ideas of van der Waals, which in turn form the basis of the very successful perturbation theories of the liquid state that we discuss in Chapter 5.

The simplest model of a fluid is a system of hard spheres, for which the pair potential $v(r)$ at a separation r is

$$\begin{aligned} v(r) &= \infty, \quad r < d, \\ &= 0, \quad r > d \end{aligned} \tag{1.2.1}$$

where d is the hard-sphere diameter. This simple potential is ideally suited to the study of phenomena in which the hard core of the potential is the dominant factor. Much of our understanding of the properties of the hard-sphere model come from computer simulations. Such calculations have revealed very clearly that the structure of a hard-sphere fluid does not differ in any significant way from that corresponding to more complicated interatomic potentials, at least under conditions close to crystallisation. The model also has some relevance to real, physical systems. For example, the osmotic equation of state of a suspension of micron-sized silica spheres in an organic solvent matches almost exactly that of a hard-sphere fluid.[1] However, although simulations show that the hard-sphere fluid undergoes a freezing transition at ρ^* $(= \rho d^3) \approx 0.945$, the absence of attractive forces means that there is only one fluid phase. A simple model that can describe a true liquid is obtained by supplementing the hard-sphere potential with a square-well attraction, as illustrated in Figure 1.2(a). This introduces two additional parameters: ε, the well depth, and $(\gamma - 1)$, the width of the well in units of d, where γ typically has a value of about 1.5. An alternative to the square-well potential with features that are of particular interest theoretically is the hard-core Yukawa potential, given by

$$\begin{aligned} v(r) &= \infty, && r^* < 1, \\ &= -\frac{\varepsilon}{r^*} \exp\bigl[-\lambda(r^* - 1)\bigr], && r^* > 1 \end{aligned} \tag{1.2.2}$$

where $r^* = r/d$ and the parameter λ measures the inverse range of the attractive tail in the potential. The two examples plotted in Figure 1.2(b) are drawn for values of λ appropriate either to the interaction between rare-gas atoms $(\lambda = 2)$ or to the short-range, attractive forces[2] characteristic of certain colloidal systems $(\lambda = 8)$.

A more realistic potential for neutral atoms can be constructed by a detailed quantum-mechanical calculation. At large separations the dominant contribution to the potential comes from the multipolar dispersion interactions between the instantaneous electric moments on one atom, created by spontaneous fluctuations in the electronic charge distribution, and moments induced in the other. All terms in the multipole series represent attractive contributions to the potential. The leading term, varying as r^{-6}, describes the dipole–dipole interaction. Higher-order terms represent dipole–quadrupole (r^{-8}), quadrupole–quadrupole (r^{-10}) interactions, and so on, but these are generally small in comparison with the term in r^{-6}.

A rigorous calculation of the short-range interaction presents greater difficulty, but over relatively small ranges of r it can be adequately represented by an exponential function of the form $\exp(-r/r_0)$, where r_0 is a range parameter. This approximation must be supplemented by requiring that $v(r) \to \infty$ for r less than some arbitrarily chosen, small value. In practice, largely for reasons of mathematical convenience, it is more usual to represent the short-range repulsion by an inverse-power law, i.e. r^{-n}, with n lying generally in the

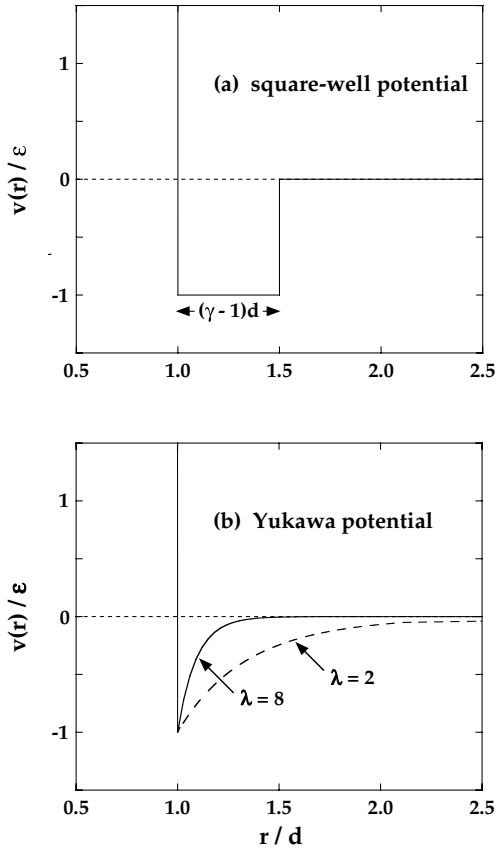

FIG. 1.2. Simple pair potentials for monatomic systems. See text for details.

range 9 to 15. The behaviour of $v(r)$ in the limiting cases $r \to \infty$ and $r \to 0$ may therefore be incorporated in a simple potential function of the form

$$v(r) = 4\varepsilon\left[(\sigma/r)^{12} - (\sigma/r)^{6}\right] \tag{1.2.3}$$

which is the famous 12-6 potential of Lennard-Jones. Equation (1.2.3) involves two parameters: the collision diameter σ, which is the separation of the particles where $v(r) = 0$; and ε, the depth of the potential well at the minimum in $v(r)$. The Lennard-Jones potential provides a fair description of the interaction between pairs of rare-gas atoms and also of quasi-spherical molecules such as methane. Computer simulations[3] have shown that the triple point of the Lennard-Jones fluid is at $\rho^* \approx 0.85$, $T^* \approx 0.68$.

Experimental information on the pair interaction can be extracted from a study of any process that involves collisions between particles.[4] The most direct method involves the measurement of atom–atom scattering cross-sections as a function of incident energy and scattering angle; inversion of the data allows, in principle, a determination of the pair po-

tential at all separations. A simpler procedure is to assume a specific form for the potential and determine the parameters by fitting to the results of gas-phase measurements of quantities such as the second virial coefficient (see Chapter 3) or the shear viscosity. In this way, for example, the parameters ε and σ in the Lennard-Jones potential have been determined for a large number of gases.

The theoretical and experimental methods we have mentioned all relate to the properties of an isolated pair of molecules. The use of the resulting pair potentials in calculations for the liquid state involves the neglect of many-body forces, an approximation that is difficult to justify. In the rare-gas liquids, the three-body, triple-dipole dispersion term is the most important many-body interaction; the net effect of triple-dipole forces is repulsive, amounting in the case of liquid argon to a few percent of the total potential energy due to pair interactions. Moreover, careful measurements, particularly those of second virial coefficients at low temperatures, have shown that the true pair potential for rare-gas atoms is not of the Lennard-Jones form, but has a deeper bowl and a weaker tail, as illustrated by the curves plotted in Figure 1.3. Apparently the success of the Lennard-Jones potential in accounting for many of the macroscopic properties of argon-like liquids is the consequence of a fortuitous cancellation of errors. A number of more accurate pair potentials have been developed for the rare gases, but their use in the calculation of condensed-phase properties requires the explicit incorporation of three-body interactions.

Although the true pair potential for rare-gas atoms is not the same as the effective pair potential used in liquid-state work, the difference is a relatively minor, quantitative one. The situation in the case of liquid metals is different, because the form of the effective ion–ion interaction is strongly influenced by the presence of a degenerate gas of conduction electrons that does not exist before the liquid is formed. The calculation of the ion–ion interaction is a complicated problem, as we shall see in Chapter 10. The ion–electron interaction is first described in terms of a "pseudopotential" that incorporates both the coulombic attraction and the repulsion due to the Pauli exclusion principle. Account

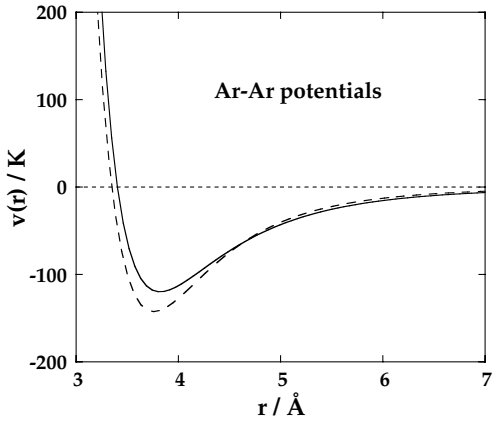

FIG. 1.3. Pair potentials for argon in temperature units. Full curve: the Lennard-Jones potential with parameter values $\varepsilon/k_B = 120$ K, $\sigma = 3.4$ Å, which is a good effective potential for the liquid; dashes: a potential based on gas-phase data.[5]

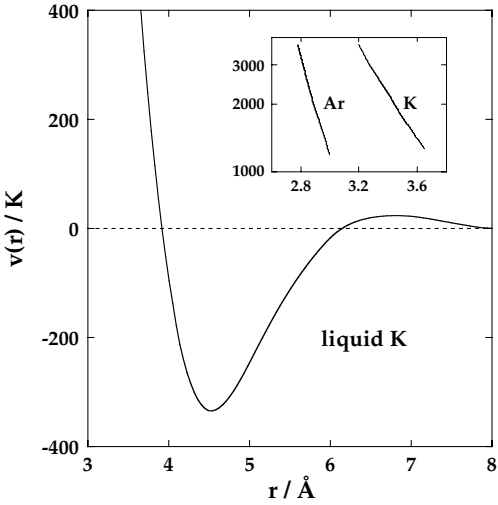

FIG. 1.4. Main figure: effective ion–ion potential (in temperature units) for liquid potassium.[6] Inset: comparison on a logarithmic scale of potentials for argon and potassium in the core region.

must then be taken of the way in which the pseudopotential is modified by interaction between the conduction electrons. The end result is a potential that represents the interaction between screened, electrically neutral "pseudoatoms". Irrespective of the detailed assumptions made, the main features of the potential are always the same: a soft repulsion, a deep attractive well and a long-range oscillatory tail. The potential, and in particular the depth of the well, are strongly density dependent but only weakly dependent on temperature. Figure 1.4 shows an effective potential for liquid potassium. The differences compared with the potentials for argon are clear, both at long range and in the core region.

For molten salts and other ionic liquids in which there is no shielding of the electrostatic forces similar to that found in liquid metals, the coulombic interaction provides the dominant contribution to the interionic potential. There must, in addition, be a short-range repulsion between ions of opposite charge, without which the system would collapse, but the detailed way in which the repulsive forces are treated is of minor importance. Polarisation of the ions by the internal electric field also plays a role, but such effects are essentially many-body in nature and cannot be adequately represented by an additional term in the pair potential.

Description of the interaction between two molecules poses greater problems than for spherical particles because the pair potential is a function both of the separation of the molecules and of their mutual orientation. The model potentials discussed in this book divide into two classes. The first consists of highly idealised models of polar liquids in which a point dipole–dipole interaction is superimposed on a spherically symmetric potential. In this case the pair potential for particles labelled 1 and 2 has the general form

$$v(1,2) = v_0(R) - \boldsymbol{\mu}_1 \cdot \boldsymbol{T}(\mathbf{R}) \cdot \boldsymbol{\mu}_2 \tag{1.2.4}$$

where $\mathbf{R}$ is the vector separation of the molecular centres, $v_0(R)$ is the spherically symmetric term, $\boldsymbol{\mu}_i$ is the dipole-moment vector of particle i and $\boldsymbol{T}(\mathbf{R})$ is the dipole–dipole interaction tensor:

$$\boldsymbol{T}(\mathbf{R}) = 3\mathbf{RR}/R^5 - \boldsymbol{I}/R^3 \tag{1.2.5}$$

where $\boldsymbol{I}$ is the unit tensor. Two examples of (1.2.4) that are of particular interest are those of dipolar hard spheres, where $v_0(R)$ is the hard-sphere potential, and the Stockmayer potential, where $v_0(R)$ takes the Lennard-Jones form. Both these models, together with extensions that include, for example, dipole–quadrupole and quadrupole–quadrupole terms, have received much attention from theoreticians. Their main limitation as models of real molecules is the fact that they ignore the angle dependence of the short-range forces. A simple way to take account of such effects is through the use of potentials of the second main type with which we shall be concerned. These are models in which the molecule is represented by a set of discrete *interaction sites* that are commonly, but not invariably, located at the sites of the atomic nuclei. The total potential energy of two interaction-site molecules is then obtained as the sum of spherically symmetric, interaction-site potentials. Let $\mathbf{r}_{i\alpha}$ be the coordinates of site α in molecule i and let $\mathbf{r}_{j\beta}$ be the coordinates of site β in molecule j. Then the total intermolecular potential energy is

$$v(1,2) = \tfrac{1}{2}\sum_{\alpha}\sum_{\beta} v_{\alpha\beta}\big(|\mathbf{r}_{2\beta} - \mathbf{r}_{1\alpha}|\big) \tag{1.2.6}$$

where $v_{\alpha\beta}(r)$ is a site–site potential and the sums on α and β run over all interaction sites in the respective molecules. Electrostatic interactions are easily allowed for by inclusion of coulombic terms in the site–site potentials. Let us take as an example the particularly simple case of a homonuclear diatomic, such as that pictured in Figure 1.5. A crude interaction-site model would be that of a "hard dumb-bell", consisting of two overlapping hard spheres of diameter d with their centres separated by a distance $L < 2d$. This should be adequate to describe the main structural features of a liquid such as nitrogen. An obvious improvement would be to replace the hard spheres by two Lennard-Jones interaction sites, with parameters chosen to fit, say, the experimentally determined equation of state. Some homonuclear diatomics also have a large quadrupole moment, which plays a significant role in determining the short-range angular correlations in the liquid. The model could in that case be further refined by placing point charges q at the Lennard-Jones sites, together

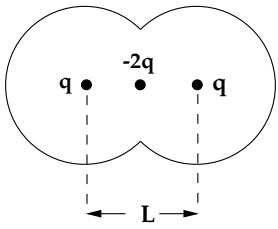

FIG. 1.5. An interaction-site model of a homonuclear diatomic.

with a compensating charge $-2q$ at the mid-point of the internuclear bond; such a charge distribution has zero dipole moment but a non-vanishing quadrupole moment proportional to qL^2. Models of this general type have proved remarkably successful in describing the properties of a wide variety of molecular liquids, both simple and complicated.

1.3 EXPERIMENTAL METHODS

The experimental methods available for studying the properties of simple liquids may be placed in one of two broad categories, depending on whether they are concerned with measurements on a macroscopic or microscopic scale. In general, the calculated microscopic properties are more sensitive to the approximations used in a theory and to the assumptions made about the pair potentials, but the macroscopic properties can usually be measured with considerably greater accuracy. The two types of measurement are therefore complementary, each providing information that is useful in the development of a statistical-mechanical theory of the liquid state.

The classic macroscopic measurements are those of thermodynamic properties, particularly of the equation of state. Integration of accurate P–ρ–T data yields information on other thermodynamic quantities, which can be supplemented by calorimetric measurements. For most liquids the pressure is known as a function of temperature and density only in the vicinity of the liquid–vapour equilibrium line, but for certain systems of particular theoretical interest experiments have been carried out at much higher pressures; the low compressibility of a liquid near its triple point means that highly specialised techniques are required. The second main class of macroscopic measurements are those relating to transport coefficients. A variety of experimental methods are used. The shear viscosity, for example, can be determined from the observed damping of torsional oscillations or from capillary-flow experiments, while the thermal conductivity can be obtained from a steady-state measurement of the transfer of heat between a central filament and a surrounding cylinder or between parallel plates. A direct method of determining the coefficient of self-diffusion involves the use of radioactive tracers, which places it in the category of microscopic measurements; in favourable cases the diffusion coefficient can be measured by nuclear magnetic resonance (NMR). NMR and other spectroscopic methods (infrared and Raman) are also useful in the study of reorientational motion in molecular liquids, while dielectric-response measurements provide information on the slow, structural relaxation in supercooled liquids near the glass transition.

Much the most important class of microscopic measurements, at least from the theoretical point of view, are the radiation-scattering experiments. Elastic scattering of neutrons or x-rays, in which the scattering cross-section is measured as a function of momentum transfer between the radiation and the sample, is the source of our experimental knowledge of the static structure of a fluid. In the case of inelastic scattering the cross-section is measured as a function of both momentum and energy transfer. It is thereby possible to extract information on wavenumber and frequency-dependent fluctuations in liquids at wavelengths comparable with the spacing between particles. This provides a very powerful method of studying microscopic time-dependent processes in liquids. Inelastic light-scattering experiments give similar information, but the accessible range of momentum transfer limits the

method to the study of fluctuations of wavelength of order 10^{-5} cm, corresponding to the hydrodynamic regime. Such experiments are, however, of considerable value in the study of colloidal dispersions and of critical phenomena.

Finally, there are a range of techniques of a quasi-experimental character, referred to collectively as computer simulation, the importance of which in the development of liquid-state theory can hardly be overstated. Simulation provides what are essentially exact results for a given potential model; its usefulness rests ultimately on the fact that a sample containing a few hundred or few thousand particles is in many cases sufficiently large to simulate the behaviour of a macroscopic system. There are two classic approaches: the *Monte Carlo* method and the method of *molecular dynamics*. There are many variants of each, but in broad terms a Monte Carlo calculation is designed to generate static configurations of the system of interest, while molecular dynamics involves the solution of the classical equations of motion of the particles. Molecular dynamics therefore has the advantage of allowing the study of time-dependent processes, but for the calculation of static properties a Monte Carlo method is often more efficient. Chapter 2 contains a brief discussion of the principles underlying the two types of calculation.

NOTES AND REFERENCES

1. Vrij, A., Jansen, J.W., Dhont, J.K.G., Pathmamanoharan, C., Kops-Werkhoven, M.M. and Fijnaut, H.M., *Faraday Disc.* **76**, 19 (1983).
2. See, e.g., Meijer, E.J. and Frenkel, D., *Phys. Rev. Lett.* **67**, 1110 (1991). The interactions in a charge-stabilised colloidal suspension can be modelled by a Yukawa potential with a positive tail.
3. Hansen, J.P. and Verlet, L., *Phys. Rev.* **184**, 151 (1969).
4. Maitland, G.C., Rigby, M., Smith, E.B. and Wakeham, W.A., "Intermolecular Forces". Clarendon Press, Oxford, 1981.
5. Model BBMS of ref. 4, p. 497.
6. Dagens, L., Rasolt, M. and Taylor, R., *Phys. Rev. B* **11**, 2726 (1975).

CHAPTER 2

Statistical Mechanics

This chapter is devoted to a summary of the principles of classical statistical mechanics, a discussion of the link between statistical mechanics and thermodynamics, and the definition of certain equilibrium and time-dependent distribution functions of fundamental importance in the theory of liquids. It also establishes much of the notation used in later parts of the book. The focus throughout is on atomic systems; some of the complications that arise in the study of molecular liquids are discussed in Chapter 11.

2.1 TIME EVOLUTION AND KINETIC EQUATIONS

Consider an isolated, macroscopic system consisting of N identical, spherical particles of mass m enclosed in a volume V. An example would be a one-component, monatomic gas or liquid. In classical mechanics the dynamical state of the system at any instant is completely specified by the $3N$ coordinates $\mathbf{r}^N \equiv \mathbf{r}_1, \ldots, \mathbf{r}_N$ and $3N$ momenta $\mathbf{p}^N \equiv \mathbf{p}_1, \ldots, \mathbf{p}_N$ of the particles. The values of these $6N$ variables define a *phase point* in a $6N$-dimensional *phase space*. Let $\mathcal{H}$ be the hamiltonian of the system, which we write in general form as

$$\mathcal{H}(\mathbf{r}^N, \mathbf{p}^N) = K_N(\mathbf{p}^N) + V_N(\mathbf{r}^N) + \Phi_N(\mathbf{r}^N) \tag{2.1.1}$$

where

$$K_N = \sum_{i=1}^{N} \frac{|\mathbf{p}_i|^2}{2m} \tag{2.1.2}$$

is the kinetic energy, V_N is the interatomic potential energy and Φ_N is the potential energy arising from the interaction of the particles with some spatially varying, external field. If there is no external field, the system will be both spatially uniform and isotropic. The motion of the phase point along its *phase trajectory* is determined by Hamilton's equations:

$$\dot{\mathbf{r}}_i = \frac{\partial \mathcal{H}}{\partial \mathbf{p}_i}, \qquad \dot{\mathbf{p}}_i = -\frac{\partial \mathcal{H}}{\partial \mathbf{r}_i} \tag{2.1.3}$$

These equations are to be solved subject to $6N$ initial conditions on the coordinates and momenta. Since the trajectory of a phase point is wholly determined by the values of $\mathbf{r}^N$, $\mathbf{p}^N$

at any given time, it follows that two different trajectories cannot pass through the same point in phase space.

The aim of equilibrium statistical mechanics is to calculate observable properties of a system of interest either as averages over a phase trajectory (the method of Boltzmann), or as averages over an ensemble of systems, each of which is a replica of the system of interest (the method of Gibbs). The main features of the two methods are reviewed in later sections of this chapter. Here it is sufficient to recall that in Gibbs's formulation of statistical mechanics the distribution of phase points of systems of the ensemble is described by a *phase-space probability density* $f^{[N]}(\mathbf{r}^N, \mathbf{p}^N; t)$. The quantity $f^{[N]}\,\mathrm{d}\mathbf{r}^N\,\mathrm{d}\mathbf{p}^N$ is the probability that at time t the physical system is in a microscopic state represented by a phase point lying in the infinitesimal, $6N$-dimensional phase-space element $\mathrm{d}\mathbf{r}^N\,\mathrm{d}\mathbf{p}^N$. This definition implies that the integral of $f^{[N]}$ over all phase space is

$$\iint f^{[N]}\big(\mathbf{r}^N, \mathbf{p}^N; t\big)\,\mathrm{d}\mathbf{r}^N \mathrm{d}\mathbf{p}^N = 1 \tag{2.1.4}$$

for all t. Given a complete knowledge of the probability density it would be possible to calculate the average value of any function of the coordinates and momenta.

The time evolution of the probability density at a fixed point in phase space is governed by the Liouville equation, which is a $6N$-dimensional analogue of the equation of continuity of an incompressible fluid; it describes the fact that phase points of the ensemble are neither created nor destroyed as time evolves. The Liouville equation may be written either as

$$\frac{\partial f^{[N]}}{\partial t} + \sum_{i=1}^{N}\left(\frac{\partial f^{[N]}}{\partial \mathbf{r}_i}\cdot\dot{\mathbf{r}}_i + \frac{\partial f^{[N]}}{\partial \mathbf{p}_i}\cdot\dot{\mathbf{p}}_i\right) = 0 \tag{2.1.5}$$

or, more compactly, as

$$\frac{\partial f^{[N]}}{\partial t} = \big\{\mathcal{H},\, f^{[N]}\big\} \tag{2.1.6}$$

where $\{A, B\}$ denotes the Poisson bracket:

$$\{A, B\} \equiv \sum_{i=1}^{N}\left(\frac{\partial A}{\partial \mathbf{r}_i}\cdot\frac{\partial B}{\partial \mathbf{p}_i} - \frac{\partial A}{\partial \mathbf{p}_i}\cdot\frac{\partial B}{\partial \mathbf{r}_i}\right) \tag{2.1.7}$$

Alternatively, by introducing the Liouville operator $\mathcal{L}$, defined as

$$\mathcal{L} \equiv i\{\mathcal{H},\ \} \tag{2.1.8}$$

the Liouville equation becomes

$$\frac{\partial f^{[N]}}{\partial t} = -i\mathcal{L} f^{[N]} \tag{2.1.9}$$

the formal solution to which is

$$f^{[N]}(t) = \exp(-i\mathcal{L}t)\, f^{[N]}(0) \tag{2.1.10}$$

The Liouville equation can be expressed even more concisely in the form

$$\frac{\mathrm{d}f^{[N]}}{\mathrm{d}t} = 0 \tag{2.1.11}$$

where $\mathrm{d}/\mathrm{d}t$ denotes the total derivative with respect to time. This result is called the Liouville theorem. The meaning of the Liouville theorem is that the probability density, as seen by an observer moving with a phase point along its phase trajectory, is independent of time. Consider the phase points that at time $t = 0$ are contained within a phase-space element $\mathrm{d}\mathbf{r}^N(0)\,\mathrm{d}\mathbf{p}^N(0)$. As time increases, the element will change in shape but no phase points will enter or leave, otherwise phase trajectories would cross each other. The Liouville theorem therefore implies that the volume of the element must remain the same: volume in phase space is said to be "conserved". In mathematical terms, conservation of volume in phase space is equivalent to the statement that the jacobian corresponding to the transformation $\mathbf{r}^N(0), \mathbf{p}^N(0) \to \mathbf{r}^N(t), \mathbf{p}^N(t)$ is equal to unity; this is easily proved explicitly.[1]

The time dependence of any function of the phase-space variables, $B(\mathbf{r}^N, \mathbf{p}^N)$ say, may be represented in a manner similar to (2.1.9). Although B is not an explicit function of t, it will in general change with time as the system moves along its phase trajectory. The time derivative of B is therefore given by

$$\frac{\mathrm{d}B}{\mathrm{d}t} = \sum_{i=1}^{N}\left(\frac{\partial B}{\partial \mathbf{r}_i}\cdot\dot{\mathbf{r}}_i + \frac{\partial B}{\partial \mathbf{p}_i}\cdot\dot{\mathbf{p}}_i\right) \tag{2.1.12}$$

or, from Hamilton's equations:

$$\frac{\mathrm{d}B}{\mathrm{d}t} = \sum_{i=1}^{N}\left(\frac{\partial B}{\partial \mathbf{r}_i}\cdot\frac{\partial \mathcal{H}}{\partial \mathbf{p}_i} - \frac{\partial B}{\partial \mathbf{p}_i}\cdot\frac{\partial \mathcal{H}}{\partial \mathbf{r}_i}\right) = i\mathcal{L}B \tag{2.1.13}$$

which has as its solution

$$B(t) = \exp(i\mathcal{L}t)\, B(0) \tag{2.1.14}$$

Note the change of sign in the propagator compared with (2.1.10).

The description of the system that the full phase-space probability density provides is for many purposes unnecessarily detailed. Normally we are interested only in the behaviour of a subset of particles of size n, say, and the redundant information can be eliminated by integrating $f^{[N]}$ over the coordinates and momenta of the other $(N - n)$ particles. We therefore define a *reduced phase-space distribution function* $f^{(n)}(\mathbf{r}^n, \mathbf{p}^n; t)$ by

$$f^{(n)}\big(\mathbf{r}^n, \mathbf{p}^n; t\big) = \frac{N!}{(N-n)!}\iint f^{[N]}\big(\mathbf{r}^N, \mathbf{p}^N; t\big)\,\mathrm{d}\mathbf{r}^{(N-n)}\,\mathrm{d}\mathbf{p}^{(N-n)} \tag{2.1.15}$$

where $\mathbf{r}^n \equiv \mathbf{r}_1, \ldots, \mathbf{r}_n$ and $\mathbf{r}^{(N-n)} \equiv \mathbf{r}_{n+1}, \ldots, \mathbf{r}_N$, etc. The quantity $f^{(n)}\,\mathrm{d}\mathbf{r}^n\,\mathrm{d}\mathbf{p}^n$ yields the probability of finding a subset of n particles in the reduced phase-space element $\mathrm{d}\mathbf{r}^n\,\mathrm{d}\mathbf{p}^n$ at time t, irrespective of the coordinates and momenta of the remaining particles; the combinatorial factor $N!/(N-n)!$ is the number of ways of choosing a subset of size n.

To find an equation of motion for $f^{(n)}$ we consider the special case when the total force acting on particle i is the sum of an external force $\mathbf{X}_i$, arising from an external potential $\phi(\mathbf{r}_i)$, and of pair forces $\mathbf{F}_{ij}$ due to other particles j, with $\mathbf{F}_{ii} = 0$. The second of Hamilton's equations (2.1.3) now takes the form

$$\frac{\partial \mathcal{H}}{\partial \mathbf{r}_i} = -\mathbf{X}_i - \sum_{j=1}^{N} \mathbf{F}_{ij} \tag{2.1.16}$$

and the Liouville equation becomes

$$\left(\frac{\partial}{\partial t} + \sum_{i=1}^{N} \frac{\mathbf{p}_i}{m} \cdot \frac{\partial}{\partial \mathbf{r}_i} + \sum_{i=1}^{N} \mathbf{X}_i \cdot \frac{\partial}{\partial \mathbf{p}_i}\right) f^{[N]} = -\sum_{i=1}^{N}\sum_{j=1}^{N} \mathbf{F}_{ij} \cdot \frac{\partial f^{[N]}}{\partial \mathbf{p}_i} \tag{2.1.17}$$

We now multiply through by $N!/(N-n)!$ and integrate over the $3(N-n)$ coordinates $\mathbf{r}_{n+1}, \ldots, \mathbf{r}_N$ and $3(N-n)$ momenta $\mathbf{p}_{n+1}, \ldots, \mathbf{p}_N$. The probability density $f^{[N]}$ is zero when $\mathbf{r}_i$ lies outside the volume occupied by the system and must vanish as $\mathbf{p}_i \to \infty$ to ensure convergence of the integrals over momenta in (2.1.4). Thus $f^{[N]}$ vanishes at the limits of integration and the derivative of $f^{[N]}$ with respect to any component of position or momentum will contribute nothing to the result when integrated with respect to that component. On integration, therefore, all terms disappear for which $i > n$ in (2.1.17). What remains, given the definition of $f^{(n)}$ in (2.1.15), is

$$\begin{aligned}
&\left(\frac{\partial}{\partial t} + \sum_{i=1}^{n} \frac{\mathbf{p}_i}{m} \cdot \frac{\partial}{\partial \mathbf{r}_i} + \sum_{i=1}^{n} \mathbf{X}_i \cdot \frac{\partial}{\partial \mathbf{p}_i}\right) f^{(n)} \\
&\quad = -\sum_{i=1}^{n}\sum_{j=1}^{n} \mathbf{F}_{ij} \cdot \frac{\partial f^{(n)}}{\partial \mathbf{p}_i} \\
&\qquad - \frac{N!}{(N-n)!} \sum_{i=1}^{n}\sum_{j=n+1}^{N} \iint \mathbf{F}_{ij} \cdot \frac{\partial f^{[N]}}{\partial \mathbf{p}_i}\,\mathrm{d}\mathbf{r}^{(N-n)}\,\mathrm{d}\mathbf{p}^{(N-n)}
\end{aligned} \tag{2.1.18}$$

Because the particles are identical, $f^{[N]}$ is symmetric with respect to interchange of particle labels and the sum of terms for $j = n+1$ to N on the right-hand side of (2.1.18) may be replaced by $(N-n)$ times the value of any one term. This simplification makes it possible to rewrite (2.1.18) in a manner that relates the behaviour of $f^{(n)}$ to that of $f^{(n+1)}$:

$$\begin{aligned}
&\left(\frac{\partial}{\partial t} + \sum_{i=1}^{n} \frac{\mathbf{p}_i}{m} \cdot \frac{\partial}{\partial \mathbf{r}_i} + \sum_{i=1}^{n} \left(\mathbf{X}_i + \sum_{j=1}^{n} \mathbf{F}_{ij}\right) \cdot \frac{\partial}{\partial \mathbf{p}_i}\right) f^{(n)} \\
&\quad = -\sum_{i=1}^{n} \iint \mathbf{F}_{i,n+1} \cdot \frac{\partial f^{(n+1)}}{\partial \mathbf{p}_i}\,\mathrm{d}\mathbf{r}_{n+1}\,\mathrm{d}\mathbf{p}_{n+1}
\end{aligned} \tag{2.1.19}$$

The system of coupled equations represented by (2.1.19) was first obtained by Yvon and subsequently rederived by others. It is known as the Bogolyubov–Born–Green–Kirkwood–Yvon or BBGKY hierarchy. The equations are exact, though limited in their applicability to systems for which the particle interactions are pairwise additive. They are not immediately useful, however, because they merely express one unknown function, $f^{(n)}$, in terms of another, $f^{(n+1)}$. Some approximate *closure relation* is therefore needed.

In practice the most important member of the BBGKY hierarchy is that corresponding to $n = 1$:

$$\left(\frac{\partial}{\partial t} + \frac{\mathbf{p}_1}{m}\cdot\frac{\partial}{\partial \mathbf{r}_1} + \mathbf{X}_1\cdot\frac{\partial}{\partial \mathbf{p}_1}\right) f^{(1)}(\mathbf{r}_1, \mathbf{p}_1; t) = -\iint \mathbf{F}_{12}\cdot\frac{\partial}{\partial \mathbf{p}_1} f^{(2)}(\mathbf{r}_1, \mathbf{p}_1, \mathbf{r}_2, \mathbf{p}_2; t)\,\mathrm{d}\mathbf{r}_2\,\mathrm{d}\mathbf{p}_2 \tag{2.1.20}$$

Much effort has been devoted to finding approximate solutions to (2.1.20) on the basis of expressions that relate the two-particle distribution function $f^{(2)}$ to the single-particle function $f^{(1)}$. From the resulting *kinetic equations* it is possible to calculate the hydrodynamic transport coefficients, but the approximations made are rarely appropriate to liquids because correlations between particles are mostly treated in a very crude way.[2] The simplest possible approximation is to ignore pair correlations altogether by writing

$$f^{(2)}(\mathbf{r}, \mathbf{p}, \mathbf{r}', \mathbf{p}'; t) \approx f^{(1)}(\mathbf{r}, \mathbf{p}; t)\, f^{(1)}(\mathbf{r}', \mathbf{p}'; t) \tag{2.1.21}$$

This leads to the Vlasov equation:

$$\left(\frac{\partial}{\partial t} + \frac{\mathbf{p}}{m}\cdot\frac{\partial}{\partial \mathbf{r}} + \left[\mathbf{X}(\mathbf{r}, t) + \overline{\mathbf{F}}(\mathbf{r}, t)\right]\cdot\frac{\partial}{\partial \mathbf{p}}\right) f^{(1)}(\mathbf{r}, \mathbf{p}; t) = 0 \tag{2.1.22}$$

where the quantity

$$\overline{\mathbf{F}}(\mathbf{r}, t) = \iint \mathbf{F}(\mathbf{r}, \mathbf{r}'; t)\, f^{(1)}(\mathbf{r}', \mathbf{p}'; t)\,\mathrm{d}\mathbf{r}'\mathrm{d}\mathbf{p}' \tag{2.1.23}$$

is the average force exerted by other particles, situated at points $\mathbf{r}'$, on a particle that at time t is at a point $\mathbf{r}$; this is an approximation of classic mean-field type. Though obviously not suitable for liquids, the Vlasov equation is widely used in plasma physics, where the long-range character of the Coulomb potential justifies a mean-field treatment of the interactions.

Equation (2.1.20) may be rewritten schematically in the form

$$\left(\frac{\partial}{\partial t} + \frac{\mathbf{p}_1}{m}\cdot\frac{\partial}{\partial \mathbf{r}_1} + \mathbf{X}_1\cdot\frac{\partial}{\partial \mathbf{p}_1}\right) f^{(1)} = \left(\frac{\partial f^{(1)}}{\partial t}\right)_{\text{coll}} \tag{2.1.24}$$

where the term $(\partial f^{(1)}/\partial t)_{\text{coll}}$ is the rate of change of $f^{(1)}$ due to collisions between particles. The collision term is given rigorously by the right-hand side of (2.1.20) but in the

Vlasov equation it is eliminated by replacing the true external force $\mathbf{X}(\mathbf{r}, t)$ by an effective force – the quantity inside square brackets in (2.1.22) – which depends in part on $f^{(1)}$ itself. For this reason the Vlasov equation is called a "collisionless" approximation. In the most famous of all kinetic equations, derived by Boltzmann more than a century ago, $(\partial f^{(1)}/\partial t)_{\text{coll}}$ is evaluated with the help of two assumptions, which in general are justified only at low densities: that two-body collisions alone are involved and that successive collisions are uncorrelated.[2] The second of these assumptions, that of "molecular chaos", corresponds formally to supposing that the factorisation represented by (2.1.21) applies prior to any collision, though not subsequently. In simple terms it means that when two particles collide, no memory is retained of any previous encounters between them, an assumption that clearly breaks down when recollisions are frequent events. A binary collision at a point $\mathbf{r}$ is characterised by the momenta $\mathbf{p}_1$, $\mathbf{p}_2$ of the two particles before collision and their momenta $\mathbf{p}_1'$, $\mathbf{p}_2'$ afterwards; the post-collisional momenta are related to their pre-collisional values by the laws of classical mechanics. With Boltzmann's approximations the collision term in (2.1.24) becomes

$$\left(\frac{\partial f^{(1)}}{\partial t}\right)_{\text{coll}} = \frac{1}{m}\iint \sigma(\Omega, \Delta p)\big[f^{(1)}(\mathbf{r}, \mathbf{p}_1'; t) f^{(1)}(\mathbf{r}, \mathbf{p}_2'; t) - f^{(1)}(\mathbf{r}, \mathbf{p}_1; t) f^{(1)}(\mathbf{r}, \mathbf{p}_2; t)\big]\, \mathrm{d}\Omega\, \mathrm{d}\mathbf{p}_2 \qquad (2.1.25)$$

where $\Delta p \equiv |\mathbf{p}_2 - \mathbf{p}_1|$ and $\sigma(\Omega, \Delta p)$ is the differential cross-section for scattering into a solid angle $\mathrm{d}\Omega$. As Boltzmann showed, this form of the collision term is able to account for the fact that many-particle systems evolve irreversibly towards an equilibrium state. This irreversibility is described by Boltzmann's H-theorem; the source of the irreversibility is the assumption of molecular chaos.

Solution of the Boltzmann equation leads to explicit expressions for the hydrodynamic transport coefficients in terms of certain "collision" integrals.[3] The differential scattering cross-section and hence the collision integrals themselves can be evaluated numerically for a given choice of two-body interaction, though for hard spheres they have a simple, analytical form. The results, however, are applicable only to dilute gases. In the case of hard spheres the Boltzmann equation was later modified semi-empirically by Enskog in a manner that extends its range of applicability to considerably higher densities. Enskog's theory retains the two key assumptions involved in the derivation of the Boltzmann equation, but it also corrects in two ways for the finite size of the colliding particles. First, allowance is made for the modification of the collision rate by the hard-sphere interaction. Because the same interaction is also responsible for the increase in pressure over its ideal-gas value, the enhancement of the collision rate relative to its low-density limit can be calculated if the hard-sphere equation of state is known. Secondly, "collisional transfer" is incorporated into the theory by rewriting (2.1.25) in a form in which the distribution functions for the two colliding particles are evaluated not the same point, $\mathbf{r}$, but at points separated by a distance equal to the hard-sphere diameter. This is an important modification of the theory, because at high densities interactions rather than particle displacements provide the dominant mechanism for the transport of energy and momentum.

The phase-space probability density of a system in thermodynamic equilibrium is a function of the time-varying coordinates and momenta, but is independent of t at each point in

phase space. We shall use the symbol $f_0^{[N]}(\mathbf{r}^N, \mathbf{p}^N)$ to denote the equilibrium probability density; it follows from (2.1.6) that a sufficient condition for a probability density to be descriptive of a system in equilibrium is that it should be some function of the hamiltonian. Integration of $f_0^{[N]}$ over a subset of coordinates and momenta in the manner of (2.1.15) yields a set of equilibrium phase-space distribution functions $f_0^{(n)}(\mathbf{r}^n, \mathbf{p}^n)$. The case $n = 1$ corresponds to the equilibrium single-particle distribution function; if there is no external field the distribution is independent of $\mathbf{r}$ and has the familiar maxwellian form, i.e.

$$f_0^{(1)}(\mathbf{r}, \mathbf{p}) = \frac{\rho \exp(-\beta|\mathbf{p}|^2/2m)}{(2\pi m k_\mathrm{B} T)^{3/2}} \equiv \rho f_\mathrm{M}(\mathbf{p}) \tag{2.1.26}$$

where $f_\mathrm{M}(\mathbf{p})$ is the Maxwell distribution of momenta, normalised such that

$$\int f_\mathrm{M}(\mathbf{p})\, \mathrm{d}\mathbf{p} = 1 \tag{2.1.27}$$

The corresponding distribution of velocities $\mathbf{u}$ is

$$\phi_\mathrm{M}(\mathbf{u}) = \left(\frac{m}{2\pi k_\mathrm{B} T}\right)^{3/2} \exp\left(-m\beta|\mathbf{u}|^2/2\right) \tag{2.1.28}$$

2.2 TIME AVERAGES AND ENSEMBLE AVERAGES

Certain thermodynamic properties of a physical system may be written as averages of functions of the coordinates and momenta of the constituent particles. These are the so-called "mechanical" properties, which include internal energy and pressure; "thermal" properties such as entropy are not expressible in this way. In a state of thermal equilibrium these averages must be independent of time. To avoid undue complications we again suppose that the system of interest consists of N identical, spherical particles. If the system is isolated from its surroundings, its total energy is constant, i.e. the hamiltonian is a constant of the motion.

As before, let $B(\mathbf{r}^N, \mathbf{p}^N)$ be some function of the $6N$ phase-space variables and let $\langle B \rangle$ be its average value, where the angular brackets represent an averaging process of a nature as yet unspecified. Given the coordinates and momenta of the particles at some instant, their values at any later (or earlier) time can in principle be obtained as the solution to Newton's equations of motion, i.e. to a set of $3N$ coupled, second-order, differential equations which, in the absence of an external field, have the form

$$m\ddot{\mathbf{r}}_i = \mathbf{F}_i = -\boldsymbol{\nabla}_i V_N\left(\mathbf{r}^N\right) \tag{2.2.1}$$

where $\mathbf{F}_i$ is the total force on particle i. It is therefore natural to view $\langle B \rangle$ as a time average over the dynamical history of the system, i.e.

$$\langle B \rangle_\mathrm{t} = \lim_{\tau \to \infty} \frac{1}{\tau} \int_0^\tau B\left[\mathbf{r}^N(t), \mathbf{p}^N(t)\right] \mathrm{d}t \tag{2.2.2}$$

A simple example of the use of (2.2.2) is the calculation of the thermodynamic temperature of the system from the time average of the total kinetic energy. If

$$\mathcal{T}(t) = \frac{2}{3Nk_{\mathrm{B}}} K_N(t) = \frac{1}{3Nk_{\mathrm{B}}m} \sum_{i=1}^{N} \left|\mathbf{p}_i(t)\right|^2 \tag{2.2.3}$$

then

$$T \equiv \langle \mathcal{T} \rangle_{\mathrm{t}} = \lim_{\tau\to\infty} \frac{1}{\tau} \int_0^\tau \mathcal{T}(t)\,\mathrm{d}t \tag{2.2.4}$$

As a more interesting application we can use (2.2.2) and (2.2.4) to show that the equation of state is related to the time average of the *virial function* of Clausius. The virial function is defined as

$$\mathcal{V}\left(\mathbf{r}^N\right) = \sum_{i=1}^{N} \mathbf{r}_i \cdot \mathbf{F}_i \tag{2.2.5}$$

From previous formulae, together with an integration by parts, we find that

$$\begin{aligned} \langle \mathcal{V} \rangle_{\mathrm{t}} &= \lim_{\tau\to\infty} \frac{1}{\tau} \int_0^\tau \sum_{i=1}^{N} \mathbf{r}_i(t) \cdot \mathbf{F}_i(t)\,\mathrm{d}t = \lim_{\tau\to\infty} \frac{1}{\tau} \int_0^\tau \sum_{i=1}^{N} \mathbf{r}_i(t) \cdot m\ddot{\mathbf{r}}_i(t)\,\mathrm{d}t \\ &= -\lim_{\tau\to\infty} \frac{1}{\tau} \int_0^\tau \sum_{i=1}^{N} m\left|\dot{\mathbf{r}}_i(t)\right|^2 \mathrm{d}t = -3Nk_{\mathrm{B}}T \end{aligned} \tag{2.2.6}$$

or

$$\langle \mathcal{V} \rangle_{\mathrm{t}} = -2\langle K_N \rangle_{\mathrm{t}} \tag{2.2.7}$$

which is the virial theorem of classical mechanics. The total virial function may be separated into two parts: one, $\mathcal{V}_{\mathrm{int}}$, comes from the forces between particles; the other, $\mathcal{V}_{\mathrm{ext}}$, arises from the forces exerted by the walls and is related in a simple way to the pressure, P. The force exerted by a surface element $\mathrm{d}\mathbf{S}$ located at $\mathbf{r}$ is $-P\mathbf{n}\,\mathrm{d}S$, where $\mathbf{n}$ is a unit vector directed outwards, and its contribution to the average virial is $-P\mathbf{r}\cdot\mathbf{n}\,\mathrm{d}S$. Integrating over the surface we find that

$$\langle \mathcal{V}_{\mathrm{ext}} \rangle = -P \int \mathbf{r}\cdot\mathbf{n}\,\mathrm{d}S = -P \int \boldsymbol{\nabla}\cdot\mathbf{r}\,\mathrm{d}V = -3PV \tag{2.2.8}$$

Equation (2.2.7) may therefore be rearranged to give the *virial equation*:

$$PV = Nk_{\mathrm{B}}T + \tfrac{1}{3}\langle \mathcal{V}_{\mathrm{int}} \rangle_{\mathrm{t}} = Nk_{\mathrm{B}}T - \tfrac{1}{3}\left\langle \sum_{i=1}^{N} \mathbf{r}_i(t) \cdot \boldsymbol{\nabla}_i V_N\left[\mathbf{r}^N(t)\right] \right\rangle_{\mathrm{t}} \tag{2.2.9}$$

or

$$\frac{\beta P}{\rho} = 1 - \frac{\beta}{3N}\left\langle \sum_{i=1}^{N} \mathbf{r}_i(t) \cdot \boldsymbol{\nabla}_i V_N\big[\mathbf{r}^N(t)\big] \right\rangle_{\mathrm{t}} \tag{2.2.10}$$

When $V_N = 0$, the virial equation reduces to the equation of state of an ideal gas, $PV = Nk_{\mathrm{B}}T$.

The alternative to the time-averaging procedure described by (2.2.2) is to average over a suitably constructed *ensemble*. A statistical-mechanical ensemble is an arbitrarily large collection of imaginary systems, each of which is a replica of the physical system of interest and characterised by the same macroscopic parameters. The systems of the ensemble differ from each other in the assignment of the coordinates and momenta of the particles and the dynamics of the ensemble as a whole is represented by the motion of a cloud of phase points distributed in phase space according to the probability density $f^{[N]}(\mathbf{r}^N, \mathbf{p}^N; t)$ introduced in Section 2.1. The equilibrium ensemble average of the function $B(\mathbf{r}^N, \mathbf{p}^N)$ is therefore given by

$$\langle B \rangle_{\mathrm{e}} = \iint B\big(\mathbf{r}^N, \mathbf{p}^N\big) f_0^{[N]}\big(\mathbf{r}^N, \mathbf{p}^N\big)\, \mathrm{d}\mathbf{r}^N\, \mathrm{d}\mathbf{p}^N \tag{2.2.11}$$

where $f_0^{[N]}$ is the equilibrium probability density. For example, the thermodynamic internal energy is the ensemble average of the hamiltonian:

$$U \equiv \langle \mathcal{H} \rangle_{\mathrm{e}} = \iint \mathcal{H} f_0^{[N]}\, \mathrm{d}\mathbf{r}^N\, \mathrm{d}\mathbf{p}^N \tag{2.2.12}$$

The explicit form of the equilibrium probability density depends on the macroscopic parameters that characterise the ensemble. The simplest case is when the systems of the ensemble are assumed to have the same number of particles, the same volume and the same total energy, E say. An ensemble constructed in this way is called a *microcanonical* ensemble and describes a system that exchanges neither heat nor matter with its surroundings. The microcanonical equilibrium probability density is

$$f_0^{[N]}\big(\mathbf{r}^N, \mathbf{p}^N\big) = C\delta(\mathcal{H} - E) \tag{2.2.13}$$

where $\delta(\cdots)$ is the Dirac δ-function and C is a normalisation constant. The systems of a microcanonical ensemble are therefore uniformly distributed over the region of phase space corresponding to a total energy E; from (2.2.13) we see that the internal energy is equal to the value of the parameter E. The constraint of constant total energy is reminiscent of the condition of constant total energy under which time averages are taken. Indeed, time averages and ensemble averages are identical if the system is *ergodic*, by which is meant that after a suitable lapse of time the phase trajectory of the system will have passed an equal number of times through every phase-space element in the region defined by (2.2.13). In practice, however, it is almost always easier to calculate ensemble averages in one of the ensembles described in the next two sections.

2.3 CANONICAL AND ISOTHERMAL–ISOBARIC ENSEMBLES

A *canonical* ensemble is a collection of systems characterised by the same values of N, V and T. The assignment of a fixed temperature is justified by imagining that the systems of the ensemble are initially brought into thermal equilibrium with each other by immersing them in a heat bath at a temperature T. The equilibrium probability density for a system of identical, spherical particles is now

$$f_0^{[N]}(\mathbf{r}^N, \mathbf{p}^N) = \frac{1}{h^{3N} N!} \frac{\exp(-\beta \mathcal{H})}{Q_N} \tag{2.3.1}$$

where h is Planck's constant and the normalisation constant Q_N is the canonical *partition function*, defined as

$$Q_N = \frac{1}{h^{3N} N!} \iint \exp(-\beta \mathcal{H}) \, \mathrm{d}\mathbf{r}^N \, \mathrm{d}\mathbf{p}^N \tag{2.3.2}$$

Inclusion of the factor $1/h^{3N}$ in these definitions ensures that both $f_0^{[N]} \, \mathrm{d}\mathbf{r}^N \, \mathrm{d}\mathbf{p}^N$ and Q_N are dimensionless and consistent in form with the corresponding quantities of quantum statistical mechanics, while division by $N!$ ensures that microscopic states are correctly counted.

The *thermodynamic potential* appropriate to a situation in which N, V and T are chosen as independent thermodynamic variables is the Helmholtz free energy, F, defined as

$$F = U - TS \tag{2.3.3}$$

where S is the entropy. Use of the term "potential" means that equilibrium at constant values of T, V and N is reached when F is a minimum with respect to variations of any internal constraint. The link between statistical mechanics and thermodynamics is established via a relation between the thermodynamic potential and the partition function:

$$F = -k_\mathrm{B} T \ln Q_N \tag{2.3.4}$$

Let us assume that there is no external field and hence that the system of interest is homogeneous. Then the change in internal energy arising from infinitesimal changes in N, V and S is

$$\mathrm{d}U = T \, \mathrm{d}S - P \, \mathrm{d}V + \mu \, \mathrm{d}N \tag{2.3.5}$$

where μ is the chemical potential. Since N, V and S are all extensive variables it follows that

$$U = TS - PV + \mu N \tag{2.3.6}$$

Combination of (2.3.5) with the differential form of (2.3.3) shows that the change in free energy in an infinitesimal process is

$$\mathrm{d}F = -S \, \mathrm{d}T - P \, \mathrm{d}V + \mu \, \mathrm{d}N \tag{2.3.7}$$

Thus N, V and T are the natural variables of F; if F is a known function of these variables, all other thermodynamic functions can be obtained by differentiation:

$$S = -\left(\frac{\partial F}{\partial T}\right)_{V,N}, \qquad P = -\left(\frac{\partial F}{\partial V}\right)_{T,N}, \qquad \mu = \left(\frac{\partial F}{\partial N}\right)_{T,V} \tag{2.3.8}$$

and

$$U = F + TS = \left(\frac{\partial (F/T)}{\partial (1/T)}\right)_{V,N} \tag{2.3.9}$$

To each such thermodynamic relation there corresponds an equivalent relation in terms of the partition function. For example, it follows from (2.2.12) and (2.3.1) that

$$U = \frac{1}{h^{3N} N! Q_N} \iint \mathcal{H} \exp(-\beta \mathcal{H}) \, \mathrm{d}\mathbf{r}^N \mathrm{d}\mathbf{p}^N = -\left(\frac{\partial \ln Q_N}{\partial \beta}\right)_V \tag{2.3.10}$$

This result, together with the fundamental relation (2.3.4), is equivalent to the thermodynamic formula (2.3.9). Similarly, the expression for the pressure given by (2.3.8) can be rewritten as

$$P = k_\mathrm{B} T \left(\frac{\partial \ln Q_N}{\partial V}\right)_{T,N} \tag{2.3.11}$$

and shown to be equivalent to the virial equation (2.2.10).[4]

If the hamiltonian is separated into kinetic and potential energy terms in the manner of (2.1.1), the integrations over momenta in the definition (2.3.2) of Q_N can be carried out analytically, yielding a factor $(2\pi m k_\mathrm{B} T)^{1/2}$ for each of the $3N$ degrees of freedom. This allows the partition function to be rewritten as

$$Q_N = \frac{1}{N!} \frac{Z_N}{\Lambda^{3N}} \tag{2.3.12}$$

where Λ is the de Broglie thermal wavelength defined by (1.1.1) and

$$Z_N = \int \exp(-\beta V_N) \, \mathrm{d}\mathbf{r}^N \tag{2.3.13}$$

is the *configuration integral*. If $V_N = 0$:

$$Z_N = \int \cdots \int \mathrm{d}\mathbf{r}_1 \cdots \mathbf{r}_N = V^N \tag{2.3.14}$$

Hence the partition function of a uniform, ideal gas is

$$Q_N^{\mathrm{id}} = \frac{1}{N!} \frac{V^N}{\Lambda^{3N}} = \frac{q^N}{N!} \tag{2.3.15}$$

where $q = V/\Lambda^3$ is the single-particle translational partition function, familiar from elementary statistical mechanics. If Stirling's approximation is used for $\ln N!$, the Helmholtz free energy is

$$\frac{F^{\mathrm{id}}}{N} = k_{\mathrm{B}}T\left(\ln \Lambda^3\rho - 1\right) \tag{2.3.16}$$

and the chemical potential is

$$\mu^{\mathrm{id}} = k_{\mathrm{B}}T \ln \Lambda^3\rho \tag{2.3.17}$$

The partition function of a system of interacting particles is conveniently written in the form

$$Q_N = Q_N^{\mathrm{id}} \frac{Z_N}{V^N} \tag{2.3.18}$$

Then, on taking the logarithm of both sides, the Helmholtz free energy separates naturally into "ideal" and "excess" parts:

$$F = F^{\mathrm{id}} + F^{\mathrm{ex}} \tag{2.3.19}$$

where F^{id} is given by (2.3.16) and the excess part is

$$F^{\mathrm{ex}} = -k_{\mathrm{B}}T \ln \frac{Z_N}{V^N} \tag{2.3.20}$$

The excess part contains the contributions to the free energy that arise from interactions between particles; in the case of an inhomogeneous fluid there will also be a contribution that depends explicitly on the external potential. A similar division into ideal and excess parts can be made of any thermodynamic function obtained by differentiation of F with respect to either V or T. For example, the internal energy derived from (2.3.10) and (2.3.18) is

$$U = U^{\mathrm{id}} + U^{\mathrm{ex}} \tag{2.3.21}$$

where $U^{\mathrm{id}} = 3Nk_{\mathrm{B}}T/2$ and

$$U^{\mathrm{ex}} = \langle V_N \rangle = \frac{1}{Z_N} \int V_N \exp(-\beta V_N)\, \mathrm{d}\mathbf{r}^N \tag{2.3.22}$$

Note the simplification compared with the expression for U given by the first equality in (2.3.10); because V_N is a function only of the particle coordinates, the integrations over momenta cancel between numerator and denominator.

In the *isothermal–isobaric* ensemble pressure, rather than volume, is a fixed parameter. The thermodynamic potential of a system characterised by fixed values of N, P and T is the Gibbs free energy, G, defined as

$$G = F + PV \tag{2.3.23}$$

and other state functions are obtained by differentiation of G with respect to the independent variables. The link with statistical mechanics is now made through the relation

$$G = -k_{\mathrm{B}} T \ln \Delta_N \tag{2.3.24}$$

where the isothermal–isobaric partition function Δ_N is generally written[5] as a Laplace transform of the canonical partition function:

$$\begin{aligned} \Delta_N &= \frac{\beta P}{h^{3N} N!} \int_0^\infty \mathrm{d}V \iint \exp\bigl[-\beta(\mathcal{H} + PV)\bigr]\, \mathrm{d}\mathbf{r}^N\, \mathrm{d}\mathbf{p}^N \\ &= \beta P \int_0^\infty \exp(-\beta P V) Q_N \, \mathrm{d}V \end{aligned} \tag{2.3.25}$$

The factor βP (or some other constant with the dimensions of an inverse volume) is included to make Δ_N dimensionless. The form of (2.3.25) implies that the process of forming the ensemble average involves first calculating the canonical-ensemble average at a volume V and then averaging over V with a weight factor $\exp(-\beta P V)$.

2.4 THE GRAND CANONICAL ENSEMBLE

The discussion of ensembles has thus far been restricted to uniform systems containing a fixed number of particles ("closed" systems). We now extend the argument to the situation where the number of particles may vary by interchange with the surroundings, but retain the assumption that the system is homogeneous. The thermodynamic state of an "open" system is defined by specifying the values of μ, V and T and the corresponding thermodynamic potential is the grand potential, Ω, defined in terms of the Helmholtz free energy by

$$\Omega = F - N\mu \tag{2.4.1}$$

When the internal energy is given by (2.3.6), the grand potential reduces to

$$\Omega = -PV \tag{2.4.2}$$

and the differential form of (2.4.1) is

$$\mathrm{d}\Omega = -S\,\mathrm{d}T - P\,\mathrm{d}V - N\,\mathrm{d}\mu \tag{2.4.3}$$

The thermodynamic functions S, P and N are therefore given as derivatives of Ω by

$$S = -\left(\frac{\partial \Omega}{\partial T}\right)_{V,\mu}, \qquad P = -\left(\frac{\partial \Omega}{\partial V}\right)_{T,\mu}, \qquad N = -\left(\frac{\partial \Omega}{\partial \mu}\right)_{T,V} \tag{2.4.4}$$

An ensemble of systems having the same values of μ, V and T is called a *grand canonical* ensemble. The phase space of the grand canonical ensemble is the union of phase

spaces corresponding to all values of the variable N, and the constancy of T and μ is ensured by supposing that the systems of the ensemble are allowed to come to equilibrium with a reservoir with which they can exchange both heat and matter. The ensemble probability density is now a function of N as well as of the phase-space variables $\mathbf{r}^N$, $\mathbf{p}^N$; at equilibrium it takes the form

$$f_0(\mathbf{r}^N, \mathbf{p}^N; N) = \frac{\exp[-\beta(\mathcal{H} - N\mu)]}{\Xi} \tag{2.4.5}$$

where

$$\Xi = \sum_{N=0}^{\infty} \frac{\exp(N\beta\mu)}{h^{3N} N!} \iint \exp(-\beta\mathcal{H})\, \mathrm{d}\mathbf{r}^N \mathrm{d}\mathbf{p}^N = \sum_{N=0}^{\infty} \frac{z^N}{N!} Z_N \tag{2.4.6}$$

is the grand partition function and

$$z = \frac{\exp(\beta\mu)}{\Lambda^3} \tag{2.4.7}$$

is the *activity*. The definition (2.4.5) means that f_0 is normalised such that

$$\sum_{N=0}^{\infty} \frac{1}{h^{3N} N!} \iint f_0(\mathbf{r}^N, \mathbf{p}^N; N)\, \mathrm{d}\mathbf{r}^N \mathrm{d}\mathbf{p}^N = 1 \tag{2.4.8}$$

and the ensemble average of a microscopic variable $B(\mathbf{r}^N, \mathbf{p}^N)$ is

$$\langle B \rangle = \sum_{N=0}^{\infty} \frac{1}{h^{3N} N!} \iint B(\mathbf{r}^N, \mathbf{p}^N) f_0(\mathbf{r}^N, \mathbf{p}^N; N)\, \mathrm{d}\mathbf{r}^N \mathrm{d}\mathbf{p}^N \tag{2.4.9}$$

The link with thermodynamics is established through the relation

$$\Omega = -k_\mathrm{B} T \ln \Xi \tag{2.4.10}$$

Equation (2.3.17) shows that $z = \rho$ for a uniform, ideal gas and in that case (2.4.6) reduces to

$$\Xi^{\mathrm{id}} = \sum_{N=0}^{\infty} \frac{\rho^N V^N}{N!} = \exp(\rho V) \tag{2.4.11}$$

which, together with (2.4.2), yields the equation of state in the form $\beta P = \rho$.

The probability, $p(N)$, that at equilibrium a system of the ensemble contains precisely N particles irrespective of their coordinates and momenta is

$$p(N) = \frac{1}{h^{3N} N!} \iint f_0\, \mathrm{d}\mathbf{r}^N\, \mathrm{d}\mathbf{p}^N = \frac{1}{\Xi} \frac{z^N}{N!} Z_N \tag{2.4.12}$$

The average number of particles in the system is

$$\langle N\rangle = \sum_{N=0}^{\infty} Np(N) = \frac{1}{\Xi}\sum_{N=0}^{\infty} N\frac{z^N}{N!}Z_N = \frac{\partial \ln \Xi}{\partial \ln z} \tag{2.4.13}$$

which is equivalent to the last of the thermodynamic relations (2.4.4). A measure of the fluctuation in particle number about its average value is provided by the mean-square deviation, for which an expression is obtained if (2.4.13) is differentiated with respect to $\ln z$:

$$\begin{aligned}\frac{\partial\langle N\rangle}{\partial \ln z} &= z\frac{\partial}{\partial z}\left(\frac{1}{\Xi}\sum_{N=0}^{\infty} N\frac{z^N}{N!}Z_N\right)\\ &= \frac{1}{\Xi}\sum_{N=0}^{\infty} N^2\frac{z^N}{N!}Z_N - \left(\frac{1}{\Xi}\sum_{N=0}^{\infty} N\frac{z^N}{N!}Z_N\right)^2\\ &= \left\langle N^2\right\rangle - \langle N\rangle^2 \equiv \left\langle (\Delta N)^2\right\rangle\end{aligned} \tag{2.4.14}$$

or, equivalently:

$$\frac{\langle(\Delta N)^2\rangle}{\langle N\rangle} = \frac{k_{\mathrm{B}}T}{\langle N\rangle}\frac{\partial\langle N\rangle}{\partial\mu} \tag{2.4.15}$$

The right-hand side of this equation is an intensive quantity and the same must therefore be true of the left-hand side. Hence the relative root-mean-square deviation, $\langle(\Delta N)^2\rangle^{1/2}/\langle N\rangle$, tends to zero as $\langle N\rangle \to \infty$. In the *thermodynamic limit*, i.e. the limit $\langle N\rangle \to \infty$, $V \to \infty$ with $\rho = \langle N\rangle/V$ held constant, the number of particles in the system of interest (the thermodynamic variable N) may be identified with the grand canonical average, $\langle N\rangle$. In the same limit thermodynamic properties calculated in different ensembles become identical.

The intensive ratio (2.4.15) is related to the isothermal compressibility χ_T, defined as

$$\chi_T = -\frac{1}{V}\left(\frac{\partial V}{\partial P}\right)_T \tag{2.4.16}$$

To show this we note first that because the Helmholtz free energy is an extensive property it must be expressible in the form

$$F = N\phi(\rho, T) \tag{2.4.17}$$

where ϕ, the free energy per particle, is a function of the intensive variables ρ and T. From (2.3.8) we find that

$$\mu = \phi + \rho\left(\frac{\partial\phi}{\partial\rho}\right)_T \tag{2.4.18}$$

$$\left(\frac{\partial\mu}{\partial\rho}\right)_T = 2\left(\frac{\partial\phi}{\partial\rho}\right)_T + \rho\left(\frac{\partial^2\phi}{\partial\rho^2}\right)_T \tag{2.4.19}$$

and

$$P = \rho^2 \left(\frac{\partial \phi}{\partial \rho} \right)_T \tag{2.4.20}$$

$$\left(\frac{\partial P}{\partial \rho} \right)_T = 2\rho \left(\frac{\partial \phi}{\partial \rho} \right)_T + \rho^2 \left(\frac{\partial^2 \phi}{\partial \rho^2} \right)_T = \rho \left(\frac{\partial \mu}{\partial \rho} \right)_T \tag{2.4.21}$$

Because $(\partial P/\partial \rho)_T = -(V^2/N)(\partial P/\partial V)_{N,T} = 1/\rho \chi_T$ and $(\partial \mu/\partial \rho)_T = V(\partial \mu/\partial N)_{V,T}$ it follows that

$$N \left(\frac{\partial \mu}{\partial N} \right)_{V,T} = \frac{1}{\rho \chi_T} \tag{2.4.22}$$

and hence, from (2.4.15):

$$\frac{\langle (\Delta N)^2 \rangle}{\langle N \rangle} = \rho k_B T \chi_T \tag{2.4.23}$$

Thus the compressibility cannot be negative, since $\langle N^2 \rangle$ is always greater than or equal to $\langle N \rangle^2$.

Equation (2.4.23) and other fluctuation formulae of similar type can also be derived by purely thermodynamic arguments. In the thermodynamic theory of fluctuations described in Appendix A, the quantity N in (2.4.23) is interpreted as the number of particles in a subsystem of macroscopic dimensions that forms part of a much larger thermodynamic system. If the system as a whole is isolated from its surroundings, the probability of a fluctuation within the subsystem is proportional to $\exp(\Delta S_t / k_B)$, where ΔS_t is the total entropy change resulting from the fluctuation. Since ΔS_t can in turn be related to changes in the properties of the subsystem, it becomes possible to calculate the mean-square fluctuations in those properties; the results thereby obtained are identical to their statistical-mechanical counterparts. Because the subsystems are of macroscopic size, fluctuations in neighbouring subsystems will in general be uncorrelated. Strong correlations can, however, be expected under certain conditions. In particular, number fluctuations in two infinitesimal volume elements will be highly correlated if the separation of the elements is comparable with the range of the interparticle forces. A quantitative measure of these correlations is provided by the equilibrium distribution functions introduced below in Sections 2.5 and 2.6.

The definitions (2.3.1) and (2.4.5), together with (2.4.12), show that the equilibrium canonical and grand canonical ensemble probability densities are related by

$$\frac{1}{h^{3N} N!} f_0(\mathbf{r}^N, \mathbf{p}^N; N) = p(N) f_0^{[N]}(\mathbf{r}^N, \mathbf{p}^N) \tag{2.4.24}$$

The grand canonical ensemble average of any microscopic variable is therefore given by a weighted sum of averages of the same variable in the canonical ensemble, the weighting factor being the probability $p(N)$ that the system contains precisely N particles.

In addition to its significance as a fixed parameter of the grand canonical ensemble, the chemical potential can also be expressed as a canonical ensemble average. This result, due to Widom,[6] provides some useful insight into the meaning of chemical potential.

From (2.3.8) and (2.3.20) we see that

$$\mu^{\mathrm{ex}} = F^{\mathrm{ex}}(N+1, V, T) - F^{\mathrm{ex}}(N, V, T) = k_{\mathrm{B}}T \ln \frac{V Z_N}{Z_{N+1}} \tag{2.4.25}$$

or

$$\frac{V Z_N}{Z_{N+1}} = \exp\bigl(\beta \mu^{\mathrm{ex}}\bigr) \tag{2.4.26}$$

where Z_N, Z_{N+1} are the configuration integrals for systems containing N or $(N+1)$ particles, respectively. The ratio Z_{N+1}/Z_N is

$$\frac{Z_{N+1}}{Z_N} = \frac{\int \exp[-\beta V_{N+1}(\mathbf{r}^{N+1})]\, \mathrm{d}\mathbf{r}^{N+1}}{\int \exp[-\beta V_N(\mathbf{r}^N)]\, \mathrm{d}\mathbf{r}^N} \tag{2.4.27}$$

If the total potential energy of the system of $(N+1)$ particles is written as

$$V_{N+1}\bigl(\mathbf{r}^{N+1}\bigr) = V_N\bigl(\mathbf{r}^N\bigr) + \varepsilon \tag{2.4.28}$$

where ε is the energy of interaction of particle $(N+1)$ with all others, (2.4.27) can be re-expressed as

$$\frac{Z_{N+1}}{Z_N} = \frac{\int \exp(-\beta\varepsilon) \exp[-\beta V_N(\mathbf{r}^N)]\, \mathrm{d}\mathbf{r}^{N+1}}{\int \exp[-\beta V_N(\mathbf{r}^N)]\, \mathrm{d}\mathbf{r}^N} \tag{2.4.29}$$

If the system is homogeneous, translational invariance allows us to take $\mathbf{r}_{N+1}$ as origin for the remaining N position vectors and integrate over $\mathbf{r}_{N+1}$; this yields a factor V and (2.4.29) becomes

$$\frac{Z_{N+1}}{Z_N} = \frac{V \int \exp(-\beta\varepsilon) \exp(-\beta V_N)\, \mathrm{d}\mathbf{r}^N}{\int \exp(-\beta V_N)\, \mathrm{d}\mathbf{r}^N} = V\bigl\langle \exp(-\beta\varepsilon) \bigr\rangle \tag{2.4.30}$$

where the angular brackets denote a canonical ensemble average for the system of N particles. Substitution of (2.4.30) in (2.4.25) gives

$$\mu^{\mathrm{ex}} = -k_{\mathrm{B}}T \ln\bigl\langle \exp(-\beta\varepsilon) \bigr\rangle \tag{2.4.31}$$

Hence the excess chemical potential is proportional to the logarithm of the mean Boltzmann factor of a test particle introduced randomly into the system.

Equation (2.4.31) has a particularly simple interpretation for a system of hard spheres. Insertion of a test hard sphere can have one of two possible outcomes: either the sphere that is added overlaps with one or more of the spheres already present, in which case ε is infinite and the Boltzmann factor in (2.4.31) is zero, or there is no overlap, in which case $\varepsilon = 0$ and the Boltzmann factor is unity. The excess chemical potential may therefore be written as

$$\mu^{\mathrm{ex}} = -k_{\mathrm{B}}T \ln p_0 \tag{2.4.32}$$

where p_0 is the probability that a hard sphere can be introduced at a randomly chosen point in the system without creating an overlap.

2.5 PARTICLE DENSITIES AND DISTRIBUTION FUNCTIONS

It was shown in Section 2.3 that a factorisation of the equilibrium phase-space probability density into kinetic and potential terms leads naturally to a separation of thermodynamic properties into ideal and excess parts. A similar factorisation can be made of the reduced phase-space distribution functions $f_0^{(n)}$ defined in Section 2.1. We assume again that there is no external-field contribution to the hamiltonian and hence that $\mathcal{H} = K_N + V_N$, where K_N is a sum of independent terms. For a system of fixed N, V and T, $f_0^{[N]}$ is given by the canonical distribution (2.3.1). If we recall from Section 2.3 that integration over each component of momentum yields a factor $(2\pi m k_\mathrm{B} T)^{1/2}$, we see that $f_0^{(n)}$ can be written as

$$f_0^{(n)}(\mathbf{r}^n, \mathbf{p}^n) = \rho_N^{(n)}(\mathbf{r}^n) f_\mathrm{M}^{(n)}(\mathbf{p}^n) \tag{2.5.1}$$

where

$$f_\mathrm{M}^{(n)}(\mathbf{p}^n) = \frac{1}{(2\pi m k_\mathrm{B} T)^{3n/2}} \exp\left(-\beta \sum_{i=1}^{n} \frac{|\mathbf{p}_i|^2}{2m}\right) \tag{2.5.2}$$

is the product of n independent Maxwell distributions of the form defined by (2.1.26) and $\rho_N^{(n)}$, the equilibrium *n-particle density* is

$$\begin{aligned} \rho_N^{(n)}(\mathbf{r}^n) &= \frac{N!}{(N-n)!} \frac{1}{h^{3N} N! Q_N} \iint \exp(-\beta\mathcal{H})\, \mathrm{d}\mathbf{r}^{(N-n)}\, \mathrm{d}\mathbf{p}^N \\ &= \frac{N!}{(N-n)!} \frac{1}{Z_N} \int \exp(-\beta V_N)\, \mathrm{d}\mathbf{r}^{(N-n)} \end{aligned} \tag{2.5.3}$$

The quantity $\rho_N^{(n)}(\mathbf{r}^n)\, \mathrm{d}\mathbf{r}^n$ yields the probability of finding n particles of the system with coordinates in the volume element $\mathrm{d}\mathbf{r}^n$, irrespective of the positions of the remaining particles and irrespective of all momenta. The particle densities and the closely related, equilibrium *particle distribution functions*, defined below, provide a complete description of the structure of a fluid, while knowledge of the low-order particle distribution functions, in particular of the pair density $\rho_N^{(2)}(\mathbf{r}_1, \mathbf{r}_2)$, is often sufficient to calculate the equation of state and other thermodynamic properties of the system.

The definition of the n-particle density means that

$$\int \rho_N^{(n)}(\mathbf{r}^n)\, \mathrm{d}\mathbf{r}^n = \frac{N!}{(N-n)!} \tag{2.5.4}$$

Thus

$$\int \rho_N^{(1)}(\mathbf{r})\, \mathrm{d}\mathbf{r} = N \tag{2.5.5}$$

The single-particle density of a uniform fluid is therefore equal to the overall number density:

$$\rho_N^{(1)}(\mathbf{r}) = N/V = \rho \quad \text{(uniform fluid)} \tag{2.5.6}$$

In the special case of a uniform, ideal gas we know from (2.3.14) that $Z_N = V^N$. Hence the pair density is

$$\rho_N^{(2)} = \rho^2\left(1 - \frac{1}{N}\right) \quad \text{(ideal gas)} \tag{2.5.7}$$

The appearance of the term $1/N$ in (2.5.7) reflects the fact that in a system containing a fixed number of particles the probability of finding a particle in the volume element $\mathrm{d}\mathbf{r}_1$, given that another particle is in the element $\mathrm{d}\mathbf{r}_2$, is proportional to $(N-1)/V$ rather than ρ.

The n-particle distribution function $g_N^{(n)}(\mathbf{r}^n)$ is defined in terms of the corresponding particle densities by

$$g_N^{(n)}\left(\mathbf{r}^n\right) = \frac{\rho_N^{(n)}(\mathbf{r}_1, \ldots, \mathbf{r}_n)}{\prod_{i=1}^n \rho_N^{(1)}(\mathbf{r}_i)} \tag{2.5.8}$$

which for a homogeneous system reduces to

$$\rho^n g_N^{(n)}\left(\mathbf{r}^n\right) = \rho_N^{(n)}\left(\mathbf{r}^n\right) \tag{2.5.9}$$

The particle distribution functions measure the extent to which the structure of a fluid deviates from complete randomness. If the system is also isotropic, the pair distribution function $g_N^{(2)}(\mathbf{r}_1, \mathbf{r}_2)$ is a function only of the separation $r_{12} = |\mathbf{r}_2 - \mathbf{r}_1|$; it is then usually called the *radial distribution function* and written simply as $g(r)$. When r is much larger than the range of the interparticle potential, the radial distribution function approaches the ideal-gas limit; from (2.5.7) this limit can be identified as $(1 - 1/N) \approx 1$.

The particle densities defined by (2.5.3) are also expressible in terms of δ-functions of position in a form that is very convenient for later purposes. From the definition of a δ-function it follows that

$$\begin{aligned}\left\langle \delta(\mathbf{r} - \mathbf{r}_1)\right\rangle &= \frac{1}{Z_N}\int \delta(\mathbf{r} - \mathbf{r}_1)\exp\left[-\beta V_N(\mathbf{r}_1, \mathbf{r}_2, \ldots, \mathbf{r}_N)\right]\mathrm{d}\mathbf{r}^N \\ &= \frac{1}{Z_N}\int \cdots \int \exp\left[-\beta V_N(\mathbf{r}, \mathbf{r}_2, \ldots, \mathbf{r}_N)\right]\mathrm{d}\mathbf{r}_2 \cdots \mathrm{d}\mathbf{r}_N\end{aligned} \tag{2.5.10}$$

The ensemble average in (2.5.10) is a function of the coordinate $\mathbf{r}$ but is independent of the particle label (here taken to be 1). A sum over all particle labels is therefore equal to N times the contribution from any one particle. Comparison with the definition (2.5.3) then shows that

$$\rho_N^{(1)}(\mathbf{r}) = \left\langle \sum_{i=1}^N \delta(\mathbf{r} - \mathbf{r}_i)\right\rangle \tag{2.5.11}$$

which represents the ensemble average of a microscopic particle density $\rho(\mathbf{r})$. Similarly, the average of a product of two δ-functions is

$$\begin{aligned}\left\langle \delta(\mathbf{r}-\mathbf{r}_1)\delta(\mathbf{r}'-\mathbf{r}_2)\right\rangle &= \frac{1}{Z_N}\int \delta(\mathbf{r}-\mathbf{r}_1)\delta(\mathbf{r}'-\mathbf{r}_2)\exp\left[-\beta V_N(\mathbf{r}_1,\mathbf{r}_2,\ldots,\mathbf{r}_N)\right]\mathrm{d}\mathbf{r}^N \\ &= \frac{1}{Z_N}\int\cdots\int \exp\left[-\beta V_N(\mathbf{r},\mathbf{r}',\mathbf{r}_3,\ldots,\mathbf{r}_N)\right]\mathrm{d}\mathbf{r}_3\cdots\mathrm{d}\mathbf{r}_N \quad (2.5.12)\end{aligned}$$

which implies that

$$\rho_N^{(2)}(\mathbf{r},\mathbf{r}') = \left\langle \sum_{i=1}^{N}\sum_{j=1}^{N}{}' \delta(\mathbf{r}-\mathbf{r}_i)\delta(\mathbf{r}'-\mathbf{r}_j)\right\rangle \quad (2.5.13)$$

where the prime on the summation sign indicates that terms for which $i=j$ must be omitted. Finally, a useful δ-function representation can be obtained for the radial distribution function. It follows straightforwardly that

$$\begin{aligned}\left\langle \frac{1}{N}\sum_{i=1}^{N}\sum_{j=1}^{N}{}' \delta(\mathbf{r}-\mathbf{r}_j+\mathbf{r}_i)\right\rangle &= \left\langle \frac{1}{N}\int \sum_{i=1}^{N}\sum_{j=1}^{N}{}' \delta(\mathbf{r}'+\mathbf{r}-\mathbf{r}_j)\delta(\mathbf{r}'-\mathbf{r}_i)\,\mathrm{d}\mathbf{r}'\right\rangle \\ &= \frac{1}{N}\int \rho_N^{(2)}(\mathbf{r}'+\mathbf{r},\mathbf{r}')\,\mathrm{d}\mathbf{r}' \quad (2.5.14)\end{aligned}$$

Hence, if the system is both homogeneous and isotropic:

$$\left\langle \frac{1}{N}\sum_{i=1}^{N}\sum_{j=1}^{N}{}' \delta(\mathbf{r}-\mathbf{r}_j+\mathbf{r}_i)\right\rangle = \frac{\rho^2}{N}\int g_N^{(2)}(\mathbf{r},\mathbf{r}')\,\mathrm{d}\mathbf{r}' = \rho g(r) \quad (2.5.15)$$

The radial distribution function plays a key role in the physics of monatomic liquids. There are several reasons for this. First, $g(r)$ is measurable by radiation-scattering experiments. The results of such an experiment on liquid argon are pictured in Figure 2.1; $g(r)$ shows a pattern of peaks and troughs that is characteristic of all monatomic liquids, tends to unity at large r, and vanishes as $r \to 0$ as a consequence of the strongly repulsive forces that act at small particle separations. Secondly, the form of $g(r)$ provides considerable insight into what is meant by the structure of a liquid, at least at the level of pair correlations. The definition of $g(r)$ implies that on average the number of particles lying within the range r to $r+\mathrm{d}r$ from a reference particle is $4\pi r^2\rho g(r)\,\mathrm{d}r$ and the peaks in $g(r)$ represent "shells" of neighbours around the reference particle. Integration of $4\pi r^2\rho g(r)$ up to the position of the first minimum therefore provides an estimate of the nearest-neighbour "coordination number". The concepts of a "shell" of neighbours and a "coordination number" are obviously more appropriate to solids than to liquids, but they provide useful measures of the structure of a liquid provided the analogy with solids is not taken too far. The coordination number (≈ 12.2) calculated from the distribution function shown in the figure is in fact very close to the number (12) of nearest neighbours in

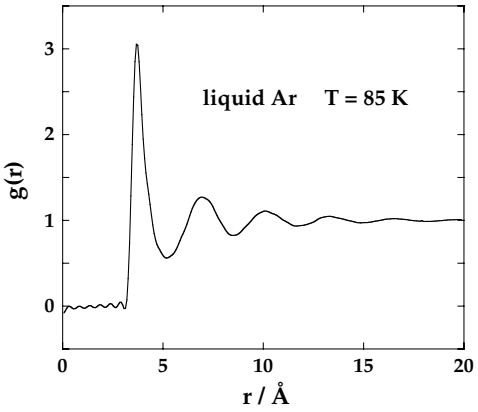

FIG. 2.1. Results of neutron-scattering experiments for the radial distribution function of liquid argon near the triple point. The ripples at small r are artefacts of the data analysis. After Yarnell *et al.*[7]

the face-centred cubic structure into which argon crystallises. Finally, if the atoms interact through pairwise-additive forces, thermodynamic properties can be expressed in terms of integrals over $g(r)$, as we shall now show.

Consider a uniform fluid for which the total potential energy is given by a sum of pair terms:

$$V_N(\mathbf{r}^N) = \sum_{i=1}^{N} \sum_{j>i}^{N} v(r_{ij}) \tag{2.5.16}$$

According to (2.3.22) the excess internal energy is

$$U^{\text{ex}} = \frac{N(N-1)}{2} \iint v(\mathbf{r}_{12}) \left(\frac{1}{Z_N} \int \cdots \int \exp(-\beta V_N)\, \mathrm{d}\mathbf{r}_3 \cdots \mathrm{d}\mathbf{r}_N \right) \mathrm{d}\mathbf{r}_1\, \mathrm{d}\mathbf{r}_2 \tag{2.5.17}$$

because the double sum over i, j in (2.5.16) gives rise to $N(N-1)/2$ terms, each of which leads to the same result after integration. Use of (2.5.3) and (2.5.9) allows (2.5.17) to be rewritten as

$$U^{\text{ex}} = \frac{N^2}{2V^2} \iint v(r_{12}) g_N^{(2)}(\mathbf{r}_1, \mathbf{r}_2)\, \mathrm{d}\mathbf{r}_1\, \mathrm{d}\mathbf{r}_2 \tag{2.5.18}$$

We can now take the position of particle 1 as the origin of coordinates, set $\mathbf{r}_{12} = \mathbf{r}_2 - \mathbf{r}_1$, and integrate over the coordinate $\mathbf{r}_1$ (which yields a factor V) to give

$$U^{\text{ex}} = \frac{N^2}{2V^2} \iint v(r_{12}) g(r_{21})\, \mathrm{d}\mathbf{r}_1\, \mathrm{d}\mathbf{r}_{12} = \frac{N^2}{2V} \int v(r) g(r)\, \mathrm{d}\mathbf{r} \tag{2.5.19}$$

or

$$\frac{U^{\text{ex}}}{N} = 2\pi\rho \int_0^\infty v(r) g(r) r^2\, \mathrm{d}r \tag{2.5.20}$$

This result, usually referred to as the *energy equation*, can also be derived in a more intuitive way. The mean number of particles at a distance between r and $r + \mathrm{d}r$ from a reference particle is $n(r)\,\mathrm{d}r = 4\pi r^2 \rho g(r)\,\mathrm{d}r$ and the total energy of interaction with the reference particle is $v(r)n(r)\,\mathrm{d}r$. The excess internal energy per particle is then obtained by integrating $v(r)n(r)$ between $r = 0$ and $r = \infty$ and dividing the result by two to avoid counting each interaction twice.

It is also possible to express the equation of state (2.2.10) as an integral over $g(r)$. Given the assumption of pairwise additivity of the interparticle forces, the internal contribution to the virial function can be written, with the help of Newton's Third Law, as

$$\mathcal{V}_{\text{int}} = \sum_{i=1}^{N} \sum_{j>i}^{N} \mathbf{r}_i \cdot \mathbf{F}_{ij} = -\sum_{i=1}^{N} \sum_{j>i}^{N} r_{ij} v'(r_{ij}) \tag{2.5.21}$$

where $v'(r) \equiv \mathrm{d}v(r)/\mathrm{d}r$. Then, starting from (2.2.10) and following the steps involved in the derivation of (2.5.20) but with $v(r_{ij})$ replaced by $r_{ij} v'(r_{ij})$, we find that

$$\frac{\beta P}{\rho} = 1 - \frac{2\pi\beta\rho}{3} \int_0^\infty v'(r) g(r) r^3\,\mathrm{d}r \tag{2.5.22}$$

Equation (2.5.22) is called either the *pressure equation* or, in common with (2.2.10), the virial equation.

Equations (2.5.20) and (2.5.22) are superficially simpler in form than (2.3.22) and (2.2.10), but the difficulty has merely shifted to that of determining the radial distribution function from the pair potential via (2.5.3) and (2.5.8). The problem is yet more complicated if there are many-body forces acting between particles or if the pair potential is not spherically symmetric. The presence of three-body forces, for example, leads to the appearance in expressions for the internal energy and pressure of integrals over the triplet distribution function $g_N^{(3)}(\mathbf{r}_1, \mathbf{r}_2, \mathbf{r}_3)$. We shall not pursue this matter further, since no new point of principle is involved, but the generalisation to systems of non-spherical particles is treated in detail in Chapter 11.

Because the pressure equation involves the derivative of the pair potential, it is not directly applicable in the calculation of the equation of state of hard spheres, or of other systems for which the pair potential contains a discontinuity. The problem can be overcome by rewriting (2.5.22) in terms of a function $y(r)$ defined as

$$y(r) = \exp\big[\beta v(r)\big] g(r) \tag{2.5.23}$$

We show in Chapter 4 that $y(r)$ is a continuous function of r even when there are discontinuities in $v(r)$ and hence in $g(r)$; $y(r)$ is called the *cavity distribution function* for reasons that will become clear in Section 4.6. On introducing the definition of $y(r)$ into (2.5.22) we find that

$$\begin{aligned} \frac{\beta P}{\rho} &= 1 - \frac{2\pi\beta\rho}{3} \int_0^\infty v'(r) e(r) y(r) r^3\,\mathrm{d}r \\ &= 1 + \frac{2\pi\rho}{3} \int_0^\infty e'(r) y(r) r^3\,\mathrm{d}r \end{aligned} \tag{2.5.24}$$

where

$$e(r) = \exp\bigl[-\beta v(r)\bigr] \tag{2.5.25}$$

is the Boltzmann factor for a pair of particles separated by a distance r and $e'(r) \equiv \mathrm{d}e(r)/\mathrm{d}r$. In the case of hard spheres, $e(r)$ is a unit step function, the derivative of which is a δ-function, i.e. $e(r) = 0$ for $r < d$, $e(r) = 1$ for $r > d$ and $e'(r) = \delta(r - d)$, where d is the hard-sphere diameter. Thus

$$\begin{aligned}\frac{\beta P}{\rho} &= 1 + \frac{2\pi\rho}{3}\int_0^\infty r^3 y(r)\delta(r-d)\,\mathrm{d}r \\ &= 1 + \frac{2\pi\rho}{3}\lim_{r\to d^+} r^3 y(r) = 1 + \frac{2\pi\rho}{3}d^3 g(d)\end{aligned} \tag{2.5.26}$$

The pressure of the hard-sphere fluid is therefore determined by the value of the radial distribution function at contact, where $g(r)$ goes discontinuously to zero. We show in the next section that $g(r) \approx e(r)$, and hence that $g(d) \to 1$, in the limit $\rho \to 0$. Thus, at low densities, $\beta P/\rho \approx 1 + 2\pi\rho d^3/3$; this expression represents the first two terms in the *virial expansion* of the equation of state in powers of the density, which we derive in a systematic way in Section 3.9.

The contact value of $g(r)$ also appears in the theory of transport processes in gases. Elementary kinetic theory[8] shows that at low densities the mean time between collisions suffered by a given particle is $\lambda/\bar{u}$, where $\bar{u} = (8k_\mathrm{B}T/\pi m)^{1/2}$ is the mean speed appropriate to a Maxwell distribution of momenta and λ is the mean free path. If the gas particles are treated as hard spheres of diameter d, the mean free path is $\lambda = 1/\sqrt{2}\pi\rho d^2$. Thus the collision rate in the dilute gas is $\Gamma_0 = \bar{u}/\lambda = 4\rho d^2(\pi k_\mathrm{B}T/m)^{1/2}$. The collision rate at higher densities is enhanced by the interactions between particles. Since the "forces" between hard spheres act only at collisions, the collision rate is proportional to the non-ideal contribution to the pressure, as given by the hard-sphere equation of state (2.5.26). It follows that $\Gamma_\mathrm{E} = g(d)\Gamma_0$ where Γ_E, the collision rate in the dense gas, is the quantity that arises in the Enskog theory discussed in Section 2.1. This enhancement of the collision rate leads to a corresponding reduction in the self-diffusion coefficient relative to the value obtained from the Boltzmann equation by a factor $1/g(d)$.

2.6 PARTICLE DENSITIES IN THE GRAND CANONICAL ENSEMBLE

The fact that in the canonical ensemble the pair distribution function behaves asymptotically as $(1 - 1/N)$ rather than tending strictly to unity is often irrelevant since the term of order N^{-1} vanishes in the thermodynamic limit. On the other hand, if a term of that order is integrated over the volume of the system, a result of order V/N is obtained, which usually cannot be ignored. The difficulties that this situation sometimes creates can be avoided by working in the grand canonical ensemble. As we shall see in later chapters, the grand canonical ensemble also provides a convenient framework for the derivation of density expansions of the particle distribution functions and, more generally, for the development of the theory of inhomogeneous fluids.

In the grand canonical ensemble the n-particle density is defined in terms of its canonical ensemble counterparts as the sum

$$\rho^{(n)}(\mathbf{r}^n) = \sum_{N \geqslant n}^{\infty} p(N)\rho_N^{(n)}(\mathbf{r}^n)$$
$$= \frac{1}{\Xi} \sum_{N=n}^{\infty} \frac{z^N}{(N-n)!} \int \exp(-\beta V_N)\, \mathrm{d}\mathbf{r}^{(N-n)} \tag{2.6.1}$$

where $p(N)$ is the probability (2.4.12). Integration of (2.6.1) over the coordinates $\mathbf{r}_1, \ldots, \mathbf{r}_n$ shows that $\rho^{(n)}$ is normalised such that

$$\int \rho^{(n)}(\mathbf{r}^n)\, \mathrm{d}\mathbf{r}^n = \left\langle \frac{N!}{(N-n)!} \right\rangle \tag{2.6.2}$$

In particular:

$$\int \rho^{(1)}\, \mathrm{d}\mathbf{r} = \langle N \rangle \tag{2.6.3}$$

and

$$\iint \rho^{(2)}(\mathbf{r}_1, \mathbf{r}_2)\, \mathrm{d}\mathbf{r}_1\, \mathrm{d}\mathbf{r}_2 = \langle N^2 \rangle - \langle N \rangle \tag{2.6.4}$$

Equation (2.6.3) confirms that the single-particle density in a homogeneous system is

$$\rho^{(1)} = \langle N \rangle / V \equiv \rho \quad \text{(uniform fluid)} \tag{2.6.5}$$

We know from Section 2.4 that for a homogeneous, ideal gas the activity z is equal to ρ, while the integral in (2.6.1) is equal to $V^{(N-n)}$. Hence the particle densities of the ideal gas are

$$\rho^{(n)} = \rho^n \quad \text{(ideal gas)} \tag{2.6.6}$$

The relation between the grand canonical n-particle density and the corresponding distribution function is the same as in the canonical ensemble, i.e.

$$g^{(n)}(\mathbf{r}^n) = \frac{\rho^{(n)}(\mathbf{r}_1, \ldots, \mathbf{r}_n)}{\prod_{i=1}^{n} \rho^{(1)}(\mathbf{r}_i)} \tag{2.6.7}$$

or $\rho^{(n)}(\mathbf{r}^n) = \rho^n g^{(n)}(\mathbf{r}^n)$ if the system is homogeneous, but now $g^{(n)}(\mathbf{r}^n) \to 1$ for all n as the mutual separations of all pairs of particles becomes sufficiently large. In particular, the *pair correlation function*, defined as

$$h^{(2)}(\mathbf{r}_1, \mathbf{r}_2) = g^{(2)}(\mathbf{r}_1, \mathbf{r}_2) - 1 \tag{2.6.8}$$

vanishes in the limit $|\mathbf{r}_2 - \mathbf{r}_1| \to \infty$. If we insert the definition (2.6.1) into (2.6.7) we obtain an expansion of the n-particle distribution function of a uniform fluid as a power series in z, which starts as

$$\Xi\left(\frac{\rho}{z}\right)^n g^{(n)}(\mathbf{r}^n) = \exp\bigl[-\beta V_n(\mathbf{r}^n)\bigr] + \mathcal{O}(z) \tag{2.6.9}$$

The first term on the right-hand side is the one corresponding to the case $N = n$ in (2.6.1). As $\rho \to 0$, it follows from earlier definitions that $z \to 0$, $\rho/z \to 1$ and $\Xi \to 1$. Hence, taking $n = 2$, we find that the low-density limit of the radial distribution function is equal to the Boltzmann factor of the pair potential:

$$\lim_{\rho \to 0} g(r) = \exp\bigl[-\beta v(r)\bigr] \tag{2.6.10}$$

The δ-function representations of $\rho_N^{(1)}(\mathbf{r})$, $\rho_N^{(2)}(\mathbf{r}, \mathbf{r}')$ and $g(r)$ provided by (2.5.11), (2.5.13) and (2.5.15), respectively, are also valid (without the subscript N) in the grand canonical ensemble, as are the energy and pressure equations, (2.5.20) and (2.5.22). On the other hand, the *compressibility equation*, which expresses χ_T as an integral over $g(r)$, can be derived only in the grand canonical ensemble because the compressibility is related to fluctuations in an open system via (2.4.23). The normalisations (2.6.3) and (2.6.4) show that

$$\iint \bigl[\rho^{(2)}(\mathbf{r}_1, \mathbf{r}_2) - \rho^{(1)}(\mathbf{r}_1)\rho^{(1)}(\mathbf{r}_2)\bigr]\,\mathrm{d}\mathbf{r}_1\,\mathrm{d}\mathbf{r}_2 = \langle N^2\rangle - \langle N\rangle - \langle N\rangle^2 \tag{2.6.11}$$

In the homogeneous case it follows immediately that

$$1 + \rho \int \bigl[g(r) - 1\bigr]\,\mathrm{d}\mathbf{r} = \frac{\langle N^2\rangle - \langle N\rangle^2}{\langle N\rangle} = \rho k_\mathrm{B} T \chi_T \tag{2.6.12}$$

Unlike the energy and pressure equations, the applicability of this relation does not rely on the assumption of pairwise additivity of the interparticle forces. For an ideal gas in the grand canonical ensemble, $g(r) = 1$ for all r; it follows from (2.6.12) that $\chi_T^{\mathrm{id}} = \beta/\rho$, in agreement with the result obtained by differentiation of the ideal-gas equation of state.

2.7 COMPUTER SIMULATION: MOLECULAR DYNAMICS AND MONTE CARLO

As we briefly mentioned at the end of Chapter 1, the behaviour of liquids, solids and dense gases at the microscopic level can be simulated in one of two ways: by the method of molecular dynamics or by the Monte Carlo method. The importance of computer simulation from the standpoint of liquid-state theory is the fact that it provides essentially exact, quasi-experimental data on well-defined models, particularly on those that are prototypical models of simple liquids. In this section we give a brief account of how classical computer simulations are carried out. Excellent books exist that provide much fuller descriptions of

the principles underlying the large variety of techniques that are now available and of the computer codes needed for their implementation.[9]

We begin by considering the method of molecular dynamics. In a conventional molecular-dynamics simulation of a bulk fluid a system of N particles is allocated a set of initial coordinates within a cell of fixed volume, most commonly a cube. A set of velocities is also assigned, usually drawn from a Maxwell distribution appropriate to the temperature of interest and selected in such a way that the net linear momentum of the system is zero. The subsequent calculation tracks the motion of the particles through space by integration of the classical equations of motion, and equilibrium properties are obtained as time averages over the dynamical history of the system in the manner outlined in Section 2.2. In modern work N is typically of order 10^3 or 10^4, though much larger systems have occasionally been studied. To minimise surface effects, and thereby simulate more closely the behaviour expected of a macroscopic system, it is customary to use a periodic boundary condition. The way in which the periodic boundary condition is applied is illustrated for the two-dimensional case in Figure 2.2. The system as a whole is divided into cells. Each cell is surrounded on all sides by periodic images of itself and particles that are images of each other have the same relative positions within their respective cells and the same momenta. When a particle enters or leaves a cell, the move is balanced by an image of that particle leaving or entering through the opposite edge. A key question is whether the properties of an infinite, periodic fluid with a unit cell containing, typically, of order 10^3 particles are representative of the properties of the macroscopic system that the calculation is designed to simulate. There is no easy or general answer to this, but broadly speaking it appears that bulk properties are only weakly dependent on sample size beyond $N \approx 500$, and that the remaining errors, relative to the $N \to \infty$ limit, are no larger than the inevitable statistical uncertainties. Nonetheless, the restriction on sample size does have some drawbacks. For example, it is impossible to study collective, spatial fluctuations of wavelength greater than L, the length of the cell. Use of a periodic boundary condition also has an effect on time correlations. In a molecular-dynamics simulation a local disturbance will

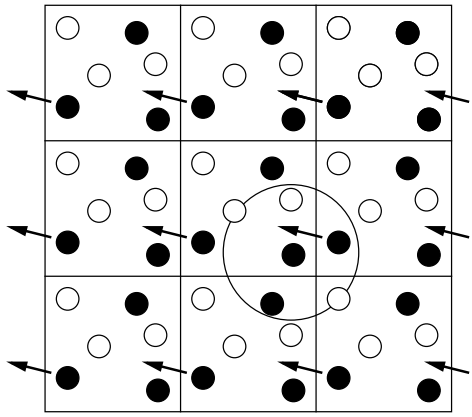

FIG. 2.2. Periodic boundary condition used in computer simulations. The circle represents the truncation sphere drawn around a black particle in the central cell. See text for details.

move through the periodic system and reappear at the same place, albeit in attenuated form, after a recurrence time of order L/c, where c is a speed of propagation that can be roughly equated to the speed of sound. The effects of periodicity will manifest themselves in spurious contributions to time correlations calculated over time intervals greater than this. Another difficulty, which is particularly acute for small samples, is the so-called quasi-ergodic problem. In the context of a computer simulation the term refers to the possibility that the system may become trapped in some region of phase space. Near the melting temperature, for example, an initial, lattice-type arrangement of particles may persist for very long times unless the density is appreciably less than the freezing density of the fluid. Whatever the starting conditions, time must be allowed for the system to equilibrate before the "production" stage of the calculation begins, while throughout the simulation it is important to monitor the properties of the system in such a way as to detect any tendency towards a long-time drift.

The interactions between particles can be of any form but in the great majority of cases they are assumed to be pairwise additive. For economy in computing time it is customary to truncate the interaction at a separation $r_c \leqslant \frac{1}{2}L$, where the cut-off radius r_c is typically a few particle diameters. When a truncation sphere is used, the interaction of a particle with its neighbours is calculated with a "nearest-neighbour" convention. The principle of this convention is illustrated in Figure 2.3: a particle i lying within a given cell is assumed to interact only with the nearest image of any other particle j (including j itself), the interaction being set equal to zero if the distance from the nearest image is greater than r_c. The significance of the restriction that r_c must be not greater than $\frac{1}{2}L$ is that there is at most one image of j (including j itself) lying with a sphere of radius $\frac{1}{2}L$ centred on i. Use of such a cut-off is inappropriate when the interparticle forces are long ranged, particularly for ionic systems, since there is not even a guarantee that the truncation sphere will be electrically neutral. One way to overcome this difficulty is to calculate the coulombic interaction of a particle not only with all other particle in the same cell but with all images in other cells. An infinite lattice sum of this type can be evaluated by the method of Ewald, the essence of which is to convert the slowly convergent sum in r^{-1} into two series that are separately rapidly convergent. One series is a sum in real space of a short-range potential that may safely be truncated, and the other is a sum over reciprocal-lattice vectors of the periodic array of cells. Strongly polar systems also require special treatment.

The earliest applications of the molecular-dynamics method were those of Alder and Wainwright[10] to systems of hard spheres and other hard-core particles. A feature of hard-sphere dynamics is that the velocities of the particles change only as the result of collisions; between collisions, the particles move in straight lines at constant speeds. The time-evolution of a many-particle, hard-sphere system may therefore be treated as a sequence of strictly binary, elastic collisions. Thus the algorithm for calculation of the trajectories consists of first advancing the coordinates of all particles until such a time as a collision occurs somewhere in the system, and then of exploiting the fact that both energy and momentum must be conserved to calculate the changes in velocities of the colliding particles. Since that calculation is exact, the trajectories of the particles can be computed with a precision limited only by round-off errors. The instantaneous temperature of the system remains constant because the total kinetic energy is conserved.

When the potentials are continuous, the trajectories of the particles, unlike those of hard spheres, can no longer be calculated exactly. In the case of spherically-symmetric potentials the equations of motion are the $3N$ coupled, second-order differential equations (2.2.1). These equations must be solved numerically by finite-difference methods, which leads unavoidably to errors in the particle trajectories. One of the simplest but also most successful algorithms is that first used by Verlet[11] in studies of the properties of the Lennard-Jones fluid. Let the coordinates of particle i at time t be $\mathbf{r}_i(t)$. The coordinates at times $t \pm \Delta t$ are given by Taylor expansions forwards and backwards in time around $\mathbf{r}_i(t)$:

$$\mathbf{r}_i(t \pm \Delta t) = \mathbf{r}_i(t) \pm \Delta t \dot{\mathbf{r}}_i(t) + \frac{\Delta t^2}{2!}\ddot{\mathbf{r}}_i(t) \pm \mathcal{O}\big(\Delta t^3\big) \tag{2.7.1}$$

By adding together the two expansions in (2.7.1), we obtain an estimate for the particle coordinates at time $t + \Delta t$:

$$\mathbf{r}_i(t + \Delta t) \approx -\mathbf{r}_i(t - \Delta t) + 2\mathbf{r}_i(t) + \frac{\Delta t^2}{m}\mathbf{F}_i(t) \tag{2.7.2}$$

where $\mathbf{F}_i(t)$ is the total force acting on particle i at time t. The error in the predicted coordinates is of order Δt^4. If we subtract the two expansions in (2.7.1), we obtain an estimate of the velocity of particle i at time t:

$$\dot{\mathbf{r}}_i(t) \approx \frac{1}{2\Delta t}\big[\mathbf{r}_i(t + \Delta t) - \mathbf{r}_i(t - \Delta t)\big] \tag{2.7.3}$$

The error now is of order Δt^2, but velocities play no part in the integration scheme and the particle trajectories are therefore unaffected. In one of a number of variants of the Verlet algorithm, the "velocity" version, the predicted coordinates are obtained solely from the forward expansion in (2.7.1), i.e.

$$\mathbf{r}_i(t + \Delta t) \approx \mathbf{r}_i(t) + \Delta t \dot{\mathbf{r}}_i(t) + \tfrac{1}{2}\Delta t^2 \ddot{\mathbf{r}}_i(t) \tag{2.7.4}$$

and the velocity is calculated as

$$\dot{\mathbf{r}}_i(t + \Delta t) \approx \dot{\mathbf{r}}_i(t) + \tfrac{1}{2}\Delta t\big[\ddot{\mathbf{r}}_i(t + \Delta t) + \ddot{\mathbf{r}}_i(t)\big] \tag{2.7.5}$$

Taken together, (2.7.4) and (2.7.5) are equivalent to (2.7.2). In other words, the particle trajectories in configuration space are identical in the two versions of the algorithm, but different estimates are obtained for the velocities.

Although simple in form, the original Verlet algorithm and its modifications are at least as satisfactory as higher-order schemes that make use of derivatives of the particle coordinates beyond $\ddot{\mathbf{r}}_i(t)$. It may be less accurate than others at short times but, more importantly, it conserves energy well even over very long times; it is also time reversible, as it should be for consistency with the equations of motion. Some understanding of the reasons for the stability of the algorithm can be obtained in the following way.[12]

The true dynamics of a system of particles is described by the action of the operator $\exp(i\mathcal{L}t)$ on the phase-space coordinates $\mathbf{r}^N$, $\mathbf{p}^N$. Let the time interval t be divided into P equal intervals of length Δt. Then

$$\exp(i\mathcal{L}t) = \left[\exp(i\mathcal{L}\Delta t)\right]^P \tag{2.7.6}$$

If the Liouville operator is divided in the from

$$i\mathcal{L} = i\mathcal{L}_{\mathbf{r}} + i\mathcal{L}_{\mathbf{p}} \tag{2.7.7}$$

where

$$i\mathcal{L}_{\mathbf{r}} \equiv \sum_{i=1}^{N} \dot{\mathbf{r}}_i \cdot \frac{\partial}{\partial \mathbf{r}_i}, \qquad i\mathcal{L}_{\mathbf{p}} = \sum_{i=1}^{N} \mathbf{F}_i \cdot \frac{\partial}{\partial \mathbf{p}_i} \tag{2.7.8}$$

and if Δt is sufficiently small, use of the so-called Trotter expansion allows the operator $\exp(i\mathcal{L}\Delta t)$ to be written as

$$\exp(i\mathcal{L}\Delta t) \approx \exp\left(i\tfrac{1}{2}\mathcal{L}_{\mathbf{p}}\Delta t\right)\exp(i\mathcal{L}_{\mathbf{r}}\Delta t)\exp\left(i\tfrac{1}{2}\mathcal{L}_{\mathbf{p}}\Delta t\right) \tag{2.7.9}$$

This relationship is only approximate, since the operators $\mathcal{L}_{\mathbf{r}}$ and $\mathcal{L}_{\mathbf{p}}$ do not commute; the error involved is of order Δt^3. The action of an exponential operator of the type appearing in (2.7.9) is

$$\exp\left(a\frac{\partial}{\partial x}\right) f(x) \equiv 1 + a\frac{\partial f}{\partial x} + \frac{a^2}{2!}\frac{\partial^2 f}{\partial x^2} + \cdots = f(x+a) \tag{2.7.10}$$

The effect of operating with $\exp(i\mathcal{L}_{\mathbf{r}}\Delta t)$ or $\exp(i\mathcal{L}_{\mathbf{p}}\Delta t)$ on $\mathbf{r}^N$, $\mathbf{p}^N$ is therefore to displace the position or momentum, respectively, of each particle according to the rules

$$\mathbf{r}_i \to \mathbf{r}_i + \Delta t\dot{\mathbf{r}}_i = \mathbf{r}_i + (\Delta t/m)\mathbf{p}_i, \qquad \mathbf{p}_i \to \mathbf{p}_i + \Delta t\dot{\mathbf{p}}_i = \mathbf{p}_i + \Delta t\mathbf{F}_i \tag{2.7.11}$$

The three operations involved in (2.7.9) may be regarded as successive steps in a simple predictor–corrector scheme. The first step yields an estimate of the momentum of the particle at time $t + \Delta t/2$:

$$\mathbf{p}_i(t + \Delta t/2) = \mathbf{p}_i(t) + \tfrac{1}{2}\Delta t\dot{\mathbf{p}}_i(t) = \mathbf{p}_i(t) + \tfrac{1}{2}\Delta t\mathbf{F}_i(t) \tag{2.7.12}$$

In the second step this estimate of the momentum is used to predict the coordinates of the particle at time $t + \Delta t$:

$$\begin{aligned}\mathbf{r}_i(t + \Delta t) &= \mathbf{r}_i(t) + (\Delta t/m)\mathbf{p}_i(t + \Delta t/2) \\ &= \mathbf{r}_i(t) + \Delta t\dot{\mathbf{r}}_i(t) + \left(\Delta t^2/2m\right)\mathbf{F}_i(t)\end{aligned} \tag{2.7.13}$$

Finally, an improved estimate is obtained for the momentum, based on the value of the force acting on the particle at its predicted position:

$$\begin{aligned}\mathbf{p}_i(t+\Delta t) &= \mathbf{p}_i(t+\Delta t/2) + \tfrac{1}{2}\Delta t\dot{\mathbf{p}}_i(t+\Delta t) \\ &= \mathbf{p}_i(t) + \tfrac{1}{2}\Delta t\big[\mathbf{F}_i(t) + \mathbf{F}_i(t+\Delta t)\big] \end{aligned} \tag{2.7.14}$$

The results obtained in this way for $\mathbf{r}_i(t+\Delta t)$, $\mathbf{p}_i(t+\Delta t)$ are precisely those that appear in the velocity version of the Verlet algorithm, (2.7.4) and (2.7.5). Although it is remarkable that a practical and widely used algorithm can be derived from a well-defined approximation for the propagator $\exp(i\mathcal{L}t)$, the greater significance of this analysis is its demonstration that not only is the Verlet algorithm time reversible but it also conserves volume in phase space in the sense of Section 2.1. Time reversibility follows from the fact that each of the steps implied in the use of (2.7.9) is separately time reversible. Similarly, for each step, the transformation of phase-space coordinates has a jacobian equal to unity. Thus the algorithm preserves the two key features of hamiltonian dynamics, which is almost certainly the reason why it is numerically so stable. Other time-reversible algorithms can be derived by dividing the Liouville operator in ways different from that adopted in (2.7.9).

A molecular-dynamics calculation is organised as a loop over time. At each step, the time is incremented by Δt, the total force acting on each particle is computed and the particles are advanced to their new positions. In the early stages of the simulation it is normal for the temperature to move away from the value at which it was set and some occasional rescaling of particle velocities is therefore needed. Once equilibrium is reached, the system is allowed to evolve undisturbed, with both potential and kinetic energies fluctuating around steady, mean values; the temperature of the system is calculated from the time-averaged kinetic energy, as in (2.2.4). The choice of time step Δt is made on the basis of how well total energy is conserved. In the case of a model of liquid argon, for example, an acceptable level of energy conservation is achieved with a time step of 10^{-14} s, and a moderately long run would be one lasting roughly 10^5 time steps, corresponding to a real time span of order 10^{-9} s. By treating argon atoms as hard spheres of diameter 3.4 Å, the mean "collision" time in liquid argon near its triple point can be estimated as roughly 10^{-13} s. Hence the criterion for the choice of time step based on energy conservation leads to the physically reasonable result that Δt should be about an order of magnitude smaller than the typical time between "collisions". As the time step is increased, the fluctuations in total energy become larger, until eventually an overall, upward drift in energy develops. Even when a small time step is used, deviations from the true dynamics are inevitable, and the phase-space trajectory of the system can be expected to diverge exponentially from that given by the exact solution of the equations of motion. In this respect an error in the algorithm plays a similar role to a small change in initial conditions. Any such change is known to lead to a divergence in phase space that grows with time as $\exp(\lambda t)$, where λ is a "Lyapunov exponent"; the consequences in terms of loss of correlation between trajectories can be dramatic.[13]

The methods outlined above are easily extended to molecular liquids if a model is adopted in which the molecules consist of independent atoms bound together by continuous intramolecular forces, but small molecules are in general better treated as rigid

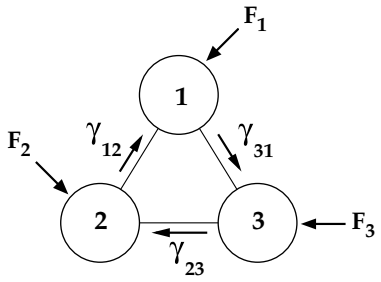

FIG. 2.3. The method of constraints applied to a triatomic molecule: $\mathbf{F}_i$ is the total intermolecular force on atom i and $\boldsymbol{\gamma}_{ij}$ is the force of constraint that maintains rigidity of the bond between i and j.

particles. One approach to the solution of the equations of motion of a rigid body involves a separation of internal and centre-of-mass coordinates. Another is based on the method of "constraints", in which the equations of motion are solved in cartesian form.[14] As an illustration of the use of constraint dynamics, consider the example of the triatomic molecule shown in Figure 2.3, in which each internuclear bond is of length L and each atom (labelled 1, 2 and 3) is of mass m. The geometry of the molecule is described by three constraints, $\sigma_{ij}(\mathbf{r}_1, \mathbf{r}_2, \mathbf{r}_3)$, such that

$$\sigma_{ij} = \tfrac{1}{2}\left(\mathbf{r}_{ij} \cdot \mathbf{r}_{ij} - L^2\right) = 0 \tag{2.7.15}$$

where $\mathbf{r}_{ij} = \mathbf{r}_j - \mathbf{r}_i$. The total force acting on atom 1, say, at time t is the sum of three terms: $\mathbf{F}_1(t)$, the force due to interactions with other molecules; a force of constraint, $\boldsymbol{\gamma}_{12}(t)$, which ensures that the bond vector $\mathbf{r}_{12}$ remains of fixed length; and a second force of constraint, $\boldsymbol{\gamma}_{13}(t)$, which preserves the bond length between atoms 1 and 3. Similar consideration apply to the other atoms. The forces of constraint are directed along the corresponding bond vectors and the law of action and reaction requires that $\boldsymbol{\gamma}_{ij} = -\boldsymbol{\gamma}_{ji}$. Thus $\boldsymbol{\gamma}_{ij} = \lambda_{ij}\mathbf{r}_{ij}$, where λ_{ij} is a time-dependent scalar quantity, with $\lambda_{ij} = \lambda_{ji}$. The newtonian equations of motion are therefore of the form

$$\begin{aligned} m\ddot{\mathbf{r}}_1(t) &= \mathbf{F}_1(t) + \lambda_{12}\mathbf{r}_{12}(t) + \lambda_{13}\mathbf{r}_{13}(t) \\ m\ddot{\mathbf{r}}_2(t) &= \mathbf{F}_2(t) - \lambda_{12}\mathbf{r}_{12}(t) + \lambda_{23}\mathbf{r}_{23}(t) \\ m\ddot{\mathbf{r}}_3(t) &= \mathbf{F}_3(t) - \lambda_{13}\mathbf{r}_{13}(t) - \lambda_{23}\mathbf{r}_{23}(t) \end{aligned} \tag{2.7.16}$$

Comparison with (2.7.15) shows that the total force of constraint on atom i, $\mathbf{G}_i$, can be written as

$$\mathbf{G}_i = -\sum_{j \neq i} \lambda_{ij} \frac{\partial \sigma_{ij}}{\partial \mathbf{r}_i} \tag{2.7.17}$$

As is to be expected, the sum of the forces of constraint is zero: $\sum_i \mathbf{G}_i = 0$.

It is possible to eliminate the unknown quantities λ_{12}, λ_{13} and λ_{23} from (2.7.16) by requiring the second time derivative of the constraint conditions (2.7.15) to vanish, i.e.

by setting $\ddot{\sigma}_{ij} = \dot{\mathbf{r}}_{ij} \cdot \dot{\mathbf{r}}_{ij} + \mathbf{r}_{ij} \cdot \ddot{\mathbf{r}}_{ij} = 0$ and replacing $\ddot{\mathbf{r}}_i$ by $(\mathbf{F}_i + \mathbf{G}_i)/m$. The resulting system of equations for the constrained coordinates can then be integrated numerically. In practice this procedure does not work: the errors inherent in any approximate algorithm cause the bond lengths to drift away rapidly from their initial values. What is done instead is to require the constraints to be satisfied exactly after each time step in a manner dictated by the chosen integration scheme. If the Verlet algorithm (2.7.2) is used, for example, we find that

$$\begin{aligned}
\mathbf{r}_1(t+\Delta t) &= \mathbf{r}_1'(t+\Delta t) + \left(\Delta t^2/m\right)\left[\lambda_{12}\mathbf{r}_{12}(t) + \lambda_{13}\mathbf{r}_{13}(t)\right] \\
\mathbf{r}_2(t+\Delta t) &= \mathbf{r}_2'(t+\Delta t) + \left(\Delta t^2/m\right)\left[-\lambda_{12}\mathbf{r}_{12}(t) + \lambda_{23}\mathbf{r}_{23}(t)\right] \\
\mathbf{r}_3(t+\Delta t) &= \mathbf{r}_3'(t+\Delta t) + \left(\Delta t^2/m\right)\left[-\lambda_{13}\mathbf{r}_{13}(t) - \lambda_{23}\mathbf{r}_{23}(t)\right]
\end{aligned} \tag{2.7.18}$$

where $\mathbf{r}_i'(t+\Delta t)$ are the predicted coordinates of atom i in the absence of constraints, given by (2.7.4). Equations (2.7.18) must be solved subject to the requirement that $|\mathbf{r}_{ij}(t+\Delta t)|^2 = L^2$ for all i, j. This leads to three simultaneous equations for the quantities $\lambda_{ij}(t)$, to which a solution can be obtained by an iterative method; three to four iterations per molecule are normally sufficient to maintain the bond lengths constant to within one part in 10^4.

Apart from its simplicity, a particular merit of the method of constraints is the fact that it can be used for both rigid and flexible molecules. A partially flexible chain molecule, for example, can be treated by employing a suitable mixture of constraints on bond angles and bond lengths in a way that allows for torsional motion and bending but freezes the fast vibrations.[15]

Given a set of initial conditions, a conventional molecular-dynamics simulation is, in principle, entirely deterministic in nature. By contrast, as the name suggests, a stochastic element is an essential part of any Monte Carlo calculation. In a Monte Carlo simulation a system of N particles, subject to the same boundary condition used in molecular-dynamics calculations and interacting through some known potentials, is again assigned a set of arbitrarily chosen, initial coordinates. A sequence of configurations is then generated by successive random displacements of the particles, usually of one particle at a time. Not all configurations that are generated are added to the sequence. The decision whether to "accept" or "reject" a trial configuration is made in such a way that asymptotically configuration space is sampled according to the probability density corresponding to a particular statistical mechanical ensemble. The ensemble average of any function of the particle coordinates, such as the total potential energy, is then obtained as an unweighted average over the resulting set of configurations. The particle momenta do not enter the calculation, there is no time scale involved, and the order in which the configurations occur has no special significance. The method is therefore limited to the calculation of static properties.

The Monte Carlo method was originally developed as a means of calculating averages in the canonical ensemble and we shall consider that case first; we also assume initially that the system consists of spherical particles. The problem of devising a scheme for sampling configuration space according to a specific probability distribution is most easily formulated in terms of the theory of Markov processes.[16] Suppose we have a sequence of random variables. Here the "variable" is the set of all coordinates of the particles and its range is

the configuration space of the system. Hence, instead of speaking of the value of the variable at a point in the sequence, it is more natural for applications in statistical mechanics to say that the system occupies a particular state at that point. If the probability of finding the system in a state n at "time" $(t+1)$ is dependent only on the state it occupied at the previous time, t, the sequence of states constitutes a Markov chain. Note that the concept of "time" is introduced merely for descriptive purposes; there is no connection with any physical time scale.

Let $q_n(t)$ be the probability that the system is in state n at time t. A Markov process is one for which

$$q_n(t) = \sum_m p_{nm} q_m(t-1) \tag{2.7.19}$$

where p_{nm} is a transition probability, with $\sum_n p_{nm} = 1$. If we regard the probabilities $\{q_n(t)\}$ as the components of a column vector $\mathbf{q}(t)$ and the quantities $\{p_{nm}\}$ as the elements of a square *transition matrix* $\boldsymbol{p}$, (2.7.19) may be rewritten in more compact form as

$$\mathbf{q}(t) = \boldsymbol{p} \cdot \mathbf{q}(t-1) \tag{2.7.20}$$

Equation (2.7.20) can be immediately generalised to yield the probability distribution at time t given an initial distribution $\mathbf{q}(0)$:

$$\mathbf{q}(t) = \overbrace{\boldsymbol{p} \cdots \boldsymbol{p}}^{t \text{ times}} \cdot \mathbf{q}(0) \equiv \boldsymbol{p}^t \cdot \mathbf{q}(0) \tag{2.7.21}$$

where $\boldsymbol{p}^t \equiv \{p_{nm}^{(t)}\}$ is the t-fold product of $\boldsymbol{p}$ with itself. If all elements of the matrix $\boldsymbol{p}^t$ are non-zero for some finite t, each state of the system can be reached from any other state in a finite number of steps (or finite "time") and the Markov chain is said to be ergodic; it is clear that this usage of the term "ergodic" is closely related to its meaning in statistical mechanics. When the chain is ergodic, it can be shown that the limits

$$\Pi_n = \lim_{t \to \infty} p_{nm}^{(t)} q_m(0) \tag{2.7.22}$$

exist and are the same for all m. In other words there exists a limiting probability distribution $\boldsymbol{\Pi} \equiv \{\Pi_n\}$ that is independent of the initial distribution $\mathbf{q}(0)$. When the limiting distribution is reached, it persists, because $\boldsymbol{p} \cdot \boldsymbol{\Pi} = \boldsymbol{\Pi}$ or, in component form:

$$\Pi_n = \sum_m p_{nm} \Pi_m \tag{2.7.23}$$

This result is called the *steady-state condition*. In the case of interest here the limits are simply the Boltzmann factors, $\Pi_n = \exp[-\beta V_N(n)]$. The task therefore is to find a set of transition probabilities that are consistent with these limits; this task is greatly simplified by seeking a transition matrix that satisfies *microscopic reversibility*, i.e. one for which

$$\Pi_n p_{mn} = \Pi_m p_{nm} \tag{2.7.24}$$

If this relation holds, the steady-state condition is automatically satisfied.

Let us suppose that the system is in state m at a given time. A trial state n can be generated by selecting a particle i at random and giving it a small, random displacement, $\mathbf{r}_i \to \mathbf{r}_i + \Delta$. If α_{nm} is the probability of choosing n as the trial state, and if this is the same as the probability α_{mn} of choosing m as the trial state when starting from n, then a choice of transition probabilities that satisfies (2.7.23) is

$$\begin{aligned} p_{nm} &= \alpha_{nm}, \qquad \text{if } \Pi_n \geqslant \Pi_m, \\ &= \alpha_{nm}\frac{\Pi_n}{\Pi_m}, \quad \text{if } \Pi_n < \Pi_m \end{aligned} \tag{2.7.25}$$

with $p_{mm} = 1 - \sum_{n \neq m} p_{nm}$. The transition matrix defined by (2.7.24) is the one proposed in the pioneering work of Metropolis and coworkers[17] and remains much the most commonly used prescription for $\boldsymbol{p}$. What it means in practice is that the trial state is accepted unconditionally if $V_N(n) \leqslant V_N(m)$ and with a probability $\exp[-\beta \Delta V_N]$, where $\Delta V_N = V_N(n) - V_N(m)$, if $V_N(n) > V_N(m)$. The procedure takes a particularly simple form for a system of hard spheres: trial configurations in which two or more spheres overlap are rejected, but all others are accepted. One important point to note about the Metropolis scheme is that the system remains in its current state if the trial state n is rejected. In that case, state m appears a further time in the Markov chain, and the contribution it makes to any ensemble average must be counted again.

Monte Carlo methods similar to that outlined above are easily devised for use in other ensembles. All that changes are the form of the probability distribution and the way in which trial states are generated. In the case of the isothermal–isobaric ensemble, for example, random displacements of the particles must be combined with random changes in volume, while in the grand-canonical ensemble displacements must be combined with random attempts to insert or remove particles. The extension to molecular systems is also straightforward. Interactions between particles are now dependent on their mutual orientation and "displacements" therefore consist of random translational moves and random reorientations.

NOTES AND REFERENCES

1. See, e.g., Reichl, L.E., "A Modern Course in Statistical Physics", 2nd edn. John Wiley, New York, 1998, p. 289.
2. Résibois, P. and DeLeener, M., "Classical Kinetic Theory of Fluids". John Wiley, New York, 1977.
3. Maitland, G.C., Rigby, M., Smith, E.B. and Wakeham, W.A., "Intermolecular Forces". Clarendon Press, Oxford, 1981, Chap. 5.
4. Hill, T.L., "Statistical Mechanics". McGraw-Hill, New York, 1956, p. 189.
5. For a different formulation of the constant-pressure ensemble, see Koper, G.J.M. and Reiss, H., *J. Phys. Chem. B* **100**, 422 (1996) and Corti, D.S. and Soto-Campos, D., *J. Chem. Phys.* **108**, 7959 (1998).
6. Widom, B., *J. Chem. Phys.* **39**, 2808 (1963). See also Shing, K.S. and Gubbins, K.E., *Mol. Phys.* **46**, 1109 (1982).
7. Yarnell, J.L., Katz, M.J., Wenzel, R.G. and Koenig, S.H., *Phys. Rev. A* **7**, 2130 (1973).
8. See, e.g., Reif, F., "Fundamentals of Statistical and Thermal Physics". McGraw-Hill, New York, 1965, pp. 268 and 471.

9. (a) Allen, M.P. and Tildesley, D.J., “Computer Simulation of Liquids”. Oxford, Clarendon Press, 1987. (b) Frenkel, D. and Smit, B., “Understanding Molecular Simulation”, 2nd edn. Academic Press, San Diego, 2002. (c) Landau, D.P. and Binder, K., “A Guide to Monte Carlo Simulations in Statistical Physics”. Cambridge University Press, Cambridge, 2000.
10. Alder, B.J. and Wainwright, T.E., *J. Chem. Phys.* **31**, 459 (1959).
11. Verlet, L., *Phys. Rev.* **159**, 98 (1967).
12. Tuckerman, M., Berne, B.J. and Martyna, G., *J. Chem. Phys.* **97**, 1990 (1992).
13. See, e.g., ref. 9(b), p. 81.
14. Ciccotti, G., Ferrario, M. and Ryckaert, J.P., *Mol. Phys.* **47**, 1253 (1982).
15. Ryckaert, J.P., *Mol. Phys.* **55**, 549 (1985).
16. Wood, W.W. and Parker, F.R., *J. Chem. Phys.* **27**, 720 (1957).
17. Metropolis, N., Rosenbluth, A.W., Rosenbluth, M.N., Teller, A.N. and Teller, E., *J. Chem. Phys.* **21**, 1087 (1953).

CHAPTER 3

Static Properties of Liquids: Thermodynamics and Structure

Liquids are homogeneous in the bulk, but inhomogeneities appear close to the confining walls or other physical boundaries and wherever different phases coexist. Although it might seem natural to develop the theory of uniform fluids first, it turns out to be equally convenient and in many ways more illuminating to treat uniform and non-uniform systems simultaneously from the outset. In the first six sections of this chapter we describe a general approach to the study of inhomogeneous fluids based on the formalism of the grand canonical ensemble.[1] The starting point is a hamiltonian that includes a term representing the interaction of the particles with some spatially varying, external field. The effect of this term is to break the translational symmetry of the system, but results for uniform fluids are easily recovered by taking the limit in which the external field vanishes. A key component of the theory is a variational principle for the grand potential, which is a classical version of a principle originally derived for the interacting electron gas.[2] The last three sections provide an introduction to the use of diagrammatic methods in the theory of liquids, with examples chosen to complement the work discussed in earlier parts of the chapter.

3.1 A FLUID IN AN EXTERNAL FIELD

We consider again a system of identical, spherical particles in a volume V. The hamiltonian of the system in the presence of an external potential $\phi(\mathbf{r})$ is given by (2.1.1), which for ease of reference we repeat here:

$$\mathcal{H}(\mathbf{r}^N, \mathbf{p}^N) = K_N(\mathbf{p}^N) + V_N(\mathbf{r}^N) + \Phi_N(\mathbf{r}^N) \tag{3.1.1}$$

The external field is assumed to couple to the microscopic particle density $\rho(\mathbf{r})$, defined as a sum of δ-functions in the form already introduced implicitly in (2.5.11), i.e.

$$\rho(\mathbf{r}) = \sum_{i=1}^{N} \delta(\mathbf{r} - \mathbf{r}_i) \tag{3.1.2}$$

Thus the total potential energy due to the field is

$$\Phi_N(\mathbf{r}^N) = \sum_{i=1}^{N} \phi(\mathbf{r}_i) = \int \rho(\mathbf{r})\phi(\mathbf{r})\,\mathrm{d}\mathbf{r} \tag{3.1.3}$$

The average density at a point $\mathbf{r}$ is the single-particle density, or *density profile*, $\rho^{(1)}(\mathbf{r})$:

$$\langle \rho(\mathbf{r}) \rangle = \rho^{(1)}(\mathbf{r}) \tag{3.1.4}$$

where the angular brackets denote an average over a grand canonical ensemble. Thus the average value of Φ_N is

$$\langle \Phi_N \rangle = \int \rho^{(1)}(\mathbf{r})\phi(\mathbf{r})\,\mathrm{d}\mathbf{r} \tag{3.1.5}$$

Fluctuations in the local density about its average value are described by a density–density correlation function, $H^{(2)}(\mathbf{r}, \mathbf{r}')$, defined as

$$\begin{aligned} H^{(2)}(\mathbf{r}, \mathbf{r}') &= \langle [\rho(\mathbf{r}) - \langle \rho(\mathbf{r}) \rangle][\rho(\mathbf{r}') - \langle \rho(\mathbf{r}') \rangle] \rangle \\ &= \rho^{(2)}(\mathbf{r}, \mathbf{r}') + \rho^{(1)}(\mathbf{r})\delta(\mathbf{r} - \mathbf{r}') - \rho^{(1)}(\mathbf{r})\rho^{(1)}(\mathbf{r}') \\ &= \rho^{(1)}(\mathbf{r})\rho^{(1)}(\mathbf{r}')h^{(2)}(\mathbf{r}, \mathbf{r}') + \rho^{(1)}(\mathbf{r})\delta(\mathbf{r} - \mathbf{r}') \end{aligned} \tag{3.1.6}$$

where $\rho^{(2)}(\mathbf{r}, \mathbf{r}')$ is given by the analogue of (2.5.13) in the grand canonical ensemble and $h^{(2)}(\mathbf{r}, \mathbf{r}')$ is the pair correlation function (2.6.8). The function $H^{(2)}(\mathbf{r}, \mathbf{r}')$ represents the first in a hierarchy of density correlation functions having the general form

$$H^{(n)}(\mathbf{r}_1, \ldots, \mathbf{r}_n) = \langle [\rho(\mathbf{r}_1) - \rho^{(1)}(\mathbf{r}_1)] \cdots [\rho(\mathbf{r}_n) - \rho^{(1)}(\mathbf{r}_n)] \rangle \tag{3.1.7}$$

for $n \geqslant 2$. Each function $H^{(n)}$ is a linear combination of all particle densities up to and including $\rho^{(n)}$.

Inclusion of the external-field term in the hamiltonian requires some modification of earlier definitions. As before, the grand partition function is related to the grand potential by $\Xi = \exp(-\beta\Omega)$, but now has the form

$$\Xi = \sum_{N=0}^{\infty} \frac{1}{N!} \int \exp(-\beta V_N) \left(\prod_{i=1}^{N} z \exp[-\beta\phi(\mathbf{r}_i)] \right) \mathrm{d}\mathbf{r}^N \tag{3.1.8}$$

and the definition of the particle densities in (2.6.1) is replaced by

$$\rho^{(n)}(\mathbf{r}^n) = \frac{1}{\Xi} \sum_{N=n}^{\infty} \frac{1}{(N-n)!} \int \exp(-\beta V_N) \left(\prod_{i=1}^{N} z \exp[-\beta\phi(\mathbf{r}_i)] \right) \mathrm{d}\mathbf{r}^{(N-n)} \tag{3.1.9}$$

Equation (3.1.8) may be recast as

$$\Xi = \sum_{N=0}^{\infty} \frac{1}{N!} \int \cdots \int \exp(-\beta V_N) \left(\prod_{i=1}^{N} \frac{1}{\Lambda^3} \exp\left[\beta \psi(\mathbf{r}_i)\right] \right) \mathrm{d}\mathbf{r}_1 \cdots \mathrm{d}\mathbf{r}_N \tag{3.1.10}$$

where

$$\psi(\mathbf{r}) = \mu - \phi(\mathbf{r}) \tag{3.1.11}$$

The quantity $\psi(\mathbf{r})$ is called the *intrinsic chemical potential*. It is the contribution to μ that is not explicitly dependent on $\phi(\mathbf{r})$.

The intrinsic chemical potential arises naturally in a thermodynamic description of the system. We suppose that the definition of $\phi(\mathbf{r})$ includes the confining potential, i.e. the interaction between the particles and the containing walls.[3] The usual thermodynamic variable V may then be replaced by $\phi(\mathbf{r})$, the volume accessible to the particles being that region of space in which $\phi(\mathbf{r})$ is finite. The change in U resulting from an infinitesimal change in equilibrium state is now

$$\delta U = T\delta S + \int \rho^{(1)}(\mathbf{r}) \delta\phi(\mathbf{r}) \, \mathrm{d}\mathbf{r} + \mu \delta N \tag{3.1.12}$$

(cf. (2.3.5)), where the integral extends over all space rather than over a large but finite volume. The definition of the Helmholtz free energy remains $F = U - TS$ and the change in F in an infinitesimal process is therefore

$$\delta F = -S\delta T + \int \rho^{(1)}(\mathbf{r}) \delta\phi(\mathbf{r}) \, \mathrm{d}\mathbf{r} + \mu \delta N \tag{3.1.13}$$

By analogy with (3.1.11), we can also define an *intrinsic free energy*, $\mathcal{F}$, as

$$\mathcal{F} = F - \int \rho^{(1)}(\mathbf{r}) \phi(\mathbf{r}) \, \mathrm{d}\mathbf{r} \tag{3.1.14}$$

with

$$\begin{aligned} \delta\mathcal{F} &= -S\delta T - \int \delta\rho^{(1)}(\mathbf{r}) \phi(\mathbf{r}) \, \mathrm{d}\mathbf{r} + \mu\delta N \\ &= -S\delta T + \int \delta\rho^{(1)}(\mathbf{r}) \psi(\mathbf{r}) \, \mathrm{d}\mathbf{r} \end{aligned} \tag{3.1.15}$$

Thus $\psi(\mathbf{r})$ appears as the field variable conjugate to $\rho^{(1)}(\mathbf{r})$. Finally, the grand potential $\Omega = F - N\mu$, when expressed in terms of $\mathcal{F}$, is

$$\Omega = \mathcal{F} + \int \rho^{(1)}(\mathbf{r}) \phi(\mathbf{r}) \, \mathrm{d}\mathbf{r} - N\mu \tag{3.1.16}$$

with a differential given by

$$\begin{aligned}\delta\Omega &= -S\delta T + \int \rho^{(1)}(\mathbf{r})\delta\phi(\mathbf{r}) - N\delta\mu \\ &= -S\delta T - \int \rho^{(1)}(\mathbf{r})\delta\psi(\mathbf{r})\,\mathrm{d}\mathbf{r} \end{aligned} \tag{3.1.17}$$

We see from (3.1.15) and (3.1.17) that it is natural to take $\mathcal{F}$ and Ω as functions of T and *functionals*, respectively, of $\rho^{(1)}$ and ψ. These relationships are expressed by use of the notation $\mathcal{F}[\rho^{(1)}]$ and $\Omega[\psi]$. Hence the change, say, in $\mathcal{F}$ created by a change in $\rho^{(1)}(\mathbf{r})$ is determined by the *functional derivative* of $\mathcal{F}$ with respect to $\rho^{(1)}$. The calculation of such derivatives requires some familiarity with the rules of functional differentiation, which are summarised in the section that follows.

The intrinsic free energy can also be written as an ensemble average. The definition (2.4.5) of the grand canonical probability density $f_0(\mathbf{r}^N, \mathbf{p}^N; N)$ shows that in the presence of an external field:

$$\ln f_0 = \beta\Omega - \beta K_N - \beta V_N - \beta\Phi_N + N\beta\mu \tag{3.1.18}$$

Thus

$$\langle K_N + V_N + k_\mathrm{B}T \ln f_0\rangle = \Omega + \int \rho^{(1)}(\mathbf{r})\psi(\mathbf{r})\,\mathrm{d}\mathbf{r} = \mathcal{F} \tag{3.1.19}$$

If there are no correlations between particles, the intrinsic chemical potential at a point $\mathbf{r}$ is given by the usual expression (2.3.17) for the chemical potential of a system of non-interacting particles, but with the overall number density ρ replaced by $\rho^{(1)}(\mathbf{r})$. Thus the chemical potential of an inhomogeneous, ideal gas is

$$\mu^{\mathrm{id}} = k_\mathrm{B}T \ln\bigl[\Lambda^3\rho^{(1)}(\mathbf{r})\bigr] + \phi(\mathbf{r}) \tag{3.1.20}$$

where the first term on the right-hand side is the intrinsic part. Equation (3.1.20) can be rearranged to give the well-known *barometric law*:

$$\rho^{(1)}(\mathbf{r}) = z^{\mathrm{id}} \exp\bigl[-\beta\phi(\mathbf{r})\bigr] \tag{3.1.21}$$

where the activity $z^{\mathrm{id}} = \Lambda^{-3}\exp(\beta\mu^{\mathrm{id}})$ is equal to the number density of the uniform gas at the same chemical potential. The intrinsic free energy of an ideal gas also has a purely "local" form, given by an integral over $\mathbf{r}$ of the free energy per unit volume of a non-interacting system of density $\rho^{(1)}(\mathbf{r})$:

$$\mathcal{F}^{\mathrm{id}} = k_\mathrm{B}T \int \rho^{(1)}(\mathbf{r})\bigl(\ln\bigl[\Lambda^3\rho^{(1)}(\mathbf{r})\bigr] - 1\bigr)\,\mathrm{d}\mathbf{r} \tag{3.1.22}$$

This expression reduces to (2.3.16) in the uniform case.

3.2 FUNCTIONALS AND FUNCTIONAL DIFFERENTIATION

A functional is a natural extension of the familiar mathematical concept of a function. The meaning of a function is that of a mapping from points in n-space to a real or complex number, n being the number of variables on which the function depends. A functional, by contrast, depends on all values of a function $u(x)$, say, in a range $a \leqslant x \leqslant b$. It can therefore be interpreted as a mapping from ∞-space to a real or complex number, the points in ∞-space being the values of $u(x)$ at the infinite number of points in the relevant range of the variable x. Functions of several variables and functionals are therefore conveniently treated as discrete and continuous versions of the same mathematical concept, making it possible to construct the rules of functional differentiation by analogy with those of elementary calculus. As usual, a sum in the discrete case is replaced by an integral in the limit in which the distribution of variables becomes continuous.

If f is a function of the n variables $\mathbf{z} \equiv z_1, \ldots, z_N$ the change in f due to an infinitesimal change in $\mathbf{z}$ is

$$\mathrm{d}f = f(\mathbf{z} + \mathrm{d}\mathbf{z}) - f(\mathbf{z}) = \sum_{i=1}^{n} A_i(\mathbf{z})\,\mathrm{d}\mathbf{z}_i \tag{3.2.1}$$

where

$$A_i(\mathbf{z}) \equiv \frac{\partial f}{\partial z_i} \tag{3.2.2}$$

Similarly, if F is a functional of $u(x)$, then

$$\delta F = F[u + \delta u] - F[u] = \int_a^b A[u; x]\delta u(x)\,\mathrm{d}x \tag{3.2.3}$$

and the functional derivative

$$A[u; x] \equiv \frac{\delta F}{\delta u(x)} \tag{3.2.4}$$

is a functional of u and a function of x. The functional derivative determines the change in F resulting from a change in u at a particular value of x; to calculate the change in F due to a variation in $u(x)$ throughout the range of x it is necessary to integrate over x, as in (3.2.3).

The rules of functional differentiation are most easily grasped by considering some specific examples. If f is a linear function of n variables we know that

$$f(\mathbf{z}) = \sum_{i=1}^{n} a_i z_i, \qquad \mathrm{d}f = \sum_{i=1}^{n} a_i\,\mathrm{d}z_i \tag{3.2.5}$$

and

$$\frac{\partial f}{\partial z_i} = a_i, \quad \text{independent of } \mathbf{z} \tag{3.2.6}$$

The analogue of (3.2.5) for a linear functional is

$$F[u] = \int a(x)u(x)\,\mathrm{d}x, \qquad \delta F = \int a(x)\delta u(x)\,\mathrm{d}x \tag{3.2.7}$$

and comparison with (3.2.3) shows that

$$\frac{\delta F}{\delta u(x)} = a(x), \quad \text{independent of } u \tag{3.2.8}$$

A more general example of the same type is when

$$F = \int \cdots \int a(x_1, \ldots, x_N)u(x_1)u(x_2)\cdots u(x_N)\,\mathrm{d}x_1 \cdots \mathrm{d}x_N \tag{3.2.9}$$

where the function $a(x_1, \ldots, x_N)$ is symmetric with respect to permutation of the labels $1, \ldots, N$. Then

$$\begin{aligned}\delta F = &\int \cdots \int a(x_1, \ldots, x_N)\delta u(x_1)u(x_2)\cdots u(x_N)\,\mathrm{d}x_2 \cdots \mathrm{d}x_N \\ &+ (N-1) \text{ other terms}\end{aligned} \tag{3.2.10}$$

The N terms on the right-hand side are all equivalent, so the change in F is N times the value of any one term. Thus

$$\frac{\delta F}{\delta u(x_1)} = N \int \cdots \int a(x_1, \ldots, x_N)u(x_2)\cdots u(x_N)\,\mathrm{d}x_1 \cdots \mathrm{d}x_N \tag{3.2.11}$$

As a slightly more complicated example, consider the non-linear functional

$$F[u] = \int u(x)\ln u(x)\,\mathrm{d}x \tag{3.2.12}$$

for which

$$\begin{aligned}\delta F &= \int \big[\delta u(x)\ln u(x) + u(x)\delta \ln u(x)\big]\,\mathrm{d}x \\ &= \int \big[\ln u(x) + 1\big]\delta u(x)\,\mathrm{d}x\end{aligned} \tag{3.2.13}$$

and hence

$$\frac{\delta F}{\delta u(x)} = \ln u(x) + 1 \tag{3.2.14}$$

This example shows how functional derivatives can be evaluated with the help of rules appropriate to ordinary differentiation.

An important special case is when

$$F[u] = u(x') = \int \delta(x - x')u(x)\,\mathrm{d}x \tag{3.2.15}$$

Then

$$\delta F = \int \delta(x - x')\delta u(x)\,\mathrm{d}x \; = \delta u(x') \tag{3.2.16}$$

and

$$\frac{\delta u(x')}{\delta u(x)} = \delta(x - x') \tag{3.2.17}$$

When u is a function of two variables the functional derivative is defined through the relation

$$\delta F = \iint \frac{\delta F}{\delta u(x_1, x_2)}\delta u(x_1, x_2)\,\mathrm{d}x_1\,\mathrm{d}x_2 \tag{3.2.18}$$

In applications in statistical mechanics symmetry often leads to a simplification similar to that seen in the example (3.2.9). Consider the functional defined as

$$F[u] = \iiint a(x_1, x_2, x_3)u(x_1, x_2)u(x_2, x_3)u(x_3, x_1)\,\mathrm{d}x_1\,\mathrm{d}x_2\,\mathrm{d}x_3 \tag{3.2.19}$$

where $a(x_1, x_2, x_3)$ is symmetrical with respect to permutation of the labels 1, 2 and 3. The change in F due to an infinitesimal change in the function u is now

$$\begin{aligned}\delta F = &\iiint a(x_1, x_2, x_3)\delta u(x_1, x_2)u(x_2, x_3)u(x_3, x_1)\,\mathrm{d}x_1\,\mathrm{d}x_2\,\mathrm{d}x_3 \\ &+ \text{two equivalent terms}\end{aligned} \tag{3.2.20}$$

Thus

$$\frac{\delta F}{\delta u(x_1, x_2)} = 3\int a(x_1, x_2, x_3)u(x_2, x_3)u(x_3, x_1)\,\mathrm{d}x_3 \tag{3.2.21}$$

Higher-order derivatives are defined in a manner similar to (3.2.3). In particular, the second derivative is defined through the relation

$$\delta A[u; x] = \int \frac{\delta A[u; x]}{\delta u(x')}\delta u(x')\,\mathrm{d}x' \tag{3.2.22}$$

The second derivative of the functional (3.2.9), for example, is

$$\frac{\delta^2 F}{\delta u(x_1)\delta u(x_2)} = N(N-1)\int \cdots \int a(x_1, \ldots, x_N)u(x_3)\cdots u(x_N)\,\mathrm{d}x_3 \cdots \mathrm{d}x_N \tag{3.2.23}$$

and is a functional of u and a function of both x and x'. If the derivatives exist, a functional $F[u]$ can be expanded in a Taylor series around a function u_0:

$$F[u] = F[u_0] + \int \left.\frac{\delta F}{\delta u(x)}\right|_{u=u_0} \big[u(x) - u_0(x)\big]\,\mathrm{d}x + \frac{1}{2!}\iint \left.\frac{\delta^2 F}{\delta u(x)\delta u(x')}\right|_{u=u_0} \big[u(x) - u_0(x)\big]\big[u(x') - u_0(x')\big]\,\mathrm{d}x\,\mathrm{d}x' + \cdots \tag{3.2.24}$$

Finally, the equivalent of the chain rule of ordinary differentiation is

$$\frac{\delta F}{\delta u(x)} = \int \frac{\delta F}{\delta v(x')}\frac{\delta v(x')}{\delta u(x)}\,\mathrm{d}x' \tag{3.2.25}$$

3.3 FUNCTIONAL DERIVATIVES OF THE GRAND POTENTIAL

The methods of the previous section can be used very straightforwardly to derive some important results involving derivatives of the grand potential. We saw in Section 3.1 that it is natural to treat the intrinsic free energy as a functional of the single-particle density. The manner in which the functional $\mathcal{F}[\rho^{(1)}]$ varies with $\rho^{(1)}$ is described by (3.1.15) and from that result, given the definition of a functional derivative, it follows immediately that

$$\frac{\delta \mathcal{F}}{\delta \rho^{(1)}(\mathbf{r})} = \psi(\mathbf{r}) \tag{3.3.1}$$

where the derivative is taken at constant T. The intrinsic free energy can be divided into ideal and excess parts in the form

$$\mathcal{F}\big[\rho^{(1)}\big] = \mathcal{F}^{\mathrm{id}}\big[\rho^{(1)}\big] + \mathcal{F}^{\mathrm{ex}}\big[\rho^{(1)}\big] \tag{3.3.2}$$

where the ideal part is given by (3.1.22). Use of example (3.2.14) confirms that the functional derivative of $\mathcal{F}^{\mathrm{id}}$ is

$$\frac{\delta \mathcal{F}^{\mathrm{id}}}{\delta \rho^{(1)}(\mathbf{r})} = k_{\mathrm{B}}T \ln\big[\Lambda^3 \rho^{(1)}(\mathbf{r})\big] \tag{3.3.3}$$

in agreement with (3.1.20). In the same way it follows from (3.1.17) that the functional derivative of $\Omega[\psi]$ with respect to ψ is

$$\frac{\delta \Omega}{\delta \psi(\mathbf{r})} = -\rho^{(1)}(\mathbf{r}) \tag{3.3.4}$$

From this result (or from (3.3.1)) it follows that the functionals $\Omega[\psi]$ and $\mathcal{F}[\rho^{(1)}]$ are related by a generalised Legendre transformation,[4] i.e.

$$\Omega[\psi] - \int \psi(\mathbf{r}) \frac{\delta \Omega}{\delta \psi(\mathbf{r})} \, \mathrm{d}\mathbf{r} \rightarrow \Omega[\psi] + \int \psi(\mathbf{r}) \rho^{(1)}(\mathbf{r}) \, \mathrm{d}\mathbf{r} = \mathcal{F}\big[\rho^{(1)}\big] \tag{3.3.5}$$

In the limit $\phi \rightarrow 0$, ψ and $\rho^{(1)}$ can be replaced by μ and $\langle N \rangle / V$, respectively, and (3.3.1) and (3.3.4) reduce to standard thermodynamic results, $\partial F / \partial N = \mu$ and $\partial \Omega / \partial \mu = -N$.

The relationship that exists between Ω and Ξ means that it must also be possible to obtain (3.3.4) by differentiation of $\ln \Xi$. We already know the outcome of this calculation, but the exercise is nonetheless a useful one, since it points the way towards the calculation of higher-order derivatives. In carrying out the differentiation it proves helpful to introduce a *local activity*, z^*, defined as

$$z^*(\mathbf{r}) = \frac{\exp[\beta \psi(\mathbf{r})]}{\Lambda^3} = z \exp\big[-\beta \phi(\mathbf{r})\big] \tag{3.3.6}$$

If we also adopt a simplified notation in which a position vector $\mathbf{r}_i$ is denoted by i, the grand partition function (3.1.10) can be rewritten in the form

$$\Xi = \sum_{N=0}^{\infty} \frac{1}{N!} \int \cdots \int \exp(-\beta V_N) \left(\prod_{i=1}^{N} z^*(i) \right) \mathrm{d}1 \cdots \mathrm{d}N \tag{3.3.7}$$

The derivative we require is

$$\frac{\delta \Omega}{\delta \psi(1)} = -k_{\mathrm{B}} T \frac{\delta \ln \Xi}{\delta \psi(1)} = -\frac{z^*(1)}{\Xi} \frac{\delta \Xi}{\delta z^*(1)} \tag{3.3.8}$$

The term for $N = 0$ in (3.3.7) vanishes on differentiation. Higher-order terms are of the general form considered in example (3.2.9) and differentiation of each term therefore yields a factor N. Thus

$$\frac{\delta \Xi}{\delta z^*(1)} = \sum_{N=1}^{\infty} \frac{1}{(N-1)!} \int \cdots \int \exp(-\beta V_N) \left(\prod_{i=2}^{N} z^*(i) \right) \mathrm{d}2 \cdots \mathrm{d}N \tag{3.3.9}$$

and combination of (3.3.8) and (3.3.9) with the definition of the particle densities in (3.1.9) leads back to (3.3.4). By further differentiation of Ξ it is easy to show that

$$\rho^{(n)}(1, \ldots, n) = \frac{z^*(1) \cdots z^*(n)}{\Xi} \frac{\delta^n \Xi}{\delta z^*(1) \cdots \delta z^*(n)} \tag{3.3.10}$$

The grand partition function is said to be the *generating functional* for the particle densities.

Calculation of the second derivative of Ω with respect to ψ is only slightly more complicated. The quantity to be determined is now

$$\frac{\delta^2 \Omega}{\delta \psi(1) \delta \psi(2)} = -\beta z^*(2) \frac{\delta}{\delta z^*(2)} \left(\frac{1}{\Xi} z^*(1) \frac{\delta \Xi}{\delta z^*(1)} \right) \tag{3.3.11}$$

Differentiation of successive factors in the product in brackets gives rise, respectively, to a term in $\rho^{(1)}(2)$, a term in $\delta(1,2)$ (as in example (3.2.17)) and a term in $\rho^{(2)}(1,2)$ (from (3.3.10)). On combining these results we find that

$$\begin{aligned}\frac{\delta^2\Omega}{\delta\psi(1)\delta\psi(2)} &= \beta\big[\rho^{(1)}(1)\rho^{(1)}(2) - \rho^{(1)}(1)\delta(1,2) - \rho^{(2)}(1,2)\big] \\ &= -\beta H^{(2)}(1,2) \end{aligned} \tag{3.3.12}$$

where $H^{(2)}(1,2)$ is the density–density correlation function defined by (3.1.6). The process of differentiation can again be extended; although the algebra becomes increasingly tedious, the general result has a simple form:

$$\frac{\delta^n\beta\Omega}{\delta\beta\psi(1)\cdots\delta\beta\psi(n)} = -H^{(n)}(1,\ldots,n), \quad n \geqslant 2 \tag{3.3.13}$$

The grand potential is therefore the generating functional for the n-fold density correlation functions.

3.4 DENSITY-FUNCTIONAL THEORY

The grand potential has temperature and intrinsic chemical potential as its natural variables. However, it turns out to be more profitable to treat $\rho^{(1)}$ rather than ψ as the fundamental field variable. The definition (3.1.9) shows that $\rho^{(1)}$ is a functional of ϕ. What is not obvious is the fact that for a given interparticle potential-energy function V_N and fixed values of T and μ, there is only one external potential that gives rise to a specific density profile. This result, the proof of which is given in Appendix B, has far-reaching implications. The grand canonical probability density f_0 defined by (2.4.5) is a functional of $\phi(\mathbf{r})$. Hence any quantity which, for given V_N, T and μ, is wholly determined by f_0 is necessarily a functional of $\rho^{(1)}$, and its functional dependence on $\rho^{(1)}$ is independent of the external potential. In particular, because the intrinsic free energy is the ensemble average of $(K_N + V_N + k_\mathrm{B}T \ln f_0)$ (see (3.1.19)), it follows that $\mathcal{F}[\rho^{(1)}]$ is a unique functional of $\rho^{(1)}$.

Let $n(\mathbf{r})$ be some average of the microscopic density, not necessarily the equilibrium one, and let $\Omega_\phi[n]$ be a functional of n, defined for fixed external potential by

$$\Omega_\phi[n] = \mathcal{F}[n] + \int n(\mathbf{r})\phi(\mathbf{r})\,\mathrm{d}\mathbf{r} - \mu\int n(\mathbf{r})\,\mathrm{d}\mathbf{r} \tag{3.4.1}$$

At equilibrium, $n(\mathbf{r}) = \rho^{(1)}(\mathbf{r})$, and Ω_ϕ reduces to the grand potential, i.e.

$$\Omega_\phi\big[\rho^{(1)}\big] = \Omega \tag{3.4.2}$$

while differentiation of (3.4.1) with respect to $n(\mathbf{r})$ gives

$$\left.\frac{\delta\Omega_\phi}{\delta n(\mathbf{r})}\right|_{n=\rho^{(1)}} = \left.\frac{\delta\mathcal{F}[n]}{\delta n(\mathbf{r})}\right|_{n=\rho^{(1)}} - \mu + \phi(\mathbf{r}) = 0 \tag{3.4.3}$$

where the right-hand side vanishes by virtue of (3.3.1). Thus Ω_ϕ is stationary with respect to variations in $n(\mathbf{r})$ around the equilibrium density. It is also straightforward to show that

$$\Omega_\phi[n] \geqslant \Omega \tag{3.4.4}$$

where the equality applies only when $n(\mathbf{r}) = \rho^{(1)}(\mathbf{r})$. In other words, the functional Ω_ϕ has a lower bound equal to the exact grand potential of the system. A proof of (3.4.4) is also given in Appendix B.

Equations (3.4.3) and (3.4.4) provide the ingredients for a variational calculation of the density profile and grand potential of an inhomogeneous fluid. What is required in order to make the theory tractable is a parametrisation of the free-energy functional $\mathcal{F}[n]$ in terms of $n(\mathbf{r})$. Since the ideal part is known exactly, the difficulty lies in finding a suitable form for $\mathcal{F}^{\mathrm{ex}}[n]$. The best estimates of $\rho^{(1)}$ and Ω are then obtained by minimising the functional $\Omega_\phi[n]$ with respect to variations in $n(\mathbf{r})$. Minimisation of a functional such as $\Omega_\phi[n]$ is the central problem in the calculus of variations and normally requires the solution to a differential equation called the Euler or Euler–Lagrange equation. Computational schemes of this type are grouped together under the title *density-functional theory*. The theory has found application to a very wide range of problems, some of which are discussed in later chapters. As in any variational calculation, the success achieved depends on the skill with which the trial functional is constructed. Because $\mathcal{F}$ is a unique functional of $\rho^{(1)}$, a good approximation would be one that was suitable for widely differing choices of external potential, but in practice most approximations are designed for use in specific physical situations.

If V_N is a sum of pair potentials, it is possible to derive an exact expression for $\mathcal{F}^{\mathrm{ex}}$ in terms of the pair density in a form that lends itself readily to approximation. The grand partition function can be written as

$$\Xi = \sum_{N=0}^{\infty} \frac{1}{N!} \int \cdots \int \left(\prod_{i<j}^{N} e(i,j) \right) \left(\prod_{i=1}^{N} z^*(i) \right) \mathrm{d}1 \cdots \mathrm{d}N \tag{3.4.5}$$

where $e(i,j) \equiv \exp[(-\beta v(i,j)]$. Then the functional derivative of Ω with respect to v at constant T and ψ is

$$\begin{aligned} \frac{\delta\Omega}{\delta v(1,2)} &= \frac{\delta \ln \Xi}{\delta \ln e(1,2)} = \frac{e(1,2)}{\Xi} \frac{\delta\Xi}{\delta e(1,2)} \\ &= \frac{1}{\Xi} \sum_{N=2}^{\infty} \frac{N(N-1)}{2N!} \int \cdots \int \left(\prod_{i<j}^{N} e(i,j) \right) \left(\prod_{i=1}^{N} z^*(i) \right) \mathrm{d}3 \cdots \mathrm{d}N \end{aligned} \tag{3.4.6}$$

where the factor $N(N-1)/2$ is the number of equivalent terms resulting from the differentiation (cf. (3.2.20)). Comparison with the definition of $\rho^{(n)}$ in (3.1.9) shows that

$$\rho^{(2)}(\mathbf{r},\mathbf{r}') = 2\frac{\delta\Omega}{\delta v(\mathbf{r},\mathbf{r}')} \tag{3.4.7}$$

and hence that

$$\rho^{(2)}(\mathbf{r},\mathbf{r}') = 2\frac{\delta\mathcal{F}^{\mathrm{ex}}[\rho^{(1)}]}{\delta v(\mathbf{r},\mathbf{r}')} \tag{3.4.8}$$

We now suppose that the pair potential can be expressed as the sum of a "reference" part, $v_0(\mathbf{r},\mathbf{r}')$, and a "perturbation", $w(\mathbf{r},\mathbf{r}')$, and define a family of intermediate potentials by

$$v_\lambda(\mathbf{r},\mathbf{r}') = v_0(\mathbf{r},\mathbf{r}') + \lambda w(\mathbf{r},\mathbf{r}'), \quad 0 \leqslant \lambda \leqslant 1 \tag{3.4.9}$$

The reference potential could, for example, be the hard-sphere interaction and the perturbation could be a weak, attractive tail, while the increase in λ from 0 to 1 would correspond to a gradual "switching on" of the perturbation. It follows from integration of (3.4.8) at constant single-particle density that the free-energy functional for the system of interest, characterised by the full potential $v(\mathbf{r},\mathbf{r}')$, is related to that of the reference system by

$$\begin{aligned}\mathcal{F}^{\mathrm{ex}}\big[\rho^{(1)}\big] &= \mathcal{F}_0^{\mathrm{ex}}\big[\rho^{(1)}\big] + \tfrac{1}{2}\int_0^1 \mathrm{d}\lambda \iint \rho^{(2)}\big(\mathbf{r},\mathbf{r}';\lambda\big) w(\mathbf{r},\mathbf{r}')\,\mathrm{d}\mathbf{r}\,\mathrm{d}\mathbf{r}' \\ &= \mathcal{F}_0^{\mathrm{ex}}\big[\rho^{(1)}\big] + \tfrac{1}{2}\iint \rho^{(1)}(\mathbf{r})\rho^{(1)}(\mathbf{r}')w(\mathbf{r},\mathbf{r}')\,\mathrm{d}\mathbf{r}\,\mathrm{d}\mathbf{r}' + \mathcal{F}_{\mathrm{corr}}\big[\rho^{(1)}\big]\end{aligned} \tag{3.4.10}$$

where $\rho^{(2)}(\mathbf{r},\mathbf{r}';\lambda)$ is the pair density for the system with potential v_λ and

$$\mathcal{F}_{\mathrm{corr}}\big[\rho^{(1)}\big] = \tfrac{1}{2}\int_0^1 \mathrm{d}\lambda \iint \rho^{(1)}(\mathbf{r})\rho^{(1)}(\mathbf{r}')h^{(2)}(\mathbf{r},\mathbf{r}';\lambda)w(\mathbf{r},\mathbf{r}')\,\mathrm{d}\mathbf{r}\,\mathrm{d}\mathbf{r}' \tag{3.4.11}$$

is the contribution to $\mathcal{F}^{\mathrm{ex}}$ due to correlations induced by the perturbation. Equation (3.4.10) provides a basis for the perturbation theories of uniform fluids discussed in Chapter 5.

3.5 DIRECT CORRELATION FUNCTIONS

We saw in Section 3.3 that the grand potential is a generating functional for the density correlation functions $H^{(n)}(\mathbf{r}^n)$. In a similar way, the excess part of the free-energy functional acts as a generating functional for a parallel hierarchy of *direct correlation functions*, $c^{(n)}(\mathbf{r}^n)$. The single-particle function is defined as the first functional derivative of $\mathcal{F}^{\mathrm{ex}}$ with respect to $\rho^{(1)}$:

$$c^{(1)}(\mathbf{r}) = -\beta\frac{\delta\mathcal{F}^{\mathrm{ex}}[\rho^{(1)}]}{\delta\rho^{(1)}(\mathbf{r})} \tag{3.5.1}$$

The pair function is defined as the functional derivative of $c^{(1)}$:

$$c^{(2)}(\mathbf{r},\mathbf{r}') = \frac{\delta c^{(1)}(\mathbf{r})}{\delta \rho^{(1)}(\mathbf{r}')} = -\beta \frac{\delta^2 \mathcal{F}^{\mathrm{ex}}[\rho^{(1)}]}{\delta \rho^{(1)}(\mathbf{r}) \delta \rho^{(1)}(\mathbf{r}')} \tag{3.5.2}$$

and similarly for higher-order functions: $c^{(n+1)}(\mathbf{r}^{n+1})$ is the derivative of $c^{(n)}(\mathbf{r}^n)$. It follows from (3.3.1), (3.3.3) and (3.5.1) that

$$\beta\psi(\mathbf{r}) = \beta \frac{\delta \mathcal{F}[\rho^{(1)}]}{\delta \rho^{(1)}(\mathbf{r})} = \ln\bigl[\Lambda^3 \rho^{(1)}(\mathbf{r})\bigr] - c^{(1)}(\mathbf{r}) \tag{3.5.3}$$

or, given that $\psi = \mu - \phi$ and $z = \exp(\beta\mu)/\Lambda^3$:

$$\rho^{(1)}(\mathbf{r}) = z \exp\bigl[-\beta\phi(\mathbf{r}) + c^{(1)}(\mathbf{r})\bigr] \tag{3.5.4}$$

Comparison with the corresponding ideal-gas result in (3.1.21) (the barometric law) shows that the effects of particle interactions on the density profile are wholly contained in the function $c^{(1)}(\mathbf{r})$. It is also clear from (3.5.3) that the quantity $-k_{\mathrm{B}}Tc^{(1)}(\mathbf{r})$, which acts in (3.5.4) as a self-consistent addition to the external potential, is the excess part of the intrinsic chemical potential. By appropriately adapting the argument of Section 2.4 it can be shown that $-k_{\mathrm{B}}Tc^{(1)}(\mathbf{r})$ is given by an expression identical to that on the right-hand side of (2.4.31), but where ε is now the energy of a test particle placed at $\mathbf{r}$ that interacts with particles of the system but not with the external field.[5] If $\phi = 0$, (3.5.4) can be rearranged to give

$$-k_{\mathrm{B}}Tc^{(1)} = \mu - k_{\mathrm{B}}T \ln \Lambda^3 \rho = \mu^{\mathrm{ex}} \tag{3.5.5}$$

To obtain a useful expression for $c^{(2)}(\mathbf{r},\mathbf{r}')$ we must return to some earlier results. Equations (3.3.4) and (3.3.12) show that, apart from a constant factor, the density–density correlation function is the functional derivative of $\rho^{(1)}$ with respect to ψ:

$$H(\mathbf{r},\mathbf{r}') = k_{\mathrm{B}}T \frac{\delta \rho^{(1)}(\mathbf{r})}{\delta \psi(\mathbf{r}')} \tag{3.5.6}$$

where, for notational simplicity, we have temporarily omitted the superscript (2). It therefore follows from (3.2.17) and (3.2.25) that the functional inverse of H, defined through the relation

$$\int H(\mathbf{r},\mathbf{r}'') H^{-1}(\mathbf{r}'',\mathbf{r}')\,\mathrm{d}\mathbf{r}'' = \delta(\mathbf{r}-\mathbf{r}') \tag{3.5.7}$$

is

$$H^{-1}(\mathbf{r},\mathbf{r}') = \beta \frac{\delta \psi(\mathbf{r})}{\delta \rho^{(1)}(\mathbf{r}')} \tag{3.5.8}$$

Functional differentiation of the expression for ψ in (3.5.3) gives

$$\beta \frac{\delta \psi(\mathbf{r})}{\delta \rho^{(1)}(\mathbf{r}')} = \frac{1}{\rho^{(1)}(\mathbf{r})}\delta(\mathbf{r}-\mathbf{r}') - c^{(2)}(\mathbf{r},\mathbf{r}') = H^{-1}(\mathbf{r},\mathbf{r}') \tag{3.5.9}$$

If we now substitute for H and H^{-1} in (3.5.7), integrate over $\mathbf{r}''$ and introduce the pair correlation function defined by (3.1.6), we obtain the *Ornstein–Zernike relation*:

$$h^{(2)}(\mathbf{r},\mathbf{r}') = c^{(2)}(\mathbf{r},\mathbf{r}') + \int c^{(2)}(\mathbf{r},\mathbf{r}'')\rho^{(1)}(\mathbf{r}'')h^{(2)}(\mathbf{r}'',\mathbf{r}')\,\mathrm{d}\mathbf{r}'' \tag{3.5.10}$$

This relation is often taken as the definition of $c^{(2)}$, but the definition as a derivative of the intrinsic free energy gives the function greater physical meaning. Equation (3.5.10) can be solved recursively to give

$$\begin{aligned} h^{(2)}(1,2) = c^{(2)}(1,2) &+ \int c^{(2)}(1,3)\rho^{(1)}(3)c^{(2)}(3,2)\,\mathrm{d}3 \\ &+ \iint c^{(2)}(1,3)\rho^{(1)}(3)c^{(2)}(3,4)\rho^{(1)}(4)c^{(2)}(4,2)\,\mathrm{d}3\,\mathrm{d}4 + \cdots \end{aligned} \tag{3.5.11}$$

This result has an obvious physical interpretation: the "total" correlation between particles 1 and 2, represented by $h^{(2)}(1,2)$, is due in part to the "direct" correlation between 1 and 2 but also to the "indirect" correlation propagated via increasingly large numbers of intermediate particles. With this physical picture in mind it is plausible to suppose that the range of $c^{(2)}(1,2)$ is comparable with that of the pair potential $v(1,2)$ and to ascribe the fact that $h^{(2)}(1,2)$ is generally much longer ranged than $v(1,2)$ to the effects of indirect correlation. The differences between the two functions for the Lennard-Jones fluid at high density and low temperature are illustrated in Figure 3.1; $c(r)$ is not only shorter ranged than $h(r)$ but also simpler in structure.

If the fluid is uniform and isotropic, the Ornstein–Zernike relation becomes

$$h(r) = c(r) + \rho \int c\big(|\mathbf{r}-\mathbf{r}'|\big)h(r')\,\mathrm{d}\mathbf{r}' \tag{3.5.12}$$

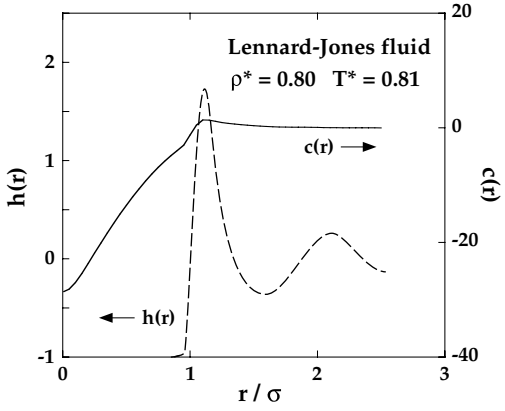

FIG. 3.1. The pair functions $h(r)$ (dashes) and $c(r)$ (full curve) obtained by Monte Carlo calculations for the Lennard-Jones fluid at a high density and low temperature. After Llano-Restrepo and Chapman.[6]

where the term representing the indirect correlation now appears as a convolution integral. We have also followed the convention adopted earlier for $g(r)$ by omitting the superscripts (2) when the system is homogeneous and shall continue to do so in circumstances where there is no risk of ambiguity. On taking the Fourier transform of both sides of (3.5.12) we obtain an algebraic relation between $\hat{h}(k)$ and $\hat{c}(k)$:

$$\hat{h}(k) = \frac{\hat{c}(k)}{1 - \rho\hat{c}(k)} \tag{3.5.13}$$

Equation (3.5.13) provides a link with thermodynamics via the compressibility equation (2.6.12). Since $h(r) = g(r) - 1$, it follows from (2.6.12) that the isothermal compressibility can be written in either of the two equivalent forms:

$$\rho k_{\mathrm{B}} T \chi_T = 1 + \rho\hat{h}(0) \tag{3.5.14}$$

or

$$\frac{1}{\rho k_{\mathrm{B}} T \chi_T} = 1 - \rho\hat{c}(0) \tag{3.5.15}$$

These results bring out particularly clearly the inverse relationship that exists between h and c.

The definitions of $c^{(1)}$ and $c^{(2)}$ in (3.5.1) and (3.5.2) are useful in characterising the nature of an approximate free-energy functional. As a simple example, consider the functional derived from the exact result (3.4.10) by discarding the term $\mathcal{F}_{\mathrm{corr}}$, which amounts to treating the effects of the perturbation $w(\mathbf{r}, \mathbf{r}')$ in a mean-field approximation. Then

$$c^{(1)}(\mathbf{r}) \approx c_0^{(1)}(\mathbf{r}) - \beta \int \rho^{(1)}(\mathbf{r}')w(\mathbf{r}, \mathbf{r}')\,\mathrm{d}\mathbf{r}' \tag{3.5.16}$$

$$c^{(2)}(\mathbf{r}, \mathbf{r}') \approx c_0^{(2)}(\mathbf{r}, \mathbf{r}') - \beta w(\mathbf{r}, \mathbf{r}') \tag{3.5.17}$$

where $c_0^{(1)}$ and $c_0^{(2)}$ are the direct correlation functions of the reference system. Substitution of (3.5.16) in (3.5.4) yields an integral equation for $\rho^{(1)}(\mathbf{r})$ that can be solved iteratively if the properties of the reference system are known or if some further approximation is made for $c_0^{(1)}$. Equation (3.5.17) is a well-known approximation in the theory of uniform fluids;[7] for historical reasons it is called the *random-phase approximation* or RPA. It is generally accepted that $c^{(2)}(\mathbf{r}, \mathbf{r}')$ behaves asymptotically as $-\beta v(\mathbf{r}, \mathbf{r}')$. The RPA should therefore be exact when $|\mathbf{r} - \mathbf{r}'|$ is sufficiently large; this assumes that the perturbation contains the long-range part of the potential, which is almost invariably the case.

The formally exact expression for the intrinsic free energy given by (3.4.10) was obtained by thermodynamic integration with respect to the interparticle potential. Another exact expression can be derived from the definitions of $c^{(1)}$ and $c^{(2)}$ by integrating with respect to the single-particle density. Let $\rho_0^{(1)}(\mathbf{r})$ and $c_0^{(1)}(\mathbf{r})$ be the single-particle density and single-particle direct correlation function, respectively, in a reference state of the system of interest. We choose a linear integration path between the reference state and the

final state of density $\rho^{(1)}(\mathbf{r})$ such that

$$\rho^{(1)}(\mathbf{r};\lambda) = \rho_0^{(1)}(\mathbf{r}) + \lambda \Delta\rho^{(1)}(\mathbf{r}) \tag{3.5.18}$$

where $\Delta\rho^{(1)} = \rho^{(1)} - \rho_0^{(1)}$. Then integration of (3.5.1) gives

$$\begin{aligned}\mathcal{F}^{\mathrm{ex}}\big[\rho^{(1)}\big] &= \mathcal{F}_0^{\mathrm{ex}}\big[\rho_0^{(1)}\big] - k_{\mathrm{B}}T \int_0^1 \mathrm{d}\lambda \int \frac{\partial\rho^{(1)}(\mathbf{r};\lambda)}{\partial\lambda} c^{(1)}(\mathbf{r};\lambda)\,\mathrm{d}\mathbf{r} \\ &= \mathcal{F}_0^{\mathrm{ex}}\big[\rho_0^{(1)}\big] - k_{\mathrm{B}}T \int_0^1 \mathrm{d}\lambda \int \Delta\rho^{(1)}(\mathbf{r}) c^{(1)}(\mathbf{r};\lambda)\,\mathrm{d}\mathbf{r}\end{aligned} \tag{3.5.19}$$

Similarly, from integration of (3.5.2):

$$c^{(1)}(\mathbf{r};\lambda) = c_0^{(1)}(\mathbf{r}) + \int_0^\lambda \mathrm{d}\lambda' \int \Delta\rho^{(1)}(\mathbf{r}') c^{(2)}(\mathbf{r},\mathbf{r}';\lambda')\,\mathrm{d}\mathbf{r}' \tag{3.5.20}$$

and hence, after substitution of (3.5.20) in (3.5.19):

$$\begin{aligned}\mathcal{F}^{\mathrm{ex}}\big[\rho^{(1)}\big] = \mathcal{F}_0^{\mathrm{ex}}\big[\rho_0^{(1)}\big] &- k_{\mathrm{B}}T \int \Delta\rho^{(1)}(\mathbf{r}) c_0^{(1)}(\mathbf{r})\,\mathrm{d}\mathbf{r} \\ &- k_{\mathrm{B}}T \int_0^1 \mathrm{d}\lambda \int_0^\lambda \mathrm{d}\lambda' \iint \Delta\rho^{(1)}(\mathbf{r}) \Delta\rho^{(1)}(\mathbf{r}') c^{(2)}(\mathbf{r},\mathbf{r}';\lambda)\,\mathrm{d}\mathbf{r}\,\mathrm{d}\mathbf{r}'\end{aligned} \tag{3.5.21}$$

The integration path defined by (3.5.18) is chosen for mathematical convenience, but the final result is independent of path, since $\mathcal{F}^{\mathrm{ex}}$ is a unique functional of $\rho^{(1)}$.

Some simplification of (3.5.21) is possible. An integration by parts shows that

$$\int_0^1 \mathrm{d}\lambda \int_0^\lambda y(\lambda')\,\mathrm{d}\lambda' = \int_0^1 (1-\lambda) y(\lambda)\,\mathrm{d}\lambda \tag{3.5.22}$$

for any function $y(\lambda)$. Thus

$$\begin{aligned}\mathcal{F}^{\mathrm{ex}}\big[\rho^{(1)}\big] = \mathcal{F}_0^{\mathrm{ex}}\big[\rho_0^{(1)}\big] &- k_{\mathrm{B}}T \int \Delta\rho^{(1)}(\mathbf{r}) c_0^{(1)}(r)\,\mathrm{d}\mathbf{r} \\ &- k_{\mathrm{B}}T \int_0^1 \mathrm{d}\lambda (1-\lambda) \iint \Delta\rho^{(1)}(\mathbf{r}) \Delta\rho^{(1)}(\mathbf{r}') c^{(2)}(\mathbf{r},\mathbf{r}';\lambda)\,\mathrm{d}\mathbf{r}\,\mathrm{d}\mathbf{r}'\end{aligned} \tag{3.5.23}$$

In contrast to (3.4.10), use of this result in constructing a trial functional requires an approximation for $c^{(2)}(\mathbf{r}',\mathbf{r}';\lambda)$ rather than $h^{(2)}(\mathbf{r}',\mathbf{r}';\lambda)$, and its derivation does not rely on the assumption of pairwise additivity of the particle interactions. If we assume that the final state is homogeneous and that the initial state is one of zero density, (3.5.23) yields an expression for the excess free energy of a uniform fluid of density ρ:

$$F^{\mathrm{ex}}(\rho) = \rho^2 k_{\mathrm{B}}T \int_0^1 \mathrm{d}\lambda\,(\lambda - 1) \int \mathrm{d}\mathbf{r} \int c\big(|\mathbf{r}' - \mathbf{r}|;\lambda\rho\big)\,\mathrm{d}(\mathbf{r}' - \mathbf{r}) \tag{3.5.24}$$

or, after integration over $\mathbf{r}$:

$$\frac{\beta F^{\mathrm{ex}}(\rho)}{N} = \rho \int_0^1 \mathrm{d}\lambda\,(\lambda - 1) \int c(r; \lambda\rho)\,\mathrm{d}\mathbf{r} \tag{3.5.25}$$

3.6 THE DENSITY RESPONSE FUNCTION

Let us suppose that a uniform fluid of number density ρ_0 is exposed to a weak, external potential $\delta\phi(\mathbf{r})$. The hamiltonian of the system is

$$\mathcal{H} = \mathcal{H}_0 + \sum_{i=1}^{N} \delta\phi(\mathbf{r}_i) \tag{3.6.1}$$

where $\mathcal{H}_0$ is the hamiltonian of the uniform fluid. The external potential acts as a perturbation on the system and creates an inhomogeneity, measured by the deviation $\delta\rho^{(1)}(\mathbf{r})$ of the single-particle density from its value in the uniform state:

$$\delta\rho^{(1)}(\mathbf{r}) = \rho^{(1)}(\mathbf{r}) - \rho_0 \tag{3.6.2}$$

Because the perturbation is weak, it can be assumed that the response is a linear but non-local function of $\delta\phi(\mathbf{r})$, expressible in terms of a *linear response function* $\chi(\mathbf{r}, \mathbf{r}')$ in the form

$$\delta\rho^{(1)}(\mathbf{r}) = \int \chi(\mathbf{r}, \mathbf{r}')\delta\phi(\mathbf{r}')\,\mathrm{d}\mathbf{r}' \tag{3.6.3}$$

It follows from the definition of a functional derivative that

$$\chi(\mathbf{r}, \mathbf{r}') = \left.\frac{\delta\rho^{(1)}(\mathbf{r})}{\delta\phi(\mathbf{r}')}\right|_{\phi=0} = -\left.\frac{\delta\rho^{(1)}(\mathbf{r})}{\delta\psi(\mathbf{r}')}\right|_{\phi=0} \tag{3.6.4}$$

and hence, from (3.5.6), that

$$\chi(\mathbf{r}, \mathbf{r}') = -\beta H^{(2)}(\mathbf{r}, \mathbf{r}') \tag{3.6.5}$$

where $H^{(2)}(\mathbf{r}, \mathbf{r}')$ is the density–density correlation function of the unperturbed system. Because the unperturbed system is homogeneous, the response function can be written as

$$\chi\big(|\mathbf{r} - \mathbf{r}'|\big) = -\beta\big[\rho_0^2 h\big(|\mathbf{r} - \mathbf{r}'|\big) + \rho_0\delta\big(|\mathbf{r} - \mathbf{r}'|\big)\big] \tag{3.6.6}$$

and the change in density due to the perturbation divides into local and non-local terms:

$$\delta\rho^{(1)}(\mathbf{r}) = -\beta\rho_0\delta\phi(\mathbf{r}) - \beta\rho_0^2 \int h\big(|\mathbf{r} - \mathbf{r}'|\big)\delta\phi(\mathbf{r}')\,\mathrm{d}\mathbf{r}' \tag{3.6.7}$$

This result is called the Yvon equation; it is equivalent to a first-order Taylor expansion of $\rho^{(1)}$ in powers of $\delta\phi$.

We now take the Fourier transform of (3.6.3) and relate the response $\delta\hat{\rho}^{(1)}(\mathbf{k})$ to the Fourier components of the external potential, defined as

$$\delta\hat{\phi}(\mathbf{k}) = \int \exp(-i\mathbf{k}\cdot\mathbf{r})\delta\phi(\mathbf{r})\,\mathrm{d}\mathbf{r} \tag{3.6.8}$$

The result is

$$\delta\hat{\rho}^{(1)}(\mathbf{k}) = \chi(\mathbf{k})\hat{\phi}(\mathbf{k}) = -\beta\rho_0 S(\mathbf{k})\delta\hat{\phi}(\mathbf{k}) \tag{3.6.9}$$

where

$$S(\mathbf{k}) = 1 + \rho_0\hat{h}(\mathbf{k}) = \frac{1}{1-\rho_0\hat{c}(k)} \tag{3.6.10}$$

is the *static structure factor* of the uniform fluid; the second equality in (3.6.10) follows from (3.5.13). The structure factor appears in (3.6.9) as a generalised response function, akin to the magnetic susceptibility of a spin system. The linear density response to an external field is therefore determined by the density–density correlation function in the absence of the field; this is an example of the *fluctuation–dissipation theorem*. More specifically, $S(\mathbf{k})$ is a measure of the density response of a system, initially in equilibrium, to a weak, external perturbation of wavelength $2\pi/k$. When the probe is a beam of neutrons, $S(\mathbf{k})$ is proportional to the total scattered intensity in a direction determined by the momentum transfer $\hbar\mathbf{k}$ between beam and sample. Use of such a probe provides an experimental means of determining the radial distribution function of a liquid, as in the example shown in Figure 2.1. Equations (3.5.14) and (3.6.10) together show that at long wavelengths $S(\mathbf{k})$ behaves as

$$\lim_{\mathbf{k}\to\infty} S(\mathbf{k}) = \rho k_{\mathrm{B}} T \chi_T \tag{3.6.11}$$

and is therefore a measure of the response in one macroscopic quantity – the number density – to a change in another – the applied pressure. If the system is isotropic, the structure factor is a function only of the wavenumber k.

An example of an experimentally determined structure factor for liquid sodium near the triple point is pictured in Figure 3.2; the dominant feature is a pronounced peak at a wavenumber approximately equal to $2\pi/\Delta r$, where Δr is the spacing of the peaks in $g(r)$. As the figure shows, the experimental structure factor is very well fitted by Monte Carlo results for a purely repulsive potential that varies as r^{-4}. Since the r^{-4} potential is only a crude representation of the effective potential for liquid sodium, the good agreement seen in the figure strongly suggests that the structure factor is insensitive to details of the atomic interactions.

The discussion until now has been limited to one-component systems, but the ideas developed in this section and the preceding one can be extended to mixtures without major complications. Consider a system containing N_ν particles of species ν, with $\nu = 1$ to n. If $N = \sum_\nu N_\nu$ is the total number of particles, the number concentration of species ν is $x_\nu = N_\nu/N$. The partial microscopic density $\rho_\nu(\mathbf{r})$ and its average value $\rho_\nu^{(1)}(\mathbf{r})$ (the

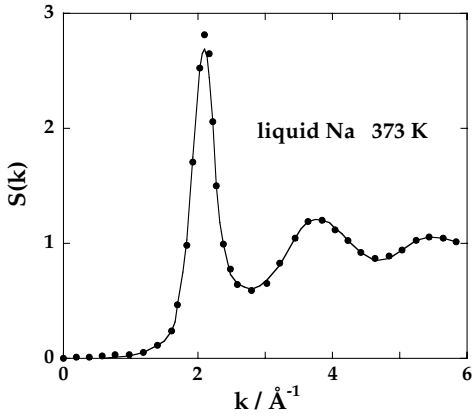

FIG. 3.2. Structure factor of liquid sodium near the normal melting temperature. The points are experimental x-ray scattering results[8] and the curve is obtained from a Monte Carlo calculation[9] for the r^{-4} potential under the same thermodynamic conditions.

single-particle density of species ν) are defined in a manner identical to (3.1.2) and (3.1.4), except that the sum on i is limited to particles of species ν. At the pair level, the structure of the fluid is described by $\frac{1}{2}n(n+1)$ partial pair correlation functions $h^{(2)}_{\nu\mu}(\mathbf{r},\mathbf{r}')$ and $\frac{1}{2}n(n+1)$ direct correlation functions $c^{(2)}_{\nu\mu}(\mathbf{r},\mathbf{r}')$. The two sets of functions are linked by a set of coupled equations, representing a generalisation of the Ornstein–Zernike relation (3.5.10), which in the homogeneous case becomes

$$h_{\nu\mu}(r) = c_{\nu\mu}(r) + \rho \sum_{\lambda} x_\lambda \int c_{\nu\lambda}\big(|\mathbf{r}-\mathbf{r}'|\big) h_{\lambda\mu}(r')\,\mathrm{d}\mathbf{r}' \tag{3.6.12}$$

The change in the single-particle density of species ν induced by a weak external potential $\delta\phi_\mu(\mathbf{r})$ that couples to the density of species μ is given by a straightforward generalisation of (3.6.7):

$$\delta\rho^{(1)}_\nu(\mathbf{r}) = -x_\nu\delta_{\nu\mu}\beta\rho\delta\phi_\mu(\mathbf{r}) - x_\nu x_\mu\beta\rho^2\int h_{\nu\mu}\big(|\mathbf{r}-\mathbf{r}'|\big)\delta\phi_\mu(\mathbf{r}')\,\mathrm{d}\mathbf{r}' \tag{3.6.13}$$

or, after Fourier transformation:

$$\delta\hat{\rho}^{(1)}_\nu(\mathbf{k}) = \chi_{\nu\mu}(\mathbf{k})\delta\hat{\phi}_\mu(\mathbf{k}) = -\beta\rho S_{\nu\mu}(\mathbf{k})\delta\hat{\phi}_\mu(\mathbf{k}) \tag{3.6.14}$$

where $\chi_{\nu\mu}(\mathbf{k})$ is a linear response function and

$$S_{\nu\mu}(\mathbf{k}) = x_\nu\delta_{\nu\mu} + x_\nu x_\mu\rho\hat{h}_{\nu\mu}(\mathbf{k}) \tag{3.6.15}$$

is a partial structure factor of the uniform fluid. Note that the local contribution to $\delta\rho^{(1)}_\nu(\mathbf{r})$ in (3.6.13) disappears unless the labels ν, μ refer to the same species. Finally, the general-

isation to mixtures of the expression for the compressibility given by (3.5.15) is

$$\frac{1}{\rho k_{\mathrm{B}} T \chi_T} = 1 - \rho \sum_{\nu} \sum_{\mu} \hat{c}_{\nu\mu}(0) \tag{3.6.16}$$

If the partial structure factors are represented as a matrix, $\boldsymbol{S}(k)$, combination of (3.6.12) and (3.6.15), together with a matrix inversion, shows that the corresponding generalisation of (3.6.11) is

$$\rho k_{\mathrm{B}} T \chi_T = \frac{|\boldsymbol{S}(0)|}{\sum_{\nu} \sum_{\mu} x_\nu x_\mu |\boldsymbol{S}(0)|_{\nu\mu}} \tag{3.6.17}$$

where $|\boldsymbol{S}(0)|_{\nu\mu}$ is the cofactor of $S_{\nu\mu}(0)$ in the determinant $|\boldsymbol{S}(0)|$. Equation (3.6.17) is called the Kirkwood–Buff formula.[10]

3.7 DIAGRAMMATIC METHODS

The grand partition function and particle densities are defined as many-dimensional integrals over particle coordinates. Such integrals are conveniently represented by *diagrams* or *graphs*, which in turn can be manipulated by graph-theoretical methods. These methods include simple prescriptions for the evaluation of functional derivatives of the type encountered in earlier sections of this chapter. As we shall see, the diagrammatic approach leads naturally to expansions of thermodynamic properties and particle distribution functions in powers of either the activity or density. While such expansions are in general more appropriate to gases than to liquids, diagrammatic methods have played a prominent role in the development of the modern theory of dense fluids. The statistical mechanics of non-uniform fluids, for example, was originally formulated in diagrammatic terms.[11] The introductory account given here is based largely on the work of Morita and Hiroike,[12] de Dominicis[13] and Stell.[14] Although the discussion is self-contained, it is limited in scope, and no attempt is made at mathematical rigour.

We consider again the case when the interparticle potential energy is a sum of pair terms. As we shall see later, it is sometimes convenient to replace the Boltzmann factor $\exp(-\beta V_N)$ by a sum of products of *Mayer functions*, $f(i, j)$, defined as

$$f(i, j) = \exp\bigl[-\beta v(i, j)\bigr] - 1 \equiv e(i, j) - 1 \tag{3.7.1}$$

Then, for example, in the definition of $\rho^{(1)}(1)$ given by (3.1.9) the term for $N = 4$ involves an integral of the form

$$I = \iiint \left(\prod_{i=1}^{4} z^*(i) \right) f(1,2)\, f(1,4)\, f(2,3)\, f(3,4)\, \mathrm{d}2\, \mathrm{d}3\, \mathrm{d}4 \tag{3.7.2}$$

To each such integral there corresponds a *labelled diagram* consisting of a number of *circles* linked by *bonds*. Circles represent particle coordinates and carry an appropriate label;

for that reason the diagrams are sometimes called "cluster" diagrams. The circles are of two types: *white circles* (or "root points"), which correspond to coordinates held constant in the integration, and *black circles* (or "field points"), which represent the variables of integration. With a circle labelled i we associate a function of coordinates, $\gamma(i)$, say. The circle is then referred to as a white or black γ-circle; a 1-circle is a circle for which $\gamma(i) = 1$. Bonds are drawn as lines between circles. With a bond between circles i and j we associate a function $\eta(i, j)$, say, and refer to it as an η-bond; a *simple* diagram is one in which no pair of circles is linked by more than one bond. The *value* of a labelled diagram is the value of the integral that the diagram represents; it is a function of the coordinates attached to the white circles and a functional of the functions associated with the black circles and bonds. Thus the integral in (3.7.2) is represented by a simple, labelled diagram consisting of z^*-circles (both white and black) and f-bonds:

$I =$ 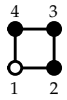

The black circles in a diagram correspond to the dummy variables of integration. The manner in which the black circles are labelled is therefore irrelevant and the labels may conveniently be omitted altogether. The value of the resulting *unlabelled diagram* involves a combinatorial factor related to the topological structure of the diagram. Consider a labelled diagram containing m black γ-circles and any number of white circles. Each of the $m!$ possible permutations of labels of the black circles leaves the value of the diagram unchanged. There is, however, a subgroup of permutations which give rise to diagrams that are *topologically equivalent*. Two labelled diagrams are said to be topologically equivalent if they are characterised by the same set of *connections*, meaning that circles labelled i and j in one diagram are linked by an η-bond if and only if they are similarly linked in the other. In the case when all black circles are associated with the same function, the *symmetry number* of a simple diagram is the order of the subgroup of permutations that leave the connections unaltered. We adopt the convention that when the word "diagram" or the symbol for a diagram appears in an equation, the quantity to be inserted is the value of that diagram. Then the value of a simple diagram Γ consisting of n white circles labelled 1 to n and m unlabelled black circles is

$$\Gamma = (1/m!)[\text{the sum of all topologically inequivalent diagrams obtained by labelling the black circles}] \tag{3.7.3}$$

The number of labelled diagrams appearing on the right-hand side of this equation is equal to $m!/S$, where S is the symmetry number, and each of the diagrams has a value equal to that of the integral it represents. The definition (3.7.3) may therefore be reformulated as

$$\begin{aligned}\Gamma &= (1/S)[\text{any diagram obtained by labelling the black circles}] \\ &= (1/S)[\text{the value of the corresponding integral}]\end{aligned} \tag{3.7.4}$$

In the example already pictured the symmetry number of the diagram is equal to two, since the connections are unaltered by interchange of the labels 2 and 4. Thus the unlabelled diagram obtained by removing the labels 2, 3 and 4 has a value equal to $\frac{1}{2}I$.

The definition of the value of a diagram can be extended to a wider class of diagrams than those we have discussed, but the definition of symmetry number may have to be modified. For example, if a diagram is *composite* rather than simple, the symmetry number is increased by a factor $n!$ for every pair of circles linked by n bonds of the same *species*. On the other hand, if the functions associated with the black circles are not all the same, the symmetry number is reduced.

The difference in value of labelled and unlabelled diagrams is important because the greater ease with which unlabelled diagrams are manipulated is due precisely to the inclusion of the combinatorial factor S. In all that follows, use of the word "diagram" without qualification should be taken as referring to the unlabelled type, though the distinction will often be irrelevant. Two unlabelled diagrams are *topologically distinct* if it is impossible to find a permutation that converts a labelled version of one diagram into a labelled version of the other. Diagrams that are topologically distinct represent different integrals. Statistical mechanical quantities usefully discussed in diagrammatic terms are frequently obtained as "the sum of all topologically distinct diagrams" having certain properties. To avoid undue repetition we shall always replace the cumbersome phrase in quotation marks by the expression "all diagrams". We also adopt the convention that any diagrams we discuss are simple unless they are otherwise described.

Two circles are *adjacent* if they are linked by a bond. A sequence of adjacent circles and the bonds that link them is called a *path*. Two paths between a given pair of circles are *independent* if they have no intermediate circle in common. A *connected* diagram is either *simply* or *multiply* connected; if there exist (at least) n independent paths between any pair of circles the diagram is (at least) *n-tuple* connected. In the examples shown below, diagram (a) is simply connected, (b) is triply connected and (c) is a *disconnected* diagram with two doubly-connected *components*.

(a) (b) (c)

A bond is said to *intersect* the circles that it links. *Removal* of a circle from a diagram means that the circle and the bonds that intersect it are erased. A *connecting* circle is a circle whose removal from a connected diagram causes the diagram to become disconnected; the *multiplicity* of a connecting circle is the number of components into which the diagram separates when the circle is removed. Removal of an *articulation* circle from a connected diagram causes the diagram to separate into two or more components, of which at least one contains no white circle; an *articulation pair* is a pair of circles whose removal has the same effect. A diagram that is free of articulation circles is said to be *irreducible*; the absence of articulation pairs implies irreducibility but not vice versa. If a diagram contains at least two white circles, a *nodal* circle is one through which all paths between two particular white circles pass. Clearly there can be no nodal circle associated with a pair of white circles linked by a bond. A nodal circle is necessarily also a connecting circle and may also be

an articulation circle if its multiplicity is three or more. The examples below illustrate the effects of removing (a) an articulation circle, (b) an articulation pair and (c) a nodal circle.

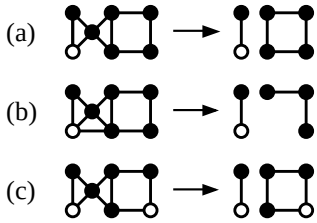

A *subdiagram* of a diagram Γ is any diagram that can be obtained from Γ by some combination of the removal of circles and erasure of bonds. A subdiagram is *maximal* with respect to a given property if it is not embedded in another subdiagram with the same property; a particularly important class of maximal subdiagrams are those that are irreducible. The *star product* of two connected diagrams Γ_1, Γ_2 is the diagram Γ_3 obtained by linking together the two diagrams in such a way that white circles carrying the same labels are superimposed, as in the example shown below:

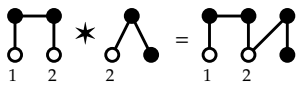

The two diagrams are said to be *connected in parallel* at the n white circles having labels that are common to both Γ_1 and Γ_2; if the two diagrams are connected in parallel at white γ-circles, the corresponding circles in Γ_3 are γ^2-circles. If Γ_1 and Γ_2 have no white circles in common, or if one or both contain only black circles, the star product is a disconnected diagram having Γ_1 and Γ_2 as its components. *Star-irreducible* diagrams are connected diagrams that cannot be expressed as the star product of two other diagrams except when one of the two is the diagram consisting of a single white circle. The definition of star-irreducibility excludes all diagrams containing white connecting circles or connecting subsets of white circles, all diagrams with adjacent white circles and, by convention, the diagram consisting of a single white circle. The star product of two star-irreducible diagrams can be uniquely decomposed into the factors that form the product; thus the properties of star-irreducible diagrams are analogous to those of prime numbers.

Diagrammatic expressions are manipulated with the aid of certain rules, the most important of which are contained in a series of lemmas derived by Morita and Hiroike.[12] The lemmas are stated here without proof and illustrated by simple examples;[15] some details of the proofs are given in Appendix C.

Lemma 1. *Let G be a set of topologically distinct, star-irreducible diagrams and let H be the set of all diagrams in G and all possible star products of diagrams in G. Then*

$$[\textit{all diagrams in } H] = \exp[\textit{all diagrams in } G] - 1$$

Illustration. If G consists of a single diagram, Γ, where

$\Gamma =$ 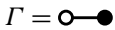

then

$\exp(\Gamma) = 1 +$ 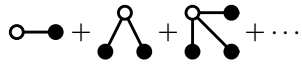

Lemma 1 is called the "exponentiation theorem". If the diagrams in G consist solely of black circles and bonds, use of the lemma makes it possible to express a sum of connected and disconnected diagrams in terms of the connected subset.

Lemmas 2 and 3 contain the diagrammatic prescriptions for the evaluation of two important types of functional derivative.

Lemma 2. *Let Γ be a diagram consisting of black γ-circles and bonds. Then*

$$\partial\Gamma/\partial\gamma(\mathbf{r}) = [\textit{all diagrams obtained by replacing a black } \gamma\textit{-circle of } \Gamma \textit{ by a white 1-circle labelled } \mathbf{r}]$$

Illustration.

$\Gamma =$  $\qquad \delta\Gamma/\delta\gamma =$ 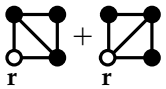

Lemma 3. *Let Γ be a diagram consisting of black circles and η-bonds. Then*

$$\partial\Gamma/\partial\eta(\mathbf{r},\mathbf{r}') = \tfrac{1}{2}[\textit{all diagrams obtained by erasing an } \eta\textit{-bond of } \Gamma, \textit{ whitening the circles that it linked and labelling the whitened circles } \mathbf{r} \textit{ and } \mathbf{r}']$$

Illustration.

$\Gamma =$  $\qquad \delta\Gamma/\delta\eta = \frac{1}{2}$ 

The example illustrated is the diagrammatic representation of example (3.2.21) for the case when $a = 1$. The numerical factor present in (3.2.21) is taken care of by the different symmetry numbers before ($S = 6$) and after ($S = 1$) differentiation.

Lemmas 4 and 5 are useful in the process of *topological reduction*.

Lemma 4. *Let G be a set of topologically distinct, connected diagrams consisting of a white circle labelled* $\mathbf{r}$*, black γ-circles and bonds, and let $\mathcal{G}(\mathbf{r})$ be the sum of all diagrams in G. If Γ is a connected diagram, if H is the set of all topologically distinct diagrams*

obtained by decorating all black circles of Γ with diagrams in G, and if each diagram in H is uniquely decomposable, then

$$[\textit{all diagrams in } H] = [\textit{the diagram obtained from } \Gamma \textit{ by replacing the black } \gamma\textit{-circles by } \mathcal{G}\textit{-circles}]$$

The process of *decorating* the diagram Γ consists of attaching one of the elements in G in such a way that its white circle is superimposed on a black circle of Γ and then blackened. For the diagrams in H to be *uniquely decomposable* it must be possible, given the structure of Γ, to determine by inspection which diagram in G has been used to decorate each black circle of Γ; this is always possible if Γ is free of black articulation circles.

Illustration. If the set G consists of the two diagrams:

and if

$\Gamma =$ 

then the set H consists of the three diagrams

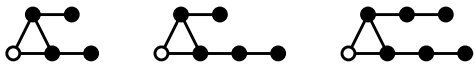

Although the example is a simple one, it illustrates the main ingredients of a topological reduction: the sum of a number of diagrams (here the diagrams in H, where the black circles are γ-circles) is replaced by a single diagram of simpler structure (here Γ, where the black circles are $\mathcal{G}$-circles).

Lemma 5. *Let G be a set of topologically distinct, connected diagrams consisting of two white circles labelled $\mathbf{r}$ and $\mathbf{r}'$, black circles and η-bonds, and let $\mathcal{G}(\mathbf{r}, \mathbf{r}')$ be the sum of all diagrams in G. If Γ is a connected diagram, if H is the set of all topologically distinct diagrams obtained by replacing all bonds of Γ by diagrams in G, and if each diagram in H is uniquely decomposable, then*

$$[\textit{all diagrams in } H] = [\textit{the diagram obtained from } \Gamma \textit{ by replacing the } \eta\textit{-bonds by } \mathcal{G}\textit{-bonds}]$$

Replacement of bonds in Γ involves superimposing the two white circles of the diagram drawn from G onto the circles of Γ and erasing the bond between them. The circles take the same colour and, if white, the same label as the corresponding circle in Γ.

Illustration. If the set G consists of the two diagrams:

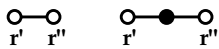

and if

$\Gamma =$ 

then the set H consists of the three diagrams

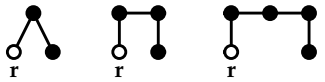

3.8 DIAGRAMMATIC EXPANSIONS OF THE DIRECT CORRELATION FUNCTIONS

We now give examples of how the definitions and lemmas of the previous section can be used to obtain results of physical interest. The examples we choose are ones that lead to series expansions of the direct correlation functions $c^{(1)}(\mathbf{r})$ and $c^{(2)}(\mathbf{r}, \mathbf{r}')$ introduced in Section 3.5. We assume again that the interparticle forces are pairwise additive and take as our starting point the expression for Ξ given by (3.4.5). It follows immediately that Ξ can be represented diagrammatically as

$\Xi = 1 +$ [all diagrams consisting of black z^*-circles with an e-bond linking each pair]

$= 1 +$ 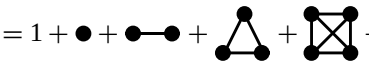 $+ \cdots$ (3.8.1)

Note that the definition of the value of a diagram takes care of the factors $1/N!$ in (3.4.5). Because $e(i, j) \to 1$ as $|\mathbf{r}_j - \mathbf{r}_i| \to \infty$, the contribution from the Nth term in (3.8.1) is of order V^N, and problems arise in the thermodynamic limit. It is therefore better to reformulate the series in terms of Mayer functions by making the substitution $f(i, j) = e(i, j) - 1$, as in example (3.7.2). The series then becomes

$\Xi = 1 +$ [all diagrams consisting of black z^*-circles and f-bonds]

$= 1 +$ 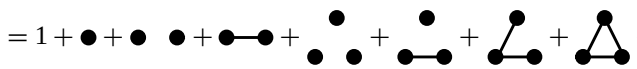 $+ \cdots$ (3.8.2)

The disconnected diagrams in (3.8.2) can be eliminated by taking the logarithm of Ξ and applying Lemma 1. This yields an expansion of the grand potential in the form

$-\beta\Omega =$ [all connected diagrams consisting of black z^*-circles and f-bonds]

$=$  $+ \cdots$ (3.8.3)

Since there is no need to consider disconnected diagrams again, the requirement that diagrams must be connected will from now on be omitted.

At each order in z^* beyond the second, many of the diagrams in the series (3.8.3) contain articulation circles; those contributing at third and fourth orders are shown below, with the articulation circles marked by arrows:

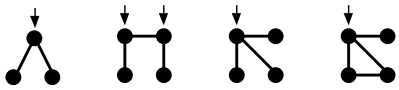

If the system were translationally invariant, the articulation circles could be chosen as the origin of coordinates in the corresponding integrals. The integrals would then factorise as products of integrals that already appear at lower order in the expansion. While this is not possible in the general case, diagrams that contain articulation circles can be eliminated by switching from an activity to a density expansion. This requires, as an intermediate step, the activity expansion of $\rho^{(1)}(\mathbf{r})$. The single-particle density at a point $\mathbf{r}$ is the functional derivative of the grand potential with respect to either $\psi(\mathbf{r})$ or, equivalently, $\ln z^*(\mathbf{r})$. From (3.3.10) and Lemma 2 it follows that

$$\rho^{(1)}(\mathbf{r})/z^*(\mathbf{r}) = 1 + [\text{all diagrams consisting of a white 1-circle labelled } \mathbf{r}\text{, at least one black } z^*\text{-circle and } f\text{-bonds}] \tag{3.8.4}$$

The diagrams in (3.8.4) fall into two classes: those in which the articulation circle is a white circle and those in which it is not and are therefore star-irreducible. The first of these classes is just the set of all diagrams that can be expressed as star products of diagrams in the second class. Use of Lemma 1 therefore eliminates the diagrams with white articulation circles to give an expansion of $\ln[\rho^{(1)}(\mathbf{r})/z^*(\mathbf{r})]$ which, from (3.5.3), is equal to $c^{(1)}(\mathbf{r})$:

$$c^{(1)}(\mathbf{r}) = [\text{all diagrams consisting of a white 1-circle labelled } \mathbf{r}\text{, at least one black } z^*\text{-circle and } f\text{-bonds, such that the white circle is not an articulation circle}] \tag{3.8.5}$$

The diagrams in (3.8.5) are all star-irreducible, but some contain black articulation circles. To eliminate the latter, we proceed as follows. For each diagram Γ in (3.8.5) we identify a maximal, irreducible subdiagram Γ_{m} that contains the single white circle.

Illustration.

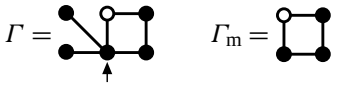

In the example shown there is one articulation circle (marked by an arrow) and there are two maximal, irreducible subdiagrams, one of which contains the white circle. It is easily proved[15] that for each Γ there is a unique choice of Γ_{m}; if Γ itself is irreducible, Γ and Γ_{m} are the same. The set $\{\Gamma_{\mathrm{m}}\}$ is a subset of the diagrams in (3.8.5). Given any Γ_{m}, the diagram from which it derives can be reconstructed by decorating the black circles with diagrams

taken from the set defined in (3.8.4). Lemma 4 can therefore be used in a topological reduction whereby the z^*-circles in (3.8.5) are replaced by $\rho^{(1)}$-circles and diagrams with black articulation circles disappear. Thus

$c^{(1)}(\mathbf{r}) =$ [all irreducible diagrams consisting of one white 1-circle labelled $\mathbf{r}$, at least one black $\rho^{(1)}$-circle and f-bonds]

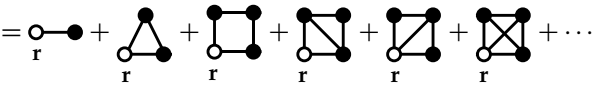

(3.8.6)

The final step is to exploit the definition (3.5.2) of the two-particle direct correlation function as a functional derivative by applying Lemma 2 to the series (3.8.6). The diagrams in (3.8.6) are irreducible; since they contain only one white circle this is equivalent to saying that they are free of connecting circles. Clearly they remain free of connecting circles when a second black circle is whitened as a result of the functional differentiation. It follows that $c^{(2)}(\mathbf{r}, \mathbf{r}')$ can be expressed diagrammatically as

$c^{(2)}(\mathbf{r}, \mathbf{r}') =$ [all diagrams consisting of two white 1-circles labelled $\mathbf{r}$ and $\mathbf{r}'$, black $\rho^{(1)}$-circles and f-bonds, and which are free of connecting circles]

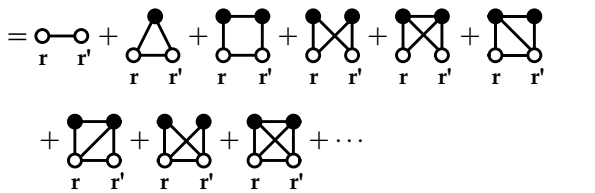

(3.8.7)

When there is no external field, (3.8.7) becomes an expansion of $c(r)$ in powers of the number density.[16]

The form of (3.8.7) suggests that the range of the direct correlation function should be roughly the range of the pair potential, as anticipated in Section 3.5. To lowest order in ρ, $c(r) \approx f(r)$ or, at large r, $c(r) \approx -\beta v(r)$. Since all higher-order diagrams in (3.8.7) are at least doubly connected, the contributions they make to $c(r)$ decay at least as fast as $[f(r)]^2$, and are therefore negligible in comparison with the leading term in the limit $r \to \infty$. However, the effects of indirect correlations are such that $h(r)$ can be significantly different from zero even for distances at which the potential is very weak. The contrast in behaviour between $c(r)$ and $h(r)$ is particularly evident close to the critical point. As the critical point is approached the compressibility χ_T becomes very large. It follows from (3.5.14) that $\hat{h}(k)$, the Fourier transform of $h(r)$, acquires a strong peak at the origin, eventually diverging as $T \to T_c$, which implies that $h(r)$ becomes very long ranged. On the other hand, (3.5.15) shows that

$$\rho\hat{c}(0) = 1 - \beta/\rho\chi_T \tag{3.8.8}$$

Close to the critical point, $\rho\hat{c}(0) \approx 1$; $c(r)$ therefore remains short ranged.

The argument concerning the relative ranges of $h(r)$ and $c(r)$ does not apply to ionic fluids. The effect of screening in ionic systems is to cause $h(r)$ to decay exponentially at large r, whereas $c(r)$ still has the range of the potential and therefore decays as r^{-1}. In this situation $c(r)$ is of longer range than $h(r)$.

3.9 VIRIAL EXPANSION OF THE EQUATION OF STATE

The derivation of the series expansion of $c^{(1)}(\mathbf{r})$ yields as a valuable by-product the *virial expansion* of the equation of state of a homogeneous fluid. If there is no external field, $c^{(1)}$ can be replaced by $-\beta\mu^{\text{ex}}$ and $\rho^{(1)}$ by ρ. Equation (3.8.6) then becomes

$$\beta\mu = \beta\mu^{\text{id}} - \sum_{i=1}^{\infty} \beta_i \rho^i \tag{3.9.1}$$

where the coefficients β_i are the irreducible "cluster integrals"; $\beta_i\rho^i$ is the sum of all diagrams in (3.8.6) that contain precisely i black circles but with $\rho^{(1)}$ replaced by ρ. The first two coefficients are

$$\beta_1 = \int f(0,1)\,\mathrm{d}1 \tag{3.9.2}$$

$$\beta_2 = \tfrac{1}{2}\iint f(0,1)\,f(0,2)\,f(1,2)\,\mathrm{d}1\,\mathrm{d}2 \tag{3.9.3}$$

where, in each case, the white circle is labelled 0. Substitution of (3.9.1) in (2.4.21) and integration with respect to ρ gives

$$\beta P = \rho - \sum_{i=1}^{\infty} \frac{i}{i+1}\beta_i \rho^{i+1} \tag{3.9.4}$$

If the *virial coefficients* are defined as $B_1 = 1$,

$$B_{i+1} = -\frac{i}{i+1}\beta_i, \quad i \geqslant 1 \tag{3.9.5}$$

we recover the virial expansion in its standard form:

$$\frac{\beta P}{\rho} = 1 + \sum_{i=2}^{\infty} B_i(T)\rho^{i-1} \tag{3.9.6}$$

The coefficients B_2 and B_3 are given by

$$B_2 = -\tfrac{1}{2}\beta_1 = -\tfrac{1}{2}\int f(r)\,\mathrm{d}\mathbf{r} \tag{3.9.7}$$

$$B_3 = -\tfrac{2}{3}\beta_2 = -\tfrac{1}{3}\iint f(r)\,f(r')\,f\left(|\mathbf{r}-\mathbf{r}'|\right)\mathrm{d}\mathbf{r}\,\mathrm{d}\mathbf{r}' \tag{3.9.8}$$

where the coordinates of the white circle have been taken as origin.

The expression for the second virial coefficient is more easily obtained by inserting in the virial equation (2.5.22) the low-density limit of $g(r)$ given by (2.6.10). Then

$$\frac{\beta P}{\rho} \approx 1 - \frac{2\pi\beta\rho}{3}\int_0^\infty v'(r)e(r)r^3\,\mathrm{d}r \tag{3.9.9}$$

If the pair potential decays faster than r^{-3} at large r, (3.9.9) can be integrated by parts to give

$$\frac{\beta P}{\rho} \approx 1 - 2\pi\rho\int_0^\infty f(r)r^2\,\mathrm{d}r \tag{3.9.10}$$

in agreement with (3.9.7). Measurements of the deviation of the equation of state of dilute gases from the ideal-gas law allow the second virial coefficient to be determined experimentally as a function of temperature. Such measurements are an important source of information on the nature of the force law between atoms or small molecules.

It is clear from the definition of the virial coefficients that the number of diagrams that contribute to the ith coefficient grows rapidly with i, while the associated integrals become increasingly more complicated. For example, the numbers of diagrams entering the expressions for B_3, B_4, B_5 and B_6 are, respectively, 1, 3, 10, 56 and 468, and the dimensions of the integrals increase each time by three. Not surprisingly, therefore, explicit calculations have been confined to the low-order coefficients. For hard spheres, B_2, B_3 and B_4 are known analytically, and B_5 to B_8 have been evaluated numerically. If we define the *packing fraction*, η, as

$$\eta = \frac{\pi\rho d^3}{6} \tag{3.9.11}$$

the virial expansion for hard spheres can be rewritten as

$$\frac{\beta P}{\rho} = 1 + \sum_{i=1}^{\infty}\mathcal{B}_i\eta^i \tag{3.9.12}$$

with

$$\mathcal{B}_i = \left(\frac{6}{\pi d^3}\right)^i B_{i+1} \tag{3.9.13}$$

The eight-term series, based on tabulated values[17] of the coefficients $\mathcal{B}_i$, is now

$$\frac{\beta P}{\rho} = 1 + 4\eta + 10\eta^2 + 18.365\eta^3 + 28.225\eta^4 + 39.74\eta^5 + 53.5\eta^6 + 70.8\eta^7 + \cdots \tag{3.9.14}$$

Figure 3.3 shows that the pressures calculated from the truncated, eight-term series are in good agreement with the results of computer simulations at all densities up to the fluid–solid transition at $\eta \approx 0.49$.

Guided by the form of (3.9.14), Carnahan and Starling[18] were able to construct a simple but very accurate hard-sphere equation of state. Noting that $\mathcal{B}_1$ and $\mathcal{B}_2$ are both integers, they chose to replace $\mathcal{B}_3$ by the nearest integer, 18, and supposed that $\mathcal{B}_i$ for all i is given by

$$\mathcal{B}_i = a_1 i^2 + a_2 i + a_3 \tag{3.9.15}$$

With $\mathcal{B}_1 = 4$, $\mathcal{B}_2 = 10$ and $\mathcal{B}_3 = 18$, the solution to (3.9.15) is $a_1 = 1, a_2 = 3$ and $a_3 = 0$. The formula then predicts that $\mathcal{B}_4 = 28$, $\mathcal{B}_5 = 40$, $\mathcal{B}_6 = 54$ and $\mathcal{B}_7 = 70$, in close agreement with the coefficients in (3.9.14). The expression

$$\frac{\beta P}{\rho} = 1 + \sum_{i=1}^{\infty} (i^2 + 3i)\eta^i \tag{3.9.16}$$

may be written as a linear combination of the first and second derivatives of the geometric series $\sum_i \eta^i$. It can therefore be summed explicitly to give

$$\frac{\beta P}{\rho} = \frac{1 + \eta + \eta^2 - \eta^3}{(1 - \eta)^3} \tag{3.9.17}$$

Equation (3.9.17) provides an excellent fit to the results of computer simulations over the entire fluid range; the largest discrepancies are of the order of 1%. Other equations of state

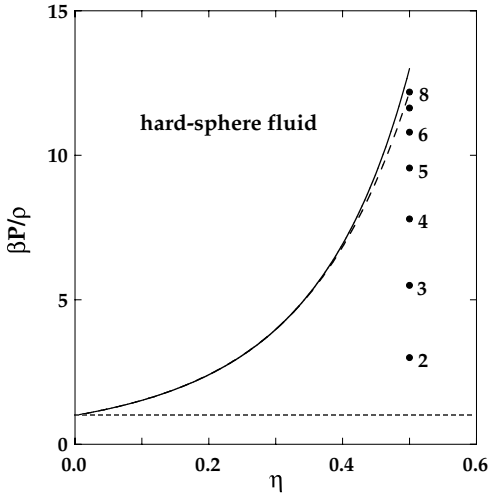

FIG. 3.3. Equation of state of hard spheres calculated from the virial series (3.9.14). The points are the values obtained for η = 0.50 when different numbers of virial coefficients are included and the full curve shows the nearly exact results given by (3.9.17).

have been devised,[19] but the simple form of the Carnahan–Starling equation makes it very convenient for use in thermodynamic calculations.[20] In particular, a closed expression for the excess Helmholtz free energy is obtained by combining (3.9.17) with the second of the thermodynamic relations (2.3.8):

$$\frac{\beta F^{\mathrm{ex}}}{N} = \int_0^{\eta} \left(\frac{\beta P}{\rho} - 1 \right) \frac{\mathrm{d}\eta'}{\eta'} = \frac{\eta(4-3\eta)}{(1-\eta)^2} \tag{3.9.18}$$

The Carnahan–Starling equation of state is widely used in perturbation theories of the type discussed in Chapter 5.

NOTES AND REFERENCES

1. Our treatment draws freely on the classic review article by Evans, R., *Adv. Phys.* **28**, 143 (1979). See also Evans, R., *In* "Fundamentals of Inhomogeneous Fluids" (D. Henderson, ed.). Marcel Decker, New York, 1991.
2. See Section 3.4. The principle was established for the ground state of the electron gas by Hohenberg, P. and Kohn, W., *Phys. Rev.* **136**, B864 (1964) and extended to finite temperatures by Mermin, N.D., *Phys. Rev.* **137**, A1441 (1964). It was first applied to classical systems by Ebner, C., Saam, W.F. and Stroud, D., *Phys. Rev. A* **14**, 226 (1976).
3. There may also be a contribution from an external source such as an electric or gravitational field.
4. See, e.g., Chandler, D., "Modern Statistical Mechanics". Oxford University Press, New York, 1987, p. 16.
5. Widom, B., *J. Stat. Phys.* **19**, 563 (1978). See also Widom, B., *J. Phys. Chem.* **86**, 869 (1982).
6. Llano-Restrepo, M. and Chapman, W.G., *J. Chem. Phys.* **97**, 2046 (1992).
7. See Chapter 5, Section 5.5.
8. Greenfield, A.J., Wellendorf, J. and Wiser, N., *Phys. Rev. A* **4**, 1607 (1971).
9. Hansen, J.P. and Schiff, D., *Mol. Phys.* **25**, 1281 (1973).
10. Kirkwood, J.G. and Buff, F.P., *J. Chem. Phys.* **19**, 774 (1951).
11. (a) Buff, F.P. and Stillinger, F.H., *J. Chem. Phys.* **25**, 312 (1956). (b) Stillinger, F.H. and Buff, F.P., *J. Chem. Phys.* **37**, 1 (1962).
12. Morita, T. and Hiroike, K., *Prog. Theor. Phys.* **25**, 537 (1961).
13. (a) de Dominicis, C., *J. Math. Phys.* **3**, 983 (1962). (b) de Dominicis, C., *J. Math. Phys.* **4**, 255 (1963).
14. Stell, G., *In* "The Equilibrium Theory of Classical Fluids" (H.L. Frisch and J.L. Lebowitz, eds). W.A. Benjamin, New York, 1964.
15. See also McDonald, I.R. and O'Gorman, S.P., *Phys. Chem. Liq.* **8**, 57 (1978).
16. This result was first obtained by Rushbrooke, G.S. and Scoins, H.I., *Proc. Roy. Soc. A* **216**, 203 (1953).
17. van Rensburg, E.J.J., *J. Phys. A* **26**, 4805 (1993). See also Vlasov, A.Y., You, X.M. and Masters, A.J., *Mol. Phys.* **100**, 3313 (2002).
18. Carnahan, N.F. and Starling, K.E., *J. Chem. Phys.* **51**, 635 (1969).
19. For a listing of many of the proposed equations and an assessment of their relative merits, see Mulero, A., Faúndez, C.A. and Cuadros, F., *Mol. Phys.* **97**, 453 (1999).
20. The Carnahan–Starling equation of state was later generalised to hard-sphere mixtures by Mansoori, G.A., Carnahan, N.F., Starling, K.E. and Leland, T.W., *J. Chem. Phys.* **54**, 1523 (1971).

CHAPTER 4

Distribution-function Theories

The greater part of this chapter is devoted to a description of the more important theoretical methods available for calculation of the pair distribution function of a uniform fluid. If the pair distribution function is known, thermodynamic properties of the system can be obtained by a number of different routes. We begin, however, by describing the way in which the distribution function is measured in radiation-scattering experiments.

4.1 THE STATIC STRUCTURE FACTOR

The structure factor of a uniform fluid was defined in Section 3.6 in terms of the Fourier transform of the pair correlation function, $h(r)$. It can be defined more generally as

$$S(\mathbf{k}) = \left\langle \frac{1}{N} \rho_{\mathbf{k}} \rho_{-\mathbf{k}} \right\rangle \tag{4.1.1}$$

where $\rho_{\mathbf{k}}$ is a Fourier component of the microscopic density (3.1.2):

$$\rho_{\mathbf{k}} = \int \rho(\mathbf{r}) \exp(-i\mathbf{k}\cdot\mathbf{r})\, \mathrm{d}\mathbf{r} = \sum_{i=1}^{N} \exp(-i\mathbf{k}\cdot\mathbf{r}_i) \tag{4.1.2}$$

Given the δ-function representation of the pair density in (2.5.13), the definition (4.1.1) implies that in the homogeneous case:

$$\begin{aligned} S(\mathbf{k}) &= \left\langle \frac{1}{N} \sum_{i=1}^{N} \sum_{j=1}^{N} \exp(-i\mathbf{k}\cdot\mathbf{r}_i) \exp(i\mathbf{k}.\mathbf{r}_j) \right\rangle \\ &= 1 + \left\langle \frac{1}{N} \sum_{i=1}^{N} \sum_{j\neq i}^{N} \exp\bigl[-i\mathbf{k}\cdot(\mathbf{r}_i - \mathbf{r}_j)\bigr] \right\rangle \\ &= 1 + \left\langle \frac{1}{N} \sum_{i=1}^{N} \sum_{j\neq i}^{N} \iint \exp\bigl[-i\mathbf{k}\cdot(\mathbf{r}-\mathbf{r}')\bigr] \delta(\mathbf{r}-\mathbf{r}_i)\delta(\mathbf{r}'-\mathbf{r}_j)\, \mathrm{d}\mathbf{r}\, \mathrm{d}\mathbf{r}' \right\rangle \end{aligned}$$

$$= 1 + \frac{1}{N} \iint \exp\bigl[-i\mathbf{k} \cdot (\mathbf{r} - \mathbf{r}')\bigr] \rho_N^{(2)}(\mathbf{r} - \mathbf{r}')\, \mathrm{d}\mathbf{r}\, \mathrm{d}\mathbf{r}'$$

$$= 1 + \rho \int g(r) \exp(-i\mathbf{k} \cdot \mathbf{r})\, \mathrm{d}\mathbf{r} \tag{4.1.3}$$

In the last step we have used the definition (2.5.8) of the pair distribution function and exploited the fact that the system is translationally invariant in order to integrate over $\mathbf{r}'$. Conversely, $g(r)$ is given by the inverse transform

$$\rho g(\mathbf{r}) = (2\pi)^{-3} \int \bigl[S(\mathbf{k}) - 1\bigr] \exp(i\mathbf{k} \cdot \mathbf{r})\, \mathrm{d}\mathbf{k} \tag{4.1.4}$$

The final result in (4.1.3) can also be written as

$$S(\mathbf{k}) = 1 + (2\pi)^3 \rho \delta(\mathbf{k}) + \rho \hat{h}(\mathbf{k}) \tag{4.1.5}$$

The definitions (3.6.10) and (4.1.1) are therefore equivalent apart from a δ-function term, which henceforth we shall ignore. Experimentally (see below) the term corresponds to radiation that passes through the sample unscattered.

The structure factor of a fluid can be determined experimentally from measurements of the cross-section for scattering of neutrons or x-rays by the fluid as a function of scattering angle. Below we give a simplified treatment of the calculation of the neutron cross-section in terms of $S(\mathbf{k})$.

Let us suppose that an incident neutron is scattered by the sample through an angle θ. The incoming neutron can be represented as a plane wave:

$$\psi_1(\mathbf{r}) = \exp(i\mathbf{k}_1 \cdot \mathbf{r}) \tag{4.1.6}$$

while at sufficiently large distances from the sample the scattered neutron can be represented as a spherical wave:

$$\psi_2(\mathbf{r}) \sim \frac{\exp(ik_2 r)}{r} \tag{4.1.7}$$

Thus, asymptotically ($r \to \infty$), the wavefunction of the neutron behaves as

$$\psi(\mathbf{r}) \sim \exp(i\mathbf{k}_1 \cdot \mathbf{r}) + f(\theta) \frac{\exp(ik_2 r)}{r} \tag{4.1.8}$$

and the amplitude $f(\theta)$ of the scattered component is related to the differential cross-section $\mathrm{d}\sigma/\mathrm{d}\Omega$ for scattering into a solid angle $\mathrm{d}\Omega$ in the direction θ, ϕ by

$$\frac{\mathrm{d}\sigma}{\mathrm{d}\Omega} = \bigl|f(\theta)\bigr|^2 \tag{4.1.9}$$

The geometry of a scattering event is illustrated in Figure 4.1. The momentum transferred from neutron to sample in units of $\hbar$ is

$$\mathbf{k} = \mathbf{k}_1 - \mathbf{k}_2 \tag{4.1.10}$$

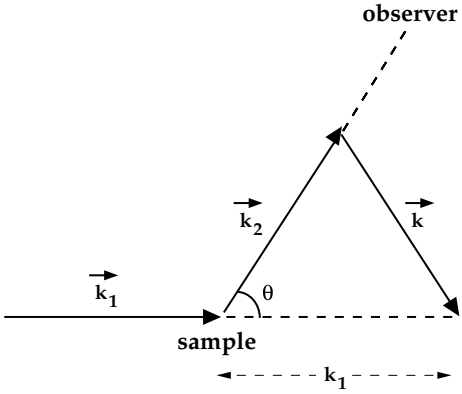

FIG. 4.1. Geometry of an elastic scattering event.

To simplify the calculation we assume that the scattering is elastic. Then $|\mathbf{k}_1| = |\mathbf{k}_2|$ and

$$k = 2k_1 \sin \tfrac{1}{2}\theta = \frac{4\pi}{\lambda} \sin \tfrac{1}{2}\theta \tag{4.1.11}$$

where λ is the neutron wavelength.

The scattering of the neutron occurs as the result of interactions with the atomic nuclei. These interactions are very short ranged, and the total scattering potential $\mathcal{V}(\mathbf{r})$ may therefore be approximated by a sum of δ-function pseudopotentials in the form

$$\mathcal{V}(\mathbf{r}) = \frac{2\pi\hbar^2}{m} \sum_{i=1}^{N} b_i \delta(\mathbf{r} - \mathbf{r}_i) \tag{4.1.12}$$

where b_i is the *scattering length* of the ith nucleus. For most nuclei, b_i is positive, but it may also be negative and even complex; it varies both with isotopic species and with the spin state of the nucleus.

The wavefunction $\psi(\mathbf{r})$ must be a solution of the Schrödinger equation:

$$\left(-\frac{\hbar^2}{2m}\nabla^2 + \mathcal{V}(\mathbf{r})\right)\psi(\mathbf{r}) = E\psi(\mathbf{r}) \tag{4.1.13}$$

The general solution having the correct asymptotic behaviour is

$$\psi(\mathbf{r}) = \exp(i\mathbf{k}_1 \cdot \mathbf{r}) - \frac{m}{2\pi\hbar^2} \int \frac{\exp(ik_1|\mathbf{r} - \mathbf{r}'|)}{|\mathbf{r} - \mathbf{r}'|} \mathcal{V}(\mathbf{r}')\psi(\mathbf{r}')\, \mathrm{d}\mathbf{r}' \tag{4.1.14}$$

The second term on the right-hand side represents a superposition of spherical waves emanating from each point in the sample.

Equation (4.1.14) is an integral equation for $\psi(\mathbf{r})$. The solution in the case when the interaction $\mathcal{V}(\mathbf{r})$ is weak is obtained by setting $\psi(\mathbf{r}) \approx \exp(i\mathbf{k}_1 \cdot \mathbf{r})$ inside the integral sign.

This substitution yields the so-called first Born approximation to $\psi(\mathbf{r})$:

$$\psi(\mathbf{r}) \approx \exp(i\mathbf{k}_1 \cdot \mathbf{r}) - \frac{m}{2\pi\hbar^2} \int \frac{\exp(ik_1|\mathbf{r}-\mathbf{r}'|)}{|\mathbf{r}-\mathbf{r}'|} \mathcal{V}(\mathbf{r}') \exp(i\mathbf{k}_1 \cdot \mathbf{r}')\, \mathrm{d}\mathbf{r}' \tag{4.1.15}$$

We can now obtain an expression for $f(\theta)$ by taking the $r \to \infty$ limit of (4.1.15) and matching the result to the known, asymptotic form of $\psi(\mathbf{r})$ given by (4.1.8). If $|\mathbf{r}| \gg |\mathbf{r}'|$, then

$$|\mathbf{r}-\mathbf{r}'| = \left(r^2 + r'^2 - 2\mathbf{r}\cdot\mathbf{r}'\right)^{1/2} \approx r - \hat{\mathbf{r}}\cdot\mathbf{r}' \tag{4.1.16}$$

where $\hat{\mathbf{r}}$ is a unit vector in the direction of $\mathbf{r}$. Since we have assumed that the scattering is elastic, $k_1\hat{\mathbf{r}} = \mathbf{k}_2$. Thus, as $r \to \infty$:

$$\psi(\mathbf{r}) \sim \exp(i\mathbf{k}_1 \cdot \mathbf{r}) - \frac{\exp(ik_1 r)}{r} \frac{m}{2\pi\hbar^2} \int \exp(-i\mathbf{k}_2 \cdot \mathbf{r}') \mathcal{V}(\mathbf{r}') \exp(i\mathbf{k}_1 \cdot \mathbf{r}')\, \mathrm{d}\mathbf{r}' \tag{4.1.17}$$

By comparing (4.1.17) with (4.1.8), and remembering that $k_1 = k_2$, we find that

$$\begin{aligned} f(\theta) &= -\frac{m}{2\pi\hbar^2} \int \exp(-i\mathbf{k}_2 \cdot \mathbf{r}) \mathcal{V}(\mathbf{r}) \exp(i\mathbf{k}_1 \cdot \mathbf{r})\, \mathrm{d}\mathbf{r} \\ &= -\frac{m}{2\pi\hbar^2} \int \mathcal{V}(\mathbf{r}) \exp(i\mathbf{k} \cdot \mathbf{r})\, \mathrm{d}\mathbf{r} \end{aligned} \tag{4.1.18}$$

Hence the amplitude of the scattered component is proportional to the Fourier transform of the scattering potential. The first line of (4.1.18) also shows that $f(\theta)$ is expressible as a matrix element of the interaction $\mathcal{V}(\mathbf{r})$ between initial and final plane-wave states of the neutron. Use of the first Born approximation is therefore equivalent to calculating the cross-section $\mathrm{d}\sigma/\mathrm{d}\Omega$ by the "golden rule" of quantum mechanical perturbation theory.

An expression for $\mathrm{d}\sigma/\mathrm{d}\Omega$ can now be derived by substituting for $\mathcal{V}(\mathbf{r})$ in (4.1.18), inserting the result in (4.1.9) and taking the thermal average. This yields the expression

$$\begin{aligned} \frac{\mathrm{d}\sigma}{\mathrm{d}\Omega} &= \left\langle \left| \sum_{i=1}^{N} b_i \exp(-i\mathbf{k} \cdot \mathbf{r}_i) \right|^2 \right\rangle \\ &= \left\langle \sum_{i=1}^{N} \sum_{j=1}^{N} b_i b_j \exp\left[-i\mathbf{k} \cdot (\mathbf{r}_j - \mathbf{r}_i)\right] \right\rangle \end{aligned} \tag{4.1.19}$$

A more useful result is obtained by taking an average of the scattering lengths over isotopes and nuclear spin states, which can be done independently of the thermal averaging over coordinates. We therefore introduce the notation

$$\begin{aligned} &\left\langle b_i^2 \right\rangle \equiv \left\langle b^2 \right\rangle, \qquad \langle b_i b_j \rangle = \langle b_i \rangle \langle b_j \rangle \equiv \langle b \rangle^2 \\ &\langle b \rangle^2 \equiv b_{\mathrm{coh}}^2, \qquad \left(\left\langle b^2 \right\rangle - \langle b \rangle^2 \right) \equiv b_{\mathrm{inc}}^2 \end{aligned} \tag{4.1.20}$$

and rewrite (4.1.19) as

$$\begin{aligned}\frac{\mathrm{d}\sigma}{\mathrm{d}\Omega} &= N\langle b^2\rangle + \langle b\rangle^2\left\langle \sum_{i=1}^{N}\sum_{j\neq i}^{N}\exp\left[-i\mathbf{k}\cdot(\mathbf{r}_j-\mathbf{r}_i)\right]\right\rangle \\ &= N\left(\langle b^2\rangle - \langle b\rangle^2\right) + \langle b\rangle^2\left\langle \left|\sum_{i=1}^{N}\exp(-i\mathbf{k}\cdot\mathbf{r}_i)\right|^2\right\rangle \\ &= Nb_{\mathrm{inc}}^2 + Nb_{\mathrm{coh}}^2 S(\mathbf{k}) \qquad (4.1.21)\end{aligned}$$

The subscripts "coh" and "inc" refer, respectively, to *coherent* and *incoherent* scattering. Information about the structure of the fluid is contained entirely within the coherent contribution to the cross-section; there is no incoherent contribution if the sample consists of a single isotopic species of zero nuclear spin. The amplitude of the wave scattered by a single, fixed nucleus is

$$f(\theta) = -b\int \delta(\mathbf{r})\exp(i\mathbf{k}\cdot\mathbf{r})\,\mathrm{d}\mathbf{r} = -b \qquad (4.1.22)$$

In the absence of incoherent scattering the cross-section for scattering by a liquid is

$$\frac{\mathrm{d}\sigma}{\mathrm{d}\Omega} = Nb^2 S(\mathbf{k}) \qquad (4.1.23)$$

where Nb^2 is the cross-section for a system of N independent nuclei and $S(\mathbf{k})$ represents the effects of spatial correlations.

A similar calculation can be made of the cross-section for elastic scattering of x-rays. There is now no separation into coherent and incoherent parts, but the expression for the differential cross-section has the same general form as in (4.1.23). One important difference is that x-rays are scattered by interaction with the atomic electrons and the analogue of the neutron scattering length is the atomic *form factor*, $f(\mathbf{k})$. The latter, unlike b, is a function of $\mathbf{k}$ and defined as

$$f(\mathbf{k}) = \left\langle \sum_{n=1}^{Z}\exp\left[i\mathbf{k}\cdot\left(\mathbf{r}_i^{(n)}-\mathbf{r}_i\right)\right]\right\rangle_{\mathrm{Q}} \qquad (4.1.24)$$

where the subscript Q denotes a quantum mechanical expectation value, $\mathbf{r}_i^{(n)}$ represents the coordinates of the nth electron of the ith atom (with nuclear coordinates $\mathbf{r}_i$) and Z is the atomic number; for large atoms, $f(\mathbf{k}) \approx Z$ over the range of $\mathbf{k}$ in which $S(\mathbf{k})$ displays a significant degree of structure.

The pair distribution function is derived from a measured structure factor, such as that pictured in Figure 3.2, by numerically transforming the experimental data according to (4.1.4). Difficulties arise in practise because measurements of $S(\mathbf{k})$ necessarily introduce a cut-off at large values of k. These difficulties are the source of the unphysical ripples seen at small r in the distribution function for liquid argon shown in Figure 2.1.

The definition of the structure factor given by (4.1.1) is easily extended to systems of more than one component. As in Section 3.6, we consider an n-component system in which the number concentration of species ν is x_ν. The microscopic partial density $\rho^\nu(\mathbf{r})$ and its Fourier components $\rho^\nu_{\mathbf{k}}$ are defined in a manner analogous to (3.1.2) and (4.1.2), except that the sums run only over the particles of species ν. Thus

$$\rho^\nu_{\mathbf{k}} = \sum_{i=1}^{N_\nu} \exp(-i\mathbf{k}\cdot\mathbf{r}_i) \tag{4.1.25}$$

If the fluid is homogeneous, the partial pair distribution function

$$g_{\nu\mu}(\mathbf{r}) = h_{\nu\mu}(\mathbf{r}) + 1 \tag{4.1.26}$$

has a δ-function representation given by

$$x_\nu x_\mu \rho g_{\nu\mu}(\mathbf{r}) = \left\langle \frac{1}{N} \sum_{i=1}^{N_\nu} \sum_{j=1}^{N_\mu}{}' \delta(\mathbf{r} + \mathbf{r}_j - \mathbf{r}_i) \right\rangle \tag{4.1.27}$$

The partial structure factor defined by a generalisation of (4.1.1) as

$$S_{\nu\mu}(\mathbf{k}) = \left\langle \frac{1}{N} \rho^\nu_{\mathbf{k}} \rho^\mu_{-\mathbf{k}} \right\rangle \tag{4.1.28}$$

is related to $g_{\nu\mu}(r)$ by

$$S_{\nu\mu}(\mathbf{k}) = x_\nu \delta_{\nu\mu} + x_\nu x_\mu \rho \int g_{\nu\mu}(r) \exp(-i\mathbf{k}\cdot\mathbf{r})\, \mathrm{d}\mathbf{r} \tag{4.1.29}$$

which again differs from the earlier definition (3.6.15) by an unimportant δ-function term.

4.2 THE YBG HIERARCHY AND THE BORN–GREEN EQUATION

It was shown in Section 2.1 that the non-equilibrium phase-space distribution functions $f^{(n)}(\mathbf{r}^n, \mathbf{p}^n; t)$ are coupled together by a set of equations called the BBGKY hierarchy. A similar hierarchy exists for the equilibrium particle densities, assuming again that the forces between particles are pairwise additive; this is generally known as the Yvon–Born–Green or YBG hierarchy.

Consider first the case when $n = 1$. At equilibrium (2.1.20) becomes

$$\left(\frac{\mathbf{p}_1}{m} . \frac{\partial}{\partial \mathbf{r}_1} + \mathbf{X}_1 . \frac{\partial}{\partial \mathbf{p}_1} \right) f_0^{(1)}(\mathbf{r}_1, \mathbf{p}_1)$$
$$= -\iint \mathbf{F}_{12} . \frac{\partial}{\partial \mathbf{p}_1} f_0^{(2)}(\mathbf{r}_1, \mathbf{p}_1, \mathbf{r}_2, \mathbf{p}_2)\, \mathrm{d}\mathbf{r}_2\, \mathrm{d}\mathbf{p}_2 \tag{4.2.1}$$

where, from the expression for $f_0^{(n)}$ given by (2.5.1) with the subscript N omitted:

$$f_0^{(1)}(\mathbf{r}_1, \mathbf{p}_1) = \rho^{(1)}(\mathbf{r}_1) f_{\mathrm{M}}(\mathbf{p}_1) \tag{4.2.2}$$

$$f_0^{(2)}(\mathbf{r}_1, \mathbf{p}_1, \mathbf{r}_2, \mathbf{p}_2) = \rho^{(2)}(\mathbf{r}_1, \mathbf{r}_2) f_{\mathrm{M}}(\mathbf{p}_1) f_{\mathrm{M}}(\mathbf{p}_2) \tag{4.2.3}$$

On inserting (4.2.2) and (4.2.3) into (4.2.1), exploiting the normalisation (2.1.27) and the fact that $(\partial/\partial\mathbf{p}) f_{\mathrm{M}}(\mathbf{p}) = -(\beta/m)\mathbf{p} f_{\mathrm{M}}(\mathbf{p})$, and finally dividing through by $(\beta/m) f_{\mathrm{M}}(\mathbf{p}_1)$, we obtain a relation between the single-particle ($n = 1$) and pair ($n = 2$) densities:

$$(k_{\mathrm{B}}T\mathbf{p}_1 \cdot \boldsymbol{\nabla}_1 - \mathbf{p}_1 \cdot \mathbf{X}_1)\rho^{(1)}(\mathbf{r}_1) = \int (\mathbf{p}_1 \cdot \mathbf{F}_{12})\rho^{(2)}(\mathbf{r}_1, \mathbf{r}_2)\, \mathrm{d}\mathbf{r}_2 \tag{4.2.4}$$

Equation (4.2.4) may be cast in the form $\mathbf{p}_i \cdot \mathbf{Q} = 0$ where $i = 1$, but because this result would be true for any choice of $\mathbf{p}_i$ it follows that $\mathbf{Q} = 0$. Thus, replacing the forces $\mathbf{X}_1$ and $\mathbf{F}_{12}$ in (4.2.4) by the negative gradients of the external potential $\phi(\mathbf{r}_1)$ and interparticle potential $v(\mathbf{r}_1, \mathbf{r}_2)$, respectively, and dividing through by $\rho^{(1)}(\mathbf{r}_1)$, we find that

$$-k_{\mathrm{B}}T\boldsymbol{\nabla}_1 \ln \rho^{(1)}(\mathbf{r}_1) = \boldsymbol{\nabla}_1\phi(\mathbf{r}_1) + \int \boldsymbol{\nabla}_1 v(\mathbf{r}_1, \mathbf{r}_2)\rho^{(1)}(\mathbf{r}_2) g^{(2)}(\mathbf{r}_1, \mathbf{r}_2)\, \mathrm{d}\mathbf{r}_2 \tag{4.2.5}$$

This expression provides a possible starting point for the calculation of the density profile of a fluid in an external field, while if there are no interactions between particles it reduces to the usual barometric law, $\rho^{(1)}(\mathbf{r}) \propto \exp[-\beta\phi(\mathbf{r})]$.

Similar manipulations for the case when $n = 2$ yield a relationship between the pair and triplet distribution functions which, in the absence of an external field, takes the form

$$\begin{aligned} &-k_{\mathrm{B}}T\boldsymbol{\nabla}_1 \ln g^{(2)}(\mathbf{r}_1, \mathbf{r}_2) \\ &\quad = \boldsymbol{\nabla}_1 v(\mathbf{r}_1, \mathbf{r}_2) + \rho \int \boldsymbol{\nabla}_1 v(\mathbf{r}_1, \mathbf{r}_3)\left(\frac{g^{(3)}(\mathbf{r}_1, \mathbf{r}_2, \mathbf{r}_3)}{g^{(2)}(\mathbf{r}_1, \mathbf{r}_2)} - g^{(2)}(\mathbf{r}_1, \mathbf{r}_3) \right) \mathrm{d}\mathbf{r}_3 \end{aligned} \tag{4.2.6}$$

where on the right-hand side we have subtracted a term that vanishes in the isotropic case. We now eliminate the triplet distribution function by use of Kirkwood's *superposition approximation*,[1] i.e.

$$g^{(3)}(\mathbf{r}_1, \mathbf{r}_2, \mathbf{r}_3) \approx g^{(2)}(\mathbf{r}_1, \mathbf{r}_2) g^{(2)}(\mathbf{r}_2, \mathbf{r}_3) g^{(2)}(\mathbf{r}_1, \mathbf{r}_3) \tag{4.2.7}$$

which becomes exact in the limit $\rho \to 0$. When this approximation is introduced into (4.2.6) the result is a non-linear integro-differential equation for the pair distribution function in terms of the pair potential:

$$\begin{aligned} &-k_{\mathrm{B}}T\boldsymbol{\nabla}_1\big[\ln g(\mathbf{r}_1, \mathbf{r}_2) + \beta v(\mathbf{r}_1, \mathbf{r}_2)\big] \\ &\quad = \rho \int \boldsymbol{\nabla}_1 v(\mathbf{r}_1, \mathbf{r}_3) g(\mathbf{r}_1, \mathbf{r}_3)\big[g(\mathbf{r}_2, \mathbf{r}_3) - 1\big]\, \mathrm{d}\mathbf{r}_3 \end{aligned} \tag{4.2.8}$$

This is the Born–Green equation.[2] Given $v(r)$, (4.2.8) can be solved numerically to yield $g(r)$, from which in turn all thermodynamic properties can be derived via the energy, pressure and compressibility equations. The work of Born and Green represented one of the earliest attempts to determine the structure and thermodynamics of a classical fluid by following a well-defined statistical mechanical route, but the results obtained are satisfactory only at low densities.[3] As we shall see later, other approximate integral equations have subsequently been proposed that work well even at high densities.

By construction, the superposition approximation satisfies the so-called core condition for hard-core systems, meaning that $g^{(3)}(\mathbf{r}_1, \mathbf{r}_2, \mathbf{r}_3)$ vanishes when any of the interparticle distances r_{12}, r_{13} or r_{23} is less than the hard-core diameter. However, it violates the sum rule

$$g^{(2)}(\mathbf{r}_1, \mathbf{r}_2) = \frac{\rho}{N-2} \int g^{(3)}(\mathbf{r}_1, \mathbf{r}_2, \mathbf{r}_3)\, \mathrm{d}\mathbf{r}_3 \tag{4.2.9}$$

which follows directly from the definitions (2.5.3) and (2.5.9). An alternative to (4.2.7) is provided by the "convolution" approximation,[4] which has the merit of satisfying (4.2.9) exactly. The approximation is most easily expressed in **k**-space, where it takes the form

$$S^{(3)}(\mathbf{k}, \mathbf{k}') \equiv \left\langle \frac{1}{N} \rho_{\mathbf{k}} \rho_{\mathbf{k}'} \rho_{-\mathbf{k}-\mathbf{k}'} \right\rangle \approx S(k) S(k') S\big(|\mathbf{k} + \mathbf{k}'|\big) \tag{4.2.10}$$

The product of structure factors in (4.2.10) transforms in **r**-space into a convolution product of pair distribution functions, but this fails to satisfy the core condition and in practice is rarely used. The convolution approximation can be derived[5] by setting the triplet function $\hat{c}^{(3)}(\mathbf{k}, \mathbf{k}')$ equal to zero in the three-particle analogue of the Ornstein–Zernike relation (3.5.10).

4.3 FUNCTIONAL EXPANSIONS AND INTEGRAL EQUATIONS

A series of approximate integral equations for the pair distribution function of a uniform fluid in which the particles interact through pairwise-additive forces can be derived systematically by an elegant method due to Percus.[6] The basis of the method is the interpretation of the quantity $\rho g(r)$ as the single-particle density at a point **r** in the fluid when a particle of the system is known to be located at the origin, $\mathbf{r} = 0$. The particle at the origin, labelled 0, is assumed to be fixed in space, while the other particles move in the force field of particle 0. Then the total potential energy of the remaining particles in the "external" field due to particle 0 is of the form (3.1.3), with

$$\phi(i) = v(0, i) \tag{4.3.1}$$

Let $\Xi[\phi]$, as given by (3.1.8), be the grand partition function in the presence of the external field. In that expression, V_N is the total interatomic potential energy of particles $1, \ldots, N$.

Alternatively, we may treat the particle at the origin as an $(N+1)$th particle. Then

$$V_N + \sum_{i=1}^{N} \phi(i) = \sum_{i=1}^{N} \sum_{j>i}^{N} v(i,j) + \sum_{i=1}^{N} v(0,i) = V_{N+1} \tag{4.3.2}$$

If we denote the partition function in the absence of the field by Ξ_0, (3.1.8) may be rewritten as

$$\begin{aligned} \Xi[\phi] &= \sum_{N=0}^{\infty} \frac{z^N}{N!} \int \cdots \int \exp(-\beta V_{N+1})\, \mathrm{d}1 \cdots \mathrm{d}N \\ &= \frac{\Xi_0}{z} \sum_{N=0}^{\infty} \frac{1}{\Xi_0} \frac{z^{N+1}}{N!} \int \cdots \int \exp(-\beta V_{N+1})\, \mathrm{d}1 \cdots \mathrm{d}N \\ &= \frac{\Xi_0}{z} \sum_{N=1}^{\infty} \frac{1}{\Xi_0} \frac{z^N}{(N-1)!} \int \cdots \int \exp(-\beta V_N)\, \mathrm{d}1 \cdots \mathrm{d}(N-1) \end{aligned} \tag{4.3.3}$$

Equation (2.5.3) shows that the sum on N in (4.3.3) is the definition of the single-particle density in a homogeneous system. Thus

$$\Xi[\phi] = \frac{\rho \Xi_0}{z} \tag{4.3.4}$$

The physical content of this result is closely related to that of (2.4.30). By a similar manipulation, but starting from (3.1.9), it can be shown that the single-particle density in the presence of the external field is related to the two-particle density in the absence of the field by

$$\rho^{(1)}(1|\phi) = \frac{\rho^{(2)}(0,1|\phi=0)}{\rho} \tag{4.3.5}$$

Because the system is spatially uniform in the absence of the field, (2.6.7) and (4.3.5) together yield the relation

$$\rho^{(1)}(1|\phi) = \rho g(0,1) \tag{4.3.6}$$

which is the mathematical expression of Percus's idea. The effect of switching on the force field of particle 0 is to change the potential $\phi(1)$ from zero to $\Delta\phi = v(0,1)$; the response, measured by the change in the single-particle density, is

$$\Delta\rho^{(1)}(1) = \rho^{(1)}(1|\phi) - \rho^{(1)}(1|\phi=0) = \rho g(0,1) - \rho = \rho h(0,1) \tag{4.3.7}$$

If the field due to particle 0 is regarded as a perturbation, it is natural to consider functional Taylor expansions of various functionals of ϕ or $\rho^{(1)}$ with respect to $\Delta\phi$. One obvious choice is to expand $\Delta\rho^{(1)}$ itself in powers of $\Delta\phi$. The first-order result is simply the

Yvon equation (3.6.7), with the infinitesimal quantities $\delta\rho^{(1)}, \delta\phi$ replaced by $\Delta\rho^{(1)}, \Delta\phi$. On combining this expression with (4.3.1) and (4.3.7) we find that

$$h(0,1) = -\beta v(0,1) + \rho \int h(1,2)\big[-\beta v(0,2)\big]\,\mathrm{d}2 \tag{4.3.8}$$

Comparison with the Ornstein–Zernike relation (3.5.12) shows that in this approximation

$$c(0,1) \approx -\beta v(0,1) \tag{4.3.9}$$

When the potential is steeply repulsive at short range, (4.3.8) and (4.3.9) are very poor approximations, because $\Delta\rho^{(1)}$ is then a highly non-linear functional of ϕ. The approach is more successful in the case of the Coulomb potential; as we shall see in Section 4.5, (4.3.9) is equivalent to the Debye–Hückel approximation.

Better results are obtained for short-ranged potentials by expansion in powers of $\Delta\rho^{(1)}$. In combination with the Ornstein–Zernike relation, each choice of functional to be expanded yields a different integral equation for the pair distribution function. Here we consider the effect of expanding the intrinsic free energy. Equation (3.5.23) is an exact relation for $\mathcal{F}^{\mathrm{ex}}[\rho^{(1)}]$ relative to the free energy of a reference system at the same temperature and chemical potential. If we take the reference system to be a uniform fluid of density ρ_0 and chemical potential μ_0, the quantities $c_0^{(1)}$, $\mathcal{F}^{\mathrm{ex}}$ can be replaced by $-\beta\mu_0^{\mathrm{ex}}$, F_0^{ex} and (3.5.23) becomes

$$\begin{aligned}\mathcal{F}^{\mathrm{ex}}\big[\rho^{(1)}\big] &= F_0^{\mathrm{ex}} + \mu_0^{\mathrm{ex}} \int \Delta\rho^{(1)}(\mathbf{r})\,\mathrm{d}\mathbf{r} \\ &\quad - k_{\mathrm{B}}T \int_0^1 \mathrm{d}\lambda\,(1-\lambda) \iint \Delta\rho^{(1)}(\mathbf{r}) c^{(2)}(\mathbf{r},\mathbf{r}';\lambda)\Delta\rho^{(1)}(\mathbf{r}')\,\mathrm{d}\mathbf{r}\,\mathrm{d}\mathbf{r}'\end{aligned} \tag{4.3.10}$$

This result is still exact, but if we make the approximation of setting $c^{(2)}(\mathbf{r},\mathbf{r}';\lambda)$ equal to the direct correlation function of the reference system, $c_0^{(2}(\mathbf{r},\mathbf{r}')$, for all values of λ, we obtain an expansion of $\mathcal{F}^{\mathrm{ex}}[\rho^{(1)}]$ correct to second order in $\Delta\rho^{(1)} \equiv \rho^{(1)} - \rho_0$:

$$\begin{aligned}\mathcal{F}^{\mathrm{ex}} &\approx F_0^{\mathrm{ex}} + \mu_0^{\mathrm{ex}} \int \Delta\rho^{(1)}(\mathbf{r})\,\mathrm{d}\mathbf{r} \\ &\quad - \tfrac{1}{2}k_{\mathrm{B}}T \iint \Delta\rho^{(1)}(\mathbf{r}) c_0^{(2)}(\mathbf{r},\mathbf{r}')\Delta\rho^{(1)}(\mathbf{r}')\,\mathrm{d}\mathbf{r}\,\mathrm{d}\mathbf{r}'\end{aligned} \tag{4.3.11}$$

or, after adding the ideal part, given by (3.1.22), and replacing μ_0^{ex} by $\mu_0 - k_{\mathrm{B}}T\ln\rho_0\Lambda^3$:

$$\begin{aligned}\mathcal{F}\big[\rho^{(1)}\big] &\approx F_0 + (\mu_0 - k_{\mathrm{B}}T)\int \Delta\rho^{(1)}(\mathbf{r})\,\mathrm{d}\mathbf{r} + k_{\mathrm{B}}T\int \rho^{(1)}(\mathbf{r})\ln\frac{\rho^{(1)}(\mathbf{r})}{\rho_0}\,\mathrm{d}\mathbf{r} \\ &\quad - \tfrac{1}{2}k_{\mathrm{B}}T \iint \Delta\rho^{(1)}(\mathbf{r}) c_0^{(2)}\big(|\mathbf{r}-\mathbf{r}'|\big)\Delta\rho^{(1)}(\mathbf{r}')\,\mathrm{d}\mathbf{r}\,\mathrm{d}\mathbf{r}'\end{aligned} \tag{4.3.12}$$

The grand-potential functional $\Omega_\phi[\rho^{(1)}]$ defined by (3.4.1) is

$$\Omega_\phi\big[\rho^{(1)}\big] = \mathcal{F}\big[\rho^{(1)}\big] + \int \rho^{(1)}(\mathbf{r})\phi(\mathbf{r})\,\mathrm{d}\mathbf{r} - \mu\int \rho^{(1)}(\mathbf{r})\,\mathrm{d}\mathbf{r} \tag{4.3.13}$$

or, after substitution for $\mathcal{F}$ from (4.3.12):

$$\begin{aligned}\Omega_\phi\big[\rho^{(1)}\big] \approx \Omega_0 &+ \int \rho^{(1)}(\mathbf{r})\phi(\mathbf{r})\,\mathrm{d}\mathbf{r} \\ &+ k_\mathrm{B}T\int\left(\rho^{(1)}(\mathbf{r})\ln\frac{\rho^{(1)}(\mathbf{r})}{\rho_0} - \Delta\rho^{(1)}(\mathbf{r})\right)\mathrm{d}\mathbf{r} \\ &- \tfrac{1}{2}k_\mathrm{B}T\iint \Delta\rho^{(1)}(\mathbf{r})c_0^{(2)}\big(|\mathbf{r}-\mathbf{r}'|\big)\Delta\rho^{(1)}(\mathbf{r}')\,\mathrm{d}\mathbf{r}\,\mathrm{d}\mathbf{r}'\end{aligned} \tag{4.3.14}$$

where

$$\Omega_0 = F_0 - \mu_0\int \rho_0\,\mathrm{d}\mathbf{r} \tag{4.3.15}$$

is the grand potential of the reference system. At equilibrium, Ω_ϕ is a minimum with respect to variations in the single-particle density, and it is straightforward to show that the density which minimises (4.3.14) is

$$\rho^{(1)}(\mathbf{r}) = \rho_0\exp\left(-\beta\phi(\mathbf{r}) + \int \Delta\rho^{(1)}(\mathbf{r}')c_0^{(2)}\big(|\mathbf{r}-\mathbf{r}'|\big)\,\mathrm{d}\mathbf{r}'\right) \tag{4.3.16}$$

The same result is obtained by minimising the total free-energy functional obtained by adding the external-field term to (4.3.12), but subject now to the constraint that the total number of particles must remain constant, i.e.

$$\int \Delta\rho^{(1)}(\mathbf{r})\,\mathrm{d}\mathbf{r} = 0 \tag{4.3.17}$$

Equation (4.3.16) may be viewed as providing either an expression for the density profile of a fluid in a true external field or, following Percus, an expression for the pair distribution function of a uniform fluid of density ρ_0 for which $\phi(r)$ can be identified with the pair potential. In the uniform case it follows from (4.3.7) that

$$g(\mathbf{r}) = \exp\left(-\beta v(\mathbf{r}) + \rho\int c\big(|\mathbf{r}-\mathbf{r}'|\big)h(\mathbf{r}')\,\mathrm{d}\mathbf{r}'\right) \tag{4.3.18}$$

or, from the Ornstein–Zernike relation (3.5.12):

$$g(\mathbf{r}) = \exp\big[-\beta v(\mathbf{r})\big]\exp\big[h(\mathbf{r}) - c(\mathbf{r})\big] \tag{4.3.19}$$

Equation (4.3.19) represents the *hypernetted-chain* or HNC approximation.[7] The corresponding expression for the grand potential is obtained by substituting (4.3.6) for $\rho^{(1)}(\mathbf{r})$ in (4.3.14). This leads, after some rearrangement and use of the Ornstein–Zernike relation, to the expression

$$\Omega = \Omega_0 + \tfrac{1}{2}\rho k_{\mathrm{B}}T \int h(\mathbf{r})\big[h(\mathbf{r}) - c(\mathbf{r})\big]\,\mathrm{d}\mathbf{r} - \rho k_{\mathrm{B}}T \int c(\mathbf{r})\,\mathrm{d}\mathbf{r} \tag{4.3.20}$$

The quantity $\Delta\Omega = \Omega - \Omega_0$ is the change in grand potential arising from the introduction of a particle that acts as the source of the external field. Since that particle is fixed in space, it makes no contribution to the ideal free energy, and the change in grand potential is therefore equal to the excess chemical potential. Thus, in the HNC approximation:

$$\beta\mu^{\mathrm{ex}} = \tfrac{1}{2}\rho \int h(\mathbf{r})\big[h(\mathbf{r}) - c(\mathbf{r})\big]\,\mathrm{d}\mathbf{r} - \rho \int c(\mathbf{r})\,\mathrm{d}\mathbf{r} \tag{4.3.21}$$

Equation (4.3.19) represents an approximate closure of the Ornstein–Zernike relation, since it provides a second, independent relation between $h(r)$ and $c(r)$. Elimination of $c(r)$ between the two relations yields the HNC integral equation:

$$\ln g(\mathbf{r}) + \beta v(\mathbf{r}) = \rho \int \big[g(\mathbf{r} - \mathbf{r}') - 1\big]\big[g(\mathbf{r}') - 1 - \ln g(\mathbf{r}') - \beta v(\mathbf{r}')\big]\,\mathrm{d}\mathbf{r}' \tag{4.3.22}$$

The HNC equation and other integral equations of a similar type can be solved numerically by an iterative approach, starting with a guess for either of the functions h or c. Perhaps the easiest method is to use the relation (3.5.13) between the Fourier transforms of h and c. An initial guess, $c_{(0)}(r)$ say, is made and its Fourier transform inserted in (3.5.13); an inverse transformation yields a first approximation for $h(r)$. The closure relation between h and c is then used to obtain an improved guess, $c_{(1)}(r)$ say. The process is repeated, with $c_{(1)}(r)$ replacing $c_{(0)}(r)$ as input, and the iteration continues until convergence is achieved.[8] To ensure convergence it is generally necessary to mix successive approximations to $c(r)$ before they are used at the next level of iteration. A variety of elaborations of this basic scheme have been worked out.

The approximation represented by (4.3.19) is equivalent to setting

$$c(\mathbf{r}) = h(\mathbf{r}) - \ln\big[h(\mathbf{r}) + 1\big] - \beta v(\mathbf{r}) \tag{4.3.23}$$

For sufficiently large r, $h(r) \ll 1$; if we expand the logarithmic term in (4.3.23), we find that $c(r) \approx -\beta v(r)$. As we shall see in Chapter 10, the r^{-1} decay of $c(r)$ at large r is crucial in determining the properties of ionic fluids. For such systems we must expect the HNC approximation to be superior to those approximations in which $c(r)$ has a different asymptotic behaviour.

4.4 THE PERCUS–YEVICK EQUATION

The derivation of (4.3.19) has a strong appeal, since it shows that the HNC closure of the Ornstein–Zernike relation corresponds to minimising a well-defined grand-potential (or free-energy) functional, albeit an approximate one. It also leads naturally to an expression for the chemical potential of a uniform fluid expressed solely in terms of the functions $h(r)$ and $c(r)$. The HNC equation can, however, be derived in a simpler way by expanding the single-particle direct correlation function $c^{(1)}(\mathbf{r})$ of an inhomogeneous fluid about that of a uniform reference system in powers of $\Delta\rho^{(1)}$ where, as before, we follow Percus's idea by supposing that the inhomogeneity is induced by "switching on" the interaction $\phi(\mathbf{r})$ with a particle fixed at the origin. To first order in $\Delta\rho^{(1)}$ the result is

$$\begin{aligned} c^{(1)}(\mathbf{r}) &\approx c_0^{(1)} + \int \Delta\rho^{(1)}(\mathbf{r}') \frac{\delta c^{(1)}(\mathbf{r})}{\delta\rho^{(1)}(\mathbf{r}')}\bigg|_{\phi=0} \mathrm{d}\mathbf{r}' \\ &= -\beta\mu_0^{\mathrm{ex}} + \int \Delta\rho^{(1)}(\mathbf{r}') c_0^{(2)}(\mathbf{r},\mathbf{r}')\,\mathrm{d}\mathbf{r}' \end{aligned} \tag{4.4.1}$$

where the subscript 0 again denotes a property of the reference system. Taken together with the relation (3.5.4) between $c^{(1)}(\mathbf{r})$ and $\rho^{(1)}(\mathbf{r})$, it is easy to show that (4.4.1) is equivalent to (4.3.16), and therefore leads again to the HNC expression (4.3.19). This method of approach is also suggestive of routes to other integral equation approximations, since there are many functionals that could be expanded to yield a possibly useful closure of the Ornstein–Zernike relation. We can, for example, choose to expand $\exp[c^{(1)}(\mathbf{r})]$ in powers of $\Delta\rho^{(1)}$. The first-order result is now

$$\begin{aligned} \exp\bigl[c^{(1)}(\mathbf{r})\bigr] &\approx \exp\bigl(-\beta\mu_0^{\mathrm{ex}}\bigr) + \int \Delta\rho^{(1)}(\mathbf{r}') \frac{\delta \exp[c^{(1)}(\mathbf{r})]}{\delta\rho^{(1)}(\mathbf{r}')}\bigg|_{\phi=0} \mathrm{d}\mathbf{r}' \\ &= \exp\bigl(-\beta\mu_0^{\mathrm{ex}}\bigr)\biggl(1 + \int \Delta\rho^{(1)}(\mathbf{r}') c_0^{(2)}(\mathbf{r},\mathbf{r}')\,\mathrm{d}\mathbf{r}'\biggr) \end{aligned} \tag{4.4.2}$$

which leads, via (3.5.4), to an expression for the pair distribution function of a uniform fluid:

$$\begin{aligned} g(\mathbf{r}) &= \exp\bigl[-\beta v(\mathbf{r})\bigr]\biggl(1 + \rho\int c\bigl(|\mathbf{r}-\mathbf{r}'|\bigr) h(\mathbf{r}')\,\mathrm{d}\mathbf{r}'\biggr) \\ &= \exp\bigl[-\beta v(\mathbf{r})\bigr]\bigl[1 + h(\mathbf{r}) - c(\mathbf{r})\bigr] \end{aligned} \tag{4.4.3}$$

This is the Percus–Yevick or PY approximation.[9] The integral equation that results from using the Ornstein–Zernike relation to eliminate $c(\mathbf{r})$ from (4.4.3) is

$$\exp\bigl[\beta v(\mathbf{r})\bigr] g(\mathbf{r}) = 1 + \rho\int \bigl[g(\mathbf{r}-\mathbf{r}') - 1\bigr] g(\mathbf{r}')\bigl(1 - \exp\bigl[\beta v(\mathbf{r}')\bigr]\bigr)\,\mathrm{d}\mathbf{r}' \tag{4.4.4}$$

The approximation (4.4.3) is equivalent to taking

$$c(\mathbf{r}) \approx \big(1 - \exp\big[\beta v(\mathbf{r})\big]\big) g(\mathbf{r}) \tag{4.4.5}$$

so that $c(\mathbf{r})$ is zero whenever the potential vanishes. The PY equation proves to be more successful than the HNC approximation when the potential is strongly repulsive and short ranged. From comparison of (4.4.3) with (4.3.19) we see that the PY approximation is recovered by linearisation of the HNC result with respect to $(h - c)$, while a diagrammatic analysis shows that the PY equation corresponds to summing a smaller class of diagrams in the density expansion of $h(r)$. To some extent, therefore, the greater success of the PY equation in the case of short-range potentials must be due to a cancellation of errors.

The HNC and PY equations are the classic integral-equation approximations of liquid-state theory. We shall deal shortly with the question of their quantitative reliability, but it is useful initially to note some general features of the two approximations. Both equations predict, correctly, that $g(r)$ behaves as $\exp[-\beta v(r)]$ in the limit $\rho \to 0$. As we shall see in Section 4.6, they also yield the correct expression for the term of order ρ in the density expansion of $g(r)$. It follows that they both give the correct second and third virial coefficients in the expansion of the equation of state. At order ρ^2 and beyond, each approximation neglects a certain number (different for each theory) of the diagrams appearing in the exact expansion of $g(r)$. Once a solution for the pair distribution function has been obtained, the internal energy, pressure and compressibility can be calculated from (2.5.20), (2.5.22) and (2.6.12), respectively. The pressure can also be determined in two other ways. First, the inverse compressibility can be integrated numerically with respect to density to yield the so-called compressibility equation of state. Secondly, the internal energy can be integrated with respect to inverse temperature to give the Helmholtz free energy (see (2.3.9)); the latter can in turn be differentiated numerically with respect to volume to give the "energy" equation of state. The results obtained via the three routes – virial, compressibility and energy – are in general different, sometimes greatly so. This lack of thermodynamic consistency is a common feature of approximate theories. The HNC equation is a special case insofar as it corresponds to a well-defined free-energy functional, and differentiation of that free energy with respect to volume can be shown[10] to give the same result as the virial equation. The energy and virial routes to the equation of state are therefore equivalent.

The PY equation is of particular interest in the theory of simple liquids because it is soluble analytically in the important case of the hard-sphere fluid. Written in terms of the cavity distribution function $y(r)$, the PY approximation (4.4.5) is

$$c(r) = y(r) f(r) \tag{4.4.6}$$

For hard spheres of diameter d, (4.4.6) is equivalent to setting

$$\begin{aligned} c(r) &= -y(r), \quad r < d, \\ &= 0, \qquad\quad r > d \end{aligned} \tag{4.4.7}$$

It follows that $c(r)$ has a discontinuity at $r = d$, since $y(r)$ is continuous everywhere (see Section 4.6). The solution is further restricted by the fact that $g(r)$ must vanish inside the

hard core, i.e.

$$g(r) = 0, \quad r < d \tag{4.4.8}$$

Given (4.4.7) and (4.4.8) it is possible to rewrite the Ornstein–Zernike relation as an integral equation for $y(r)$ in the form

$$y(r) = 1 + \rho \int_{r'<d} y(r')\,\mathrm{d}\mathbf{r}' - \rho \int_{\substack{r'<d \\ |\mathbf{r}-\mathbf{r}'|>d}} y(r')y\big(|\mathbf{r}-\mathbf{r}'|\big)\,\mathrm{d}\mathbf{r}' \tag{4.4.9}$$

which can be solved by Laplace transform methods.[11] The final result for $c(r)$ is

$$\begin{aligned} c(x) &= -\lambda_1 - 6\eta\lambda_2 x - \tfrac{1}{2}\eta\lambda_1 x^3, \quad && x < 1, \\ &= 0, && x > 1 \end{aligned} \tag{4.4.10}$$

where $x \equiv r/d$, η is the packing fraction and

$$\lambda_1 = (1+2\eta)^2/(1-\eta)^4, \qquad \lambda_2 = -(2+\eta)^2/4(1-\eta)^4 \tag{4.4.11}$$

Appendix D describes a different method of solution, due to Baxter;[12] this has the advantage of being easily generalised to cases where the potential consists of a hard-sphere core and a tail. The analytical solution to the PY equation has also been found for the case of binary mixtures of hard spheres with different but additive diameters.[13]

The compressibility of the hard-sphere fluid is obtained by substitution of (4.4.10) in (3.5.15), and integration with respect to η yields the compressibility equation of state:

$$\frac{\beta P^{\mathrm{c}}}{\rho} = \frac{1+\eta+\eta^2}{(1-\eta)^3} \tag{4.4.12}$$

Alternatively, substitution of

$$\lim_{r\to d^+} g(r) = y(d) = -\lim_{r\to d^-} c(r) \tag{4.4.13}$$

in (2.5.26) leads to the virial equation of state:

$$\frac{\beta P^{\mathrm{v}}}{\rho} = \frac{1+2\eta+3\eta^2}{(1-\eta)^2} \tag{4.4.14}$$

The difference between P^{c} and P^{v} increases with increasing density. The general expressions for the nth virial coefficient, obtained by expanding the two equations in powers of η, are

$$\begin{aligned} B_n^{\mathrm{c}}/b^{n-1} &= 2\big[2+3n(n-1)\big]/4^n \\ B_n^{\mathrm{v}}/b^{n-1} &= 8[3n-4]/4^n \end{aligned} \tag{4.4.15}$$

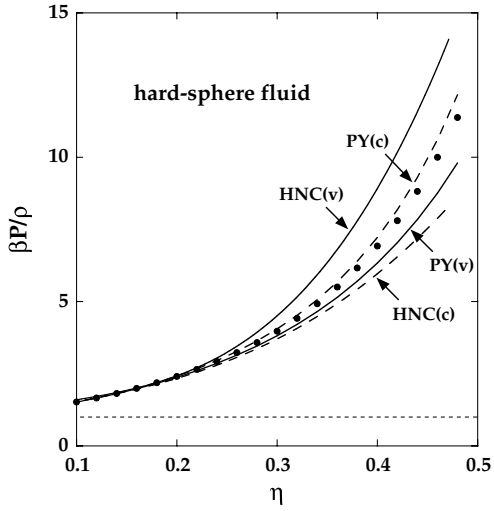

FIG. 4.2. Equation of state of the hard-sphere fluid in the PY and HNC approximations. The full curves and dashes show results from the virial and compressibility equations, respectively, and the points are calculated from the Carnahan–Starling equation (3.9.17).

where $b \equiv B_2 = (2\pi/3)d^3$. Both equations yield the exact values of B_2 and B_3, but give incorrect (and different) values for the higher-order coefficients.

The full equations of state are plotted in Figure 4.2 for comparison with results predicted by the Carnahan–Starling formula (3.9.17), which is nearly exact. The pressures calculated from the compressibility equation lie systematically closer to and above the Carnahan–Starling results at all densities, while the virial pressures lie below them. It appears that the Carnahan–Starling formula interpolates accurately between the two PY expressions; in fact (3.9.17) is recovered if (4.4.12) and (4.4.14) are added together with weights, respectively, of two-thirds and one-third:

$$\frac{\beta P}{\rho} = \frac{\beta}{3\rho}\left(2P^{\mathrm{c}} + P^{\mathrm{v}}\right) = \frac{1+\eta+\eta^2-\eta^3}{(1-\eta)^3} \tag{4.4.16}$$

Results obtained by numerical solution of the HNC equation are also shown in Figure 4.2. They are clearly inferior to the PY results.

The PY approximation to the pair distribution function is obtained by substitution of (4.4.10) into the Ornstein–Zernike relation; as a consequence of the discontinuity in $c(x)$ at $x = 1$, $g(x)$ is only a piecewise-analytical function.[14] A comparison of the calculated distribution function with the results of a Monte Carlo simulation of the hard-sphere fluid at a density ($\eta = 0.49$) close to the fluid–solid transition is shown in Figure 4.3. Although the general agreement is good, the theoretical curve shows two significant defects. First, the value at contact is too low. Secondly, the oscillations are slightly out of phase with the Monte Carlo results. In addition, the amplitude of the oscillations decreases too slowly with increasing distance, with the consequence that the main peak in the structure factor is

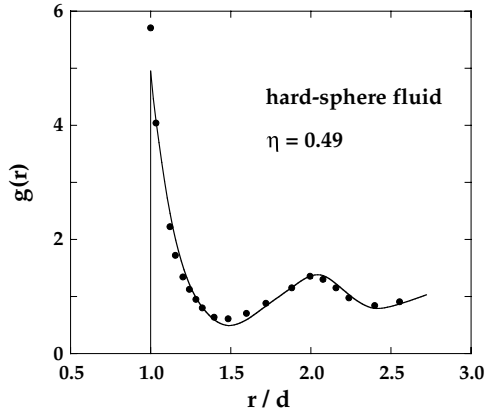

FIG. 4.3. Radial distribution function of the hard-sphere fluid at a density close to the fluid–solid transition. The curve shows the PY solution and the points are the results of Monte Carlo calculations.

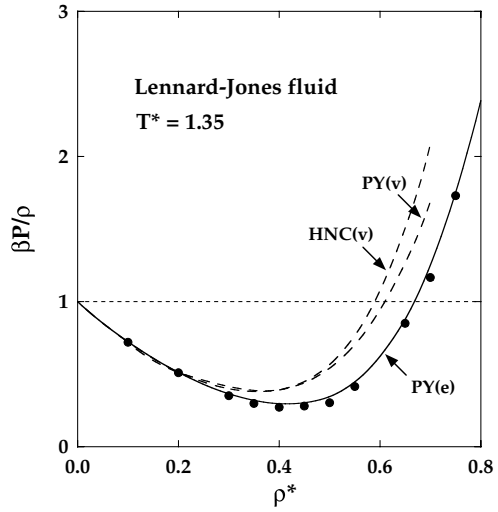

FIG. 4.4. Equation of state of the Lennard-Jones fluid along the isotherm $T^* = 1.35$. The curves show results obtained from the PY and HNC equations via the virial (v) and energy (e) routes and the points are the results of Monte Carlo calculations.[16]

too high, reaching a maximum value of 3.05 rather than the value 2.85 obtained by simulation. An accurate representation of the pair distribution function of the hard-sphere fluid is an important ingredient of many theories. To meet that need, a simple, semi-empirical modification of the PY result has been devised in which the faults seen in Figure 4.3 are corrected.[15]

Solutions to the PY and HNC equations have been obtained for a variety of other pair potentials over wide ranges of temperature and density. Comparison of results for the

Lennard-Jones potential with those of computer simulations show that the PY approximation is superior at all thermodynamic states for which calculations have been made.[3] At high temperatures the agreement with simulations is excellent both for internal energy and for pressure, but it worsens rapidly as the temperature is reduced. Figure 4.4 shows results for the virial and energy equations of state along the isotherm $T^* = 1.35$, which corresponds to a near-critical temperature. Although the pressures calculated by the energy route are in good agreement with those obtained by simulation,[17] the more significant feature of the results is the serious thermodynamic inconsistency that they reveal, which becomes more severe as the temperature is lowered further. The deficiencies in the PY approximation at low temperatures are also evident in the behaviour of the pair distribution function. The main peak in $g(r)$ has too great a height and occurs at too small a value of r, while the later oscillations are out of phase with the results of simulations; in the latter respect, the situation is markedly worse than it is for hard spheres. These weaknesses show that the PY approximation cannot be regarded as a quantitatively satisfactory theory of the liquid state.

4.5 THE MEAN SPHERICAL APPROXIMATION

There are a variety of model fluids of interest in the theory of liquids for which the pair potential consists of a hard-sphere interaction plus a tail. The tail is normally attractive, but not necessarily spherically symmetric. Such systems have been widely studied in the *mean spherical approximation* or MSA. The name comes from the fact that the approximation was first proposed as a generalisation of the mean spherical model of Ising spin systems. The general form of the potential in the spherically symmetric case is

$$\begin{aligned} v(r) &= \infty, \qquad r < d, \\ &= v_1(r), \quad r > d \end{aligned} \tag{4.5.1}$$

where d is the hard-sphere diameter. The MSA is defined in terms of the pair distribution function and direct correlation function by

$$\begin{aligned} g(r) &= 0, \qquad\qquad r < d \\ c(r) &= -\beta v_1(r), \quad r > d \end{aligned} \tag{4.5.2}$$

When supplemented by the Ornstein–Zernike relation, these two expressions combine to yield an integral equation for $g(r)$. The first expression is exact, while the second extends the asymptotic behaviour of $c(r)$ to all $r > d$ and is clearly an approximation. Despite the crude form assumed for $c(r)$, the MSA gives good results in many cases. For example, it provides a much better description of the properties of the square-well fluid[18] than is given by either the PY or HNC approximation. However, the most attractive feature of the MSA is the fact that the integral equation can be solved analytically for a number of potential models of physical interest, including the hard-core Yukawa fluid defined by (1.2.2) as well as simple models of electrolyte solutions (discussed in Chapter 10) and polar liquids (Chapter 11).

The PY equation for hard spheres is the special case of the MSA when the tail in the potential is absent and the analytical solution of the MSA for certain pair potentials is closely linked to the method of solution of the PY hard-sphere problem. The two theories also have a common diagrammatic structure,[19] but the connection between them can be established more easily in the following way. The basic PY approximation (4.4.3) may be expressed in the form

$$c(r) = f(r) + f(r)\big[h(r) - c(r)\big] \tag{4.5.3}$$

where $f(r)$ is the Mayer function for the potential $v(r)$. In the low-density limit, $h(r)$ and $c(r)$ become the same, and the right-hand side of (4.5.3) reduces to $f(r)$. Equation (4.5.3) can therefore be rewritten as

$$c(r) = c_0(r) + f(r)\big[h(r) - c(r)\big] \tag{4.5.4}$$

where $c_0(r)$, the limiting value of $c(r)$ at low density, is equal to $f(r)$ both in an exact theory and in the PY approximation. If we choose another form for $c_0(r)$ in (4.5.3), we generate a different theory. For a potential of the type defined by (4.5.1) the exact $c_0(r)$ is

$$c_0(r) = \exp\big[-\beta v(r)\big] - 1 = \big[1 + f_d(r)\big]\exp\big[-\beta v_1(r)\big] - 1 \tag{4.5.5}$$

where $f_d(r)$ is the Mayer function for hard spheres. The MSA is equivalent to linearising (4.5.5) with respect to $v_1(r)$ by setting

$$c_0(r) \approx \big[1 + f_d(r)\big]\big[1 - \beta v_1(r)\big] - 1 = f_d(r) - \beta v_1(r)\big[1 + f_d(r)\big] \tag{4.5.6}$$

and at the same time replacing f by f_d in (4.5.4). Taken together, these two approximations give rise to the expression

$$f_d(r)\big[1 + h(r)\big] = \big[c(r) + \beta v_1(r)\big]\big[1 + f_d(r)\big] \tag{4.5.7}$$

which is equivalent to the closure relation (4.5.2). This characterisation of the MSA shows that it involves approximations additional to those underlying the PY equation. One would therefore not expect the MSA to be of comparable accuracy to the PY approximation. In practice, as the results for the square-well fluid show, this is not necessarily true.

The structure of (4.5.7) suggests a natural way in which the MSA can be extended to a class of pair potentials wider than that defined by (4.5.1).[20] Let us suppose that the potential $v(r)$ is divided in the form

$$v(r) = v_0(r) + v_1(r) \tag{4.5.8}$$

The conventional MSA is applicable only when v_0 is the hard-sphere potential. When v_0 is strongly repulsive but continuous, the natural generalisation of the closure relation (4.5.7) is obtained by replacing f_d by f_0, the Mayer function for the potential v_0. The resulting equation can then be rearranged to give

$$g(r) = \exp\big[-\beta v_0(r)\big]\big[1 + h(r) - c(r) - \beta v_1(r)\big] \tag{4.5.9}$$

which reduces to the PY approximation (4.4.3) when $v_1(r)$ is very weak. When applied to the Lennard-Jones fluid, the "soft-core" MSA gives good results when the potential is divided at its minimum in the manner that has also proved very successful when used in thermodynamic perturbation theory (see Section 5.4).

4.6 DIAGRAMMATIC EXPANSIONS OF THE PAIR FUNCTIONS

In Section 3.8 we derived the density expansion of the two-particle direct correlation function $c^{(2)}(1,2)$. We now wish to do the same for other pair functions. One of our main goals is to obtain a precise, diagrammatic characterisation of the HNC approximation of Section 4.3. The simplest way to proceed is to take as starting point the iterative solution of the Ornstein–Zernike relation in (3.5.11). That solution can be expressed in diagrammatic terms as

$$h(1,2) = [\text{all chain diagrams consisting of two terminal white 1-circles labelled 1 and 2, black } \rho^{(1)}\text{-circles and } c\text{-bonds}]$$

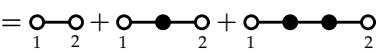

(4.6.1)

where the meaning of the terms "chain" diagram and "terminal" circle is self-evident. We now replace the c-bonds in (4.6.1) by their series expansion. The first term on the right-hand side of (4.6.1) yields the complete set of diagrams that contribute to $c(1,2)$ and are therefore free of connecting circles, which means they contain neither articulation circles nor nodal circles. The black circles appearing at higher order are all nodal circles; they remain nodal circles when the c-bonds are replaced by diagrams drawn from the series (3.8.7), but no articulation circles appear. The topology of the resulting diagrams is therefore similar to that of the diagrams in the series for $c(1,2)$ except that nodal circles are now permitted. Thus[21]

$$h(1,2) = [\text{all irreducible diagrams consisting of two white 1-circles labelled 1 and 2, black } \rho^{(1)}\text{-circles and } f\text{-bonds}] \tag{4.6.2}$$

Equation (4.6.2) contains more diagrams than (3.8.7) at each order in density beyond the zeroth-order term; the additional diagrams contain at least one nodal circle. For example, of the two second-order terms shown below, (a) appears in both expansions but (b) appears only in (4.6.2), because in (b) the black circles are nodal circles.

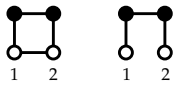

(a) (b)

Diagrams (a) and (b) differ only by the presence in (a) of an f-bond between the white circles. If we recall that $e(1,2) = f(1,2) + 1$, we see that the sum of (a) and (b) is given

by a single diagram in which the white circles are linked by an e-bond. All diagrams in (4.6.2) can be paired uniquely in this way, except that the lowest-order diagram

appears alone. We therefore add to (4.6.2) the disconnected diagram consisting of two white 1-circles:

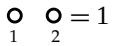

and obtain an expansion of $g(1,2) = h(1,2) + 1$ in terms of diagrams in which the white circles are linked by an e-bond and all other bonds are f-bonds. Alternatively, on dividing through by $e(1,2)$, we find that the cavity distribution function $y(1,2) = g(1,2)/e(1,2)$ can be expressed in the form

$$y(1,2) = [\text{all irreducible diagrams consisting of two non-adjacent white 1-circles labelled 1 and 2, black } \rho^{(1)}\text{-circles and } f\text{-bonds}]$$

$$= 1 + \quad + \quad + \quad + \quad + \quad + \cdots \tag{4.6.3}$$

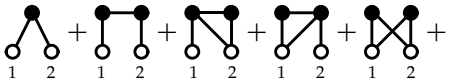

If the system is homogeneous and the factor $e(1,2)$ is restored, (4.6.3) becomes an expansion of $g(1,2)$ in powers of ρ with coefficients $g_n(r)$ such that

$$g(r) = \exp\bigl[-\beta v(r)\bigr]\left(1 + \sum_{n=1}^{\infty} \rho^n g_n(r)\right) \tag{4.6.4}$$

Both $g_1(r)$ and $g_2(r)$ have been evaluated analytically for hard spheres.[22]

The form of the series (4.6.4) leads immediately to two important results. First, $g(r)$ behaves as $\exp[-\beta v(r)]$ as $\rho \to 0$, as we proved in a different way in Section 2.6. Secondly, $y(r)$ is a continuous function of r even for hard spheres, for which the discontinuity in $g(r)$ at $r = d$ is wholly contained in the factor $\exp[-\beta v(r)]$. This useful property has already been exploited in the derivation of the hard-sphere equation of state (2.5.26). It is also clear from (4.6.3) that $y(1,2)$ can be interpreted as the distribution function for a pair 1, 2 in a "mixed" system in which the interaction between those particles is suppressed (and hence $e(1,2) = 1$) but other interactions remain the same. For a system of hard spheres, two such particles would correspond to spheres that can overlap each other, but not other particles, and therefore play a role equivalent to that of spherical cavities. Figure 4.5 shows the calculated cavity distribution function for the Lennard-Jones fluid in a high-density, low-temperature thermodynamic state. The very rapid increase in $y(r)$ as $r \to 0$ implies that there is a high probability of finding the two "cavity" particles at very small separations.

The pair distribution function is sometimes written as

$$g(1,2) = \exp\bigl[-\beta\psi(1,2)\bigr] \tag{4.6.5}$$

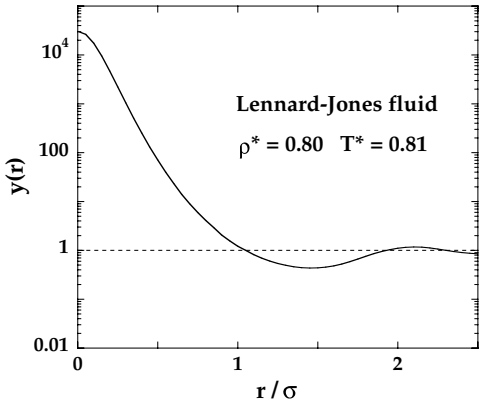

FIG. 4.5. Monte Carlo results for the cavity distribution function of the Lennard-Jones fluid. After Llano-Restrepo and Chapman.[23]

where $\psi(1,2)$ is the *potential of mean force*. The name is justified by the fact that the quantity $-\nabla_1\psi(1,2)$ is the force on particle 1, averaged over all positions of particles $3, 4, \ldots$, with particles 1 and 2 held at $\mathbf{r}_1$ and $\mathbf{r}_2$, respectively. This can be proved[24] by taking the logarithm of both sides of the definition of $g(1,2)$ provided by (2.5.3) and (2.5.8) and differentiating with respect to the coordinates of particle 1. It is clear from the behaviour of the pair-distribution function at low-density that $\psi(1,2) \to v(1,2)$ as $\rho \to 0$. If we define a function $\omega(1,2)$ by

$$\omega(1,2) = \beta\big[v(1,2) - \psi(1,2)\big] \tag{4.6.6}$$

then

$$g(1,2) = e(1,2)\exp\big[\omega(1,2)\big] \tag{4.6.7}$$

and therefore

$$\omega(1,2) = \ln y(1,2) \tag{4.6.8}$$

An application of Lemma 1 of Section 3.7 to the diagrams in (4.6.3) shows that

$$\begin{aligned}\omega(1,2) = [&\text{all diagrams consisting of two non-adjacent white 1-circles}\\ &\text{labelled 1 and 2, black } \rho^{(1)}\text{-circles and } f\text{-bonds, such that}\\ &\text{the white circles are not an articulation pair}]\end{aligned} \tag{4.6.9}$$

The effect of this operation is to eliminate those diagrams in the expansion of $y(1,2)$ that are star products of other diagrams in the same expansion. The fact that the white circles are not an articulation pair means that there exists at least one path between each pair of black circles which does not pass through either white circle.

From the earlier discussion we know that $c(1,2)$ is the sum of all diagrams in $h(1,2)$ that are free of nodal circles. We therefore define a function $b(1,2)$ such that

$$b(1,2) = h(1,2) - c(1,2) \tag{4.6.10}$$

where

$b(1,2) =$ [all irreducible diagrams consisting of two white 1-circles labelled 1 and 2, black $\rho^{(1)}$-circles and f-bonds, and which contain at least one nodal circle]

$$= \quad + \quad + \quad + \quad + \cdots \tag{4.6.11}$$

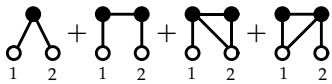

Diagrams belonging to the set (4.6.11) are called *series* diagrams; the function $b(1,2)$ is given by the convolution integral on the right-hand side of the Ornstein–Zernike relation (3.5.10) and is therefore termed the *indirect* correlation function.

All series diagrams are also members of the set (4.6.9). The function $\omega(1,2)$ can therefore be re-expressed as

$$\omega(1,2) = b(1,2) + d(1,2) \tag{4.6.12}$$

where $d(1,2)$ is the sum of the diagrams in (4.6.9) that are free of nodal circles; these are called the *bridge* or *elementary* diagrams and $d(1,2)$ is called the *bridge function*. To second order in density the only bridge diagram is

On combining (4.6.7), (4.6.10) and (4.6.12), we obtain the following, exact relation:

$$\ln\big[h(1,2)+1\big] = -\beta v(1,2) + d(1,2) + h(1,2) - c(1,2) \tag{4.6.13}$$

Since $h(1,2)$ and $c(1,2)$ are linked by the Ornstein–Zernike relation, (4.6.13) would be transformed into an integral equation for h (or c) if the unknown function $d(1,2)$ were replaced by some function of h (or c). For example, the f-bond expansion of $d(1,2)$ can be rewritten as an h-bond expansion[25] and inserted in (4.6.13). The result, together with the Ornstein–Zernike relation, constitutes an exact integral equation for $h(1,2)$, but because the h-bond expansion introduces an infinite series of many-dimensional integrals of products of h, the equation is intractable. If instead we set $d(1,2) = 0$, we recover the HNC approximation, which was arrived at in a very different way in Section 4.3. By rewriting the exact relation (4.6.13) as

$$y(1,2) = \exp\big[b(1,2) + d(1,2)\big] \quad \text{(exact)} \tag{4.6.14}$$

we see that the HNC and PY approximations are equivalent to taking either

$$y(1,2) \approx \exp\big[b(1,2)\big] \quad \text{(HNC)} \tag{4.6.15}$$

or

$$y(1,2) \approx b(1,2) + 1 \quad \text{(PY)} \tag{4.6.16}$$

In each case differences with respect to the exact result arise initially only at second order in density. From comparison of (4.6.14) with (4.6.16) it also follows that the PY approximation can be viewed as one for which the bridge function is approximated by

$$d(1,2) \approx \ln\big[b(1,2)+1\big] - b(1,2) \quad \text{(PY)} \tag{4.6.17}$$

While this interpretation is certainly correct it is important not to misunderstand its meaning. In particular, it does not imply that the PY approximation represents a partial summation of the diagrammatic expansion of $d(r)$. On the contrary, the diagrammatic effect of (4.6.17) is to replace the sum of all bridge diagrams by a sum of star products of series diagrams.

The derivation of the Debye–Hückel expression for the radial distribution function of a system of charged particles provides a simple but useful example of the application of diagrammatic techniques to the calculation of pair functions. Consider a homogeneous, one-component plasma of point charges q, for which the pair potential[26] is

$$v(r) = q^2/r \tag{4.6.18}$$

Use of (4.6.18) in expansions of the pair functions leads to divergent integrals but convergent results can be obtained if entire classes of diagrams are summed. The most strongly divergent integrals in the expansion of $\omega(1,2)$ are those associated with the most weakly connected diagrams, namely the chain diagrams. If the chain diagrams are summed to all orders in ρ, but all other diagrams are ignored, the result is an approximation for $\omega(1,2)$ of the form

$\omega(1,2) \approx$ [all chain diagrams consisting of two terminal white 1-circles labelled 1 and 2, one or more black ρ-circles and f-bonds]

$=$ 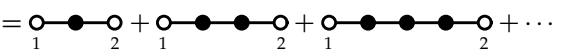 $+\cdots$ (4.6.19)

By analogy with (3.5.10) and (4.6.1), $\omega(1,2)$ is given by

$$\omega(1,2) = \rho \int f(1,3)\big[f(3,2) + \omega(3,2)\big]\,\mathrm{d}3 \tag{4.6.20}$$

On taking Fourier transforms (4.6.20) becomes

$$\hat{\omega}(k) = \frac{\rho[\hat{f}(k)]^2}{1 - \rho\hat{f}(k)} \tag{4.6.21}$$

TABLE 4.1. *Selected pair functions and their definitions*

Function	Symbol	Definition
Pair distribution function	$g(r)$	(2.5.9)
Pair correlation function	$h(r)$	$g(r)-1$
Direct correlation function	$c(r)$	(3.5.2), (3.5.10)
Cavity distribution function	$y(r)$	$\exp[\beta v(r)]g(r)$
Potential of mean force	$\psi(r)$	$-k_{\mathrm{B}}T\ln g(r)$
[Unnamed]	$\omega(r)$	$\beta[v(r)-\psi(r)]$
Indirect correlation function	$b(r)$	$h(r)-c(r)$
Bridge function	$d(r)$	$\omega(r)-b(r)$

with

$$\rho\hat{f}(k)=\rho\int\exp(-i\mathbf{k}\cdot\mathbf{r})f(r)\,\mathrm{d}\mathbf{r}$$
$$\approx-\beta\rho q^2\int\frac{\exp(-i\mathbf{k}\cdot\mathbf{r})}{r}\,\mathrm{d}\mathbf{r}=-\frac{k_{\mathrm{D}}^2}{k^2} \tag{4.6.22}$$

where

$$k_{\mathrm{D}}=\left(4\pi\beta\rho q^2\right)^{1/2} \tag{4.6.23}$$

is the Debye wavenumber. We now substitute for $\rho\hat{f}(k)$ in (4.6.21) and find that

$$\rho\left[\hat{\omega}(k)-\beta\hat{v}(k)\right]=\frac{k_{\mathrm{D}}^2}{k_{\mathrm{D}}^2+k^2} \tag{4.6.24}$$

or

$$\omega(r)-\beta v(r)=-\beta\psi(r)=-\frac{\beta q^2}{r}\exp(-k_{\mathrm{D}}r) \tag{4.6.25}$$

We see that summing the chain diagrams leads to a potential of mean force or "renormalised" potential equal to $v(r)\exp(-k_{\mathrm{D}}r)$. This damping of the Coulomb potential by the factor $\exp(-k_{\mathrm{D}}r)$ is familiar from elementary Debye–Hückel theory and corresponds physically to the effects of screening. It follows from (4.6.5) that the corresponding approximation for the radial distribution function is

$$g(r)=\exp\left(-\frac{\beta q^2}{r}\exp(-k_{\mathrm{D}}r)\right) \tag{4.6.26}$$

Equation (4.6.26) is more familiar in its linearised form, valid for $k_{\mathrm{D}}r\gg1$, i.e.

$$g(r)\approx1-\frac{\beta q^2}{r}\exp(-k_{\mathrm{D}}r) \tag{4.6.27}$$

This result could have been obtained more directly by replacing $c(r)$ by $-\beta v(r)$ in (4.6.1). A serious weakness of the linearised approximation is the fact that it allows $g(r)$ to become negative at small r; this failing is rectified in the non-linear version (4.6.26).

The pair functions discussed in this section, together with their definitions, are summarised in Table 4.1.

4.7 EXTENSIONS OF INTEGRAL EQUATIONS

We saw in the previous section that the development of an accurate integral equation for $g(r)$ can be reduced to the problem of devising a satisfactory approximation for the bridge function $d(r)$. The HNC approximations consists in taking $d(r) = 0$. Hence the integral equations to which some other approximation, $d(r) \approx d_0(r)$ say, gives rise can be regarded as a modified HNC equation in which the exact relation (4.6.13) is replaced by

$$\ln g(r) = -\beta\big[v(r) - k_{\mathrm{B}}T d_0(r)\big] + h(r) - c(r) \tag{4.7.1}$$

The task of solving the modified equation is therefore equivalent to finding the solution to the HNC equation for an effective potential $v_{\mathrm{eff}}(r)$ defined as

$$v_{\mathrm{eff}}(r) = v(r) - k_{\mathrm{B}}T d_0(r) \tag{4.7.2}$$

It is possible to improve the HNC approximation systematically by including successively higher-order terms in the series expansion of the bridge function, but the calculations are computationally demanding and the slow convergence of the series means that in general only modest improvement is achieved.[27]

The true bridge function for a given system can be calculated from (4.6.14) if $c(r)$, $h(r)$ and $y(r)$ are known. A conventional simulation provides values of $h(r)$ at separations where $g(r)$ is non-zero, from which $c(r)$ for all r can be obtained via the Ornstein–Zernike relation; in this range of r the calculation of $y(r)$ from $h(r)$ is a trivial task. To determine $d(r)$ at smaller separations, where $h(r) \approx -1$, an independent calculation of $y(r)$ is required. This can be achieved by simulation of the mixed system, described in the previous section, in which the particles labelled 1 and 2 do not interact with each other. The calculation is straightforward in principle, but the very rapid rise in $y(r)$ as $r \to 0$ means that special techniques are needed to ensure that the full range of r is adequately sampled.[23,28]

Figure 4.6 shows the bridge function derived from Monte Carlo calculations for the Lennard-Jones fluid in a thermodynamic state not far from the triple point and compares the results with those given by the PY approximation (4.6.17). In the example illustrated, the bridge function makes a contribution to the effective potential (4.7.2) that is both short ranged and predominantly repulsive, but the same is true for the Lennard-Jones fluid at other thermodynamic states and also for other model fluids. The PY approximation is poor at small values of r, but in that region the pair potential is so strongly repulsive that errors in the effective potential are unimportant for many purposes. So far as the calculation of thermodynamic properties is concerned, the most serious deficiencies in the PY approximation occur in the region of the main peak in $g(r)$ ($r/\sigma \approx 1.0$ to 1.6).

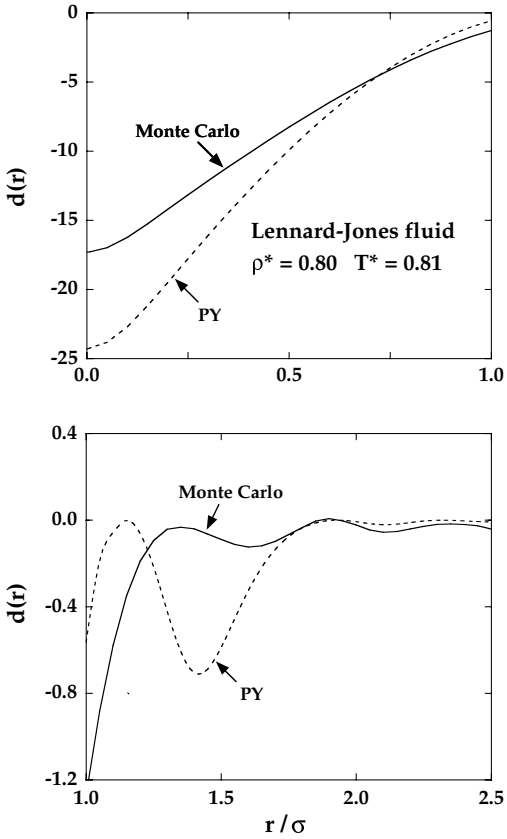

FIG. 4.6. Bridge function of the Lennard-Jones fluid for $r < \sigma$ (above) and $r > \sigma$ (below). The PY results are those given by (4.6.17). After Llano-Restrepo and Chapman.[23]

Alternatives to the PY approximation have been proposed[29] that resemble (4.6.17) insofar as $d(r)$ is written as a function of $b(r)$. These approximations give results for the hard-sphere fluid that improve on those obtained from the PY equation and they have also been applied, though with generally less success, to systems having an attractive term in the potential. There is no reason to suppose, however, that the functional relationship between $d(r)$ and $b(r)$ is the same for all potentials, or even for different thermodynamic states of a given system.[23,30] To improve on the PY or PY-like approximations it seems necessary to make the assumed form of $d(r)$ explicitly dependent on $v(r)$. The soft-core MSA (SMSA) discussed in Section 4.5 provides an example of how this can be done. The SMSA expression for $g(r)$ given by (4.5.9) may be rewritten as

$$y(r) \approx 1 + b(r) - \beta v_1(r) \tag{4.7.3}$$

where $v_1(r)$ is the tail in the potential. Comparison with (4.6.13) shows that this is in turn equivalent to approximating the bridge function by

$$d(r) \approx \ln\big[b^*(r)+1\big] - b^*(r) \quad \text{(SMSA)} \tag{4.7.4}$$

where

$$b^*(r) = b(r) - \beta v_1(r) \tag{4.7.5}$$

Equation (4.7.4) is identical to its PY counterpart (4.6.17), except that $b(r)$ is replaced by $b^*(r)$. The result, as we have seen, is a marked improvement relative to the PY approximation in the case of the Lennard-Jones fluid.

We showed in Section 4.3 that the HNC approximation can be derived by minimising the grand-potential functional obtained from a functional Taylor expansion of the intrinsic free energy truncated at second order. The question therefore arises as to whether any significant improvement is obtained when the third-order term is included.[5] Equation (4.3.10) again provides the starting point of the calculation, but $c^{(2)}(\mathbf{r},\mathbf{r}';\lambda)$ is now replaced, not by $c_0^{(2)}(\mathbf{r},\mathbf{r}')$, but by

$$\begin{aligned} c^{(2)}(\mathbf{r},\mathbf{r}';\lambda) &\approx c_0^{(2)}(\mathbf{r},\mathbf{r}') + \lambda \int \Delta\rho^{(1)}(\mathbf{r}'') \frac{\delta c_0^{(2)}(\mathbf{r},\mathbf{r}')}{\delta\rho^{(1)}(\mathbf{r}'')}\,\mathrm{d}\mathbf{r}'' \\ &= c_0^{(2)}(\mathbf{r},\mathbf{r}') + \lambda \int \Delta\rho^{(1)}(\mathbf{r}'') c_0^{(3)}(\mathbf{r},\mathbf{r}',\mathbf{r}'')\,\mathrm{d}\mathbf{r}'' \end{aligned} \tag{4.7.6}$$

where $c_0^{(3)}(\mathbf{r},\mathbf{r}',\mathbf{r}'')$ is the three-particle direct correlation function of the reference fluid. The effect is to add to the grand-potential functional (4.3.14) the term

$$-\tfrac{1}{6}k_{\mathrm{B}}T \iiint \Delta\rho^{(1)}(\mathbf{r})\Delta\rho^{(1)}(\mathbf{r}')\Delta\rho^{(1)}(\mathbf{r}'')c_0^{(3)}(\mathbf{r},\mathbf{r}',\mathbf{r}'')\,\mathrm{d}\mathbf{r}\,\mathrm{d}\mathbf{r}'\,\mathrm{d}\mathbf{r}''$$

If we now follow the steps that previously led to the HNC approximation (4.3.19), we obtain an expression for the pair distribution function of a uniform fluid having the form (4.7.1), with

$$d_0(r) = \tfrac{1}{2}\rho^2 \iint c^{(3)}(\mathbf{r}-\mathbf{r}',\mathbf{r}-\mathbf{r}'')h(r')h(r'')\,\mathrm{d}\mathbf{r}'\,\mathrm{d}\mathbf{r}'' \tag{4.7.7}$$

Solution of the integral equation for $g(r)$ requires some further approximation[5] to be made for the triplet function $c^{(3)}$. Equation (4.7.7) is equivalent to the lengthier expression in terms of $g^{(3)}$ obtained from an expansion of $c^{(1)}(\mathbf{r})$ taken to second order, the so-called HNC2 approximation.[31]

Results based on (4.7.7) show a clear improvement over the HNC approximation for a number of model fluids but the method is computationally demanding. The HNC equation can more easily and successfully be extended by identifying $d_0(r)$ with the bridge function of a suitable reference system, a step that leads to the "reference" HNC (RHNC) approximation.[32] The obvious choice of reference system is a fluid of hard spheres, since

TABLE 4.2. *Thermodynamic properties of the Lennard-Jones fluid: comparison between molecular-dynamics results (MD) and calculations based on the RHNC approximation. After Lado et al.*[32(c)]

		$\beta P/\rho$		$\beta U^{\mathrm{ex}}/N$	
ρ^*	T^*	MD	RHNC	MD	RHNC
0.85	0.719	0.36	0.424	−6.12	−6.116
0.85	2.889	4.36	4.364	−4.25	−4.240
0.75	1.071	0.89	0.852	−5.17	−5.166
0.65	1.036	−0.11	−0.155	−4.52	−4.522
0.65	2.557	2.14	2.136	−3.78	−3.786
0.45	1.552	0.57	0.552	−2.98	−2.982
0.45	2.935	1.38	1.377	−2.60	−2.608
0.40	1.424	0.38	0.382	−2.73	−2.728

this is the only potential model for which the bridge function is known with sufficient accuracy over the full range of state conditions.[33] Equation (4.7.1) then represents a one-parameter theory in which the only unknown quantity is the hard-sphere diameter d. It was originally argued that the bridge function was likely to be highly insensitive to details of the potential and that its representation by a hard-sphere function should therefore be a good approximation. Although it is now recognised that the bridge function does not have a genuinely "universal" character,[34] this approach has been applied successfully in calculations for a variety of different systems. The overall agreement with the results of simulations is very good, as illustrated by the results for thermodynamic properties of the Lennard-Jones fluid given in Table 4.2; the errors in the corresponding pair distribution functions are barely discernible, even under conditions close to the triple point. In the work on which Table 4.2 is based, the hard-sphere diameter was chosen in such a way as to minimise an approximate free-energy functional. So far as internal consistency of the theory is concerned, use of this procedure gives the RHNC approximation a status comparable with that of the HNC equation. The method has also been applied to mixtures of Lennard-Jones fluids, again with very good results.[32(e)]

A number of attempts have been made to combine different closure relations in hybrid schemes that ensure a degree of thermodynamic consistency. For example, whereas the HNC approximation is correct at large separations, the PY approximation, being much superior for strongly repulsive potentials, is presumably more accurate at short distances. It is therefore plausible to mix the two closures in such a way that the function $y(r)$ in (4.6.14) reduces to its PY value as $r \to 0$ and to its HNC value as $r \to \infty$.[35] The parameter that determines the proportions in which the two approximations are mixed at intermediate values of r can then be chosen to force consistency between the compressibility and virial equations of state. The method works well for systems of particles interacting through purely repulsive potentials, but breaks down for the Lennard-Jones potential for which, at low temperatures, it is impossible to find a value of the mixing parameter that provides thermodynamic consistency.[36] Where successful, the method relies heavily on the fact that the HNC and PY approximations in some sense bracket the exact solution for the system

of interest. The difficulty in the case of the Lennard-Jones fluid lies in the fact that the PY approximation is poor at low temperatures. The problem can be overcome by interpolating instead between the HNC approximation and the soft-core MSA, an approach – called the HMSA – that yields results comparable in quality with those obtained by the RHNC approximation.[36]

A more ambitious method of building thermodynamic consistency into an integral-equation theory is to write the direct correlation function in a form that can be adjusted so as to satisfy some consistency criterion. This is the basis of the self-consistent Ornstein–Zernike approximation or SCOZA developed by Stell and coworkers.[37] The SCOZA is most easily applied when the potential consists of a hard core and a tail, $v_1(r)$ say, as in (4.5.1). Since $g(r)$ vanishes inside the hard core, closure of the Ornstein–Zernike is achieved by making some approximation for $c(r)$ in the range $r > d$; this approximation is typically of the form

$$c(r) = c_d(r) - \beta A(\rho, T) v_1(r), \quad r > d \tag{4.7.8}$$

where $c_d(r)$ is the direct correlation function of the hard-sphere fluid. The function $A(\rho, T)$ can then be chosen in such a way as to enforce consistency between the compressibility and energy routes to the equation of state. Equation (4.7.8) resembles certain other closure relations insofar as the range of $c(r)$ is the same as that of the pair potential, but in contrast, say, to the MSA, its amplitude is now density dependent. If the compressibility and internal energy are to be consistent with each other, they must come from the same free energy, and hence must satisfy the relation[38]

$$-\frac{\partial \hat{c}(k=0)}{\partial \beta} = \frac{\partial^2 u}{\partial \rho^2} \tag{4.7.9}$$

where $u \equiv U^{\text{ex}}/V$ and $\hat{c}(k=0)$ is related to the compressibility by (3.5.15). Published calculations based on the SCOZA are largely concerned with the hard-core Yukawa model (1.2.2), a system for which the analytical solution to the MSA is known.[39] A major simplification of the problem is then possible. If $c_d(r)$ is represented by a second Yukawa term, $\hat{c}(k=0)$ and u can be related analytically and (4.7.10) becomes a partial differential equation for the variable $u(\rho, T)$, which can be solved numerically; the two free parameters in the second Yukawa term are chosen so as to reproduce the Carnahan–Starling equation of state in the limit $T \to \infty$. The method gives good results for the structure and thermodynamics of the Yukawa fluid over a range of state conditions and choices of the Yukawa parameter λ, but its chief merit is the fact that it remains accurate in the critical region, where the performance of other integral-equation theories is mostly poor.

NOTES AND REFERENCES

1. Kirkwood, J.G., *J. Chem. Phys.* **3**, 300 (1935).
2. Born, M. and Green, M.S., "A General Kinetic Theory of Liquids". Cambridge University Press, Cambridge, 1949.
3. Levesque, D., *Physica* **32**, 1985 (1966).

4. Ichimaru, S., *Phys. Rev. A* **2**, 494 (1970).
5. Barrat, J.L., Hansen, J.P. and Pastore, G., *Mol. Phys.* **63**, 747 (1988).
6. (a) Percus, J.K., *Phys. Rev. Lett.* **8**, 462 (1962). (b) Percus, J.K., *In* "The Equilibrium Theory of Classical Fluids" (H.L. Frisch and J.L. Lebowitz, eds). W.A. Benjamin, New York, 1964.
7. The HNC approximation was developed independently by several workers. For some historical background, see Rowlinson, J.S., *Rep. Prog. Phys.* **28**, 169 (1965).
8. Gillan, M.J., *Mol. Phys.* **38**, 1781 (1979).
9. The PY equation was originally derived in a very different way by Percus, J.K. and Yevick, G.J., *Phys. Rev.* **110**, 1 (1958).
10. Morita, T., *Prog. Theor. Phys.* **23**, 423, 829 (1960). See also Schlijper, A.G., Telo da Gama, M.M. and Ferreira, P.G., *J. Chem. Phys.* **98**, 1534 (1993).
11. (a) Thiele, E., *J. Chem. Phys.* **39**, 474 (1963). (b) Wertheim, M.S., *Phys. Rev. Lett.* **10**, 321 (1963). (c) Wertheim, M.S., *J. Math. Phys.* **5**, 643 (1964).
12. Baxter, R.J., *Aust. J. Phys.* **21**, 563 (1968).
13. Lebowitz, J.L., *Phys. Rev.* **133**, A895 (1964).
14. Analytical expressions covering the range $x = 1$ to 5 are given by Smith, W.R. and Henderson, D., *Mol. Phys.* **19**, 411 (1970). See also Chang, J. and Sandler, S.I., *Mol. Phys.* **81**, 735 (1994).
15. Verlet, L. and Weis, J.J., *Phys. Rev. A* **5**, 939 (1972). The implementation of certain theories also requires a knowledge of the hard-sphere $y(r)$ inside the hard core, a parametrisation of which is given by Grundke, E.W. and Henderson, D., *Mol. Phys.* **24**, 269 (1972).
16. Hansen, J.P. and Verlet, L., *Phys. Rev.* **184**, 151 (1969).
17. Chen, M., Henderson, D. and Barker, J.A., *Can. J. Phys.* **54**, 703 (1969).
18. Smith, W.R., Henderson, D. and Tago, Y., *J. Chem. Phys.* **67**, 5308 (1977).
19. Madden, W.G., *J. Chem. Phys.* **75**, 1984 (1981).
20. Madden, W.G. and Rice, S.A., *J. Chem. Phys.* **72**, 4208 (1980).
21. This result was first derived by Mayer, J.E. and Montroll, E., *J. Chem. Phys.* **9**, 2 (1941).
22. Nijboer, B.R.A. and van Hove, L., *Phys. Rev.* **85**, 177 (1952).
23. Llano-Restrepo, M. and Chapman, W.G., *J. Chem. Phys.* **97**, 2046 (1992).
24. Hill, T.L., "Introduction to Statistical Thermodynamics". Addison-Wesley, Reading, 1960, p. 313.
25. This transformation is achieved by a topological reduction based on Lemma 5 of Section 3.7.
26. We use electrostatic units (esu).
27. See, e.g., Perkyns, J.S., Dyer, K.M. and Pettitt, B.M., *J. Chem. Phys.* **116**, 9404 (2002).
28. Torrie, G. and Patey, G.N., *Mol. Phys.* **34**, 1623 (1977).
29. For examples of this approach, see Caccamo, C., *Phys. Rep.* **274**, 1 (1996).
30. Fantoni, R. and Pastore, G., *J. Chem. Phys.* **120**, 10681 (2004).
31. (a) Verlet, L., *Physica* **30**, 95 (1964). (b) Verlet, L., *Physica* **31**, 959 (1965).
32. (a) Lado, F., *Phys. Rev. A* **8**, 2548 (1973). (b) Rosenfeld, Y. and Ashcroft, N.W., *Phys. Rev. A* **20**, 1208 (1979). (c) Lado, F., Foiles, S.M. and Ashcroft, N.W., *Phys. Rev. A* **28**, 2374 (1983). (d) Foiles, S.M., Ashcroft, N.W. and Reatto, L., *J. Chem. Phys.* **80**, 4441 (1984). (e) Enciso, E., Lado, F., Lombardero, M., Abascal, J.L.F. and Lago, S., *J. Chem. Phys.* **87**, 2249 (1987). Note that the "bridge function" in these and related papers is sometimes defined, in the present notation, as $-d(r)$.
33. See note 14. The hard-sphere bridge function has also been parametrised as a function of packing fraction by Malijevský, A. and Labík, S., *Mol. Phys.* **60**, 663 (1987).
34. See, e.g., Kambayashi, S. and Chihara, J., *Phys. Rev. E* **50**, 1317 (1994).
35. Rogers, F.J. and Young, D.A., *Phys. Rev. A* **30**, 999 (1984).
36. Zerah, G. and Hansen, J.P., *J. Chem. Phys.* **84**, 2336 (1986).
37. (a) Pini, D., Stell, G. and Høye, J.S., *Int. J. Thermophys.* **19**, 1029 (1998). (b) Pini, D., Stell, G. and Wilding, N.B., *Mol. Phys.* **95**, 483 (1998). (c) Caccamo, C., Pellicane, G., Costa, D., Pini, D. and Stell, G., *Phys. Rev. E* **60**, 5533 (1999).
38. This result follows straightforwardly from the thermodynamic relations (2.3.8) and (2.3.9).
39. Waisman, E., *Mol. Phys.* **25**, 45 (1973). For later developments see, e.g., Høye, J.S. and Blum, L., *J. Stat. Phys.* **16**, 399 (1977), Ginoza, M., *Mol. Phys.* **71**, 145 (1990) and Tang, Y., *J. Chem. Phys.* **118**, 4140 (2003).

CHAPTER 5

Perturbation Theory

5.1 INTRODUCTION: THE VAN DER WAALS MODEL

The intermolecular pair potential often separates in a natural way into two parts: a harsh, short-range repulsion and a smoothly varying, long-range attraction. A separation of this type is an explicit ingredient of many empirical representations of the intermolecular forces, including the Lennard-Jones potential. It is now generally accepted that the structure of most simple liquids, at least at high density, is largely determined by the way in which the molecular hard cores pack together. By contrast, the attractive interactions may, in a first approximation, be regarded as giving rise to a uniform background potential that provides the cohesive energy of the liquid but has little effect on its structure. A further plausible approximation consists in modelling the short-range forces by the infinitely steep repulsion of the hard-sphere potential. The properties of the liquid of interest can in this way be related to those of a hard-sphere reference system, the attractive part of the potential being treated as a perturbation. The choice of the hard-sphere fluid as a reference system is an obvious one, since its thermodynamic and structural properties are well known.

The idea of representing a liquid as a system of hard spheres moving in a uniform, attractive potential is an old one, providing as it does the physical basis for the famous van der Waals equation of state. At the time of van der Waals, little was known of the properties of the dense hard-sphere fluid. The approximation that van der Waals made was to take the excluded volume per sphere of diameter d as equal to $\frac{2}{3}\pi d^3$ (or four times the hard-sphere volume), which leads to an equation of state of the form

$$\frac{\beta P_0}{\rho} = \frac{1}{1-4\eta} \tag{5.1.1}$$

where, as before, η is the packing fraction. Equation (5.1.1) gives the second virial coefficient correctly (see (3.9.14)), but it fails badly at high densities. In particular, the pressure diverges as $\eta \to 0.25$, a packing fraction lying well below that of the fluid–solid transition ($\eta \approx 0.49$).

Considerations of thermodynamic consistency[1] show that the equation of state compatible with the hypothesis of a uniform, attractive background is necessarily of the form

$$\frac{\beta P}{\rho} = \frac{\beta P_0}{\rho} - \beta\rho a \tag{5.1.2}$$

where a is a positive constant; this is equivalent to supposing that the chemical potential is lowered with respect to that of the hard spheres by an amount proportional to the density and equal to $2a\rho$. The classic van der Waals equation is then recovered by substituting for P_0 from (5.1.1). It is clear that a first step towards improving on van der Waals's result is to replace (5.1.1) by a more accurate hard-sphere equation of state, such as that of Carnahan and Starling, (3.9.17). A calculation along these lines was first carried out by Longuet-Higgins and Widom,[2] who thereby were able to account successfully for the melting properties of rare-gas solids.

The sections that follow are devoted to perturbation methods that may be regarded as attempts to improve the theory of van der Waals in a systematic fashion. The methods we describe have as a main ingredient the assumption that the structure of a dense, monatomic fluid resembles that of an assembly of hard spheres. Justification for this intuitively appealing idea is provided by the great success of the perturbation theories to which it gives rise, and which mostly reduce to (5.1.2) in some well-defined limit, but more direct evidence exists to support it. For example, it has long been known[3] that the experimental structure factors of a variety of liquid metals near their normal melting points can to a good approximation be superimposed on the structure factor of an "equivalent" hard-sphere fluid, and Figure 5.1 shows the results of a similar but more elaborate analysis of data obtained by molecular-dynamics calculations for the Lennard-Jones fluid. The fact that the attractive forces play such an apparently minor role in these examples is understandable through the following argument.[4] Equation (3.6.9) shows that the structure factor determines the density response of the fluid to a weak, external field. If the external potential is identified with the potential due to a test particle placed at the origin, the long-range part of that potential gives rise to a long-wavelength response in the density. In the long-wavelength limit ($k \to 0$), the response is proportional to $S(k = 0)$ and hence, through (3.6.11), to the compressibility. Under triple-point conditions the compressibility of a liquid is very small: typically the ratio of χ_T to its ideal-gas value is approximately 0.02. The effects of long-wavelength perturbations are therefore greatly reduced. At lower densities, particularly in the

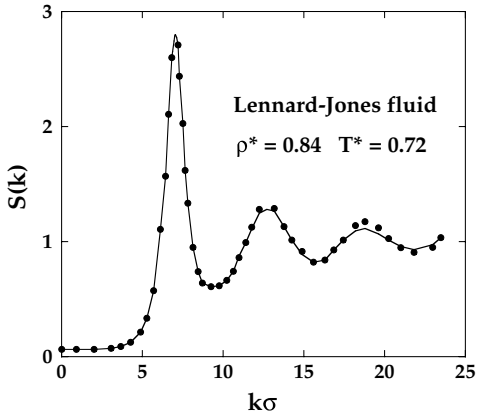

FIG. 5.1. Structure factor of the Lennard-Jones fluid close to the triple point (curve) and its representation by a hard-sphere model (points). After Verlet.[4]

critical region, the compressibility can become very large. The role of the attractive forces is then important and the simple van der Waals model no longer has a sound physical basis.

We shall assume throughout this chapter that the interactions between particles are pairwise additive, though there is no difficulty in principle in extending the treatment to include three-body and higher-order forces. We also suppose that the system of interest is homogeneous. The basis of all the perturbation theories we discuss is a division of the pair potential of the form

$$v(1,2) = v_0(1,2) + w(1,2) \tag{5.1.3}$$

where $v_0(1,2)$ is the pair potential of the reference system and $w(1,2)$ is the perturbation. The calculation then usually proceeds in two stages. The first step is to compute the effects of the perturbation on the thermodynamic properties and pair distribution function of the reference system. This can be done systematically via an expansion in powers either of inverse temperature (the "λ-expansion") or of a parameter that measures the range of the perturbation (the "γ-expansion"). When hard spheres themselves are the reference system, this completes the calculation, but in the more general situation the properties of some "soft-core" reference system must in turn be related to those of the hard-sphere fluid.

5.2 THE λ-EXPANSION

Consider a pair potential $v_\lambda(1,2)$ of the form

$$v_\lambda(1,2) = v_{\lambda_0}(1,2) + w_\lambda(1,2) \tag{5.2.1}$$

where λ is a parameter that varies between λ_0 and λ_1. When $\lambda = \lambda_0$, w_λ vanishes and the potential $v_{\lambda_0} \equiv v_0$ reduces to that of a reference system, the properties of which are assumed to be known, whereas for $\lambda = \lambda_1$ the potential $v_{\lambda_0} \equiv v$ is the one that characterises the system of interest. The quantity λ has the meaning of a coupling parameter: the effect of varying λ continuously from λ_0 to λ_1 is that of gradually increasing the perturbation $w_\lambda(1,2)$. The commonest example of such a potential is

$$v_\lambda(1,2) = v_0(1,2) + \lambda w(1,2) \tag{5.2.2}$$

with $\lambda_0 = 0$ and $\lambda_1 = 1$; when $\lambda = 1$, the potential is the same as that introduced in (5.1.3).

Let $V_N(\lambda)$, given by

$$V_N(\lambda) = \sum_{i=1}^{N} \sum_{j>i}^{N} v_\lambda(i,j) \tag{5.2.3}$$

be the total potential energy of a system of particles interacting through the potential (5.2.1). From the definitions of the configuration integral, (2.3.13), and the excess free energy (here denoted simply by F), (2.3.20), it follows immediately that the derivative of $F(\lambda)$ with respect to the coupling parameter is

$$\beta \frac{\partial F(\lambda)}{\partial \lambda} = \frac{1}{Z_N(\lambda)} \int \exp\bigl[-\beta V_N(\lambda)\bigr] \beta V_N'(\lambda)\, \mathrm{d}\mathbf{r}^N = \beta \bigl\langle V_N'(\lambda) \bigr\rangle_\lambda \tag{5.2.4}$$

where $V_N'(\lambda) \equiv \partial V_N(\lambda)/\partial\lambda$ and $\langle\cdots\rangle_\lambda$ denotes a canonical ensemble average for the system characterised by the potential $v_\lambda(1,2)$. Integration of (5.2.4) gives

$$\beta F(\lambda_1) = \beta F_0 + \beta \int_{\lambda_0}^{\lambda_1} \langle V_N'(\lambda)\rangle_\lambda \, \mathrm{d}\lambda \tag{5.2.5}$$

where $F_0 \equiv F_{\lambda_0}$ is the excess free energy of the reference system. A series expansion of the ensemble average $\langle V_N'(\lambda)\rangle_\lambda$ can now be made around its value for $\lambda = \lambda_0$:

$$\langle V_N'(\lambda)\rangle_\lambda = \langle V_N'(\lambda)\rangle_{\lambda_0} + (\lambda - \lambda_0)\frac{\partial}{\partial\lambda}\langle V_N'(\lambda)\rangle_\lambda\Big|_{\lambda=\lambda_0} + \mathcal{O}(\lambda-\lambda_0)^2 \tag{5.2.6}$$

The derivative with respect to λ in (5.2.6) is

$$\frac{\partial}{\partial\lambda}\langle V_N'(\lambda)\rangle_\lambda = \langle V_N''(\lambda)\rangle_\lambda - \beta\big(\langle[V_N'(\lambda)]^2\rangle_\lambda - \langle V_N'(\lambda)\rangle_\lambda^2\big) \tag{5.2.7}$$

and insertion of this result in (5.2.5) yields an expansion of the free energy in powers of $(\lambda_1 - \lambda_0)$:

$$\begin{aligned}\beta F(\lambda_1) = {} & \beta F_0 + (\lambda_1-\lambda_0)\beta\langle V_N'(\lambda_0)\rangle_{\lambda_0} \\ & + \tfrac{1}{2}(\lambda_1-\lambda_0)^2\big(\beta\langle V_N''(\lambda_0)\rangle_{\lambda_0} - \beta^2\big(\langle[V_N'(\lambda_0)]^2\rangle_{\lambda_0} - \langle V_N'(\lambda_0)\rangle_{\lambda_0}^2\big)\big) \\ & + \mathcal{O}(\lambda_1-\lambda_0)^3\end{aligned} \tag{5.2.8}$$

We now restrict ourselves to the important special case when $v_\lambda(1,2)$ is given by (5.2.2). If we define the total perturbation energy for $\lambda = 1$ as

$$W_N = \sum_{i=1}^{N}\sum_{j>i}^{N} w(i,j) \tag{5.2.9}$$

then $V_N' = W_N$, $V_N'' = 0$ and (5.2.8) simplifies to give

$$\beta F = \beta F_0 + \beta\langle W_N\rangle_0 - \tfrac{1}{2}\beta^2\big(\langle W_N^2\rangle_0 - \langle W_N\rangle_0^2\big) + \mathcal{O}\big(\beta^3\big) \tag{5.2.10}$$

The series (5.2.10) is called the *high-temperature expansion*, but the name is not entirely appropriate. Although successive terms are multiplied by increasing powers of β, the ensemble averages are also, in general, functions of temperature. However, when the reference system is a hard-sphere fluid, the averages depend only on density and the λ-expansion reduces to a Taylor series in T^{-1}. Equation (5.2.10) was first derived by Zwanzig,[5] who showed that the nth term in the series can be written in terms of the mean fluctuations $\langle[(W_N - \langle W_N\rangle_0)]^\nu\rangle_0$, with $\nu \leqslant n$. Thus every term in the expansion corresponds to a statistical average evaluated in the reference-system ensemble. The third and

fourth-order terms, for example, are

$$\begin{aligned}\beta F_3 &= \frac{\beta^3}{3!}\langle\big[W_N - \langle W_N\rangle_0\big]^3\rangle_0 \\ \beta F_4 &= -\frac{\beta^4}{4!}\big(\langle\big[W_N - \langle W_N\rangle_0\big]^4\rangle_0 - 3\langle\big[W_N - \langle W_N\rangle_0\big]^2\rangle_0^2\big)\end{aligned} \tag{5.2.11}$$

The assumption of pairwise additivity of the potential (including the perturbation) means that (5.2.5) can be written as

$$\frac{\beta F}{N} = \frac{\beta F_0}{N} + \frac{\beta}{2N}\int_0^1 \mathrm{d}\lambda \iint \rho_\lambda^{(2)}(1,2)w(1,2)\,\mathrm{d}1\,\mathrm{d}2 \tag{5.2.12}$$

where $\rho_\lambda^{(2)}(1,2)$ is the pair density for the system with potential $v_\lambda(1,2)$; this is a special case of the general result contained in (3.4.10). The pair density can then be expanded in powers of λ:

$$\rho_\lambda^{(2)}(1,2) = \rho_0^{(2)}(1,2) + \lambda\frac{\partial\rho_\lambda^{(2)}(1,2)}{\partial\lambda}\bigg|_{\lambda=0} + \mathcal{O}(\lambda^2) \tag{5.2.13}$$

When this result is inserted in (5.2.12) the term of zeroth order in λ yields the first-order term in the high-temperature expansion of the free energy:

$$\frac{\beta F_1}{N} = \frac{\beta}{2N}\iint \rho_0^{(2)}(1,2)w(1,2)\,\mathrm{d}1\,\mathrm{d}2 = \frac{\beta\rho}{2}\int g_0(1,2)w(1,2)\,\mathrm{d}\mathbf{r}_{12} \tag{5.2.14}$$

In this approximation the structure of the fluid is unaltered by the perturbation. At second order in λ, however, calculation of the free energy involves the derivative $\partial\rho_\lambda^{(2)}/\partial\lambda$. Care is needed in passing to the thermodynamic limit and the differentiation is easier to perform in the grand canonical ensemble. The final result for a closed system[6] is

$$\begin{aligned}\frac{\beta F_2}{N} = -\frac{\beta^2}{2}\Bigg(&\frac{\rho}{2}\int g_0(1,2)\big[w(1,2)\big]^2\,\mathrm{d}2 \\ &+ \rho^2\iint g_0^{(3)}(1,2,3)w(1,2)w(1,3)\,\mathrm{d}2\,\mathrm{d}3 \\ &+ \frac{\rho^3}{4}\iiint\big[g_0^{(4)}(1,2,3,4) - g_0^{(2)}(1,2)g_0^{(2)}(3,4)\big] \\ &\qquad\times w(1,2)w(3,4)\,\mathrm{d}2\,\mathrm{d}3\,\mathrm{d}4\Bigg) \\ &- \tfrac{1}{4}S_0(0)\left(\frac{\partial}{\partial\rho}\left(\rho^2\int g_0(1,2)w(1,2)\,\mathrm{d}2\right)^2\right)\end{aligned} \tag{5.2.15}$$

where $S_0(k)$ is the structure factor of the reference system.

We see from (5.2.15) that a calculation of the second-order term requires a knowledge of the three- and four-particle distribution functions of the reference system. The situation is even more complicated for higher-order terms, since the calculation of F_n requires the distribution functions of all orders up to and including $2n$. By the same rule, calculation of the first-order term requires only the pair distribution function of the reference system. If ε defines the energy scale of the perturbation, truncation at first order is likely to be justified whenever $\beta\varepsilon \ll 1$. The fact that second- and higher-order terms are determined by fluctuations in the total perturbation energy suggests that they should be small, relative to F_1, whenever the perturbing potential is a very smoothly varying function of particle separation. Schemes that simplify the calculation of F_2 have been devised, but the high-temperature expansion remains easiest to apply in situations where terms beyond first order are negligible. The question of whether or not a first-order treatment is adequate depends on the thermodynamic state, the form of the potential $v(1,2)$, and the manner in which $v(1,2)$ is divided into a reference-system potential and a perturbation.

If the reference system is the hard-sphere fluid and the perturbation potential $w(1,2)$ is very long ranged, the high-temperature expansion limited to first order reduces to the van der Waals equation (5.1.2). It is necessary only that the range of $w(1,2)$ be large compared with the range of interparticle separations over which $g_0(1,2)$ is significantly different from its asymptotic value. Then, to a good approximation:

$$\frac{\beta F_1}{N} \approx \frac{\beta\rho}{2}\int w(\mathbf{r})\,\mathrm{d}\mathbf{r} = -\beta\rho a \tag{5.2.16}$$

where a is positive when the perturbing potential is attractive. On differentiating with respect to density we recover (5.1.2):

$$\frac{\beta P}{\rho} = \rho\frac{\partial}{\partial\rho}\left(\frac{\beta F_0}{N} + \frac{\beta F_1}{N}\right) = \frac{\beta P_0}{\rho} - \beta\rho a \tag{5.2.17}$$

Another important feature of the high-temperature expansion is the fact that the first-order approximation yields a rigorous upper bound on the free energy of the system of interest irrespective of the choice of reference system. This result is a further consequence of the Gibbs–Bogoliubov inequalities discussed in Appendix B in connection with the density-functional theory of Section 3.4. Consider two integrable, non-negative but otherwise arbitrary configuration-space functions $A(\mathbf{r}^N)$ and $B(\mathbf{r}^N)$, defined such that[7]

$$\int A\left(\mathbf{r}^N\right)\mathrm{d}\mathbf{r}^N = \int B\left(\mathbf{r}^N\right)\mathrm{d}\mathbf{r}^N \tag{5.2.18}$$

The argument in Appendix B shows that the two functions satisfy the inequality

$$\int A\left(\mathbf{r}^N\right)\ln A\left(\mathbf{r}^N\right)\mathrm{d}\mathbf{r}^N \geqslant \int A\left(\mathbf{r}^N\right)\ln B\left(\mathbf{r}^N\right)\mathrm{d}\mathbf{r}^N \tag{5.2.19}$$

We now make two particular choices for A and B. First, let

$$\begin{aligned} A(\mathbf{r}^N) &= \exp\bigl(\beta\bigl[F_0 - V_N(0)\bigr]\bigr) \\ B(\mathbf{r}^N) &= \exp\bigl(\beta\bigl[F_0 - V_N(1)\bigr]\bigr) \end{aligned} \tag{5.2.20}$$

It follows from (5.2.19) that

$$F \leqslant F_0 + \bigl[\bigl\langle V_N(1)\bigr\rangle_0 - \bigl\langle V_N(0)\bigr\rangle_0\bigr] = F_0 + \langle W_N\rangle_0 \tag{5.2.21}$$

This is precisely the inequality announced earlier. If we interchange the definitions of A and B, i.e. if we set

$$\begin{aligned} A(\mathbf{r}^N) &= \exp\bigl(\beta\bigl[F_0 - V_N(1)\bigr]\bigr) \\ B(\mathbf{r}^N) &= \exp\bigl(\beta\bigl[F_0 - V_N(0)\bigr]\bigr) \end{aligned} \tag{5.2.22}$$

then we find from (5.2.19) that

$$F \geqslant F_0 + \langle W_N\rangle_1 \tag{5.2.23}$$

where the average of the perturbation energy is now taken over the ensemble of the system of interest. This result is less useful than (5.2.21), because the properties of the system of interest are in general unknown. With the assumption of pairwise additivity, (5.2.21) and (5.2.23) may be combined in the form

$$\frac{\beta F_0}{N} + \frac{\beta\rho}{2}\int g(\mathbf{r})w(\mathbf{r})\,\mathrm{d}\mathbf{r} \leqslant \frac{\beta F}{N} \leqslant \frac{\beta F_0}{N} + \frac{\beta\rho}{2}\int g_0(\mathbf{r})w(\mathbf{r})\,\mathrm{d}\mathbf{r} \tag{5.2.24}$$

The second of the inequalities (5.2.24) can be used as the basis for a variational approach to the calculation of thermodynamic properties.[8] The variational procedure consists in choosing a reference-system potential that depends on one or more parameters and then of minimising the last term on the right-hand side of (5.2.24) with respect to those parameters. As we shall see in the next section, the method has been applied with particular success[9] to systems of particles interacting through an inverse-power or "soft-sphere" potential of the form

$$v(r) = \varepsilon(\sigma/r)^n \tag{5.2.25}$$

In these calculations the reference system is taken to be a fluid of hard spheres and the hard-sphere diameter is treated as the single variational parameter. Still better results are obtained if a correction is made for the fact that the configuration space accessible to the hard-sphere and soft-sphere fluids is different for the two systems. The effect of this correction is to add to the right-hand side of (5.2.14) a term[10] involving a ratio of configuration integrals:

$$\frac{\beta\Delta F}{N} = \frac{1}{N}\ln\frac{\int_{\Omega_d}\exp[-\beta V_N(\mathbf{r}^N)]\,\mathrm{d}\mathbf{r}^N}{\int_{\Omega}\exp[-\beta V_N(\mathbf{r}^N)]\,\mathrm{d}\mathbf{r}^N} \tag{5.2.26}$$

where $V_N(\mathbf{r}^N)$ is the total potential energy of the system of interest (the soft-sphere fluid), Ω represents the full configuration space and Ω_d represents that part of configuration space

in which there is no overlap between hard spheres of diameter d. Since Ω_d is smaller than Ω, the correction is always negative, thereby lowering the upper bound on the free energy provided by the inequality (5.2.21). The correction term can be evaluated numerically by a Monte Carlo method,[10(b)] and an approximate but accurate expression for the term has been derived[9] that involves only the pair distribution function of the hard-sphere fluid.

5.3 SOFT-CORE REFERENCE SYSTEMS

Perturbation theories are useful only if they relate the properties of the system of interest to those of a well understood reference system. Hard spheres are an obvious choice of reference system, for the reasons discussed in Section 5.1. On the other hand, realistic intermolecular potentials do not have an infinitely steep repulsive core, and there is no natural separation into a hard-sphere part and a weak perturbation. Instead, an arbitrary division of the potential is made, as in (5.2.1), and the properties of the reference system, with potential $v_0(r)$, are then usually related to those of hard spheres in a manner independent of the way in which the perturbation is treated. In this section we discuss how the relation between the reference system and the system of hard spheres can be established, postponing the question of how best to separate the potential until Section 5.4. We describe in detail only the "blip-function" method of Andersen, Weeks and Chandler,[11] but we also show how results obtained earlier by Rowlinson[12] and by Barker and Henderson[13] can be recovered from the same analysis. In each case the free energy of the reference system is equated to that of a hard-sphere fluid at the same temperature and density. The hard-sphere diameter is, in general, a functional of $v_0(r)$ and a function of ρ and T, and the various methods of treating the reference system differ from each other primarily in the prescription used to determine d.

If the reference-system potential is harshly repulsive but continuous, the Boltzmann factor $e_0(r) = \exp[-\beta v_0(r)]$ typically has the appearance shown in Figure 5.2 and is not very different from the Boltzmann factor $e_d(r)$ of a hard-sphere potential. Thus, for a well chosen value of d, the function

$$\Delta e(r) = e_0(r) - e_d(r) \tag{5.3.1}$$

is effectively non-zero only over a small range of r which we denote by ξd. The behaviour of $\Delta e(r)$ as a function of r is sketched in Figure 5.2; the significance of the name "blip function" given to it is obvious from the figure.

When ξ is small it is natural to seek an expansion of the properties of the reference system about those of hard spheres in powers of ξ. Such a series can be derived by making a functional Taylor expansion of the reduced free-energy density $\phi = -\beta F^{\text{ex}}/V$ in powers of $\Delta e(r)$, i.e.

$$\phi = \phi_d + \int \left.\frac{\delta\phi}{\delta e(\mathbf{r})}\right|_{e=e_d} \Delta e(\mathbf{r})\,\mathrm{d}\mathbf{r} + \tfrac{1}{2}\iint \left.\frac{\delta^2\phi}{\delta e(\mathbf{r})\delta e(\mathbf{r}')}\right|_{e=e_d} \mathrm{d}\mathbf{r}\,\mathrm{d}\mathbf{r}' + \cdots \tag{5.3.2}$$

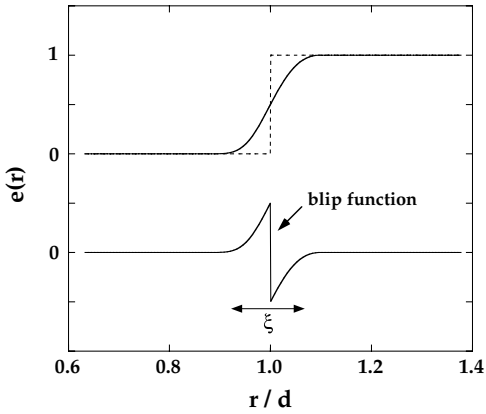

FIG. 5.2. The blip function. The upper part of the figure shows the Boltzmann factors $e_0(r)$ and $e_d(r)$ for soft-core (full curve) and hard-sphere (dashes) potentials, respectively; the lower part shows the blip function, $\Delta e(r) = e_0(r) - e_d(r)$.

where ϕ_d is the free-energy density of the hard-sphere fluid. We know from (2.5.23) and (3.4.8) that the functional derivative of ϕ with respect to $e(\mathbf{r})$ is

$$\frac{\delta\phi}{\delta e(\mathbf{r})} = \tfrac{1}{2}\rho^2 y(\mathbf{r}) \tag{5.3.3}$$

Equation (5.3.2) can therefore be rewritten as

$$\phi = \phi_d + \tfrac{1}{2}\rho^2 \int y_d(\mathbf{r})\,\Delta e(\mathbf{r})\,\mathrm{d}\mathbf{r} + \cdots \tag{5.3.4}$$

The expression for the second-order term involves the three- and four-particle distribution functions of the hard-sphere system, but terms beyond first order are not needed for steep potentials.

Since the range of $\Delta e(r)$ is ξd, the first-order term in the expansion (5.3.2) is of order ξ. A natural choice of d is one that causes the first-order term to vanish; d is then determined by the implicit relation

$$\int y_d(r)\,\Delta e(r)\,\mathrm{d}\mathbf{r} = 0 \tag{5.3.5}$$

With this choice of d, the second-order term in (5.3.2), which would normally be of order ξ^2, becomes of order ξ^4. Thus the free-energy density of the reference system is related to that of the hard-sphere fluid by

$$\phi_0 = \phi_d + \mathcal{O}(\xi^4) \tag{5.3.6}$$

where d is defined by (5.3.5).

Equation (5.3.5) represents only one of many possible prescriptions for calculating the diameter of the "equivalent" hard spheres. Because $\Delta e(r)$ is non-zero only in a narrow range of r, the factor $r^2 y_d(r)$ in (5.3.5) can be expanded in a Taylor series about $r = d$ in the form

$$r^2 y_d(r) = \sigma_0 + \sigma_1\left(\frac{r}{d} - 1\right) + \sigma_2\left(\frac{r}{d} - 1\right)^2 + \cdots \tag{5.3.7}$$

with

$$\frac{\sigma_m}{d^m} = \frac{d^m}{dr^m} r^2 y_d(r)\bigg|_{r=d} \tag{5.3.8}$$

Substitution of the expansion (5.3.7) in (5.3.5) gives

$$\sum_{m=0}^{\infty} \frac{\sigma_m}{m!} I_m = 0 \tag{5.3.9}$$

where

$$\begin{aligned} I_m &= \int_0^\infty \left(\frac{r}{d} - 1\right)^m \Delta e(r)\, \mathrm{d}(r/d) \\ &= -\frac{1}{m+1}\int_0^\infty \left(\frac{r}{d} - 1\right)^{m+1} \frac{\mathrm{d}}{\mathrm{d}r} \exp\bigl[-\beta v_0(r)\bigr]\, \mathrm{d}r \end{aligned} \tag{5.3.10}$$

If $v_0(r)$ varies rapidly with r, the derivative in (5.3.10) is approximately a δ-function at $r = d$ and the series (5.3.9) is rapidly convergent. If only the first term is retained, then $I_0 = 0$, and a straightforward integration shows that

$$d = \int_0^\infty \bigl(1 - \exp\bigl[-\beta v_0(r)\bigr]\bigr)\, \mathrm{d}r \tag{5.3.11}$$

This expression is identical to one derived in a different way by Barker and Henderson.[13] In the case when $v_0(r)$ is a soft-sphere potential of the form (5.2.25), the integral in (5.3.11) can be evaluated explicitly in terms of the Γ-function to give

$$d = \sigma(\varepsilon/k_\mathrm{B}T)^{1/n}\Gamma\left(\frac{n-1}{n}\right) = \sigma(\varepsilon/k_\mathrm{B}T)^{1/n}(1 + \gamma/n) + \mathcal{O}\bigl(1/n^2\bigr) \tag{5.3.12}$$

where $\gamma = 0.5772\ldots$ is Euler's constant. On discarding terms of order $1/n^2$ we recover an expression due to Rowlinson.[12] Rowlinson's calculation is based on an expansion of the free energy in powers of the inverse steepness parameter $\lambda = 1/n$ about $\lambda = 0$ (hard spheres); the work of Barker and Henderson may be regarded as a generalisation of Rowlinson's method to a repulsive potential of arbitrary form.

The main difference between (5.3.5) and (5.3.11) lies in the fact that the former yields a hard-sphere diameter that is a function of both density and temperature, whereas the

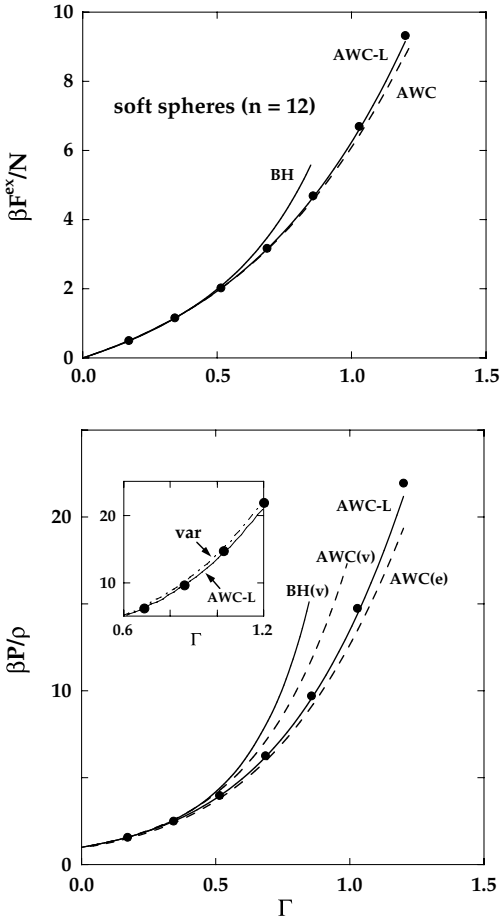

FIG. 5.3. Thermodynamic properties of the r^{-12} fluid.[9,11,13,15] The points are Monte Carlo results[14] and the curves show the predictions of perturbation theory: BH, method of Barker and Henderson, based on (5.3.11); AWC and AWC-L, method of Andersen, Weeks and Chandler, based on (5.3.5) and (5.3.16), respectively. Pressures are calculated from either the virial, (v), or energy, (e), routes, which yield identical results when (5.3.16) is used. The curve labelled "var" in the inset shows the results of a variational calculation[9] in which the correction represented by (5.2.26) is included.

Barker–Henderson diameter is dependent only on temperature. The greater flexibility provided by the use of (5.3.5) ensures that the predictions of the Andersen–Weeks–Chandler approach are, in general, superior to those of the Barker–Henderson theory. The agreement with the results of computer simulations is illustrated for the case of the potential (5.2.25) with $n = 12$ (the r^{-12} fluid) in Figure 5.3. The differences between the results of the two theories becomes smaller as the potential $v_0(r)$ becomes steeper. For inverse-power potentials of this type the excess thermodynamic properties have simple scaling properties, and quantities such as those plotted in the figure are determined by the single, dimensionless

parameter Γ defined as

$$\Gamma = \rho\sigma^3\left(\frac{\varepsilon}{k_{\mathrm{B}}T}\right)^{3/n} \tag{5.3.13}$$

The Andersen–Weeks–Chandler theory also yields a very simple expression for the pair distribution function of the reference system. It follows from (5.3.3) and (5.3.4) that

$$y_0(r) = y_d(r) + \text{higher-order terms} \tag{5.3.14}$$

where the higher-order terms are of order ξ^2 or smaller if d is chosen to satisfy (5.3.5). Thus

$$g_0(r) = \exp\bigl[-\beta v_0(r)\bigr] y_0(r) \approx \exp\bigl[-\beta v_0(r)\bigr] y_d(r) \tag{5.3.15}$$

This expression for the reference-system pair distribution function can now be used, via (5.2.14), to compute the correction to the free energy that results from a perturbing potential $w(r)$. It also allows us to rewrite (5.3.5) in terms of the $k \to 0$ limits of the reference-system and hard-sphere structure factors in the form $S_0(0) = S_d(0)$. Use of the hard-sphere diameter defined by (5.3.5) therefore has the effect of setting the compressibility of the reference system equal to that of the underlying hard-sphere fluid. Equation (5.3.15) is expected to be less accurate than the expression for the free energy, (5.3.6), because the neglected terms are now of order ξ^2 rather than ξ^4. This is borne out by calculations made for the r^{-12}-fluid; the approximate $g_0(r)$ is in only moderate agreement with the results of simulations[14] whereas the agreement obtained for the free energy is very good, as illustrated in Figure 5.3. The situation improves markedly when a much steeper reference potential is involved.

Although the blip-function method works satisfactorily so far as the calculation of thermodynamic properties is concerned, it is clear from Figure 5.3 that there is scope for improvement at large values of Γ, i.e. at high densities or low temperatures. There is also a lack of internal consistency in the theory: pressures calculated from the virial equation (2.5.22) via (5.3.15) differ significantly from those obtained by numerical differentiation of the free energy. The results derived from the free energy are the more reliable, but they are also more troublesome to compute. Equivalence of the two routes to the equation of state is guaranteed, however, if the hard-sphere diameter is calculated, not from (5.3.5), but from the relation[15]

$$\int \frac{\partial y_d(r)}{\partial d}\,\Delta e(\mathbf{r})\,\mathrm{d}\mathbf{r} = 0 \tag{5.3.16}$$

Equation (5.3.16) is derived by requiring that the free energy of the system of interest be a minimum with respect to variations in the hard-sphere function $y_d(r)$. As Figure 5.3 shows, the results obtained for the pressure of the r^{-12}-fluid are thereby much improved.

The blip-function expansion was designed specifically to treat the case of strongly repulsive potentials. This is the case for the Lennard-Jones fluid, which we discuss in the next section. In the repulsive region the Lennard-Jones potential varies much more rapidly than r^{-12}, and the accuracy of the blip-function method in such circumstances could

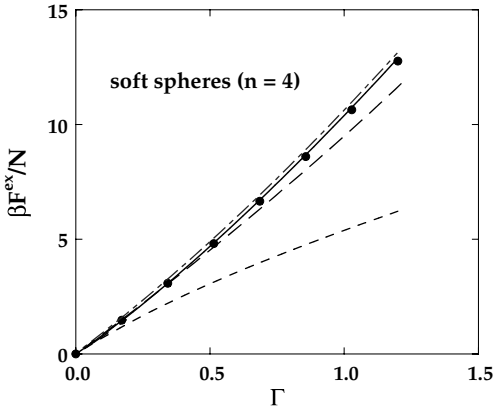

FIG. 5.4. Thermodynamic properties of the r^{-4} fluid. The points are Monte Carlo results and the curves show the predictions of different theories: blip-function method based on (5.3.5) (short dashes) or (5.3.16) (long dashes), and variational theory based on a hard-sphere reference system with (full curve) or without (chain curve) the correction represented by (5.2.26). After Ben-Amotz and Stell.[9]

scarcely be improved upon. The method is less satisfactory for the softer repulsions relevant to liquid metals, because truncation of the expansion (5.3.2) after the first-order term is no longer justified. By contrast, though we see from Figure 5.3 that the hard-sphere variational approach described in Section 5.2 is comparable in accuracy with blip-function theory for $n = 12$, it also retains its accuracy even for $n = 4$ while the first-order blip-function method does not. This is clear from the results shown in Figure 5.4. We also see that within blip-function theory the two prescriptions for the hard-sphere diameter, (5.3.5) and (5.3.16), give rise to significantly larger differences in free energy as the potential is softened. The correction (5.2.26) to the variational calculation is small but not negligible.

5.4 AN EXAMPLE: THE LENNARD-JONES FLUID

The λ-expansion described in Section 5.2 is suitable for treating perturbations that vary slowly in space, while the blip-function expansion and related methods of Section 5.3 provide a good description of reference systems for which the potential is rapidly varying but localised. In this section we show how the two approaches can be combined in a case where the pair potential has both a steep but continuous, repulsive part and a weak, longer ranged attraction. The example we choose is that of the Lennard-Jones fluid, a system for which sufficient data are available from computer simulations to allow a complete test to be made of different perturbation schemes.[16]

At first sight it might appear that the complications due to softness of the core would make it more difficult to obtain satisfactory results by perturbation theory than in situations where the potential consists of a hard-sphere interaction and a tail. This is not necessarily true, however, because there is now the extra flexibility provided by the arbitrary separation of the potential into a reference part, $v_0(r)$, and a perturbation, $w(r)$. A judicious choice of separation can significantly enhance the rate of convergence of the resulting perturbation

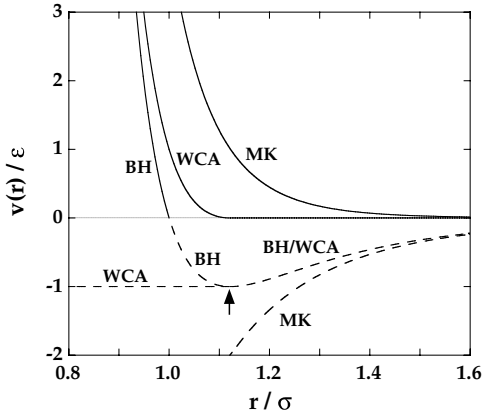

FIG. 5.5. Three separations of the Lennard-Jones potential that have been used in perturbation-theory calculations: MK, by McQuarrie and Katz:[17] BH, by Barker and Henderson;[13] WCA, by Weeks, Chandler and Andersen.[19] Full curves: the reference-system potential; dashes: the perturbation. The arrow marks the position of the minimum in the full pair potential; at larger values of r the Barker–Henderson and WCA choices of perturbation are the same.

series. A number of separations have been proposed for the Lennard-Jones potential, the best known of which are the three illustrated in Figure 5.5.

In the method of McQuarrie and Katz[17] the r^{-12} term is chosen as the reference-system potential and the r^{-6} term is treated as a perturbation. Given a scheme in which the properties of the reference system are calculated accurately, the method works well at temperatures above $T^* \approx 3$. At lower temperatures, however, the results are much less satisfactory. This is understandable, since the reference-system potential is considerably softer than the full potential in the region close to the minimum in $v(r)$. In the separation used by Barker and Henderson[13] the reference system is defined by that part of the full potential which is positive ($r < \sigma$) and the perturbation consists of the part that is negative ($r > \sigma$). The reference-system properties are then related to those of hard spheres of diameter d given by (5.3.11). In contrast to the case of the r^{-12} potential (see Figure 5.3), this treatment of the reference system yields very accurate results. The corrections due to the perturbation are handled in the framework of the λ-expansion; the first-order term is calculated from (5.2.14), with $g_0(r)$ taken to be the pair distribution function of the equivalent hard-sphere fluid. At $T^* = 0.72$ and $\rho^* = 0.85$, which is close to the triple point of the Lennard-Jones fluid, the results are $\beta F_0/N = 3.37$ and $\beta F_1/N = -7.79$. Thus the sum of the two leading terms is equal to -4.42, whereas the resulted obtained for the total excess free energy from Monte Carlo calculations[16] is $\beta F/N = -4.87$. The sum of all higher-order terms in the λ-expansion is therefore far from negligible; detailed calculations show that the second-order term accounts for most of the remainder.[16(a)] The origin of the large second-order term lies in the way in which the potential is separated. As Figure 5.5 reveals, the effect of dividing $v(r)$ at $r = \sigma$ is to include in the perturbation the rapidly varying part of the potential between $r = \sigma$ and the minimum at $r = r_m \approx 1.122\sigma$. Since the pair distribution function has its maximum value in the same range of r, fluctuations in the total perturbation energy W_N, and hence the numerical values of F_2, are large.

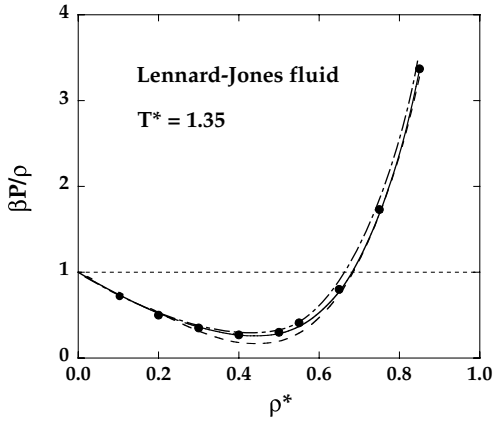

FIG. 5.6. Equation of state of the Lennard-Jones fluid along the isotherm $T^* = 1.35$. The points are Monte Carlo results and the curves show the predictions of perturbation theory. Dashes: WCA theory; chain curve: first-order Barker–Henderson theory; full curve: second-order Barker–Henderson theory. After Barker and Henderson.[18]

The work of Barker and Henderson is a landmark in the development of liquid-state theory, since it demonstrated for the first time that thermodynamic perturbation theory is capable of yielding quantitatively reliable results even for states close to the triple point of the system of interest. A drawback to their method is the fact that its successful implementation requires a careful evaluation of the second-order term in the λ-expansion. The calculation of F_2 from (5.2.15) requires further approximations to be made, and although the hard-sphere data that allow such a calculation are available in analytical form[18] the theory is inevitably more awkward to handle than is the case when a first-order treatment is adequate. Nonetheless, as Figure 5.6 illustrates, the calculated equation of state is in excellent agreement with the results of simulations.

The problem of the second-order term can be overcome by dividing the potential in the manner of Weeks, Chandler and Andersen,[19] usually called the WCA separation. In this method, the potential is split at $r = r_m$ into its purely repulsive ($r < r_m$) and purely attractive ($r > r_m$) parts; the former defines the reference system and the latter constitutes the perturbation. To avoid a discontinuity at $r = r_m$, $w(r)$ is set equal to $-\varepsilon$ for $r < r_m$ and $v_0(r)$ is shifted upwards by a compensating amount. Compared with the Barker–Henderson separation, the perturbation now varies more slowly over the range of r corresponding to the first peak in $g(r)$, and the perturbation series is therefore more rapidly convergent. For example, at $T^* = 0.72$, $\rho^* = 0.85$, the reference-system free energy is $\beta F_0/N = 4.49$ and the first-order correction in the λ-expansion is -9.33; the sum of the two terms is -4.84, which differs by less than 1% from the Monte Carlo result for the full potential.[16(b)] Agreement of the same order is found throughout the high-density region and the perturbation series may confidently be truncated after the first-order term. The difficulties associated with the calculation of the second- and higher-order terms are thereby avoided. At high densities, on the other hand, the hard-sphere diameter calculated for the WCA separation may correspond to a packing fraction lying in the metastable region beyond the fluid–solid transition. This limits the range of applicability of the theory at supercritical temperatures.[20]

In the calculations summarised above, and in most of those based on the WCA separation, the free energy of the reference system is related to that of hard spheres through (5.3.5) and (5.3.6). At high densities, the error (of order ξ^4) thereby introduced is very small. Under the same conditions, use of the approximate relation (5.3.15) to calculate the first-order correction from (5.2.14) also involves only a very small error. Some results for the Lennard-Jones fluid along a near-critical isotherm are shown in Figure 5.6. The general level of agreement with the results of computer simulations is good and at high densities is comparable with that achieved by the Barker–Henderson method taken to second order. At low densities the attractive forces play an important role in determining the structure and the key assumption of a first-order theory, namely that $g(r) \approx g_0(r)$, is no longer valid. New methods are then required, as we discuss in detail in the next section.

5.5 TREATMENT OF ATTRACTIVE FORCES

Situations in which the influence of the attractive forces on the structure cannot be ignored may be treated by methods similar to those used when the perturbation is both weak and very long ranged relative to the reference-system potential. In such cases the natural expansion parameter is the inverse range rather than the strength of the perturbation; this leads to the so-called γ-expansion,[21] the nature of which differs significantly from that of the λ-expansion described in Section 5.2. The early work on the γ-expansion was motivated by the fact that an exact solution can be found for the one-dimensional model of hard rods of length d that attract each other via the potential

$$w_\gamma(x) = -a\gamma \exp(-\gamma x), \quad a\gamma > 0 \tag{5.5.1}$$

where γ is an inverse-range parameter; the integral of $w_\gamma(x)$ over all one-dimensional space is independent of γ and equal to $-a$. Kac, Uhlenbeck and Hemmer[22] have shown that in the limit $\gamma \to 0$, taken *after* the thermodynamic limit, the pressure is given by the one-dimensional van der Waals equation, i.e.

$$\lim_{\gamma \to 0} \frac{\beta P}{\rho} = \frac{1}{1-\rho d} - \beta\rho a \tag{5.5.2}$$

where the first term on the right-hand side represents the exact equation of state of the hard-rod reference system. This result was later extended to three dimensions and it was proved rigorously that in the limit where the perturbation is both infinitesimally strong and infinitely long ranged, the equation of state is given exactly by the generalised van der Waals equation (5.1.2).

The γ-expansion is obtained by considering perturbations of the general form

$$w_\gamma(r) = -\gamma^3 f(\gamma r) \tag{5.5.3}$$

and expanding the properties of the system of interest in powers of γ. If R is the range of the reference-system potential (e.g. the hard-sphere diameter), the dimensionless parameter of the expansion is $\delta = (\gamma R)^3$; δ is roughly the ratio of the reference-system interaction

volume (e.g. the volume of a hard sphere) to the total interaction volume. In most simple liquids the attractive forces are not truly long ranged in the sense of (5.5.3), but many of the results of the γ-expansion can usefully be carried over to such systems by setting $\gamma = 1$. However, rather than following the original derivation of the γ-expansion, we describe instead the closely related but simpler method of Andersen and Chandler.[23] In doing so, we make use of the diagrammatic definitions and lemmas of Section 3.7. We assume throughout that the pair potential has the general form given by (5.1.3).

We first require the diagrammatic expansion of the excess Helmholtz free energy. This can be derived from the corresponding expansion of the single-particle direct correlation function given by (3.8.6), taken for the case of zero external field. By comparison of (3.8.6) with the definition of $c^{(1)}(\mathbf{r})$ in (3.5.1) it can be deduced that the reduced free-energy density $\phi = -\beta F^{\text{ex}}/V$ introduced in Section 5.3 is expressible diagrammatically as

$V\phi =$ [all irreducible diagrams consisting of two or more black ρ-circles and f-bonds]

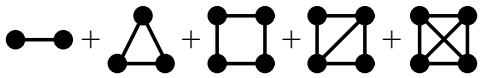

(5.5.4)

If (5.5.4) is inserted in (3.5.1), a simple application of Lemma 2 leads back to (3.8.6).

The separation of the pair potential in (5.1.3) means that the Mayer function $f(1,2)$ can be factorised as

$$f(1,2) = f_0(1,2) + \big[1 + f_0(1,2)\big]\big(\exp\big[\Psi(1,2)\big] - 1\big) \tag{5.5.5}$$

where $f_0(1,2)$ is the Mayer function of the reference system and

$$\Psi(1,2) = -\beta w(1,2) \tag{5.5.6}$$

Since the perturbation is weak, the exponential term in (5.5.5) can be expanded to give

$$f(1,2) = f_0(1,2) + \big[1 + f_0(1,2)\big]\sum_{n=1}^{\infty} \frac{[\Psi(1,2)]^n}{n!} \tag{5.5.7}$$

The form of (5.5.7) suggests the introduction of two different types of bond: short-range f_0-bonds and long-range Ψ-bonds. The presence of two types of bond transforms the simple diagrams in (5.5.4) into composite diagrams in which two circles are linked by at most one f_0-bond but an arbitrary number of Ψ-bonds. We recall from Section 3.7 that if two circles in a diagram are linked by n bonds of a given species, the symmetry number of the diagram is increased, and its value decreased, by a factor $n!$; this takes care of the factors $1/n!$ in (5.5.7). The complete expansion of a in terms of composite diagrams is

$V\phi =$ [all irreducible diagrams consisting of two or more black ρ-circles, f_0-bonds and Ψ-bonds, where each pair of circles is linked by any number of Ψ-bonds but at most one f_0-bond] (5.5.8)

The corresponding expansion of the pair distribution function can be obtained from (3.4.8). Written in the notation of the present section the latter becomes

$$\rho^2 g(1,2) = 2V \frac{\delta \phi}{\delta \Psi(1,2)} \tag{5.5.9}$$

and the diagrammatic prescription for $g(1,2)$ follows immediately from application of Lemma 3.

The sum of all diagrams in (5.5.8) in which only f_0-bonds appear yields the free-energy density ϕ_0 of the reference system. The f_0-bonds in the other diagrams can be replaced in favour of h_0-bonds by a process of topological reduction based on Lemma 5. This leads to the elimination of diagrams containing "reference articulation pairs", which are pairs of circles linked by one or more independent paths consisting exclusively of black circles linked by reference-system bonds.[24] Of the diagrams that remain after the topological reduction there are two of order ρ^2 that contain only a single Ψ-bond. The sum of the two is written as

$V\phi_{\mathrm{HTA}} =$ 

$$= \tfrac{1}{2}\rho^2 \iint \left[\Psi(1,2) + h_0(1,2)\Psi(1,2)\right] \mathrm{d}1\,\mathrm{d}2$$

$$= -\frac{V\beta\rho^2}{2} \int g_0(\mathbf{r}) w(\mathbf{r})\, \mathrm{d}\mathbf{r} \tag{5.5.10}$$

where a broken line represents an h_0-bond, a solid line represents a Ψ-bond and HTA stands for "high-temperature approximation". Comparison of (5.5.10) with (5.2.14) shows that the HTA is equivalent to truncation of the λ-expansion after the first-order term, with

$$\phi_{\mathrm{HTA}} = -\frac{\beta F_1}{V} \tag{5.5.11}$$

The corresponding approximation to $g(1,2)$ is given by a trivial application of Lemma 3. If $\phi \approx \phi_{\mathrm{HTA}}$ we find from (5.5.10) that

$$\rho^2 g(1,2) \approx 2V \frac{\delta \phi_{\mathrm{HTA}}}{\delta \Psi(1,2)}$$

$$= \rho^2 + \rho^2 h_0(1,2) = \rho^2 g_0(1,2) \tag{5.5.12}$$

in agreement with the results of Section 5.3.

To proceed beyond the HTA it is necessary to sum a larger class of diagrams in the expansion of ϕ. An approximation similar in spirit to the Debye–Hückel theory of ionic fluids is

$$\phi \approx \phi_0 + \phi_{\mathrm{HTA}} + \phi_{\mathrm{R}} \tag{5.5.13}$$

where

$V\phi_{\mathrm{R}} =$ 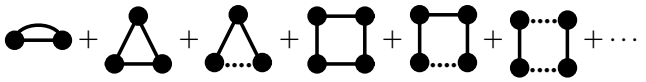 (5.5.14)

is the sum of all simple "ring" diagrams plus the diagram consisting of two black circles linked by two Ψ-bonds; the absence of reference articulation pairs means that none of the ring diagrams in (5.5.14) contains two successive h_0-bonds. The approximation to $g(1,2)$ obtained by applying Lemma 3 is now

$$g(1,2) \approx g_0(1,2) + C(1,2) \tag{5.5.15}$$

where the function $C(1,2)$ is given by

$$\begin{aligned}\rho^2 C(1,2) = [&\text{all chain diagrams consisting of two terminal white}\\ &\rho\text{-circles labelled 1 and 2, black } \rho\text{-circles, } \Psi\text{-bonds}\\ &\text{and } h_0\text{-bonds, where there are never two successive}\\ &h_0\text{-bonds}]\end{aligned} \tag{5.5.16}$$

If the reference system is the ideal gas and if $w(r)$ is the Coulomb potential, then $-k_{\mathrm{B}}TC(1,2)$ is the screened potential $\psi(r)$ of (4.6.25) and (5.5.15) reduces to the linearised Debye–Hückel result (4.6.27). For the systems of interest here, $-k_{\mathrm{B}}TC(1,2)$ is a renormalised potential in which the perturbation is screened by the order imposed on the fluid by the short-range interaction between particles.

The function $C(1,2)$ can be evaluated by Fourier transform techniques similar to those used in the derivation of the Debye–Hückel result. We first group the chain diagrams according to the number of Ψ-bonds they contain. Let $C^{(n)}(1,2)$ be the sum of all chain diagrams with precisely n Ψ-bonds. Then

$$\rho^2 C(1,2) = \rho^2 \sum_{n=1}^{\infty} C^{(n)}(1,2) \tag{5.5.17}$$

where

$\rho^2 C^{(1)}(1,2) =$ 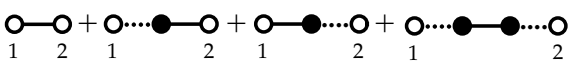 (5.5.18)

and so on. Any diagram that contributes to $C^{(n)}$ contains at most $(n+1)$ h_0-bonds and $C^{(n)}$ consists of 2^{n+1} topologically distinct diagrams.

The sum of all diagrams in $C^{(n)}(1,2)$ may be represented by a single "generalised chain" in which circles are replaced by *hypervertices*. A hypervertex of order n is associated with a function of n coordinates, $\Sigma(1,\ldots,n)$, and is pictured as a large circle surrounded by

n white circles; the latter correspond, as usual, to the coordinates $\mathbf{r}_1, \ldots, \mathbf{r}_n$. For present purposes we need consider only the hypervertex of order two associated with the reference-system function $\Sigma_0(1,2)$ defined as

$$\Sigma_0(1,2) = \rho\delta(1,2) + \rho^2 h_0(1,2)$$
$$= \quad 1 \quad 2 \tag{5.5.19}$$

We can then re-express $C^{(n)}(1,2)$ for $n=1$ and $n=2$ in the form

$$\rho^2 C^{(1)}(1,2) = \iint \Sigma_0(1,3)\Psi(3,4)\Sigma_0(4,2)\,\mathrm{d}3\,\mathrm{d}4 \tag{5.5.20}$$
$$= \quad 1 \quad 2$$

$$\rho^2 C^{(2)}(1,2) = \quad 1 \quad 2 \tag{5.5.21}$$

and $\rho^2 C^{(n)}(1,2)$ for any n is represented by a generalised chain consisting of n Ψ-bonds and $(n+1)$ Σ_0-hypervertices. Each generalised chain corresponds to a convolution integral with a Fourier transform given by

$$\rho^2 \widehat{C}^{(n)}(\mathbf{k}) = \left[\widehat{\Sigma}_0(\mathbf{k})\widehat{\Psi}(\mathbf{k})\right]^n \widehat{\Sigma}_0(\mathbf{k}) \tag{5.5.22}$$

where $\widehat{\Sigma}_0(\mathbf{k})$ is related to the structure factor of the reference system by $\widehat{\Sigma}_0(\mathbf{k}) = \rho S_0(\mathbf{k})$ and $\widehat{\Psi}(\mathbf{k}) = -\beta\widehat{w}(\mathbf{k})$. If $|\widehat{\Sigma}_0(\mathbf{k})\widehat{\Psi}(\mathbf{k})| < 1$, the Fourier transform of the function $C(1,2)$ is obtained as the sum of a geometric series:

$$\rho^2 \widehat{C}(\mathbf{k}) = \sum_{n=1}^{\infty} \rho^2 \widehat{C}^{(n)}(\mathbf{k}) = \frac{[\widehat{\Sigma}_0(\mathbf{k})]^2 \widehat{\Psi}(\mathbf{k})}{1 - \widehat{\Sigma}_0(\mathbf{k})\widehat{\Psi}(\mathbf{k})} = -\frac{\rho^2 [S_0(\mathbf{k})]^2 \beta\widehat{w}(\mathbf{k})}{1 + \rho S_0(\mathbf{k})\beta\widehat{w}(\mathbf{k})} \tag{5.5.23}$$

The derivation of (5.5.23) tends to obscure the basic simplicity of the theory. If (4.1.5), (5.5.15) and (5.5.23) are combined, we find that the structure factor of the system of interest is related to that of the reference fluid by

$$S(\mathbf{k}) = S_0(\mathbf{k}) - \frac{\rho[S_0(\mathbf{k})]^2 \beta\widehat{w}(\mathbf{k})}{1 + \rho S_0(\mathbf{k})\beta\widehat{w}(\mathbf{k})} = \frac{S_0(\mathbf{k})}{1 + \rho S_0(\mathbf{k})\beta\widehat{w}(\mathbf{k})} \tag{5.5.24}$$

On the other hand, we find with the help of (3.6.10) that the exact relation between the two structure factors is given in terms of the corresponding direct correlation functions by

$$S(\mathbf{k}) = \frac{S_0(\mathbf{k})}{1 - \rho[\hat{c}(\mathbf{k}) - \hat{c}_0(\mathbf{k})]S_0(\mathbf{k})} \tag{5.5.25}$$

Use of (5.5.24) is therefore equivalent to replacing the true direct correlation function by the random-phase approximation (RPA) of (3.5.17), i.e.

$$c(r) \approx c_0(r) - \beta w(r) \tag{5.5.26}$$

which is asymptotically correct if the perturbation contains the long-range part of the potential. The Debye–Hückel approximation corresponds to writing $c(r) \approx -\beta w(r)$; (5.5.26) improves on this by building in the exact form of the direct correlation function of the reference system.

The RPA approximation for the free energy is obtained by combining (5.5.10), (5.5.13) and (5.5.14). When functionally differentiated with respect to $\Psi(1,2)$ according to the rule (5.5.12), the total ring-diagram contribution to ϕ yields the function $C(1,2)$. It follows that $V\phi_{\mathrm{R}}$ can be expressed diagrammatically as

$$V\phi_{\mathrm{R}} = \sum_{n=2}^{\infty} R^{(n)} \tag{5.5.27}$$

where $R^{(n)}$ is a generalised ring consisting of Σ_0-hypervertices and Ψ-bonds. A generalised ring can be derived from a generalised chain by inserting a Ψ-bond between the white circles and integrating over the coordinates associated with those circles. Thus

$$\begin{aligned} R^{(n)} &= \frac{\rho^2}{2n} \iint C^{(n-1)}(1,2)\Psi(1,2)\,\mathrm{d}1\,\mathrm{d}2 \\ &= \frac{V\rho^2}{2n} \int C^{(n-1)}(\mathbf{r})\Psi(\mathbf{r})\,\mathrm{d}\mathbf{r} \\ &= \frac{V\rho^2}{2n}(2\pi)^{-3} \int \widehat{C}^{(n-1)}(\mathbf{k})\widehat{\Psi}(\mathbf{k})\,\mathrm{d}\mathbf{k} \end{aligned} \tag{5.5.28}$$

where the factor $1/2n$ comes from the symmetry number of the generalised ring. If we now substitute for $\widehat{C}^{(n-1)}(\mathbf{k})$ from (5.5.22) and assume again that $|\widehat{\Sigma}_0(\mathbf{k})\widehat{\Psi}(\mathbf{k})| < 1$, we find that the contribution to ϕ from the ring diagrams is

$$\begin{aligned} \phi_{\mathrm{R}} &= \left(\frac{1}{2\pi}\right)^3 \int \sum_{n=2}^{\infty} \frac{1}{2n}\left[\widehat{\Sigma}_0(\mathbf{k})\widehat{\Psi}(\mathbf{k})\right]^n \mathrm{d}\mathbf{k} \\ &= -\tfrac{1}{2}(2\pi)^{-3} \int \left(\widehat{\Sigma}_0(\mathbf{k})\widehat{\Psi}(\mathbf{k}) + \ln\left[1 - \widehat{\Sigma}_0(\mathbf{k})\widehat{\Psi}(\mathbf{k})\right]\right) \mathrm{d}\mathbf{k} \end{aligned} \tag{5.5.29}$$

This result is used in the discussion of hierarchical reference theory in Section 5.7.

We saw in Section 4.6 that a defect of the linearised Debye–Hückel approximation is the fact that it yields a pair distribution function that behaves unphysically at small separations. A similar problem arises here. Consider, for simplicity, the case in which the reference system is a fluid of hard spheres of diameter d. In an exact theory, $g(r)$ necessarily vanishes

for $r < d$, but in the approximation represented by (5.5.15) there is no guarantee that this will be so, since in general $C(r)$ will be non-zero in that region. There is, however, some flexibility in the choice of $C(r)$, and this fact can be usefully exploited. Although $C(r)$ is a functional of $w(r)$, it is obvious on physical grounds that the true properties of the fluid must be independent of the choice of perturbation for $r < d$. The unphysical behaviour of the RPA can therefore be eliminated by choosing $w(r)$ for $r < d$ in such a way that

$$C(r) = 0, \quad r < d \tag{5.5.30}$$

Comparison of (5.5.15) with the general rule (5.5.9) shows that this condition is equivalent to requiring the free energy to be stationary with respect to variations in the perturbing potential within the hard core. The RPA together with the condition (5.5.30) is called the "optimised" random-phase approximation or ORPA. The ORPA may also be regarded as a solution to the Ornstein–Zernike relation that satisfies both the closure relation (5.5.26) and the restriction that $g(r) = 0$ for $r < d$. It is therefore similar in spirit to the MSA of Section 4.5, the difference being that the treatment of the hard-sphere system is exact in the ORPA.

The derivation of (5.5.24) did not involve any assumption about the range of the potential $w(r)$. However, as we have seen in Section 3.5, the RPA can also be derived by treating the effects of the perturbation in a mean-field way, an approximation that is likely to work best when the perturbation is both weak and long ranged. In practice the optimised version of the theory gives good results for systems such as the Lennard-Jones fluid.[25] Not surprisingly, however, it is less successful when the attractive well in the potential is both deep and narrow.[26] In that case better results are obtained by replacing $-\beta w(r)$ in (5.5.26) by the corresponding Mayer function; this modification also ensures that $c(r)$ behaves correctly in the low-density limit.

A different method of remedying the unphysical behaviour of the RPA pair distribution function can be developed by extending the analogy with Debye–Hückel theory. If the reference system is the ideal gas, the RPA reduces to

$$g(1, 2) \approx 1 + C(1, 2) \tag{5.5.31}$$

When $w(r)$ is the Coulomb potential, this result is equivalent to the linearised Debye–Hückel approximation (4.6.27). If we add to the right-hand side of (5.5.28) the sum of all diagrams in the exact expansion of $h(1, 2)$ that can be expressed as star products of the diagram $C(1, 2)$ with itself, and then apply Lemma 1, we obtain an improved approximation in the form

$$\begin{aligned} g(1, 2) &\approx \exp C(1, 2) \\ &= 1 + \underset{1\quad 2}{\circ\!\!-\!\!\circ} + \underset{1\quad 2}{\circ\!\!\frown\!\!\circ} + \underset{1\quad 2}{\circ\!\!\rightleftharpoons\!\!\circ} + \cdots \end{aligned} \tag{5.5.32}$$

which is equivalent to the non-linear equation (4.6.26). In the present case a generalisation of the same approach replaces the RPA of (5.5.15) by the approximation

$$g(1, 2) \approx g_0(1, 2) \exp C(1, 2) \tag{5.5.33}$$

This is called the "exponential" or EXP approximation. At low density the renormalised potential behaves as $C(r) \approx \Psi(r) = -\beta w(r)$. In the same limit, $g_0(r) \approx \exp[-\beta v_0(r)]$. Thus, from (5.5.33):

$$\lim_{\rho \to 0} g(1,2) = \exp\bigl[-\beta v_0(r)\bigr] \exp\bigl[-\beta w(r)\bigr] = \exp\bigl[-\beta v(r)\bigr] \tag{5.5.34}$$

The EXP approximation, unlike either the HTA or the ORPA, is therefore exact in the low-density limit. Andersen and Chandler[23] give arguments to show that the contribution from diagrams neglected in the EXP approximation is minimised if the optimised $C(1,2)$ is used in the evaluation of (5.5.33) and the related expression for the free energy.

The ORPA and the EXP approximation with optimised $C(1,2)$ both correspond to a truncation of the diagrammatic expansion of the free energy in terms of ρ-circles, h_0-bonds and Ψ-bonds in which the perturbation inside the hard core is chosen so as to increase the rate of convergence. Each is therefore an approximation within a general theoretical framework called "optimised cluster theory". The optimised cluster expansion is not in any obvious way a systematic expansion in powers of a small parameter, but it has the great advantage of yielding successive approximations that are easy to evaluate if the pair distribution function of the reference system is known. The γ-expansion provides a natural ordering of the perturbation terms in powers of γ^3, but it leads to more complicated expressions for properties of the system of interest. If the perturbation is of the form of (5.5.3), the terms of order γ^3 in the expansion of the free energy consist of the second of the two diagrams in (5.5.10) (the HTA) and the sum of all diagrams in (5.5.14) (the ring diagrams). There is, in addition, a term of zeroth order in γ, given by the first of the two diagrams in (5.5.10), which in this case has the value

$$\frac{V\beta\rho^2\gamma^3}{2} \int f\bigl(\gamma^3 \mathbf{r}\bigr)\, \mathrm{d}\mathbf{r} = V\beta\rho^2 a \tag{5.5.35}$$

where a is the constant introduced in (5.2.16). We see that the effect of the volume integration is to reduce the apparent order of the term from γ^3 to γ^0. As a consequence, the free energy does not reduce to that of the reference system in zeroth order. It yields instead the van der Waals approximation; the latter is therefore exact in the limit $\gamma \to 0$. Through order γ^3, the free energy (with $\gamma = 1$) is the same as in the RPA. On the other hand, the sum of all terms of order γ^3 in the expansion of $g(1,2)$ contains diagrams additional to the chain diagrams included in (5.5.15).[27]

Results obtained by the optimised cluster approach for a potential model consisting of a hard-sphere core plus a Lennard-Jones tail at two different thermodynamic states are compared with the results of Monte Carlo calculations in Figure 5.7. In the lower-density state, the HTA, ORPA and EXP pair distribution functions represent successively improved approximations to the "exact" results. At the higher density, where the perturbation is heavily screened and the renormalised potential is correspondingly weak, the HTA is already very satisfactory. The difference in behaviour between the two states reflects the diminishing role of the attractive forces on the structure of the fluid as the density increases. Similar conclusions have been reached for other model fluids. Overall the results obtained by opti-

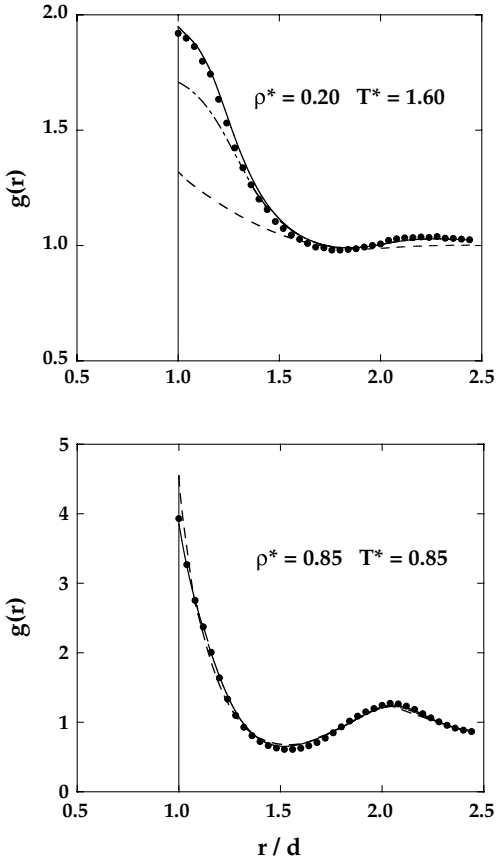

FIG. 5.7. Radial distribution function for a fluid of hard spheres with a Lennard-Jones tail at two different thermodynamic states. The points are Monte Carlo results and the curves show the predictions of perturbation theory. Dashes: HTA; chain curve; ORPA; full curves: EXP. After Stell and Weis.[28]

mised cluster methods are comparable in accuracy with those of conventional perturbation theory taken to second order.

5.6 MEAN-FIELD THEORY OF LIQUID–VAPOUR COEXISTENCE

Coexistence of liquid and vapour arises from a balance between repulsive and attractive intermolecular forces. In the absence of any attractive interactions, there is no liquid–vapour transition, and only one fluid phase appears. Since perturbation theory is based explicitly on a division of the pair potential into repulsive and attractive parts, it is a natural choice for the description of phenomena associated with condensation. The integral-equation approximations described in Chapter 4 provide another possible approach, but for the most part they either lead to spurious solutions or do not converge numerically in the thermody-

namic region of interest.[29] These failings are a consequence of the underlying singularities in thermodynamic properties, in particular the divergence of the isothermal compressibility at the critical point.

For a two-phase system to be in equilibrium, each phase must be at the same pressure (mechanical equilibrium) and temperature (thermal equilibrium). However, the pressure and temperature of a two-phase system are not independent variables, since equality of the chemical potentials or, equivalently, of the molar Gibbs free energies is also required. Thus, at equilibrium between liquid (L) and gas (G) in a one-component system:

$$\mu_{\mathrm{L}}(P,T)=\mu_{\mathrm{G}}(P,T) \tag{5.6.1}$$

If μ_{L} and μ_{G} are known from some approximate theory, (5.6.1) can be solved for P as a function of T to yield the phase-coexistence curve in the pressure–temperature plane. Condensation is a first-order phase transition, since it coincides with discontinuities in the first-order thermodynamic derivatives of the Gibbs free energy. The volume change, ΔV, corresponds to a discontinuity in $(\partial G/\partial P)_T$, while the change in entropy, ΔS, corresponds to a discontinuity in $(\partial G/\partial T)_P$; ΔS is related to the latent heat of the transition by $L = T\Delta S$. Differentiation of the equilibrium condition (5.6.1) with respect to temperature leads to the Clapeyron equation:

$$\frac{\mathrm{d}P}{\mathrm{d}T}=\frac{\Delta S}{\Delta V}=\frac{L}{T\Delta V} \tag{5.6.2}$$

Since V and S both increase on vaporisation, it follows that the slope of the coexistence curve is always positive.

We consider again a system for which the pair potential $v(r)$ consists of a hard-sphere repulsion supplemented by an attractive term, $w(r)$, for $r > d$, where, as usual, d is the hard-sphere diameter. If $w(r)$ is sufficiently long ranged, the free energy may be approximated by the first two terms of the λ-expansion of Section 5.2 or, within the mean-field approximation (5.2.16), by

$$\frac{\beta F}{N}=\frac{\beta F_0}{N}-\beta\rho a \tag{5.6.3}$$

where F_0, the free energy of the hard-sphere reference system, is a function only of the packing fraction η. The equation of state is then given by (5.2.17). We are interested primarily in the calculation of thermodynamic properties in the critical region. Since the critical density ρ_{c} is typically less than half that of the triple point, it is reasonable to approximate the hard-sphere pressure by the Percus–Yevick compressibility equation (4.4.12), which is very accurate at low to moderate densities. Thus

$$\frac{\beta P}{\rho}=\frac{1+\eta+\eta^2}{(1-\eta)^3}-\beta\rho a \tag{5.6.4}$$

Above a critical temperature T_{c}, to be determined below, the pressure isotherms calculated from (5.6.4) are single-valued, increasing functions of ρ, as sketched in Figure 5.8. Below T_{c}, however, so-called van der Waals loops appear, which contain an unphysical section between their maxima and minima where the isothermal compressibility would

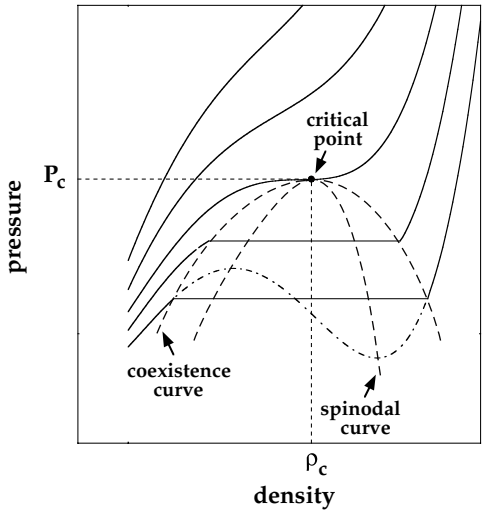

FIG. 5.8. Isotherms of a simple fluid in the pressure–density plane. The chain curve shows a van der Waals loop. Note that the Maxwell construction applies in the pressure–volume, not the pressure–density plane.

be negative, thereby violating one of the conditions necessary for stability of the system against fluctuations (see Appendix A). The unstable states are eliminated by replacing the loops by horizontal portions between points on the isotherm determined via the Maxwell equal-area construction in the P–V plane. The Maxwell construction is a graphical formulation of the requirement for equality of the pressures and chemical potentials of the two phases; it is equivalent[30] to the double-tangent construction on a plot of free energy versus volume, which ensures that F is always a convex function, i.e. that $(\partial^2 F/\partial V^2)_T > 0$. The end-points of the horizontal portions lie on the coexistence curve, while the locus of maxima and minima of the van der Waals loops, which separates the P–ρ plane into stable and unstable regions, forms the *spinodal* curve. States lying between the coexistence and spinodal curves are metastable, but can be reached experimentally if sufficient care is taken to prevent formation of the thermodynamically stable phase. As the temperature increases towards the critical value, the horizontal portion of the isotherm shrinks, eventually reducing to a point of inflection with a horizontal tangent. The critical parameters T_c and ρ_c are therefore determined by the conditions

$$\left(\frac{\partial P}{\partial \rho}\right)_{T=T_c} = 0, \qquad \left(\frac{\partial^2 P}{\partial \rho^2}\right)_{T=T_c} = 0 \tag{5.6.5}$$

The first of these conditions confirms that the compressibility diverges at the critical point; it also diverges everywhere along the spinodal curve, the apex of which coincides with the critical point. The two coexisting phases, liquid and vapour, merge at the critical point, so the transition, which is of first order below T_c, becomes of second order. Second-order transitions are characterised by discontinuities in the second derivatives of the free energy, of which the compressibility is one.

Equations (5.6.4) and (5.6.5) can be solved for the three unknowns: ρ_c, T_c and P_c (the critical pressure). Elimination of T and P leads to a cubic equation in ρ having two unphysical, negative roots and one positive root:

$$\rho_c d^3 \approx 0.245 \tag{5.6.6a}$$

with a corresponding critical temperature given by

$$k_B T_c \approx 0.179 a/d^3 \tag{5.6.6b}$$

and a critical compressibility ratio

$$Z_c = \frac{P_c}{\rho_c k_B T_c} \approx 0.359 \tag{5.6.6c}$$

Both ρ_c and Z_c are independent of the strength of the interparticle attraction, as measured by the value of the quantity a. The theoretical results can be compared with those obtained by molecular-dynamics calculations for a square-well fluid.[31] In this case, $a = \frac{2}{3}\varepsilon\pi d^3(\gamma^3 - 1)$, where γd is the range of the potential and ε is the depth of the square well (see Figure 1.2(a)). The simulations give $\rho_c d^3 \approx 0.34$, $k_B T_c \approx 0.25 a/d^3$ and $Z_c \approx 0.28$, so the agreement with theory is only semi-quantitative. The discrepancies can be ascribed to the use in the theory of the mean-field approximation for the first-order term in the high-temperature expansion and the neglect of higher-order terms. Although the fluctuations corresponding to the higher-order terms are small for liquids at densities close to freezing, they increase rapidly as the density is reduced.

The deficiencies of mean-field theory are also evident in the predictions to which it leads for the behaviour of thermodynamic properties in the immediate vicinity of the critical point. In the approximation represented by (5.6.4) the pressure is an analytic function of ρ and T over a range of packing fraction that extends well beyond the value corresponding to close packing, i.e. $\eta = \pi\sqrt{2}/6 \approx 0.74$. It is therefore legitimate to expand P around P_c in powers of the deviations $\Delta\rho = \rho - \rho_c$ and $\Delta T = T - T_c$. Expansion up to third order gives

$$P = P_c + P_{10}\Delta T + P_{11}\Delta T\,\Delta\rho + P_{03}(\Delta\rho)^3 + \cdots \tag{5.6.7}$$

where the coefficients P_{ij} are

$$P_{ij} = \left(\frac{\partial^{i+j} P}{\partial T^i \partial \rho^j}\right)_{\rho=\rho_c, T=T_c} \tag{5.6.8}$$

Terms in $\Delta\rho$ and $(\Delta\rho)^2$ are zero by virtue of the conditions (5.6.5) and other omitted terms play no role in the derivation that follows. Along the critical isotherm, $\Delta T = 0$, and (5.6.7) simplifies to

$$\Delta P = P - P_c \sim (\Delta\rho)^3, \qquad T = T_c \tag{5.6.9}$$

Thus the critical isotherm is predicted to have an antisymmetric, cubic form. Division of both sides of (5.6.7) by $\Delta\rho$ gives

$$P_{03}(\Delta\rho)^2 = \frac{\Delta P}{\Delta\rho} - P_{10}\frac{\Delta T}{\Delta\rho} - P_{11}\Delta T \tag{5.6.10}$$

On taking the limit $\Delta T \to 0$, we find that

$$\begin{aligned} \frac{\Delta P}{\Delta\rho} &\to \left(\frac{\partial P}{\partial\rho}\right)_{T=T_c} = 0 \\ \frac{\Delta T}{\Delta\rho} &\to \left(\frac{\partial T}{\partial\rho}\right)_P = -\left(\frac{\partial P}{\partial\rho}\right)_{T=T_c} \Bigg/ \left(\frac{\partial P}{\partial T}\right)_{\rho=\rho_c} = 0 \end{aligned} \tag{5.6.11}$$

where the second result follows from the fact that $(\partial P/\partial T)_\rho$ is always positive. Thus (5.6.10) reduces to

$$\Delta\rho = \pm B|\Delta T|^{1/2}, \quad T < T_c \tag{5.6.12}$$

where $B^2 = P_{11}/P_{03} > 0$. The coexistence curve close to the critical point should therefore be symmetrical about $\rho = \rho_c$, i.e. $(\rho_G - \rho_c) = -(\rho_L - \rho_c)$ and $\rho_L + \rho_G = 2\rho_c$. This is a special case of the empirical law of "rectilinear diameters", according to which $\rho_L + \rho_G$ is a linear function of temperature.

Next we consider the behaviour of the isothermal compressibility. From (5.6.7) we see that near the critical point:

$$\left(\frac{\partial P}{\partial\rho}\right)_T \approx P_{11}\Delta T + P_{03}(\Delta\rho)^2 \tag{5.6.13}$$

Along the critical isotherm, where $\Delta\rho = 0$, we find that

$$\chi_T = \frac{1}{\rho}\left(\frac{\partial\rho}{\partial P}\right)_T \approx \frac{1}{P_{11}\rho_c}(\Delta T)^{-1}, \quad T \to T_c^+ \tag{5.6.14a}$$

Along the coexistence curve, (5.6.12) applies. Thus

$$\chi_T \approx \frac{1}{2P_{11}\rho_c}|\Delta T|^{-1}, \quad T \to T_c^- \tag{5.6.14b}$$

Finally, it is easy to show that the specific heat C_V exhibits a finite discontinuity as the critical point is approached along either the critical isochore or the coexistence curve.

Equations (5.6.9), (5.6.12) and (5.6.14) are examples of the *scaling laws* that characterise the behaviour of a fluid close to the critical point, some of which are summarised in Table 5.1. Scaling laws are expressed in terms of certain experimentally measurable *critical exponents* (α, β, γ, etc.), which have the same values for all fluids, irrespective of their chemical nature.[33] This *universality* extends to the behaviour of the Ising model and

TABLE 5.1. *Definitions of the critical scaling laws and numerical values of the exponents*

	Definition	$T - T_c$	$\rho - \rho_c$	Expt[32]	Classical
α	$C_V = A(T - T_c)^{-\alpha}$	>0	0	0.10 ± 0.05	0*
α'	$C_V = A'\lvert T - T_c\rvert^{-\alpha'}$	<0	$\neq 0$		0*
β	$\rho_L - \rho_G = B\lvert T - T_c\rvert^{\beta}$	<0	$\neq 0$	0.32 ± 0.01	$\frac{1}{2}$
γ	$\chi_T = C(T - T_c)^{-\gamma}$	>0	0	1.24 ± 0.1	1
γ'	$\chi_T = C\lvert T - T_c\rvert^{-\gamma'}$	<0	$\neq 0$		1
δ	$\lvert P - P_c\rvert = D\lvert\rho - \rho_c\rvert^{\delta}$	0	$\neq 0$	4.8 ± 0.2	3
ν	$\xi = \xi_0(T - T_c)^{-\nu}$	>0	0	0.63 ± 0.04	$\frac{1}{2}$
ν'	$\xi = \xi_0'\lvert T - T_c\rvert^{-\nu'}$	<0	$\neq 0$		$\frac{1}{2}$

*Finite discontinuity.

other magnetic systems near the paramagnetic–ferromagnetic transition. By comparing the definitions of the scaling laws in Table 5.1 with the results of the mean-field calculations, we can identify the so-called classical values of some of the critical exponents: $\alpha = \alpha' = 0$ (a finite discontinuity), $\beta = \frac{1}{2}$, $\gamma = \gamma' = 1$ and $\delta = 3$. These results differ significantly from the experimental values listed in the table. The classical values are independent of the explicit form of the equation of state. They follow solely from the assumption that the pressure or, equivalently, the free energy is an analytic function of ρ and T close to the critical point and can therefore be expanded in a Taylor series.[34] Analyticity also implies that the classical exponents should be independent of the spatial dimensionality, which is in contradiction both with experimental findings and with exact, theoretical results for the Ising model. The hypothesis of analyticity at the critical point, inherent in mean-field theory, must therefore be rejected. The presence of mathematical singularities in the free energy, reflected in the fact that the true critical exponents are neither integers nor simple, rational numbers, can be traced back to the appearance of large-scale density fluctuations near the critical point. For any finite system, the partition function and free energy are analytic functions of the independent thermodynamic variables. Singularities appear only in the thermodynamic limit, where fluctuations of very long wavelength become possible. Finite systems therefore behave classically, as the results of computer simulations have shown. Extrapolation techniques based on finite-size scaling ideas are needed if non-classical values of the exponents are to be obtained by simulation.[35]

On approaching the critical point, the amplitude of density fluctuations increases and local fluctuations become correlated over increasingly long distances. The compressibility equation (2.6.12) shows that the divergence of the compressibility must be linked to a divergence in the range of the pair correlation function $h(r)$; the range of $h(r)$ is called the *correlation length*, ξ. The behaviour of ξ for $T \approx T_c$ is described by critical exponents ν (along the critical isochore as $T \to T_c^+$) and ν' (along the coexistence curve as $T \to T_c^-$). These exponents are measurable by light and x-ray scattering experiments. Anomalies in the intensity of light scattered from a fluid near its critical point, particularly the phenomenon known as critical opalescence, were first studied theoretically by Ornstein and Zernike as far back as 1914; it was in the course of this work that the direct correlation function

was introduced. Equation (3.5.15) shows that close to the critical point, $\hat{c}(k)$ is of order $1/\rho$ at $k = 0$. Thus the range of $c(r)$ remains finite, which is consistent with the conjecture that $c(r) \to -\beta v(r)$ as $r \to \infty$ (see the discussion following (3.8.7)). If we also assume that $\hat{c}(k)$ has no singularities, it can be expanded in a Taylor series about $k = 0$ in the form

$$\rho\hat{c}(k) = c_0(\rho, T) + c_2(\rho, T)k^2 + \mathcal{O}(k^4) \tag{5.6.15}$$

with

$$\begin{aligned} c_0(\rho, T) &= \rho\hat{c}(0) = 1 - 1/\rho k_B T \chi_T \\ c_2(\rho, T) &= -\tfrac{1}{6}\rho \int c(r) r^2 \, d\mathbf{r} \equiv -R^2 \end{aligned} \tag{5.6.16}$$

The characteristic length R is sometimes called the Debye persistence length. Note that the conjecture regarding the asymptotic behaviour of $c(r)$ means that c_2 and higher-order coefficients in (5.6.16) are strictly defined only for pair potentials $v(r)$ of sufficiently short range.

The key assumption of Ornstein–Zernike theory is that R remains finite at the critical point. Equations (3.6.10) and (5.6.15) then imply that

$$\frac{1}{S(k)} = 1 - \rho\hat{c}(k) \approx 1 - c_0(\rho, T) - c_2(\rho, T)k^2 \tag{5.6.17a}$$

or, from (5.6.16):

$$S(k) = 1 + \rho\hat{h}(k) \approx \frac{R^{-2}}{K^2 + k^2} \tag{5.6.17b}$$

where $K^2 = (1 - c_0)R^{-2} = R^{-2}/\rho k_B T \chi_T$. The asymptotic form of the pair correlation function is obtained by taking the Fourier transform of (5.6.17b):

$$h(r) \sim \frac{1}{4\pi\rho R^2} \frac{\exp(-Kr)}{r}, \quad r \to \infty \tag{5.6.18}$$

The form of this expression makes it natural to identify K with the inverse range of $h(r)$, i.e. with the inverse correlation length:

$$\xi = K^{-1} = R(\rho k_B T \chi_T)^{1/2} \tag{5.6.19}$$

From (5.6.19) and Table 5.1 it is obvious that within the Ornstein–Zernike approximation the critical exponents for ξ and χ_T are related by $\nu = \frac{1}{2}\gamma$. There are indications, however, that the theory is not entirely correct at the critical point. First, it breaks down in two dimensions, where it predicts that $h(r) \sim \ln r$ for large r, which is clearly absurd. Secondly, careful study of plots of $1/S(k)$ versus k^2 shows that the experimental data are not strictly linear, as suggested by (5.6.17a), but curve slightly downwards in the limit $k^2 \to 0$. These difficulties can be circumvented[34] by the introduction of another exponent, η, which allows

$h(r)$ for large r to be written as

$$h(r) \sim \frac{A \exp(-r/\xi)}{r^{\mathcal{D}-2+\eta}} \tag{5.6.20}$$

where $\mathcal{D}$ is the dimensionality; the Ornstein–Zernike approximation is recovered by putting $\eta = 0$. In the limit $\xi \to \infty$, the Fourier transform of (5.6.20) is

$$\hat{h}(k) \sim \frac{A}{k^{2-\eta}} \tag{5.6.21}$$

and a non-zero value of η can account for the non-linearity of the plots of $1/S(k)$ versus k^2. Substitution of (5.6.21) in the compressibility equation (2.6.12) yields a relation between the exponents γ, ν and η:

$$\nu(2-\eta) = \gamma \tag{5.6.22}$$

This result is independent of dimensionality. The value of η is difficult to determine experimentally, but the available evidence suggests that it is a small, positive number, approximately equal to 0.05.

5.7 SCALING CONCEPTS AND HIERARCHICAL REFERENCE THEORY

The shortcomings of mean-field theory in the critical region are linked to its inability to describe the onset of large-scale density fluctuations close to the critical point, where the correlation length ξ diverges. The scaling concepts introduced by Widom[36] and Kadanoff[37] in the 1960s, and later formalised by Wilson within renormalisation-group theory,[38] are ultimately based on the recognition that ξ is the only relevant length scale near criticality. The divergence of ξ as $T \to T_c$ causes the fluid to become "scale invariant", meaning that fluctuations on all length scales are self-similar; this in turn implies that critical behaviour is universal.

Scaling laws follow from an explicit assumption concerning the functional form of thermodynamic potentials near the critical point. The basic idea is perhaps most easily illustrated in the case of the chemical potential, which is the "ordering field" conjugate to the "order parameter" $(\rho_L - \rho_G)$. These two variables play roles analogous to the external field and magnetisation in the Ising model, which belongs to the same universality class as simple fluids. At the critical point we see from (2.4.21) and (5.6.5) that the chemical potential satisfies the conditions

$$\left(\frac{\partial \mu}{\partial \rho}\right)_{T=T_c} = \left(\frac{\partial^2 \mu}{\partial \rho^2}\right)_{T=T_c} = 0 \tag{5.7.1}$$

If μ is assumed to be an analytic function of ρ and T at the critical point, a Taylor expansion similar to (5.6.7) can be made. By introducing the reduced variables

$$\mu^* = \frac{\mu \rho_c}{P_c}, \qquad \Delta\rho^* = \frac{\rho - \rho_c}{\rho_c}, \qquad \Delta T^* = \frac{T - T_c}{T_c} \tag{5.7.2}$$

and taking account of (5.7.1), the result to first order in ΔT^* may be written as

$$\begin{aligned}\Delta\mu^* &= \mu^*(\rho, T) - \mu^*(\rho_c, T) \\ &\approx \frac{(\mu - \mu_c)\rho_c}{P_c} - \mu^*_{10}\Delta T^* \approx \mu^*_{11}\Delta\rho^*\Delta T^* + \mu^*_{03}(\Delta\rho^*)^3 \end{aligned} \tag{5.7.3}$$

where

$$\mu^*_{ij} = \left(\frac{\partial^{i+j}\mu^*}{\partial\Delta T^{*i}\,\partial\Delta\rho^{*j}}\right)_{\rho=\rho_c, T=T_c} \tag{5.7.4}$$

The classical values of the critical exponents are now easily recovered. In particular, since ΔT^* is zero along the critical isotherm:

$$\Delta\mu^* = \pm D^*|\Delta\rho^*|^\delta = D^*\Delta\rho^*|\Delta\rho^*|^{\delta-1} \tag{5.7.5}$$

where $\delta = 3$ and $D^* = \mu^*_{03}$. Similarly, because $\Delta\mu^*$ vanishes along the coexistence curve:

$$\Delta\rho^* = \pm B^*|\Delta T^*|^\beta \tag{5.7.6}$$

where $\beta = \frac{1}{2}$ and $B^* = (\mu^*_{11}/\mu^*_{03})^\beta$.

We now introduce a dimensionless *scaling parameter*, defined as

$$x = \Delta T^*/|\Delta\rho^*|^{1/\beta} \tag{5.7.7}$$

Clearly x is zero along the critical isotherm and is infinite along the critical isochore, while along the coexistence curve $x = -x_0 = -(B^*)^{1/\beta}$. Equation (5.7.3) can therefore be rewritten in generic form as

$$\Delta\mu^* = \Delta\rho^*|\Delta\rho^*|^{\delta-1}h(x) \tag{5.7.8}$$

where, in the classical theory:

$$h(x) = \mu^*_{03}(1 + x/x_0) \tag{5.7.9}$$

One way of formulating the scaling hypothesis is to postulate that non-classical critical behaviour still yields a result having the general form of (5.7.8), but with non-classical values of the exponents β and δ and a different (but unspecified) expression for $h(x)$, assumed to be an analytic function of x for $-x_0 < x < \infty$ and to vanish as $x \to x_0$.[39]

The scaling hypothesis leads to relations between the critical exponents, from which the values of all exponents can be obtained once two are specified. Consider, for example, the exponent γ', which describes the behaviour of the isothermal compressibility along the coexistence curve. Given that $x = -x_0$ and $h(x) = 0$, it follows from (5.7.6) and (5.7.8) that

$$\left(\frac{\partial\Delta\mu^*}{\partial\Delta\rho^*}\right)_{\Delta T^*} = -\frac{1}{\beta}|\Delta\rho^*|^{\delta-1-1/\beta}\Delta T^* h'(-x_0) \sim |\Delta T^*|^{\beta(\delta-1)} \tag{5.7.10}$$

where $h'(x) \equiv \mathrm{d}h(x)/\mathrm{d}x$. Then, since $\chi_T^{-1} = \rho^2(\partial\mu/\partial\rho)_T$ (see (2.4.22)), comparison with the definition of the exponent γ' in Table 5.1 shows that

$$\gamma' = \beta(\delta - 1) \tag{5.7.11}$$

In a similar way it is possible to establish the relations

$$\gamma = \gamma', \qquad \alpha' + 2\beta + \gamma' = 2, \qquad \alpha' + \beta(1 + \delta) = 2 \tag{5.7.12}$$

However, since this analysis rests on a hypothesis that refers only to thermodynamic quantities, it yields no information about the correlation-length exponents ν, ν' and η. Relations involving those quantities can be derived by exploiting scale invariance near the critical point within Kadanoff's "block-spin" construction for magnetic systems.[37] That approach leads back to the exponent relation (5.6.22) and to the "hyperscaling" relation, which involves the dimensionality $\mathcal{D}$ of the system:

$$\nu\mathcal{D} = 2 - \alpha \tag{5.7.13}$$

Although scaling arguments lead to relations between the critical exponents, they cannot be used to derive numerical values of the exponents given only the hamiltonian of the system. That goal can be reached within renormalisation-group theory, which is basically an iterative scheme whereby the total number of degrees of freedom contained in a volume of order $\xi^{\mathcal{D}}$ is systematically reduced to a smaller set of effective degrees of freedom. The reduction is brought about by successive elimination of fluctuations of wavelength $\lambda < L$, where the length L is progressively allowed to approach ξ. Scaling laws turn out to be a natural consequence of the theory. The set of transformations τ associated with the progressive reduction in the numbers of degrees of freedom gradually transforms a given initial hamiltonian, belonging to some universality class, into a fixed point of τ, i.e. a hamiltonian that is invariant under the transformation; the existence of a fixed point is equivalent to the principle of universality. The theory shows that for dimensionality $\mathcal{D} > 4$, fluctuations of wavelength λ become negligible as λ increases, and mean-field theory is therefore exact. Deviations from classical behaviour for $\mathcal{D} < 4$ can be expanded in powers of $\varepsilon = 4 - \mathcal{D}$ by the use of field-theoretic techniques; this allows the calculation of the non-classical exponents in three dimensions.[40]

Renormalisation-group ideas have been combined with those of thermodynamic perturbation theory in the hierarchical reference theory or HRT of Parola, Reatto and coworkers,[41] which leads to a non-classical description of criticality. The starting point of HRT is closely related to the treatment of long-range interactions in Section 5.5. We assume again that the total pair potential is divided into a repulsive, reference part, $v_0(r)$, and an attractive perturbation, $w(r)$. Then, in the random-phase approximation (5.5.13) and (5.5.29), the reduced free-energy density $\phi = -\beta F^{\mathrm{ex}}/V$ is given by

$$\begin{aligned}\phi = \phi_0 &+ \tfrac{1}{2}\rho^2 \int g_0(r)\Psi(r)\,\mathrm{d}\mathbf{r} \\ &- \tfrac{1}{2}(2\pi)^{-3} \int \left(\widehat{\Sigma}_0(k)\widehat{\Psi}(k) + \ln\left[1 - \widehat{\Sigma}_0(k)\widehat{\Psi}(k)\right]\right)\mathrm{d}\mathbf{k}\end{aligned} \tag{5.7.14}$$

where a subscript 0 denotes a property of the reference system, $\Psi(r) = -\beta w(r)$ and $\widehat{\Sigma}_0(k) = \rho S_0(k) = \rho^2/[1 - \rho\hat{c}_0(k)]$. Use of Parseval's relation allows (5.7.14) to be rewritten as

$$\phi = \phi_0 + \tfrac{1}{2}\rho^2 \int \Psi(r)\,\mathrm{d}\mathbf{r} - \tfrac{1}{2}(2\pi)^{-3} \int \big(\rho\widehat{\Psi}(k) + \ln\big[1 - \widehat{\Sigma}_0(k)\widehat{\Psi}(k)\big]\big)\,\mathrm{d}\mathbf{k} \qquad (5.7.15)$$

where the first two terms on the right-hand side correspond to the mean-field approximation (5.6.3) and the final term is the contribution made by fluctuations. The non-analyticities in the free energy that characterise the critical region mean, however, that a straightforward perturbative treatment of the effect of fluctuations is bound to fail. The renormalisation-group approach provides a hint of how to go beyond conventional perturbation theory. Density fluctuations must be introduced selectively and recursively, starting from short-wavelength fluctuations, which modify the local structure of the reference fluid, up to longer wavelengths, which eventually lead to condensation. The gradual switching on of fluctuations is brought about by passing from the reference-system pair potential to the full potential via an infinite sequence of intermediate potentials

$$v^{(Q)}(r) = v_0(r) + w^{(Q)}(r) \qquad (5.7.16)$$

where the perturbation $w^{(Q)}(r)$ contains only those Fourier components of $w(r)$ corresponding to wavenumbers $k > Q$. In other words:

$$\begin{aligned} \widehat{w}^{(Q)} &= \widehat{w}(k), \quad k > Q, \\ &= 0, \qquad k < Q \end{aligned}$$

and the reference-system and full potentials are recovered in the limits $Q \to \infty$ and $Q \to 0$, respectively:

$$\lim_{Q\to\infty} v^{(Q)}(r) = v_0(r), \qquad \lim_{Q\to 0} v^{(Q)}(r) = v(r) \qquad (5.7.17)$$

The "Q-system", i.e. the fluid with pair potential $v^{(Q)}(r)$, serves as the reference system for a fluid of particles interacting through the potential $v^{(Q-\delta Q)}(r)$, corresponding to an infinitesimally lower cut-off in $\mathbf{k}$-space. The parameter Q, like the inverse-range parameter γ in (5.5.3), has no microscopic significance; its role, as we shall see, is merely to generate a sequence of approximations that interpolate between the mean-field result and the exact solution for the fully interacting system.

The cut-off in $\widehat{w}(k)$ at $k = Q$ leads to discontinuities in the free energy and pair functions of the Q-system. To avoid the difficulties that this would create, a modified free-energy density $\bar{\phi}^{(Q)}$ is introduced, defined as

$$\bar{\phi}^{(Q)} = \phi^{(Q)} + \tfrac{1}{2}\rho^2\big[\widehat{\Psi}(0) - \widehat{\Psi}^{(Q)}(0)\big] - \tfrac{1}{2}\rho\big[\Psi(0) - \Psi^{(Q)}(0)\big] \qquad (5.7.18)$$

together with a modified direct correlation function $\widehat{\mathcal{C}}^{(Q)}$, given by

$$\widehat{\mathcal{C}}^{(Q)}(k) = \hat{c}^{(Q)}(k) - 1/\rho + \widehat{\Psi}(k) - \widehat{\Psi}^{(Q)}(k) \qquad (5.7.19)$$

where $c^{(Q)}(k)$ is the direct correlation function of the Q-system, defined in the usual way, and $\Psi^{(Q)}(r) = -\beta w^{(Q)}(r)$. Inclusion of the last two terms[42] on the right-hand side of (5.7.19) compensates for the discontinuity, equal to $\beta\widehat{w}(k)$, that appears in the function $\hat{c}^{(Q)}(k)$ at $k = Q$. Thus

$$\begin{aligned}\widehat{\mathcal{C}}^{(Q)}(k) &= -\frac{1}{\widehat{\Sigma}^{(Q)}(k)}, \qquad k > Q, \\ &= -\frac{1}{\widehat{\Sigma}^{(Q)}(k)} + \widehat{\Psi}(k), \quad k < Q\end{aligned} \tag{5.7.20}$$

with $\widehat{\Sigma}^{(Q)}(k) = \rho S^{(Q)}(k)$. With these definitions, the expression derived from (5.7.15) for $\bar{\phi}^{(Q-\delta Q)}$ in terms of $\bar{\phi}^{(Q)}$ can be written as

$$\bar{\phi}^{(Q-\delta Q)} = \bar{\phi}^{(Q)} + \tfrac{1}{2}(2\pi)^{-3}\int \ln\left(1 - \frac{\widehat{\Psi}(k)}{\widehat{\mathcal{C}}^{(Q)}(k)}\right)\mathrm{d}\mathbf{k} \tag{5.7.21}$$

where the integration is confined to the interval $Q - \delta Q < k < Q$. By taking the limit $\delta Q = 0$ we arrive at an exact, differential equation for $\bar{\phi}^{(Q)}$, which describes the evolution of the free energy with Q:

$$-\frac{\mathrm{d}\bar{\phi}^{(Q)}}{\mathrm{d}Q} = \frac{Q^2}{4\pi^2}\ln\left(1 - \frac{\widehat{\Psi}(Q)}{\widehat{\mathcal{C}}^{(Q)}(Q)}\right) \tag{5.7.22}$$

The initial condition is imposed at $Q = \infty$, where the free energy takes its mean-field value, i.e.

$$\phi^{(\infty)} = \phi_0 + \tfrac{1}{2}\rho^2\widehat{\Psi}(0) - \tfrac{1}{2}\rho\Psi(0) \tag{5.7.23}$$

or, equivalently, $\bar{\phi}^{(\infty)} = \phi_0$.

Methods similar to those sketched above can be used to derive a formally exact, infinite hierarchy of differential equations that link the pair function $\mathcal{C}^{(Q)}(k)$ to all higher-order direct correlation functions $\hat{c}_n^{(Q)}(\mathbf{r}_1, \ldots, \mathbf{r}_n)$, $n \geqslant 3$. Close to the critical point some simplification occurs at small values of Q, i.e. when critical fluctuations begin to make a contribution to the free energy. The definitions (5.7.18) and (5.7.19) imply that a generalisation of the compressibility relation (3.5.15):

$$\widehat{\mathcal{C}}^{(Q)}(k=0) = -\frac{\partial^2\bar{\phi}^{(Q)}}{\partial\rho^2} \tag{5.7.24}$$

applies for all Q. The resulting divergence of $1/\widehat{\mathcal{C}}^{(Q)}(k)$ in the limit $k \to 0$ means that the argument of the logarithmic function in (5.7.21) is dominated by the term describing pair correlations. Thus the evolution of the free energy with Q in its final stages has a universal character, being essentially independent of the interaction term $\widehat{\Psi}(k)$. Similar simplifications appear at all levels of the hierarchy, and the distinctive features of renormalisation-group theory, such as scaling laws and the expansion in powers of $\varepsilon = 4 - \mathcal{D}$, emerge

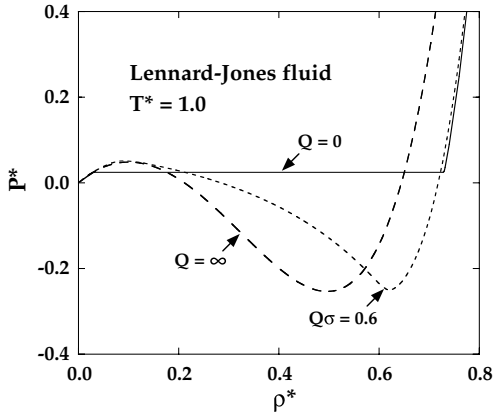

FIG. 5.9. An isotherm of the Lennard-Jones fluid in the pressure–density plane, calculated at three different stages in the integration of (5.7.22); $P^* = P\sigma^3/\varepsilon$ is the reduced pressure. The limits $Q = \infty$ and $Q = 0$ correspond, respectively, to the mean-field and final solutions. For $Q = 0$ the theory yields an isotherm that is rigorously flat in the two-phase region, while at finite Q van der Waals loops are obtained.

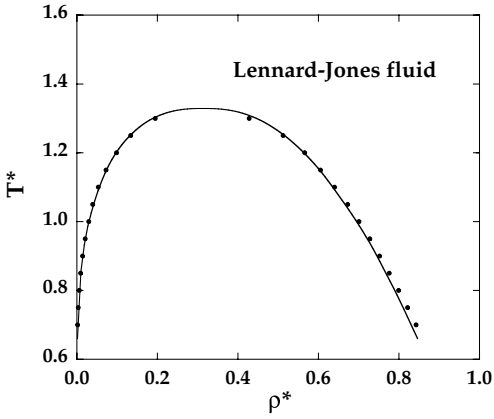

FIG. 5.10. Liquid–vapour coexistence curve for the Lennard-Jones fluid. The curve is calculated from HRT and the points are the results of Monte Carlo calculations.[45] After Tau *et al.*[43]

from the formalism without recourse to field-theoretical models. Away from the critical region some approximate closure of the hierarchy is required if numerical results are to be obtained. In practice this is achieved at the level of the free energy by approximating the function $\widehat{\mathcal{C}}^{(Q)}(k)$ in a form that is consistent both with (5.7.24) and with the Ornstein–Zernike assumption that $\widehat{\mathcal{C}}^{(Q)}(k)$ is analytic in k^2 (see (5.6.17)). The first equation of the hierarchy is thereby transformed into a partial differential equation in the variables Q and ρ. Closures of this general type, having features in common with other approximate theories, have been used in calculations for a variety of simple fluids.[43,44] Overall the theory yields a very satisfactory description of liquid–vapour coexistence. Non-classical values

are obtained for the critical exponents, though these differ somewhat from the nearly exact results derived from the ε expansion.[41(b)] For example, within HRT, $\beta \approx 0.345$, while the ε expansion gives $\beta \approx 0.327$. Below T_c the theory leads to rigorously flat isotherms in the two-phase region, illustrated by the results for the Lennard-Jones fluid shown in Figure 5.9. The coexistence curve can therefore be determined without use of the Maxwell construction, with results in excellent agreement with those obtained by simulation, as Figure 5.10 reveals. A fault in the theory is the fact that it leads to an artificial divergence of the isothermal compressibility along the coexistence curve, which therefore coincides with the spinodal everywhere, not just at the critical point (cf. Figure 5.8). The source of this error is the analyticity imposed on $\widehat{\mathcal{C}}^{(Q)}(k)$.

NOTES AND REFERENCES

1. Widom, B., *J. Chem. Phys.* **39**, 2808 (1963).
2. Longuet-Higgins, H.C. and Widom, B., *Mol. Phys.* **8**, 549 (1964).
3. Ashcroft, N.W. and Lekner, J., *Phys. Rev.* **145**, 83 (1966).
4. Verlet, L., *Phys. Rev.* **163**, 201 (1968).
5. Zwanzig, R., *J. Chem. Phys.* **22**, 1420 (1954).
6. Henderson, D. and Barker, J.A., *In* "Physical Chemistry: An Advanced Treatise", vol. VIIIA (H. Eyring, D. Henderson and W. Jost, eds). Academic Press, New York, 1971.
7. Isihara, A., *J. Phys. A* **1**, 539 (1968).
8. (a) Mansoori, G.A. and Canfield, F.B., *J. Chem. Phys.* **51**, 4958 (1969). (b) Rasaiah, J.C. and Stell, G., *Mol. Phys.* **18**, 249 (1970).
9. Ben-Amotz, D. and Stell, G., *J. Chem. Phys.* **120**, 4844 (2004).
10. (a) Mon, K.K., *J. Chem. Phys.* **112**, 3245 (2000). (b) Mon, K.K., *J. Chem. Phys.* **115**, 4766 (2001).
11. Andersen, H.C., Weeks, J.D. and Chandler, D., *Phys. Rev. A* **4**, 1597 (1971).
12. Rowlinson, J.S., *Mol. Phys.* **8**, 107 (1964).
13. Barker, J.A. and Henderson, D., *J. Chem. Phys.* **47**, 4714 (1967).
14. Hansen, J.P. and Weis, J.J., *Mol. Phys.* **23**, 853 (1972).
15. Lado, F., *Mol. Phys.* **52**, 871 (1984). See also Ben-Amotz, D. and Stell, G., *J. Phys. Chem. B* **108**, 6877 (2004).
16. (a) Levesque, D. and Verlet, L., *Phys. Rev.* **182**, 307 (1969). (b) Verlet, L. and Weis, J.J., *Mol. Phys.* **24**, 1013 (1972).
17. McQuarrie, D.A. and Katz, J.L., *J. Chem. Phys.* **44**, 2398 (1966).
18. Barker, J.A. and Henderson, D., *Rev. Mod. Phys.* **48**, 587 (1976).
19. Weeks, J.D., Chandler, D. and Andersen, H.C., *J. Chem. Phys.* **54**, 5237 (1971).
20. Talbot, J., Lebowitz, J.L., Waisman, E.M., Levesque, D. and Weis, J.J., *J. Chem. Phys.* **85**, 2187 (1986).
21. (a) Hemmer, P.C., *J. Math. Phys.* **5**, 75 (1964). (b) Lebowitz, J.L., Stell, G. and Baer, S., *J. Math. Phys.* **6**, 1282 (1965).
22. Kac, M., Uhlenbeck, G.E. and Hemmer, P.C., *J. Math. Phys.* **4**, 216 (1963). For the extension to three dimensions, see van Kampen, N.G., *Phys. Rev.* **135**, 362 (1964) and Lebowitz, J.L. and Penrose, O., *J. Math. Phys.* **7**, 98 (1966).
23. Andersen, H.C. and Chandler, D., *J. Chem. Phys.* **57**, 1918 (1972).
24. Except in trivial cases, removal of a reference articulation pair causes a diagram to separate into two or more components, of which at least one contains only reference-system bonds.
25. See, e.g., Tables VIII and IX of ref. 18.
26. Pini, D., Parola, A. and Reatto, L., *Mol. Phys.* **100**, 1507 (2002).
27. For a discussion of the relationship between the two expansions, see Stell, G., *J. Chem. Phys.* **55**, 1485 (1971).
28. Stell, G. and Weis, J.J., *Phys. Rev. A* **21**, 645 (1980).
29. See, e.g., Caccamo, C., *Phys. Rep.* **274**, 1 (1996).

30. Huang, K., “Statistical Mechanics”, 2nd edn. John Wiley, New York, 1987, p. 41.
31. Alder, B.J., Young, D.A. and Mark, M.A., *J. Chem. Phys.* **56**, 3013 (1972).
32. (a) Rowlinson, J.S. and Swinton, F.L., “Liquids and Liquid Mixtures”, 3rd edn. Butterworth, London, 1982. (b) Chaikin, P.M. and Lubensky, T.C., “Principles of Condensed Matter Physics”. Cambridge University Press, Cambridge, 1995.
33. Note that the prefactors (the critical amplitudes) that appear in the scaling laws are not universal quantities.
34. Fisher, M.E., *J. Math. Phys.* **5**, 944 (1964).
35. See, e.g., Ferrenberg, A.M. and Landau, D.P., *Phys. Rev. B* **44**, 5081 (1991) (Ising model) and Wilding, N.B., *Phys. Rev. E* **52**, 602 (1995) (Lennard-Jones fluid).
36. Widom, B., *J. Chem. Phys.* **43**, 3898 (1965).
37. (a) Kadanoff, L.P., *Physics* **2**, 263 (1966). (b) Kadanoff, L.P., “Statistical Physics: Statics, Dynamics and Renormalization”. World Scientific, Singapore, 1999.
38. (a) Wilson, K.G., *Phys. Rev. B* **4**, 3174 and 3184 (1971). (b) Fisher, M.E., *Rev. Mod. Phys.* **70**, 653 (1998). For introductory treatments, see the book by Huang, ref. 30, and Plischke, M. and Bergersen, B., “Equilibrium Statistical Physics”, 2nd edn. World Scientific, Singapore, 1994.
39. Griffiths, R.B., *Phys. Rev.* **158**, 176 (1967).
40. (a) Wilson, K.G. and Kogut, J., *Phys. Rep.* **12**, 75 (1974). (b) Amit, D.J., “Field Theory, the Renormalization Group and Critical Phenomena”, 2nd edn. World Scientific, Singapore, 1993.
41. (a) Parola, A. and Reatto, L., *Phys. Rev. A* **31**, 3309 (1985). (b) Parola, A. and Reatto, L., *Adv. Phys.* **44**, 211 (1995).
42. The second term is introduced in order to simplify the resulting expressions.
43. See, e.g., Tau, M., Parola, A., Pini, D. and Reatto, L., *Phys. Rev. E* **52**, 2644 (1995). For a description of the numerical implementation, see Reiner, A. and Kahl, G., *Phys. Rev. E* **65**, 046701 (2002).
44. HRT has also been successfully generalised to binary systems. See, e.g., Pini, D., Tau, M., Parola, A. and Reatto, L., *Phys. Rev. E* **67**, 046116 (2003).
45. Lotfi, A., Vrabec, J. and Fischer, J., *Mol. Phys.* **76**, 1319 (1992).

CHAPTER 6

Inhomogeneous Fluids

Chapters 4 and 5 were concerned with theories designed primarily for the calculation of thermodynamic and structural properties of bulk, uniform fluids. We now turn our attention to non-uniform systems. The translational symmetry characteristic of a homogeneous fluid is broken by exposure to an external force field, in the vicinity of a confining surface (which may be regarded as the source of an external field), or in the presence of an interface between coexisting phases. Static properties of inhomogeneous fluids are most effectively studied within the framework of density-functional theory, the foundations of which were laid in Sections 3.1 and 3.4. As we saw there, use of the theory requires as a starting point some approximate expression for the intrinsic free energy as a functional of the single-particle density, or density profile, $\rho^{(1)}(\mathbf{r})$. In this chapter we show how useful approximations can be devised and describe their application to a variety of physical problems.

6.1 LIQUIDS AT INTERFACES

Molecular interactions at fluid interfaces are responsible for many familiar, physical processes, from lubrication and bubble formation to the wetting of solids and the capillary rise of liquids in narrow tubes. Questions of a fundamental character that a theory needs to address include the nature of the interface that arises spontaneously between, say, a liquid and its vapour or between two immiscible liquids; the layering of dense fluids near a solid substrate; the properties of liquids confined to narrow pores; the formation of electric double layers in electrolyte solutions; and the factors that control interfacial phase transitions, such as the capillary condensation of under-saturated vapour in porous media. In all these situations, surface contributions to the thermodynamic potentials (proportional to the surface area) are no longer negligible compared with the contributions from the bulk (proportional to the volume). The equilibrium values of the potentials are therefore determined by the competition between bulk and surface effects.[1]

The change in grand potential associated with an infinitesimal change in thermodynamic state of a system containing an interface is given by a generalisation of (2.4.3):

$$\mathrm{d}\Omega = -S\,\mathrm{d}T - P\,\mathrm{d}V - N\mathrm{d}\mu + \gamma\,\mathrm{d}\mathcal{A} \tag{6.1.1a}$$

or, in the case of a mixture:

$$\mathrm{d}\Omega = -S\,\mathrm{d}T - P\,\mathrm{d}V - \sum_{\nu} N_\nu\,\mathrm{d}\mu_\nu + \gamma\,\mathrm{d}\mathcal{A} \tag{6.1.1b}$$

where ν labels a species, $\mathcal{A}$ is the interfacial area and γ, the variable conjugate to $\mathcal{A}$, is the surface tension. The corresponding change in Helmholtz free energy is

$$\mathrm{d}F = -S\,\mathrm{d}T - P\,\mathrm{d}V + \sum_{\nu} \mu_\nu\,\mathrm{d}N_\nu + \gamma\,\mathrm{d}\mathcal{A} \tag{6.1.2}$$

The surface tension is the work required to increase the interface by unit area. It is positive for any real liquid, since intermolecular forces tend to reduce the interfacial area. Hence, in the absence of gravity, formation of a spherical interface is always favoured. From (6.1.1) and (6.1.2) it follows that γ may be written as a thermodynamic derivative in either of two different ways:

$$\gamma = \left(\frac{\partial\Omega}{\partial\mathcal{A}}\right)_{V,T,\{\mu_\nu\}} = \left(\frac{\partial F}{\partial\mathcal{A}}\right)_{V,T,\{N_\nu\}} \tag{6.1.3}$$

In addition, since Ω is a homogeneous function of first order in V and $\mathcal{A}$, (6.1.1) can be integrated at constant μ_ν and T to give

$$\Omega = -PV + \gamma\mathcal{A} \tag{6.1.4}$$

which is the generalisation to interfacial systems of the thermodynamic relation (2.4.2). Thus the surface tension can also be written as:

$$\gamma = \frac{1}{\mathcal{A}}(\Omega + PV) \equiv \frac{\Omega^{(\mathrm{s})}}{\mathcal{A}} \tag{6.1.5}$$

where $\Omega^{(\mathrm{s})}$ is the *surface excess* grand potential.

The concept of a surface excess property is easily extended to other thermodynamic quantities. Consider, for example, the interface between a one-component liquid and its vapour. Under the influence of gravity, the interface is planar and horizontal, and the density profile depends only on the vertical coordinate, z. Macroscopically the interface appears sharp, but on the molecular scale it varies smoothly over a few molecular diameters. A typical density profile, $\rho^{(1)}(z)$, is shown schematically in Figure 6.1, where the z-axis is drawn perpendicular to the interface. The physical interface is divided into two parts by an imaginary plane located at $z = z_0$, called the *Gibbs dividing surface*. The liquid phase extends below $z = z_0$, where $\rho^{(1)}(z)$ rapidly approaches its bulk-liquid value, ρ_{L}, while for $z > z_0$, $\rho^{(1)}(z)$ tends towards the bulk-gas value, ρ_{G}. The liquid and gas *adsorptions*, Γ_{L} and Γ_{G}, are defined as integrals over the regions labelled 1 and 2 in the figure:

$$\Gamma_{\mathrm{L}} = \int_{-\infty}^{z_0} \left[\rho^{(1)}(z) - \rho_{\mathrm{L}}\right]\mathrm{d}z < 0, \qquad \Gamma_{\mathrm{G}} = \int_{z_0}^{\infty} \left[\rho^{(1)}(z) - \rho_{\mathrm{G}}\right]\mathrm{d}z > 0 \tag{6.1.6}$$

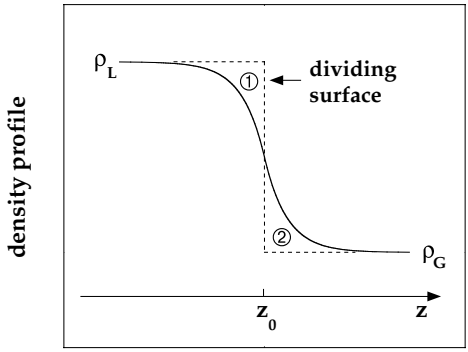

FIG. 6.1. Density profile at the liquid–vapour interface. The z-axis is perpendicular to the interface and the Gibbs dividing surface is located at $z = z_0$; ρ_L and ρ_G are the bulk densities of liquid and gas, respectively.

Though the location of the dividing surface is arbitrary, it is commonly positioned so as to make the two labelled regions equal in area, in which case the total adsorption, $\Gamma = \Gamma_L + \Gamma_G$, is zero. We shall follow this convention. If the interface were infinitely sharp, with the two bulk phases meeting discontinuously at the dividing surface, the total number of particles would be

$$N_L + N_G = V_L \rho_L + V_G \rho_G \tag{6.1.7}$$

where V_L, V_G are the volumes occupied by the two phases. The total number of particles in the inhomogeneous system contained in the volume $V = V_L + V_G$ may therefore be written as

$$N = N_L + N_G + N^{(s)} \tag{6.1.8}$$

where $N^{(s)}$ is the surface excess number of particles, and the total adsorption is $\Gamma = N^{(s)}/\mathcal{A}$. With the conventional choice of z_0, $N^{(s)} = 0$. In a solution, z_0 may be chosen such that the adsorption of the solvent vanishes, but the adsorptions of the solutes will then in general be non-zero. Expressions analogous to (6.1.8) serve as definitions of the other surface excess quantities.

The surface excess grand potential is related to the surface tension by (6.1.5). When that relation is combined with (6.1.1) and the corresponding expressions for the two bulk phases, we find that

$$\mathrm{d}\Omega^{(s)} = \gamma\,\mathrm{d}\mathcal{A} + \mathcal{A}\,\mathrm{d}\gamma = -S^{(s)}\,\mathrm{d}T - \sum_\nu N_\nu^{(s)}\,\mathrm{d}\mu_\nu + \gamma\,\mathrm{d}\mathcal{A} \tag{6.1.9}$$

which leads, after division by $\mathcal{A}$, to

$$s^{(s)}\,\mathrm{d}T + \sum_\nu \Gamma_\nu\,\mathrm{d}\mu_\nu + \mathrm{d}\gamma = 0 \tag{6.1.10}$$

where $s^{(s)} \equiv S^{(s)}/\mathcal{A}$ is the surface excess entropy per unit area. Equation (6.1.10) is called the *Gibbs adsorption equation*. This is the surface equivalent of the Gibbs–Duhem relation

in the bulk phase and shows that the adsorptions of the different species are related to the surface tension by

$$\Gamma_\nu = -\left(\frac{\partial\gamma}{\partial\mu_\nu}\right)_{T,\{\mu_{\nu'\neq\nu}\}} \tag{6.1.11}$$

Equations (6.1.10) and (6.1.11) have been derived with the example of a liquid–gas interface in mind, but their applicability is more general. They hold also in the case of a fluid in contact with a solid surface. There, depending on the nature of the solid–fluid interaction, the adsorptions may be either positive or negative.

Thus far we have assumed that the system contains a single, planar (or weakly curved) interface, well-separated from any other surface. When a fluid is narrowly confined, an additional control variable comes into play, namely the quantity that characterises the spacing between the bounding surfaces. In the simplest case, that of a liquid confined to a slit-like pore between two parallel plates of area $\mathcal{A}$, the new variable is the spacing L of the plates. The necessary generalisation of (6.1.1) is

$$\mathrm{d}\Omega = -S\,\mathrm{d}T - P\,\mathrm{d}V - \sum_\nu N_\nu\,\mathrm{d}\mu_\nu + 2\gamma\,\mathrm{d}\mathcal{A} - f_S\mathcal{A}\,\mathrm{d}L \tag{6.1.12}$$

where $\gamma = \frac{1}{2}(\partial\Omega/\partial\mathcal{A})_{V,T,\{\mu_\nu\},L}$ is the substrate–fluid interfacial tension. The quantity $-f_S$ is the variable per unit area conjugate to L; f_S has the dimensions of pressure, but is commonly referred to as the "solvation force". Physically, f_S is the force over and above any direct interaction between the plates that must be exerted on the plates in order to maintain them at a separation L; when $f_S > 0$, the force is repulsive. If Γ_ν, $\rho_\nu^{(1)}(z)$ and $\rho_{\nu\mathrm{L}}$ are, respectively, the total adsorption, density profile and bulk-liquid density of species ν, then

$$\Gamma_\nu = \int_0^L \left[\rho_\nu^{(1)}(z) - \rho_{\nu\mathrm{L}}\right]\mathrm{d}z \tag{6.1.13}$$

and the differential of the surface excess grand potential is

$$\mathrm{d}\Omega^{(\mathrm{s})} = -2s^{(\mathrm{s})}\mathcal{A}\,\mathrm{d}T - \mathcal{A}\sum_\nu \Gamma_\nu\,\mathrm{d}\mu_\nu + 2\gamma\,\mathrm{d}\mathcal{A} - f_S\mathcal{A}\,\mathrm{d}L \tag{6.1.14}$$

The interfacial tension is again the surface excess grand potential per unit area, i.e. $\gamma = \Omega^{(s)}(\mu, T, L)/2\mathcal{A}$, and the solvation force is

$$f_S = -2\left(\frac{\partial\gamma}{\partial L}\right)_{T,\{\mu_\nu\}} = -\frac{1}{\mathcal{A}}\left(\frac{\partial\Omega}{\partial L}\right)_{\mathcal{A},T,\{\mu_\nu\}} - P \tag{6.1.15}$$

since $\mathrm{d}V = \mathcal{A}\,\mathrm{d}L$. In the limit $L \to \infty$, the first term on the right-hand side of (6.1.15) becomes equal to the bulk pressure and the solvation force vanishes. In the same limit, the total adsorptions Γ_ν become equal to the sum of the adsorptions at each plate 1, 2 considered separately, i.e. $\Gamma_\nu \to \Gamma_\nu^{(1)} + \Gamma_\nu^{(2)}$, and $2\gamma \to \gamma^{(1)} + \gamma^{(2)}$. The "solvation potential"

per unit area is defined as

$$W(L) = \frac{1}{\mathcal{A}}\big[\Omega^{(\mathrm{s})}(L) - \Omega^{(\mathrm{s})}(L \to \infty)\big] = \big(2\gamma - \gamma^{(1)} - \gamma^{(2)}\big) - f_{\mathrm{S}} L \tag{6.1.16}$$

with $f_{\mathrm{S}} = -\partial W(L)/\partial L$. In the limit $L \to 0$, the confined fluid is completely expelled and $\gamma \to 0$. Thus $W(L=0) = -\gamma^{(1)} - \gamma^{(2)}$.

6.2 APPROXIMATE FREE-ENERGY FUNCTIONALS

We saw in Chapter 3 that the grand potential of an inhomogeneous fluid is a functional of the intrinsic chemical potential $\psi(\mathbf{r}) = \mu - \phi(\mathbf{r})$, where $\phi(\mathbf{r})$ is the external potential. Equation (3.3.13) shows that Ω is also the generating functional for the set of n-particle correlation functions $H^{(n)}(\mathbf{r}_1, \ldots, \mathbf{r}_n)$. Similarly, the Helmholtz free energy is a functional of the single-particle density, and its excess (non-ideal) part is the generating functional for the set of n-particle direct correlation functions $c^{(n)}(\mathbf{r}_1, \ldots, \mathbf{r}_n)$. Implementation of density-functional theory is based on the variational principle embodied in (3.4.3), according to which the functional $\Omega_\phi[n] = \mathcal{F}[n] - \int n(\mathbf{r})\psi(\mathbf{r})\,\mathrm{d}\mathbf{r}$ reaches its minimum value when the trial density $n(\mathbf{r})$ coincides with the equilibrium density, while the minimum value itself is the grand potential of the system. This in turn requires the construction of an intrinsic free-energy functional $\mathcal{F}$ in a form appropriate to the physical problem of interest. While the ideal part is given exactly by (3.1.22), the non-trivial, excess part is in general unknown, and some approximation must be invoked.

We consider first the case of a small-amplitude modulation of the single-particle density of the form $\delta\rho^{(1)}(\mathbf{r}) = \rho^{(1)}(\mathbf{r}) - \rho_0$, where ρ_0 is the number density of the uniform, reference fluid. If the modulation is produced by a weak, external potential $\delta\phi(\mathbf{r})$, the Fourier components of $\delta\rho^{(1)}$ are related to those of $\delta\phi$ by the linear-response formula (3.6.9), the constant of proportionality being the density response function $\chi(k)$. A similar result emerges if $\mathcal{F}$ is assumed to be a quadratic functional of the density modulation, i.e.

$$\mathcal{F}\big[\rho^{(1)}\big] = V f_0 + \tfrac{1}{2}\int \mathrm{d}\mathbf{r} \int \mathrm{d}\mathbf{r}'\, \delta\rho^{(1)}(\mathbf{r}) X_0(\mathbf{r}, \mathbf{r}') \delta\rho^{(1)}(\mathbf{r}') + \mathcal{O}\big(\big(\delta\rho^{(1)}\big)^3\big) \tag{6.2.1}$$

where f_0 is the free-energy per unit volume of the reference system; the function $X_0(\mathbf{r}, \mathbf{r}')$ is also a property of the reference system and therefore dependent only on the separation $\mathbf{r} - \mathbf{r}'$. The absence from (6.2.1) of a term linear in $\delta\rho^{(1)}$ is explained by the fact that when $\phi(\mathbf{r}) = 0$, $\mathcal{F}[\rho^{(1)}]$ has its minimum value for a uniform density. When written in terms of Fourier components, (6.2.1) becomes

$$\mathcal{F}\big[\rho^{(1)}\big] = V f_0 + \frac{1}{2V}\sum_{\mathbf{k}} \delta\hat{\rho}^{(1)}(\mathbf{k}) \widehat{X}_0(\mathbf{k}) \delta\hat{\rho}^{(1)}(-\mathbf{k}) + \mathcal{O}\big(\delta\rho^{(1)}\big)^3 \tag{6.2.2}$$

Then, on applying the variational formula (3.4.3), where the derivative is now taken with respect to $\delta\hat{\rho}^{(1)}(\mathbf{k})$, we find that $\delta\hat{\rho}^{(1)}(\mathbf{k})$ and $\delta\hat{\phi}(\mathbf{k})$ are linearly related in the form

$$\widehat{X}_0(\mathbf{k}) \delta\hat{\rho}^{(1)}(\mathbf{k}) = -\delta\hat{\phi}(\mathbf{k}) \tag{6.2.3}$$

Comparison of (6.2.3) with the linear-response expression (3.6.9) shows that

$$\widehat{X}_0(\mathbf{k}) \equiv -\frac{1}{\chi(k)} = \frac{k_{\mathrm{B}}T}{\rho_0 S(\mathbf{k})} \tag{6.2.4}$$

where $S(\mathbf{k})$ is the static structure factor of the uniform fluid. The free-energy cost $\delta\mathcal{F}$ of creating a weak density modulation of wavevector $\mathbf{k}$ is therefore proportional to $1/S(\mathbf{k})$.

Next we consider the slow-modulation limit, corresponding to the case of an inhomogeneity of wavelength such that $|\nabla\rho^{(1)}(\mathbf{r})|/\rho_0 = 1/\xi \ll 1/\xi_0$, where ξ_0 is a typical correlation length in the bulk system. The simplest assumption to make is that macroscopic thermodynamics applies locally, i.e. within volume elements of order ξ^3, and hence that a local free energy can be defined at each point in the fluid. In this *local-density approximation* the intrinsic free energy is written as

$$\mathcal{F}\big[\rho^{(1)}\big] = \int f\big(\rho^{(1)}\big)\,\mathrm{d}\mathbf{r} \tag{6.2.5}$$

where $f(\rho^{(1)})$ is the free-energy per unit volume of the homogeneous fluid at a density $\rho^{(1)}(\mathbf{r})$. Because the ideal contribution to the free-energy functional is precisely of the local form represented by (6.2.5), the approximation is needed only for the excess part, $\mathcal{F}^{\mathrm{ex}}$. The Euler–Lagrange formula that results from substitution of (6.2.5) in the variational formula (3.4.3) is

$$f'\big(\rho^{(1)}\big) = \mu - \phi(\mathbf{r}) \tag{6.2.6}$$

where, here and below, the prime denotes a derivative of a function with respect to its argument, in this case $\rho^{(1)}(\mathbf{r})$. If we now take the gradient of both sides of (6.2.6) and use the second of the thermodynamic relations (2.3.8), we find that (6.2.6) is equivalent to the macroscopic condition of mechanical equilibrium:

$$\nabla P(\mathbf{r}) = -\rho^{(1)}(\mathbf{r})\nabla\phi(\mathbf{r}) \tag{6.2.7}$$

The local-density approximation has proved successful in predicting the concentration profiles of colloidal dispersions in sedimentation equilibrium, where the external potential is either gravity or a centrifugal potential and the slow-modulation criterion is therefore well satisfied.[2]

To go beyond the local-density approximation we suppose initially that the inhomogeneity extends in only one direction, as is true, for example, of the interface pictured in Figure 6.1. The density profile is then a function of a single coordinate, which we take to be z. The free-energy functional can be formally expanded in powers of $1/\xi$, the inverse range of the inhomogeneity. Thus, since $\mathrm{d}\rho^{(1)}(z)/\mathrm{d}z$ is of order $1/\xi$, a natural generalisation of (6.2.5) is one in which the free-energy density f is taken to be a function not only of $\rho^{(1)}(z)$ but also of its low-order derivatives, i.e.

$$\mathcal{F}\big[\rho^{(1)}\big] = \int_{-\infty}^{\infty} f\left(\rho^{(1)}(z), \frac{\mathrm{d}\rho^{(1)}(z)}{\mathrm{d}z}, \frac{\mathrm{d}^2\rho^{(1)}(z)}{\mathrm{d}z^2}\right)\mathrm{d}z \tag{6.2.8}$$

with

$$f = f_0 + f_1 \frac{\mathrm{d}\rho^{(1)}(z)}{\mathrm{d}z} + f_{2'} \left(\frac{\mathrm{d}\rho^{(1)}(z)}{\mathrm{d}z} \right)^2 + f_{2''} \frac{\mathrm{d}^2\rho^{(1)}(z)}{\mathrm{d}z^2} + \mathcal{O}\big(1/\xi^4\big) \tag{6.2.9}$$

where the coefficients f_n on the right-hand side are all functions of $\rho^{(1)}(z)$. Terms beyond f_0 in (6.2.9) represent successive "gradient" corrections to the local-density approximation. However, the coefficient f_1 is zero, since the functional must be invariant under reflection. Indeed, if $\rho^{(1)}(z)$ is a solution of (3.4.3), the mirror-image profile $\rho^{(1)}(-z)$ must also be a solution. A change of variable from z to $z' = -z$ in the integral (6.2.8) proves that this is possible only if $f_1 = 0$; a similar argument shows that all odd coefficients must also vanish. When (6.2.9) is substituted in (6.2.8), the term involving $\mathrm{d}^2\rho^{(1)}(z)/\mathrm{d}z^2$ can be transformed into one proportional to $[\mathrm{d}\rho^{(1)}(z)/\mathrm{d}z]^2$ through an integration by parts. The resulting expression for $\mathcal{F}$ is called the *square-gradient* functional:

$$\mathcal{F}\big[\rho^{(1)}\big] = \int_{-\infty}^{\infty} \left(f_0 + f_2 \left(\frac{\mathrm{d}\rho^{(1)}(z)}{\mathrm{d}z} \right)^2 \right) \mathrm{d}z \tag{6.2.10}$$

Substitution of (6.2.10) in (3.4.3) yields a differential equation for $\rho^{(1)}(z)$ of the form

$$f_0' - f_2' \left(\frac{\mathrm{d}\rho^{(1)}(z)}{\mathrm{d}z} \right)^2 - 2 f_2 \frac{\mathrm{d}^2\rho^{(1)}(z)}{\mathrm{d}z^2} = \mu - \phi(z) \tag{6.2.11}$$

The generalisation of these results to the three-dimensional case is straightforward, requiring only the replacement of $\mathrm{d}\rho^{(1)}(z)/\mathrm{d}z$ by $\boldsymbol{\nabla}\rho^{(1)}(\mathbf{r})$. Thus (6.2.10) becomes

$$\mathcal{F}\big[\rho^{(1)}\big] = \int \big(f_0 + f_2 \big| \boldsymbol{\nabla}\rho^{(1)}(\mathbf{r}) \big|^2 \big) \, \mathrm{d}\mathbf{r} \tag{6.2.12}$$

where f_0 and f_2 are functions of $\rho^{(1)}(\mathbf{r})$.

The coefficient f_2 can be determined by considering again the case of a slowly varying, small-amplitude inhomogeneity $\delta\rho^{(1)}(\mathbf{r})$ around a bulk density ρ_0. If the integrand in (6.2.12) is expanded to second order in $\delta\rho^{(1)}(\mathbf{r})$ and the result expressed in terms of Fourier components, we find that

$$\begin{aligned} \mathcal{F}\big[\rho^{(1)}\big] &\approx \int \big(f_0 + \tfrac{1}{2} f_0'' \big(\delta\rho^{(1)}\big)^2 + f_2 \boldsymbol{\nabla}\delta\rho^{(1)}(\mathbf{r}) \cdot \boldsymbol{\nabla}\delta\rho^{(1)}(\mathbf{r}) \big) \, \mathrm{d}\mathbf{r} \\ &= V f_0 + \frac{1}{2V} \sum_{\mathbf{k}} \big(f_0'' + 2 f_2 k^2 \big) \delta\hat{\rho}^{(1)}(\mathbf{k}) \delta\hat{\rho}^{(1)}(-\mathbf{k}) \end{aligned} \tag{6.2.13}$$

where f_0 and f_2 are now functions of ρ_0. This result should be compared with the quadratic functional (6.2.2). Both approximations assume that the inhomogeneity is small in amplitude, but whereas (6.2.2) is valid for any $\mathbf{k}$, (6.2.13) holds only in the long-wavelength limit. The structure factor and two-particle direct correlation function of the reference fluid

are related by (3.6.10). If $\hat{c}(\mathbf{k})$ is expanded in even powers of k in the manner of (5.6.15), the quantity $\widehat{X}_0(\mathbf{k})$ in (6.2.2) can be replaced by

$$\widehat{X}_0(\mathbf{k}) = \frac{k_B T}{\rho_0}\big(1 - \rho_0 \hat{c}(k)\big) = \frac{k_B T}{\rho_0}\big(1 - c_0 - c_2 k^2 + \mathcal{O}\big(k^4\big)\big) \tag{6.2.14}$$

where the coefficients c_0 and c_2 are given by (5.6.16). Then, on identifying the resulting expression with (6.2.13), we find that

$$f_0''(\rho_0) = k_B T \int c(r)\, \mathrm{d}\mathbf{r} \tag{6.2.15a}$$

$$f_2(\rho_0) = \tfrac{1}{12} k_B T \int c(r) r^2\, \mathrm{d}\mathbf{r} \tag{6.2.15b}$$

Equation (6.2.15a) is merely a restatement of the compressibility relation (3.5.15), while (6.2.15b) shows that the coefficient f_2 is determined by the second moment of the direct correlation function of the homogeneous system.

The form of the results obtained for f_0 and f_2 suggests that terms of order higher than quadratic are likely to involve still higher-order moments of $c(r)$, thereby exposing a limitation inherent in an expansion in powers of the density-profile gradient (or powers of $1/\xi$). Because $c(r)$ decays as $v(r)$ at large r, moments of any given order will diverge for sufficiently long ranged potentials. For example, if the potential contains a contribution from dispersion forces, $c(r)$ will decay as r^{-6}, leading to a divergence of the fourth and higher-order moments and hence of the coefficients f_n for $n \geqslant 4$. Even within the square-gradient approximation there is the further difficulty that in the presence of attractive interactions the equilibrium state of the reference system may be one in which liquid and vapour coexist, and neither f_0 nor f_2 is properly defined in the two-phase region. The square-gradient functional has nonetheless proved extremely useful in studies of the liquid–gas interface, as the work described in the next section will illustrate.[3] Long-range interactions can be treated by dividing the pair potential into a short-range reference part and long-range perturbation in the spirit of the perturbation theories of Chapter 5. This separation leads to the formally exact expression for the excess part of the free-energy functional given by (3.4.10), from which an approximate, mean-field functional is obtained if the correlation term is ignored. The mean-field approach provides the basis for the Poisson–Boltzmann theory of the electric double layer described in Chapter 10.

The local-density and square-gradient functionals are both designed for use in cases where the inhomogeneity is both weak and slowly varying. Two different strategies have been devised to deal with situations in which these conditions are not met. The first, already discussed in a different context in Section 4.3, is based on a functional Taylor expansion of $\mathcal{F}^{\mathrm{ex}}$ in powers of the deviation from the bulk density. Truncation of the expansion at second order, and replacement of the direct correlation function by that of the reference system, leads to the expression for the density profile given by (4.3.16); the quadratic functional (6.2.1) is then recovered if the ideal contribution to the free energy is also expanded to second order. Equation (4.3.16) provides the starting point for a theory of freezing described in Section 6.6. The alternative approach involves the concept of a weighted or

coarse-grained local density. There are some circumstances in which the local density can reach values greater than that corresponding to close packing. This is true, for example, of a dense hard-sphere fluid close to a solid surface. In such cases the local-density approximation becomes meaningless. However, a non-local approximation with a structure not unlike (6.2.5) can be devised by introducing a coarse-grained density $\bar{\rho}(\mathbf{r})$, defined as a weighted average of $\rho^{(1)}(\mathbf{r})$ over a volume comparable with the volume of a particle, i.e.

$$\bar{\rho}(\mathbf{r}) = \int w\big(|\mathbf{r}-\mathbf{r}'|\big)\rho^{(1)}(\mathbf{r}')\,\mathrm{d}\mathbf{r}' \tag{6.2.16}$$

where $w(|\mathbf{r}|)$ is some suitable weight function, normalised such that

$$\int w\big(|\mathbf{r}|\big)\,\mathrm{d}\mathbf{r} = 1 \tag{6.2.17}$$

The excess part of the free-energy functional is then taken to be

$$\mathcal{F}^{\mathrm{ex}}\big[\rho^{(1)}\big] = \int \phi^{\mathrm{ex}}(\bar{\rho})\rho^{(1)}(\mathbf{r})\,\mathrm{d}\mathbf{r} \tag{6.2.18}$$

where $\phi^{\mathrm{ex}}(\bar{\rho}) = f^{\mathrm{ex}}(\bar{\rho})/\bar{\rho}$ is the excess free energy per particle of the homogeneous fluid at a density $\bar{\rho}(\mathbf{r})$; the exact form (3.1.22) is retained for the ideal part. Equation (6.2.18) represents a *weighted-density approximation*.

The difficulty in implementing a weighted-density approximation lies in making an appropriate choice of weight function.[4] A useful guide is obtained by considering the low-density limit. The virial expansion developed in Section 3.9 shows that to lowest order in density the excess free energy per particle of a homogeneous fluid of density ρ_0 is $\phi^{\mathrm{ex}}(\rho_0) = k_{\mathrm{B}}T\rho_0 B_2$, where B_2 is the second virial coefficient (3.9.7). In the case of hard spheres, B_2 is given by the integral

$$B_2 = \tfrac{1}{2}\int \Theta\big(|\mathbf{r}|-d\big)\,\mathrm{d}\mathbf{r} \tag{6.2.19}$$

where d is the hard-sphere diameter and $\Theta(x)$ is a unit step function: $\Theta(x) = 1$, $x < 0$; $\Theta(x) = 0$, $x > 0$. The total excess free energy of the homogeneous fluid can therefore be written as

$$\beta F^{\mathrm{ex}} = \beta\int \rho_0\phi^{\mathrm{ex}}(\rho_0)\,\mathrm{d}\mathbf{r} = \tfrac{1}{2}\int \mathrm{d}\mathbf{r}\int \mathrm{d}\mathbf{r}'\,\rho_0^2\Theta\big(|\mathbf{r}-\mathbf{r}'|-d\big) \tag{6.2.20}$$

This result is immediately generalisable to the inhomogeneous case in the form

$$\begin{aligned}\beta\mathcal{F}^{\mathrm{ex}}\big[\rho^{(1)}\big] &= \tfrac{1}{2}\int \mathrm{d}\mathbf{r}\int \mathrm{d}\mathbf{r}'\,\rho^{(1)}(\mathbf{r})\Theta\big(|\mathbf{r}-\mathbf{r}'|-d\big)\rho^{(1)}(\mathbf{r}') \\ &= \tfrac{1}{2}\beta\int \phi^{\mathrm{ex}}(\bar{\rho})\rho^{(1)}(\mathbf{r})\,\mathrm{d}\mathbf{r}\end{aligned} \tag{6.2.21}$$

where $\bar{\rho}(\mathbf{r})$ is the weighted density defined by (6.2.16), with a weight function given by

$$w\big(|\mathbf{r}|\big) = \frac{1}{2B_2}\Theta\big(|\mathbf{r}| - d\big) = \frac{3}{4\pi d^3}\Theta\big(|\mathbf{r}| - d\big) \tag{6.2.22}$$

which corresponds to averaging the density uniformly over a sphere of radius d. The same approximation may be used at higher densities if combined with a suitable expression for $\phi^{\mathrm{ex}}(\bar{\rho})$, such as that derived from the Carnahan–Starling equation of state. This leads to qualitatively satisfactory results for the oscillatory density profiles of hard spheres near hard, planar walls;[5] an example is shown later in Figure 6.4, from which the quantitative deficiencies in the approximation are evident. Significant improvement is achievable, at the cost of greater computational effort, if the weight function itself is made dependent on the weighted density.[6] For example, we can retain (6.2.18) but replace (6.2.16) by

$$\bar{\rho}(\mathbf{r}) = \int w\big(|\mathbf{r} - \mathbf{r}'|, \bar{\rho}\big)\rho^{(1)}(\mathbf{r}')\,\mathrm{d}\mathbf{r}' \tag{6.2.23}$$

Alternatively, we can write the free-energy functional in the form

$$\mathcal{F}^{\mathrm{ex}}\big[\rho^{(1)}\big] = N\phi^{\mathrm{ex}}(\bar{\rho}) \tag{6.2.24}$$

where $\bar{\rho}$ is a position-independent, weighted density given by

$$\bar{\rho} = \frac{1}{N}\int \mathrm{d}\mathbf{r}\,\rho^{(1)}(\mathbf{r}) \int \mathrm{d}\mathbf{r}'\, w\big(|\mathbf{r} - \mathbf{r}'|, \bar{\rho}\big)\rho^{(1)}(\mathbf{r}') \tag{6.2.25}$$

In either case, a solution for $w(|\mathbf{r}|, \bar{\rho})$ can be obtained by functionally differentiating $\mathcal{F}^{\mathrm{ex}}$ twice with respect to $\rho^{(1)}$ to give $c(\mathbf{r})$ (see (3.5.2)) and matching the results to those for the reference system. Numerical calculations therefore require as input not only the free energy of the uniform fluid but also the direct correlation function, which would normally be obtained from some approximate integral equation. For many purposes, however, these methods has been superseded by the *fundamental-measure theory* of Rosenfeld,[7] a discussion of which we defer until Section 6.4.

6.3 THE LIQUID–VAPOUR INTERFACE

An interface between bulk phases will form spontaneously whenever the thermodynamic conditions necessary for phase coexistence are met. The most familiar example is the interface that forms between a liquid and its coexisting vapour, for which the density profile $\rho^{(1)}(z)$ varies smoothly with the single coordinate z in the manner illustrated schematically in Figure 6.1. At low temperatures the width of the interface is of the order of a few particle diameters, but since the distinction between the two phases vanishes continuously at the critical temperature, the width is expected to increase rapidly as the critical point is approached and the densities ρ_{L} and ρ_{G} merge towards a common value, the critical density ρ_{c}. The smoothness of the profile makes this a problem to which the square-gradient

approximation is well suited. Such a calculation was first carried out by van der Waals, whose work is the earliest known example of the use in statistical mechanics of what are now called density-functional methods. The Euler–Lagrange equation to be solved is (6.2.11) in the limit in which the gravitational potential $\phi(z) = mgz$ becomes vanishingly small. So long as the inhomogeneity is of small amplitude, i.e. $(\rho_L - \rho_G) \ll \rho_c$, the coefficient f_2 of the square-gradient term is related by (6.2.15b) to the direct correlation function of the bulk, reference system. For condensation to occur, the interparticle potential must contain an attractive term, $w(r)$ say. Within the random-phase approximation, $c(r) \approx c_0(r) - \beta w(r)$ (see (3.5.17)), but the presence of a factor r^4 in the integrand means that the contribution to the integral in (6.2.15b) from the short-range function $c_0(r)$ can be ignored. Thus

$$f_2 \approx -\tfrac{1}{3}\pi \int_0^\infty w(r) r^4 \, \mathrm{d}r = \tfrac{1}{2}m \tag{6.3.1}$$

where m is a positive, density-independent constant. Equation (6.2.11) then takes the simpler form

$$m \frac{\mathrm{d}^2 \rho^{(1)}(z)}{\mathrm{d}z^2} = -\frac{\mathrm{d}W(\rho^{(1)})}{\mathrm{d}\rho^{(1)}} \tag{6.3.2}$$

where $W(\rho^{(1)}) = -f_0(\rho^{(1)}) + \mu\rho^{(1)}$. The analogy between this expression and Newton's equation of motion is obvious, with m, z, $\rho^{(1)}(z)$ and $W(\rho^{(1)})$ playing the roles of mass, time, position and potential energy, respectively. Equation (6.3.2) is a non-linear differential equation that must be solved subject to the boundary conditions $\lim_{z\to\pm\infty} W(\rho^{(1)}) = W(\rho_B) = -f_0(\rho_B) + \mu\rho_B = P$, where ρ_B is the bulk density of either liquid (as $z \to -\infty$) or gas (as $z \to +\infty$) and P is the bulk pressure. When integrated, (6.3.2) becomes

$$W\big(\rho^{(1)}\big) + \tfrac{1}{2}m\left(\frac{\mathrm{d}\rho^{(1)}(z)}{\mathrm{d}z}\right)^2 = P \tag{6.3.3}$$

which is the analogue of the conservation of mechanical energy, while a second integration yields a parametric representation of the density profile in the form of a quadrature:

$$z = -\left(\frac{m}{2}\right)^{1/2} \int_{\rho^{(1)}(0)}^{\rho^{(1)}(z)} \big[P - W(\rho)\big]^{-1/2} \, \mathrm{d}\rho \tag{6.3.4}$$

By definition, $W(\rho) = -\omega(\rho)$, where $\omega = \Omega/V$ is the grand potential per unit volume of the fluid at a density $\rho = \rho^{(1)}(z)$. At liquid–gas coexistence, $\omega(\rho)$ has two minima of equal depth, situated at $\rho = \rho_L$ and $\rho = \rho_G$, with $\omega(\rho_L) = \omega(\rho_G) = -P$. A simple parametrisation of $\omega(\rho)$, valid near the critical point is

$$\omega(\rho) = \tfrac{1}{2}C(\rho - \rho_L)^2(\rho - \rho_G)^2 - P \tag{6.3.5}$$

where both C and the pressure at coexistence, P, are functions of temperature. Substitution of (6.3.5) in (6.3.4) gives

$$z = -\left(\frac{m}{C}\right)^{1/2} \int_{\rho^{(1)}(0)}^{\rho^{(1)}(z)} \frac{\mathrm{d}\rho}{(\rho_{\mathrm{L}} - \rho)(\rho - \rho_{\mathrm{G}})} = -\zeta \ln\left(\frac{\rho^{(1)}(z) - \rho_{\mathrm{G}}}{\rho_{\mathrm{L}} - \rho^{(1)}(z)}\right) \tag{6.3.6}$$

where $\zeta = (m/C)^{1/2}/(\rho_{\mathrm{L}} - \rho_{\mathrm{G}})$ is a characteristic length that provides a measure of the interfacial width. Equation (6.3.6) is easily solved to give $\rho^{(1)}$ as a function of z:

$$\begin{aligned} \rho^{(1)}(z) &= \frac{\rho_{\mathrm{G}}}{1 + \exp(-z/\zeta)} + \frac{\rho_{\mathrm{L}}}{1 + \exp(z/\zeta)} \\ &= \tfrac{1}{2}(\rho_{\mathrm{L}} + \rho_{\mathrm{G}}) - \tfrac{1}{2}(\rho_{\mathrm{L}} - \rho_{\mathrm{G}}) \tanh\left(\frac{z}{2\zeta}\right) \end{aligned} \tag{6.3.7}$$

which has the general shape pictured in Figure 6.1. The predicted profile is therefore antisymmetric with respect to the mid-point, a result consequent on the symmetric form assumed for the grand potential in (6.3.5) and the neglect of the density dependence of the coefficient f_2. In reality, the profile is steeper on the liquid than on the vapour side. Equation (6.3.7) also implies that the width of the interface diverges at the critical point. Within the mean-field theory of phase transitions, $(\rho_{\mathrm{L}} - \rho_{\mathrm{G}})$ behaves as $(T_{\mathrm{c}} - T)^{1/2}$ as the critical temperature is approached from below,[8] so ζ diverges as $(T_{\mathrm{c}} - T)^{-1/2}$. Note, however, that density-functional theory provides only an "intrinsic" or averaged description of the density profile. The physical interface is a fluctuating object; these "capillary" fluctuations lead to a thermal broadening of the interface that can be comparable with the theoretical, intrinsic thickness.

The surface tension is defined thermodynamically as the additional free energy per unit area due to the presence of an interface. Accordingly, within the square-gradient approximation:

$$\gamma = \int_{-\infty}^{\infty} \left(f_0\big(\rho^{(1)}\big) + \tfrac{1}{2}m\big(\mathrm{d}\rho^{(1)}/\mathrm{d}z\big)^2 - f_{\mathrm{B}}\right) \mathrm{d}z \tag{6.3.8}$$

where f_{B} is the bulk free-energy density, equal to f_{L} for $z < z_0$ and to f_{G} for $z > z_0$. Now $f_0(\rho) = -W(\rho) + \mu\rho$ and $W(\rho)$ is given by (6.3.3), from which the bulk pressure can be eliminated by use of the thermodynamic relation $P = f_{\mathrm{B}} - \mu\rho_{\mathrm{B}}$. Equation (6.3.8) therefore reduces to

$$\begin{aligned} \gamma &= \int_{-\infty}^{\infty} \left(-P + \mu\rho^{(1)}(z) + m\big(\mathrm{d}\rho^{(1)}/\mathrm{d}z\big)^2 - f_B\right) \mathrm{d}z \\ &= \int_{-\infty}^{\infty} \left(\mu\big[\rho^{(1)}(z) - \rho_{\mathrm{B}}\big] + m\big(\mathrm{d}\rho^{(1)}/\mathrm{d}z\big)^2\right) \mathrm{d}z = m \int_{-\infty}^{\infty} \big(\mathrm{d}\rho^{(1)}/\mathrm{d}z\big)^2 \, \mathrm{d}z \end{aligned} \tag{6.3.9}$$

Use of (6.3.3) and (6.3.5) allows (6.3.9) to be recast in the equivalent form:

$$\gamma = m \int_{-\infty}^{\infty} \frac{\mathrm{d}\rho^{(1)}}{\mathrm{d}z} \, \mathrm{d}\rho^{(1)} = (2m)^{1/2} \int_{\rho_{\mathrm{L}}}^{\rho_{\mathrm{G}}} \big[P + \omega(\rho)\big]^{1/2} \, \mathrm{d}\rho$$

$$= -(mC)^{1/2} \int_{\rho_L}^{\rho_G} (\rho_L - \rho)(\rho - \rho_G)\, d\rho = \tfrac{1}{6}(mC)^{1/2}(\rho_L - \rho_G)^3 \qquad (6.3.10)$$

Thus, close to the critical point, the surface tension is predicted to behave as $\gamma \sim (T_c - T)^{3/2}$. Experimentally the critical exponent is found to be somewhat smaller than $\frac{3}{2}$.

6.4 FUNDAMENTAL-MEASURE THEORY

Fundamental-measure theory is a generalised form of weighted-density approximation for fluids consisting of hard particles. In contrast to similar approximations discussed in Section 6.2, the free-energy density is taken to be a function not just of one but of several different weighted densities, defined by weight functions that emphasise the geometrical characteristics of the particles. The theory was originally formulated for hard-sphere mixtures, but for the sake of simplicity we consider in detail only the one-component case. Its development[7] was inspired by the link that exists between scaled-particle theory[9] – described in Appendix E – and the Percus–Yevick approximation for hard spheres. Scaled-particle theory provides only thermodynamic properties, while the PY approximation is a theory of pair structure, but the PY equation of state obtained via the compressibility route is identical to the scaled-particle result; the same is true for binary mixtures.

The derivation of the theory starts from the observation that the PY expression (4.4.10) for the two-particle direct correlation function of the hard-sphere fluid can be rewritten in terms of quantities that characterise the geometry of two intersecting spheres of radius R ($= \frac{1}{2}d$) and separated by a distance $r < 2R$, as pictured in Figure 6.2. The quantities involved are the overlap volume $\Delta V(r)$, the overlap surface area $\Delta S(r)$ and the "overlap radius" $\Delta R(r) = 2R - \overline{R}$, where $\overline{R} = R + r/4$ is the mean radius of the convex envelope

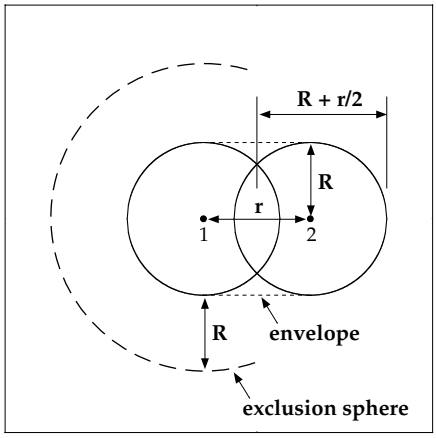

FIG. 6.2. Geometry of two overlapping hard spheres of radius R and separation r. The exclusion sphere of radius $2R$ drawn around sphere 1 defines the region into which the centre of another sphere cannot enter without creating an overlap.

surrounding the spheres. Written in this way, (4.4.10) becomes

$$-c(r) = \chi^{(3)}\Delta V(r) + \chi^{(2)}\Delta S(r) + \chi^{(1)}\Delta R(r) + \chi^{(0)}\Theta\big(|\mathbf{r}| - 2R\big) \tag{6.4.1}$$

where the step function $\Theta(|\mathbf{r}| - 2R)$, defined in the previous section, is the "characteristic" volume function of the exclusion sphere shown in the figure. The density-dependent coefficients $\chi^{(\alpha)}$ can be expressed in the form

$$\begin{aligned}
\chi^{(0)} &= \frac{1}{1-\xi_3}, \qquad \chi^{(1)} = \frac{\xi_2}{(1-\xi_3)^2} \\
\chi^{(2)} &= \frac{\xi_1}{(1-\xi_3)^2} + \frac{\xi_2^2}{4\pi(1-\xi_3)^3} \\
\chi^{(3)} &= \frac{\xi_0}{(1-\xi_3)^2} + \frac{2\xi_1\xi_2}{(1-\xi_3)^3} + \frac{\xi_2^3}{4\pi(1-\xi_3)^4}
\end{aligned} \tag{6.4.2}$$

with $\xi_\alpha = \rho\mathcal{R}^{(\alpha)}$, where the quantities $\mathcal{R}^{(\alpha)}$ are the "fundamental geometric measures" of a sphere:

$$\begin{aligned}
&\mathcal{R}^{(3)} = \tfrac{4}{3}\pi R^3 \quad \text{(volume)}, && \mathcal{R}^{(2)} = 4\pi R^2 \quad \text{(surface area)} \\
&\mathcal{R}^{(1)} = R \quad \text{(radius)}, && \mathcal{R}^{(0)} = 1
\end{aligned} \tag{6.4.3}$$

The variables ξ_α also arise naturally in scaled-particle theory. In particular, the scaled-particle free-energy density (see Appendix E) can be written as

$$\frac{\beta F^{\text{ex}}}{V} = -\xi_0\ln(1-\xi_3) + \frac{\xi_1\xi_2}{1-\xi_3} + \frac{\xi_2^3}{24\pi(1-\xi_3)^2} \tag{6.4.4}$$

The same result applies to mixtures if the scaled-particle variables are replaced by their multi-component generalisations, i.e. $\xi_\alpha = \sum_\nu \rho_\nu \mathcal{R}_\nu^{(\alpha)}$, where ρ_ν is the number density of spheres of radius R_ν and fundamental measures $\mathcal{R}_\nu^{(\alpha)}$.

The overlap volume, surface and radius are geometric measures associated with a pair of overlapping spheres, but they are also expressible in terms of convolutions of the characteristic volume and surface functions of individual spheres:

$$\omega^{(3)}(\mathbf{r}) = \Theta\big(|\mathbf{r}| - R\big) \quad \text{(volume)}, \qquad \omega^{(2)}(\mathbf{r}) = \delta\big(|\mathbf{r}| - R\big) \quad \text{(surface)} \tag{6.4.5}$$

via the relations

$$\begin{aligned}
\Delta V(r) = \omega^{(3)} \otimes \omega^{(3)} &= \int \Theta\big(|\mathbf{r}'| - R\big)\Theta\big(|\mathbf{r} - \mathbf{r}'| - R\big)\,\mathrm{d}\mathbf{r}' \\
&= \tfrac{2}{3}\pi\big(2R^3 - 3R^2 r + r^3\big)\Theta\big(|\mathbf{r}| - 2R\big) \\
\Delta S(r) = 2\omega^{(3)} \otimes \omega^{(2)} &= 2\int \Theta\big(|\mathbf{r}'| - R\big)\delta\big(|\mathbf{r} - \mathbf{r}'| - R\big)\,\mathrm{d}\mathbf{r}' \\
&= 4\pi R^2(1 - r/2R)\Theta\big(|\mathbf{r}| - 2R\big)
\end{aligned}$$

$$\Delta R(r) = \frac{\Delta S(r)}{8\pi R} + \tfrac{1}{2} R\Theta\big(|\mathbf{r}| - 2R\big) = (R - r/4)\Theta\big(|\mathbf{r}| - 2R\big) \tag{6.4.6}$$

When results are brought together, it is straightforward to show that (6.4.1) is identical to (4.4.10); in particular, $c(r)$ is strictly zero for $r > 2R$ and $c(r) \to -\Theta(|\mathbf{r}| - 2R)$ as $\rho \to 0$. It is, in addition, clear that if $c(r)$ is to be written solely in terms of functions characteristic of individual spheres, the pair function $\Theta(|\mathbf{r}| - 2R)$ must be replaced by some convolution of single-sphere functions; this can be achieved with a basis set consisting of the two scalar functions (6.4.5), a vector function

$$\boldsymbol{\omega}^{(2)}(\mathbf{r}) = \nabla\omega^{(3)}(\mathbf{r}) = \frac{\mathbf{r}}{r}\delta\big(|\mathbf{r}| - R\big) \tag{6.4.7}$$

and three further functions proportional to either $\omega^{(2)}(\mathbf{r})$ or $\boldsymbol{\omega}^{(2)}(\mathbf{r})$:

$$\omega^{(1)}(\mathbf{r}) = \frac{\omega^{(2)}(\mathbf{r})}{4\pi R}, \qquad \omega^{(0)}(\mathbf{r}) = \frac{\omega^{(2)}(\mathbf{r})}{4\pi R^2}, \qquad \boldsymbol{\omega}^{(1)}(\mathbf{r}) = \frac{\boldsymbol{\omega}^{(2)}(\mathbf{r})}{4\pi R} \tag{6.4.8}$$

The vector functions are needed to account for the discontinuity in the step function. Then

$$\Theta\big(|\mathbf{r}| - 2R\big) = 2\big(\omega^{(3)} \otimes \omega^{(0)} + \omega^{(2)} \otimes \omega^{(1)} + \boldsymbol{\omega}^{(2)} \otimes \boldsymbol{\omega}^{(1)}\big) \tag{6.4.9}$$

where the convolution of two vector functions also implies a scalar product; this result is most easily verified by taking Fourier transforms. In the limit $\mathbf{k} \to 0$, the transforms of the scalar characteristic functions are related to the scaled-particle variables by

$$\rho\hat{\omega}^{(\alpha)}(\mathbf{k} = 0) = \xi_\alpha, \quad \alpha = 0 \text{ to } 3 \tag{6.4.10}$$

while the transforms of the vector functions vanish:

$$\hat{\boldsymbol{\omega}}^{(\alpha')}(\mathbf{k} = 0) = 0, \quad \alpha' = 1,\ 2 \tag{6.4.11}$$

Use of the characteristic functions (6.4.5), (6.4.7) and (6.4.8) as a basis therefore allows the PY direct correlation function to be expressed as a linear combination of convolutions in the form

$$c(r) = \sum_\alpha \sum_\beta c_{\alpha\beta}\, \omega^{(\alpha)} \otimes \omega^{(\beta)} \tag{6.4.12}$$

where a simplified notation is adopted in which the sums on α and β run over both scalar and vector functions; the density-dependent coefficients $c_{\alpha\beta}$ are proportional[7] to the functions $\chi^{(\alpha)}$ defined by (6.4.2). A different set of basis functions that does not involve vector functions has been proposed, but this turns out to be equivalent to the one we have described in the sense that it leads ultimately to the same free-energy functional.[10]

The key assumption of fundamental-measure theory is that the excess free-energy functional has the form

$$\beta\mathcal{F}^{\text{ex}}\big[\rho^{(1)}\big] = \int \Phi^{\text{ex}}\big(\{\bar{\rho}_\alpha(\mathbf{r}')\}\big)\, \mathrm{d}\mathbf{r}' \tag{6.4.13}$$

where the free-energy density Φ^{ex} (in units of $k_{\text{B}}T$) is a function of a set of weighted densities, each defined in the manner of (6.2.16), i.e.

$$\bar{\rho}_\alpha(\mathbf{r}) = \int w_\alpha\big(|\mathbf{r}-\mathbf{r}'|\big)\rho^{(1)}(\mathbf{r}')\,\mathrm{d}\mathbf{r}' \tag{6.4.14}$$

It follows from (3.5.2) that if the scheme contained in (6.4.13) and (6.4.14) is adopted, the direct correlation function of the uniform fluid is of the form

$$c(r) = -\sum_\alpha \sum_\beta \frac{\partial^2 \Phi^{\text{ex}}}{\partial\bar{\rho}_\alpha \partial\bar{\rho}_\beta} w_\alpha \otimes w_\beta \tag{6.4.15}$$

Comparison of (6.4.15) with (6.4.12) suggests immediately that the appropriate choice of weight functions in (6.4.14) are the characteristic functions $\omega^{(\alpha)}(\mathbf{r})$ and $\boldsymbol{\omega}^{(\alpha')}(\mathbf{r})$, and hence that the set $\{\bar{\rho}_\alpha\}$ is one consisting of four scalar and two vector densities:

$$\begin{aligned}
\bar{\rho}_\alpha(\mathbf{r}) &= \int \omega^{(\alpha)}\big(|\mathbf{r}-\mathbf{r}'|\big)\rho^{(1)}(\mathbf{r}')\,\mathrm{d}\mathbf{r}', \quad \alpha = 0 \text{ to } 3 \\
\bar{\boldsymbol{\rho}}_{\alpha'}(\mathbf{r}) &= \int \boldsymbol{\omega}^{(\alpha')}(\mathbf{r}-\mathbf{r}')\rho^{(1)}(\mathbf{r}')\,\mathrm{d}\mathbf{r}', \quad \alpha' = 1,\ 2
\end{aligned} \tag{6.4.16}$$

If the system is homogeneous, the scalar weighted densities reduce to the scaled-particle variables (6.4.2) and the vectorial densities vanish. The scalar densities have the dimensions of the corresponding ξ_α, i.e. $[\text{L}]^{\alpha-3}$; $\bar{\boldsymbol{\rho}}_1$ and $\bar{\boldsymbol{\rho}}_2$ have the same dimensions as $\bar{\rho}_1$ and $\bar{\rho}_2$, respectively.

The precise functional form of the free-energy density remains to be specified. One obvious possibility, in the spirit of a virial expansion, is to write Φ^{ex} as a linear combination of the lowest powers of the weighted densities and their products. In that case, since Φ^{ex} is a scalar with the dimensions of density, it can only be a sum of terms in $\bar{\rho}_0$, $\bar{\rho}_1\bar{\rho}_2$, $\bar{\rho}_2^3$, $\bar{\boldsymbol{\rho}}_1 \cdot \bar{\boldsymbol{\rho}}_2$ and $\bar{\rho}_2(\bar{\boldsymbol{\rho}}_2 \cdot \bar{\boldsymbol{\rho}}_2)$, with coefficients that are functions of the dimensionless density $\bar{\rho}_3$. Thus

$$\Phi^{\text{ex}}\big(\{\bar{\rho}_\alpha\}\big) = \phi_0\bar{\rho}_0 + \phi_1\bar{\rho}_1\bar{\rho}_2 + \phi_2\bar{\rho}_2^3 + \phi_3\bar{\boldsymbol{\rho}}_1 \cdot \bar{\boldsymbol{\rho}}_2 + \phi_4\bar{\rho}_2(\bar{\boldsymbol{\rho}}_2 \cdot \bar{\boldsymbol{\rho}}_2) \tag{6.4.17a}$$

or, in the case of a uniform fluid:

$$\Phi^{\text{ex}}\big(\{\xi_\alpha\}\big) = \phi_0\xi_0 + \phi_1\xi_1\xi_2 + \phi_2\xi_2^3 \tag{6.4.17b}$$

The excess free-energy functional follows from (6.4.13) and the corresponding excess grand potential is

$$\Omega^{\text{ex}}\big[\rho^{(1)}\big] \equiv -\int P^{\text{ex}}\big[\rho^{(1)}\big]\,\mathrm{d}\mathbf{r} = \mathcal{F}^{\text{ex}}\big[\rho^{(1)}\big] - \int \rho^{(1)}(\mathbf{r})\frac{\delta\mathcal{F}^{\text{ex}}}{\delta\rho^{(1)}(\mathbf{r})}\,\mathrm{d}\mathbf{r} \tag{6.4.18}$$

Hence the excess-pressure $P^{\rm ex}$ (a functional of $\rho^{(1)}$) is given by the expression

$$\beta P^{\rm ex}\big[\rho^{(1)}\big] = -\Phi^{\rm ex} + \sum_{\alpha} \bar{\rho}_{\alpha}(\mathbf{r}) \frac{\partial \Phi^{\rm ex}}{\partial \bar{\rho}_{\alpha}} \tag{6.4.19}$$

where the sum runs over all densities in the set $\{\bar{\rho}_{\alpha}\}$.

Now consider the problem from the point of view of scaled-particle theory, which provides an approximation for the excess chemical potential $\mu_{\nu}^{\rm ex}$ of a solute particle of radius R_{ν} in a uniform fluid of hard spheres. It is shown in Appendix E that in the limit $R_{\nu} \to \infty$, $\mu_{\nu}^{\rm ex} \to P V_{\nu}$, where V_{ν} is the volume of the particle and P is the bulk pressure. But it follows from (6.4.17b), as applied to a mixture, that the chemical potential of the solute, $\mu_{\nu}^{\rm ex} = k_{\rm B}T(\partial \Phi^{\rm ex}/\partial \rho_{\nu})$, must also satisfy the relation

$$\beta \mu_{\nu}^{\rm ex} = \sum_{\alpha} \frac{\partial \Phi^{\rm ex}}{\partial \xi_{\alpha}} \frac{\partial \xi_{\alpha}}{\partial \rho_{\nu}} = \frac{\partial \Phi^{\rm ex}}{\partial \xi_3} V_{\nu} + \mathcal{O}\big(R_{\nu}^2\big) \tag{6.4.20}$$

Thus the derivative $\partial \Phi^{\rm ex}/\partial \xi_3$ can be identified as βP. Within fundamental-measure theory the further assumption is now made that the analogous relation is valid for the inhomogeneous fluid, i.e. that

$$\frac{\partial \Phi^{\rm ex}}{\partial \bar{\rho}_3} = \beta P^{\rm ex}\big[\rho^{(1)}\big] + \bar{\rho}_0 \tag{6.4.21}$$

and combination of (6.4.19) and (6.4.21) yields a differential equation for the free-energy density in the form

$$-\Phi^{\rm ex} + \sum_{\alpha} \bar{\rho}_{\alpha} \frac{\partial \Phi^{\rm ex}}{\partial \bar{\rho}_{\alpha}} + \bar{\rho}_0 = \frac{\partial \Phi^{\rm ex}}{\partial \bar{\rho}_3} \tag{6.4.22}$$

Substitution of (6.4.17a) into (6.4.22), and identification of the coefficients of the basis functions in the expansion (6.4.17a), then leads to five, first-order differential equations, one for each of the coefficients ϕ_i; these equations are easily solved to give

$$\begin{aligned} &\phi_0 = -\ln(1-\bar{\rho}_3) + c_0, \qquad \phi_1 = \frac{c_1}{1-\bar{\rho}_3} \\ &\phi_2 = \frac{c_2}{(1-\bar{\rho}_3)^2}, \qquad \phi_3 = \frac{c_3}{1-\bar{\rho}_3}, \qquad \phi_4 = \frac{c_4}{(1-\bar{\rho}_3)^2} \end{aligned} \tag{6.4.23}$$

The constants of integration, c_i, are chosen to ensure that both the free energy and its second functional derivative, i.e. the two-particle direct correlation function (see (3.5.2)), go over correctly to their known, low-density limits in the case of a uniform fluid.[11] These constraints give $c_0 = 0$, $c_1 = 1$, $c_2 = 1/24\pi$, $c_3 = -1$ and $c_4 = -1/8\pi$.[12] The excess free-energy density is thereby completely determined and may be written in the form

$$\Phi^{\rm ex}\big(\{\bar{\rho}_{\alpha}\}\big) = \Phi_1 + \Phi_2 + \Phi_3 \tag{6.4.24}$$

with

$$\Phi_1 = -\bar{\rho}_0 \ln(1-\bar{\rho}_3), \qquad \Phi_2 = \frac{\bar{\rho}_1\bar{\rho}_2 - \bar{\boldsymbol{\rho}}_1 \cdot \bar{\boldsymbol{\rho}}_2}{1-\bar{\rho}_3}$$
$$\Phi_3 = \frac{\bar{\rho}_2^3 - 3\bar{\rho}_2(\bar{\boldsymbol{\rho}}_2 \cdot \bar{\boldsymbol{\rho}}_2)}{24\pi(1-\bar{\rho}_3)^2} \tag{6.4.25}$$

which reduces to the scaled-particle result (6.4.4) for a uniform fluid. The two-particle direct correlation function obtained by differentiation of the free energy reduces in turn to the PY expression (6.4.1), while the third functional derivative yields a three-particle function in good agreement with the results of Monte Carlo calculations.[13] As Figure 4.2 shows, the scaled-particle (or PY compressibility) equation of state slightly overestimates the pressure of the hard-sphere fluid. Some improvement in performance can therefore be expected if the assumed form of the free-energy density is modified in such a way as to recover the Carnahan–Starling equation of state (3.9.17) in the uniform-fluid limit.[14]

The theory is easily generalised to the case of hard-sphere mixtures. Scalar and vectorial characteristic functions $\omega_\nu^{(\alpha)}(\mathbf{r})$ and $\boldsymbol{\omega}_\nu^{(\alpha)}$ are defined for each species ν in a manner completely analogous to the one-component case, with R_ν replacing R. The characteristic functions are then used as weight functions in the definition of a set of global weighted densities:

$$\bar{\rho}_\alpha(\mathbf{r}) = \sum_\nu \int \omega_\nu^{(\alpha)}\big(|\mathbf{r}-\mathbf{r}'|\big)\rho_\nu^{(1)}(\mathbf{r}')\,\mathrm{d}\mathbf{r}', \quad \alpha = 0 \text{ to } 3$$
$$\bar{\boldsymbol{\rho}}_{\alpha'}(\mathbf{r}) = \sum_\nu \int \boldsymbol{\omega}_\nu^{(\alpha')}\big(|\mathbf{r}-\mathbf{r}'|\big)\rho_\nu^{(1)}(\mathbf{r}')\,\mathrm{d}\mathbf{r}', \quad \alpha' = 1,\ 2 \tag{6.4.26}$$

where $\rho_\nu^{(1)}$ is the density profile of species ν, and the free-energy density of the mixture is again given by (6.4.25), or some other, improved form.

The same general approach[15] can be used to derive free-energy functionals for hard-core systems in dimensions $\mathcal{D} = 1$ (hard rods) or $\mathcal{D} = 2$ (hard disks). For $\mathcal{D} = 1$, where only two weight functions are required, this leads to the exact hard-rod functional due to Percus.[16] For $\mathcal{D} = 2$, the procedure is less straightforward, since the decomposition of the Mayer function analogous to (6.4.9) is not achievable with any finite set of basis functions and the PY equation does not have an analytical solution. One and two-dimensional hard-core systems may be regarded as special cases of a hard-sphere fluid confined to a cylindrical pore ($\mathcal{D} = 1$) or a narrow slit ($\mathcal{D} = 2$) for which the diameter of the cylinder or width of the slit is equal to the hard-sphere diameter. Narrow confinement therefore corresponds to a reduction in effective dimensionality or "dimensional crossover", the most extreme example of which ($\mathcal{D} = 0$) occurs when a hard sphere is confined to a spherical cavity large enough to accommodate at most one particle. If the $\mathcal{D} = 3$ functional is to be used in studies of highly confined fluids, it is clearly desirable that it should reduce to the appropriate one- or two-dimensional functional for density profiles of the form $\rho^{(1)}(\mathbf{r}) = \rho^{(1)}(x)\delta(y)\delta(z)$ (for $\mathcal{D} = 1$) or $\rho^{(1)}(\mathbf{r}) = \rho^{(1)}(x, y)\delta(z)$ (for $\mathcal{D} = 2$). This turns out not to be the case. The

exact results for $\mathcal{D}=0$ and $\mathcal{D}=1$ are recovered if the term Φ_3 in (6.4.25) is omitted, but this leads to a considerable deterioration in the results for $\mathcal{D}=3$. A good compromise is achieved[17] if Φ_3 is replaced by

$$\Phi_3' = \frac{\bar{\rho}_2^3}{24\pi(1-\bar{\rho}_3)^2}\left(1-\xi^2\right)^3 \tag{6.4.27}$$

where $\xi(\mathbf{r}) = |\bar{\boldsymbol{\rho}}_2(\mathbf{r})/\bar{\rho}_2(\mathbf{r})|$. The modified term vanishes for $\mathcal{D}=0$ and is numerically small, except at the highest densities, for $\mathcal{D}=1$. In addition, since Φ_3' differs from Φ_3 only by terms of order ξ^4, differentiation of the resulting functional still leads to the PY result for the direct correlation function of the uniform fluid. However, the modification is essentially empirical in nature. A more systematic method of constructing free-energy functionals with the correct dimensional-crossover properties is to start from the exact result for $\mathcal{D}=0$ and build in successively the additional terms needed in higher dimensions.[18] That the functional should have at least the correct qualitative behaviour for $\mathcal{D}=0$ is essential for application to the solid phase, where each particle is confined to the nearly spherical cage formed by its nearest neighbours. The contribution from Φ_3 diverges to negative infinity in the zero-dimensional limit. Thus the theory in its unmodified form cannot account for solid–fluid coexistence, since the solid is always the stable phase.

6.5 CONFINED FLUIDS

The density-functional formalism has been successfully applied to a wide range of physical problems involving inhomogeneous fluids. In this section we describe some of the results obtained from calculations for fluids in confined geometries. The simplest example, illustrated in Figure 6.3, is that of a fluid near a hard, planar wall that confines the fluid strictly to a half-space $z \geqslant 0$, say, where the normal to the wall is taken as the z-axis. The particles of the fluid interact with the wall via a potential $\phi(z)$, which plays the role of the external potential in the theoretical treatment developed in earlier sections. For a hard wall the potential has a purely excluded-volume form, i.e. $\phi(z)=\infty,\ z<0,\ \phi(z)=0,\ z>0$, but more generally it will contain a steeply repulsive term together with a longer ranged, attractive part. If the particles making up the wall are assumed to interact with those of the fluid through a Lennard-Jones potential with parameters ε and σ, integration over a continuous distribution of particles within the wall leads to a wall–fluid potential given by

$$\phi(z) = \tfrac{2}{3}\pi\rho_{\mathrm{W}}\sigma^3\varepsilon\left[\tfrac{2}{15}(\sigma/z)^9 - (\sigma/z)^3\right] \tag{6.5.1}$$

where ρ_{W} is the density of particles in the wall; the surface of the wall is now at $z=0$. This so-called 9-3 potential has been widely adopted as a model of the wall–fluid interaction.

The density profile of a fluid against a planar wall is a function of the single coordinate z. If the bulk density ρ_{B} (the density far from the wall) is sufficiently large, the profile has a pronounced layer structure that extends several particle diameters into the fluid. When all interactions are of hard-core type, $\rho^{(1)}(z)$ may be calculated by density-functional theory

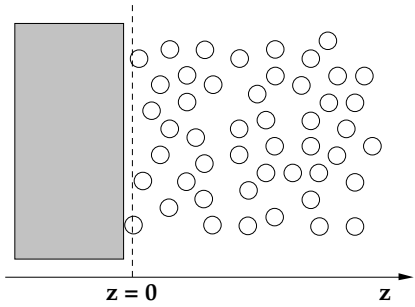

FIG. 6.3. A fluid confined by a hard wall; the centres of interaction of the particles are restricted to the region $z > 0$. For hard spheres of diameter d, the surface of the wall is at $z = -\frac{1}{2}d$.

with the boundary conditions:

$$\lim_{z\to\infty} \rho^{(1)}(z) = \rho_{\mathrm{B}} \tag{6.5.2a}$$

$$\lim_{z\to 0+} \rho^{(1)}(z) = \beta P \tag{6.5.2b}$$

where P is the bulk pressure; these conditions must be supplemented by the requirement that $\rho^{(1)}(z) = 0$ for $z < 0$. Equation (6.5.2b) is an expression of the *contact theorem*, $z = 0$ being the distance of closest approach of a hard sphere of diameter d to a hard wall with a surface at $z = -\frac{1}{2}d$ (see Figure 6.3). The proof of the contact theorem is similar to that of the relation (2.5.26) between the pressure of a uniform hard-sphere fluid and the value of the pair distribution function at contact. The density profile of a fluid against a hard wall is discontinuous at $z = 0$, but whatever the nature of the wall–fluid interaction the density profile can always be written in the form $\rho^{(1)}(z) = \exp[-\beta\phi(z)]y(z)$, where $y(z)$ is a continuous function of z, analogous to the cavity distribution function of a homogeneous fluid. The pressure exerted by the fluid on the wall must be balanced by the force per unit area exerted by the wall on the fluid, i.e.

$$P = -\int_0^\infty \frac{\mathrm{d}\phi(z)}{\mathrm{d}z}\rho^{(1)}(z)\,\mathrm{d}z = k_{\mathrm{B}}T\int_0^\infty \frac{\mathrm{d}}{\mathrm{d}z}\exp\bigl[-\beta\phi(z)\bigr]y(z)\,\mathrm{d}z \tag{6.5.3a}$$

and hence, in the case of a hard wall:

$$P = k_{\mathrm{B}}T\int_0^\infty \delta(z)y(z)\,\mathrm{d}z = k_{\mathrm{B}}T\rho^{(1)}(z = 0+) \tag{6.5.3b}$$

which is (6.5.2b).

The layering of a high-density, hard-sphere fluid near a hard wall is illustrated in Figure 6.4, where comparison is made between the density profile derived from fundamental-measure theory and results obtained by Monte Carlo calculations. Agreement between theory and simulation is excellent. The only significant discrepancies (not visible in the figure)

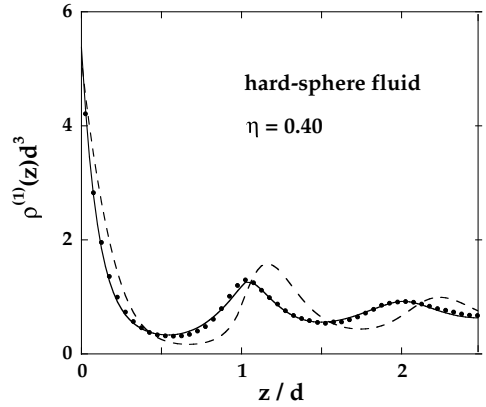

FIG. 6.4. Density profile of a hard-sphere fluid close to a hard wall at a packing fraction $\eta = 0.40$. The full curve is calculated from fundamental-measure theory and the points show the results of Monte Carlo calculations.[19] The dashed curve is calculated from the simpler weighted-density approximation provided by (6.2.22).

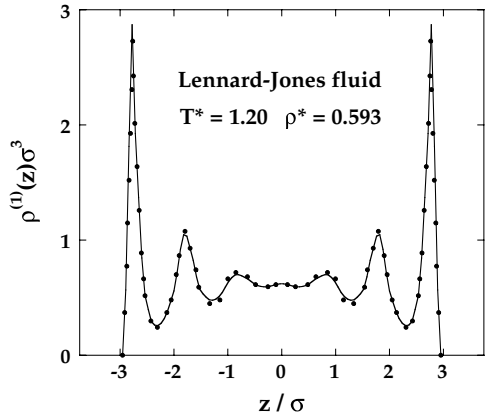

FIG. 6.5. Density profile of a Lennard-Jones fluid in a slit of width $L = 7.5\sigma$. The curve is calculated from fundamental-measure theory and the points show the results of a Monte Carlo simulation.[20] After Kierlik and Rosinberg.[21]

occur close to contact, where the theoretical values are too high. The source of these small errors lies in the fact that in the theory as implemented here the value at contact is determined, via the boundary condition (6.5.2b), by the pressure calculated from scaled-particle theory. As discussed in Section 6.4, such errors can be largely eliminated if the free-energy functional is tailored to reproduce a more accurate equation of state.

Though designed for systems of hard particles, fundamental-measure theory can also be used to calculate the density profiles and associated thermodynamic properties of a wider class of fluids if combined with the methods of perturbation theory described in Chapter 5. We suppose, as usual, that the pair potential $v(r)$ of the system of interest can be divided

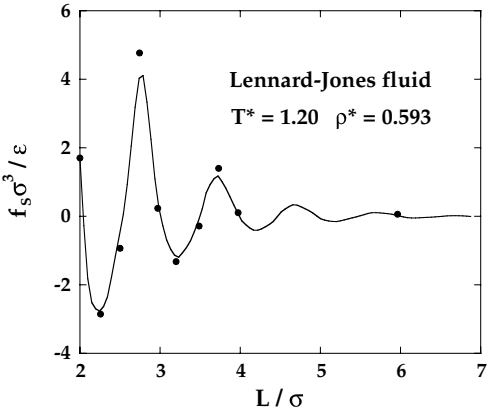

FIG. 6.6. Solvation force for a Lennard-Jones fluid in a slit as a function of slit width L. The curve is calculated from fundamental-measure theory and the points show the results of a Monte Carlo simulation.[22] After Kierlik and Rosinberg.[21]

into a reference part, $v_0(r)$, and a perturbation, $w(r)$. Then (3.4.10) provides an exact relation between the free-energy functional corresponding to the full potential, $\mathcal{F}[\rho^{(1)}]$, and that of the reference system, $\mathcal{F}_0[\rho^{(1)}]$. The obvious choice of reference system is again a fluid of hard spheres of diameter d given, say, by the Barker–Henderson prescription (5.3.11). If the perturbation is sufficiently weak to be treated in a mean-field approximation, the correlation term in (3.4.10) can be ignored. The grand-potential functional to be minimised is then of the form

$$\Omega_\phi[n] = \mathcal{F}_d[n] + \tfrac{1}{2}\iint n(\mathbf{r})w(\mathbf{r},\mathbf{r}')n(\mathbf{r}')\,\mathrm{d}\mathbf{r}\,\mathrm{d}\mathbf{r}' + \int n(\mathbf{r})\big[\phi(\mathbf{r}) - \mu\big]\,\mathrm{d}\mathbf{r} \qquad (6.5.4)$$

where $\mathcal{F}_d[\rho^{(1)}]$ is the free-energy functional of the hard-sphere system, taken to be of fundamental-measure form, and $n(\mathbf{r})$ is a trial density. This approximation has been widely used in a variety of applications to confined fluids. An example of the results obtained for the density profile of a Lennard-Jones fluid confined to a slit formed by two parallel plates separated by a distance L is pictured in Figure 6.5; the wall–fluid potential has a form similar to (6.5.1). When $L/\sigma \approx 3$, the density profile has a double-peaked structure, with maxima close to the walls of the slit. As the slit width increases, the number of layers of particles that can be accommodated also increases, with a third peak appearing initially mid-way between the walls. In the example shown, corresponding to $L/\sigma = 7.5$, six clearly defined layers can be detected, together with a weak maximum at the centre of the slit. The agreement with simulations is again outstandingly good. Figure 6.6 shows the solvation force as a function of L for the same system, calculated from the microscopic expression

$$f_S = -\int_0^L \frac{\mathrm{d}\phi(z)}{\mathrm{d}z}\rho^{(1)}(z)\,\mathrm{d}z - P \qquad (6.5.5)$$

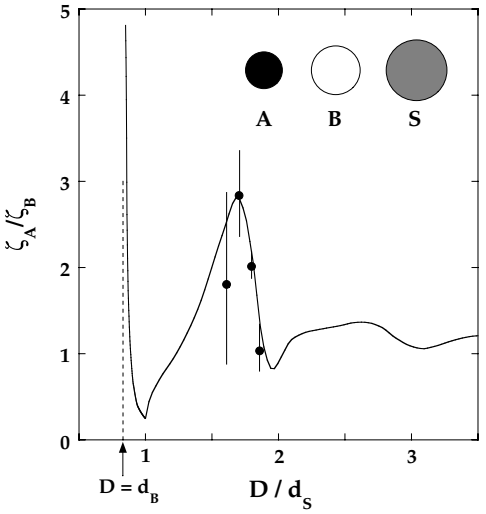

FIG. 6.7. Selective absorption by a cylindrical pore of solute hard-spheres (A, B) at low concentration in a solvent of larger spheres (S) as a function of the cylinder diameter. The curve is calculated from fundamental-measure theory and the points with error bars show the results of Monte Carlo calculations. See text for details. After Goulding *et al*.[24]

which is easily derived from the definition (6.1.15). The force is seen to oscillate around zero, its asymptotic value as $L \to \infty$. Oscillatory solvation forces are a direct consequence of the layering evident in Figure 6.5; they have been observed experimentally with the aid of "surface-force machines", which have a spatial resolution better than 1 Å. The amplitude of oscillation decreases rapidly with L, and is already negligible for $L = 7.5\sigma$ despite the high degree of layering still observed at this separation.

Functionals of the general form represented by (6.5.4), with various levels of approximation for the reference-system contribution, have also been used extensively in studies of phenomena such as capillary condensation in a narrow pore and the wetting of solid substrates.[23] The two effects are closely related and each is strongly dependent on the nature of the interaction between the fluid and the confining surface. Capillary condensation is the phenomenon whereby a confined gas condenses to a liquid at a chemical potential below that corresponding to liquid–vapour coexistence in the bulk. Wetting is an interfacial phase transition for which the adsorption defined by (6.1.13) (with $L \to \infty$) acts as an order parameter by providing a measure of the thickness of the liquid film adsorbed on the substrate. As the temperature increases along the liquid–vapour coexistence line, the film thickness, which is of microscopic dimensions at low temperatures, diverges either continuously (corresponding to a second-order wetting transition) or discontinuously (a first-order transition) as the wetting temperature T_w, with $T_t < T_w < T_c$, is reached (T_t and T_c being the triple-point and critical temperatures, respectively).

A different type of problem to which density-functional theory has been successfully applied concerns the size selectivity of porous materials in which the pores have a confining length of molecular dimensions. As a simple example, consider an infinitely long,

cylindrical pore of diameter D connecting two reservoirs that contain a three-component mixture of hard spheres under identical physical conditions (packing fraction and concentrations). The fluid in the reservoirs consists of a majority component – the "solvent" S – at a packing fraction $\eta = 0.41$, and two "solute" components, A and B, at concentrations of 0.05 M, with relative hard-sphere diameters $d_A : d_B : d_S$ appropriate to water (S) and the ions Na^+ (A) and K^+ (B).[24] Spheres of different diameters will permeate the pore to different extents, and at equilibrium the chemical potentials of each species will be the same inside the pore as in the reservoirs. The density profiles within the pore depend only on the radial distance r from axis of the cylinder; they can be calculated by minimising a fundamental-measure functional, modified in the manner represented by (6.4.27) to cater for the quasi-one-dimensional nature of the confinement. The degree of permeation (or "absorbance") ζ_ν of species ν may be defined as the ratio of the mean density of particles of that species inside the pore to the density of the same species in the reservoirs. When the cylinder diameter D is comparable with the sphere diameters, the pore absorbs preferentially one of the two solutes. The selectivity of the pore is measured by the relative absorbance ζ_A/ζ_B, plotted as a function of cylinder diameter in Figure 6.7. This varies with D by a factor of order 10, in fair agreement with calculations by a grand-canonical Monte Carlo method, though the low concentrations of solute particle mean that the statistical uncertainties in the results of the simulations are large. When $d_B < d_S$, only A-particles can be absorbed. Thus, for cylinder diameters only slightly larger than d_B, the selectivity is initially very large but falls rapidly as D increases. When $D \approx d_S$, the larger solute is up to four times more likely to be adsorbed than the smaller one, a purely entropic effect that is somewhat counterintuitive. However, when the cylinder diameter exceeds d_S and solvent particles can enter the pore, the selectivity rises, reaching a maximum value of about 2.8 at $D \approx 1.7 d_S$. The degree of selectivity can be greatly enhanced by changes in the relative diameters of the species involved.

6.6 DENSITY-FUNCTIONAL THEORY OF FREEZING

If cooled or compressed sufficiently gently, a liquid will freeze into an ordered, solid phase. The transition is accompanied by a discontinuous change in volume, $\Delta V = V_L - V_S$, which is usually positive (water is a notable exception), and by a latent heat, $T\Delta S$, which is always positive. The discontinuities in V and S, both of which are first derivatives of the free energy, are the signatures of a first-order phase transition. Freezing of simple liquids is largely driven by entropic factors, a fact most obvious in the case of the hard-sphere fluid, since the nature of the hard-sphere interaction means that the difference in free energy of the solid and fluid phases at a given temperature is equal to $-T\Delta S$. One of the most significant findings to emerge from the earliest molecular simulations[25] was that the hard-sphere fluid freezes into a stable, face-centred cubic crystal; accurate calculations[26] of the free energies of the fluid and solid as functions of density subsequently showed that the packing fractions at coexistence are $\eta_F \approx 0.494$ and $\eta_S \approx 0.545$. We can obtain a rough estimate of the configurational entropy in the two phases by temporarily ignoring the correlations between particles brought about by excluded-volume effects. If we treat the fluid

as a system of non-interacting particles moving freely in a volume V and the solid as a system of localised (and hence distinguishable) particles in which each particle is confined by its neighbours to a region of order V/N around its lattice site, a simple calculation shows that the configurational entropy per particle of the solid lies below that of the fluid by an amount equal to k_B. In reality, of course, correlations make a large contribution to the entropy, which at densities beyond $\eta \approx 0.5$ must be appreciably larger for the "ordered" solid than for the "disordered" fluid, since the solid is the stable phase. The explanation of this apparent paradox is the fact that the free volume available to a particle is larger in the solid than in the "jammed" configurations that are generated when a fluid is over-compressed. This ties in with Bernal's observation that the maximum density achievable by random packing of hard spheres ($\eta \approx 0.65$) lies well below that of the face-centred cubic structure ($\eta \approx 0.74$).

The relative volume change on freezing of a hard-sphere fluid is $|\Delta V|/V \approx 0.10$ and the entropy change per particle is $\Delta S/Nk_B \approx 1.16$. Simple perturbation theory shows that the effect of adding an attractive term to the hard-sphere interaction is to broaden the freezing transition, i.e. to increase the relative volume change, but the opposite effect occurs if the short-range repulsion is softened. In the case of the soft-sphere potentials defined by (5.2.25), for example, the relative volume change is found to decrease rapidly[27] with reduction in the exponent n, becoming strictly zero[28] in the limiting case of the one-component plasma ($n = 1$). The change in entropy also decreases with n, but much more slowly, and remains close to k_B per particle. Both experiments and simulations show that for a wide variety of systems consisting of spherical or nearly spherical particles the amplitude of the main peak in the static structure factor at freezing is approximately 2.85. This provides a useful criterion for freezing that appears to be independent of the crystal structure of the solid phase.[29] It applies, for example, to the family of soft-sphere fluids, for which the stable crystal phase is face-centred cubic at large values of n but body-centred cubic for softer potentials.

The lattice structure of a crystalline solid means that the density profile must be a periodic function of $\mathbf{r}$ such that

$$\rho^{(1)}(\mathbf{r} + \mathbf{R}_i) = \rho^{(1)}(\mathbf{r}) \tag{6.6.1}$$

where the set $\{\mathbf{R}_i\}$ represents the lattice coordinates of the particles in the perfectly ordered crystal. Let $\mathbf{u}_i = \mathbf{r}_i - \mathbf{R}_i$ be the displacement of particle i from its equilibrium position. Then the Fourier transform of the density profile can be written (see (3.1.4)) as

$$\hat{\rho}^{(1)}(\mathbf{k}) = \sum_{i=1}^{N} \langle \exp(-i\mathbf{k}\cdot\mathbf{r}_i) \rangle = \sum_{i=1}^{N} \exp(-i\mathbf{k}\cdot\mathbf{R}_i) \langle \exp(-i\mathbf{k}\cdot\mathbf{u}_i) \rangle \tag{6.6.2}$$

Away from any interface, all lattice sites are equivalent, and the second statistical average in (6.6.2) is therefore independent of i. Thus

$$\hat{\rho}^{(1)}(\mathbf{k}) = \langle \exp(-i\mathbf{k}\cdot\mathbf{u}) \rangle \sum_{i=1}^{N} \exp(-i\mathbf{k}\cdot\mathbf{R}_i) \tag{6.6.3}$$

The sum over lattice sites is non-zero only if $\mathbf{k}$ coincides with a reciprocal lattice vector $\mathbf{G}$. Hence

$$\sum_{i=1}^{N} \exp(-i\mathbf{k}\cdot\mathbf{R}_i) = N\delta_{\mathbf{k},\mathbf{G}} \tag{6.6.4}$$

and the only non-zero Fourier components of the density are

$$\hat{\rho}^{(1)}(\mathbf{G}) = N\big\langle \exp(-i\mathbf{G}\cdot\mathbf{u})\big\rangle \tag{6.6.5}$$

In the harmonic-phonon approximation, valid for small-amplitude vibrations of the particles around their lattice positions, the displacement vectors $\mathbf{u}$ have a gaussian distribution:

$$\big\langle \exp(-i\mathbf{G}\cdot\mathbf{u})\big\rangle = \exp\big(-\tfrac{1}{6}G^2\langle u^2\rangle\big) \tag{6.6.6}$$

where $\langle u^2\rangle$ is the mean-square displacement of a particle from its lattice site. If we substitute (6.6.6) in (6.6.5) and take the inverse transform, we find that

$$\begin{aligned}
\rho^{(1)}(\mathbf{r}) &= \frac{1}{V}\sum_{\mathbf{G}}\sum_{i=1}^{N} \exp\big(i\mathbf{G}\cdot(\mathbf{r}-\mathbf{R}_i)\big)\exp\big(-\tfrac{1}{6}G^2\langle u^2\rangle\big) \\
&\approx \frac{1}{(2\pi)^3}\sum_{i=1}^{N}\int \exp\big(i\mathbf{G}\cdot(\mathbf{r}-\mathbf{R}_i)\big)\exp\big(-\tfrac{1}{6}G^2\langle u^2\rangle\big)\,\mathrm{d}\mathbf{G} \\
&= \left(\frac{\alpha}{\pi}\right)^{3/2}\sum_{i=1}^{N}\exp\big(-\alpha(\mathbf{r}-\mathbf{R}_i)^2\big)
\end{aligned} \tag{6.6.7}$$

where $\alpha = (3/2\langle u^2\rangle)$ is an inverse-width parameter. The density profile of the crystal therefore appears as the sum of N gaussian peaks, each centred on a lattice site $\mathbf{R}_i$. As α increases, the particles become more strongly localised and the peaks become narrower. The most general representation of $\rho^{(1)}(\mathbf{r})$ compatible with lattice periodicity is

$$\rho^{(1)}(\mathbf{r}) = \rho_{\mathrm{S}}\left(1 + \sum_{\mathbf{G}\neq 0}\zeta(\mathbf{G})\exp(i\mathbf{G}\cdot\mathbf{r})\right) \tag{6.6.8}$$

where ρ_{S} is the overall number density of the solid. In the harmonic approximation the coefficients of the "density waves" $\exp(i\mathbf{G}\cdot\mathbf{r})$ are related to the parameter α by

$$\zeta(\mathbf{G}) = \exp\big(-G^2/4\alpha\big) \tag{6.6.9}$$

The vibrational mean-square displacement $\langle u^2\rangle$ can be determined by analysis of the lineshape of the Bragg peaks observed in x-ray or neutron-scattering experiments; it is found to decrease sharply as the crystal is cooled along an isochore or compressed along an isotherm. The quantity $L = \langle u^2\rangle^{1/2}/R_0$, where R_0 is the nearest-neighbour distance in

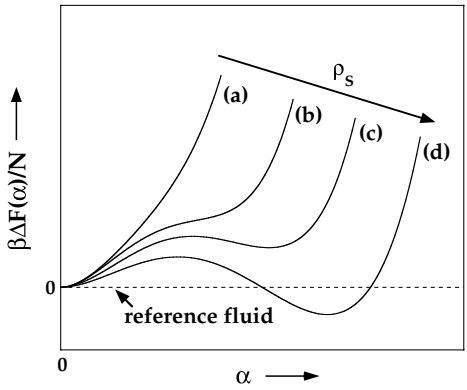

FIG. 6.8. Typical behaviour of the free-energy difference defined by (6.6.11) as a function of the variational parameter α for increasing values of the density ρ_S. Curve (d) corresponds to a density at which the ordered crystal is the stable phase. See text for details.

the crystal, is called the Lindemann ratio. According to the "Lindemann rule", melting should occur when L reaches a value that is only weakly material-dependent and equal to about 0.15. Simulations have shown that for hard spheres the value at melting is approximately 0.13, but is slightly larger for softer potentials. That such a criterion exists is not surprising: instability of the solid can be expected once the vibrational amplitude of the particles becomes a significant fraction of the spacing between neighbouring lattice sites.

The idea that underpins much of the density-functional approach to freezing goes back to the work of Kirkwood and Monroe.[30] While the periodic density profile is clearly very different from the uniform density of the fluid, it is reasonable to assume that the short-range pair correlations in the solid are similar to those of some effective, reference fluid. In other words, a crystal may be regarded as a highly inhomogeneous fluid, and different versions of the theory differ mostly in the choice made for the density of the reference fluid.[31]

We showed in Section 4.3 that expansion of the free-energy functional in powers of $\delta\rho^{(1)}(\mathbf{r})$ around that of a homogeneous fluid of density ρ_0 leads, when truncated at second order, to the expression for the density profile given by (4.3.16). In the application to freezing, there is no external field, and (4.3.16) becomes

$$\rho^{(1)}(\mathbf{r}) = \rho_0 \exp\left(\int c_0^{(2)}(\mathbf{r}-\mathbf{r}')\left[\rho^{(1)}(\mathbf{r}) - \rho_0\right] \mathrm{d}\mathbf{r}' \right) \tag{6.6.10}$$

Higher-order terms in the expansion are easily derived, but explicit calculations become increasingly involved and are therefore rarely attempted. Equation (6.6.10) always has the trivial solution $\rho^{(1)}(\mathbf{r}) = \rho_0$, but at sufficiently high densities there exist, in addition, periodic solutions of the form (6.6.8). In order to decide whether the uniform or periodic solution corresponds to the stable phase, it is necessary to compute the free energies of the two phases. The free energy of the solid phase is related to that of the reference fluid by (4.3.12), where the choice of ρ_0 remains open. It is clear, however, that ρ_0 should be

comparable with ρ_S, the mean number density in the solid, since the density change on freezing is typically less than 10%. One obvious possibility is to set $\rho_0 = \rho_S$, which simplifies the problem because the linear term in (4.3.12) then vanishes, but other choices have been made.[32] If we substitute (6.6.8) (with $\rho_0 = \rho_S$) into the quadratic term in (4.3.12) and use the convolution theorem, we find that

$$\begin{aligned}\frac{\beta \Delta F}{N} &\equiv \frac{\beta \mathcal{F}[\rho^{(1)}]}{N} - \frac{\beta F_0(\rho_S)}{N} \\ &= \int \rho^{(1)}(\mathbf{r}) \ln\left(\frac{\rho^{(1)}(\mathbf{r})}{\rho_S}\right) d\mathbf{r} - \tfrac{1}{2}\rho_S \sum_{\mathbf{G}\neq 0} \hat{c}_0^{(2)}(\mathbf{G}) |\zeta \mathbf{G}|^2 \end{aligned} \tag{6.6.11}$$

The free-energy difference ΔF must now be minimised with respect to $\rho^{(1)}(\mathbf{r})$, i.e. with respect to the order parameters $\zeta_{\mathbf{G}}$. In practice, most calculations are carried out using the gaussian form (6.6.9), in which case the inverse width α is the only variational parameter. The ideal contribution to the free energy favours the homogeneous phase; the quadratic, excess term favours the ordered phase provided the quantities $\hat{c}_0^{(2)}(\mathbf{G})$ are positive for the smallest reciprocal-lattice vectors, since the contributions thereafter decrease rapidly with increasing G. The competition between ideal and excess contributions leads to curves of ΔF versus α of the Landau type, shown schematically in Figure 6.8. When the density ρ_S is low (curves (a) and (b)), there is a single minimum at $\alpha = 0$, corresponding to a homogeneous, fluid phase. At higher densities (curve (c)), a minimum appears at a positive value of ΔF, signalling the appearance of a metastable, crystalline phase. Further increase in density leads to a lowering of the value of ΔF at the second minimum, which eventually becomes negative (curve (d)); the ordered crystal is now the stable phase. Once the free energies of fluid and solid along a given isotherm are known, the densities of the coexisting phases can be determined from the Maxwell double-tangent construction, which ensures equality of the chemical potentials and pressures of the two phases.[8] The calculations are carried out for a given Bravais lattice and hence for a given set of reciprocal-lattice vectors. If the relative stability of different crystal structures is to be assessed, separate calculations are needed for each lattice.

The method we have outlined is essentially that advanced by Ramakrishnan and Yussouff,[33] reformulated in the language of density-functional theory.[34] It works satisfactorily in the case of hard spheres, but the quality of the results deteriorates for softer potentials, for which the stable solid has a body-centred cubic structure. In that case, if the potential is sufficiently soft, the contribution to the sum over $\mathbf{G}$ in (6.6.11) from the second shell of reciprocal-lattice vectors is negative. The resulting contribution to ΔF is therefore positive and sufficiently large to destabilise the solid. This defect in the method can be overcome by inclusion of the third-order term in the expansion of the free-energy functional, but that requires some approximation to be made for the three-particle direct correlation function of the reference system.[35] Other approaches to the problem of freezing have also been used. The most successful of these are variants of fundamental-measure theory of the type discussed at the end of Section 6.4, which lead to values for the densities at coexistence of the hard-sphere fluid and solid that agree with those obtained by simulation to within one percent.

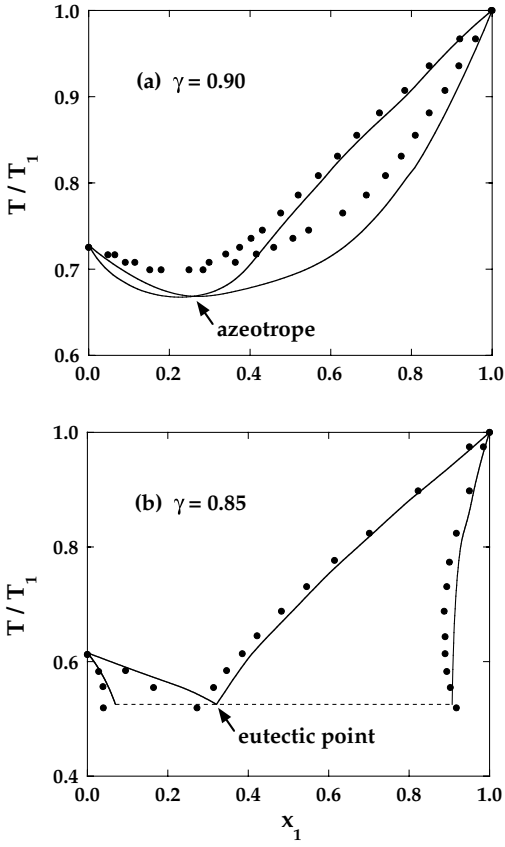

FIG. 6.9. Phase diagrams of binary hard-sphere mixtures at a fixed pressure for two values of the diameter ratio γ; x_1 and T_1 are, respectively, the number concentration of the larger spheres and the freezing temperature for $x_1 = 1$. (a) An azeotropic-type diagram; (b) a eutectic-type diagram. The full curves are calculated from density-functional theory and the points are the results of Monte Carlo calculations;[37] the broken line in (b) shows the miscibility gap at the eutectic temperature. After Zeng and Oxtoby.[36]

The theory can be extended to mixtures and in that form has been used to study the freezing of binary hard-sphere mixtures into substutionally disordered, face-centred-cubic structures, where the nature of the resulting phase diagram depends critically on the value of the diameter ratio, $\gamma = d_1/d_2$. Figure 6.9 shows phase diagrams in the temperature–concentration plane calculated from a version of density-functional theory[36] in which the free-energy of the solid is calculated from a generalisation of the weighted-density approximation (6.2.24); earlier calculations based on a generalisation of (6.6.11) had led to qualitatively similar results.[38] When γ is greater than approximately 0.94, the two species are miscible in all proportions in both phases, the concentration of large spheres being slightly higher in the solid. At lower values of γ ($0.88 < \gamma < 0.93$), the phase diagram has the form shown in part (a) of the figure, in which we see the appearance of an azeotrope, i.e. a point where the coexistence curves pass through a minimum and solid and fluid have identical

compositions. When γ is reduced below 0.88, as in part (b), the azeotrope is replaced by a eutectic point. There is now a wide range of concentration over which the two species are immiscible in the solid; the solubilities of large spheres in a solid consisting mostly of small spheres or vice versa are each less than 10% and become rapidly smaller as γ is further reduced. This behaviour is broadly consistent with the empirical Hume–Rothery rule, according to which the disordered solid phases of metallic alloys become unstable for diameter ratios less than about 0.85. As the figure shows, there is good agreement with the results of simulations both here and in the azeotropic case. Other density-functional calculations[39] have shown that ordered phases of AB_n-type structure remain stable at values of γ below 0.8, which is consistent both with simulations of hard-sphere mixtures and with experimental studies of colloidal suspensions.[40]

NOTES AND REFERENCES

1. For a more detailed treatment of the material discussed in this section, see Evans, R., *In* "Liquids at Interfaces: Les Houches, Session XLVIII" (J. Charvolin, J.F. Joanny and J. Zinn-Justin, eds). Elsevier, Amsterdam, 1990.
2. Biben, T., Hansen, J.P. and Barrat, J.L., *J. Chem. Phys.* **98**, 7330 (1993).
3. It also played a central role in early theoretical work on the wetting transition. See Cahn, J.W., *J. Chem. Phys.* **66**, 3667 (1977).
4. For a critical survey of different approximations, see Evans, R., *In* "Fundamentals of Inhomogeneous Fluids" (D. Henderson, ed.). Marcel Dekker, New York, 1991.
5. Tarazona, P. and Evans, R., *Mol. Phys.* **52**, 847 (1984).
6. (a) Tarazona, P., *Phys. Rev. A* **31**, 2672 (1985). (b) Curtin, W.A. and Ashcroft, N.W., *Phys. Rev. A* **32**, 2909 (1985). (c) Denton, A.R. and Ashcroft, N.W., *Phys. Rev. A* **39**, 4701 (1989).
7. (a) Rosenfeld, Y., *Phys. Rev. Lett.* **63**, 980 (1989). (b) Rosenfeld, Y., Levesque, D. and Weis, J.J., *J. Chem. Phys.* **92**, 6818 (1990).
8. See Chapter 5, Section 5.6.
9. Reiss, H., Frisch, H.L. and Lebowitz, J.L., *J. Chem. Phys.* **31**, 369 (1959).
10. (a) Kierlik, E. and Rosinberg, M.L., *Phys. Rev. A* **42**, 3382 (1990). (b) Phan, S., Kierlik, E., Rosinberg, M.L., Bildstein, B. and Kahl, G., *Phys. Rev. E* **48**, 618 (1993).
11. The detailed calculation for a different but related system (parallel hard cubes) is given by Cuesta, J.A. and Martínez-Ratón, Y., *J. Chem. Phys.* **107**, 6379 (1997).
12. Note that in refs. 7 the signs of the coefficients c_3 and c_4 are incorrect.
13. See Figure 1 in ref. 10(a). The correct results are those given by the full curves: for an explanation, see ref. 10(b).
14. Roth, R., Evans, R., Lang, A. and Kahl, G., *J. Phys. Condens. Matter* **14**, 12063 (2002).
15. Rosenfeld, Y., *Phys. Rev. A* **42**, 5978 (1990).
16. Percus, J.K., *J. Stat. Phys.* **15**, 505 (1976).
17. Rosenfeld, Y., Schmidt, M., Löwen, H. and Tarazona, P., *Phys. Rev. E* **55**, 4245 (1997).
18. Tarazona, P. and Rosenfeld, Y., *Phys. Rev. E* **55**, R4873 (1997). See also González, A., White, J.A. and Evans, R., *J. Phys. Condens. Matter* **9**, 2375 (1997).
19. Groot, R.D., Faber, N.M. and van der Eerden, J.P., *Mol. Phys.* **62**, 861 (1987).
20. Snook, I.K. and van Megen, W., *J. Chem. Phys.* **72**, 2907 (1980).
21. Kierlik, E. and Rosinberg, M.L., *Phys. Rev. A* **44**, 5025 (1991).
22. Magda, J.J., Tirell, M. and Davis, H.T., *J. Chem. Phys.* **83**, 1888 (1985).
23. (a) Evans, R., *J. Phys. Condens. Matter* **2**, 8989 (1990). (b) Gelb, L.V., Gubbins, K.E., Radhakrishnan, R. and Sliwinska-Bartkowiak, M., *Rep. Prog. Phys.* **62**, 1573 (1999).
24. Goulding, D., Melchionna, S. and Hansen, J.P., *Phys. Chem. Chem. Phys.* **3**, 1644 (2001).
25. (a) Alder, B.J. and Wainwright, T.E., *J. Chem. Phys.* **27**, 1208 (1957). (b) Wood, W.W. and Jacobson, J.D., *J. Chem. Phys.* **27**, 1207 (1957).

26. Hoover, W.G. and Ree, F.H., *J. Chem. Phys.* **49**, 3609 (1968).
27. (a) Hoover, W.G., Gray, S.G. and Johnson, K.W., *J. Chem. Phys.* **55**, 1128 (1971). (b) Agrawal, R. and Kofke, D.A., *Phys. Rev. Lett.* **74**, 122 (1995).
28. Weeks, J.D., *Phys. Rev. B* **24**, 1530 (1981).
29. (a) Hansen, J.P. and Verlet, L., *Phys. Rev.* **184**, 151 (1969). (b) Hansen, J.P. and Schiff, D., *Mol. Phys.* **25**, 1281 (1973).
30. Kirkwood, J.G. and Monroe, E., *J. Chem. Phys.* **9**, 511 (1941).
31. Fundamental-measure theory is an exception to this rule.
32. Baus, M., *J. Phys. Condens. Matter* **2**, 2111 (1990).
33. Ramakrishnan, T.V. and Yussouff, M., *Phys. Rev. B* **19**, 2775 (1979).
34. Haymet, A.D.J. and Oxtoby, D.W., *J. Chem. Phys.* **74**, 2559 (1981).
35. See, e.g., Barrat, J.L., Hansen, J.P. and Pastore, G., *Mol. Phys.* **63**, 747 (1988).
36. Zeng, X.C. and Oxtoby, D.W., *J. Chem. Phys.* **93**, 4357 (1990). See also Denton, A.R. and Ashcroft, N.W., *Phys. Rev.* **42**, 7312 (1990).
37. Kranendonk, W.G.T. and Frenkel, D., *Mol. Phys.* **72**, 679 (1991).
38. Barrat, J.L., Baus, M. and Hansen, J.P., *J. Phys. C* **20**, 1413 (1987).
39. Xu, H. and Baus, M., *J. Phys. Condens. Matter* **4**, L663 (1992).
40. Bartlett, P., Ottewill, R.H. and Pusey, P.N., *Phys. Rev. Lett.* **68**, 3801 (1992).

CHAPTER 7

Time-dependent Correlation and Response Functions

The next three chapters are devoted to a discussion of the transport properties and microscopic dynamics of simple, dense fluids.[1] The present chapter deals with the general formalism of time-correlation functions and with linear response theory; Chapter 8 is concerned with the behaviour of time-dependent fluctuations in the long-wavelength, low-frequency limit, where contact can be made with the macroscopic equations of hydrodynamics; and Chapter 9 describes methods that allow the explicit calculation of time-correlation functions.

7.1 GENERAL PROPERTIES OF TIME-CORRELATION FUNCTIONS

A dynamical variable, $A(t)$ say, of a system consisting of N structureless particles is a function of some or all of the time-varying coordinates $\mathbf{r}_i$ and momenta $\mathbf{p}_i$, $i = 1$ to N. We recall from Section 2.1 that the time evolution of A is determined by the equation of motion $A(t) = \exp(i\mathcal{L}t)A(0)$, where $\mathcal{L}$ is the Liouville operator. It follows that A has the signature $\varepsilon_A = +1$ or -1 under time reversal depending on whether or not it changes sign under the transformation $\mathbf{p}_i \to -\mathbf{p}_i$. Now consider two such variables, A and B, each of which may be either real or complex. Their equilibrium time-correlation function is written as

$$C_{AB}(t', t'') = \langle A(t')B^*(t'')\rangle \tag{7.1.1}$$

with the convention that $t' \geqslant t''$. The superscript * denotes a complex conjugate and the angular brackets represent either an average over time or an ensemble average over initial conditions. Thus $C_{AB}(t', t'')$ is defined either as

$$\langle A(t')B^*(t'')\rangle = \lim_{\tau\to\infty} \frac{1}{\tau}\int_0^\tau A(t'+t)B^*(t''+t)\,\mathrm{d}t \tag{7.1.2}$$

or as

$$\langle A(t')B^*(t'')\rangle = \iint f_0^{[N]}(\mathbf{r}^N, \mathbf{p}^N)B^*(\mathbf{r}^N, \mathbf{p}^N) \times \exp\big[i\mathcal{L}(t'-t'')\big]A(\mathbf{r}^N, \mathbf{p}^N)\,\mathrm{d}\mathbf{r}^N\mathrm{d}\mathbf{p}^N \tag{7.1.3}$$

The average in (7.1.3) is taken over all possible states of the system at time t'', weighted by the equilibrium probability density $f_0^{[N]}$; for a system characterised by fixed values of N, V and T, $f_0^{[N]}$ is given by the canonical distribution (2.3.1). Equations (7.1.2) and (7.1.3) yield the same result in the thermodynamic limit if the system is ergodic. The most important class of time-correlation functions are the *autocorrelation* functions $C_{AA}(t)$, for which A and B are the same variable.

Since the equilibrium probability density is independent of time, the ensemble average in (7.1.3) is independent of the choice of time origin t'', and the correlation function $C_{AB}(t', t'')$ is invariant under time translation. If we put $t'' = s$ and $t' = s + t$ the correlation function is a function only of the time difference t and is said to be *stationary* with respect to s. It is therefore customary to set $s = 0$ and use the more compact notation

$$C_{AB}(t) = \langle A(t) B^* \rangle \tag{7.1.4}$$

where $B^* \equiv B^*(0)$. The stationary character of the correlation function means that

$$\frac{\mathrm{d}}{\mathrm{d}s}\langle A(t+s)B^*(s)\rangle = \langle \dot{A}(t+s)B^*(s)\rangle + \langle A(t+s)\dot{B}^*(s)\rangle = 0 \tag{7.1.5}$$

and hence that

$$\langle \dot{A}(t) B^* \rangle = -\langle A(t)\dot{B}^* \rangle \tag{7.1.6}$$

In particular:

$$\langle \dot{A} A^* \rangle = 0 \tag{7.1.7}$$

Repeated differentiation with respect to s leads to a number of useful relations; these can also be deduced by exploiting the definition (7.1.2). For example:

$$\begin{aligned}\frac{\mathrm{d}^2}{\mathrm{d}t^2}\langle A(t)B^*\rangle &= \langle \ddot{A}(t)B^*\rangle \\ &= \lim_{\tau\to\infty}\frac{1}{\tau}\int_0^\tau \ddot{A}(t+t')B^*(t')\,\mathrm{d}t' \\ &= -\lim_{\tau\to\infty}\frac{1}{\tau}\int_0^\tau \dot{A}(t+t')\dot{B}^*(t')\,\mathrm{d}t' \\ &= -\langle \dot{A}(t)\dot{B}^*\rangle \end{aligned} \tag{7.1.8}$$

The invariance of correlation functions under time translation implies that

$$\begin{aligned} C_{AB}(t) &= \varepsilon_A\varepsilon_B C_{AB}(-t) = \varepsilon_A\varepsilon_B\langle A(-t)B^*\rangle \\ &= \varepsilon_A\varepsilon_B\langle AB^*(t)\rangle = \varepsilon_A\varepsilon_B C^*_{BA}(t) \end{aligned} \tag{7.1.9}$$

where $\varepsilon_A, \varepsilon_B$ are the time-reversal signatures of the two variables.

It is clear that

$$\lim_{t\to 0} C_{AB}(t) = \langle AB^* \rangle \tag{7.1.10}$$

where $\langle AB^* \rangle$ is a static correlation function. In the limit $t \to \infty$ the variables $A(t)$ and B become uncorrelated and

$$\lim_{t\to\infty} C_{AB}(t) = \langle A \rangle \langle B^* \rangle \tag{7.1.11}$$

However, it is usually more convenient to define the dynamical variables in such a way as to exclude their average values and to consider only the time correlation of their fluctuating parts, i.e.

$$C_{AB}(t) = \big\langle \big[A(t) - \langle A \rangle\big]\big[B^* - \langle B^* \rangle\big] \big\rangle \tag{7.1.12}$$

With this convention, $C_{AB}(t) \to 0$ as $t \to \infty$. Because

$$\big\langle \big[A(t) \pm A\big]\big[A(t) \pm A\big]^* \big\rangle \geqslant 0 \tag{7.1.13}$$

it is also true that

$$-\langle AA^* \rangle \leqslant C_{AA}(t) \leqslant \langle AA^* \rangle \tag{7.1.14}$$

The magnitude of an autocorrelation function is therefore bounded above by its initial value. This is to be expected, since an autocorrelation function describes the averaged way in which spontaneous (thermal) fluctuations in a variable A decay in time.

If $C_{AB}(t)$ is defined as in (7.1.12), it is also possible to define its Fourier transform or *power spectrum*:

$$C_{AB}(\omega) = \frac{1}{2\pi} \int_{-\infty}^{\infty} C_{AB}(t) \exp(i\omega t)\, \mathrm{d}t \tag{7.1.15}$$

and its Laplace transform:

$$\widetilde{C}_{AB}(z) = \int_0^{\infty} C_{AB}(t) \exp(izt)\, \mathrm{d}t \tag{7.1.16}$$

where z is a complex frequency. Since $C_{AB}(t)$ is bounded, $\widetilde{C}_{AB}(z)$ is analytic in the upper half of the complex z plane ($\mathrm{Im}\, z > 0$); it is also related to $C_{AB}(\omega)$ by a Hilbert transform, i.e.

$$\begin{aligned} \widetilde{C}_{AB}(z) &= \int_0^{\infty} \mathrm{d}t \exp(izt) \int_{-\infty}^{\infty} C_{AB}(\omega) \exp(-i\omega t)\, \mathrm{d}\omega \\ &= i \int_{-\infty}^{\infty} \frac{C_{AB}(\omega)}{z - \omega}\, \mathrm{d}\omega \end{aligned} \tag{7.1.17}$$

From the results in (7.1.9) it follows that an autocorrelation function $C_{AA}(t)$ and its power spectrum $C_{AA}(\omega)$ are real, even functions of t and ω, respectively. An integral such as

that in (7.1.17) can be evaluated with the help of a standard relation commonly written in short-hand form as

$$\lim_{\varepsilon\to 0}\frac{1}{x\pm i\varepsilon}\equiv\mathcal{P}\left(\frac{1}{x}\right)\mp i\pi\delta(x) \tag{7.1.18}$$

where $\mathcal{P}$ denotes the principal value. Thus, since $C_{AA}(\omega)$ is necessarily real:

$$\begin{aligned}\lim_{\varepsilon\to 0}\operatorname{Re}\widetilde{C}_{AA}(\omega+i\varepsilon)&=\lim_{\varepsilon\to 0}\operatorname{Re}\left(i\int_{-\infty}^{\infty}\frac{C_{AA}(\omega')}{\omega-\omega'+i\varepsilon}\,\mathrm{d}\omega'\right)\\&=\pi C_{AA}(\omega)\end{aligned} \tag{7.1.19}$$

It can also be shown that $C_{AA}\geqslant 0$ for all ω. Consider an auxiliary variable, $A_T(\omega)$, defined as

$$A_T(\omega)=\frac{1}{\sqrt{2T}}\int_{-T}^{T}A(t)\exp(i\omega t)\,\mathrm{d}t \tag{7.1.20}$$

The statistical average of $\langle A_T(\omega)A_T^*(\omega)\rangle$ cannot be negative. Hence

$$\left\langle A_T(\omega)A_T^*(\omega)\right\rangle=\frac{1}{2T}\int_{-T}^{T}\mathrm{d}t\int_{-T}^{T}\mathrm{d}t'\left\langle A(t)A^*(t')\right\rangle\exp\left[i\omega(t-t')\right]\geqslant 0 \tag{7.1.21}$$

If we now make a change of variable from t' to $\tau=t-t'$ and take the limit $T\to\infty$, we find that

$$\begin{aligned}\lim_{T\to\infty}\left\langle A_T(\omega)A_T^*(\omega)\right\rangle&=\int_{-\infty}^{\infty}C_{AA}(\tau)\exp(i\omega\tau)\,\mathrm{d}\tau\\&=C_{AA}(\omega)\geqslant 0\end{aligned} \tag{7.1.22}$$

The experimental significance of time-correlation functions lies in the fact that the spectra measured by various spectroscopic techniques are the power spectra of well-defined dynamical variables. This connection between theory and experiment will be made explicit in Section 7.5 for the special but important case of inelastic neutron scattering. In addition, as we shall see later, the linear transport coefficients of hydrodynamics are related to time integrals of certain autocorrelation functions. Finally, time-correlation functions provide a quantitative description of the microscopic dynamics in liquids. Computer simulations play a key role here, since they give access to a large variety of correlation functions, many of which are not measurable by laboratory experiments.

Apart from the limitation to classical mechanics, the properties of time-correlation functions given thus far are completely general. We now restrict the discussion to systems of particles for which the interaction potential is continuous; the hamiltonian is therefore differentiable and the Liouville operator has the form given by (2.1.8). An autocorrelation function of such a system is an even function of time and can be expanded in a Taylor

series in even powers of t around $t = 0$. Thus

$$C_{AA}(t) = \sum_{n=0}^{\infty} \frac{t^{2n}}{(2n)!} \langle A^{(2n)} A^* \rangle = \sum_{n=0}^{\infty} \frac{t^{2n}}{(2n)!} (-1)^n \langle A^{(n)} A^{(n)*} \rangle$$
$$= \sum_{n=0}^{\infty} \frac{t^{2n}}{(2n)!} (-1)^n \langle |(i\mathcal{L})^n A|^2 \rangle \tag{7.1.23}$$

where the superscript $(2n)$ denotes a $2n$-fold derivative and repeated use has been made of (7.1.8). Differentiation of the inverse Fourier transform of (7.1.15) $2n$ times with respect to t gives

$$\langle \omega^{2n} \rangle_{AA} \equiv \int_{-\infty}^{\infty} \omega^{2n} C_{AA}(\omega)\, \mathrm{d}\omega = (-1)^n C_{AA}^{(2n)}(t = 0) \tag{7.1.24}$$

Thus, apart from a possible change of sign, the frequency moments of the power spectrum are equal to the derivatives of the autocorrelation function taken at $t = 0$; these derivatives are static correlation functions that are expressible as integrals over the particle distribution functions. On expanding the right-hand side of (7.1.17) in powers of $1/z$ it becomes clear that the frequency moments defined by (7.1.24) are also the coefficients in the high-frequency expansion of the Laplace transform:

$$\tilde{C}_{AA}(z) = \frac{i}{z} \sum_{n=0}^{\infty} \frac{\langle \omega^{2n} \rangle_{AA}}{z^{2n}} \tag{7.1.25}$$

Expansions of the type displayed in (7.1.23) cannot be used for systems such as the hard-sphere fluid. The impulsive nature of the forces between particles with hard cores means that the Liouville operator no longer has the form[2] shown in (2.1.8). As a result, the time-correlation functions are non-analytic at $t = 0$, and their power spectra have frequency moments that are infinite.

The definition of a time-correlation function provided by (7.1.3) has the form of an inner product of the "vectors" $A(t)$ and B in the infinite-dimensional, Hilbert space of dynamical variables, usually called Liouville space. A useful notation based on this identification is one in which a time-correlation function is written as

$$\langle A(t) B^* \rangle \equiv \big(B, A(t)\big) \tag{7.1.26}$$

where $(\cdots, \cdots)$ denotes an inner product. The usual requirements of an inner product are therefore satisfied. In particular, $(A, A) \geqslant 0$ and $(A, B) = (B, A)^*$. Formal properties of time-correlation functions can then be deduced from the fact that the Liouville operator is hermitian (and hence $i\mathcal{L}$ is anti-hermitian) with respect to the inner product, i.e.

$$(B, \mathcal{L}A) = (A, \mathcal{L}B)^* = (\mathcal{L}B, A) \tag{7.1.27}$$

Because $\mathcal{L}$ is hermitian, the propagator $\exp(i\mathcal{L}t)$ is a unitary operator with an hermitian conjugate given by $\exp(-i\mathcal{L}t)$. It follows that

$$\begin{aligned}\langle A(t)B^*\rangle &\equiv \big(B, \exp(i\mathcal{L}t)A\big) = \big(B, \exp(-i\mathcal{L}s)A(t+s)\big) \\ &= \big(A(t+s), \exp(i\mathcal{L}s)B\big)^* \equiv \langle A(t+s)B^*(s)\rangle \end{aligned} \tag{7.1.28}$$

thereby proving that the correlation function is stationary. Note that the effect of the operation $A(t) = \exp(i\mathcal{L}t)A$ is to "rotate" A through an angle $\mathcal{L}t$ in Liouville space. By exploiting the fact that $i\mathcal{L}A = \dot{A}$, properties of time-correlation functions that involve time derivatives of dynamical variables are also easily derived. For example:

$$\begin{aligned}\langle \dot{A}(t)B^*\rangle &\equiv \big(B, i\mathcal{L}A(t)\big) \\ &= -\big(A(t), i\mathcal{L}B\big)^* \equiv -\langle A(t)\dot{B}^*\rangle \end{aligned} \tag{7.1.29}$$

in agreement with (7.1.6).

The proof that the Liouville operator is hermitian requires an integration by parts of the derivatives appearing in the Poisson-bracket representation (2.1.8). The inner product is sometimes defined without the weighting factor $f_0^{(N)}$, but the Liouville operator retains its hermitian character, since $\mathcal{L}f_0^{(N)} = 0$.

7.2 AN ILLUSTRATION: THE VELOCITY AUTOCORRELATION FUNCTION AND SELF-DIFFUSION

The ideas introduced in Section 7.1 can be usefully illustrated by considering one of the simplest but most important examples of a time-correlation function, namely the autocorrelation function of the velocity $\mathbf{u} = \mathbf{p}/m$ of a tagged particle moving through a fluid. The velocity autocorrelation function, defined as

$$Z(t) = \tfrac{1}{3}\langle \mathbf{u}(t)\cdot\mathbf{u}\rangle = \langle u_x(t)u_x\rangle \tag{7.2.1}$$

is a measure of the projection of the particle velocity onto its initial value, averaged over initial conditions. Its value at $t = 0$ is given by the equipartition theorem:

$$Z(0) = \tfrac{1}{3}\langle u^2\rangle = \frac{k_B T}{m} \tag{7.2.2}$$

At times long compared with any microscopic relaxation time the initial and final velocities will be completely uncorrelated. Thus $Z(t\to\infty) = 0$. The results of computer simulations of argon-like liquids show that the velocities are already largely decorrelated after times of order 10^{-12} s, but in general $Z(t)$ also has a weak, slowly decaying part. The detailed behaviour at long times varies with thermodynamic state, as is evident from the examples plotted in Figure 7.1. We shall return later to a discussion of the main features of curves such as these, but first we show that there exists a general relationship between the self-diffusion coefficient D and the time integral of $Z(t)$.

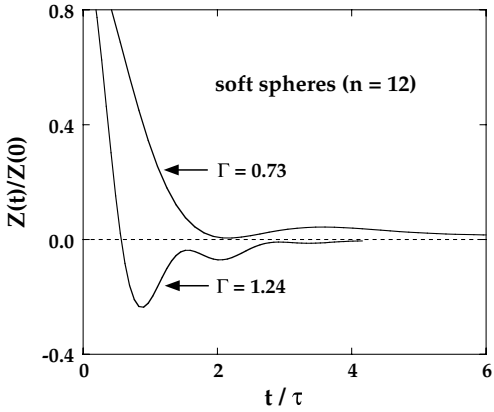

FIG. 7.1. Normalised velocity autocorrelation function of the r^{-12}-fluid at two different values of the dimensionless coupling parameter Γ defined by (5.3.13). The higher value of Γ represents a thermodynamic state close to the fluid–solid transition and the unit of time is $\tau = (m\sigma^2/48\varepsilon)^{1/2}$. After Heyes *et al.*[3]

Consider a set of identical, tagged particles having initial positions $\{\mathbf{r}_i(0)\}$. If the particles diffuse in time t to positions $\{\mathbf{r}_i(t)\}$, the self-diffusion coefficient is given by a well-known relation due to Einstein:

$$D = \lim_{t\to\infty} \frac{\langle |\mathbf{r}_i(t) - \mathbf{r}_i(0)|^2 \rangle}{6t} \tag{7.2.3}$$

This result is a direct consequence of Fick's law of diffusion, as we shall see in Section 8.2. It is also a relation characteristic of a "random walk", in which the mean-square displacement of the walker becomes a linear function of time after a sufficiently large number of random steps. The nature of the limiting process involved in (7.2.3) highlights the general importance of taking the thermodynamic limit before the limit $t \to \infty$. For a system of finite volume V, the diffusion coefficient defined by (7.2.3) is strictly zero, since the maximum achievable mean-square displacement is of order $V^{2/3}$. In practice, for a system of macroscopic dimensions, the ratio on the right-hand side of (7.2.3) will reach a plateau value at times much shorter than those required for the diffusing particles to reach the boundaries of the system; it is the plateau value that provides the definition of D for a finite system.

We now rewrite the Einstein relation in terms of the velocity autocorrelation function. The displacement in a time interval t of any tagged particle is

$$\mathbf{r}(t) - \mathbf{r}(0) = \int_0^t \mathbf{u}(t')\,\mathrm{d}t' \tag{7.2.4}$$

When squared and averaged over initial conditions, (7.2.4) becomes

$$\left\langle \left|\mathbf{r}(t) - \mathbf{r}(0)\right|^2 \right\rangle = \left\langle \int_0^t \mathbf{u}(t')\,\mathrm{d}t' \cdot \int_0^t \mathbf{u}(t'')\,\mathrm{d}t'' \right\rangle$$

$$= 2\int_0^t \mathrm{d}t' \int_0^{t'} \mathrm{d}t'' \langle \mathbf{u}(t') \cdot \mathbf{u}(t'') \rangle$$

$$= 6\int_0^t \mathrm{d}t' \int_0^{t'} \mathrm{d}t'' Z(t' - t'') \tag{7.2.5}$$

A change of variable from t'' to $s = t' - t''$ followed by an integration by parts with respect to t' shows that

$$\left\langle \left| \mathbf{r}(t) - \mathbf{r}(0) \right|^2 \right\rangle = 6\int_0^t \mathrm{d}t' \int_0^{t'} \mathrm{d}s\, Z(s)$$

$$= 6t \int_0^t \left(1 - \frac{s}{t}\right) Z(s)\, \mathrm{d}s \tag{7.2.6}$$

and substitution of (7.2.5) in (7.2.3) gives the required result:

$$D = \int_0^\infty Z(t)\, \mathrm{d}t \tag{7.2.7}$$

Equation (7.2.7) is an example of a *Green–Kubo formula*, an important class of relations in which a macroscopic dynamical property is written as the time integral of a microscopic time-correlation function.

If the interparticle potential is continuous, the short-time expansion of $Z(t)$ starts as

$$Z(t) = \frac{k_\mathrm{B}T}{m}\left(1 - \Omega_0^2 \frac{t^2}{2} + \cdots\right) \tag{7.2.8}$$

Equation (7.1.23) shows that the coefficient of $\frac{1}{2}t^2$ is

$$\Omega_0^2 = \frac{m}{3k_\mathrm{B}T} \langle \dot{\mathbf{u}} \cdot \dot{\mathbf{u}} \rangle = \frac{\langle |\mathbf{F}|^2 \rangle}{3mk_\mathrm{B}T} \tag{7.2.9}$$

where $\mathbf{F}$ is the total force exerted on the diffusing particle by its neighbours. If the tagged particle is identical to all other particles in the fluid, $\mathbf{F} = -\nabla V_N$, where V_N is the total potential energy. When V_N is a sum of pair terms, Ω_0^2 can be expressed in terms of the equilibrium pair distribution function and the interparticle potential. To show this, we first derive a useful, general result. Let $A(\mathbf{r}^N)$ be some function of the particle coordinates. Then

$$\left\langle A(\mathbf{r}^N) \frac{\partial V_N}{\partial x_i} \right\rangle$$

$$= \frac{1}{Z_N} \int \cdots \int A(\mathbf{r}^N) \frac{\partial V_N}{\partial x_i} \exp(-\beta V_N)\, \mathrm{d}\mathbf{r}_1 \cdots \mathrm{d}x_i\, \mathrm{d}y_i\, \mathrm{d}z_i \cdots \mathrm{d}\mathbf{r}_N$$

$$= \frac{k_\mathrm{B}T}{Z_N} \int \cdots \int \frac{\partial A(\mathbf{r}^N)}{\partial x_i} \exp(-\beta V_N)\, \mathrm{d}\mathbf{r}_1 \cdots \mathrm{d}x_i\, \mathrm{d}y_i\, \mathrm{d}z_i \cdots \mathrm{d}\mathbf{r}_N \tag{7.2.10}$$

or

$$\left\langle A\left(\mathbf{r}^N\right)\frac{\partial V_N}{\partial x_i}\right\rangle = k_{\mathrm{B}}T\left\langle\frac{\partial A(\mathbf{r}^N)}{\partial x_i}\right\rangle \tag{7.2.11}$$

The second equality in (7.2.10) follows from an integration by parts with respect to x_i. Equation (7.2.11) is called the Yvon theorem. When applied to the current problem it shows that the mean-square force on a particle is

$$\left\langle|\mathbf{F}|^2\right\rangle = k_{\mathrm{B}}T\left\langle\nabla^2 V_N\right\rangle \tag{7.2.12}$$

With the assumption of pairwise additivity, manipulations similar to those used in Section 2.5 now allow (7.2.9) to be rewritten in the form

$$\Omega_0^2 = \frac{(N-1)}{3m}\left\langle\nabla^2 v(r)\right\rangle = \frac{\rho}{3m}\int \nabla^2 v(r)g(r)\,\mathrm{d}\mathbf{r} \tag{7.2.13}$$

The quantity Ω_0 is called the Einstein frequency, since it represents the frequency at which the tagged particle would vibrate if it were undergoing small oscillations in the potential well produced by the surrounding particles when maintained at their mean equilibrium positions around the tagged particle. Numerically, Ω_0 is of order 10^{13} s^{-1} for liquid argon near its triple point.

Equation (7.2.8) does not apply to systems of hard spheres because the hard-sphere potential is not differentiable.[4] The short-time behaviour of $Z(t)$ now takes the form

$$\left\langle\mathbf{u}(t)\cdot\mathbf{u}\right\rangle = \left\langle u^2\right\rangle + t\left(\frac{\mathrm{d}}{\mathrm{d}t}\left\langle\mathbf{u}(t)\cdot\mathbf{u}\right\rangle\right)_{t=0} + \cdots \tag{7.2.14}$$

where the differentiation with respect to time must be carried out after the ensemble averaging. Thus

$$Z(t) = \tfrac{1}{3}\left\langle u^2\right\rangle(1 - \Omega_0' t + \cdots) \tag{7.2.15}$$

where the frequency Ω_0' is

$$\Omega_0' = -\frac{1}{\langle u^2\rangle}\lim_{\Delta t\to 0}\frac{\langle\Delta\mathbf{u}\cdot\mathbf{u}\rangle}{\Delta t} \tag{7.2.16}$$

Consider a tagged hard sphere of diameter d moving in a fluid of untagged but otherwise identical hard spheres.[5] Over a sufficiently short time interval the tagged sphere will suffer at most one collision with a sphere from the bath. To evaluate Ω_0' from its definition (7.2.16), let us suppose that the tagged sphere, of momentum $\mathbf{p}$, collides with a sphere of momentum $\mathbf{p}'$, as pictured in Figure 7.2. Because the collision is elastic, the momentum gained by the tagged particle is $\Delta\mathbf{p} = -(\mathbf{p}\cdot\hat{\mathbf{r}} - \mathbf{p}'\cdot\hat{\mathbf{r}})\hat{\mathbf{r}}$, where $\hat{\mathbf{r}} = \mathbf{r}/r$ is a unit vector along the line joining the two centres of mass. Thus $-\Delta\mathbf{p}\cdot\mathbf{p} = p(p - p')$ where p, p' are the components of $\mathbf{p}$ and $\mathbf{p}'$, respectively, along $\hat{\mathbf{r}}$. If $p > p'$, the separation of the two spheres will decrease in a short time Δt by an amount $\Delta r = (p - p')\Delta t/m$. On average, given

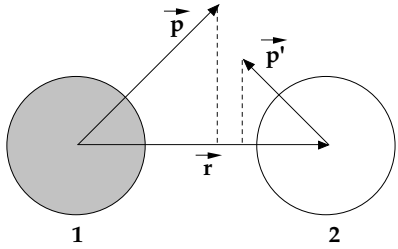

FIG. 7.2. A collision between a tagged hard sphere, (1), and a sphere from the bath, (2).

that Δr is small, the number of spheres that initially lie within a distance d to $d + \Delta r$ of the tagged sphere will be $n(\Delta r) \approx 4\pi d^2 g(d)(p - p')\Delta t/m$, where $g(d)$ is the pair distribution function at contact, and the probability that the tagged sphere will suffer a collision with a sphere having a component of momentum p' along $\hat{\mathbf{r}}$ is $P(p') = n(\Delta r) f_{\mathrm{M}}(p')\,\mathrm{d}p'$, where f_{M} is the maxwellian distribution (2.1.26) in its component form. The statistical average of $-\Delta\mathbf{p}\cdot\mathbf{p}$ is therefore obtained by multiplying $P(p')$ by $p(p - p') f_{\mathrm{M}}(p)\,\mathrm{d}p$ and integrating over p and p'. Bringing these results together we find that

$$\begin{aligned}\Omega_0' &= -\frac{1}{3mk_{\mathrm{B}}T}\lim_{\Delta t\to 0}\frac{\langle\Delta\mathbf{p}\cdot\mathbf{p}\rangle}{\Delta t} \\ &= \frac{4\pi d^2 g(d)}{3m^2 k_{\mathrm{B}}T}\iint_{p>p'} p(p-p')^2 f_{\mathrm{M}}(p) f_{\mathrm{M}}(p')\,\mathrm{d}p\,\mathrm{d}p' \end{aligned} \tag{7.2.17}$$

or, on changing variables from p, p' to $p_+ = (p + p')/\sqrt{2}$, $p_- = (p - p')/\sqrt{2}$:

$$\Omega_0' = \frac{4\sqrt{2}\pi d^2 g(d)}{3m^2 k_{\mathrm{B}}T}\int_{-\infty}^{\infty}\mathrm{d}p_+\int_0^{\infty}\mathrm{d}p_- p_-^3 f_{\mathrm{M}}(p_-) f_{\mathrm{M}}(p_+) \tag{7.2.18}$$

The double integral is now easily evaluated to give

$$\Omega_0' = \frac{8\rho d^2 g(d)}{3}\left(\frac{\pi k_{\mathrm{B}}T}{m}\right)^{1/2} = \frac{2\Gamma_{\mathrm{E}}}{3} \tag{7.2.19}$$

where Γ_{E} is the Enskog collision rate introduced in Section 2.5.

The derivation of (7.2.19) shows that the Enskog approximation makes allowance for static correlations in the fluid, but the key assumption underlying the Boltzmann equation is retained, namely that successive collisions are completely uncorrelated. The velocity of a tagged particle immediately following a collision is therefore dependent on its velocity immediately prior to the collision, but not on its velocity at earlier times. Because collisions between hard spheres are instantaneous events, this is tantamount to saying that the "memory" associated with the tagged-particle velocity is of infinitesimally short duration, with the consequence, as we shall see in later sections, that the velocity autocorrelation function is exponential in time. By identifying the right-hand side of (7.2.14) with the

leading terms in the expansion of an exponential function, we do in fact recover Enskog's approximation[6] for the velocity autocorrelation function of hard spheres:

$$Z_{\mathrm{E}}(t) = \frac{k_{\mathrm{B}}T}{m}\exp\bigl(-2\Gamma_{\mathrm{E}}|t|/3\bigr) \tag{7.2.20}$$

where the absolute value of t appears because $Z(t)$ must be an even function of t. The corresponding approximation for the diffusion coefficient is obtained by substitution of (7.2.20) in (7.2.7):

$$D_{\mathrm{E}} = \frac{3k_{\mathrm{B}}T}{2m\Gamma_{\mathrm{E}}} = \frac{3}{8\rho d^2 g(d)}\left(\frac{k_{\mathrm{B}}T}{\pi m}\right)^{1/2} \tag{7.2.21}$$

This expression is nearly exact in the low-density limit[7] while its applicability at higher densities has been thoroughly tested in molecular dynamics calculations.[8] From Figure 7.3 we see that the diffusion coefficient obtained by simulation exceeds the Enskog value at intermediate densities, but falls below it at densities close to crystallisation.[9] The high-density deviations arise from back-scattering effects, corresponding to the fact that collisions lead, on average, to the reversal of the velocity of a tagged particle into a comparatively narrow range of angles. This gives rise to an extended negative region in $Z(t)$; the same effect is seen for other potential models, as exemplified in Figure 7.1. The increase in the ratio D/D_{E} at intermediate densities is attributable in large part to an enhancement of velocity correlations due to the excitation of slowly decaying, collective motions in the fluid. The motion of the tagged particle induces a backflow pattern in the surrounding fluid that reacts on the particle at later times, giving rise to persistence (or "memory") effects and an unexpectedly slow ($\sim t^{-3/2}$) decay of $Z(t)$ at very long times; this behaviour is again not specific to hard spheres. We shall return to the question of the "long-time tails"

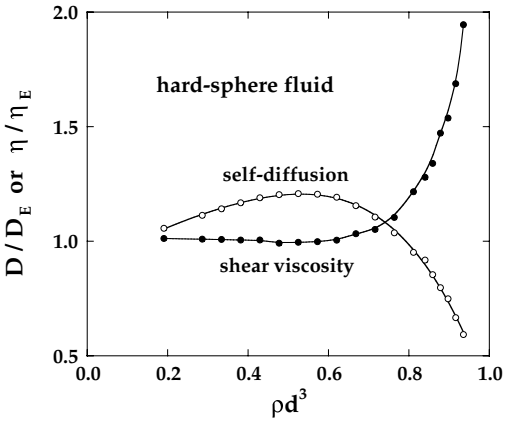

FIG. 7.3. Molecular-dynamics results for the self-diffusion coefficient D and shear viscosity η of the hard-sphere fluid relative to their values in the Enskog approximation. The curves are drawn as a guide to the eye. After Sigurgeirsson and Heyes.[8(b)]

of correlation functions in Section 8.7. Figure 7.3 also shows the corresponding results for the shear viscosity of the hard-sphere fluid, but we postpone discussion of these until Section 8.4.

A treatment of self-diffusion by kinetic theory that goes beyond the Enskog approximation must take account of the correlated sequences of binary collisions that a tagged particle experiences. In such a sequence the tagged particle collides initially with a particle from the bath, then diffuses through the fluid, suffering collisions with other bath particles, before colliding either with the same particle it met initially or with another particle whose motion is correlated in some way with that of the initial collision partner. Examples of collision sequences are illustrated in Figure 7.4; in each case the tagged particle is labelled 1 and A, B represent two different space-time points. In example (a), the two collisions are uncorrelated. In (b) and (c), particles 1 and 2 first meet at A, then recollide at B; in (b) the recollision involves one intermediate collision between 2 and 3 (a three-body event) and in (c) it involves intermediate collisions between 1 and 4 and between 2 and 3 (a four-body event). Example (d) is a different type of four-body event in which the initial (at A) and final (at B) collision partners are different but the collisions suffered by 1 at A and B are nonetheless correlated. Sequences (b), (c) and (d) are all examples of "ring-collision" events.

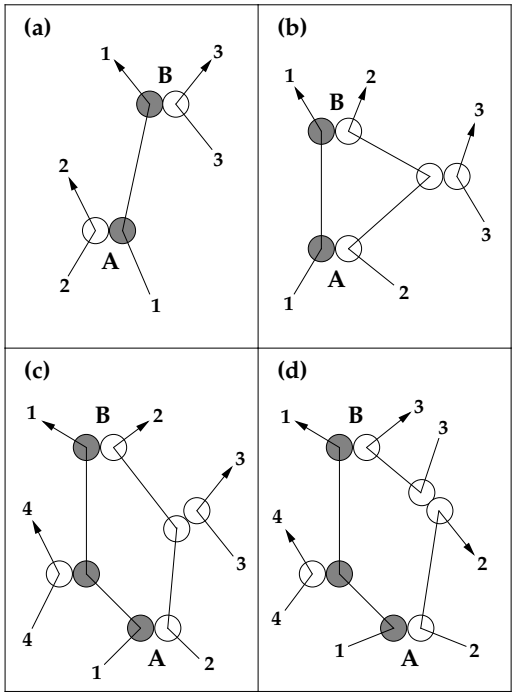

FIG. 7.4. Examples of uncorrelated (a) and correlated (b, c, d) sequences of binary collisions. A and B represent two different space-time points. See text for details.

7.3 BROWNIAN MOTION AND THE GENERALISED LANGEVIN EQUATION

Calculations of the velocity autocorrelation function either by the Enskog method or by other, more sophisticated versions of kinetic theory are largely limited to hard-sphere systems, though efforts have been made to apply similar techniques in calculations for continuous potentials. In this section we describe a different approach that is more phenomenological in character, but has found wide application in the theory of transport processes in liquids. Its basis is the stochastic theory used by Langevin to describe the brownian motion of a large and massive particle in a bath of particles that are much smaller and lighter than itself. The problem is characterised by two very different timescales, one associated with the slow relaxation of the initial velocity of the brownian particle and another linked to the frequent collisions that the brownian particle suffers with particles of the bath. Langevin assumed that the force acting on the brownian particle consists of two parts: a systematic, frictional force proportional to the velocity $\mathbf{u}(t)$, but acting in the opposite sense, and a randomly fluctuating force, $\mathbf{R}(t)$, which arises from collisions with surrounding particles. The equation of motion of a brownian particle of mass m is therefore written as

$$m\dot{\mathbf{u}}(t) = -m\xi\mathbf{u}(t) + \mathbf{R}(t) \tag{7.3.1}$$

where ξ is the *friction coefficient*. The random force is assumed to vanish in the mean:

$$\langle \mathbf{R}(t) \rangle = 0 \tag{7.3.2}$$

to be uncorrelated with the velocity at any earlier time:

$$\langle \mathbf{R}(t) \cdot \mathbf{u} \rangle = 0, \quad t > 0 \tag{7.3.3}$$

and to have an infinitesimally short correlation time, i.e.

$$\langle \mathbf{R}(t+s) \cdot \mathbf{R}(s) \rangle = 2\pi R_0 \delta(t) \tag{7.3.4}$$

which in turn means that the power spectrum of the random force is a constant, R_0 (a "white" spectrum):

$$\frac{1}{2\pi} \int_{-\infty}^{\infty} \langle \mathbf{R}(t) \cdot \mathbf{R} \rangle \exp(i\omega t)\, \mathrm{d}t = R_0 \tag{7.3.5}$$

These are reasonable assumptions when the brownian particle is much larger than its neighbours, because even on a short timescale its motion will be determined by a very large number of essentially uncorrelated collisions. When all particles are of the same size, the assumptions are less well justified, and a generalisation of a type to be described later is required.

The two terms on the right-hand side of the Langevin equation (7.3.1) are not independent. To see the connection between them we first write the solution to (7.3.1) in the form

$$m\mathbf{u}(t) = m\mathbf{u}(0)\exp(-\xi t) + \exp(-\xi t) \int_0^t \exp(\xi s)\mathbf{R}(s)\, \mathrm{d}s \tag{7.3.6}$$

On squaring and taking the statistical average we find, using (7.3.3) and (7.3.4), that

$$\begin{aligned} m^2\langle|\mathbf{u}(t)|^2\rangle &= m^2\langle|\mathbf{u}(0)|^2\rangle\exp(-2\xi t) \\ &\quad + \exp(-2\xi t)\int_0^t \mathrm{d}s\int_0^t \mathrm{d}s'\exp\bigl[\xi(s+s')\bigr]2\pi R_0\delta(s-s') \\ &= m^2\langle|\mathbf{u}(0)|^2\rangle\exp(-2\xi t) + \frac{\pi R_0}{\xi}\bigl[1-\exp(-2\xi t)\bigr] \end{aligned} \tag{7.3.7}$$

We now take the limit $t\to\infty$; the brownian particle will then be in thermal equilibrium with the bath regardless of the initial conditions. Hence $\langle|\mathbf{u}(\infty)|^2\rangle = 3k_\mathrm{B}T/m$ and (7.3.7) can be rearranged to give an expression for the friction coefficient:

$$\xi = \frac{\pi\beta R_0}{3m} = \frac{\beta}{3m}\int_0^\infty \langle\mathbf{R}(t)\cdot\mathbf{R}\rangle\,\mathrm{d}t \tag{7.3.8}$$

From a physical point of view it is not surprising to find a link between the frictional and random forces. If the brownian particle were to be drawn through the bath by an external field, random collisions suffered by the particle would give rise to a systematic retarding force proportional to the particle velocity. Equation (7.3.8) is a further illustration of the fluctuation–dissipation theorem already discussed in Section 3.5 and which we shall establish more generally in Section 7.6.

The friction coefficient is also related to the diffusion coefficient. Consider the case when the brownian particle is initially ($t=0$) situated at the origin ($\mathbf{r}=0$). We wish to calculate the mean-square displacement of the particle after a time t. By multiplying through (7.3.1) by $\mathbf{r}(t)$ and using the results

$$\mathbf{r}\cdot\mathbf{u} = \mathbf{r}\cdot\dot{\mathbf{r}} = \tfrac{1}{2}\frac{\mathrm{d}}{\mathrm{d}t}r^2 \tag{7.3.9}$$

$$\mathbf{r}\cdot\dot{\mathbf{u}} = \mathbf{r}\cdot\ddot{\mathbf{r}} = \tfrac{1}{2}\frac{\mathrm{d}^2}{\mathrm{d}t^2}r^2 - u^2 \tag{7.3.10}$$

we find that

$$\tfrac{1}{2}m\frac{\mathrm{d}^2}{\mathrm{d}t^2}|\mathbf{r}(t)|^2 + \tfrac{1}{2}\xi m\frac{\mathrm{d}}{\mathrm{d}t}|\mathbf{r}(t)|^2 = m|\mathbf{u}(t)|^2 + \mathbf{r}(t)\cdot\mathbf{R}(t) \tag{7.3.11}$$

In the statistical mean (7.3.11) becomes

$$\frac{\mathrm{d}^2}{\mathrm{d}t^2}\langle|\mathbf{r}(t)|^2\rangle + \xi\frac{\mathrm{d}}{\mathrm{d}t}\langle|\mathbf{r}(t)|^2\rangle = \frac{6k_\mathrm{B}T}{m} \tag{7.3.12}$$

The solution to (7.3.12) that satisfies the boundary conditions $\langle|\mathbf{r}(0)|^2\rangle = 0$ and

$$\frac{\mathrm{d}}{\mathrm{d}t}\langle|\mathbf{r}(t)|^2\rangle\Big|_{t=0} = 2\langle\mathbf{r}(0)\cdot\mathbf{u}(0)\rangle = 0 \tag{7.3.13}$$

is

$$\left\langle \left|\mathbf{r}(t)\right|^2 \right\rangle = \frac{6k_{\mathrm{B}}T}{\xi m}\left(t - \frac{1}{\xi} + \frac{1}{\xi}\exp(-\xi t)\right) \tag{7.3.14}$$

At very short times, such that $\xi t \ll 1$, the solution becomes

$$\left\langle \left|\mathbf{r}(t)\right|^2 \right\rangle \approx \left(\frac{3k_{\mathrm{B}}T}{m}\right)t^2 = \langle u^2 \rangle t^2 \tag{7.3.15}$$

which corresponds to free-particle motion. At very large times ($\xi t \gg 1$), (7.3.14) reduces to

$$\left\langle \left|\mathbf{r}(t)\right|^2 \right\rangle \approx \left(\frac{6k_{\mathrm{B}}T}{\xi m}\right)t \tag{7.3.16}$$

and comparison with (7.2.3) leads to Einstein's expression for the diffusion coefficient:

$$D = \frac{k_{\mathrm{B}}T}{\xi m} \tag{7.3.17}$$

An estimate of ξ can be obtained from a hydrodynamic calculation of the frictional force on a sphere of diameter d moving with constant velocity $\mathbf{u}$ in a fluid of shear viscosity η. This leads to a famous result due to Stokes, the precise form of which depends on the assumptions made about the behaviour at the surface of the sphere of the velocity field created by the fluid. If the "stick" boundary condition is used, the fluid velocity at the surface is everywhere taken equal to $\mathbf{u}$; in the "slip" approximation, the normal component of the fluid velocity is set equal to the normal component of $\mathbf{u}$, thereby ensuring that no fluid can enter or leave the sphere, and the tangential force acting on the sphere is assumed to vanish. The stress tensor at the surface is then obtained by solving the linearised Navier–Stokes equation (see Section 8.3) subject to one of these boundary conditions, supplemented by the requirement that the fluid velocity must vanish at infinite distance from the sphere. When the stress tensor is known, the total frictional force $\mathbf{F}$ can be calculated by integration over the surface. The final result has the form $\mathbf{F} = -\xi\mathbf{u}$, with

$$\xi = \frac{3\pi\eta d}{m} \quad \text{(stick)}, \qquad \xi = \frac{2\pi\eta d}{m} \quad \text{(slip)} \tag{7.3.18}$$

Combination of (7.3.17) with (7.3.18) leads to the two familiar forms of Stokes's law:

$$D\eta = \frac{k_{\mathrm{B}}T}{3\pi d} \quad \text{(stick)}, \qquad D\eta = \frac{k_{\mathrm{B}}T}{2\pi d} \quad \text{(slip)} \tag{7.3.19}$$

It is a remarkable feature of Stokes's law that although it is derived from purely macroscopic considerations, and is apparently limited to brownian particles, it also provides a good, empirical correlation of experimental data on simple liquids, use of the slip boundary condition generally leading to more reasonable values of the effective diameter d.

The form of the velocity autocorrelation function of the brownian particle is easily deduced. If we multiply through (7.3.1) by $\mathbf{u}(0)$ and take the thermal average we find that

$$Z(t) = \tfrac{1}{3}\langle \mathbf{u}(t) \cdot \mathbf{u}(0) \rangle = \left(\frac{k_B T}{m} \right) \exp(-\xi t) \tag{7.3.20}$$

where $t \geqslant 0$. The expression for the diffusion coefficient given by (7.3.17) is then recovered by inserting (7.3.20) in (7.2.7). Note that the autocorrelation function is of the same, exponential form as the Enskog result for the hard-sphere fluid. This is to be expected, since a markovian hypothesis underlies both calculations. In practice, as is evident from Figure 7.1, the velocity autocorrelation function of a simple liquid may be very far from exponential. Moreover, the power spectrum of an exponential correlation function has an infinite second moment, which for continuous potentials is not consistent with the result shown in (7.2.8). The inconsistency arises because the applicability of (7.3.20) does not extend to very short times. In a time interval t such that $\xi t \ll 1$ the brownian particle experiences very few collisions and the basic assumptions of the Langevin theory are no longer valid.

When the dimensions of the diffusing particle are similar to those of its neighbours, the weakest part of the theory is the markovian approximation whereby the frictional force on the particle at a given time is assumed to be proportional only to its velocity at the same time. The implication of this assumption is that the motion of the particle adjusts itself instantaneously to changes in the surrounding medium. It would obviously be more realistic to suppose that the frictional force acting on a particle reflects the previous history of the system. In other words, we should associate a certain "memory" with the motion of the particle. This can be achieved by introducing a friction coefficient $\xi(t-s)$ that is non-local in time and determines the contribution to the systematic force at time t coming from the velocity at earlier times s. Mathematically this amounts to writing the frictional force as a convolution in time, giving rise to a non-markovian generalisation of the Langevin equation, which we write as

$$m\dot{\mathbf{u}}(t) = -m \int_0^t \xi(t-s)\mathbf{u}(s)\,\mathrm{d}s + \mathbf{R}(t) \tag{7.3.21}$$

The properties of $\mathbf{R}(t)$ expressed by (7.3.2) and (7.3.3) are assumed to be unaltered. If, therefore, we multiply through (7.3.21) by $\mathbf{u}(0)$ and take the thermal average, we arrive at an equation for the velocity autocorrelation function in the form

$$\dot{Z}(t) = -\int_0^t \xi(t-s)Z(s)\,\mathrm{d}s \tag{7.3.22}$$

The quantity $\xi(t)$ is called the *memory function* for the autocorrelation function $Z(t)$. An equation analogous to (7.3.22) can be written down for the autocorrelation function of an arbitrary dynamical variable, A say. Such an expression may be regarded as a generalised Langevin equation in which the random "force" is proportional to that part of $A(t)$ which is uncorrelated with $A(0)$ (cf. (7.3.3)). All that is lost in extending the use of the generalised

Langevin equation to other dynamical variables is a feeling for the physical meaning of the "friction" coefficient and random "force".

If we take the Laplace transform of (7.3.22), we obtain a simple, algebraic relation between $\tilde{Z}(z)$ and $\tilde{\xi}(z)$:

$$\tilde{Z}(z) = \frac{k_B T/m}{-iz + \tilde{\xi}(z)} \tag{7.3.23}$$

On replacing the frequency-dependent friction coefficient in (7.3.23) by a constant, ξ, and inverting the transform, we recover the exponential form of $Z(t)$ given by (7.3.20); this amounts to choosing a purely local (markovian) memory function, $\xi(t) = \xi\delta(t)$, which leads back to the original Langevin equation (7.3.1). Similarly, the Enskog approximation (7.2.20) corresponds to taking $\xi(t) = (3/2\Gamma_E)\delta(t)$. Equation (7.3.22) is exact, however, since it acts as a definition of the unknown function $\xi(t)$. What is lacking at this stage is any statistical-mechanical definition of either $\mathbf{R}(t)$ or $\xi(t)$, nor is it obvious that $\xi(t)$ is a simpler object to understand than $Z(t)$ itself; if it were not, (7.3.22) would be of little value. The interpretation of the generalised Langevin equation and the memory-function equation in terms of statistical mechanics is described in detail in Chapter 9. Here it is sufficient to say that $\xi(t)$ is expected to decay much faster than $Z(t)$. If this is so, it suggests that a phenomenological model of a complicated dynamical process can be devised by postulating a rather simple form for the appropriate memory function that satisfies, in particular, the low-order sum rules on the autocorrelation function. For example, to describe the diffusion process, we could suppose that the memory function decays exponentially[10] with a characteristic time τ:

$$\xi(t) = \xi(0)\exp\bigl(-|t|/\tau\bigr) \tag{7.3.24}$$

If we differentiate (7.3.22) with respect to time, set $t = 0$ and use (7.2.9), we find that

$$\xi(0) = -\frac{\ddot{Z}(0)}{Z(0)} = \Omega_0^2 \tag{7.3.25}$$

Then, by taking the Laplace transform of (7.3.24) and substituting the result in (7.3.23), we obtain the expression

$$\tilde{Z}(z) = \frac{k_B T/m}{-iz + \frac{\Omega_0^2}{-iz+\tau^{-1}}} \tag{7.3.26}$$

It follows from (7.2.7) that the diffusion coefficient is

$$D = \tilde{Z}(0) = \frac{k_B T}{m\Omega_0^2 \tau} \tag{7.3.27}$$

and inverse Laplace transformation of (7.3.26) shows that the velocity autocorrelation function is given by

$$Z(t) = \left(\frac{k_B T/m}{\alpha_+ - \alpha_-}\right)\bigl[\alpha_+ \exp\bigl(-\alpha_-|t|\bigr) - \alpha_- \exp\bigl(-\alpha_+|t|\bigr)\bigr] \tag{7.3.28}$$

where α_+, α_- are the two poles of $\tilde{Z}(z = i\alpha)$:

$$\alpha_\pm = \frac{1}{2\tau}\left[1 \mp \left(1 - 4\Omega_0^2\tau^2\right)^{1/2}\right] \tag{7.3.29}$$

If $\tau < 1/2\Omega_0$, the poles are real and positive and $Z(t)$ decays monotonically with the correct curvature (Ω_0^2) at the origin. On the other hand, if $\tau > 1/2\Omega_0$, which from (7.3.27) is equivalent to the condition

$$\frac{mD\Omega_0}{k_\mathrm{B}T} < 2 \tag{7.3.30}$$

then the poles are a complex-conjugate pair and the velocity autocorrelation function behaves as

$$Z(t) = \left(\frac{k_\mathrm{B}T}{m}\right)\exp\left(-|t|/2\tau\right)\left[\cos\Omega_1|t| + (1/2\Omega_1\tau)\sin\Omega_1|t|\right] \tag{7.3.31}$$

where $\Omega_1^2 = \Omega_0^2 - 1/4\tau^2$. The function defined by (7.3.31) exhibits a negative region at intermediate times, in qualitative agreement with simulation results on simple liquids at low temperatures and high densities (see Figure 7.1), where the condition (7.3.30) is indeed well satisfied. The argument that leads to (7.3.28) is nonetheless inadequate in certain respects. First, it provides no prescription for the relaxation time τ, though the value of τ can be derived from (7.3.27) if D is known. Secondly, use of the simple memory function (7.3.24) yields a spectrum $Z(\omega)$ for which the even frequency moments beyond the second are all infinite. Both defects can be overcome by postulating a gaussian rather than an exponential memory function and forcing agreement with the fourth frequency moment of $Z(\omega)$, which in turn requires a knowledge of the equilibrium triplet distribution function. However, none of the phenomenological memory-function calculations that use as their basic ingredients only the short-time behaviour of the correlation function are capable of reproducing the observed slow ($\sim t^{-3/2}$) decay at long times ($\Omega_0 t \gg 1$).

7.4 CORRELATIONS IN SPACE AND TIME

A detailed description of the time evolution of spatial correlations in liquids requires the introduction of time-dependent generalisations of the static distribution functions defined in Sections 2.5 and 2.6. The relevant dynamical variable is the microscopic particle density (3.1.2), where account must now be taken of the time-dependence of the particle coordinates $\mathbf{r}_i$. More generally, we define a microscopic dynamical variable as

$$A(\mathbf{r}, t) = \sum_{i=1}^{N} a_i(t)\delta\left[\mathbf{r} - \mathbf{r}_i(t)\right] \tag{7.4.1}$$

where a_i is some physical quantity such as the mass, velocity or energy of particle i. The spatial Fourier components of $A(\mathbf{r}, t)$ are

$$A_{\mathbf{k}}(t) = \int A(\mathbf{r}, t) \exp(-i\mathbf{k} \cdot \mathbf{r})\, d\mathbf{r} = \sum_{i=1}^{N} a_i(t) \exp\bigl[-i\mathbf{k} \cdot \mathbf{r}_i(t)\bigr] \tag{7.4.2}$$

A microscopic dynamical variable is said to be *conserved* if it satisfies a continuity equation of the form

$$\frac{\partial A(\mathbf{r}, t)}{\partial t} + \nabla \cdot \mathbf{j}^A(\mathbf{r}, t) = 0 \tag{7.4.3}$$

where $\mathbf{j}^A$ is the *current* associated with the variable A. Equation (7.4.3) is a local expression of the fact that $\int A(\mathbf{r}, t)\, d\mathbf{r} = \sum_i a_i(t)$ is independent of time; the corresponding equation for the Fourier components of A is

$$\frac{\partial A_{\mathbf{k}}(t)}{\partial t} + i\mathbf{k} \cdot \mathbf{j}^A_{\mathbf{k}}(t) = 0 \tag{7.4.4}$$

which shows that spontaneous fluctuations in a conserved variable decay very slowly at long wavelengths.

The time-dependent, microscopic particle density

$$\rho(\mathbf{r}, t) = \sum_{i=1}^{N} \delta\bigl[\mathbf{r} - \mathbf{r}_i(t)\bigr] \tag{7.4.5}$$

corresponds to the case when $a_i = 1$ and is a particularly important example of a conserved local variable. The associated particle current is

$$\mathbf{j}(\mathbf{r}, t) = \sum_{i=1}^{N} \mathbf{u}_i(t) \delta\bigl[\mathbf{r} - \mathbf{r}_i(t)\bigr] \tag{7.4.6}$$

with Fourier components

$$\mathbf{j}_{\mathbf{k}}(t) = \sum_{i=1}^{N} \mathbf{u}_i(t) \exp\bigl[-i\mathbf{k} \cdot \mathbf{r}_i(t)\bigr] \tag{7.4.7}$$

where $\mathbf{u}_i$ is the velocity of particle i. Each Fourier component may be separated into longitudinal (l) and transverse (t) parts, the two parts being parallel and perpendicular, respectively, to the wavevector $\mathbf{k}$. The longitudinal component, $\mathbf{j}_{\mathbf{k}l}$, is related to the microscopic density via the continuity equation (7.4.4).

The time-correlation function of two space-dependent dynamical variables is defined as in (7.1.2) or (7.1.3) but is now, in general, non-local in space:

$$C_{AB}(\mathbf{r}', \mathbf{r}''; t', t'') = \bigl\langle A(\mathbf{r}', t') B^*(\mathbf{r}'', t'') \bigr\rangle \tag{7.4.8}$$

while the correlation functions of the Fourier components are defined as

$$C_{AB}(\mathbf{k}', \mathbf{k}''; t', t'') = \left\langle A_{\mathbf{k}'}(t') B^*_{\mathbf{k}''}(t'') \right\rangle = \left\langle A_{\mathbf{k}'}(t') B_{-\mathbf{k}''}(t'') \right\rangle \tag{7.4.9}$$

These correlation functions have all the properties given in Section 7.1, in particular those associated with stationarity. In addition, for homogeneous liquids, translational invariance in space means that the correlation function (7.4.8) depends only on the relative coordinates $\mathbf{r} = \mathbf{r}' - \mathbf{r}''$. Thus

$$C_{AB}(\mathbf{r}', \mathbf{r}''; t', t'') = C_{AB}(\mathbf{r}' - \mathbf{r}'', t' - t'') \tag{7.4.10}$$

Translational invariance also implies that correlations between Fourier components $A_{\mathbf{k}'}(t')$ and $B_{\mathbf{k}''}(t'')$ are non-zero only if $\mathbf{k}' = \mathbf{k}''$, i.e.

$$C_{AB}(\mathbf{k}', \mathbf{k}''; t) = \left\langle A_{\mathbf{k}'}(t) B_{-\mathbf{k}''} \right\rangle \delta_{\mathbf{k}', \mathbf{k}''} \tag{7.4.11}$$

Clearly $C_{AB}(\mathbf{k}, t)$ is the spatial Fourier transform of $C_{AB}(\mathbf{r}, t)$:

$$C_{AB}(\mathbf{k}, t) = \int C_{AB}(\mathbf{r}, t) \exp(-i\mathbf{k} \cdot \mathbf{r}) \, \mathrm{d}\mathbf{r} \tag{7.4.12}$$

If the fluid is also isotropic, the correlation functions (7.4.10) and (7.4.11) share with their static counterparts the property that they are functions, respectively, of the scalar quantities r and k. The frequency moments of the power spectrum of an autocorrelation function $C_{AA}(k, t)$ are again given by (7.1.24), but are now wavenumber-dependent. The continuity equation for conserved variables leads to simple expressions for the second frequency moments, called f-sum rules. From (7.1.24) and (7.4.4) it follows that

$$\left\langle \omega^2 \right\rangle_{AA} = \langle \dot{A}_{\mathbf{k}} \dot{A}_{-\mathbf{k}} \rangle = k^2 \left\langle \left| \mathbf{j}^A_{\mathbf{k}'} \right|^2 \right\rangle \tag{7.4.13}$$

The memory function, M_{AA} say, associated with a space-dependent autocorrelation function C_{AA} must allow for non-local effects in space as well as in time. The memory-function equation satisfied by C_{AA} is therefore written as

$$\dot{C}_{AA}(\mathbf{r}, t) + \int_0^t \mathrm{d}t' \int \mathrm{d}\mathbf{r}' M_{AA}(\mathbf{r} - \mathbf{r}', t - t') C_{AA}(\mathbf{r}', t') = 0 \tag{7.4.14}$$

or, by exploiting the convolution theorem:

$$\dot{C}_{AA}(\mathbf{k}, t) + \int_0^t \mathrm{d}t' M_{AA}(\mathbf{k}, t - t') C_{AA}(\mathbf{k}, t') = 0 \tag{7.4.15}$$

We now focus specifically on the way in which time-dependent correlations in the microscopic density and particle current are described. A convenient starting point is provided by the space and time-dependent distribution function introduced by van Hove. The van

Hove function for a uniform fluid is defined as

$$G(\mathbf{r},t)=\left\langle \frac{1}{N}\sum_{i=1}^{N}\sum_{j=1}^{N}\int \delta\big[\mathbf{r}-\mathbf{r}_j(t)+\mathbf{r}_i(0)\big]\right\rangle \tag{7.4.16}$$

which can be rewritten successively as

$$\begin{aligned} G(\mathbf{r},t)&=\left\langle \frac{1}{N}\int \sum_{i=1}^{N}\sum_{j=1}^{N}\delta\big[\mathbf{r}'+\mathbf{r}-\mathbf{r}_j(t)\big]\delta\big[\mathbf{r}'-\mathbf{r}_i(0)\big]\,\mathrm{d}\mathbf{r}'\right\rangle \\ &=\left\langle \frac{1}{N}\int \rho(\mathbf{r}'+\mathbf{r},t)\rho(\mathbf{r}',0)\,\mathrm{d}\mathbf{r}'\right\rangle=\frac{1}{\rho}\big\langle\rho(\mathbf{r},t)\rho(\mathbf{0},0)\big\rangle \end{aligned} \tag{7.4.17}$$

The van Hove function therefore has the meaning of a density–density time-correlation function which for $t=0$ is closely related to the static correlation function (3.1.6). It separates naturally into two terms, usually called the "self" (s) and "distinct" (d) parts, i.e.

$$G(\mathbf{r},t)=G_{\mathrm{s}}(\mathbf{r},t)+G_{\mathrm{d}}(\mathbf{r},t) \tag{7.4.18}$$

where

$$G_{\mathrm{s}}(\mathbf{r},t)=\left\langle \frac{1}{N}\sum_{i=1}^{N}\delta\big[\mathbf{r}-\mathbf{r}_i(t)+\mathbf{r}_i(0)\big]\right\rangle \tag{7.4.19a}$$

$$G_{\mathrm{d}}(\mathbf{r},t)=\left\langle \frac{1}{N}\sum_{i=1}^{N}\sum_{j\neq i}^{N}\delta\big[\mathbf{r}-\mathbf{r}_j(t)+\mathbf{r}_i(0)\big]\right\rangle \tag{7.4.19b}$$

Hence $G_{\mathrm{s}}(\mathbf{r},0)=\delta(\mathbf{r})$ and (from (2.5.15)) $G_{\mathrm{d}}(\mathbf{r},0)=\rho g(\mathbf{r})$. The physical interpretation of the van Hove function is that $G(\mathbf{r},t)\,\mathrm{d}\mathbf{r}$ is the number of particles j in a region $\mathrm{d}\mathbf{r}$ around a point $\mathbf{r}$ at time t given that there was a particle i at the origin at time $t=0$; the division into self and distinct parts corresponds to the possibilities that i and j may be the same particle or different ones. As t increases, G_{s} broadens into a bell-shaped curve and the peaks in G_{d} gradually disappear. In the limit $t\to\infty$, both functions become independent of r, with $G_{\mathrm{s}}(\mathbf{r},t\to\infty)\sim 1/V$ and $G_{\mathrm{d}}(\mathbf{r},t\to\infty)\sim\rho$; the behaviour at large r is the same as that at large t.

Rather than considering the density–density correlation in real space, it is often more convenient to focus attention on the correlation function of the Fourier components $\rho_{\mathbf{k}}$:

$$F(\mathbf{k},t)=\frac{1}{N}\big\langle\rho_{\mathbf{k}}(t)\rho_{-\mathbf{k}}\big\rangle \tag{7.4.20}$$

The function $F(\mathbf{k},t)$ is called the *intermediate scattering function*; as we shall see later, $F(\mathbf{k},t)$ is closely related to the cross-section measured in an inelastic scattering experiment. By following steps almost identical to those that establish the relation (4.1.3) between the static structure factor and the pair distribution function it is easy to show that

$F(\mathbf{k}, t)$ is the spatial Fourier transform of the van Hove function, i.e.

$$F(\mathbf{k}, t) = \int G(\mathbf{r}, t) \exp(-i\mathbf{k} \cdot \mathbf{r})\, \mathrm{d}\mathbf{r} \tag{7.4.21}$$

The power spectrum of the intermediate scattering function:

$$S(\mathbf{k}, \omega) = \frac{1}{2\pi} \int_{-\infty}^{\infty} F(\mathbf{k}, t) \exp(i\omega t)\, \mathrm{d}t \tag{7.4.22}$$

is called the *dynamic structure factor*. Combination of (4.1.1) and (7.1.24) shows that the static and dynamic structure factors are related by

$$\int_{-\infty}^{\infty} S(\mathbf{k}, \omega)\, \mathrm{d}\omega = F(\mathbf{k}, 0) = S(\mathbf{k}) \tag{7.4.23}$$

The physical significance of this sum rule will become clear in the next section. Finally, we define the autocorrelation function of the Fourier components (7.4.7) of the current associated with the microscopic density. Because $\mathbf{j}_\mathbf{k}$ is a vector, the corresponding correlation function is a second-rank tensor, but rotational invariance implies that the longitudinal and transverse projections of the particle current are uncorrelated if the fluid is isotropic. When that is so, the correlation-function tensor has only two independent components and may therefore be written in the form

$$\begin{aligned} C_{\alpha\beta}(\mathbf{k}, t) &= \frac{k^2}{N} \left\langle j_\mathbf{k}^\alpha(t)\, j_{-\mathbf{k}}^\beta \right\rangle \\ &= \hat{k}_\alpha \hat{k}_\beta C_l(k, t) + (\delta_{\alpha\beta} - \hat{k}_\alpha \hat{k}_\beta) C_t(k, t) \end{aligned} \tag{7.4.24}$$

where $\alpha, \beta = x,\ y$ or z and $\hat{k}_\alpha,\ \hat{k}_\beta$ are cartesian components of the unit vector $\hat{\mathbf{k}} = \mathbf{k}/k$. If the z-axis is chosen parallel to $\mathbf{k}$, the longitudinal and transverse current autocorrelation functions are given by

$$C_l(k, t) = \frac{k^2}{N} \left\langle j_\mathbf{k}^z(t)\, j_{-\mathbf{k}}^z \right\rangle \tag{7.4.25a}$$

$$C_t(k, t) = \frac{k^2}{N} \left\langle j_\mathbf{k}^x(t)\, j_{-\mathbf{k}}^x \right\rangle \tag{7.4.25b}$$

The continuity equation (7.4.4) (with $A = \rho$) and the general property (7.1.8) imply that the density and longitudinal-current correlation functions are not independent, since

$$C_l(k, t) = \frac{1}{N} \left\langle \dot{\rho}_\mathbf{k}(t) \dot{\rho}_\mathbf{k} \right\rangle = -\frac{\mathrm{d}^2}{\mathrm{d}t^2} F(k, t) \tag{7.4.26}$$

Written in terms of Laplace transforms, (7.4.26) becomes

$$\widetilde{C}_l(k, z) = z^2 \widetilde{F}(k, z) - izS(k) \tag{7.4.27}$$

or, on taking the real part and making use of (7.1.19):

$$C_l(k,\omega) = \omega^2 S(k,\omega) \tag{7.4.28}$$

The function $C_l(k,\omega)$ describes the spectrum of longitudinal-current fluctuations in the liquid. Fluctuations in density are therefore intimately related to fluctuations in longitudinal current, but are independent of the transverse current.

In classical statistical mechanics, positions and velocities at a given instant are uncorrelated. Thus the definitions of the current autocorrelation functions show that their zero-time values are the same and given by

$$C_{l,t}(k,0) = k^2\left(\frac{k_\mathrm{B}T}{m}\right) = \omega_0^2, \quad \text{say} \tag{7.4.29}$$

From (7.4.26) and the general f-sum rule (7.4.13) it follows that the second frequency moment of the dynamic structure factor is given by

$$\langle\omega^2\rangle_{\rho\rho} = \int_{-\infty}^{\infty} \omega^2 S(k,\omega)\,\mathrm{d}\omega = -\ddot{F}(k,0) = \omega_0^2 \tag{7.4.30}$$

Since the f-sum rule is a consequence of the continuity equation, the second moment is purely kinetic in origin, but higher-order moments depend on the interparticle potential. If the potential is continuous, the general results contained in (7.1.23) and (7.1.24) imply that the odd frequency moments of $S(k,\omega)$ are all zero and the fourth moment is equal, by virtue of the relation (7.4.28), to the second moment of $C_l(k,\omega)$. We may therefore base a calculation of the fourth moment on the short-time expansion of $C_l(k,t)$, which we write as

$$C_l(k,t) = \omega_0^2\left(1 - \omega_{1l}^2\frac{t^2}{2!} + \cdots\right) \tag{7.4.31}$$

Equations (7.1.8) and (7.4.31) show that

$$\omega_0^2\omega_{1l}^2 = -\frac{\mathrm{d}^2}{\mathrm{d}t^2}C_l(k,t)\bigg|_{t=0} = \frac{\mathrm{d}^4}{\mathrm{d}t^4}F(k,t)\bigg|_{t=0} = \frac{1}{N}\langle\ddot{\rho}_{\mathbf{k}}\ddot{\rho}_{-\mathbf{k}}\rangle \tag{7.4.32}$$

If again we take the z-axis along the direction of $\mathbf{k}$ and make the substitution $\dot{u}_{iz} = -(1/m)(\partial V_N/\partial z_i)$, (7.4.32) becomes

$$\omega_0^2\omega_{1l}^2 = k^4\langle u_{iz}^4\rangle + k^2\left(\frac{k_\mathrm{B}T}{m}\right)\left\langle\sum_{i=1}^{N}\sum_{j=1}^{N}\frac{\partial V_N}{\partial z_i}\frac{\partial V_N}{\partial z_j}\exp\bigl[ik(z_i - z_j)\bigr]\right\rangle \tag{7.4.33}$$

For a maxwellian distribution of velocities, $\langle u_{iz}^4 \rangle = 3\langle u_{iz}^2 \rangle^2$, and the statistical average in (7.4.33) can be simplified with the help of Yvon's theorem (7.2.11) to give

$$\left\langle \sum_{i=1}^{N}\sum_{j=1}^{N} \frac{\partial V_N}{\partial z_i}\frac{\partial V_N}{\partial z_j} \exp\bigl[ik(z_i - z_j)\bigr] \right\rangle$$

$$= k_{\mathrm{B}}T\left\langle N\frac{\partial^2 V_N}{\partial z_1^2} + N(N-1)\frac{\partial^2 V_N}{\partial z_1 \partial z_2}\exp\bigl[ik(z_1 - z_2)\bigr]\right\rangle \tag{7.4.34}$$

where 1 and 2 are the labels of two, arbitrarily chosen particles. Hence, if V_N is a sum of pair terms:

$$\omega_{1l}^2 = 3\omega_0^2 + \frac{\rho}{m}\int (1 - \cos kz)\frac{\partial^2 v(r)}{\partial z^2} g(r)\,\mathrm{d}\mathbf{r} \tag{7.4.35}$$

where $v(r)$ is the pair potential. At large k, the kinetic contribution dominates, corresponding to free-particle behaviour. From (7.4.28) we see that ω_{1l}^2 is related to the second and fourth frequency moments of $S(k,\omega)$ by $\omega_{1l}^2 = \langle\omega^4\rangle_{\rho\rho}/\langle\omega^2\rangle_{\rho\rho}$.

A similar calculation can be made for the transverse current. The short-time expansion of the correlation function is now

$$C_t(k,t) = \omega_0^2\left(1 - \omega_{1t}^2\frac{t^2}{2!} + \cdots\right) \tag{7.4.36}$$

with

$$\omega_0^2\omega_{1t}^2 = -\frac{\mathrm{d}^2}{\mathrm{d}t^2}C_t(k,t)\bigg|_{t=0} \tag{7.4.37}$$

By pursuing the methods already used in the longitudinal case we find that the analogue of (7.4.35) is

$$\omega_{1t}^2 = \omega_0^2 + \frac{\rho}{m}\int (1 - \cos kz)\frac{\partial^2 v(r)}{\partial x^2} g(r)\,\mathrm{d}\mathbf{r} \tag{7.4.38}$$

Higher-order moments of $C_l(k,\omega)$ and $C_t(k,\omega)$ involve correlations between increasingly large numbers of particles and rapidly become very tedious to evaluate.

7.5 INELASTIC NEUTRON SCATTERING

We now show how the Fourier transforms of the van Hove functions $G(\mathbf{r},t)$ and $G_{\mathrm{s}}(\mathbf{r},t)$ are related to measurements of the inelastic scattering of slow (or "thermal") neutrons. To do so, we require a generalisation of the calculation of Section 4.1 that allows for the exchange of energy between the neutrons and the target.[11] Neutrons are particularly useful as probes of the microscopic dynamics of liquids because their momentum $\hbar\mathbf{k}$ and energy $E = \hbar\omega$ are related by $E = \hbar^2k^2/2m$, where m is the neutron mass. It follows that when E is of order $k_{\mathrm{B}}T$, and therefore comparable with the thermal energies of particles in the

liquid, the wavelength $\lambda = 2\pi/k$ associated with the neutron is approximately 2 Å, which is similar to the distance between neighbouring particles.

In a typical scattering event a neutron of momentum $\hbar\mathbf{k}_1$ and energy $\hbar\omega_1$ is scattered into a solid angle $\mathrm{d}\Omega$. Let the momentum and energy of the neutron after the event be $\hbar\mathbf{k}_2$ and $\hbar\omega_2$ and let the momentum and energy transfer from neutron to sample be $\hbar\mathbf{k}$ and $\hbar\omega$. The dynamical conservation laws require that

$$\hbar\omega = E_2 - E_1 \equiv \hbar\omega_{12} \tag{7.5.1}$$

$$\hbar\mathbf{k} = \hbar\mathbf{k}_1 - \hbar\mathbf{k}_2 \tag{7.5.2}$$

where E_1 and E_2 are the initial and final energies of the sample. The probability per unit time, W_{12}, for the transition $|1, \mathbf{k}_1\rangle \rightarrow |2, \mathbf{k}_2\rangle$, where $|1\rangle$ and $|2\rangle$ denote the initial and final states of the sample, is given by Fermi's "golden rule":

$$W_{12} = \frac{2\pi}{\hbar}\left|\left\langle 1, \mathbf{k}_1|\mathcal{V}|2, \mathbf{k}_2\right\rangle\right|^2 \delta(\hbar\omega - \hbar\omega_{12}) \tag{7.5.3}$$

where $\mathcal{V}$ represents the perturbation, i.e. the interaction between the neutron and the atomic nuclei. For the sake of simplicity we have ignored the spin state of the neutron. The partial differential cross-section for scattering into the solid angle $\mathrm{d}\Omega$ in a range of energy transfer $\hbar\,\mathrm{d}\omega$ is calculated by averaging W_{12} over all initial states $|1\rangle$ with their statistical weights $P_1 \propto \exp(-\beta E_1)$, summing over all final states $|2\rangle$ allowed by energy conservation, multiplying by the density of final states of the neutron, namely

$$\mathrm{d}\mathbf{k}_2/(2\pi)^3 = k_2^2\,\mathrm{d}k_2\,\mathrm{d}\Omega/(2\pi)^3 = \left(m/\hbar^2\right)\hbar k_2\,\mathrm{d}\omega\,\mathrm{d}\Omega/(2\pi)^3 \tag{7.5.4}$$

and dividing by the flux $\hbar k_1/m$ of incident neutrons, with the final result having the form

$$\frac{\mathrm{d}^2\sigma}{\mathrm{d}\Omega\,\mathrm{d}\omega} = \frac{k_2}{k_1}\left(\frac{m}{2\pi\hbar^2}\right)^2 \sum_{\{1\}}\sum_{\{2\}} P_1\left|\left\langle 1, \mathbf{k}_1|\mathcal{V}|2, \mathbf{k}_2\right\rangle\right|^2 \delta(\omega - \omega_{12}) \tag{7.5.5}$$

The differential cross-section (4.1.9) is obtained by integrating over all energy transfers:

$$\frac{\mathrm{d}\sigma}{\mathrm{d}\Omega} = \int \frac{\mathrm{d}\sigma}{\mathrm{d}\Omega\,\mathrm{d}\omega}\,\mathrm{d}\omega \tag{7.5.6}$$

The structure and dynamics of the liquid enter the calculation through the interaction of the neutron with the atomic nuclei. We assume again that $\mathcal{V}$ is given by the sum (4.1.12) of δ-function pseudopotentials between a neutron located at $\mathbf{r}$ and nuclei at positions $\mathbf{r}_i$. If the initial and final states of the neutron are taken as plane-wave states of the form (4.1.6), the matrix element in (7.5.5) may be rewritten as

$$\left\langle 1, \mathbf{k}_1|\mathcal{V}|2, \mathbf{k}_2\right\rangle = \frac{2\pi\hbar^2}{m}\sum_{i=1}^{N}\left\langle 1\left|b_i \exp(-i\mathbf{k}\cdot\mathbf{r}_i)\right|2\right\rangle \tag{7.5.7}$$

where $\hbar\mathbf{k}$ is the momentum transfer already defined and b_i is the scattering length of nucleus i.

Consider first the case when all nuclei in the sample have the same scattering length. By incorporating (7.5.7) into (7.5.5), exploiting the definition (4.1.2) and introducing the integral representation of the δ-function, we obtain an expression for the cross-section in terms of the Fourier components of the microscopic density:

$$\begin{aligned}\frac{\mathrm{d}^2\sigma}{\mathrm{d}\Omega\,\mathrm{d}\omega} &= b^2\left(\frac{k_2}{k_1}\right)\sum_{\{1\}}\sum_{\{2\}} P_1\left|\langle 1|\rho_{\mathbf{k}}|2\rangle\right|^2\delta(\omega-\omega_{12}) \\ &= b^2\left(\frac{k_2}{k_1}\right)\sum_{\{1\}}\sum_{\{2\}} P_1\frac{1}{2\pi}\int_{-\infty}^{\infty}\left|\langle 1|\rho_{\mathbf{k}}|2\rangle\right|^2\exp\left[i(\omega-\omega_{12})t\right]\mathrm{d}t \qquad (7.5.8)\end{aligned}$$

Equation (7.5.8) can be simplified by recognising that

$$\begin{aligned}&\exp(-i\omega_{12}t)\left|\langle 1|\rho_{\mathbf{k}}|2\rangle\right|^2 \\ &\quad= \exp(-iE_2t/\hbar)\exp(iE_1t/\hbar)\langle 1|\rho_{\mathbf{k}}|2\rangle\langle 2|\rho_{-\mathbf{k}}|1\rangle \\ &\quad= \langle 1|\exp(iE_1t/\hbar)\rho_{\mathbf{k}}\exp(-iE_2t/\hbar)|2\rangle\langle 2|\rho_{-\mathbf{k}}|1\rangle \\ &\quad= \langle 1|\exp(i\mathcal{H}t/\hbar)\rho_{\mathbf{k}}\exp(-i\mathcal{H}t/\hbar)|2\rangle\langle 2|\rho_{-\mathbf{k}}|1\rangle \\ &\quad= \langle 1|\rho_{\mathbf{k}}(t)|2\rangle\langle 2|\rho_{-\mathbf{k}}|1\rangle \qquad (7.5.9)\end{aligned}$$

where $\mathcal{H}$ is the hamiltonian of the sample.

It remains only to sum over the initial states of the sample, which is equivalent to taking an ensemble average, and over the final states, which is done by exploiting the closure property, $\sum_j |j\rangle\langle j| = 1$, of a complete set of quantum states $|j\rangle$. The final result for the cross-section is

$$\begin{aligned}\frac{\mathrm{d}^2\sigma}{\mathrm{d}\Omega\,\mathrm{d}\omega} &= b^2\left(\frac{k_2}{k_1}\right)\frac{1}{2\pi}\int_{-\infty}^{\infty}\langle\rho_{\mathbf{k}}(t)\rho_{-\mathbf{k}}\rangle\exp(i\omega t)\,\mathrm{d}t \\ &= Nb^2\left(\frac{k_2}{k_1}\right)S(\mathbf{k},\omega) \qquad (7.5.10)\end{aligned}$$

where $S(\mathbf{k},\omega)$ is the dynamic structure factor defined by (7.4.22). Equation (7.5.10) shows that a measurement of the experimental cross-section as a function of $\mathbf{k}$ and ω is equivalent, at least in principle, to a determination of the van Hove correlation function $G(\mathbf{r},t)$. The connection with the elastic cross-section is made via (7.5.6); comparison of (4.1.23) with (7.5.10), taken for the case $k_1 = k_2$, shows that (7.5.6) provides the physical content of the so-called "elastic" sum rule (7.4.23).

By analogy with (7.4.21) and (7.4.22), it is customary to define a *self dynamic structure factor* $S_{\mathrm{s}}(\mathbf{k},\omega)$ as the double Fourier transform of the self part of the van Hove function, i.e.

$$S_{\mathrm{s}}(\mathbf{k},\omega) = \frac{1}{2\pi}\int_{-\infty}^{\infty}\mathrm{d}t\exp(i\omega t)\int G_{\mathrm{s}}(\mathbf{r},t)\exp(-i\mathbf{k}\cdot\mathbf{r})\,\mathrm{d}\mathbf{r} \qquad (7.5.11)$$

together with a self intermediate scattering function $F_s(\mathbf{k}, t)$, defined through the transform

$$S_s(\mathbf{k}, \omega) = \frac{1}{2\pi} \int_{-\infty}^{\infty} F_s(\mathbf{k}, t) \exp(i\omega t)\, \mathrm{d}t \tag{7.5.12}$$

with $F_s(\mathbf{k}, 0) = 1$. The self functions are important for the discussion of inelastic scattering in situations where more than one scattering length is involved. As in Section 4.1, the averaging over scattering lengths can be carried out independently of the thermal average over nuclear coordinates. A generalisation of the result in (4.1.21) allows the inelastic cross-section to be written as the sum of incoherent and coherent parts in the form

$$\frac{\mathrm{d}^2\sigma}{\mathrm{d}\Omega\, \mathrm{d}\omega} = \left(\frac{\mathrm{d}^2\sigma}{\mathrm{d}\Omega\, \mathrm{d}\omega}\right)_{\mathrm{inc}} + \left(\frac{\mathrm{d}^2\sigma}{\mathrm{d}\Omega\, \mathrm{d}\omega}\right)_{\mathrm{coh}} \tag{7.5.13}$$

with

$$\begin{aligned} \left(\frac{\mathrm{d}^2\sigma}{\mathrm{d}\Omega\, \mathrm{d}\omega}\right)_{\mathrm{inc}} &= N b_{\mathrm{inc}}^2 \left(\frac{k_2}{k_1}\right) S_s(\mathbf{k}, \omega) \\ \left(\frac{\mathrm{d}^2\sigma}{\mathrm{d}\Omega\, \mathrm{d}\omega}\right)_{\mathrm{coh}} &= N b_{\mathrm{coh}}^2 \left(\frac{k_2}{k_1}\right) S(\mathbf{k}, \omega) \end{aligned} \tag{7.5.14}$$

By varying the isotopic composition of the sample, or by using polarised neutrons, it is possible to measure separately the coherent and incoherent cross-sections and thereby, again in principle, to separate G_s and G_d.

For systems with inversion symmetry, which includes all fluids, the dynamic structure factor is invariant under a change of sign of $\mathbf{k}$. In the classical limit, $S(\mathbf{k}, \omega)$ is also an even function of ω, but a measured cross-section cannot be strictly even with respect to ω; if that were the case, thermal equilibrium between radiation and sample would never be reached. The principle of detailed balance requires that the cross-sections for the scattering processes $|\mathbf{k}_1, 1\rangle \rightarrow |\mathbf{k}_2, 2\rangle$ and $|\mathbf{k}_2, 2\rangle \rightarrow |\mathbf{k}_1, 1\rangle$ be equal to the ratio of the statistical weights of the states $|1\rangle$ and $|2\rangle$, i.e. $S(\mathbf{k}, \omega)/S(\mathbf{k}, -\omega) = \exp(\beta\hbar\omega)$. Experimental scattering data are therefore frequently reported in the form of a "symmetrised" dynamic structure factor, $\overline{S}(\mathbf{k}, \omega)$, defined as

$$\overline{S}(\mathbf{k}, \omega) = \exp\left(-\tfrac{1}{2}\beta\hbar\omega\right) S(\mathbf{k}, \omega) \tag{7.5.15}$$

This is an even function of frequency for both classical and quantum systems.

In the limit $\mathbf{r}, t \rightarrow 0$, particles in a fluid move freely at constant velocity. These conditions correspond to the limit $k, \omega \rightarrow \infty$, where $S(k, \omega)$ behaves in the manner appropriate to an ideal gas. The limiting form of $S(k, \omega)$ is easily derived, since positions of different particles are uncorrelated in an ideal gas ($G_d = \rho$); the calculation of $S(k, \omega)$ is therefore equivalent to a calculation of $G_s(r, t)$. The probability that an ideal-gas particle will move a distance r in a time t is equal to the probability, given by the Maxwell distribution (2.1.28), that the particle has a velocity in the range $\mathbf{u}$ to $\mathbf{u} + \mathrm{d}\mathbf{u}$, where $\mathbf{u} = \mathbf{r}/t$. Thus

$$G_s(\mathbf{r}, t) = \left(\frac{\beta m}{2\pi t^2}\right)^{3/2} \exp\left(-\beta m r^2/2t^2\right) \tag{7.5.16}$$

where the form of the pre-exponential factor is determined by the requirement that $\int G_s(\mathbf{r}, t)\, d\mathbf{r} = 1$. The corresponding result for $S(k, \omega)$ is

$$S(k, \omega) = \left(\frac{\beta m}{2\pi k^2}\right)^{1/2} \exp\left(-\beta m \omega^2 / 2k^2\right) \tag{7.5.17}$$

Equation (7.5.17) provides a reasonable fit to data on simple liquids at wavelengths significantly shorter than the spacing between particles, typically for k greater than about 10 Å^{-1}; small deviations from the free-particle result can be allowed for by calculating the correction to $S(k, \omega)$ due to a single, binary collision. At longer wavelengths correlations between particles become increasingly important and the ideal-gas model is no longer valid. Very small values of k correspond to the hydrodynamic regime, where thermodynamic equilibrium is brought by frequent collisions between particles; this is the opposite extreme to the free-particle limit represented by (7.5.17).

Inelastic neutron-scattering experiments designed for the study of both single-particle and collective dynamical properties have been carried out for a number of monatomic liquids. These experiments have been complemented by simulations of the Lennard-Jones and hard-sphere fluids and a variety of models of the liquid alkali metals. Most of the interest lies in the behaviour of the dynamic structure factor as a function of k and all the existing experiments and simulations reveal broadly the same features. At reduced wavenumbers $kd \approx 1$ or smaller, where d is the atomic diameter, $S(k, \omega)$ has a sharp peak at zero frequency and two more or less well defined side peaks, one on each side of the central peak. As k increases, the peaks shift to higher frequencies with a dispersion that is approximately linear. We shall see in Chapter 8 that the side peaks observed at long wavelengths correspond to propagating sound waves; they are clearly visible in the results of neutron scattering experiments on liquid caesium, some of which are plotted in Figure 7.5. At shorter wavelengths the sound waves are strongly damped and disappear when $kd \approx 2$, leaving only a central, lorentzian-like peak. The width of the central peak first increases with k, but then shows a marked decrease at wavenumbers close to the peak in the static structure factor (see curve (d) in Figure 7.5). This last effect is called "de Gennes narrowing"; it corresponds to a dramatic slowing down in the decay of the density autocorrelation function $F(k, t)$, which in turn has its origins in the strong spatial correlations existing at these wavelengths. At still larger values of k, the spectrum broadens again, going over finally to its free-particle limit. The behaviour of $S_s(k, \omega)$ is much simpler; this has only a single, central peak, the width of which increases smoothly with k.

Measurements of $S(k, \omega)$ can also be made by the inelastic scattering of light or x-rays. Both techniques measure only the coherent cross-section and cannot be used as probes of the single-particle motion, though this also simplifies analysis of the experimental data. In thermal-neutron scattering experiments the smallest momentum transfers correspond to wavelengths of the order of the nearest-neighbour spacing, but in light scattering the wavelengths involved are much larger, of order 5000 Å. It is therefore possible to calculate the spectral distribution of scattered light from the macroscopic equations of hydrodynamics, which are discussed in detail in Chapter 8. Light is scattered by fluctuations in the local dielectric constant of the sample, but for most liquids these are directly proportional to the fluctuations in density and the measured spectrum is proportional to $S(k, \omega)$. Inelastic x-ray

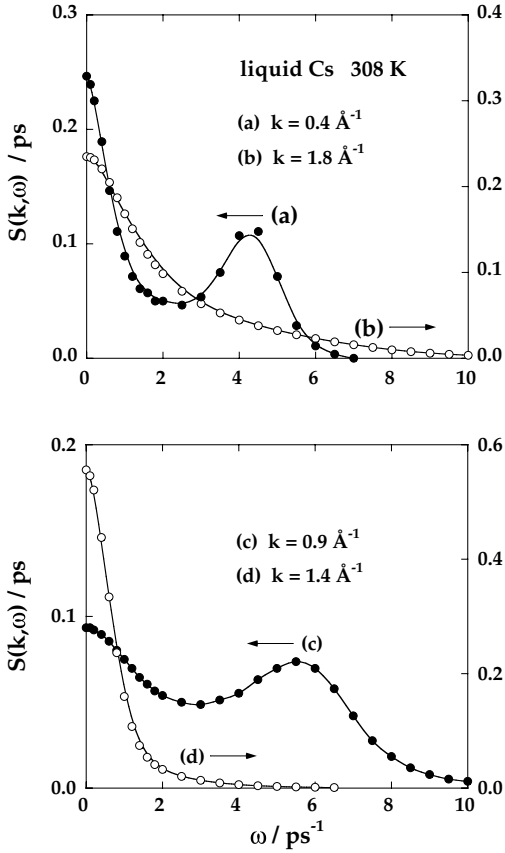

FIG. 7.5. Results from inelastic neutron-scattering experiments for the dynamic structure factor of liquid caesium near the normal melting temperature. The spectra have been normalised to unit area and only the energy-gain side is shown. The main peak in $S(k)$ is at $k \approx 1.4$ Å^{-1}. After Bodensteiner *et al.*[12]

scattering experiments have become feasible only with the development of high-resolution synchrotron radiation facilities. The momentum-energy relation for the neutron means that there exists a maximum possible energy transfer for a given momentum transfer, with a value determined by the velocity of the incoming neutron. This constraint does not apply in the case of x-ray scattering, thereby allowing measurements of $S(k, \omega)$ to be made over a wider range of the frequency-wavenumber plane.

7.6 LINEAR-RESPONSE THEORY

We turn now to an investigation of the behaviour of a system under the perturbing influence of an external field to which the system is weakly coupled. As we shall see, the response of the system can be described entirely in terms of time-correlation functions characteristic of

the system at equilibrium, i.e. in the *absence* of the field; the expression already obtained for the inelastic neutron-scattering cross-section in terms of the dynamic structure factor is an example of this relationship. The derivation of the general result requires only a straightforward calculation of the change produced in a dynamical variable B by an applied space and time-dependent field $\mathcal{F}$ conjugate to a variable A. Both A and B are to be regarded in general as functions of the coordinates and momenta of all particles in the system. The mean value of B in the equilibrium state is assumed to be zero.

The hamiltonian of the system in the presence of the external field is

$$\mathcal{H} = \mathcal{H}_0 + \mathcal{H}'(t) \tag{7.6.1}$$

where $\mathcal{H}_0$ characterises the unperturbed system and $\mathcal{H}'(t)$ represents the perturbation:

$$\mathcal{H}'(t) = -\int A(\mathbf{r})\mathcal{F}(\mathbf{r}, t)\,\mathrm{d}\mathbf{r} \tag{7.6.2}$$

The external field can always be treated as a superposition of monochromatic plane waves. Since we are interested in the linear response of the system, it is sufficient to consider a single plane wave:

$$\mathcal{F}(\mathbf{r}, t) = \frac{1}{V}\mathcal{F}_{\mathbf{k}} \exp\bigl[i(\mathbf{k}\cdot\mathbf{r} - \omega t)\bigr] \tag{7.6.3}$$

in which case (7.6.2) becomes

$$\mathcal{H}'(t) = -A_{-\mathbf{k}}\mathcal{F}_{\mathbf{k}} \exp(-i\omega t) \tag{7.6.4}$$

As a further simplification we shall temporarily suppose that the external field is spatially homogeneous and ignore the dependence on $\mathbf{k}$; the latter is trivially reintroduced at a later stage. We also assume that the system was in thermal equilibrium in the infinite past ($t \to -\infty$). Then $\mathcal{H}'(t)$ may be written as

$$\mathcal{H}'(t) = -A\mathcal{F}(t) = -A\mathcal{F}_0 \exp\bigl[-i(\omega + i\varepsilon)t\bigr] \tag{7.6.5}$$

where A and B are now taken to be real. The factor $\exp(\varepsilon t)$ ($\varepsilon > 0$) is included to ensure that $\mathcal{F} \to 0$ as $t \to -\infty$; the limit $\varepsilon \to 0$ is taken at the end of the calculation. The time evolution of the phase-space probability density $f^{[N]}(t) \equiv f^{[N]}(\mathbf{r}^N, \mathbf{p}^N; t)$ in the presence of the perturbation is determined by the Liouville equation (2.1.9). Thus

$$\begin{aligned}\frac{\partial f^{[N]}(t)}{\partial t} = -i\mathcal{L}f^{[N]}(t) &= \bigl\{\mathcal{H}_0 + \mathcal{H}',\, f^{[N]}(t)\bigr\} \\ &= -i\mathcal{L}_0 f^{[N]}(t) - \bigl\{A,\, f^{[N]}(t)\bigr\}\mathcal{F}(t)\end{aligned} \tag{7.6.6}$$

where $\mathcal{L}_0$ is the Liouville operator corresponding to the unperturbed hamiltonian. Equation (7.6.6) must be solved subject to the initial condition that $f^{[N]}(-\infty) = f_0^{[N]}$.

We are interested only in the response to a weak external field. We may therefore write the probability density as

$$f^{[N]}(t) = f_0^{[N]} + \Delta f^{[N]}(t) \tag{7.6.7}$$

and linearise (7.6.6) in the form

$$\frac{\partial \Delta f^{[N]}(t)}{\partial t} = -i\mathcal{L}_0 \Delta f^{[N]}(t) - \left\{A, f_0^{[N]}\right\}\mathcal{F}(t) \tag{7.6.8}$$

The solution to (7.6.8) is

$$\Delta f^{[N]}(t) = -\int_{-\infty}^{t} \exp\left[-i(t-s)\mathcal{L}_0\right]\left\{A, f_0^{[N]}\right\}\mathcal{F}(s)\,\mathrm{d}s \tag{7.6.9}$$

That this is the solution for all t is easily checked by differentiation, since it is obviously correct for $t = -\infty$. In the canonical ensemble, $f_0^{[N]} \propto \exp(-\beta\mathcal{H}_0)$, and the Poisson bracket appearing in (7.6.9) can be re-expressed as

$$\begin{aligned}\left\{A, f_0^{[N]}\right\} &= \sum_{i=1}^{N}\left(\frac{\partial A}{\partial \mathbf{r}_i}\cdot\frac{\partial f_0^{[N]}}{\partial \mathbf{p}_i} - \frac{\partial A}{\partial \mathbf{p}_i}\cdot\frac{\partial f_0^{[N]}}{\partial \mathbf{r}_i}\right)\\ &= -\beta\sum_{i=1}^{N}\left(\frac{\partial A}{\partial \mathbf{r}_i}\cdot\frac{\partial \mathcal{H}_0}{\partial \mathbf{p}_i} - \frac{\partial A}{\partial \mathbf{p}_i}\cdot\frac{\partial \mathcal{H}_0}{\partial \mathbf{r}_i}\right) f_0^{[N]}\\ &= -\beta(i\mathcal{L}_0 A) f_0^{[N]} = -\beta\dot{A} f_0^{[N]}\end{aligned} \tag{7.6.10}$$

The mean change in the variable $B(\mathbf{r}^N, \mathbf{r}^N)$ arising from the change in the distribution function is therefore

$$\begin{aligned}\left\langle \Delta B(t)\right\rangle &= \iint B\left(\mathbf{r}^N, \mathbf{p}^N\right)\Delta f^{[N]}(t)\,\mathrm{d}\mathbf{r}^N\,\mathrm{d}\mathbf{p}^N\\ &= \beta\int_{-\infty}^{t}\mathcal{F}(s)\,\mathrm{d}s\iint f_0^{[N]} B\exp\left[-i(t-s)\mathcal{L}_0\right]\dot{A}\,\mathrm{d}\mathbf{r}^N\mathrm{d}\mathbf{p}^N\\ &= \beta\int_{-\infty}^{t}\mathcal{F}(s)\,\mathrm{d}s\iint f_0^{[N]}\dot{A}\exp\left[i(t-s)\mathcal{L}_0\right]B\,\mathrm{d}\mathbf{r}^N\mathrm{d}\mathbf{p}^N\end{aligned} \tag{7.6.11}$$

where we have used a result contained in (7.1.28). The response of the system can therefore be written in the form

$$\left\langle \Delta B(t)\right\rangle = \int_{-\infty}^{t}\Phi_{BA}(t-s)\mathcal{F}(s)\,\mathrm{d}s \tag{7.6.12}$$

in terms of an *after-effect function* $\Phi_{BA}(t)$, defined as

$$\Phi_{BA}(t) = \beta\left\langle B(t)\dot{A}\right\rangle = -\beta\left\langle \dot{B}(t)A\right\rangle \tag{7.6.13}$$

The thermal averages in (7.6.13) are taken over the unperturbed system because in the linear approximation represented by (7.6.11) the variable B evolves in time under the influence of the reference-system propagator $\exp(i\mathcal{L}_0 t)$. It is sometimes convenient to use as an alternative definition of the after-effect function the expression

$$\theta_{BA}(t) = -\beta\langle \dot{B}(t)A\rangle\theta(t) \tag{7.6.14}$$

where $\theta(t)$ is the Heaviside step-function. Since $\theta_{BA}(t) = 0$ for $t < 0$, the upper limit of the integral in (7.6.12) can then be extended to $+\infty$.

The physical meaning of (7.6.12) and (7.6.13) is that the response, i.e. the change in the variable B at time t, is a superposition of delayed effects and the response to a unit δ-function force applied at $t = 0$ is proportional to the after-effect function itself. The basic result of linear-response theory embodied in these two equations can also be derived by calculating the changes in the phase-space trajectories of the particles to first order in the applied force. That method of derivation emphasises the assumption of mechanical linearity which underlies linear-response theory. Mechanical linearity cannot hold for macroscopic times, however, since it is known that the perturbed and unperturbed phase-space trajectories diverge exponentially on a macroscopic timescale even when the external field is very weak. On the other hand, the corresponding deviation in the phase-space distribution function is expected to behave smoothly as a function of the perturbation. Linearisation of the statistically averaged response should therefore be justified, in agreement with experimental observations. The apparent contradiction between mechanical non-linearity and statistical linearity is resolved by noting that the decay times of the relevant correlations, i.e. the times after which randomisation sets in, are generally quite short, and that use of a linear approximation for the divergence of the trajectories in phase space is valid for time intervals over which the after-effect function differs significantly from zero.

Equation (7.6.12) is easily generalised to the case in which the external field also varies in space. If the unperturbed system is spatially uniform, the response is determined by an after-effect function $\Phi_{BA}(\mathbf{r}, t)$ through the relation

$$\langle \Delta B(\mathbf{r}, t)\rangle = \int_{-\infty}^{t} \mathrm{d}s \int \Phi_{BA}(\mathbf{r} - \mathbf{r}', t - s)\mathcal{F}(\mathbf{r}', s)\,\mathrm{d}\mathbf{r}' \tag{7.6.15}$$

or, in terms of Fourier components, by

$$\langle \Delta B_{\mathbf{k}}(t)\rangle = \int_{-\infty}^{t} \mathrm{d}s \int \Phi_{BA}(\mathbf{k}, t - s)\mathcal{F}_{\mathbf{k}}(s)\,\mathrm{d}s \tag{7.6.16}$$

where

$$\Phi_{BA}(\mathbf{k}, t) = -\frac{\beta}{V}\langle \dot{B}_{\mathbf{k}}(t)A_{-\mathbf{k}}\rangle \tag{7.6.17}$$

Equation (7.6.16) shows that in the linear regime a perturbation of given wavevector induces a response only of the same wavevector; this is a consequence of the assumed uniformity of the unperturbed system and the property (7.4.11).

We now restrict the discussion to the case of isotropic fluids. If the external field has the monochromatic form of (7.6.5), the expression for the response becomes

$$\begin{aligned}\langle \Delta B_{\mathbf{k}}(t)\rangle &= \int_{-\infty}^{t} \Phi_{BA}(k,t-s)\mathcal{F}_{\mathbf{k}} \exp\bigl[-i(\omega+i\varepsilon)s\bigr]\,\mathrm{d}s \\ &= \mathcal{F}_{\mathbf{k}} \exp\bigl[-i(\omega+i\varepsilon)t\bigr] \int_{-\infty}^{t} \Phi_{BA}(k,t-s) \exp\bigl[-i(\omega+i\varepsilon)(s-t)\bigr]\,\mathrm{d}s \\ &= \mathcal{F}_{\mathbf{k}} \exp\bigl[-i(\omega+i\varepsilon)t\bigr] \int_{0}^{\infty} \Phi_{BA}(k,t) \exp\bigl[i(\omega+i\varepsilon)t\bigr]\,\mathrm{d}t \end{aligned} \tag{7.6.18}$$

or, taking the limit $\varepsilon \to 0$:

$$\langle \Delta B_{\mathbf{k}}(t)\rangle = \chi_{BA}(k,\omega)\mathcal{F}_{\mathbf{k}} \exp(-i\omega t) \tag{7.6.19}$$

where $\chi_{BA}(k,\omega)$ is a complex *dynamic susceptibility* or *dynamic response function*:

$$\begin{aligned}\chi_{BA}(k,\omega) &= \chi'_{BA}(k,\omega) + i\chi''_{BA}(k,\omega) \\ &= \lim_{\varepsilon\to 0+} \int_{0}^{\infty} \Phi_{BA}(k,t) \exp\bigl[i(\omega+i\varepsilon)t\bigr]\,\mathrm{d}t \end{aligned} \tag{7.6.20}$$

If we substitute for $\Phi_{BA}(k,t)$ from (7.6.17) and integrate by parts, we find that

$$\chi_{BA}(k,\omega) = \frac{\beta}{V}\bigl[C_{BA}(k,t=0) + i(\omega+i\varepsilon)\widetilde{C}_{BA}(k,\omega+i\varepsilon)\bigr] \tag{7.6.21}$$

When A and B are the same, it follows from (7.1.19) that

$$C_{AA}(k,\omega) = \frac{Vk_{\mathrm{B}}T}{\pi\omega}\chi''_{AA}(k,\omega) \tag{7.6.22}$$

The zero-frequency limit of $\chi_{AA}(k,\omega)$, i.e. the static susceptibility $\chi_{AA}(k)$, is obtained from (7.6.21) as

$$\chi_{AA}(k) \equiv \chi_{AA}(k,\omega=0) = \frac{\beta}{V}C_{AA}(k,t=0) \tag{7.6.23}$$

Thus the static version of (7.6.19) for the case when A and B are the same is

$$\langle \Delta A_{\mathbf{k}}\rangle = \frac{\beta}{V}\langle A_{\mathbf{k}}A_{-\mathbf{k}}\rangle\mathcal{F}_{\mathbf{k}} \tag{7.6.24}$$

Equation (7.6.22) is a particular form of the fluctuation–dissipation theorem. Indeed the name is often applied specifically to this relation between the power spectrum of the auto-correlation function of a dynamical variable and the imaginary part of the corresponding response function. Use of the term "dissipation" is connected to the fact, well known in

spectroscopy, that the energy absorbed from the external field and later dissipated as heat is proportional to $\omega\chi''_{AA}(k,\omega)$.

When A is the microscopic density some minor changes are needed to the formulae we have derived. Let $\phi_{\mathbf{k}}\exp(-i\omega t)$ be a Fourier component of an external potential that couples to the component $\rho_{-\mathbf{k}}$ of the density. The term $\mathcal{H}'(t)$ in the hamiltonian (7.6.1) now has the form

$$\mathcal{H}'(t) = \frac{1}{V}\rho_{-\mathbf{k}}\phi_{\mathbf{k}}\exp(-i\omega t) \tag{7.6.25}$$

The resulting change in density is

$$\left\langle \Delta\rho_{\mathbf{k}}(t)\right\rangle = \chi_{\rho\rho}(k,\omega)\phi_{\mathbf{k}}\exp(-i\omega t) \tag{7.6.26}$$

which is a generalisation to non-zero frequencies of the static result (3.6.9). The after-effect function is

$$\Phi_{\rho\rho}(k,t) = \frac{\beta}{V}\left\langle \dot{\rho}_{\mathbf{k}}(t)\rho_{-\mathbf{k}}\right\rangle = \beta\rho\dot{F}(k,t) \tag{7.6.27}$$

and the imaginary part of the response function is related to the dynamic structure factor by

$$S(k,\omega) = -\frac{k_{\mathrm{B}}T}{\pi\rho\omega}\chi''_{\rho\rho}(k,\omega) \tag{7.6.28}$$

The changes in sign relative to (7.6.17) and (7.6.22) arise from the difference in sign between the hamiltonian terms (7.6.4) and (7.6.25); the density response function is conventionally defined in terms of the response to an external potential rather than an external field. Similarly, the static susceptibility is now

$$\chi_{\rho\rho}(k) = -\frac{\beta}{V}\langle\rho_{\mathbf{k}}\rho_{-\mathbf{k}}\rangle = -\beta\rho S(k) \tag{7.6.29}$$

in agreement with (3.6.9).

The properties of the after-effect function $\Phi_{BA}(k,t)$ follow directly from its definition (7.6.17) and the general properties of time-correlation functions. If A and B are different, we see from (7.1.9) and (7.6.17) that

$$\Phi_{BA}(k,t) = \varepsilon_A\varepsilon_{\dot{B}}\Phi_{AB}(k,t) = -\varepsilon_A\varepsilon_B\Phi_{AB}(k,t) \tag{7.6.30}$$

Equation (7.6.30) is an expression of the Onsager *reciprocity relations*. If A and B are real, $\Phi_{BA}(k,t)$ is also real, and from (7.6.20) we see that on the real axis

$$\chi_{BA}(k,-\omega) = \chi^*_{BA}(k,\omega) = \chi'_{BA}(k,\omega) - i\chi''_{BA}(k,\omega) \tag{7.6.31}$$

Thus the real and imaginary parts of χ_{BA} are, respectively, even and odd functions of frequency.

The response function $\chi_{BA}(k,\omega)$ can be interpreted as the limit of a Laplace transform $\chi(k,z)$ defined in the entire upper half of the complex plane ($\mathrm{Im}\, z > 0$):

$$\chi_{BA}(k,z) = \int_0^\infty \Phi_{BA}(k,t)\exp(izt)\,\mathrm{d}t \tag{7.6.32}$$

If we confine ourselves to the important special case when the variables B and A are the same we may discard the subscripts and consider the behaviour of the susceptibility $\chi(k,z) \equiv \chi_{AA}(k,z)$ as a function of the complex variable $z = \omega + i\varepsilon$, with $\varepsilon > 0$. By restricting ε to positive values we ensure that $\chi(k,z)$ is analytic in the upper half-plane, but the function is undefined in the lower half-plane because the integral in (7.6.32) diverges. Since (7.6.13) implies that the after-effect function (with $A = B$) is linear in t at short times, it follows that $\chi(k,z)$ behaves asymptotically as z^{-2} at large z.

Let the contour C in the complex plane be $C = C_1 + C_2$, where C_1 is the real axis and C_2 is the infinite semicircle in the upper half-plane. Application of Cauchy's integral formula shows that

$$\chi(k,z) = \frac{1}{2\pi i}\int_C \frac{\chi(k,z')}{z'-z}\,\mathrm{d}z' \tag{7.6.33}$$

where z is any point inside C. On the other hand, because the conjugate variable z^* lies outside C, the function $\chi(k,z')/(z'-z^*)$ is analytic in and on the contour C. It follows from Cauchy's theorem that

$$\int_C \frac{\chi(k,z')}{z'-z^*}\,\mathrm{d}z' = 0 \tag{7.6.34}$$

The contributions to the integrals (7.6.33) and (7.6.34) from the contour C_2 are both zero, because $\chi(k,z)$ vanishes rapidly as $z \to \infty$. By adding quantities that are zero to the right-hand side of (7.6.33) and discarding the integral around C_2, $\chi(k,z)$ can be re-expressed either as

$$\chi(k,z) = \frac{1}{2\pi i}\int_{C_1} \chi(k,z')\left(\frac{1}{z'-z} + \frac{1}{z'-z^*}\right)\mathrm{d}z' \tag{7.6.35a}$$

or as

$$\chi(k,z) = \frac{1}{2\pi i}\int_{C_1} \chi(k,z')\left(\frac{1}{z'-z} - \frac{1}{z'-z^*}\right)\mathrm{d}z' \tag{7.6.35b}$$

Two further expressions for $\chi(k,z)$ are obtained by adding the real part of (a) to i times the imaginary part of (b) and vice versa:

$$\chi(k,z) = \frac{1}{\pi}\int_{-\infty}^{\infty} \frac{\chi''(k,\omega)}{\omega - z}\,\mathrm{d}\omega \tag{7.6.36a}$$

$$\chi(k,z) = \frac{1}{\pi i}\int_{-\infty}^{\infty} \frac{\chi'(k,\omega)}{\omega - z}\,\mathrm{d}\omega \tag{7.6.36b}$$

We now let $\varepsilon \to 0$ in (7.6.36a), so that $\chi(k,\omega+i\varepsilon) \to \chi'(k,\omega)+i\chi''(k,\omega)$, and use the identity (7.1.18). In this way we find that

$$\chi'(k,\omega) = \mathcal{P}\frac{1}{\pi}\int_{-\infty}^{\infty}\frac{\chi''(k,\omega')}{\omega'-\omega}\,\mathrm{d}\omega' \tag{7.6.37}$$

which is the Kramers–Kronig relation for $\chi'(k,\omega)$ in terms of $\chi''(k,\omega)$. The inverse relation, obtained by applying the rule (7.1.18) to (7.6.36b), is

$$\chi''(k,\omega) = -\mathcal{P}\frac{1}{\pi}\int_{-\infty}^{\infty}\frac{\chi'(k,\omega')}{\omega'-\omega} \tag{7.6.38}$$

These results show that the real and imaginary parts of $\chi(k,\omega)$ are not independent of each other and a knowledge of one part is sufficient to determine the full response function.

The dispersion and damping of the collective modes associated with a dynamical variable A are governed, respectively, by the real and imaginary parts of the poles (corresponding to resonances) of the analytic continuation of $\chi_{AA}(k,z)$ into the lower half-plane. Much of the early theoretical work on density fluctuations in liquids was based on attempts to modify the density response function of an ideal gas to allow for the effects of particle interactions through a variety of mean-field or "effective-field" approximations. The problem with such approximations is that they account only for static and not for dynamic correlations between particles; they therefore fare badly at densities characteristic of the liquid state.

7.7 APPLICATIONS OF THE LINEAR-RESPONSE FORMALISM

The best known and most important of the applications of linear-response theory is its use in the derivation of expressions for the transport coefficients of hydrodynamics, through which induced fluxes are related to certain gradients within the fluid. The simplest example concerns the mobility of a tagged particle under the action of a constant external force $\mathcal{F}$ that acts only on the tagged particles. We suppose that the force is applied along the x-direction from $t=0$ onwards. Then the perturbation term in the hamiltonian is $\mathcal{H}'(t) = -\mathcal{F}x(t)\theta(t)$, where $x(t)$ is the x-coordinate of a tagged particle; if the fluid is isotropic, the drift velocity $\mathbf{u}$ of the particle will be in the same direction as the applied force. From (7.6.12) and (7.6.13) it follows that

$$\langle u_x(t)\rangle = \beta\int_{-\infty}^{t}\langle u_x(t')\dot{x}\rangle\mathcal{F}\theta(t')\,\mathrm{d}t' = \beta\mathcal{F}\int_0^t\langle u_x(t')u_x\rangle\,\mathrm{d}t' \tag{7.7.1}$$

This leads to the Einstein relation for the mobility μ, defined as the ratio of the limiting drift velocity to the applied force:

$$\mu = \lim_{t\to\infty}\frac{1}{k_\mathrm{B}T}\int_0^t\langle u_x(t')u_x\rangle\,\mathrm{d}t' = \frac{D}{k_\mathrm{B}T} \tag{7.7.2}$$

where D is the diffusion coefficient. Equation (7.7.2) is a further example of the fluctuation–dissipation theorem: D is a quantity that characterises spontaneous fluctuations in the velocity of a tagged particle and μ is a measure of the response of the tagged particle to an applied force.

It is instructive to consider an alternative derivation of (7.7.2). If the tagged particles are subjected to a weak, external force derived from a potential $\exp(\varepsilon t)\phi(\mathbf{r})$ $(\varepsilon > 0)$, a concentration gradient is set up. The resulting induced current is

$$\left\langle \mathbf{j}^{(s)}(\mathbf{r}, t)\right\rangle = -\mu\rho_s \exp(\varepsilon t)\nabla\phi(\mathbf{r}) - D\nabla\left\langle \rho^{(s)}(\mathbf{r}, t)\right\rangle \tag{7.7.3}$$

or, in terms of Fourier components:

$$\left\langle \mathbf{j}_{\mathbf{k}}^{(s)}(t)\right\rangle = -i\mu\rho_s \exp(\varepsilon t)\mathbf{k}\phi_{\mathbf{k}} - iD\mathbf{k}\left\langle \rho_{\mathbf{k}}^{(s)}(t)\right\rangle \tag{7.7.4}$$

where ρ_s is the number of tagged particles per unit volume. The first term on the right-hand side of (7.7.3) represents the contribution to the current from the drift velocity of the tagged particles and the second term arises from Fick's law of diffusion (see Section 8.2). If the field is turned on sufficiently slowly, i.e. if $\varepsilon \ll Dk^2$, the system will remain in a steady state. The two contributions to the current then cancel and (7.7.4) reduces to

$$\left\langle \rho_{\mathbf{k}}^{(s)}\right\rangle = -\frac{\mu\rho_s}{D}\phi_{\mathbf{k}} \tag{7.7.5}$$

If the concentration of tagged particles is sufficiently low for interactions between them to be negligible, it follows from (3.6.9) that $\langle\rho_{\mathbf{k}}^{(s)}\rangle$ and $\phi_{\mathbf{k}}$ are also related by[13]

$$\left\langle \rho_{\mathbf{k}}^{(s)}\right\rangle = -\beta\rho_s\phi_{\mathbf{k}} \tag{7.7.6}$$

where $-\beta\rho_s$ is the static susceptibility of a non-interacting system of density ρ_s. Combination of (7.7.5) and (7.7.6) leads back to the Einstein expression (7.7.2).

The calculation of the electrical conductivity provides an example of a different type, in which a collective response of a system to an external field is involved. Suppose that a time-dependent electric field $\mathbf{E}(t)$ is applied to a system of charged particles. The field gives rise to a charge current, defined as

$$e\mathbf{j}^{Z}(t) = \sum_{i=1}^{N} z_i e\dot{\mathbf{r}}_i(t) = \dot{\mathbf{M}}(t) \tag{7.7.7}$$

where $z_i e$ is the charge carried by the ith particle (e is the elementary charge) and $\mathbf{M}(t)$ is the total dipole moment of the sample. The interaction with the applied field is described by the hamiltonian

$$\mathcal{H}'(t) = -\sum_{i=1}^{N} \mathbf{M}(t)\cdot\mathbf{E}(t) \tag{7.7.8}$$

If the system is isotropic and the field is applied, say, along the x-axis, then, in the statistical mean, only the x-component of the induced current will survive. The linear response to a real, periodic field can therefore be written as

$$e\langle j_x^Z(t)\rangle = \mathrm{Re}\,\sigma(\omega)E_0\exp(-i\omega t) \tag{7.7.9}$$

where, according to the general formulae (7.6.13) and (7.6.20), the electrical conductivity per unit volume is given by

$$\begin{aligned}\sigma(\omega) &= \frac{\beta e}{V}\int_0^\infty \sum_{i=1}^N \langle j_x^Z(t) z_i e\dot{x}_i\rangle \exp(i\omega t)\,\mathrm{d}t \\ &= \frac{\beta e^2}{V}\int_0^\infty \langle j_x^Z(t) j_x^Z\rangle \exp(i\omega t)\,\mathrm{d}t \end{aligned} \tag{7.7.10}$$

The usual static electrical conductivity σ is then identified as $\sigma = \lim_{\omega\to 0}\sigma(\omega)$. The statistical average in the second line of (7.7.10) is the autocorrelation function of the fluctuating charge current in the absence of the electrical field. In deriving this result we have ignored any spatial variation of the electric field, thereby avoiding the difficulties which arise when taking the long-wavelength limit for coulombic systems; we shall return to a discussion of this problem in Chapter 10.

Correlation-function formulae for transport coefficients have been obtained by many authors in a variety of ways. The derivation from linear-response theory is not always as straightforward as it is in the case of electrical conductivity, the difficulty being that the dissipative behaviour described by hydrodynamics is generally not induced by external forces but by gradients of local thermodynamic variables, which cannot be represented by a perturbation term in the hamiltonian. The thermal conductivity provides an example; this is the transport coefficient that relates the induced heat flux to an imposed temperature gradient via Fourier's law. A temperature gradient is a manifestation of boundary conditions and cannot be formulated in mechanical terms because temperature is a statistical property of the system. However, a linear-response argument can still be invoked by introducing an inhomogeneous field that couples to the energy density of the system and sets up a heat flow. Einstein's argument relating the diffusion coefficient to the mobility can then be extended to yield a correlation-function expression for the thermal conductivity. We postpone a derivation of the microscopic expressions for thermal conductivity and shear and bulk viscosities to Chapter 8, where it is shown that these coefficients are related to the long-wavelength, low-frequency (or "hydrodynamic") limit of certain space and time-dependent correlation functions.

The response to a weak, applied field can be measured directly in a molecular dynamics simulation in a way that allows the accurate calculation of transport coefficients with relatively modest computational effort.[14] To understand what is involved, we return to the problem of the electrical conductivity. Clearly we could hope to mimic a real experiment by adding to the equations of motion of the particles the force due to a steady electrical field and computing the steady-state charge current to which the field gives rise. The practical

value of such an approach is seriously limited by the fact that a very large field must be applied in order to produce a systematic response that is significantly greater than the natural fluctuations. Use of a large field leads to a rapid heating-up of the system, non-conservation of energy and other undesirable effects.

The problems associated with the use of large fields can be overcome either by imposing constraints that maintain the system at constant kinetic energy or by a "subtraction" technique closely related to linear-response theory. In the subtraction method the response is computed as the difference in the property of interest along two phase-space trajectories; both start from the same phase point at time $t = 0$ but in one case a very small perturbing force is applied. In the example of electrical conductivity the response is the difference in charge current after a time t, given by

$$\Delta j_x^Z(t) = \exp(i\mathcal{L}t)\, j_x^Z - \exp(i\mathcal{L}_0 t)\, j_x^Z \tag{7.7.11}$$

where $\mathcal{L}$ and $\mathcal{L}_0$ are the Liouville operators that determine the perturbed and unperturbed trajectories, respectively. The statistical response is obtained by averaging (7.7.11) over initial conditions:

$$\begin{aligned}\left\langle \Delta j_x^Z(t) \right\rangle &= \iint f_0^{[N]} \left[\exp(i\mathcal{L}t) - \exp(i\mathcal{L}_0 t) \right] j_x^Z \, \mathrm{d}\mathbf{r}^N \, \mathrm{d}\mathbf{p}^N \\ &= \left\langle j_x^Z(t) \right\rangle_{\mathcal{L}} - \left\langle j_x^Z(t) \right\rangle_{\mathcal{L}_0}\end{aligned} \tag{7.7.12}$$

where the brackets denote averages over the unperturbed equilibrium distribution function and the nature of the mechanical evolution is indicated by the subscripts $\mathcal{L}$ and $\mathcal{L}_0$. The success of the method rests mostly on the fact that random fluctuations in the two terms in (7.7.12) are highly correlated and therefore largely cancel, leaving only the systematic part, i.e. the response to the perturbation. It is therefore possible to use a perturbing force that is very small. In principle, because the hamiltonian in the absence of the perturbation is symmetric under reflection ($x_i \to -x_i$), the second term in (7.7.12) should vanish, but in practice this is not the case because the average is taken over a limited number of trajectories. The form of the statistical response depends on the time-dependence of the applied field. If a constant electric field is applied along the x-axis from $t = 0$ onwards, acting in opposite senses on charges of different sign, the mean response is proportional to the integral of the current autocorrelation function and therefore reaches a plateau value from which the conductivity can be calculated via (7.7.10); if a δ-function force is applied at $t = 0$, the response is proportional to the current autocorrelation function itself. The length of the trajectories must, of course, exceed the relevant relaxation time of the system, in this case the lifetime of spontaneous fluctuations in the electric current.

As a final example we show how the density response function of a non-interacting system can be calculated by a linear-response argument. The time evolution of the single-particle phase-space distribution function $f^{(1)}(\mathbf{r}, \mathbf{p}; t)$ of an ideal gas in an external potential $\phi(\mathbf{r}, t)$ is determined by the Boltzmann equation (2.1.24) with the collision term set equal to zero, i.e.

$$\left(\frac{\partial}{\partial t} + \frac{\mathbf{p}}{m} \cdot \frac{\partial}{\partial \mathbf{r}} - \frac{\partial \phi(\mathbf{r}, t)}{\partial \mathbf{r}} \cdot \frac{\partial}{\partial \mathbf{p}} \right) f^{(1)}(\mathbf{r}, \mathbf{p}; t) = 0 \tag{7.7.13}$$

If we write the distribution function as

$$f^{(1)}(\mathbf{r},\mathbf{p};t) = \rho f_{\mathrm{M}}(\mathbf{p}) + \Delta f^{(1)}(\mathbf{r},\mathbf{p};t) \tag{7.7.14}$$

where $f_{\mathrm{M}}(\mathbf{p})$ is the Maxwell distribution (2.1.26), the change $\Delta f^{(1)}$ induced by the external potential is linear in ϕ when the potential is weak. Substitution of (7.7.14) in (7.7.13) yields an equation of motion for $\Delta f^{(1)}$:

$$\left(\frac{\partial}{\partial t} + \frac{\mathbf{p}}{m}\cdot\frac{\partial}{\partial \mathbf{r}} - \frac{\partial\phi(\mathbf{r},t)}{\partial \mathbf{r}}\cdot\frac{\partial}{\partial \mathbf{p}}\right)\Delta f^{(1)}(\mathbf{r},\mathbf{p};t) - \rho\frac{\partial\phi(\mathbf{r},t)}{\partial \mathbf{r}}\cdot\frac{\partial f_{\mathrm{M}}(\mathbf{p})}{\partial \mathbf{p}} = 0 \tag{7.7.15}$$

and a double, Fourier–Laplace transform leads (in an obvious notation) to

$$\left(\omega + i\varepsilon - \frac{\mathbf{p}\cdot\mathbf{k}}{m}\right)\Delta f^{(1)}(\mathbf{k},\mathbf{p};\omega+i\varepsilon) + \rho\phi(\mathbf{k},\omega+i\varepsilon)\mathbf{k}\cdot\frac{\partial f_{\mathrm{M}}}{\partial \mathbf{p}} = 0 \tag{7.7.16}$$

The mean change in microscopic density due to the external potential is

$$\left\langle \Delta\rho(\mathbf{r},t)\right\rangle = \int \Delta f^{(1)}(\mathbf{r},\mathbf{p};t)\,\mathrm{d}\mathbf{p} \tag{7.7.17}$$

or, in terms of Fourier components:

$$\left\langle \rho_{\mathbf{k}}(\omega)\right\rangle = \int \Delta f^{(1)}(\mathbf{k},\mathbf{p};\omega)\,\mathrm{d}\mathbf{p} \tag{7.7.18}$$

Dividing through (7.7.16) by $(\omega + i\varepsilon - \mathbf{p}\cdot\mathbf{k}/m)$ and integrating over $\mathbf{p}$ we find that

$$\left\langle \rho_{\mathbf{k}}(\omega+i\varepsilon)\right\rangle = -\rho\phi(\mathbf{k},\omega+i\varepsilon)\int \frac{\mathbf{k}\cdot(\partial f_{\mathrm{M}}/\partial \mathbf{p})}{\omega + i\varepsilon - \mathbf{p}\cdot\mathbf{k}/m}\,\mathrm{d}\mathbf{p} \tag{7.7.19}$$

Thus the density response function is

$$\begin{aligned}\chi_{\rho\rho}(k,\omega+i\varepsilon) &= -\rho\int \frac{\mathbf{k}\cdot(\partial f_{\mathrm{M}}/\partial \mathbf{p})}{\omega + i\varepsilon - \mathbf{p}\cdot\mathbf{k}/m}\,\mathrm{d}\mathbf{p}\\ &= \beta\rho\int \frac{(\mathbf{p}\cdot\mathbf{k}/m)\,f_{\mathrm{M}}(\mathbf{p})}{\omega + i\varepsilon - \mathbf{p}\cdot\mathbf{k}/m}\,\mathrm{d}\mathbf{p}\\ &= -\beta\rho + (\omega+i\varepsilon)\beta\rho\int \frac{f_{\mathrm{M}}(\mathbf{p})}{\omega + i\varepsilon - \mathbf{p}\cdot\mathbf{k}/m}\,\mathrm{d}\mathbf{p}\end{aligned} \tag{7.7.20}$$

In the limit $\varepsilon \to 0$ the imaginary part of (7.7.20) is

$$\chi''_{\rho\rho}(k,\omega) = -\pi\beta\rho\omega\int f_{\mathrm{M}}(\mathbf{p})\delta(\omega - \mathbf{p}\cdot\mathbf{k}/m)\,\mathrm{d}\mathbf{p} \tag{7.7.21}$$

This result follows immediately from the identity (7.1.18). On substituting for $f_{\mathrm{M}}(\mathbf{p})$ and integrating over $\mathbf{p}$ we find that

$$\chi''_{\rho\rho}(k,\omega) = -\beta\rho\omega\left(\frac{\pi\beta m}{2k^2}\right)^{1/2}\exp\left(-\beta m\omega^2/2k^2\right) \tag{7.7.22}$$

which, combined with (7.6.28), is equivalent to the expression (7.5.17) derived earlier for the dynamic structure factor of an ideal gas.

NOTES AND REFERENCES

1. Some of the material discussed in Chapters 7 to 9 is dealt with at greater length in a number of specialised texts. (a) Berne, B.J. and Pecora, R., "Dynamic Light Scattering". John Wiley, New York, 1976. (b) Résibois, P. and DeLeener, M., "Classical Kinetic Theory of Fluids". John Wiley, New York, 1977. (c) Boon, J.P. and Yip, S., "Molecular Hydrodynamics". Dover Publications, New York, 1991. (d) Mazo, R.M., "Brownian Motion". Clarendon Press, Oxford, 2002.
2. See, e.g., ref. 1(b), p. 240.
3. Heyes, D.M., Powles, J.G. and Rickayzen, G., *Mol. Phys.* **100**, 595 (2002).
4. Lebowitz, J.L., Percus, J.K. and Sykes, J., *Phys. Rev.* **188**, 487 (1969).
5. Longuet-Higgins, H.C. and Pople, J.A., *J. Chem. Phys.* **25**, 884 (1956).
6. See, e.g., ref. 1(b), p. 324.
7. When $g(d) = 1$, (7.2.2) reduces to the result obtained by solution of the Boltzmann equation in a first-order approximation; higher-order corrections are of order 2%. See, e.g., Chapman, S. and Cowling, T.G., "The Mathematical Theory of Non-Uniform Gases", 3rd edn. Cambridge University Press, Cambridge, 1970, p. 258.
8. (a) Alder, B.J., Gass, D.M. and Wainwright, T.E., *Phys. Rev. A* **1**, 18 (1970). (b) Sigurgeirsson, H. and Heyes, D.M., *Mol. Phys.* **101**, 469 (2003).
9. Comparison of molecular-dynamics results for the Lennard-Jones fluid with an extended form of Enskog theory reveals a different behaviour at intermediate densities. See Miyazaki, K., Srinivas, G. and Bagchi, B., *J. Chem. Phys.* **114**, 6276 (2001).
10. Berne, B.J., Boon, J.P. and Rice, S.A., *J. Chem. Phys.* **45**, 1086 (1966).
11. (a) Lovesey, S.W., "Theory of Neutron Scattering from Condensed Matter", vol. 1. Clarendon Press, Oxford, 1984. (b) Squires, G.L., "Introduction to the Theory of Thermal Neutron Scattering". Dover Publications, New York, 1996.
12. Bodensteiner, T., Morkel, C., Gläser, W. and Dorner, B., *Phys. Rev. A* **45**, 5709 (1992); erratum: *Phys. Rev. A* **46**, 3574 (1992).
13. Equation (7.7.6) is just the ideal-gas form of (3.6.9).
14. Ciccotti, G., Jacucci, G. and McDonald, I.R., *J. Stat. Phys.* **21**, 1 (1979).

CHAPTER 8

Hydrodynamics and Transport Coefficients

Chapter 7 was concerned largely with the formal definition and general properties of time-correlation functions and with the link that exists between spontaneous, time-dependent fluctuations and the response of a fluid to an external probe. The main objectives of the present chapter are, first, to show how the decay of fluctuations is described within the framework of linearised hydrodynamics and, secondly, to obtain explicit expressions for the macroscopic transport coefficients in terms of microscopic quantities. The hydrodynamic approach is valid only on scales of length and time much larger than those characteristic of the molecular level, but we show how the gap between the microscopic and macroscopic descriptions can be bridged by an essentially phenomenological extrapolation of the hydrodynamic results to shorter wavelengths and higher frequencies. The same problem is taken up in a more systematic way in Chapter 9.

8.1 THERMAL FLUCTUATIONS AT LONG WAVELENGTHS AND LOW FREQUENCIES

We have seen in Section 4.1 that the microscopic structure of a liquid is revealed experimentally by the scattering of radiation of wavelength comparable with the interparticle spacing. Examination of a typical pair distribution function, such as the one pictured in Figure 2.1, shows that positional correlations decay rapidly in space and are negligibly small at separations beyond a few molecular diameters. From a static point of view, therefore, a fluid behaves, for longer wavelengths, essentially as a continuum. When discussing the dynamics, however, it is necessary to consider simultaneously the scales both of length and time. In keeping with traditional kinetic theory it is conventional to compare wavelengths with the mean free path l_c and times with the mean collision time τ_c. The wavenumber–frequency plane may then be divided into three parts. The region in which $kl_c \ll 1,\ \omega\tau_c \ll 1$ corresponds to the *hydrodynamic* regime, in which the behaviour of the fluid is described by the phenomenological equations of macroscopic fluid mechanics. The range of intermediate wavenumbers and frequencies ($kl_c \approx 1, \omega\tau_c \approx 1$) forms the *kinetic* regime, where allowance must be made for the molecular structure of the fluid and a treatment based on the microscopic equations of motion is required. Finally, the region where $kl_c \gg 1,\ \omega\tau_c \gg 1$ represents the *free-particle* regime; here the distances and times involved are so short that the particles move almost independently of each other.

In this chapter we shall be concerned mostly with the hydrodynamic regime, where the local properties of the fluid vary slowly on microscopic scales of length and time. The set of *hydrodynamic variables* or *hydrodynamic fields* include the densities of mass (or particle number), energy and momentum; these are closely related to the conserved microscopic variables introduced in Section 7.4. Like their microscopic counterparts, the conserved hydrodynamic variables satisfy continuity equations of the form (7.4.3), which express the conservation of matter, energy and momentum. In addition, there exist certain *constitutive relations* between the fluxes (or currents) and gradients of the local variables, expressed in terms of phenomenological *transport coefficients*. Fick's law of diffusion and Fourier's law of heat transport are two of the more familiar examples of a constitutive relation.

One of the main tasks of the present chapter is to obtain microscopic expressions for the transport coefficients that are similar in structure to the formula (7.7.10) already derived for the electrical conductivity of an ionic fluid. This is achieved by calculating the *hydrodynamic limit* of the appropriate time-correlation function. To understand what is involved in such a calculation it is first necessary to clarify the relationship between hydrodynamic and microscopic dynamical variables. As an example, consider the local density. The microscopic particle density $\rho(\mathbf{r}, t)$ is defined by (7.4.5); its integral over all volume is equal to N, the total number of particles in the system. The hydrodynamic local density $\bar{\rho}(\mathbf{r}, t)$ is obtained by averaging the microscopic density over a subvolume v around the point $\mathbf{r}$ that is macroscopically small but still sufficiently large to ensure that the relative fluctuation in the number of particles inside v is negligible. Then

$$\bar{\rho}(\mathbf{r}, t) = \frac{1}{v} \int_v \rho(\mathbf{r}' - \mathbf{r}, t)\, \mathrm{d}\mathbf{r}' \tag{8.1.1}$$

Strictly speaking, the definition of $\bar{\rho}(\mathbf{r}, t)$ also requires a smoothing or "coarse graining" in time. This can be realised by averaging (8.1.1) over a time interval that is short on a macroscopic scale but long in comparison with the mean collision time. In practice, however, smoothing in time is already achieved by (8.1.1) if the subvolume is sufficiently large. The Fourier components of the hydrodynamic density are defined as

$$\bar{\rho}_{\mathbf{k}}(t) = \int \bar{\rho}(\mathbf{r}, t) \exp(-i\mathbf{k} \cdot \mathbf{r})\, \mathrm{d}\mathbf{r} \tag{8.1.2}$$

where the wavevector $\mathbf{k}$ must be such that k is less than about $2\pi/v^{1/3}$. The corresponding density autocorrelation function is then defined as in (7.4.20), except that the Fourier components of the microscopic density are replaced by $\bar{\rho}_{\mathbf{k}}$. Since we are now working at the macroscopic level, the average to be taken is not an ensemble average, but an average over initial conditions, weighted by the probability density of thermodynamic fluctuation theory (see Appendix A). By forming such an average, we are implicitly invoking the hypothesis of *local thermodynamic equilibrium*. In other words, we are assuming that although the hydrodynamic densities vary over macroscopic lengths and times, the fluid contained in each of the subvolumes is in a state of thermodynamic equilibrium, and that the local density, pressure and temperature satisfy the usual relations of equilibrium thermodynamics. These assumptions are particularly plausible at high densities, since in that case local equilibrium is rapidly brought about by collisions between particles.

Once the calculation we have described in words has been carried out, the relations of interest are obtained by supposing that in the limit of long wavelengths ($\lambda \gg l_c$) and long times ($t \gg \tau_c$) or, equivalently, of small wavenumbers and low frequencies, correlation functions derived from the hydrodynamic equations are identical to the correlation functions of the corresponding microscopic variables. This intuitively appealing hypothesis, which is due to Onsager, can be justified on the basis of the fluctuation–dissipation theorem discussed in Section 7.6. In the example of the density autocorrelation function the assumption can be expressed by the statement that

$$\left\langle \rho_{\mathbf{k}}(t)\rho_{-\mathbf{k}} \right\rangle \sim \left\langle \bar{\rho}_{\mathbf{k}}(t)\bar{\rho}_{-\mathbf{k}} \right\rangle, \quad kl_c \ll 1,\ t/\tau_c \gg 1 \tag{8.1.3}$$

with the qualification, explained above, that the meaning of the angular brackets is different for the two correlation functions. As the sections that follow are concerned almost exclusively with the calculation of correlation functions of hydrodynamic variables, no ambiguity is introduced by dropping the bar we have used to distinguish the latter from the corresponding microscopic quantities.

One important implication of the assumption of local thermodynamic equilibrium is that the Maxwell distribution of velocities applies at the local level. The local velocity is defined via the relation

$$\mathbf{p}(\mathbf{r}, t) = \rho_m(\mathbf{r}, t)\mathbf{u}(\mathbf{r}, t) \tag{8.1.4}$$

where $\mathbf{p}(\mathbf{r}, t)$ is the momentum density and $\rho_m(\mathbf{r}, t) = m\rho(\mathbf{r}, t)$ is the mass density (we assume that the fluid contains only one component). The single-particle distribution function is now a function of $\mathbf{r}$ and t and (2.1.26) is replaced by

$$f_{\text{l.e.}}(\mathbf{u}, \mathbf{r}; t) = \rho(\mathbf{r}, t)\left(\frac{m}{2\pi k_{\text{B}} T(\mathbf{r}, t)}\right)^{3/2} \exp\left(\frac{-m|\mathbf{u} - \mathbf{u}(\mathbf{r}, t)|^2}{2k_{\text{B}} T(\mathbf{r}, t)}\right) \tag{8.1.5}$$

where $T(\mathbf{r}, t)$ is the local temperature. The function $f_{\text{l.e.}}(\mathbf{u}, \mathbf{r}; t)$ is called the "local-equilibrium" Maxwell distribution.

8.2 SPACE-DEPENDENT SELF MOTION

As an illustration of the general procedure described in the previous section, we first consider the relatively simple problem of the diffusion of tagged particles. If the tagged particles are physically identical to the other particles in the fluid, and if their concentration is sufficiently low that their mutual interactions can be ignored, the problem is equivalent to that of single-particle motion as described by the self part of the van Hove correlation function $G_{\text{s}}(\mathbf{r}, t)$ (see Section 7.4). The macroscopic tagged-particle density $\rho^{(s)}(\mathbf{r}, t)$ and current $\mathbf{j}^{(s)}(\mathbf{r}, t)$ satisfy a continuity equation of the form

$$\frac{\partial \rho^{(s)}(\mathbf{r}, t)}{\partial t} + \nabla \cdot \mathbf{j}^{(s)}(\mathbf{r}, t) = 0 \tag{8.2.1}$$

and the corresponding constitutive equation is provided by Fick's law:

$$\mathbf{j}^{(s)}(\mathbf{r},t) = -D\nabla\rho^{(s)}(\mathbf{r},t) \tag{8.2.2}$$

where the interdiffusion constant D is in this case the same as the self-diffusion constant. Combination of (8.2.1) and (8.2.2) yields the *diffusion equation*:

$$\frac{\partial\rho^{(s)}(\mathbf{r},t)}{\partial t} = D\nabla^2\rho^{(s)}(\mathbf{r},t) \tag{8.2.3}$$

or, in reciprocal space:

$$\frac{\partial\rho_{\mathbf{k}}^{(s)}(t)}{\partial t} = -Dk^2\rho_{\mathbf{k}}^{(s)}(t) \tag{8.2.4}$$

Equation (8.2.4) can be integrated immediately to give

$$\rho_{\mathbf{k}}^{(s)}(t) = \rho_{\mathbf{k}}^{(s)}\exp\bigl(-Dk^2t\bigr) \tag{8.2.5}$$

where $\rho_{\mathbf{k}}^{(s)}$ is a Fourier component of the tagged-particle density at $t = 0$. If we multiply both sides of (8.2.5) by $\rho_{-\mathbf{k}}^{(s)}$ and take the thermal average, we find that the normalised autocorrelation function is

$$\frac{1}{n}\bigl\langle\rho_{\mathbf{k}}^{(s)}(t)\rho_{-\mathbf{k}}^{(s)}\bigr\rangle = \frac{1}{n}\bigl\langle\rho_{\mathbf{k}}^{(s)}\rho_{-\mathbf{k}}^{(s)}\bigr\rangle\exp\bigl(-Dk^2t\bigr) = \exp\bigl(-Dk^2t\bigr) \tag{8.2.6}$$

where n is the total number of tagged particles. Here we have used the fact that because the concentration of tagged particles is low, their coordinates are mutually uncorrelated. It then follows from the general hypothesis discussed in Section 8.1 that in the hydrodynamic limit the self part of the density autocorrelation function (7.4.21), i.e. the self intermediate scattering function defined by (7.5.12), behaves as

$$F_{\mathrm{s}}(k,t) \sim \exp\bigl(-Dk^2t\bigr), \quad kl_c \ll 1,\ t/\tau_c \gg 1 \tag{8.2.7}$$

The long-wavelength, low-frequency limit of the van Hove self correlation function is the spatial Fourier transform of (8.2.7):

$$G_{\mathrm{s}}(r,t) = \frac{1}{(4\pi Dt)^{3/2}}\exp\bigl(-r^2/4Dt\bigr) \tag{8.2.8}$$

In the same limit the self dynamic structure factor is

$$S_{\mathrm{s}}(k,\omega) = \frac{1}{\pi}\frac{Dk^2}{\omega^2 + (Dk^2)^2} \tag{8.2.9}$$

Equation (8.2.9) represents a single, lorentzian curve centred at $\omega = 0$ with a width at half-height equal to $2Dk^2$. A spectrum of this type is typical of any diffusive process described

by an equation similar to (8.2.3). Alternatively, the structure of the Laplace transform of (8.2.7), i.e.

$$\widetilde{F}_s(k,z) = \frac{1}{-iz + Dk^2} \tag{8.2.10}$$

shows that a diffusive process is characterised by a purely imaginary pole at $z = -iDk^2$. It should be emphasised again that the simple result expressed by (8.2.9) is valid only for $kl_c \ll 1,\ \omega\tau_c \ll 1$. Its breakdown at high frequencies is reflected in the fact that the even frequency moments (beyond zeroth order) of $S_s(k,\omega)$ are all infinite. Note also that the transport coefficient D is related to the behaviour of $S_s(k,\omega)$ in the limit $k,\ \omega \to 0$. From (8.2.9) we see that

$$D = \lim_{\omega\to 0}\lim_{k\to 0}\frac{\omega^2}{k^2}\pi S_s(k\cdot\omega) \tag{8.2.11}$$

where it is crucial that the limits are taken in the correct order, i.e. $k \to 0$ before $\omega \to 0$. In principle, (8.2.11) provides a means of determining D from the results of inelastic neutron-scattering experiments.

Equations (7.5.16) and (8.2.8) show that the van Hove self correlation function is a gaussian function of r both for $t \to 0$ (free-particle behaviour) and $t \to \infty$ (the hydrodynamic limit); it is therefore tempting to suppose that the function is gaussian at all times. To study this point in more detail we write $G_s(r,t)$ as a generalised gaussian function of r in the form

$$G_s(r,t) = \left(\frac{\alpha(t)}{\pi}\right)^{3/2}\exp\bigl[-\alpha(t)r^2\bigr] \tag{8.2.12}$$

where $\alpha(t)$ is a function of t but not of r; the hydrodynamic limit corresponds to taking $\alpha(t) = 1/4Dt$ and the ideal-gas model to $\alpha(t) = m/2k_BTt^2$. The mean-square displacement of tagged particles after a time t is the second moment of $G_s(r,t)$, i.e.

$$\bigl\langle r^2(t)\bigr\rangle \equiv \bigl\langle\bigl|\mathbf{r}(t) - \mathbf{r}(0)\bigr|^2\bigr\rangle = \int r^2 G_s(r,t)\,\mathrm{d}\mathbf{r} \tag{8.2.13}$$

and is therefore related to the unknown function $\alpha(t)$ by $\langle r^2(t)\rangle = 3/2\alpha(t)$. If we insert this result in (8.2.12) and take the Fourier transform, we find that in the gaussian approximation the self intermediate scattering function has the form

$$F_s(k,t) = \exp\left(-\frac{k^2}{6}\bigl\langle r^2(t)\bigr\rangle\right) \tag{8.2.14}$$

Systematic corrections to the gaussian approximation can be obtained from a cumulant expansion of $F_s(k,t)$ in powers of k^2. Comparison with molecular-dynamics results for argon-like liquids shows that in the intermediate range of k between the free-particle and hydrodynamic regimes the first correction (of order k^4) to (8.2.14) is typically 10% or less and positive; corrections of higher order are even smaller.[1]

The Einstein expression for the long-time limit of the mean-square displacement of a tagged particle is a direct consequence of the hydrodynamic result for $G_s(r,t)$; substitution

of (8.2.8) into the definition (8.2.13) leads immediately to (7.2.3). Since the mean-square displacement is also related to the velocity autocorrelation function through (7.2.6), there is a close connection between the functions $G_s(r,t)$ (or $F_s(k,t)$) and $Z(t)$. In fact, in the gaussian approximation represented by (8.2.14), $F_s(k,t)$ is entirely determined by $Z(t)$ and vice versa; more generally, only the second of these statements is true. To see the significance of this connection we return briefly to the description of the system in terms of microscopic variables. If we define the Fourier components of the microscopic current associated with a tagged particle i having velocity $\mathbf{u}_i$ as

$$\mathbf{j}_{\mathbf{k}i}(t) = \mathbf{u}_i(t)\exp\bigl[-i\mathbf{k}\cdot\mathbf{r}_i(t)\bigr] \tag{8.2.15}$$

and the self-current autocorrelation function as

$$C_s(k,t) = \bigl\langle \mathbf{k}\cdot\mathbf{j}_{\mathbf{k}i}(t)\mathbf{k}\cdot\mathbf{j}_{-\mathbf{k}i}\bigr\rangle \tag{8.2.16}$$

it is clear that

$$Z(t) = \bigl\langle u_{iz}(t)u_{iz}\bigr\rangle = \lim_{k\to 0}\frac{1}{k^2}C_s(k,t) = -\lim_{k\to 0}\frac{1}{k^2}\frac{\mathrm{d}^2}{\mathrm{d}t^2}F_s(k,t) \tag{8.2.17}$$

where we have chosen $\mathbf{k}$ to lie along the z-axis and used the single-particle version of (7.4.26). The relation between the corresponding power spectra is

$$Z(\omega) = \frac{\omega^2}{2\pi}\lim_{k\to 0}\frac{1}{k^2}\int_{-\infty}^{\infty}F_s(k,t)\exp(i\omega t)\,\mathrm{d}t = \omega^2\lim_{k\to 0}\frac{S_s(k,\omega)}{k^2} \tag{8.2.18}$$

Equation (8.2.18) may be regarded as a generalisation of (8.2.11) to non-zero frequencies in which $Z(\omega)$ appears as a frequency-dependent diffusion coefficient; it also provides a possible route to an experimental determination of the velocity autocorrelation function.

The relationship between $Z(t)$ and $F_s(k,t)$ (or $C_s(k,t)$) is further reflected in the short-time expansions of these functions. By analogy with (7.4.31) the expansion of $C_s(k,t)$ in powers of t can be written as

$$C_s(k,t) = \omega_0^2\left(1 - \omega_{1s}^2\frac{t^2}{2!} + \cdots\right) \tag{8.2.19}$$

From the general result (7.1.23) and the continuity equation (8.2.1) it follows that

$$\begin{aligned}\omega_0^2\omega_{1s}^2 &= -\bigl\langle \mathbf{k}\cdot\dot{\mathbf{j}}_{\mathbf{k}i}\mathbf{k}\cdot\dot{\mathbf{j}}_{-\mathbf{k}i}\bigr\rangle = \langle\ddot{\rho}_{\mathbf{k}i}\ddot{\rho}_{-\mathbf{k}i}\rangle \\ &= k^4\bigl\langle u_{iz}^4\bigr\rangle + k^2\bigl\langle \dot{u}_{iz}^2\bigr\rangle = 3\omega_0^4 + \bigl(k^2/m^2\bigr)\bigl\langle F_{iz}^2\bigr\rangle\end{aligned} \tag{8.2.20}$$

and hence, from the definition (7.2.9), that

$$\omega_{1s}^2 = 3\omega_0^2 + \Omega_0^2 \tag{8.2.21}$$

The next term (of order t^4) in the Taylor expansion of $C_s(k,t)$ involves integrals over the triplet distribution function. Short-time expansions such as (8.2.19) are useful in extending the validity of hydrodynamic results to microscopic scales of length and time.

8.3 THE NAVIER–STOKES EQUATION AND HYDRODYNAMIC COLLECTIVE MODES

We turn now to the problem of describing the decay of long-wavelength fluctuations in the collective dynamical variables. For a one-component fluid the macroscopic local densities associated with the conserved variables are the number density $\rho(\mathbf{r},t)$, energy density $e(\mathbf{r},t)$ and momentum density $\mathbf{p}(\mathbf{r},t)$. The conservation laws for the local densities have the form

$$m\frac{\partial}{\partial t}\rho(\mathbf{r},t)+\nabla\cdot\mathbf{p}(\mathbf{r},t)=0 \tag{8.3.1}$$

$$\frac{\partial}{\partial t}e(\mathbf{r},t)+\nabla\cdot\mathbf{J}^e(\mathbf{r},t)=0 \tag{8.3.2}$$

$$\frac{\partial}{\partial t}\mathbf{p}(\mathbf{r},t)+\nabla\cdot\boldsymbol{\Pi}(\mathbf{r},t)=0 \tag{8.3.3}$$

where $\mathbf{J}^e$ is the energy current and $\boldsymbol{\Pi}$ is the momentum current or *stress tensor*. These equations must be supplemented by two constitutive relations in which $\mathbf{J}^e$ and $\boldsymbol{\Pi}$ are expressed in terms of quantities representing dissipative processes in the fluid. We choose a frame of reference in which the mean velocity of the fluid is zero, i.e. $\langle\mathbf{u}(\mathbf{r},t)\rangle=0$, and assume that the local deviations of the hydrodynamic variables from their average values are small. The equations may then be linearised with respect to the deviations. We consider in turn each of the three conservation laws.

Conservation of particle number. Equation (8.3.1) is easily dealt with. The assumption that the local deviation in number density is small means that the momentum density can be written as

$$\mathbf{p}(\mathbf{r},t)=m\big[\rho+\delta\rho(\mathbf{r},t)\big]\mathbf{u}(\mathbf{r},t)\approx m\rho\mathbf{u}(\mathbf{r},t)\equiv m\mathbf{j}(\mathbf{r},t) \tag{8.3.4}$$

which also serves as the definition of the local particle current $\mathbf{j}(\mathbf{r},t)$. With this approximation, (8.3.1) becomes

$$\frac{\partial}{\partial t}\delta\rho(\mathbf{r},t)+\nabla\cdot\mathbf{j}(\mathbf{r},t)=0 \tag{8.3.5}$$

Conservation of energy. The macroscopic energy current $\mathbf{J}^e$ is defined as

$$\mathbf{J}^e(\mathbf{r},t)=(e+P)\mathbf{u}(\mathbf{r},t)-\lambda\nabla T(\mathbf{r},t) \tag{8.3.6}$$

where $e=U/V$ is the equilibrium energy density, λ is the thermal conductivity and $T(\mathbf{r},t)$ is the local temperature already introduced in (8.1.5); terms corresponding to viscous heating have been omitted, since these are quadratic in the local velocity. Equations (8.3.2),

(8.3.5) and (8.3.6) can now be combined to give the *energy equation*, i.e.

$$\frac{\partial}{\partial t}\delta q(\mathbf{r},t) - \lambda\nabla^2\delta T(\mathbf{r},t) = 0 \tag{8.3.7}$$

where $\delta q(\mathbf{r},t)$ is the fluctuation in a quantity

$$q(\mathbf{r},t) = e(\mathbf{r},t) - \left(\frac{e+P}{\rho}\right)\rho(\mathbf{r},t) \tag{8.3.8}$$

which can be interpreted as a density of heat energy. If the number of particles is held constant, the entropy change of the system in an infinitesimal process is $T\,\mathrm{d}S = \mathrm{d}U + P\,\mathrm{d}V$. Hence

$$T\,\mathrm{d}S = \mathrm{d}(eV) + P\,\mathrm{d}V = V\,\mathrm{d}e - \frac{eV}{\rho}\,\mathrm{d}\rho - \frac{PV}{\rho}\,\mathrm{d}\rho = V\,\mathrm{d}q \tag{8.3.9}$$

A change in q is therefore equal to the heat lost or gained by the system per unit volume when the change is carried out reversibly and $\delta q(\mathbf{r},t)$ is related to the change in entropy density $s(\mathbf{r},t)$ by

$$\delta q(\mathbf{r},t) = T\delta s(\mathbf{r},t) \tag{8.3.10}$$

If we invoke the hypothesis of local thermodynamic equilibrium, the deviation of a local thermodynamic variable such as $s(\mathbf{r},t)$ from its average value can be expressed in terms of a set of statistically independent quantities. We choose as independent variables the density and temperature (see Appendix A) and expand $q(\mathbf{r},t)$ to first order in the deviations $\delta\rho(\mathbf{r},t)$ and $\delta T(\mathbf{r},t)$. Then, from (8.3.10), and remembering that N is fixed:

$$\begin{aligned}\delta q(\mathbf{r},t) &= \frac{T}{V}\left(\frac{\partial S}{\partial\rho}\right)_T \delta\rho(\mathbf{r},t) + \frac{T}{V}\left(\frac{\partial S}{\partial T}\right)_\rho \delta T(\mathbf{r},t)\\ &= -\frac{T\beta_V}{\rho}\,\delta\rho(\mathbf{r},t) + \rho c_V \delta T(\mathbf{r},t)\end{aligned} \tag{8.3.11}$$

where

$$\beta_V = \left(\frac{\partial P}{\partial T}\right)_\rho = -\rho\left(\frac{\partial(S/V)}{\partial\rho}\right)_T \tag{8.3.12}$$

is the thermal pressure coefficient, c_V is the heat capacity per particle at constant volume and use has been made of the Maxwell relation $(\partial S/\partial V)_T = (\partial P/\partial T)_V$. If we now substitute (8.3.11) in (8.3.7), eliminate $(\partial/\partial t)\rho(\mathbf{r},t)$ with the help of (8.3.5) and divide through by ρc_V, the energy equation becomes

$$\left(\frac{\partial}{\partial t} - a\nabla^2\right)\delta T(\mathbf{r},t) + \frac{T\beta_V}{\rho^2 c_V}\boldsymbol{\nabla}\cdot\mathbf{j}(\mathbf{r},t) = 0 \tag{8.3.13}$$

where

$$a = \frac{\lambda}{\rho c_V} \tag{8.3.14}$$

Conservation of momentum. The stress tensor $\boldsymbol{\Pi}$ in (8.3.3) is given macroscopically by

$$\begin{aligned}\Pi^{\alpha\beta}(\mathbf{r},t) = \delta_{\alpha\beta}P(\mathbf{r},t) - \eta\left(\frac{\partial u_\alpha(\mathbf{r},t)}{\partial r_\beta} + \frac{\partial u_\beta(\mathbf{r},t)}{\partial r_\alpha}\right) \\ + \delta_{\alpha\beta}\left(\tfrac{2}{3}\eta - \zeta\right)\boldsymbol{\nabla}\cdot\mathbf{u}(\mathbf{r},t)\end{aligned} \tag{8.3.15}$$

where $P(\mathbf{r},t)$ is the local pressure, η is the shear viscosity, ζ is the bulk viscosity and the bracketed quantity in the second term on the right-hand side is the rate-of-strain tensor.[2] Substitution of (8.3.15) in (8.3.3) and use of (8.3.5) leads to the Navier–Stokes equation in its linearised form:

$$\frac{\partial}{\partial t}\mathbf{j}(\mathbf{r},t) + \frac{1}{m}\boldsymbol{\nabla}P(\mathbf{r},t) - \nu\nabla^2\mathbf{j}(\mathbf{r},t) - \frac{\frac{1}{3}\eta+\zeta}{\rho m}\boldsymbol{\nabla}\boldsymbol{\nabla}\cdot\mathbf{j}(\mathbf{r},t) = 0 \tag{8.3.16}$$

where

$$\nu = \frac{\eta}{\rho m} \tag{8.3.17}$$

is the kinematic shear viscosity. To first order in $\delta\rho(\mathbf{r},t)$ and $\delta T(\mathbf{r},t)$ the fluctuation in local pressure is

$$\begin{aligned}\delta P(\mathbf{r},t) &= \left(\frac{\partial P}{\partial \rho}\right)_T \delta\rho(\mathbf{r},t) + \left(\frac{\partial P}{\partial T}\right)_\rho \delta T(\mathbf{r},t) \\ &= \frac{1}{\rho\chi_T}\,\delta\rho(\mathbf{r},t) + \beta_V \delta T(\mathbf{r},t)\end{aligned} \tag{8.3.18}$$

where χ_T is the isothermal compressibility (2.4.16). The Navier–Stokes equation can therefore be rewritten as

$$\frac{1}{\rho m\chi_T}\boldsymbol{\nabla}\delta\rho(\mathbf{r},t) + \frac{\beta_V}{m}\boldsymbol{\nabla}\delta T(\mathbf{r},t) + \left(\frac{\partial}{\partial t} - \nu\nabla^2 - \frac{\frac{1}{3}\eta+\zeta}{\rho m}\boldsymbol{\nabla}\boldsymbol{\nabla}\cdot\right)\mathbf{j}(\mathbf{r},t) = 0 \tag{8.3.19}$$

Equations (8.3.5), (8.3.13) and (8.3.19) form a closed set of linear equations for the variables $\delta\rho(\mathbf{r},t)$, $\delta T(\mathbf{r},t)$ and $\mathbf{j}(\mathbf{r},t)$. These are readily solved by taking the double transforms with respect to space (Fourier) and time (Laplace) to give

$$-iz\tilde{\rho}_{\mathbf{k}}(z) + i\mathbf{k}\cdot\tilde{\mathbf{j}}_{\mathbf{k}}(z) = \rho_{\mathbf{k}} \tag{8.3.20}$$

$$\left(-iz + ak^2\right)\widetilde{T}_{\mathbf{k}}(z) + \frac{T\beta_V}{\rho^2 c_V} i\mathbf{k}\cdot\tilde{\mathbf{j}}_{\mathbf{k}}(z) = T_{\mathbf{k}} \tag{8.3.21}$$

$$\frac{1}{\rho m \chi_T} i\mathbf{k}\tilde{\rho}_{\mathbf{k}}(z) + \frac{\beta_V}{m} i\mathbf{k}\widetilde{T}_{\mathbf{k}}(z) + \left(-iz + \nu k^2 + \frac{\frac{1}{3}\eta + \zeta}{\rho m}\mathbf{k}\mathbf{k}\cdot\right)\tilde{\mathbf{j}}_{\mathbf{k}}(z) = \mathbf{j}_{\mathbf{k}} \tag{8.3.22}$$

where, for example:

$$\tilde{\rho}_{\mathbf{k}}(z) = \int_0^\infty \mathrm{d}t\ \exp(izt) \int \delta\rho(\mathbf{r}, t) \exp(-i\mathbf{k}\cdot\mathbf{r})\, \mathrm{d}\mathbf{r} \tag{8.3.23}$$

and $\rho_{\mathbf{k}}$, $T_{\mathbf{k}}$ and $\mathbf{j}_{\mathbf{k}}$ are the spatial Fourier components at $t = 0$. We now separate the components of the current $\mathbf{j}_{\mathbf{k}}$ into their longitudinal and transverse parts. Taking $\mathbf{k}$ along the z-axis, we rewrite (8.3.22) as

$$\frac{1}{\rho m \chi_T} ik\tilde{\rho}_{\mathbf{k}}(z) + \frac{\beta_V}{m} ik\widetilde{T}_{\mathbf{k}}(z) + \left(-iz + bk^2\right)\tilde{j}^z_{\mathbf{k}}(z) = j^z_{\mathbf{k}} \tag{8.3.24a}$$

$$\left(-iz + \nu k^2\right)\tilde{j}^\alpha_{\mathbf{k}} = j^\alpha_{\mathbf{k}}, \quad \alpha = x, y \tag{8.3.24b}$$

where

$$b = \frac{\frac{4}{3}\eta + \zeta}{\rho m} \tag{8.3.25}$$

is the kinematic longitudinal viscosity.

Equations (8.3.20), (8.3.21) and (8.3.24) are conveniently summarised in matrix form:

$$\begin{pmatrix} -iz & 0 & ik & 0 & 0 \\ 0 & -iz + ak^2 & \dfrac{T\beta_V ik}{\rho^2 c_V} & 0 & 0 \\ \dfrac{ik}{\rho m \chi_T} & \dfrac{\beta_V ik}{m} & -iz + bk^2 & 0 & 0 \\ 0 & 0 & 0 & -iz + \nu k^2 & 0 \\ 0 & 0 & 0 & 0 & -iz + \nu k^2 \end{pmatrix} \begin{pmatrix} \tilde{\rho}_{\mathbf{k}}(z) \\ \widetilde{T}_{\mathbf{k}}(z) \\ \tilde{j}^z_{\mathbf{k}}(z) \\ \tilde{j}^x_{\mathbf{k}}(z) \\ \tilde{j}^y_{\mathbf{k}}(z) \end{pmatrix} = \begin{pmatrix} \rho_{\mathbf{k}} \\ T_{\mathbf{k}} \\ j^z_{\mathbf{k}} \\ j^x_{\mathbf{k}} \\ j^y_{\mathbf{k}} \end{pmatrix} \tag{8.3.26}$$

The matrix of coefficients in (8.3.26) is called the *hydrodynamic matrix*. Its block-diagonal structure shows that the transverse-current fluctuations are completely decoupled from fluctuations in the other, longitudinal variables. The determinant of the hydrodynamic matrix therefore factorises into the product of purely longitudinal (l) and purely transverse (t) parts, i.e.

$$D(k, z) = D_l(k, z) D_t(k, z) \tag{8.3.27}$$

with

$$D_l(k, z) = -iz\left(-iz + ak^2\right)\left(-iz + bk^2\right) + \left(-iz + ak^2\right)\frac{k^2}{\rho m \chi_T} - iz\frac{T\beta_V^2 k^2}{\rho^2 m c_V} \tag{8.3.28}$$

and

$$D_t(k,z) = \left(-iz + \nu k^2\right)^2 \tag{8.3.29}$$

The dependence of frequency on wavenumber or *dispersion relation* for the collective modes is determined by the poles of the inverse of the hydrodynamic matrix and hence by the complex roots of the equation

$$D(k,z) = 0 \tag{8.3.30}$$

The factorisation in (8.3.27) shows that (8.3.30) has a double root associated with the two transverse modes, namely

$$z = -i\nu k^2 \tag{8.3.31}$$

while the complex frequencies corresponding to longitudinal modes are obtained as the solution to the cubic equation

$$iz^3 - z^2(a+b)k^2 - iz\left(abk^2 + c_s^2\right)k^2 + (a/\gamma)c_s^2 k^4 = 0 \tag{8.3.32}$$

where $\gamma = c_P/c_V$ is the ratio of specific heats, c_s is the adiabatic speed of sound, given by

$$c_s^2 = \frac{\gamma}{\rho m \chi_T} \tag{8.3.33}$$

and use has been made of the thermodynamic relation[3]

$$c_P = c_V + \frac{T\chi_T \beta_V^2}{\rho} \tag{8.3.34}$$

Since the hydrodynamic calculation is valid only in the long-wavelength limit, it is sufficient to calculate the complex frequencies to order k^2. The algebra is simplified by introducing the reduced variables $s = z/c_s k$; it is then straightforward to show[4] that the approximate solution to (8.3.32) is

$$z_0 = -iD_T k^2 \tag{8.3.35a}$$

$$z_\pm = \pm c_s k - i\Gamma k^2 \tag{8.3.35b}$$

where

$$D_T = \frac{a}{\gamma} = \frac{\lambda}{\rho c_P} \tag{8.3.36}$$

is the thermal diffusivity and

$$\Gamma = a(\gamma - 1)/2\gamma + b/2 \tag{8.3.37}$$

is the sound attenuation coefficient. The imaginary roots in (8.3.31) and (8.3.35a) represent diffusive processes of the type already discussed in the preceding section, and the pair of complex roots in (8.3.35b) correspond to propagating sound waves, as we shall see in Section 8.5.

8.4 TRANSVERSE-CURRENT CORRELATIONS

Equation (8.3.24b) shows that in the time domain the hydrodynamic behaviour of the transverse-current fluctuations is governed by a first-order differential equation of the form

$$\frac{\partial}{\partial t} j^x_{\mathbf{k}}(t) = -\nu k^2 j^x_{\mathbf{k}}(t) \tag{8.4.1}$$

This result has precisely the same structure as the diffusion equation (8.2.4) and the kinematic shear viscosity has the same dimensions as the self-diffusion coefficient, but is typically two orders of magnitude larger than D for, say, an argon-like liquid near its triple point. If we multiply through (8.4.1) by $j^x_{-\mathbf{k}}$ and take the thermal average we find that the transverse current autocorrelation function satisfies the equation

$$\frac{\partial}{\partial t} C_t(k,t) + \nu k^2 C_t(k,t) = 0 \tag{8.4.2}$$

Equation (8.4.2) is easily solved to give

$$C_t(k,t) = C_t(k,0)\exp\bigl(-\nu k^2 t\bigr) = \omega_0^2 \exp\bigl(-\nu k^2 t\bigr) \tag{8.4.3}$$

where ω_0 is the frequency defined by (7.4.29). The exponential decay in (8.4.3) is typical of a diffusive process (see Section 8.2).

The diffusive behaviour of the hydrodynamic "shear" mode is also apparent in the fact that the Laplace transform of $C_t(k,t)$ has a purely imaginary pole corresponding to the root (8.3.31) of $D(k,z)$:

$$\widetilde{C}_t(k,z) = \frac{\omega_0^2}{-iz + \nu k^2} \tag{8.4.4}$$

Let $z = \omega + i\varepsilon$ approach the real axis from above ($\varepsilon \to 0+$). Then $\widetilde{C}_t(k,\omega)$ at small k is given approximately by

$$\widetilde{C}_t(k,\omega) = \frac{\omega_0^2}{-i\omega}\left(1 - \frac{\nu k^2}{i\omega}\right)^{-1} \approx \frac{\omega_0^2}{-i\omega}\left(1 + \frac{\nu k^2}{i\omega}\right) \tag{8.4.5}$$

If we substitute for ω_0^2 and recall the definition (8.3.17) of ν, we find that the shear viscosity, which must be real, is related to the long-wavelength, low-frequency behaviour of

$\widetilde{C}_t(k,\omega)$ by

$$\eta = \beta\rho m^2 \lim_{\omega\to 0}\lim_{k\to 0}\frac{\omega^2}{k^4}\mathrm{Re}\,\widetilde{C}_t(k,\omega)$$
$$= \pi\beta\rho m^2 \lim_{\omega\to 0}\lim_{k\to 0}\frac{\omega^2}{k^4}C_t(k,\omega) \tag{8.4.6}$$

where $C_t(k,\omega)$ is the spectrum of transverse-current fluctuations, i.e. the Fourier transform of $C_t(k,t)$; this result is the analogue of the expression (8.2.11) for the self-diffusion coefficient. From the properties of the Laplace transform and the definition of $C_t(k,t)$ it follows that

$$\frac{k^2}{N}\int_0^\infty \langle \dot{j}^x_{\mathbf{k}}(t)\dot{j}^x_{-\mathbf{k}}\rangle \exp(i\omega t)\,\mathrm{d}t = -\int_0^\infty \frac{\mathrm{d}^2}{\mathrm{d}t^2}C_t(k,t)\exp(i\omega t)\,\mathrm{d}t$$
$$= \omega^2\widetilde{C}_t(k,\omega) - i\omega\omega_0^2 \tag{8.4.7}$$

We may therefore rewrite (8.4.6) as

$$\eta = \frac{\beta m^2}{V}\lim_{\omega\to 0}\lim_{k\to 0}\mathrm{Re}\int_0^\infty \frac{1}{k^2}\langle \dot{j}^x_{\mathbf{k}}(t)\dot{j}^x_{-\mathbf{k}}\rangle \exp(i\omega t)\,\mathrm{d}t \tag{8.4.8}$$

The time derivative of the transverse current can be expressed in terms of the stress tensor via the conservation law (8.3.3). Taking the Fourier transform of (8.3.3), and remembering that $\mathbf{k}$ lies along the z-axis and that $\mathbf{p}(\mathbf{r},t) = m\mathbf{j}(\mathbf{r},t)$, we find that

$$\frac{\partial}{\partial t}j^x_{\mathbf{k}}(t) + \frac{ik}{m}\Pi^{xz}_{\mathbf{k}}(t) = 0 \tag{8.4.9}$$

Combination of (8.4.8) and (8.4.9) shows that the shear viscosity is proportional to the time integral of the autocorrelation function of an off-diagonal element of the stress tensor in the limit $k \to 0$:

$$\eta = \frac{\beta}{V}\int_0^\infty \langle \Pi^{xz}_0(t)\Pi^{xz}_0\rangle \mathrm{d}t \equiv \int_0^\infty \eta(t)\,\mathrm{d}t \tag{8.4.10}$$

In order to relate the shear viscosity to the intermolecular forces it is necessary to have a microscopic expression for the stress tensor. It follows from the definition (7.4.7) of the microscopic particle current that

$$m\frac{\partial}{\partial t}j^\alpha_{\mathbf{k}} = m\sum_{i=1}^N\left(\dot{u}_{i\alpha} - \sum_\beta ik_\beta u_{i\alpha}u_{i\beta}\right)\exp(-i\mathbf{k}\cdot\mathbf{r}_i) \tag{8.4.11}$$

where α, β denote any of x, y or z; the relation to the stress tensor is then established by use of (8.4.9), with $\alpha = x$ and $\beta = z$. To introduce the pair potential $v(r)$ we note that

$\mathbf{r}_{ji} = -\mathbf{r}_{ij}$, and rewrite the first term on the right-hand side of (8.4.11) successively as

$$\begin{aligned} & m\sum_{i=1}^{N} \dot{u}_{i\alpha} \exp(-i\mathbf{k}\cdot\mathbf{r}_i) \\ &= \sum_{i=1}^{N}\sum_{j\neq i}^{N} \frac{r_{ij\alpha}}{|\mathbf{r}_{ij}|} v'(r_{ij}) \exp(-i\mathbf{k}\cdot\mathbf{r}_i) \\ &= \tfrac{1}{2}\sum_{i=1}^{N}\sum_{j\neq i}^{N} \frac{r_{ij\alpha}}{|\mathbf{r}_{ij}|} v'(r_{ij}) \big[\exp(-i\mathbf{k}\cdot\mathbf{r}_i) - \exp(-i\mathbf{k}\cdot\mathbf{r}_j)\big] \\ &= \tfrac{1}{2} ik_\beta \sum_{i=1}^{N}\sum_{j\neq i}^{N} \frac{r_{ij\alpha} r_{ij\beta}}{ik_\beta r_{ij\beta}|\mathbf{r}_{ij}|} v'(r_{ij}) \big[\exp(-i\mathbf{k}\cdot\mathbf{r}_i) - \exp(-i\mathbf{k}\cdot\mathbf{r}_j)\big] \end{aligned} \tag{8.4.12}$$

where $v'(r) \equiv \mathrm{d}v(r)/\mathrm{d}r$; the second step is taken by writing each term in the double sum as half the sum of two equal terms. Introducing a quantity $\Phi_{\mathbf{k}}(\mathbf{r})$ defined as

$$\Phi_{\mathbf{k}}(\mathbf{r}) = r v'(r) \left(\frac{\exp(i\mathbf{k}\cdot\mathbf{r}) - 1}{i\mathbf{k}\cdot\mathbf{r}} \right) \tag{8.4.13}$$

we finally obtain a microscopic expression for $\Pi_{\mathbf{k}}^{\alpha\beta}$ in the form

$$\Pi_{\mathbf{k}}^{\alpha\beta} = \sum_{i=1}^{N} \left(m u_{i\alpha} u_{i\beta} + \tfrac{1}{2} \sum_{j\neq i}^{N} \frac{r_{ij\alpha} r_{ij\beta}}{r_{ij}^2} \Phi_{\mathbf{k}}(\mathbf{r}_{ij}) \right) \exp(-i\mathbf{k}\cdot\mathbf{r}_i) \tag{8.4.14}$$

The Green–Kubo relation for the shear viscosity analogous to (7.2.7) is then obtained by inserting (8.4.14) (taken for $\mathbf{k} = 0$) in (8.4.10). Note that it follows from the virial theorem that

$$\left\langle \Pi_0^{\alpha\alpha} \right\rangle = PV \tag{8.4.15}$$

whereas

$$\left\langle \Pi_0^{\alpha\beta} \right\rangle = 0, \quad \alpha \neq \beta \tag{8.4.16}$$

Equation (8.4.10) is not directly applicable to the hard-sphere fluid because the potential $v(r)$ has a singularity at $r = d$ (the hard-sphere diameter). However, the microscopic expression for the shear viscosity, together with formulae to be derived later for other transport coefficients, can be recast in a form that resembles the Einstein relation (7.2.3) for the self-diffusion coefficient and is valid even for hard spheres. A Green–Kubo formula for a transport coefficient K, including both (7.7.10) (taken for $\omega = 0$) and (8.4.10), can always be written as

$$K = \frac{\beta}{V} \int_0^\infty \left\langle \dot{A}(t) \dot{A} \right\rangle \mathrm{d}t \tag{8.4.17}$$

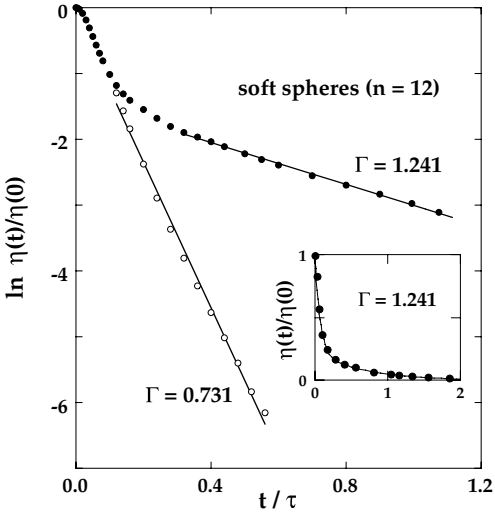

FIG. 8.1. Normalised Green–Kubo integrand for the shear viscosity of a soft-sphere (r^{-12}) fluid at two values of the coupling parameter Γ defined by (5.3.13). The unit of time is $\tau = (m\sigma^2/48\varepsilon)^{1/2}$. The inset shows the results of a two-exponential fit to $\eta(t)$ at the higher value of Γ. Unpublished results of D.M. Heyes.

where A is some microscopic dynamical variable. The argument used to derive (7.2.7) from (7.2.3) can be extended to show that (8.4.17) is equivalent to writing

$$K = \frac{\beta}{V} \lim_{t\to\infty} \frac{1}{2t} \left\langle \left| A(t) - A(0) \right|^2 \right\rangle \tag{8.4.18}$$

which may be regarded as a generalised form of the Einstein relation for D. In the case of the shear viscosity we see from (8.4.8) that the variable $A(t)$ is

$$\begin{aligned} A(t) &= \lim_{k\to 0} \frac{im}{k} j^x_{\mathbf{k}}(t) \\ &= \lim_{k\to 0} \frac{im}{k} \sum_{i=1}^{N} u_{ix}(t)\left[1 - ikr_{iz}(t) + \cdots\right] = m \sum_{i=1}^{N} u_{ix}(t) r_{iz}(t) \end{aligned} \tag{8.4.19}$$

where a frame of reference has been chosen in which the total momentum of the particles (a conserved quantity) is zero. Hence the generalised Einstein relation for the shear viscosity is

$$\eta = \frac{\beta m^2}{V} \lim_{t\to\infty} \frac{1}{2t} \left\langle \left| \sum_{i=1}^{N} \left[u_{ix}(t) r_{iz}(t) - u_{ix}(0) r_{iz}(0) \right] \right|^2 \right\rangle \tag{8.4.20}$$

The quantity Π_0^{xz} in the Green–Kubo formula (8.4.10) is the sum of a kinetic and a potential term. There are consequently three distinct contributions to the shear viscosity:

a purely kinetic term, corresponding to the transport of transverse momentum via the displacement of particles; a purely potential term, arising from the action of the interparticle forces ("collisional" transport); and a cross term. At liquid densities the potential term is much the largest of the three. In Enskog's theory (see Section 7.2) the shear viscosity of the hard-sphere fluid is

$$\frac{\eta_{\mathrm{E}}}{\eta_0} = \frac{2\pi\rho d^3}{3}\left(\frac{1}{y} + 0.8 + 0.761y\right) \tag{8.4.21}$$

where $y = \beta P/\rho - 1 = (2\pi\rho d^3/3)g(d)$ and $\eta_0 = (5/16d^2)(mk_{\mathrm{B}}T/\pi)^{1/2}$ is the limiting, low-density result derived from the Boltzmann equation.[5] The three terms between brackets in (8.4.21) represent, successively, the kinetic, cross and potential contributions; the last of these is dominant close to the fluid–solid transition, where $g(d)$ (the pair distribution function at contact) ≈ 6 and $y \approx 10$. Note that the kinetic contribution scales with $g(d)$ in exactly the same way as the diffusion constant (see Section 2.5); this is not surprising, since diffusion is a purely kinetic phenomenon. Figure 7.3 compares the results of molecular-dynamics calculations of the shear viscosity of the hard-sphere fluid with those obtained from the Enskog expression (8.4.21). Agreement is very good for densities up to $\rho d^3 \approx 0.7$. Near solidification, however, where η increases rapidly with density, Enskog's theory underestimates the shear viscosity by a factor of approximately two. As the same figure also shows, the behaviour of the self-diffusion constant at high densities is the reverse of this. The net result is that the product $D\eta$ calculated from the molecular-dynamics data is roughly constant for ρd^3 greater than about 0.2; at the highest densities its value is within a few percent of that predicted by Stokes's law (7.3.19) with slip boundary conditions. The increase in shear viscosity at high densities is linked numerically to the appearance of a slowly decaying, quasi-exponential tail in the stress-tensor autocorrelation function, colloquially called the "molasses" tail.[6] The effect is not peculiar to hard spheres. For example, a persisting, positive tail is clearly present in the results shown in Figure 8.1 for a soft-sphere (r^{-12}) fluid at a high value of the coupling constant Γ, where $\eta(t)$ is well represented by the sum of two exponentials. At the lower value, corresponding to lower densities or higher temperatures, the tail in $\eta(t)$ – if any – is not perceptible.

8.5 LONGITUDINAL COLLECTIVE MODES

The longitudinal collective modes are those associated with fluctuations in density, temperature and the projection of the particle current along the direction of the wavevector $\mathbf{k}$. It is clear from the structure of the hydrodynamic matrix in (8.3.26) that the variables $\tilde{\rho}_{\mathbf{k}}(z)$, $\widetilde{T}_{\mathbf{k}}(z)$ and $\tilde{j}^z_{\mathbf{k}}(z)$ are coupled to each other. The analysis is therefore more complicated than in the case of the transverse-current fluctuations discussed in Section 8.4. There are three longitudinal modes, corresponding to the roots z_0, z_+ and z_- displayed in (8.3.35). The significance of the different roots is most easily grasped by solving the system of coupled, longitudinal equations represented by (8.3.26) to obtain the hydrodynamic limiting form of the dynamic structure factor $S(k, \omega)$. The solution for $\tilde{\rho}_{\mathbf{k}}(z)$ involves terms proportional to the initial values $\rho_{\mathbf{k}}$, $T_{\mathbf{k}}$ and $j^z_{\mathbf{k}}$. We may omit the term proportional to $j^z_{\mathbf{k}}$ because $\mathbf{k}$ can

always be chosen to make $\mathbf{u}_\mathbf{k}$ (the Fourier transform of the initial local velocity $\mathbf{u}(\mathbf{r}, 0)$) perpendicular to $\mathbf{k}$, thereby ensuring that $j_\mathbf{k}^z = 0$. We can also ignore the term proportional to $T_\mathbf{k}$; this contributes nothing to the final expression for $S(k, \omega)$, since fluctuations in temperature and density are instantaneously uncorrelated, i.e. $\langle T_\mathbf{k} \rho_{-\mathbf{k}} \rangle = 0$ (see Appendix A). With these simplifications the solution for $\tilde{\rho}_\mathbf{k}(z)$ is

$$\frac{\tilde{\rho}_\mathbf{k}(z)}{\rho_\mathbf{k}} = \frac{(-iz + ak^2)(-iz + bk^2) + (\gamma - 1)c_s^2 k^2/\gamma}{D_l(k, z)} \tag{8.5.1}$$

where all quantities are as defined in Section 8.3. Separation of the right-hand side of (8.5.1) into partial fractions shows that on the real axis $\tilde{\rho}_\mathbf{k}$ is given by

$$\begin{aligned}\frac{\tilde{\rho}_\mathbf{k}(\omega)}{\rho_\mathbf{k}} = &\left(\frac{\gamma - 1}{\gamma}\right)\frac{1}{-i\omega + D_T k^2} \\ &+ \frac{1}{2\gamma}\left(\frac{1}{-i\omega + \Gamma k^2 - ic_s k} + \frac{1}{-i\omega + \Gamma k^2 + ic_s k}\right)\end{aligned} \tag{8.5.2}$$

which, via an inverse transform, yields an expression for $\rho_\mathbf{k}(t)$ given by

$$\rho_\mathbf{k}(t) = \rho_\mathbf{k}\left[\left(\frac{\gamma - 1}{\gamma}\right)\exp\left(-D_T k^2 t\right) + \frac{1}{\gamma}\exp\left(-\Gamma k^2 t\right)\cos c_s k t\right] \tag{8.5.3}$$

The form of (8.5.3) shows that the purely imaginary root in (8.3.35a) represents a fluctuation that decays without propagating, the lifetime of the fluctuation being determined by the thermal diffusivity D_T. By contrast, the complex roots correspond to a fluctuation that propagates through the fluid at the speed of sound, eventually decaying through the combined effects of viscosity and thermal conduction. The definition of Γ in (8.3.37) implies that the thermal damping of the sound mode is small when $\gamma \approx 1$, which is the case for many liquid metals. On multiplying through (8.5.3) by $\rho_{-\mathbf{k}}$, dividing by N and taking the thermal average, we obtain an expression for the density autocorrelation function $F(k, t)$; this is easily transformed to give

$$\begin{aligned}S(k, \omega) = \frac{S(k)}{2\pi}&\left[\left(\frac{\gamma - 1}{\gamma}\right)\frac{2D_T k^2}{\omega^2 + (D_T k^2)^2}\right. \\ &\left. + \frac{1}{\gamma}\left(\frac{\Gamma k^2}{(\omega + c_s k)^2 + (\Gamma k^2)^2} + \frac{\Gamma k^2}{(\omega - c_s k)^2 + (\Gamma k^2)^2}\right)\right]\end{aligned} \tag{8.5.4}$$

The spectrum of density fluctuations therefore consists of three components: the *Rayleigh line*, centred at $\omega = 0$, and two *Brillouin lines* at $\omega = \pm c_s k$; a typical spectrum is plotted in Figure 8.2. The two shifted components correspond to propagating sound waves and are analogous to the longitudinal acoustic phonons of a solid, whereas the central line corresponds to the diffusive, thermal mode. The total integrated intensity of the Rayleigh line is

$$\mathcal{I}_R = \frac{\gamma - 1}{\gamma} S(k) \tag{8.5.5}$$

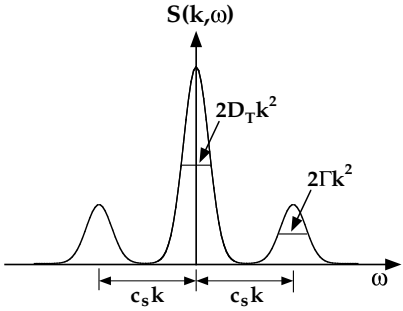

FIG. 8.2. Dynamic structure factor in the hydrodynamic limit. D_T is the thermal diffusivity, Γ is the sound-attenuation coefficient and c_S is the adiabatic speed of sound.

and that of each of the two Brillouin lines is

$$\mathcal{I}_B = \frac{1}{2\gamma} S(k) \tag{8.5.6}$$

Thus

$$\mathcal{I}_R + 2\mathcal{I}_B = S(k) \tag{8.5.7}$$

which is a particular case of the sum rule (7.4.23). The ratio

$$\frac{\mathcal{I}_R}{2\mathcal{I}_B} = \gamma - 1 \tag{8.5.8}$$

is called the Landau–Placzek ratio. As the values of C_P/C_V listed in Table 1.2 suggest, the Landau–Placzek ratio is typically an order of magnitude larger for the rare-gas liquids than for simple liquid metals. In passing from (8.5.1) to (8.5.2) we have, for the sake of simplicity, omitted a non-lorentzian term that in practice makes only a negligibly small, asymmetric correction to the Brillouin lines.

We have chosen to discuss the behaviour of the longitudinal modes in terms of local fluctuations in density and temperature, but it would have been equally appropriate to choose the pressure and entropy as variables, since these are also statistically independent (see Appendix A). The calculation is instructive, since it shows that the first term in (8.5.2) can be identified with the decay of entropy fluctuations. It follows that the Brillouin doublet is associated with propagating pressure fluctuations at constant entropy (hence the appearance of the adiabatic speed of sound) while the Rayleigh line corresponds to non-propagating fluctuations in entropy at constant pressure.[4]

The wavelength of visible light is much greater than the nearest-neighbour spacing in liquids. Light-scattering experiments are therefore ideally suited to measurements of the Rayleigh–Brillouin spectrum at long wavelengths and provide an accurate means of measurement of properties such as the thermal diffusivity, speed of sound and sound-attenuation coefficient. However, the spectral lineshape is determined by a small number of

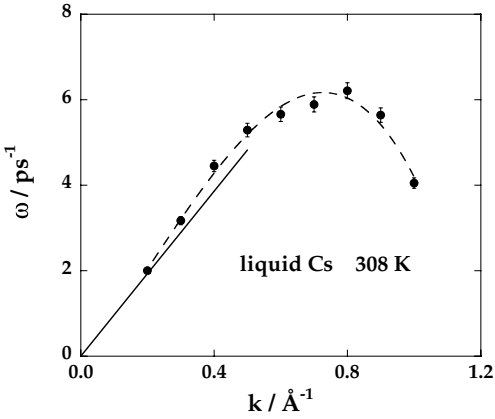

FIG. 8.3. Dispersion of the Brillouin peak in liquid caesium near the normal melting temperature. The points are the results of inelastic neutron-scattering experiments and the line shows the hydrodynamic dispersion corresponding to the experimental speed of sound, $c_S = 965\ \mathrm{m\,s^{-1}}$. After Bodensteiner *et al.*[10]

macroscopic properties that are insensitive to details either of the interactions between particles or of the molecular structure of the fluid. From the standpoint of microscopic theory the more interesting question is whether the propagating density fluctuations characteristic of the hydrodynamic regime can also be supported in simple liquids at wavelengths comparable with the spacing between particles. We have already seen in Section 7.5 that well-defined, collective excitations of the hydrodynamic type, manifesting themselves in a three-peak structure in $S(k, \omega)$, have been detected in neutron-scattering experiments on liquid caesium, but similar results have been obtained by neutron or x-ray scattering for the other alkali metals as well as for lead, mercury and aluminium.[7] Brillouin-type sidepeaks have also been seen in molecular-dynamics calculations on a variety of systems, including both the hard-sphere[8] and Lennard-Jones[9] fluids. The spectra are therefore qualitatively similar to those predicted by hydrodynamics, though there are some major differences in detail. Figure 8.3, for example, shows the dispersion of the sound-wave peak observed in neutron-scattering experiments on liquid caesium. At the smallest wavenumbers the dispersion is approximately linear, in agreement with hydrodynamics, but corresponds to a speed of propagation significantly higher than the adiabatic speed of sound. The widths of the Rayleigh and Brillouin lines are also poorly described by the hydrodynamic result. As we shall see in Section 8.6 and again in Chapter 9, a description of the density fluctuations in the range of k explored in neutron or x-ray scattering experiments requires a generalisation of the hydrodynamic approach, the effect of which is to replace the transport coefficients and thermodynamic derivatives in (8.5.4) by quantities dependent on frequency and wavenumber.

For later purposes we also require an expression for the hydrodynamic limit of the longitudinal-current autocorrelation function $C_l(k, t)$. We proceed, as before, by solving the system of equations (8.3.26) for the variable of interest, which in this case is the longitudinal particle current $\tilde{j}^z_{\mathbf{k}}(z)$. The terms in $\rho_{\mathbf{k}}$ and $T_{\mathbf{k}}$ may be omitted, since they are

uncorrelated with $\tilde{j}^z_{-\mathbf{k}}$. For z on the real axis the result is

$$\tilde{j}^z_{\mathbf{k}}(\omega) = j^z_{\mathbf{k}} \frac{-i\omega(-i\omega + ak^2)}{D_l(k,\omega)} \tag{8.5.9}$$

Thus

$$\widetilde{C}_l(k,\omega) = \frac{\omega_0^2}{-i\omega + bk^2 + c_s^2 k^2 \left(\dfrac{1}{-i\omega} + \dfrac{\gamma - 1}{-i\omega + ak^2} \right)} \tag{8.5.10}$$

The same result can be obtained from (7.4.28) and the hydrodynamic result (8.5.4).

According to (8.5.10), the spectrum of longitudinal-current fluctuations at small k behaves as

$$C_l(k,\omega) = \frac{1}{\pi} \mathrm{Re}\, \widetilde{C}_l(k,\omega) \approx \frac{\omega_0^2}{\pi\omega^2} \left(bk^2 + \frac{(\gamma - 1)ac_s^2 k^4}{\omega^2 + (ak^2)^2} \right) \tag{8.5.11}$$

Hence the longitudinal viscosity is given by a limiting operation analogous to (8.4.6) for the shear viscosity, i.e.

$$\tfrac{4}{3}\eta + \zeta = \rho m b = \pi\beta\rho m^2 \lim_{\omega\to 0} \lim_{k\to 0} \frac{\omega^2}{k^4} C_l(k,\omega) \tag{8.5.12}$$

If we now follow steps similar to those that lead to the Green–Kubo formula (8.4.10), we find that the longitudinal viscosity can be expressed in terms of the autocorrelation function of a diagonal element of the microscopic stress tensor (8.4.14):

$$\tfrac{4}{3}\eta + \zeta = \lim_{\omega\to 0} \frac{\beta}{V} \int_0^\infty \left\langle \Pi_0^{zz}(t) \Pi_0^{zz} \right\rangle \exp(i\omega t)\, \mathrm{d}t \tag{8.5.13}$$

In taking the limit $\omega = 0$ in (8.5.13) we find a discontinuity: the thermal average of Π_0^{zz} is non-zero (see (8.4.15)), so the integrand in (8.5.13) goes to a non-zero value as $t \to \infty$. The problem is overcome by subtracting the invariant part, the transport coefficient being linked only to fluctuations in the local variables. Thus

$$\tfrac{4}{3}\eta + \zeta = \frac{\beta}{V} \int_0^\infty \left\langle \left[\Pi_0^{zz}(t) - PV \right] \left[\Pi_0^{zz} - PV \right] \right\rangle \mathrm{d}t \tag{8.5.14}$$

To obtain the Green–Kubo relation for the thermal conductivity we require an expression for the rate of decay of a fluctuation in $q(\mathbf{r},t)$, the macroscopic density of heat energy; $q(\mathbf{r},t)$ is related to the entropy density by (8.3.10). We first use (8.3.11) to eliminate the local temperature from the energy equation (8.3.13). The result is

$$\left(\frac{\partial}{\partial t} - a\nabla^2 \right) \delta q(\mathbf{r},t) - \frac{\lambda T \beta_V}{\rho^2 c_V} \nabla^2 \delta\rho(\mathbf{r},t) = 0 \tag{8.5.15}$$

which, after transformation to Fourier–Laplace variables and use of (8.3.12) and the thermodynamic chain rule

$$\left(\frac{\partial S}{\partial \rho}\right)_T = -\left(\frac{\partial S}{\partial T}\right)_\rho \left(\frac{\partial T}{\partial \rho}\right)_S = -\frac{Nc_V}{T}\left(\frac{\partial T}{\partial \rho}\right)_S \tag{8.5.16}$$

gives

$$\left(-iz + ak^2\right)\tilde{q}_{\mathbf{k}}(z) + \lambda k^2 \left(\frac{\partial T}{\partial \rho}\right)_S \tilde{\rho}_{\mathbf{k}}(z) = q_{\mathbf{k}} \tag{8.5.17}$$

Next, an equation relating $\tilde{\rho}_{\mathbf{k}}(z)$ to $\widetilde{P}_{\mathbf{k}}(z)$ is obtained by taking the divergence of the Navier–Stokes equation (8.3.16) and transforming again to the variables k and z; the result in this case is

$$izm\left(-iz + bk^2\right)\tilde{\rho}_{\mathbf{k}}(z) - k^2 \widetilde{P}_{\mathbf{k}}(z) = -m\left(-iz + bk^2\right)\rho_{\mathbf{k}} \tag{8.5.18}$$

where $\mathbf{k}$ has once more been chosen perpendicular to the initial particle current. Equation (8.5.18) can now be converted into a relation for $\tilde{q}_{\mathbf{k}}(z)$ by making the substitutions

$$\widetilde{P}_{\mathbf{k}}(z) = \left(\frac{\partial P}{\partial \rho}\right)_S \tilde{\rho}_{\mathbf{k}}(z) + \frac{V}{T}\left(\frac{\partial P}{\partial S}\right)_\rho \tilde{q}_{\mathbf{k}}(z) \tag{8.5.19}$$

and

$$\rho_{\mathbf{k}} = \left(\frac{\partial \rho}{\partial P}\right)_S P_{\mathbf{k}} + \frac{V}{T}\left(\frac{\partial \rho}{\partial S}\right)_\rho q_{\mathbf{k}} \tag{8.5.20}$$

The final step is to eliminate $\tilde{\rho}_{\mathbf{k}}(z)$ between (8.5.17) and (8.5.18). The resulting expression for $\tilde{q}_{\mathbf{k}}(z)$ has some similarities with that obtained previously for $\tilde{\rho}_{\mathbf{k}}(z)$ in (8.5.1). In particular, there are two complex-conjugate poles and a single imaginary pole. At small k the local pressure and entropy are uncorrelated (see Appendix A). The problem can therefore be simplified by discarding terms proportional to $P_{\mathbf{k}}$. The lowest-order solution for $\tilde{q}_{\mathbf{k}}(z)$ then reduces to

$$\tilde{q}_{\mathbf{k}}(z) = \frac{q_{\mathbf{k}}}{-iz + D_{\mathrm{T}}k^2} \tag{8.5.21}$$

where D_{T} is the thermal diffusivity defined by (8.3.36). Equation (8.5.21) describes a purely diffusive mode, thereby confirming the fact that the Rayleigh peak in $S(k, \omega)$ is associated with the decay of non-propagating entropy fluctuations.

Our main concern is with the behaviour at small k. Since $\lim_{k\to 0} q_{\mathbf{k}} = T\Delta S$, it follows from (A.8) of Appendix A that $\langle q_{\mathbf{k}} q_{-\mathbf{k}}\rangle$ can be replaced by

$$\left\langle q_0^2 \right\rangle = T^2 N k_{\mathrm{B}} c_P \tag{8.5.22}$$

We now proceed as in the cases of the shear and longitudinal viscosities. On multiplying (8.5.21) through by $q_{-\mathbf{k}}$ and taking the thermal average, we obtain an expression for the

thermal conductivity of the form

$$\lambda = \rho c_P D_T = \frac{\beta}{VT} \lim_{\omega\to 0}\lim_{k\to 0} \frac{\omega^2}{k^2} \mathrm{Re}\langle \tilde{q}_{\mathbf{k}}(\omega) q_{-\mathbf{k}}\rangle \tag{8.5.23}$$

If we introduce a fluctuating heat current $\mathbf{J}^q_{\mathbf{k}}(t)$ defined, by virtue of (8.3.8), as the Fourier transform of

$$\mathbf{J}^q(\mathbf{r},t) = \mathbf{J}^e(\mathbf{r},t) - \frac{e+P}{\rho}\mathbf{j}(\mathbf{r},t) \tag{8.5.24}$$

we see that the energy-conservation equation (8.3.2) may be re-expressed as

$$\frac{\partial}{\partial t} q_{\mathbf{k}}(t) + i\mathbf{k}\cdot\mathbf{J}^q_{\mathbf{k}}(t) = 0 \tag{8.5.25}$$

Hence, if the z-axis is taken parallel to $\mathbf{k}$, we can rewrite (8.5.23) in typical Green–Kubo form as

$$\lambda = \frac{\beta}{VT}\int_0^\infty \langle J_0^{qz}(t) J_0^{qz}\rangle \,\mathrm{d}t \tag{8.5.26}$$

For (8.5.26) to be useful we require a microscopic expression for the heat current. Taking the Fourier transform of (8.3.2), we find that the component of the microscopic energy current in the direction of $\mathbf{k}$ is

$$-ikJ^{ez}_{\mathbf{k}} = \frac{\partial}{\partial t} e_{\mathbf{k}} = \frac{\partial}{\partial t}\sum_{i=1}^N \left(\tfrac{1}{2}m|\mathbf{u}_i|^2 + \tfrac{1}{2}\sum_{j\neq i}^N v(r_{ij})\right)\exp(-i\mathbf{k}\cdot\mathbf{r}_i) \tag{8.5.27}$$

where we have adopted the convention that the total potential energy of interaction of two particles is shared equally between them. Differentiation of the quantity inside large brackets gives rise to a term that can be treated by the methods used in calculating the microscopic stress tensor; the final result for $\mathbf{k} = 0$ is

$$J_0^{ez} = \sum_{i=1}^N u_{iz}\left(\tfrac{1}{2}m|\mathbf{u}_i|^2 + \tfrac{1}{2}\sum_{j\neq i}^N v(r_{ij})\right) - \tfrac{1}{2}\sum_{i=1}^N\sum_{j\neq i}^N \mathbf{u}_i\cdot\mathbf{r}_{ij}\frac{\partial v(r_{ij})}{\partial z_{ij}} \tag{8.5.28}$$

The current J_0^{qz} is obtained from J_0^{ez} by subtracting the term $(e+P)\sum_i u_{iz}$; with a suitable choice of frame of reference this term will be zero. Thus we can equally well write the Green–Kubo formula for λ as

$$\lambda = \frac{\beta}{VT}\int_0^\infty \langle J_0^{ez}(t) J_0^{ez}\rangle \,\mathrm{d}t \tag{8.5.29}$$

The correlation-function formulae (or the equivalent Einstein expressions) for D, η, ζ and λ have been used in simulations to determine the transport coefficients of a number of model fluids. A particularly large body of results exists for the hard-sphere fluid, some

of which have already been discussed in Section 8.4. As we saw there, the shear viscosity is in good agreement with the predictions of Enskog theory at densities up to about 80% of that corresponding to the fluid–solid transition, but close to the transition it is larger than the Enskog value by a factor of nearly two. The enhancement of the shear viscosity at high densities is linked numerically to the existence of a long-lived positive tail in the corresponding autocorrelation function. The bulk viscosity is purely potential in origin and vanishes as $\rho \to 0$, but the Enskog result for the thermal conductivity has a structure similar to that displayed for η in (8.4.21), i.e.

$$\frac{\lambda_E}{\lambda_0} = \frac{2\pi\rho d^3}{3}\left(\frac{1}{y} + 1.2 + 0.757y\right) \tag{8.5.30}$$

where $\lambda_0 = (75k_B/64d^2)(k_BT/\pi m)^{1/2}$ is the value in the low-density limit.[5] The potential term (the last term within brackets) again provides the dominant contribution at high densities, but good agreement with molecular-dynamics results is now maintained up to the freezing transition. The success of Enskog theory in the case of λ can be plausibly attributed to the absence of a significant tail in the energy-current autocorrelation function.

8.6 GENERALISED HYDRODYNAMICS

In the earlier sections of this chapter we have shown in some detail how the equations of hydrodynamics can be used to calculate the time-correlation functions of conserved variables in the long-wavelength, low-frequency limit. Two questions then arise. First, what are the scales of length and time over which it is possible to maintain the continuum description that underlies the hydrodynamic approach? Secondly, how can the hydrodynamic equations be modified to make their predictions applicable on the atomic scale, where lengths are typically of order a few ångström units and times are of order 10^{-13} s? We have seen in Chapter 7 that the behaviour of the correlation functions at short times is related to frequency sum rules involving static distribution functions descriptive of the molecular structure of the fluid. It is precisely these sum rules that are violated by hydrodynamic expressions such as (8.4.5) and (8.5.4), since the resulting frequency moments beyond zeroth order all diverge. In addition, an exponential decay, such as that in (8.4.3), cannot satisfy certain of the general properties of time-correlation functions discussed in Section 7.1. The failure of the hydrodynamic approach at short times (or high frequencies) is linked to the presence of dissipative terms in the basic hydrodynamic equations; the latter, unlike the microscopic equations of motion, are not invariant under time reversal. In this section we describe some phenomenological generalisations of the hydrodynamic equations, based on the introduction of frequency and wavenumber-dependent transport coefficients, that have been developed in attempts to bridge the gap between the hydrodynamic (small k, ω) and kinetic (large k, ω) regimes. The use of non-local transport coefficients is closely related to the memory-function approach of Section 7.3, which we develop in more systematic fashion in Chapter 9.

The ideas of *generalised hydrodynamics* are most easily illustrated by considering the example of the transverse-current correlations. Equation (8.4.3) shows that in the hydrodynamic limit the correlation function $C_t(k, t)$ decays exponentially with a relaxation time

equal to $1/\nu k^2$, where ν is the kinematic shear viscosity. The corresponding power spectrum is of lorentzian form:

$$C_t(k,\omega) = \frac{1}{\pi}\mathrm{Re}\,\widetilde{C}_t(k,\omega) = \frac{\omega_0^2}{\pi}\frac{\nu k^2}{\omega^2 + (\nu k^2)^2} \tag{8.6.1}$$

The ω^{-2} behaviour at large ω is not compatible with the exact, high-frequency sum rules such as (7.4.38), nor does (8.6.1) yield the correct free-particle limit of $C_t(k,\omega)$ at large k; that limit is gaussian in form, similar to the longitudinal free-particle limit displayed in (7.5.17). Moreover, molecular-dynamics calculations, which are the only source of "experimental" information on transverse-current fluctuations in atomic liquids, show that in an intermediate wavenumber range $C_t(k,t)$ decays in an oscillatory manner and its power spectrum has a peak at non-zero frequency, suggestive of the existence of a propagating shear mode. (Examples of the power spectra are shown later in Chapter 9, Figure 9.3.) What this means physically is that at high frequencies the fluid has insufficient time to flow in response to an applied strain rate, and instead reacts elastically in the manner of a solid. To account for the appearance of shear waves we need to extend the hydrodynamic description to include the effects of elasticity. Suppose that a shearing force is applied to a fluid. The strain at a point (x, y, z) is expressible in terms of the displacement $\mathbf{r}$ at that point and the rate of strain is expressible in terms of the velocity $\dot{\mathbf{r}}$. If the flow is purely viscous, the shearing stress (an off-diagonal component of the stress tensor $\boldsymbol{\Pi}$) is proportional to the rate-of-strain tensor and can be written as

$$\Pi^{xz} = -\eta\frac{\partial}{\partial t}\left(\frac{\partial r_x}{\partial z} + \frac{\partial r_z}{\partial x}\right) \tag{8.6.2}$$

which is the hydrodynamic form (see (8.3.15)). By contrast, if the force is applied suddenly, the instantaneous displacement is determined by the stress through a typical stress–strain relation, i.e.

$$\Pi^{xz} = -G_\infty\left(\frac{\partial r_x}{\partial z} + \frac{\partial r_z}{\partial x}\right) \tag{8.6.3}$$

where G_∞ is an instantaneous (high-frequency) modulus of rigidity. We can interpolate between these two extremes by making a *viscoelastic* approximation such that

$$\left(\frac{1}{\eta} + \frac{1}{G_\infty}\frac{\partial}{\partial t}\right)\Pi^{xz} = -\frac{\partial}{\partial t}\left(\frac{\partial r_x}{\partial z} + \frac{\partial r_z}{\partial x}\right) \tag{8.6.4}$$

By taking the Laplace transform of (8.6.4) it is easy to show that the viscoelastic approximation is equivalent to replacing η in (8.6.2) by a complex, frequency-dependent shear viscosity given by

$$\tilde{\eta}(\omega) = \frac{G_\infty}{-i\omega + 1/\tau_\mathrm{M}} \tag{8.6.5}$$

The constant $\tau_\mathrm{M} = \eta/G_\infty$ is called the Maxwell relaxation time. If $\omega\tau_\mathrm{M} \ll 1$, $\tilde{\eta}(\omega) \approx \eta$, which corresponds to purely viscous flow, but if $\omega\tau_\mathrm{M} \gg 1$, substitution of (8.6.5) in (8.6.4)

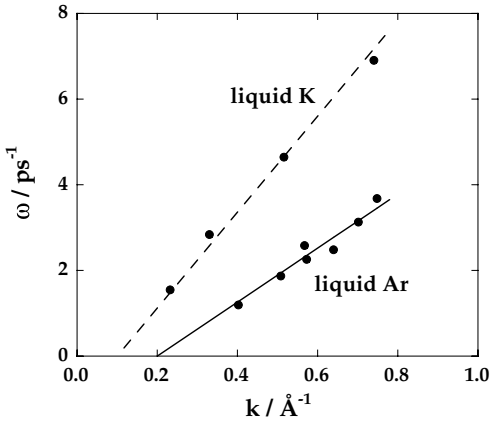

FIG. 8.4. Dispersion of the shear-wave peak derived from molecular-dynamics simulations of liquid argon[9,11] and potassium[12] for state conditions close to the triple point. The dashed line through the data for potassium is a guide to the eye; the full line for argon is drawn with a slope given by the viscoelastic expression (8.6.6) for the speed of propagation (630 m s^{-1}). Results are shown only for the range of k in which the dispersion is approximately linear.

yields a dispersion relation of the form $\omega^2 \approx (G_\infty/\rho m)k^2$, corresponding to elastic waves propagating at a speed

$$c_t = (G_\infty/\rho m)^{1/2} \tag{8.6.6}$$

Figure 8.4 shows the dispersion of the shear-wave peak observed in molecular-dynamics simulations of liquid argon and potassium at state conditions close to their respective triple points. Over the wavenumber range covered by the figure the dispersion is well described by a relation of the form $\omega = c_t(k - k_t)$, where k_t is the wavenumber below which the propagating mode vanishes. In the case of argon, for which a value of G_∞ is available from simulation, the slope of the dispersion curve is in surprisingly good agreement with that calculated from the viscoelastic approximation (8.6.6).

If account is also to be taken of non-local effects in space, the generalised shear viscosity must be a function of wavenumber as well as of frequency. The rigidity modulus is also dependent on k and related in a simple way to the second frequency moment ω_{1t}^2. These ideas can be formalised via a phenomenological generalisation of the hydrodynamic equation (8.4.2):

$$\frac{\partial}{\partial t}C_t(k,t) + k^2 \int_0^t \nu(k, t-s)C_t(k,s)\,\mathrm{d}s = 0 \tag{8.6.7}$$

The quantity $\nu(k,t)$ is a memory function; it describes a response that is non-local in both space and time and its Laplace transform $\tilde{\nu}(k,\omega)$ plays the role of a generalised kinematic viscosity. If we take the Laplace transform of (8.6.7) and compare the result with (8.4.4), we find that $\tilde{\nu}(k,\omega)$ must satisfy the constraint that

$$\lim_{\omega\to 0}\lim_{k\to 0}\tilde{\nu}(k,\omega) = \nu \tag{8.6.8}$$

where ν is the macroscopic kinematic viscosity, given by the Green–Kubo formula (8.4.10). If, on the other hand, we differentiate (8.6.7) with respect to t, set $t = 0$ and use (7.4.37), we find that

$$\nu(k, t = 0) = \frac{\omega_{1t}^2}{k^2} \equiv \frac{G_\infty(k)}{\rho m} \tag{8.6.9}$$

which acts as the definition of the k-dependent shear modulus $G_\infty(k)$. Equations (8.6.8) and (8.6.9) are useful in the construction of approximate forms of $\nu(k, t)$ that reduce to the hydrodynamic and viscoelastic expressions in the limits, respectively, $\omega \to 0$ and $\omega \to \infty$.

If molecular-dynamics results for $C_t(k, t)$ are available, values of the generalised shear viscosity $\tilde{\eta}(k, \omega) = \rho m \tilde{\nu}(k, \omega)$ can be obtained by numerical inversion of (8.6.7) while its value at infinite wavelength, $\tilde{\eta}(k = 0, \omega) \equiv \tilde{\eta}(\omega)$, is given by the Laplace transform of the stress autocorrelation function $\eta(t)$ in (8.4.10). The generalised shear viscosity is believed to be a non-analytic function of both k and ω. For example, molecular-dynamics calculations for hard spheres[13] have shown that $\eta(t)$ decays as $t^{-3/2}$ beyond about ten mean collision times, implying that $\tilde{\eta}(\omega)$ behaves as $\omega^{1/2}$ at low frequencies. If the zero-frequency shear viscosity $\eta(k) \equiv \tilde{\eta}(k, \omega = 0)$ could be expanded in a Taylor series in k about its macroscopic limit, $\eta \equiv \eta(k = 0)$, the series would start as

$$\eta(k) = \eta + \eta_2 k^2 + \cdots \tag{8.6.10}$$

since invariance under space inversion means that only even powers of k can appear. The quantity η_2 is called a Burnett coefficient. Burnett coefficients were introduced in an attempt to extend the range of validity of hydrodynamic equations through the addition of terms of higher order in the gradients of the hydrodynamic fields. However, the indications from mode-coupling theories[14] of the type to be discussed in the section that follows are that the coefficients diverge, implying that the relation between the applied gradients and the induced hydrodynamic fluxes is non-analytic in character. This conclusion is supported by the results of computer simulations of a soft-sphere (r^{-12}) fluid,[15] which are compatible with a small-k behaviour of the form

$$\eta(k) = \eta - \eta_{3/2} k^{3/2} + \cdots \tag{8.6.11}$$

where $\eta_{3/2}$ is a positive quantity. These and related calculations[16] suggest that $\eta(k)$ and other generalised transport coefficients decrease smoothly with increasing wavenumber, becoming an order of magnitude smaller than their macroscopic ($k = 0$) values when the wavelength is comparable with the interparticle spacing.

The longitudinal projections of the hydrodynamic equations can be treated in the same way through the introduction of wavenumber and frequency-dependent quantities that are generalisations of the coefficients a and b defined by (8.3.14) and (8.3.25). Similarly, the thermodynamic derivatives, which are related to static correlation functions, become functions of wavelength.[17] In particular, the macroscopic compressibility is replaced by its k-dependent generalisation, i.e. the structure factor $S(k)$ (see (3.6.11)), while the thermal pressure coefficient, which determines the coupling between momentum and energy, now contains a part that is explicitly dependent on frequency and vanishes in the limit $k \to 0$.

A scheme in which the various thermodynamic and transport coefficients are assumed to be functions only of wavenumber and not of frequency has been found to reproduce satisfactorily a large part of the molecular-dynamics results obtained for the dynamic structure factor of the hard-sphere fluid.[8] This approach breaks down, however, both for wavelengths shorter than the mean free path (corresponding to free-particle behaviour), and at densities close to crystallisation, where viscoelastic effects becomes important.

8.7 LONG-TIME TAILS IN TIME-CORRELATION FUNCTIONS

Fluctuations in the conserved hydrodynamic variables decay infinitely slowly in the long-wavelength limit. The rates of relaxation are determined by the hydrodynamic eigenvalues (8.3.31) and (8.3.35) (multiplied by $-i$), all of which vanish with k. No such property holds for the non-conserved currents that enter the Green–Kubo integrands for the transport coefficients; if it did, the transport coefficients would not be well defined. Until the late 1960s it was generally believed that away from critical points the autocorrelation functions of non-conserved variables decay exponentially at long times. This, for example, is the behaviour predicted by the Boltzmann and Enskog equations. It therefore came as a surprise when analysis of the molecular-dynamics results of Alder and Wainwright[18] on self diffusion in hard-disk ($\mathcal{D} = 2$) and hard-sphere ($\mathcal{D} = 3$) fluids showed that the velocity autocorrelation function apparently decays asymptotically as $t^{-\mathcal{D}/2}$, where $\mathcal{D}$ denotes the dimensionality of the system. Later simulations of hard-core fluids and other systems have also detected the presence of a long-time tail in the stress-tensor autocorrelation function.

The presence of a slowly decaying tail in $Z(t)$ suggests that highly collective effects make a significant contribution to the process of self diffusion. The apparent involvement of large numbers of particles makes it natural to analyse the long-time behaviour in hydrodynamic terms, and Alder and Wainwright were led in this way to a simple but convincing explanation of their results. Underlying their argument is the idea that the initial motion of a tagged particle creates around that particle a vortex or backflow, which in turn causes a retarded current to develop in the direction of the initial velocity. At low densities, where the initial direction of motion is likely to persist, the effect of the current is to reduce the drag on the particle, thereby "pushing" it onwards in the initial direction. This results in a long-lasting, positive correlation between the initial velocity and its value at later times. At high densities, on the other hand, the initial direction of motion is on average soon reversed. In this case the retarded current gives rise to an extra drag at later times and hence to an extended negative region in $Z(t)$; at very large times an enhancement of the forward motion can again be expected but the effect is likely to be undetectable. That this physical picture is basically correct was confirmed in striking fashion by observation of the velocity field that forms around a moving particle in a fluid of hard disks. A vortex pattern quickly develops; this, after a few mean collision times, matches closely the pattern obtained by numerical solution of the Navier–Stokes equation. The persistence of the tail in $Z(t)$ is therefore associated with a coupling between the motion of the tagged particle and the hydrodynamic modes of the fluid. As we shall now show, this argument can be formalised in such a way as to predict the observed $t^{-\mathcal{D}/2}$ decay at long times.[19]

Suppose that at time $t = 0$ a particle i has a component of velocity $u_{ix}(0)$ in the x-direction. After a short time, τ say, collisions will have caused the initial momentum of particle i to be shared among the ρV_τ particles in a $\mathcal{D}$-dimensional volume V_τ centred on i. Local equilibrium now exists within the volume V_τ, and particle i will be moving with a velocity $u_{ix}(\tau) \approx u_{ix}(0)/\rho V_\tau$. (We have assumed, for simplicity, that the neighbours of i are initially at rest.) Further decay in the velocity $u_{ix}(t)$ for $t > \tau$ will occur as the result of enlargement of the volume V_τ, i.e. from the spread of the velocity field around particle i. At large times the dominant contribution to the growth of V_τ will come from diffusion of the transverse component of the velocity field and the radius of V_τ will therefore increase as $(\nu t)^{1/2}$. Thus $V_\tau \sim (\nu t)^{3/2}$ in the three-dimensional case, from which it follows that $Z(t) \sim (\nu t)^{-3/2}$. This argument assumes that particle i remains at the centre of V_τ; if the diffusive motion of i is taken into account it can be shown that

$$Z(t) \sim \left[(D + \nu)t\right]^{-3/2} \tag{8.7.1}$$

The analogous result in two dimensions implies that a self-diffusion coefficient does not exist, because the integral of $Z(t)$ diverges logarithmically.

The form of (8.7.1) has been confirmed by a number of more sophisticated calculations. In the case of hard-core fluids these include a microscopic treatment based on kinetic theory in which account is taken of the effect of correlated collision sequences (the ring collisions of Section 7.2) along with that of uncorrelated, binary collisions.[20] Though limited to low densities, the calculation shows that the velocity, stress-tensor and energy-current autocorrelation functions all decay as $t^{-\mathcal{D}/2}$; it also yields explicit expressions for the coefficients of the long-time tails. A more phenomenological approach has also been developed in which the existence of the long-time tails is explained by simple arguments concerning the decay of fluctuations into pairs of hydrodynamic modes. Since the physical content of this work is closely related to the mode-coupling formalism to be discussed in Chapter 9, we give here a brief derivation of the result obtained in three dimensions for the velocity autocorrelation function.[21]

The definition (7.1.3) of a time-correlation function involves an equilibrium ensemble average over the initial phase-space coordinates of the system. This average can be replaced by a constrained ensemble average, characterised by an initial position $\mathbf{r}_0$ and initial velocity $\mathbf{u}_0$ of a tagged particle i, which is then integrated over all $\mathbf{r}_0$ and $\mathbf{u}_0$. The definition of $Z(t)$ is thereby reformulated as

$$\begin{aligned} Z(t) &= \langle u_{ix}(t)u_{ix}\rangle \\ &= \int \mathrm{d}\mathbf{r}_0 \int \mathrm{d}\mathbf{u}_0\, u_{0x}\langle u_{ix}(t)\delta(\mathbf{u}_i - \mathbf{u}_0)\delta(\mathbf{r}_i - \mathbf{r}_0)\rangle \end{aligned} \tag{8.7.2}$$

The constrained average in (8.7.2) can be written as a non-equilibrium ensemble average (subscript n.e.), defined through the relation

$$\langle u_{ix}(t)\delta(\mathbf{u}_i - \mathbf{u}_0)\delta(\mathbf{r}_i - \mathbf{r}_0)\rangle = \langle u_{ix}(t)\rangle_{\text{n.e.}}\langle\delta(\mathbf{u}_i - \mathbf{u}_0)\delta(\mathbf{r}_i - \mathbf{r}_0)\rangle \tag{8.7.3}$$

In the canonical ensemble the equilibrium average on the right-hand side of (8.7.3) is equal to $1/N$ times the single-particle distribution function defined by (2.1.15) (taken for $n = 1$)

but with $\mathbf{p}$ replaced by $\mathbf{u}$ as independent variable. Equations (8.7.2) and (8.7.3) can therefore be combined to give

$$Z(t) = \frac{1}{V}\int \mathrm{d}\mathbf{r}_0 \int \mathrm{d}\mathbf{u}_0\, \phi_{\mathrm{M}}(\mathbf{u}_0) u_{0x} \langle u_{ix}(t)\rangle_{\mathrm{n.e.}} \tag{8.7.4}$$

where $\phi_{\mathrm{M}}(\mathbf{u}_0)$ is the Maxwell distribution (2.1.28). By defining a tagged-particle distribution function in the non-equilibrium ensemble as

$$f^{(s)}(\mathbf{r}, \mathbf{u}; t) = \langle \delta[\mathbf{r}_i(t) - \mathbf{r}]\delta[\mathbf{u}_i(t) - \mathbf{u}]\rangle_{\mathrm{n.e.}} \tag{8.7.5}$$

we can rewrite the non-equilibrium average in (8.7.4) as

$$\langle u_{ix}(t)\rangle_{\mathrm{n.e.}} = \int \mathrm{d}\mathbf{r} \int \mathrm{d}\mathbf{u}\, u_x f^{(s)}(\mathbf{r}, \mathbf{u}; t) \tag{8.7.6}$$

The calculation thus far is exact. To make progress we assume that $f^{(s)}(\mathbf{r}, \mathbf{u}; t)$ relaxes towards the corresponding local-equilibrium form on a timescale that is fast in comparison with the rate of decay of $Z(t)$. The long-time behaviour of the non-equilibrium average (8.7.6) is then obtained by replacing $f^{(s)}(\mathbf{r}, \mathbf{u}; t)$ by the tagged-particle analogue of (8.1.5) to give

$$\langle u_{ix}(t)\rangle_{\mathrm{n.e.}} = \int \rho^{(s)}(\mathbf{r}, t) u_x(\mathbf{r}, t)\, \mathrm{d}\mathbf{r} \tag{8.7.7}$$

If this result is in turn substituted in (8.7.4), and the hydrodynamic variables $\mathbf{u}(\mathbf{r}, t)$ and $\rho^{(s)}(\mathbf{r}, t)$ are replaced by the sums of their Fourier components, we find that

$$\begin{aligned} Z(t) = \frac{1}{3V}\int \mathrm{d}\mathbf{r}_0 \int \mathrm{d}\mathbf{u}_0\, \phi_{\mathrm{M}}(\mathbf{u}_0) \\ \times \frac{1}{V^2}\sum_{\mathbf{k}}\sum_{\mathbf{k}'} \rho^{(s)}_{\mathbf{k}'}(t)\mathbf{u}_{\mathbf{k}}(t)\cdot\mathbf{u}_0 \int \exp[-i(\mathbf{k}+\mathbf{k}')\cdot\mathbf{r}]\,\mathrm{d}\mathbf{r} \end{aligned} \tag{8.7.8}$$

The integral over $\mathbf{r}$ is equal to $V\delta_{\mathbf{k},-\mathbf{k}'}$ and (8.7.8) therefore reduces to

$$Z(t) = \frac{1}{3V}\int \mathrm{d}\mathbf{r}_0 \int \mathrm{d}\mathbf{u}_0\, \phi_{\mathrm{M}}(\mathbf{u}_0) \frac{1}{V}\sum_{\mathbf{k}} \rho^{(s)}_{-\mathbf{k}}(t)\mathbf{u}_{\mathbf{k}}(t)\cdot\mathbf{u}_0 \tag{8.7.9}$$

Equation (8.7.9) is said to be of "mode-coupling" form, because $Z(t)$ is expressed as a sum of products of pairs of hydrodynamic variables. We assume, in addition, that at times much longer than the mean collision time the decay of $Z(t)$ is dominated by the long-wavelength components of the hydrodynamic fields and that the time evolution of the latter is described by the equations of linearised hydrodynamics. The quantity $\rho^{(s)}_{-\mathbf{k}}(t)$ is then given by (8.2.5), while the hydrodynamic velocity field is conveniently divided into its longitudinal and transverse parts:

$$\mathbf{u}_{\mathbf{k}}(t) = \mathbf{u}_{\mathbf{k}l}(t) + \mathbf{u}_{\mathbf{k}t}(t) \tag{8.7.10}$$

The term $\mathbf{u}_{\mathbf{k}t}(t)$ satisfies the transverse-current diffusion equation (8.4.1) (with $\mathbf{j}_{\mathbf{k}t} = \rho\mathbf{u}_{\mathbf{k}t}$), the solution to which is

$$\mathbf{u}_{\mathbf{k}t}(t) = \mathbf{u}_{\mathbf{k}t}\exp\bigl(-\nu k^2 t\bigr) \tag{8.7.11}$$

The longitudinal velocity field may be treated in a similar way, but its contribution to $Z(t)$ turns out to decay exponentially, the physical reason for this being the fact that the momentum of the tagged particle is carried away by the propagating sound waves. Hence the long-time behaviour of $Z(t)$ is entirely determined by the transverse velocity field. Finally, the choice of initial conditions implies that

$$\rho_{-\mathbf{k}}^{(s)} = \exp(i\mathbf{k}\cdot\mathbf{r}_0) \tag{8.7.12a}$$

$$\mathbf{j}_{\mathbf{k}} = \rho\mathbf{u}_{\mathbf{k}} = \mathbf{u}_0\exp(-i\mathbf{k}\cdot\mathbf{r}_0) \tag{8.7.12b}$$

An expression for $Z(t)$ is now obtained by substituting (8.7.11), (8.7.12a) and the transverse projection of (8.7.12b) into (8.7.9) (remembering that there are two transverse components), and integrating over $\mathbf{r}_0$ and $\mathbf{u}_0$. The result is

$$Z(t) = \frac{2k_{\mathrm{B}}T}{3\rho m V}\sum_{\mathbf{k}}\exp\bigl[-(D+\nu)k^2 t\bigr] \tag{8.7.13}$$

or, in the thermodynamic limit:

$$Z(t) = \frac{2k_{\mathrm{B}}T}{3\rho m}(2\pi)^{-3}\int\exp\bigl[-(D+\nu)k^2 t\bigr]\,\mathrm{d}\mathbf{k} \tag{8.7.14}$$

Integration over all wavevectors is a questionable procedure, since the hydrodynamic equations on which (8.7.14) is based are not valid when k is large. However, we are interested only in the asymptotic form of $Z(t)$, and the main contribution to the integral comes from wavenumbers such that $k \approx [(D+\nu)t]^{-1/2}$; this is in the hydrodynamic range whenever t is much larger than typical microscopic times ($\sim 10^{-13}$) s. Alternatively, a natural upper limit on k can be introduced by a more careful choice of the initial spatial distribution of tagged particles. Use of such a cut-off has no effect on the predicted long-time behaviour that results from carrying out the integration in (8.7.14), namely

$$Z(t) \sim \frac{2k_{\mathrm{B}}T}{3\rho m}\bigl[4\pi(D+\nu)t\bigr]^{-3/2}, \quad t\to\infty \tag{8.7.15}$$

This has the same general form as (8.7.1) but it also provides an explicit expression for the coefficient of the long-time tail.

The result in (8.7.15) has been confirmed by molecular-dynamics calculations for systems of hard discs and of particles interacting through a Lennard-Jones potential truncated at $r = 2^{1/6}\sigma$, the separation at which $v(r)$ has its minimum value; the simulations are difficult to carry out with the necessary precision because the long-time tail is very weak.[22] Results obtained for the truncated Lennard-Jones potential are shown in Figure 8.5, where

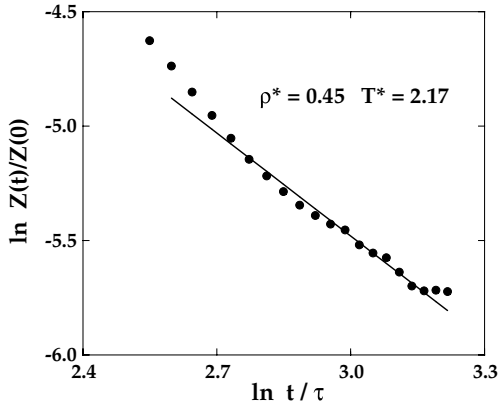

FIG. 8.5. Log–log plot of the velocity autocorrelation function versus time for a system of particles interacting through a truncated Lennard-Jones potential. The points are molecular-dynamics results and the line is drawn with a slope equal to $-\frac{3}{2}$. The unit of time is $\tau = (m\sigma^2/48\varepsilon)^{1/2}$. After Levesque and Ashurst.[22]

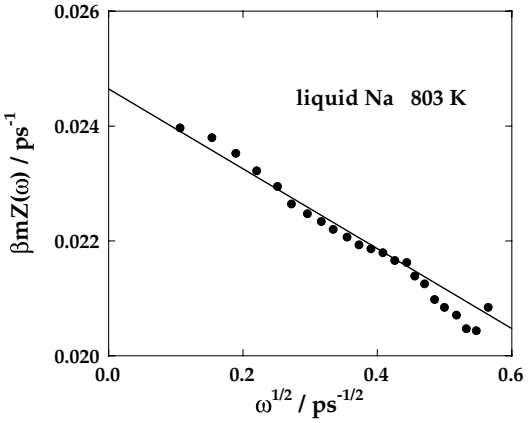

FIG. 8.6. Power spectrum of the velocity autocorrelation function of liquid sodium as a function of $\omega^{1/2}$. The points are derived from inelastic neutron-scattering measurements and the line is a least-squares fit to the data. After Morkel *et al*.[23]

$Z(t)$ is plotted versus t on a log–log scale. If (5.3.5) is used to define an effective hard-sphere diameter for the particles, the onset of the asymptotic behaviour is found to come after approximately 18 mean collision times. The predicted long-time behaviour of $Z(t)$ implies that at low frequencies its Fourier transform behaves as

$$Z(\omega) = \frac{D}{\pi}\left[1 - (\omega_0/\omega)^{1/2} + \cdots\right] \tag{8.7.16}$$

where ω_0 is related to the transport coefficients D and ν. Experimentally, evidence for the presence of a long-time tail can be derived from neutron-scattering measurements of the

self dynamic structure factor, provided results are obtained at sufficiently small values of k to allow the extrapolation required in (8.2.18) to be successfully carried through. Figure 8.6 shows some results obtained for liquid sodium at a temperature well above the melting point (the effect at low temperatures is too weak to be detectable). Not only is the square-root dependence on ω well reproduced, but the value obtained for ω_0 from a least-squares fit to the data lies within 2% of that predicted by mode-coupling theory.

8.8 DYNAMICS OF SUPERCOOLED LIQUIDS

When a liquid is slowly cooled (or compressed) it normally undergoes a transition to an ordered, crystalline phase at a temperature located on the equilibrium liquid–solid coexistence curve. However, if the rate of cooling (or compression) is sufficiently rapid, crystallisation can be by-passed; in that case the liquid is gradually transformed into an amorphous solid or glass. The glass-transition temperature T_G is less than the freezing temperature, but its value depends on factors such as the cooling rate and the diagnostic used to locate the transition; it is not an intrinsic property of the system. Relaxation times in the supercooled liquid measured, for example, in dielectric or shear-stress relaxation experiments, increase dramatically with decreasing temperature and close to the glass transition become comparable with macroscopic time-scales. A rough but useful estimate of T_G is provided by the viscoelastic theory of Section 8.6, which shows that a crossover from viscous to elastic behaviour can be expected when the structural relaxation time of the system becomes of the order of the Maxwell relaxation time, defined as the ratio of shear viscosity to shear modulus, $\tau_M = \eta/G_\infty$. The shear modulus is of order 10^{10} erg cm^{-1} for most materials and is only weakly dependent on temperature, but the shear viscosity rises by many orders of magnitude as the temperature approaches T_G. An implicit definition of T_G is obtained by identifying τ_M with some experimental time-scale, τ_{exp}. A choice of 10^3 s for τ_{exp} leads to the conventional definition of T_G as the temperature at which the viscosity reaches a value of 10^{13} poise (1 P $\equiv$ 0.1 N s m^{-2}). Below this temperature, the system exists in a metastable state having a disordered, liquid-like structure but with mechanical properties similar to those of a crystalline solid. The freezing-out of the translational and rotational degrees of freedom at the glass transition leads in many cases to anomalies in the temperature dependence of thermodynamic properties such as the specific heat. The change in behaviour at T_G is therefore described as a "thermodynamic" or "calorimetric" phase transition, though its nature is very different from that of an equilibrium phase transition.

Glass-forming liquids appear to fall into one of two broad classes: "strong" and "fragile".[24] The difference between the two is particularly evident in the way in which the viscosity changes with temperature, as exemplified by the Arrhenius plots shown in Figure 8.7. Strong glass formers are covalently bonded, network-forming substances such as silica; the network already exists in the high-temperature melt and gradually strengthens as the liquid is supercooled. The calorimetric anomalies near T_G are weak, or may be absent altogether, and the Arrhenius plots are essentially linear, implying that transport in the liquid is largely governed by thermally activated processes or "barrier hopping". The anomalies are stronger for the ionic and organic liquids that make up the class of fragile glass formers. The Arrhenius plots of such materials show a marked change in curvature

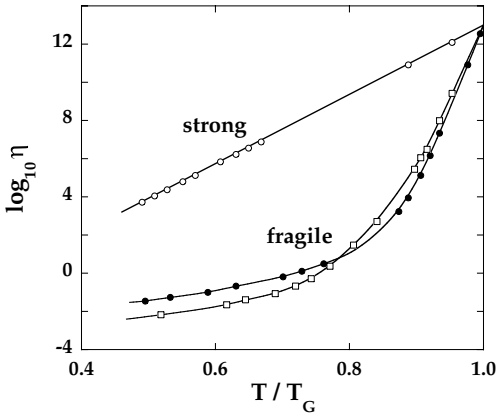

FIG. 8.7. Arrhenius plots of the shear viscosities (in poise) of three glass-forming liquids, showing the difference in behaviour between strong and fragile glass formers. Open circles: silica; squares: o-terphenyl; filled circles: an ionic melt of composition $[KNO_3]_{0.6}[Ca(NO)_3)_2]_{0.4}$. After Angell.[24]

at a temperature T_C lying some 10 to 20% above T_G; this is suggestive of a qualitative change in character of the microscopic dynamics over a narrow temperature interval. When $T \approx T_C$, the Maxwell relaxation time is in the nanosecond range. This is a time-scale well suited to studies of the dynamics by neutron and light-scattering experiments and other experimental probes as well as by molecular-dynamics simulation, and there is now ample evidence to show that as the temperature is lowered towards T_C there is a dramatic slowing down in the decay of time-dependent correlation functions. The crossover in behaviour near T_C seen, for example, in Figure 8.7, corresponds to what is called a *kinetic glass transition*. Experiment and simulation also show that structural and thermodynamic properties vary smoothly with temperature in the region of the transition. It is therefore reasonable to suppose that the supercooled liquid remains in a state of thermodynamic equilibrium and that equilibrium statistical mechanics applies once crystallisation has been by-passed. This is the key assumption underlying the mode-coupling theory of the transition, which we describe later in Section 9.6.

The nature of the changes that take place at the kinetic glass transition are well illustrated by the results shown in Figures 8.8 and 8.9. Those in Figure 8.8 are taken from a simulation of a binary,[26] soft-sphere (r^{-12}) fluid and show the behaviour for one of the two species of the probability density

$$W(r,t) = 4\pi r^2 G_s(r,t) \tag{8.8.1}$$

where $G_s(r,t)$ is the self part (7.4.19a) of the van Hove function; the quantity $W(r,t)\,\mathrm{d}r$ is the probability of finding a particle at time t at a distance r from its position at $t = 0$. The thermodynamic state of the system is specified by a single coupling constant, Γ, defined in a manner similar to (5.3.13) but generalised to allow for the two-component nature of the system. A decrease in temperature is therefore strictly equivalent to an increase in density. The inset to the figure shows the results obtained for three different times at a value of Γ corresponding to a temperature above T_C. The curve has a single peak, which moves

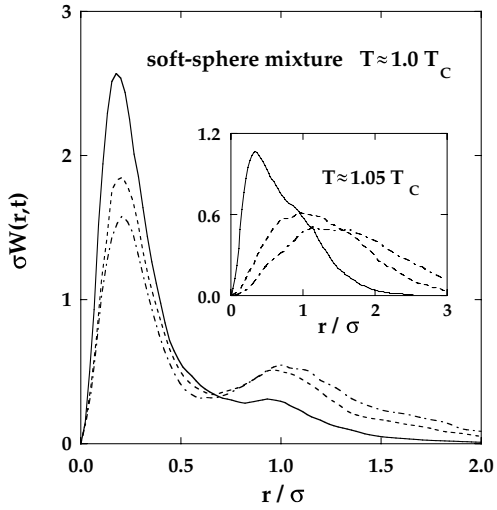

FIG. 8.8. Molecular-dynamics results for the probability density for diffusion of particles of one species in a two-component soft-sphere fluid at temperatures in the supercooled region. See text for details. Results are shown for three different values of the reduced time $t^* = t/\tau$. Full curves: $t^* = 100$; dashes: $t^* = 300$; chain curves: $t^* = 500$. For argon-like values of the potential parameters and particle masses, $\tau \approx 2$ ps; σ is an averaged size parameter. After Barrat *et al.*[25]

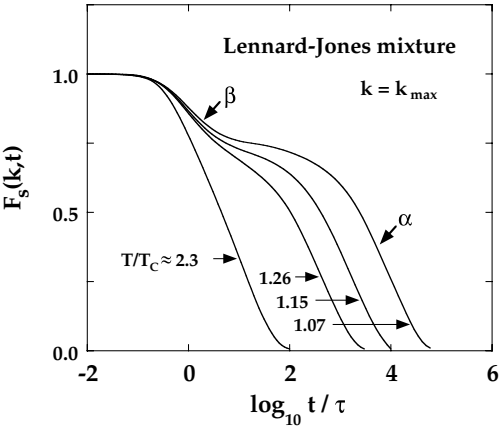

FIG. 8.9. Molecular-dynamics results for the self intermediate scattering function for particles of one species in a two-component Lennard-Jones fluid at temperatures in the supercooled region; $k_{\max}$ is the wavenumber corresponding to the main peak in the static structure factor. The labels α, β mark the two different relaxation regimes discussed in the text. For argon-like values of the potential parameters and particle masses, the unit of time is $\tau \approx 0.3$ ps. After Kob and Andersen.[27]

to larger r according to a $t^{1/2}$ law, in agreement with the result derived from Fick's law (see (8.2.8)). However, the qualitative behaviour changes dramatically above a threshold value of Γ, which can be identified with the crossover value Γ_{C}. The peak in $W(r,t)$ now

appears to be frozen at a fixed value of r and its amplitude decreases only slowly with time as a secondary maximum builds up at a distance from the main peak roughly equal to the mean spacing between particles. The physical interpretation of this bimodal distribution is clear: most atoms vibrate around fixed, disordered positions, but some diffuse slowly by correlated hopping to neighbouring sites. The two values of Γ for which the results are shown correspond to temperatures differing by less than 6%. Thus the diffusion mechanism changes very rapidly from one that is hydrodynamic-like to one consisting of a succession of activated jumps.

The same, pronounced slowing down of the single-particle motion as a threshold temperature is reached is also visible in the behaviour of the self intermediate scattering function $F_s(k,t)$. Some results obtained by molecular-dynamics calculations for a binary Lennard-Jones system are shown in Figure 8.9, where time is plotted on a logarithmic scale. At high temperatures, $F_s(k,t)$ relaxes to zero in nearly exponential fashion. However, as the temperature is lowered into the supercooled region, the decay becomes very much slower and its exponential character is lost. As T approaches T_C, the relaxation proceeds in two, increasingly well-separated steps. After a fast initial decay on the time-scale of an inverse Einstein frequency, a first step (β-relaxation) leads to a plateau, where the function remains almost constant over two or more decades in time. The plateau is followed by a second step (α-relaxation) in which the correlation function finally decays to zero. The width of the plateau increases rapidly as the temperature is reduced. Eventually, when the temperature is sufficiently low, α-relaxation can be expected to set in only at times longer than those accessible in a simulation. The correlation function will then appear to level off at a non-zero value, signalling the onset of non-ergodic behaviour, at least on the (nanosecond) time-scale of the simulation. The plateau value varies with k, but the general pattern seen in Figure 8.9 remains much the same over a wide range of molecular-scale wavenumber.

The decay of collective density fluctuations, as described by the full intermediate scattering function $F(k,t)$ defined by (7.4.20) and measurable either experimentally or by simulation, shows a qualitatively similar behaviour to that of the single-particle function. The plateau value of $F(k,t)$ is analogous to the Debye–Waller factor of a solid; it provides a measure of the "structural arrest" in the fluid, which persists for times that increase rapidly with decreasing temperature. Over a temperature range just above T_C, the decay of either function in the α-relaxation regime, normalised by its value at $t = 0$, can be accurately represented by a function of the form

$$f(t) = f_k \Phi(t^*) \tag{8.8.2}$$

where f_k is the plateau value, $t^* \equiv t/\tau_k(T)$ and $\Phi(t^*)$ is a universal scaling function. The wavenumber and temperature dependence of the decay enter only through the relaxation time $\tau_k(T)$ and the correlation functions are said to satisfy a "time–temperature superposition" principle. The scaling function is distinctly non-exponential, but is generally well-approximated by a Kohlrausch stretched-exponential function, i.e.

$$\Phi(t^*) \approx \exp\left[-(t^*)^\beta\right] \tag{8.8.3}$$

where the exponent β (< 1 for "stretching") is material and wavenumber dependent but independent of temperature.[28] Stretched-exponential behaviour is typical of relaxation

processes in which the observed rate is determined by a wide distribution of relaxation times.

NOTES AND REFERENCES

1. Rahman, A., *Phys. Rev.* **136**, A405 (1964). Deviations from gaussian behaviour increase rapidly as a liquid is supercooled: see, e.g., Bernu, B., Hansen, J.P., Hiwatari, Y. and Pastore, G., *Phys. Rev. A* **36**, 4891 (1987).
2. Landau, L.D. and Lifshitz, E.M., "Fluid Mechanics", 2nd edn. Butterworth-Heinemann, Oxford, 1987, p. 44.
3. See, e.g., Reif, F., "Fundamentals of Statistical and Thermal Physics". McGraw-Hill, New York, 1965, p. 168.
4. (a) Mountain, R.D., *Rev. Mod. Phys.* **38**, 205 (1966). (b) Berne, B.J. and Pecora, R., "Dynamic Light Scattering". John Wiley, New York, 1976.
5. Chapman, S. and Cowling, T.G., "The Mathematical Theory of Non-Uniform Gases", 3rd edn. Cambridge University Press, Cambridge, 1970, p. 308. For a simplified discussion of the Boltzmann and Enskog equations see, e.g., Reed, T.M. and Gubbins, K.E., "Applied Statistical Mechanics". McGraw-Hill, New York, 1973.
6. This is not the same effect as the $t^{-3/2}$ tail referred to in Sections 8.6 and 8.8.
7. A particularly comprehensive neutron-scattering study is that of liquid Rb by Copley, J.R.D. and Rowe, J.M., *Phys. Rev. A* **9**, 1656 (1974). For inelastic x-ray scattering and references to earlier scattering experiments on liquid metals see, e.g., Scopigno, T., Balucani, U., Ruocco, G. and Sette, F., *Phys. Rev. E* **65**, 031205 (2002).
8. Alley, W.E., Alder, B.J. and Yip, S., *Phys. Rev. A* **27**, 3174 (1983).
9. Levesque, D., Verlet, L. and Kürkijarvi, J., *Phys. Rev. A* **7**, 1690 (1973).
10. Bodensteiner, T., Morkel, C., Gläser, W. and Dorner, B., *Phys. Rev. A* **45**, 5709 (1992); erratum: *Phys. Rev. A* **46**, 3574 (1992).
11. Rahman, A., *In* "Neutron Inelastic Scattering", vol. 1. IAEA, Vienna, 1968.
12. Jacucci, G. and McDonald, I.R., *Mol. Phys.* **39**, 515 (1980).
13. Erpenbeck, J.J. and Wood, W.W., *J. Stat. Phys.* **24**, 455 (1981).
14. Keyes, T. and Oppenheim, I., *Physica* **70**, 100 (1973).
15. Evans, D.J., *Mol. Phys.* **47**, 1165 (1982).
16. (a) Alley, W.E. and Alder, B.J., *Phys. Rev. A* **27**, 3158 (1983). (b) Kambayashi, S. and Kahl, G., *Phys. Rev. A* **46**, 3255 (1992).
17. Schofield, P., *Proc. Phys. Soc.* **88**, 149 (1966).
18. Alder, B.J. and Wainwright, T.E., *Phys. Rev. Lett.* **18**, 988 (1967). (b) Alder, B.J. and Wainwright, T.E., *Phys. Rev. A* **1**, 18 (1970).
19. Pomeau, Y. and Résibois, P., *Phys. Rep.* **19**, 63 (1975).
20. (a) Dorfman, J.R. and Cohen, E.G.D., *Phys. Rev. A* **6**, 776 (1972). (b) Dorfman, J.R. and Cohen, E.G.D., *Phys. Rev. A* **12**, 292 (1975).
21. (a) Ernst, M.H., Hauge, E.H. and van Leeuwen, J.M.J., *Phys. Rev. A* **4**, 2055 (1971). (b) Erpenbeck, J.J. and Wood, W.W., *Phys. Rev. A* **26**, 1648 (1982).
22. Levesque, D. and Ashurst, W.T., *Phys. Rev. Lett.* **33**, 277 (1974). The conclusions of this paper were later confirmed, with much higher precision, by simulations of a lattice-gas model for which the equations of motion can be solved exactly: see van der Hoef, M.A. and Frenkel, D., *Phys. Rev. A* **41**, 4277 (1990).
23. Morkel, C., Gronemeyer, C., Gläser, W. and Bosse, J., *Phys. Rev. Lett.* **58**, 1873 (1987).
24. This classification is due to Angell, C.A., *J. Phys. Chem. Solids* **49**, 863 (1988).
25. Barrat, J.L., Roux, J.N. and Hansen, J.P., *Chem. Phys.* **149**, 198 (1990).
26. Simulations of the glass transition are commonly carried out on mixed systems as a device to inhibit crystallisation.
27. Kob, W. and Andersen, H.C., *Phys. Rev. E* **52**, 4134 (1995).
28. The conventional use of β for the Kohlrausch exponent is unfortunate, since it refers to the decay in the α-relaxation regime.

CHAPTER 9

Theories of Time-correlation Functions

We turn now to the problem of devising a general theoretical scheme for the calculation of time-correlation functions at wavelengths and frequencies on the molecular scale. Memory functions play a key role in the theoretical development and we begin by showing how the memory-function approach can be formalised through use of the projection-operator methods of Zwanzig[1] and Mori.[2] The calculation of the memory function in a specific problem is a separate task that can be tackled along two different lines. The first represents a systematic extension of the ideas of generalised hydrodynamics introduced in Section 8.6; the second is more microscopic in nature and based on the mode-coupling approach already used in Section 8.7.

9.1 THE PROJECTION-OPERATOR FORMALISM

Let A be some dynamical variable, dependent in general on the coordinates and momenta of all particles in the system. The definition of A is assumed to be made in such a way that its mean value is zero, but this involves no loss of generality. We have seen in Section 7.1 that if the phase function A is represented by a vector in Liouville space, the inner product $(B, A(t))$ of $A(t)$ with the vector representing a second variable B may be identified with the equilibrium time-correlation function $C_{AB}(t)$. We can also use a vector in Liouville space to represent a set of dynamical variables of the system, but for the present we restrict ourselves to the single-variable case.

The time variation of the vector $A(t)$ is given by the exact equation of motion (2.1.14). Our aim is to find an alternative to (2.1.14) that is also exact but more easily usable. We proceed by considering the time evolution both of the projection of $A(t)$ onto A (the *projected* part), and of the component of $A(t)$ normal to A (the *orthogonal* part), which we denote by the symbol $A'(t)$. The projection of a second variable $B(t)$ onto A can be written in terms of a linear *projection operator* $\mathcal{P}$ as

$$\mathcal{P}B(t) = (A, A)^{-1}\big(A, B(t)\big)A \tag{9.1.1}$$

Thus

$$\big(\mathcal{P}B(t), A\big) = \big(A, B(t)\big) \equiv \big\langle B(t)A^*\big\rangle \tag{9.1.2}$$

The complementary operator $\mathcal{Q} = 1 - \mathcal{P}$ projects onto the subspace orthogonal to A. Hence the orthogonal part of $A(t)$ is

$$A'(t) = \mathcal{Q}A(t) \tag{9.1.3}$$

Both $\mathcal{P}$ and $\mathcal{Q}$ satisfy the fundamental properties of projection operators:

$$\mathcal{P}^2 = \mathcal{P}, \qquad \mathcal{Q}^2 = \mathcal{Q}, \qquad \mathcal{P}\mathcal{Q} = \mathcal{Q}\mathcal{P} = 0 \tag{9.1.4}$$

The projection of $A(t)$ along A is proportional to $Y(t)$, the normalised time autocorrelation function of the variable A, i.e.

$$\mathcal{P}A(t) = Y(t)A \tag{9.1.5}$$

with

$$Y(t) = \big(A, A(t)\big)(A, A)^{-1} \equiv \big\langle A(t)A^* \big\rangle \langle AA^* \rangle^{-1} = C_{AA}(t)/C_{AA}(0) \tag{9.1.6}$$

The definitions (9.1.1) to (9.1.3) ensure that

$$\big(A, A'(t)\big) = 0 \tag{9.1.7}$$

The first step is to derive an equation for the time evolution of the projected part, $Y(t)$. The Laplace transform of the equation of motion (2.1.14) is

$$(z + \mathcal{L})\tilde{A}(z) \equiv (z + \mathcal{L})(\mathcal{P} + \mathcal{Q})\tilde{A}(z) = iA \tag{9.1.8}$$

Thus

$$\begin{aligned} \widetilde{Y}(z) &= \left(A, \int_0^\infty \exp(izt) \exp(i\mathcal{L}t) A \, \mathrm{d}t \right) (A, A)^{-1} \\ &= \big(A, i(z + \mathcal{L})^{-1} A\big)(A, A)^{-1} = \big(A, \tilde{A}(z)\big)(A, A)^{-1} \end{aligned} \tag{9.1.9}$$

where the "resolvent" operator $i(z + \mathcal{L})^{-1}$ is the Laplace transform of the propagator $\exp(i\mathcal{L}t)$. We now project (9.1.8) parallel and perpendicular to A by application, respectively, of the operators $\mathcal{P}$ and $\mathcal{Q}$. Use of the properties (9.1.4) shows that

$$z\mathcal{P}\tilde{A}(z) + \mathcal{P}\mathcal{L}\mathcal{P}\tilde{A}(z) + \mathcal{P}\mathcal{L}\mathcal{Q}\tilde{A}(z) = iA \tag{9.1.10}$$

$$z\mathcal{Q}\tilde{A}(z) + \mathcal{Q}\mathcal{L}\mathcal{P}\tilde{A}(z) + \mathcal{Q}\mathcal{L}\mathcal{Q}\mathcal{Q}\tilde{A}(z) = 0 \tag{9.1.11}$$

and elimination of $\mathcal{Q}\tilde{A}(z)$ between (9.1.10) and (9.1.11) gives

$$z\mathcal{P}\tilde{A}(z) + \mathcal{P}\mathcal{L}\mathcal{P}\tilde{A}(z) - \mathcal{P}\mathcal{L}\mathcal{Q}(z + \mathcal{Q}\mathcal{L}\mathcal{Q})^{-1}\mathcal{Q}\mathcal{L}\mathcal{P}\tilde{A}(z) = iA \tag{9.1.12}$$

If we now take the inner product with A and multiply through by $-i(A, A)^{-1}$, (9.1.12) becomes

$$-iz\tilde{Y}(z) - i\big(A, \mathcal{L}\mathcal{P}\tilde{A}(z)\big)(A, A)^{-1} + i\big(A, \mathcal{L}\mathcal{Q}(z + \mathcal{Q}\mathcal{L}\mathcal{Q})^{-1}\mathcal{Q}\mathcal{L}\mathcal{P}\tilde{A}(z)\big)(A, A)^{-1} = 1 \tag{9.1.13}$$

Since $i\mathcal{L}\mathcal{P}\tilde{A}(z) = (A, A)^{-1}(A, \tilde{A}(z))\dot{A}$, this expression can be rewritten as

$$(-iz - i\Omega)\tilde{Y}(z) + \big(K, \tilde{R}(z)\big)(A, A)^{-1}\tilde{Y}(z) = 1 \tag{9.1.14}$$

where

$$K = \mathcal{Q}\dot{A} = \mathcal{Q}(i\mathcal{L})A \tag{9.1.15}$$

is the projection of $\dot{A}$ orthogonal to A and we have introduced the quantity

$$\tilde{R}(z) = i(z + \mathcal{Q}\mathcal{L}\mathcal{Q})^{-1}K \tag{9.1.16}$$

and defined a frequency Ω as

$$i\Omega = (A, \dot{A})(A, A)^{-1} = \dot{Y}(0) \tag{9.1.17}$$

In the single-variable case the frequency Ω is identically zero for systems with continuous interactions, since all autocorrelation functions are even functions of time, but we retain the term in Ω here to facilitate the later generalisation to the multi-variable description.

The projection K is conventionally termed a "random force". If A is the momentum of particle i, $\dot{A}$ is the total force acting on i and K is then the random force of the classic Langevin theory described in Section 7.3. In other cases, however, K is not a force in the mechanical sense. Instantaneously, K and $\dot{A}$ are the same, but the two quantities evolve differently in time. The time-dependence of the random force is given by the Laplace transform of $\tilde{R}(z)$:

$$R(t) = \exp(i\mathcal{Q}\mathcal{L}\mathcal{Q}t)K \tag{9.1.18}$$

with $R(0) = K$. The special form of its propagator means that $R(t)$ remains at all times in the subspace orthogonal to A, i.e.

$$\big(A, R(t)\big) = 0 \quad \text{for all } t \tag{9.1.19}$$

This is easily proved by expanding the right-hand side of (9.1.18) in powers of t, since it is clear by inspection that every term in the series is orthogonal to A. The expansion also makes it clear that the propagator in (9.1.18) can equally well be written as $\exp(i\mathcal{Q}\mathcal{L}t)$ and both forms appear in the literature. The autocorrelation function of the random force defines the memory function $M(t)$ for the evolution of the dynamical variable A:

$$M(t) = \big(R, R(t)\big)(A, A)^{-1} \tag{9.1.20}$$

or

$$\widetilde{M}(z) = \big(R, \widetilde{R}(z)\big)(A, A)^{-1} \tag{9.1.21}$$

Equation (9.1.14) can be rewritten in terms of the memory function as

$$\widetilde{Y}(z) = \big[-iz - i\Omega + \widetilde{M}(z)\big]^{-1} \tag{9.1.22}$$

or, in the time domain, as

$$\dot{Y}(t) - i\Omega Y(t) + \int_0^t M(t-s)Y(s)\,\mathrm{d}s = 0 \tag{9.1.23}$$

The equation describing the time evolution of the orthogonal component $A'(t)$ is obtained along similar lines. From (9.1.11) we find that for $\tilde{A}'(z) = \mathcal{Q}\tilde{A}(z)$:

$$\begin{aligned}(z + \mathcal{Q}\mathcal{L}\mathcal{Q})\tilde{A}'(z) &= -\mathcal{Q}\mathcal{L}\mathcal{P}\tilde{A}(z) \\ &= -\mathcal{Q}\mathcal{L}\widetilde{Y}(z)A = i\widetilde{Y}(z)K\end{aligned} \tag{9.1.24}$$

If we substitute for $\widetilde{Y}(z)$ from (9.1.22) and use the definition of $\widetilde{R}(z)$ in (9.1.16), (9.1.24) becomes

$$\widetilde{R}(z) = \big[-iz - i\Omega + \widetilde{M}(z)\big]\tilde{A}'(z) \tag{9.1.25}$$

or, in the time domain:

$$\dot{A}'(t) - i\Omega A'(t) + \int_0^t M(t-s)A'(s)\,\mathrm{d}s = R(t) \tag{9.1.26}$$

Equations (9.1.23) and (9.1.26) are the projections parallel and perpendicular to the variable A of a generalised Langevin equation for A:

$$\dot{A}(t) - i\Omega A(t) + \int_0^t M(t-s)A(s)\,\mathrm{d}s = R(t) \tag{9.1.27}$$

Apart from the introduction of the term in Ω, (9.1.27) has the same general form as the Langevin equation (7.3.21), but the random force $R(t)$ and memory function $M(t)$ now have the explicit definitions provided by (9.1.18) and (9.1.20).

There is a close connection between the behaviour of the functions $Y(t)$ and $M(t)$ at short times, a fact we have already exploited in Section 7.3. When differentiated with respect to time the memory-function equation (9.1.23) becomes

$$\ddot{Y}(t) - i\Omega\dot{Y}(t) + M(0)Y(t) + \int_0^t \dot{M}(t-s)Y(s)\,\mathrm{d}s = 0 \tag{9.1.28}$$

Since $Y(0) = 1$ and $\dot{Y}(0) = i\Omega$, we see that

$$M(0) = -\ddot{Y}(0) - \Omega^2 = (\dot{A}, \dot{A})(A, A)^{-1} - \Omega^2 \tag{9.1.29}$$

Repeated differentiation leads to relations between the initial time derivatives of $Y(t)$ and $M(t)$ or, equivalently, given (7.1.24), between the frequency moments of the power spectra $Y(\omega)$ and $M(\omega)$. These relations are useful in constructing simple, approximate forms for $M(t)$ that satisfy the low-order sum rules on $Y(t)$. A link also exists between the autocorrelation function of the random force, i.e. the memory function, and that of the total force, $\dot{A}$. Let $\Phi(t)$ be the autocorrelation function of $\dot{A}$, defined as

$$\Phi(t) = \big(\dot{A}, \dot{A}(t)\big)(A, A)^{-1} = -\ddot{Y}(t) \tag{9.1.30}$$

It follows from the properties of the Laplace transform that the functions $\widetilde{\Phi}(z)$ and $\widetilde{Y}(z)$ are related by

$$\widetilde{\Phi}(z) = z^2\widetilde{Y}(z) - iz + i\Omega \tag{9.1.31}$$

Since the term $i\Omega$ vanishes in the one-variable case, we may temporarily discard it. Then elimination of $\widetilde{Y}(z)$ between (9.1.22) and (9.1.31) leads to the expression

$$\frac{1}{\widetilde{M}(z)} = \frac{1}{\widetilde{\Phi}(z)} + \frac{1}{iz} \tag{9.1.32}$$

The two autocorrelation functions therefore vary with time in different ways except in the high-frequency (short-time) limit: the time dependence of $\Phi(t)$ is determined by the full Liouville operator $\mathcal{L}$ and that of $M(t)$ by the projected operator $\mathcal{Q}\mathcal{L}\mathcal{Q}$.

There are two important ways in which the projection-operator formalism can be extended. First, (9.1.23) may be regarded as the leading member in a hierarchy of memory-function equations. If we apply the methods already used to the case when R is treated as the dynamical variable, we obtain an equation similar to (9.1.23) for the time evolution of the projection of $R(t)$ along R. The kernel of the integral equation is now the autocorrelation function of a second-order random force that is orthogonal at all times to both R and A. As an obvious generalisation of this procedure we can write a memory-function equation of the form

$$\dot{M}_n(t) - i\Omega_n M_n(t) + \int_0^t M_{n+1}(t-s)\Delta_{n+1}^2 M_n(s)\,\mathrm{d}s = 0 \tag{9.1.33}$$

where

$$M_n(t) = \big(R_n, R_n(t)\big)(R_n, R_n)^{-1} \tag{9.1.34a}$$

$$R_n(t) = \exp(i\mathcal{Q}_n\mathcal{L}\mathcal{Q}_n t)\mathcal{Q}_n\dot{R}_{n-1} \tag{9.1.34b}$$

and

$$\Delta_n^2 = (R_n, R_n)(R_{n-1}, R_{n-1})^{-1} \tag{9.1.35}$$

The operator $\mathcal{P}_n$ projects a dynamical variable along R_{n-1} according to the rule (9.1.1). By construction, therefore, the complementary operator

$$\mathcal{Q}_n = 1 - \sum_{j=1}^{n} \mathcal{P}_j \tag{9.1.36}$$

projects onto the subspace orthogonal to all R_j for $j < n$. Thus the nth-order random force $R_n(t)$ is uncorrelated at all times with random forces of lower order. Equation (9.1.23) is a special case of (9.1.33) with $Y \equiv M_0$. Repeated application of the Laplace transform to equations of the hierarchy leads to an expression for $\widetilde{Y}(z)$ in the form of a continued fraction:

$$\widetilde{Y}(z) = \cfrac{1}{-iz - i\Omega_0 + \cfrac{\Delta_1^2}{-iz - i\Omega_1 + \cfrac{\Delta_2^2}{-iz - i\Omega_2 + \cdots}}} \tag{9.1.37}$$

A second extension of the method, which has proved particularly useful for the description of collective modes in liquids, is one we have already mentioned. This is the generalisation to the case where the dynamical quantity of interest is not a single fluctuating property of the system but a set of n independent variables $A_1,\ A_2, \ldots,\ A_n$. We represent this set by a column vector $\mathbf{A}$ and its hermitian conjugate by the row vector $\mathbf{A}^*$. The derivation of the generalised Langevin equation for $\mathbf{A}$ follows the lines already laid down, due account being taken of the fact that the quantities involved are no longer scalars. The result may be written in matrix form as

$$\dot{\mathbf{A}}(t) - i\boldsymbol{\Omega} \cdot \mathbf{A}(t) + \int_0^t \mathbf{M}(t-s) \cdot \mathbf{A}(s)\, \mathrm{d}s = \mathbf{R}(t) \tag{9.1.38}$$

The definitions of the random-force vector $\mathbf{R}(t)$, frequency matrix $\boldsymbol{\Omega}$ and memory-function matrix $\mathbf{M}(t)$ are analogous to those of $R(t)$, Ω and $M(t)$ in the single-variable case, the scalars A and A^* being replaced by the vectors $\mathbf{A}$ and $\mathbf{A}^*$. If we multiply (9.1.38) from the right by $\mathbf{A}^* \cdot (\mathbf{A}, \mathbf{A})^{-1}$ and take the thermal average we find that

$$\dot{\mathbf{Y}}(t) - i\boldsymbol{\Omega} \cdot \mathbf{Y}(t) + \int_0^t \mathbf{M}(t-s) \cdot \mathbf{Y}(s)\, \mathrm{d}s = \mathbf{0} \tag{9.1.39}$$

where $\mathbf{Y}(t) = (\mathbf{A}, \mathbf{A}(t)) \cdot (\mathbf{A}, \mathbf{A})^{-1}$ is the correlation-function matrix. Equation (9.1.39) is the multivariable generalisation of (9.1.23); its solution in terms of Laplace transforms is

$$\widetilde{\mathbf{Y}}(z) = \left[-iz\mathbf{I} - i\boldsymbol{\Omega} + \widetilde{\mathbf{M}}(z)\right]^{-1} \tag{9.1.40}$$

where $\mathbf{I}$ is the identity matrix. Note that each diagonal element of $\mathbf{Y}(t)$ is an autocorrelation function, normalised by its value at $t = 0$, and the off-diagonal elements are cross-correlation functions.

The value of the memory-function formalism is most easily appreciated by considering specific examples of its use. Before doing so, however, it is helpful to look at the problem from a wider point of view. Equation (9.1.38) represents an equation of motion for $\mathbf{A}(t)$ in which terms linear in $\mathbf{A}$ are displayed explicitly on the left-hand side while the random-force vector describes the effects of non-linear terms, initial transient processes and the dependence of $\mathbf{A}(t)$ on variables not included in the set $\{A_i\}$. This separation of effects is most useful in cases where the random force fluctuates rapidly and the non-zero elements of the memory-function matrix decay much faster than the correlation functions of interest. It is then not unreasonable to represent $\mathbf{M}(t)$ in some simple way, in particular by invoking a markovian approximation whereby the non-zero elements are replaced by δ-functions in t. For this representation to be successful the vector $\mathbf{A}$ should contain as its components not only the variables of immediate interest but also those to which they are strongly coupled. If the set of variables is well chosen, the effect of projecting $\mathbf{A}(t)$ onto the subspace spanned by $\mathbf{A}$ is to project out all the slowly varying properties of the system. The markovian assumption can then be used with greater confidence in approximating the memory-function matrix. By extending the dimensionality of $\mathbf{A}$, an increasingly detailed description can be obtained without departing from the markovian hypothesis. In practice, as we shall see in later sections, this ideal state of affairs is often difficult to achieve, and some of the elements of $\mathbf{M}(t)$ may not be truly short ranged in time. The calculation of the frequency matrix $\boldsymbol{\Omega}$ is generally a straightforward problem, since it involves only static quantities; the same is true of the static correlation matrix $(\mathbf{A}, \mathbf{A})$.

As an alternative to the multidimensional description it is possible to work with a smaller set of variables and exploit the continued-fraction expansion, truncating the hierarchy at a suitable point in some simple, approximate way. This approach is particularly useful when insufficient is known about the dynamical behaviour of the system to permit an informed choice of a larger set of variables. Its main disadvantage is the fact that the physical significance of the memory function becomes increasingly obscure as the expansion is carried to higher orders.

9.2 SELF CORRELATION FUNCTIONS

As a simple example we consider first the application of projection-operator methods to the calculation of the self intermediate scattering function $F_s(k, t)$. This function is of interest because of its link to the velocity autocorrelation function via (8.2.17) and because its power spectrum, the self dynamic structure factor $S_s(k, \omega)$, is closely related to the cross-section for incoherent scattering of neutrons.

The most straightforward approach to the problem is to choose as the single variable A the fluctuating density $\rho_{\mathbf{k}i}$ of a tagged particle i and write a memory-function equation for $\tilde{F}_s(k, z)$ in the form

$$\tilde{F}_s(k, z) = \frac{1}{-iz + \tilde{M}_s(k, z)} \tag{9.2.1}$$

Results given in Section 8.2 show that the short-time expansion of $F_s(k,t)$ starts as

$$F_s(k,t) = 1 - \omega_0^2 \frac{t^2}{2!} + \omega_0^2\left(3\omega_0^2 + \Omega_0^2\right)\frac{t^4}{4!} + \cdots \tag{9.2.2}$$

where the coefficients of successive powers of t are related to the frequency moments of $S_s(k,\omega)$ via the general expression (7.1.24) and the quantities Ω_0 (the Einstein frequency) and ω_0 are defined by (7.2.9) and (7.4.29) respectively. Thus, from (9.1.29), the effect of setting $M_s(k,t=0) = \omega_0^2 = k^2(k_B T/m)$ is to ensure that $S_s(k,\omega)$ has the correct second moment. We may also rewrite $\widetilde{M}_s$ in the form $\widetilde{M}_s(k,z) = k^2\widetilde{D}(k,z)$ where, by analogy with (8.2.10), $\widetilde{D}(k,z)$ plays the role of a generalised self-diffusion coefficient such that $\lim_{z\to 0}\lim_{k\to 0}\widetilde{D}(k,z) = D$. If the continued-fraction expansion is taken to second order we find that

$$\widetilde{F}_s(k,z) = \cfrac{1}{-iz + \cfrac{\omega_0^2}{-iz + \widetilde{N}_s(k,z)}} \tag{9.2.3}$$

By extension of the calculation that leads to (9.1.29) it is easy to show that the initial value of the second-order memory function $N_s(k,t)$ is related to the short-time behaviour of $M_s(k,t)$ by $N_s(k,0) = -\ddot{M}_s(k,0)/M_s(k,0) = \omega_0^2(2\omega_0^2 + \Omega_0^2)$. Thus, if

$$\widetilde{N}_s(k,z) = \left(2\omega_0^2 + \Omega_0^2\right)\tilde{n}_s(k,z) \tag{9.2.4}$$

where $n_s(k,t=0) = 1$, the resulting expression for $S_s(k,\omega)$ also has the correct fourth moment, regardless of the time dependence of $n_s(k,t)$.

As an alternative to making a continued-fraction expansion of $\widetilde{F}_s(k,z)$ we can consider the multivariable description of the problem that comes from the choice

$$\mathbf{A} = \begin{pmatrix} \rho_{\mathbf{k}i} \\ \dot{\rho}_{\mathbf{k}i} \\ \sigma_{\mathbf{k}i} \end{pmatrix} \tag{9.2.5}$$

where the variable $\sigma_{\mathbf{k}i}$, given by

$$\sigma_{\mathbf{k}i} = \ddot{\rho}_{\mathbf{k}i} - (\rho_{\mathbf{k}i}, \ddot{\rho}_{\mathbf{k}i})(\rho_{\mathbf{k}i}, \rho_{\mathbf{k}i})^{-1}\rho_{\mathbf{k}i} \tag{9.2.6}$$

is orthogonal to both $\rho_{\mathbf{k}i}$ and $\dot{\rho}_{\mathbf{k}i}$. From results derived in Sections 7.4 and 8.2 it is straightforward to show that the corresponding static correlation matrix is diagonal and given by

$$(\mathbf{A},\mathbf{A}) = \begin{pmatrix} 1 & 0 & 0 \\ 0 & \omega_0^2 & 0 \\ 0 & 0 & \omega_0^2(2\omega_0^2 + \Omega_0^2) \end{pmatrix} \tag{9.2.7}$$

while the frequency matrix is purely off-diagonal:

$$i\boldsymbol{\Omega} = (\mathbf{A}, \dot{\mathbf{A}}) \cdot (\mathbf{A}, \mathbf{A})^{-1} = \begin{pmatrix} 0 & 1 & 0 \\ -\omega_0^2 & 0 & 1 \\ 0 & -2\omega_0^2 - \Omega_0^2 & 0 \end{pmatrix} \tag{9.2.8}$$

Both $\dot{A}_1$ and $\dot{A}_2$ form part of the space spanned by the vector $\mathbf{A}$. In the case of $\dot{A}_1$ this is easy to see, since $\dot{A}_1 = A_2$. To understand why it is also true for $\dot{A}_2$ it is sufficient to note that the projection of $\dot{A}_2$ along A_1 is obviously part of the space of $\mathbf{A}$, whereas the component orthogonal to A_1 is, according to the definition (9.2.6), the same as A_3. It follows that the random-force vector has only one non-zero component and the memory-function matrix has only one non-zero entry:

$$\mathbf{M}(k,t) = \begin{pmatrix} 0 & 0 & 0 \\ 0 & 0 & 0 \\ 0 & 0 & \mathcal{M}(k,t) \end{pmatrix} \tag{9.2.9}$$

On collecting results and inserting them in (9.1.40), we find that the correlation-function matrix has the form

$$\widetilde{\mathbf{Y}}(k,z) = \begin{pmatrix} -iz & -1 & 0 \\ \omega_0^2 & -iz & -1 \\ 0 & 2\omega_0^2 + \Omega_0^2 & -iz + \widetilde{\mathcal{M}}(k,z) \end{pmatrix} \tag{9.2.10}$$

Inversion of (9.2.10) shows that $\widetilde{F}_s(k,z)$ is given by

$$\widetilde{F}_s(k,z) = \widetilde{Y}_{11}(k,z) = \cfrac{1}{-iz + \cfrac{\omega_0^2}{-iz + \cfrac{2\omega_0^2 + \Omega_0^2}{-iz + \widetilde{\mathcal{M}}(k,z)}}} \tag{9.2.11}$$

and comparison with (9.2.3) and (9.2.4) makes it possible to identify $\mathcal{M}(k,t)$ as the memory function of $N_s(k,t)$. Similarly, the Laplace transform of the self-current autocorrelation function $C_s(k,t)$ is

$$\begin{aligned} \widetilde{C}_s(k,z) &= \omega_0^2 \widetilde{Y}_{22}(k,z) \\ &= \frac{\omega_0^2}{-iz + (2\omega_0^2 + \Omega_0^2)\tilde{n}_s(k,z) + \dfrac{\omega_0^2}{-iz}} \end{aligned} \tag{9.2.12}$$

The same result can be derived from (9.2.3) via the relation (8.2.17) between $C_s(k,t)$ and $F_s(k,t)$, which in turn implies that $\widetilde{C}_s(k,z) = z^2 \widetilde{F}_s(k,z) - iz$.

In the long-wavelength limit the memory function $n_s(k,t)$ is directly related to the memory function of the velocity autocorrelation function $Z(t)$. From (7.2.8), (8.2.17) and

(9.2.12) we find that

$$\widetilde{Z}(z) = \frac{k_B T/m}{-iz + \Omega_0^2 \tilde{n}_s(0,z)} \tag{9.2.13}$$

Thus

$$N_s(0,t) = \Omega_0^2 n_s(0,t) \equiv \xi(t) \tag{9.2.14}$$

where $\xi(t)$ is the memory function of $Z(t)$, introduced earlier in Section 7.3. Since $N_s(k,t)$ is also the memory function of $M_s(k,t)$ and $M_s(k,0) = k^2 Z(0)$, we see that $k^2 Z(t)$ becomes the memory function of $F_s(k,t)$ as $k \to 0$. For consistency with the hydrodynamic result (8.2.10) we also require that

$$\Omega_0^2 \tilde{n}_s(0,0) = \frac{k_B T}{mD} \tag{9.2.15}$$

A particularly simple (markovian) approximation is to replace $N_s(k,t)$ by a quantity independent of t, $1/\tau_s(k)$ say, which is equivalent to assuming an exponential form for $M_s(k,t)$:

$$M_s(k,t) = \omega_0^2 \exp\bigl[-|t|/\tau_s(k)\bigr] \tag{9.2.16}$$

with the constraint, required to satisfy (9.2.15), that

$$\tau_s(0) = \frac{mD}{k_B T} \tag{9.2.17}$$

As we have seen in Section 7.3, this approximation leads to an exponential velocity autocorrelation function of the Langevin type, the quantity $1/\tau_s(0)$ appearing as a frequency-independent friction coefficient. Better results are obtained by choosing an exponential form for $N_s(k,t)$, i.e.

$$N_s(k,t) = \bigl(2\omega_0^2 + \Omega_0^2\bigr) \exp\bigl[-|t|/\tau_s(k)\bigr] \tag{9.2.18}$$

with

$$\tau_s(0) = \frac{k_B T}{mD\Omega_0^2} \tag{9.2.19}$$

This second approximation is equivalent to neglecting the frequency dependence of $\widetilde{\mathcal{M}}(k,z)$; it leads to an analytic form for $S_s(k,\omega)$ having the correct zeroth, second and fourth moments:

$$S_s(k,\omega) = \frac{1}{\pi} \frac{\tau_s(k)\omega_0^2(2\omega_0^2 + \Omega_0^2)}{\omega^2 \tau_s^2(k)(\omega^2 - 3\omega_0^2 - \Omega_0^2)^2 + (\omega^2 - \omega_0^2)^2} \tag{9.2.20}$$

The corresponding expression for $\widetilde{Z}(z)$ is that given in (7.3.26) (with $\tau \equiv \tau_s(0)$).

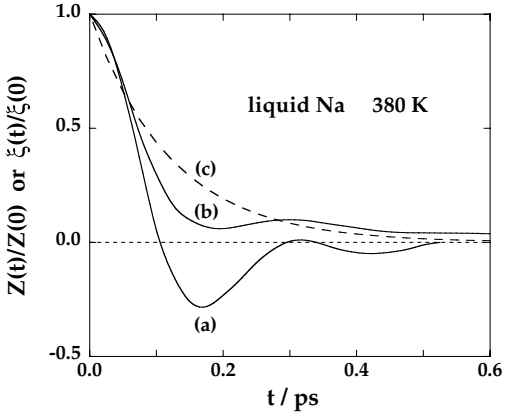

FIG. 9.1. Velocity autocorrelation function, curve (a), and the associated memory function, curve (b), derived from molecular-dynamics calculations for liquid sodium at state conditions close to the normal melting point. Curve (c) shows the exponential approximation (9.2.18) for the memory function, with $\tau_s(0)$ chosen to give the correct self-diffusion coefficient. After Balucani *et al*.[5]

In the absence of any well-based microscopic theory it is perhaps best to treat the relaxation time $\tau_s(k)$ as an adjustable parameter, but it is also tempting to look for some relatively simple prescription for this quantity. An argument based on a scaling of the memory function $M_s(k,t)$ has been used to derive the expression[3]

$$\tau_s^{-1}(k) = \gamma\left(2\omega_0^2 + \Omega_0^2\right)^{1/2} \tag{9.2.21}$$

where the parameter γ is taken to be independent of k, an assumption that is reasonably well borne out in practice. If, in the limit $k \to 0$, we require (9.2.21) to yield the correct diffusion coefficient, it follows that $\gamma = mD\Omega_0/k_BT$; this leads to a value of γ of approximately 0.9 at the triple point of liquid argon. On the other hand, for large wavenumbers, $S_s(k,0)$ goes over correctly to the ideal-gas result if $\gamma = 2/\pi^{1/2} \approx 1.13$.

Although the exponential approximation (9.2.18) has been used with some success in the interpretation of experimental neutron-scattering data,[4] the true situation is known to be much less simple, at least at small wavenumbers. In particular, molecular-dynamics calculations for a range of simple liquids have shown that the memory function of $Z(t)$, i.e. $N_s(0,t)$, cannot be adequately described by a model involving only a single relaxation time. Figure 9.1 shows the memory function obtained from a simulation of liquid sodium in which a clear separation of time-scales is apparent; the presence of the long-time tail in the memory function has the effect of reducing the self-diffusion coefficient by about 30%. In their analysis of the self correlation functions of the Lennard-Jones fluid Levesque and Verlet[6] found it necessary to use a rather complicated expression for $N_s(k,t)$, which for $k = 0$ reduces to

$$N_s(0,t) = \Omega_0^2 \exp\left(-At^2/2\right) + Bt^4 \exp(-\alpha t) \tag{9.2.22}$$

where A, B and α are adjustable parameters. A separation into a rapidly decaying part and a longer-lived term that starts as t^4 is also an explicit ingredient of modern versions of

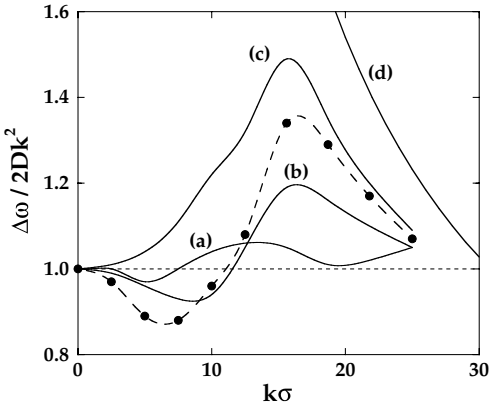

FIG. 9.2. Width at half-height of the self dynamic structure factor relative to its value in the hydrodynamic limit. The points are molecular-dynamics data for the Lennard-Jones fluid at a high density and low temperature ($\rho^* = 0.844,\ T^* = 0.722$) and the broken curve is drawn as an aid to the eye. The full curves show the results predicted (a) by the single-relaxation-time approximation (9.2.18), (b) by the k-dependent generalisation of (9.2.22), (c) by the gaussian approximation (8.2.14) and (d) in the ideal-gas ($k \to \infty$) limit. After Levesque and Verlet.[6]

kinetic theory, in which account is taken of correlated as well as uncorrelated collisions. The long-lived term represents collective effects and lends itself to calculation by mode-coupling methods similar to that employed in Section 8.7 and which we shall meet again later in this chapter.

The importance of including a long-time tail in the memory function $N_s(k,t)$ for $k > 0$ is illustrated for the case of the Lennard-Jones fluid close to the triple point in Figure 9.2. The quantity plotted there, as a function of k, is the width at half-height of $S_s(k,\omega)$ relative to its value in the hydrodynamic limit (where $\Delta\omega = 2Dk^2$). Comparison with results for $S_s(k\omega)$ itself is not very illuminating, since the spectrum is largely featureless, but the dependence of $\Delta\omega/k^2$ on k shows a structure that is not even qualitatively reproduced by the single-exponential approximation; the same is true of the gaussian approximation (8.2.14).

9.3 TRANSVERSE COLLECTIVE MODES

As we saw in Section 8.6, the appearance of propagating shear waves in dense fluids can be explained in qualitative or even semi-quantitative terms by a simple, viscoelastic model based on a generalisation of the hydrodynamic approach. In this section we show how such a theory can be developed in systematic fashion by use of the projection-operator formalism.

Taking the viscoelastic relation (8.6.4) as a guide, we choose as components of the vector **A** the x-component of the mass current and the xz-component of the stress tensor,

assuming as usual that the z-axis is parallel to $\mathbf{k}$. Thus

$$\mathbf{A} = \begin{pmatrix} m j_{\mathbf{k}}^{x} \\ \Pi_{\mathbf{k}}^{xz} \end{pmatrix} \tag{9.3.1}$$

and

$$(\mathbf{A}, \mathbf{A}) = V k_{\mathrm{B}} T \begin{pmatrix} \rho m & 0 \\ 0 & G_{\infty}(k) \end{pmatrix} \tag{9.3.2}$$

where $G_{\infty}(k)$ is the generalised elastic constant defined by (8.6.9). To calculate the frequency matrix we use the relations

$$(A_1, \dot{A}_1) = (A_2, \dot{A}_2) = 0 \tag{9.3.3}$$

$$(A_2, \dot{A}_1) = (A_1, \dot{A}_2) = -ikV k_{\mathrm{B}} T G_{\infty}(k) \tag{9.3.4}$$

and find that

$$i\boldsymbol{\Omega} = \begin{pmatrix} 0 & -ik \\ \dfrac{-ikG_{\infty}(k)}{\rho m} & 0 \end{pmatrix} \tag{9.3.5}$$

Because $\dot{A}_1$ is proportional to A_2, the projection of $\dot{A}_1$ orthogonal to $\mathbf{A}$ is identically zero. The memory-function matrix therefore has only one non-zero element, which we denote by $M_t(k, t)$:

$$\mathbf{M}(k, t) = \begin{pmatrix} 0 & 0 \\ 0 & M_t(k, t) \end{pmatrix} \tag{9.3.6}$$

When these results are substituted in (9.1.40) we obtain an expression for the Laplace transform of the correlation-function matrix in the form

$$\widetilde{\mathbf{Y}}(k, z) = \begin{pmatrix} -iz & ik \\ \dfrac{ikG_{\infty}(k)}{\rho m} & -iz + \widetilde{M}_t(k, z) \end{pmatrix}^{-1} \tag{9.3.7}$$

Thus the Laplace transform of the transverse-current autocorrelation function is

$$\widetilde{C}_t(k, z) = \omega_0^2 \widetilde{Y}_{11}(k, z) = \cfrac{\omega_0^2}{-iz + \cfrac{\omega_{1t}^2}{-iz + \widetilde{M}_t(k, z)}} \tag{9.3.8}$$

where ω_{1t}^2, defined by (7.4.38), is related to $G_{\infty}(k)$ by (8.6.9). Consistency with the hydrodynamic result (8.4.4) in the long-wavelength, low-frequency limit is achieved by setting

$$\widetilde{M}_t(0, 0) = \frac{G_{\infty}(0)}{\eta} \tag{9.3.9}$$

The function $\widetilde{M}_t(k,z)$ is the memory function of the generalised kinematic shear viscosity introduced in Section 8.6. This identification follows immediately from comparison of (9.3.8) with the Laplace transform of (8.6.7), which shows that

$$\widetilde{C}_t(k,z) = \frac{\omega_0^2}{-iz + k^2\tilde{\nu}(k,z)} \tag{9.3.10}$$

The viscoelastic approximation corresponds to ignoring the frequency dependence of $\widetilde{M}_t(k,z)$ and replacing it by a constant, $1/\tau_t(k)$ say, implying that $\nu(k,t)$ decays exponentially with a characteristic time $\tau_t(k)$ and hence, from (8.6.9), that

$$\nu(k,t) = \frac{G_\infty(k)}{\rho m}\exp\bigl[-|t|/\tau_t(k)\bigr] \tag{9.3.11}$$

Use of (9.3.11) ensures that the spectrum of transverse-current fluctuations:

$$C_t(k,\omega) = \frac{1}{\pi}\operatorname{Re}\widetilde{C}_t(k,\omega) = \frac{1}{\pi}\frac{\omega_0^2\omega_{1t}^2\tau_t(k)}{\omega^2 + \tau_t^2(k)(\omega_{1t}^2-\omega^2)^2} \tag{9.3.12}$$

has the correct second moment irrespective of the choice of $\tau_t(k)$. If, as in Section 8.6, we define a wavenumber-dependent shear viscosity $\eta(k)$ as the zero-frequency limit of $\rho m\tilde{\nu}(k,\omega)$, we find in the approximation represented by (9.3.11) that

$$\eta(k) = \tau_t(k)G_\infty(k) \tag{9.3.13}$$

so that $\tau_t(k)$ appears as a k-dependent Maxwell relaxation time (see (8.6.5)). In particular:

$$\eta \equiv \eta(0) = \tau_t(0)G_\infty(0) \tag{9.3.14}$$

in agreement with (9.3.9).

It is easy to establish the criterion for the existence of propagating transverse modes within the context of the single-relaxation-time approximation represented by (9.3.12). The condition for $C_t(k,\omega)$ to have a peak at non-zero frequency at a given value of k is

$$\omega_{1t}^2\tau_t^2(k) > \tfrac{1}{2} \tag{9.3.15}$$

and the peak, if it exists, is at a frequency ω such that $\omega^2 = \omega_{1t}^2 - \frac{1}{2}\tau_t^{-2}(k)$. It follows from the inequality (9.3.15) that shear waves will appear for values of k greater than k_c, where k_c is a critical wavevector given by

$$k_c^2 = \frac{\rho m}{2\tau_t^2(k)G_\infty(k)} \tag{9.3.16}$$

We can obtain an estimate for k_c by taking the $k \to 0$ limit of (9.3.16); this gives

$$k_c^2 \approx \frac{\rho m G_\infty(0)}{2\eta^2} \tag{9.3.17}$$

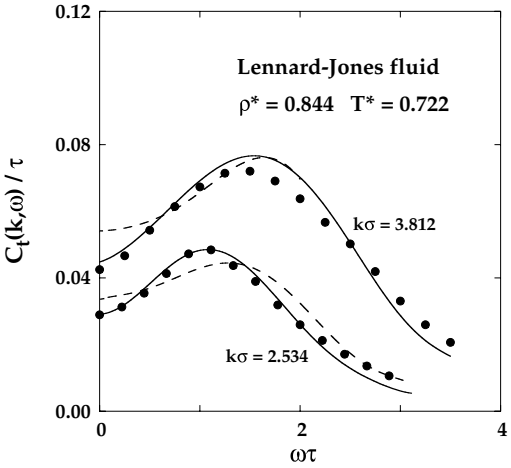

FIG. 9.3. Spectrum of transverse-current fluctuations for the Lennard-Jones fluid near its triple point. The points are molecular-dynamics results and the curves show results calculated from the viscoelastic approximation (9.3.11) (broken lines) and the two-exponential memory function (9.3.20) (full lines). The unit of time is $\tau = (m\sigma^2/48\varepsilon)^{1/2}$. After Levesque *et al.*[7]

On inserting the values of η and $G_\infty(0)$ obtained by molecular-dynamics calculations for the Lennard-Jones fluid close to its triple point we find that $k_c\sigma \approx 0.79$. This is apparently a rather good guide to what occurs in practice: the dispersion curve for liquid argon plotted in Figure 8.4 shows that shear waves first appear at $k_c \approx 2.0$ Å or, taking a value (3.4 Å) for σ appropriate to argon, $k_c\sigma \approx 0.7$. At sufficiently large values of k the shear waves again disappear as the role of the interparticle forces becomes less important.

Given its simplicity, the viscoelastic approximation provides a very satisfactory description of the transverse-current fluctuations over a wide range of wavelength. Careful study reveals, however, that there are some systematic discrepancies with the molecular-dynamics data that persist even when the parameter $\tau_t(k)$ is chosen to fit the observed spectrum rather than calculated from some semi-empirical prescription. In particular, the shear-wave peaks at long wavelengths are significantly too broad and flat, as the results for the Lennard-Jones fluid shown in Figure 9.3 reveal. The structure of the correlation-function matrix (9.3.7) gives a clue to the origin of the deficiencies in the viscoelastic model. The element $\widetilde{Y}_{22}(k,z)$ of the matrix is the Laplace transform of the normalised autocorrelation function of the xz-component of the stress tensor. Thus

$$\begin{aligned}\widetilde{Y}_{22}(k,z) &= \frac{\beta}{VG_\infty(k)}\int_0^\infty \left\langle \Pi_{\mathbf{k}}^{xz}(t)\Pi_{-\mathbf{k}}^{xz}\right\rangle \exp(izt)\,\mathrm{d}t \\ &= \frac{1}{-iz + \widetilde{M}_t(k,z) + \dfrac{\omega_{1t}^2}{-iz}}\end{aligned} \tag{9.3.18}$$

where the form of the normalisation factor follows from (8.4.10) and (8.6.9). If we again replace $\widetilde{M}_t(k,z)$ by $1/\tau_t(k)$ and take the limit $k \to 0$, (9.3.18) can be inverted to give

$$\eta(t) = G_\infty(0)Y_{22}(0,t) = G_\infty(0)\exp\bigl[-G_\infty(0)|t|/\eta\bigr] \tag{9.3.19}$$

which is consistent with (8.4.10). We saw in Section 8.6 that the memory function $\nu(k,t)$ and the stress autocorrelation function $\eta(t)$ become identical (apart from a multiplicative factor) as k tends to zero; within the viscoelastic approximation the identity is apparent immediately from intercomparison of (9.3.11), (9.3.14) and (9.3.19). At high densities, as Figure 8.1 illustrates, the correlation function $\eta(t)$ has a pronounced, slowly decaying tail and it is reasonable to suppose that the transverse-current fluctuations at small wavevectors can be adequately described only if a comparably long-lived contribution is included in the memory function $\nu(k,t)$. In their classic analysis of the collective dynamical properties of the Lennard-Jones fluid, Levesque, Verlet and Kürkijarvi[7] suggested the use of a two-exponential memory function of the form

$$\nu(k,t)/\nu(k,0) = (1-\alpha_k)\exp\bigl[-|t|/\tau_1(k)\bigr] + \alpha_k \exp\bigl[-|t|/\tau_2(k)\bigr] \tag{9.3.20}$$

which, as the inset to Figure 8.1 suggests, is also a useful approximation for other systems. In practise, for the Lennard-Jones fluid, τ_2 turns out to be almost independent of k and some seven times larger than $\tau_1(0)$, while the parameter α_k decreases rapidly with increasing k. Thus, for large k, the single-relaxation-time approximation is recovered. At small k, however, inclusion of the long-lived tail in the memory function leads to a marked enhancement of the shear-wave peaks and significantly improved agreement with the molecular-dynamics results, as illustrated in Figure 9.3; the price paid is the introduction of an additional two parameters. Broadly similar conclusions have emerged from calculations for liquid metals.[8]

9.4 DENSITY FLUCTUATIONS

The description of the longitudinal-current fluctuations on the basis of the generalised Langevin equation is necessarily a more complicated task than in the case of the transverse modes. This is obvious from the much more complicated structure of the hydrodynamic formula (8.5.10) compared with (8.4.4). The problem of particular interest is to account for the dispersion and eventual disappearance of the collective mode associated with sound-wave propagation.

In discussion of the longitudinal modes a natural choice of components of the dynamical vector $\mathbf{A}$ is the set of conserved variables consisting of $\rho_{\mathbf{k}}$, $\mathbf{j}_{\mathbf{k}}$ and the microscopic energy density $e_{\mathbf{k}}$ defined via (8.5.27). The variables $\rho_{\mathbf{k}}$ and $e_{\mathbf{k}}$ are both orthogonal to $\mathbf{j}_{\mathbf{k}}$. In place of $e_{\mathbf{k}}$, however, it is more convenient to choose that part which is also orthogonal to $\rho_{\mathbf{k}}$ and plays the role of a microscopic temperature fluctuation; this we write as $T_{\mathbf{k}}$. Thus

$$T_{\mathbf{k}} = e_{\mathbf{k}} - (\rho_{\mathbf{k}}, e_{\mathbf{k}})(\rho_{\mathbf{k}}, \rho_{\mathbf{k}})^{-1}\rho_{\mathbf{k}} \tag{9.4.1}$$

The static correlation matrix is then diagonal. Since our attention is focused on the longitudinal fluctuations, we include only the projection of the current along $\mathbf{k}$, which we label $j^z_{\mathbf{k}}$. The vector $\mathbf{A}$ specified in this way, i.e.

$$\mathbf{A} = \begin{pmatrix} \rho_{\mathbf{k}} \\ j^z_{\mathbf{k}} \\ T_{\mathbf{k}} \end{pmatrix} \tag{9.4.2}$$

is only one of many possible choices; larger sets of variables that include both the stress tensor and heat current have also been considered. The static correlation matrix arising from (9.4.2) is

$$(\mathbf{A}, \mathbf{A}) = \begin{pmatrix} NS(k) & 0 & 0 \\ 0 & \dfrac{Nk_{\mathrm{B}}T}{m} & 0 \\ 0 & 0 & \langle T_{\mathbf{k}} T_{-\mathbf{k}} \rangle \end{pmatrix} \tag{9.4.3}$$

and the corresponding frequency matrix is

$$-i\boldsymbol{\Omega} = \begin{pmatrix} 0 & -ik & 0 \\ \dfrac{-ik}{S(k)}\left(\dfrac{k_{\mathrm{B}}T}{m}\right) & 0 & \dfrac{\langle \dot{j}^z_{\mathbf{k}} T_{-\mathbf{k}} \rangle}{\langle T_{\mathbf{k}} T_{-\mathbf{k}} \rangle} \\ 0 & -\dfrac{\langle T_{\mathbf{k}} \dot{j}^z_{-\mathbf{k}} \rangle}{Nk_{\mathrm{B}}T/m} & 0 \end{pmatrix} \tag{9.4.4}$$

It is unnecessary for our purposes to write more explicit expressions for the statistical averages appearing in (9.4.3) and (9.4.4).

Since $\dot{A}_1$ is proportional to A_2, it follows that the component R_1 of the random-force vector is zero and the memory-function matrix reduces to

$$\mathbf{M}(k,t) = \begin{pmatrix} 0 & 0 & 0 \\ 0 & M_{22}(k,t) & M_{23}(k,t) \\ 0 & M_{32}(k,t) & M_{33}(k,t) \end{pmatrix} \tag{9.4.5}$$

The correlation-function matrix is therefore given by

$$\widetilde{\mathbf{Y}}(k,z) = \begin{pmatrix} -iz & ik & 0 \\ \dfrac{ik}{S(k)}\left(\dfrac{k_{\mathrm{B}}T}{m}\right) & -iz + \widetilde{M}_{22}(k,z) & -i\Omega_{23} + \widetilde{M}_{23}(k,z) \\ 0 & -i\Omega_{32} + \widetilde{M}_{32}(k,z) & -iz + \widetilde{M}_{33}(k,z) \end{pmatrix}^{-1} \tag{9.4.6}$$

and the Laplace transform of the longitudinal-current autocorrelation function is

$$\begin{aligned} \widetilde{C}_l(k,z) &= \omega_0^2 \widetilde{Y}_{22}(k,z) \\ &= \frac{\omega_0^2}{-iz + \dfrac{\omega_0^2}{-izS(k)} + \widetilde{N}_l(k,z)} \end{aligned} \tag{9.4.7}$$

where the memory function $N_l(k,t)$ is defined through its Laplace transform as

$$\widetilde{N}_l(k,z) = \widetilde{M}_{22}(k,z) - \frac{\Theta(k,z)}{-iz + \widetilde{M}_{33}(k,z)} \tag{9.4.8}$$

with

$$\Theta(k,z) = \left(\widetilde{M}_{23}(k,z) - \frac{\langle \dot{j}^z_{\mathbf{k}} T_{-\mathbf{k}}\rangle}{\langle T_{\mathbf{k}} T_{-\mathbf{k}}\rangle}\right)\left(\widetilde{M}_{32}(k,z) + \frac{\langle T_{\mathbf{k}} \dot{j}^z_{-\mathbf{k}}\rangle}{N(k_{\mathrm{B}}T/m)}\right) \tag{9.4.9}$$

The physical significance of the four unknown memory functions in (9.4.5) is easily inferred from their definitions in terms of the random forces $\mathcal{Q}\dot{j}^z_{\mathbf{k}}$ and $\mathcal{Q}\dot{T}_{\mathbf{k}}$. The functions M_{23} and M_{32} describe a coupling between the momentum current (the stress tensor) and heat flux whereas M_{22} and M_{33} represent, respectively, the relaxation processes associated with viscosity and thermal conduction. By comparison of (9.4.7) to (9.4.9) with the hydrodynamic result in (8.5.10) we can make the following identifications in the limit $k \to 0$:

$$\lim_{k\to 0} \widetilde{M}_{22}(k,0) = \frac{\left(\frac{4}{3}\eta + \zeta\right)k^2}{\rho m} = bk^2 \tag{9.4.10}$$

$$\lim_{k\to 0} \widetilde{M}_{33}(k,0) = \frac{\lambda k^2}{\rho m} = ak^2 \tag{9.4.11}$$

and

$$\lim_{k\to 0} \frac{|\langle \dot{j}^z_{\mathbf{k}} T_{-\mathbf{k}}\rangle|^2}{\langle T_{\mathbf{k}} T_{-\mathbf{k}}\rangle} = Nk^2\left(\frac{k_{\mathrm{B}}T}{m}\right)^2 \frac{\gamma - 1}{S(k)} \tag{9.4.12}$$

Finally, by requiring that

$$N_l(k, t=0) = \omega_{1l}^2 - \frac{\omega_0^2}{S(k)} \tag{9.4.13}$$

with ω_{1l}^2 given by (7.4.35), we guarantee that the first three non-zero moments of $S(k,\omega)$ are correct.

The derivation of (9.4.6) brings out clearly the advantage of working with a multivariable description of a problem such as that provided by (9.4.2). For example, we can immediately write down an expression for the fluctuations in temperature analogous to (9.4.7) for the current fluctuations. If we define a temperature autocorrelation function as

$$C_T(k,t) = \left\langle T_{\mathbf{k}}(t) T_{-\mathbf{k}}\right\rangle \tag{9.4.14}$$

we find from (9.4.6) that

$$\begin{aligned}\widetilde{C}_T(k,z) &= \langle T_{\mathbf{k}} T_{-\mathbf{k}}\rangle \widetilde{Y}_{33}(k,z) \\ &= \frac{\langle T_{\mathbf{k}} T_{-\mathbf{k}}\rangle}{-iz - \dfrac{\Theta(k,z)}{-iz + \dfrac{\omega_0^2}{-izS(k)} + \widetilde{M}_{22}(k,z)} + \widetilde{M}_{33}(k,z)}\end{aligned} \tag{9.4.15}$$

The key point to note is that $\widetilde{C}_T(k,z)$ can be expressed in terms of the same memory functions used to describe $\widetilde{C}_l(k,z)$. Similarly, by solving for $\widetilde{Y}_{11}(k,z)$, we obtain an expression for the density autocorrelation function:

$$\begin{aligned}\widetilde{F}(k,z) &= S(k)\widetilde{Y}_{11}(k,z) \\ &= \frac{S(k)}{-iz + \dfrac{1}{S(k)}\left(\dfrac{\omega_0^2}{-iz + \widetilde{N}_l(k,z)}\right)}\end{aligned} \tag{9.4.16}$$

This is a less interesting result than that obtained for $\widetilde{C}_T(k,z)$, because $F(k,t)$ and $C_l(k,t)$ are in any case related by (7.4.26). It nevertheless brings out a second important feature of the multivariable approach. An expression for $\widetilde{F}(k,z)$ having the same form as (9.4.16) can more easily be obtained by setting $A = \rho_{\mathbf{k}}$ and making a continued-fraction expansion of $\widetilde{F}(k,z)$ truncated at second order. What the more elaborate calculation yields is detailed information on the structure of the memory function $N_l(k,t)$, enabling contact to be made with the hydrodynamic result and allowing approximations to be introduced in a controlled way.

If we write the complex function $\widetilde{N}_l(k,z)$ on the real axis ($z = \omega + i\varepsilon,\ \varepsilon \to 0+$) as the sum of its real and imaginary parts, i.e.

$$\widetilde{N}_l(k,\omega) = N_l'(k,\omega) + iN_l''(k,\omega) \tag{9.4.17}$$

we find from (9.4.7) that the spectrum of longitudinal-current fluctuations is given by

$$C_l(k,\omega) = \frac{1}{\pi}\frac{\omega^2\omega_0^2 N_l'(k,\omega)}{[\omega^2 - \omega_0^2/S(k) - \omega N_l''(k,\omega)]^2 + [\omega N_l'(k,\omega]^2} \tag{9.4.18}$$

If the memory function were small, there would be a resonance at a frequency determined by the static structure of the fluid, i.e. at $\omega^2 \approx \omega_0^2/S(k)$. The physical role of the memory function – the generalised "friction" – is therefore to shift and damp the resonance.

The task of calculating the function $N_l(k,t)$ remains a formidable one, even with the restrictions we have discussed. Some recourse to modelling is therefore needed if tractable expressions for $C_l(k,\omega)$ and $S(k,\omega)$ are to be obtained. The limiting form of $\widetilde{N}_l(k,\omega)$ when $k,\ \omega \to 0$ (hydrodynamic limit) follows from (9.4.8) to (9.4.12):

$$\lim_{\omega\to 0}\lim_{k\to 0}\widetilde{N}_l(k,\omega) = bk^2 + \frac{\omega_0^2}{S(k)}\frac{\gamma - 1}{-i\omega + ak^2} \tag{9.4.19}$$

The first-term on the right-hand side of this expression describes viscous relaxation and corresponds to $\widetilde{M}_{22}(k,\omega)$ in (9.4.8), while the second term arises from temperature

fluctuations. We now require a generalisation of (9.4.19) that is valid for microscopic wavelengths and frequencies. An obvious first approximation is to assume that the coupling between the momentum and heat currents, represented by the memory functions $M_{23}(k,t)$ and $M_{32}(k,t)$, makes no contribution to the density fluctuations. This is true in the hydrodynamic limit and it is true instantaneously at finite wavelengths because the random forces $\mathcal{Q}\dot{j}^z_{\mathbf{k}}$ and $\mathcal{Q}\dot{T}_{\mathbf{k}}$ are instantaneously uncorrelated; the two memory functions therefore vanish at $t = 0$. If we also assume that the effect of thermal fluctuations is negligible, an approximation that can be justified at large wavenumbers, we are left only with the problem of representing the generalised longitudinal viscosity $\widetilde{M}_{22}(k,\omega)$. Since the viscoelastic model (9.3.11) works moderately well in the case of the transverse currents, it is natural to make a similar approximation here by writing

$$N_l(k,t) = \left(\omega_{1l}^2 - \frac{\omega_0^2}{S(k)}\right)\exp\bigl[-|t|/\tau_l(k)\bigr] \tag{9.4.20}$$

which is compatible with the constraint (9.4.13). The resulting expression for the dynamic structure factor is

$$S(k,\omega) = \frac{1}{\pi}\frac{\tau_l(k)\omega_0^2[\omega_{1l}^2 - \omega_0^2/S(k)]}{\omega^2\tau_l^2(k)(\omega^2 - \omega_{1l}^2)^2 + [\omega^2 - \omega_0^2/S(k)]^2} \tag{9.4.21}$$

A variety of proposals have been made for the calculation of the relaxation time $\tau_l(k)$. For example, arguments similar to those used in the derivation of (9.2.21) lead in this case to the expression[9]

$$\tau_l^{-1}(k) = \frac{2}{\pi^{1/2}}\left(\omega_{1l}^2 - \frac{\omega_0^2}{S(k)}\right)^{1/2} \tag{9.4.22}$$

The usefulness of this approach is illustrated in Figure 9.4, which shows the dispersion of the sound-wave peak obtained from molecular-dynamics calculations for liquid rubidium and compares the results with those predicted by the viscoelastic approximation (9.4.21) in conjunction with (9.4.22). The agreement is good but the detailed shape of $S(k,\omega)$ is less well reproduced, particularly at small k. As the example shown in the lower part of the figure reveals, the discrepancies occur mostly at low frequencies. This is not surprising, since the low-frequency region of the spectrum is dominated by temperature fluctuations, which the viscoelastic model ignores.

The type of scheme outlined above is clearly an oversimplification. Analysis of results obtained by inelastic x-ray scattering at small wavenumbers has confirmed the inadequacy of the viscoelastic approximation for liquid metals[12] and in other cases the method is not even qualitatively satisfactory. In particular, the viscoelastic model is unable to account for the Brillouin peak observed in molecular-dynamics calculations for the Lennard-Jones fluid, as pictured in Figure 9.5. It can be shown from (9.4.22) that the viscoelastic model predicts the existence of such a propagating mode whenever

$$\omega_{1l}^2 < \frac{3\omega_0^2}{S(k)} \tag{9.4.23}$$

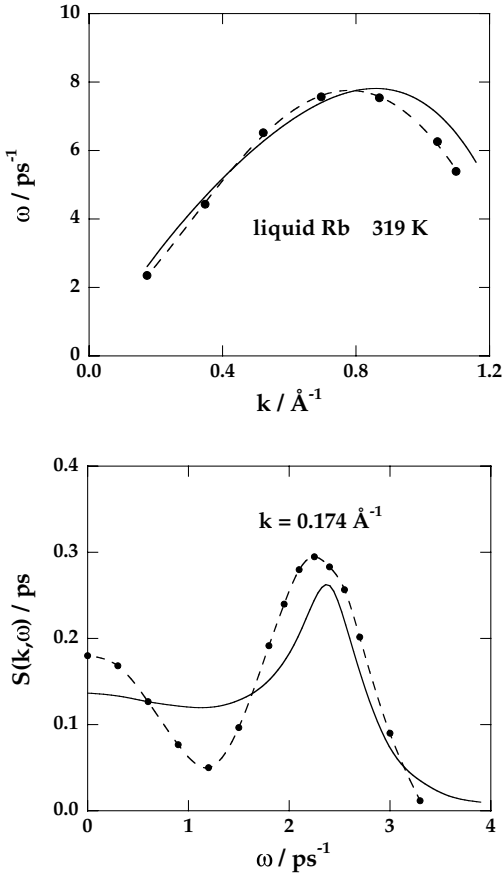

FIG. 9.4. Sound-wave dispersion curve (above) and dynamic structure factor (below) for a model of liquid rubidium near the normal melting temperature. The points are molecular-dynamics results[10] and the broken curves are drawn as guides to the eye. The full curves are calculated from the viscoelastic approximation (9.4.21) in conjunction with (9.4.22). After Copley and Lovesey.[11]

If k is small this inequality can be rewritten as

$$\chi_T\left[\tfrac{4}{3}G_\infty(0) + K_\infty(0)\right] < 3 \tag{9.4.24}$$

when ω_{1l}^2 is expressed in terms of the long-wavelength limits of the instantaneous shear modulus (8.6.9) and the instantaneous bulk modulus $K_\infty(k)$ defined by the relation

$$\tfrac{4}{3}G_\infty(k) + K_\infty(k) = \frac{\rho m \omega_{1l}^2}{k^2} \tag{9.4.25}$$

In the case of the alkali metals the inequality (9.4.24) is easily satisfied, but for the Lennard-Jones fluid under triple-point conditions the left-hand side of (9.4.24) has a value of ap-

proximately 4.9. Given the structure of (9.4.24), it seems plausible to conclude that the persistence of the sound-wave peak in liquid metals to relatively much larger wavenumbers than in rare-gas liquids is associated with the lower compressibility of the metals (see Table 1.2). This difference in behaviour can in turn be correlated with the softer nature of the interatomic potentials in metals compared with those in the rare gases.

In order to describe the small-k behaviour of the Lennard-Jones system it is necessary to go beyond the viscoelastic approximation (9.4.20) by including the effect of temperature fluctuations. A generalisation of the hydrodynamic result (9.4.19) that satisfies the short-time constraint (9.4.13) is obtained by setting

$$\widetilde{N}_l(k,\omega) = \left(\omega_{1l}^2 - \frac{\omega_0^2\gamma(k)}{S(k)}\right)\tilde{n}_{1l}(k,\omega) + \frac{\omega_0^2}{S(k)}\frac{\gamma(k)-1}{-i\omega + a(k)k^2} \tag{9.4.26}$$

with $n_{1l}(k,t=0)=1$; this ignores any frequency dependence of the generalised thermal diffusivity $a(k)$ (the quantity $a(0)$ is defined by (8.3.14)). If, in addition, $\gamma(k)$ (a k-dependent ratio of specific heats) is set equal to one, the term representing temperature fluctuations disappears and (9.4.26) reduces to the viscoelastic approximation; the latter, as we have seen, works reasonably well for liquid metals, for which $\gamma(0)\approx 1$. The first term on the right-hand side of (9.4.26) can be identified as $\widetilde{M}_{22}(k,\omega)$. Then, if we assume a simple, exponential form for $n_{1l}(k,t)$, i.e.

$$n_{1l}(k,t) = \exp\bigl[-|t|/\tau_l(k)\bigr] \tag{9.4.27}$$

we find that in the hydrodynamic limit $\widetilde{M}_{22}(k,0)$ approaches the value

$$\lim_{k\to 0}\frac{\widetilde{M}_{22}(k,0)}{k^2} = \frac{\tau_l(0)}{\rho m}\bigl[\tfrac{4}{3}G_\infty(0) + K_\infty(0) - \gamma/\chi_T\bigr] \tag{9.4.28}$$

Comparison of (9.4.28) with (9.4.10) shows that $\tau_l(0)$ is given by

$$\tau_l(0) = \frac{\frac{4}{3}\eta + \zeta}{\frac{4}{3}G_\infty(0) + K_\infty(0) - \gamma/\chi_T} \tag{9.4.29}$$

Equations (9.4.26) to (9.4.29) make up the set of generalised hydrodynamic equations used by Levesque, Verlet and Kürkijarvi[7] in their study of the Lennard-Jones fluid; together they yield a good fit to the dynamic structure factor over a wide range of k. Among the satisfying features of the analysis is the fact that at long wavelengths $\tau_l(k)$, as determined by a least-squares fitting procedure, tends correctly to its limiting value (9.4.29) as $k\to 0$. Moreover, $\gamma(k)\approx 1$ beyond $k\sigma\approx 2$. The large-k behaviour of $\gamma(k)$ implies that the viscoelastic model is a good approximation at short wavelengths because the coupling with the thermal mode becomes negligible. On the other hand, at small k, $\gamma(k)$ tends to a value that is larger by a factor of approximately two than the thermodynamic value derived from the simulation. This fault can be eliminated by inclusion of a slowly relaxing part in the generalised longitudinal viscosity $\widetilde{M}_{22}(k,\omega)$. If a two-exponential form is used for $n_{1l}(k,t)$, and if the two decay times are given the same values as the corresponding relaxation times in

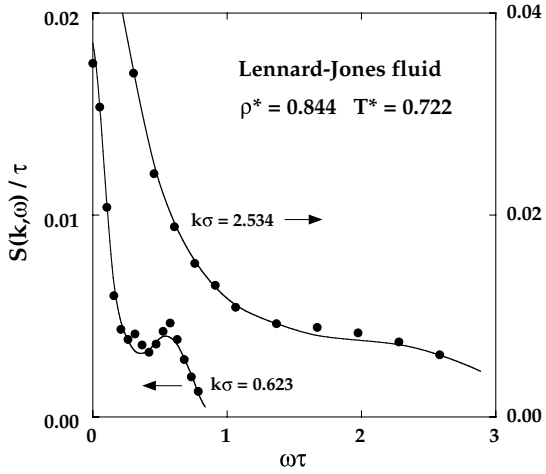

FIG. 9.5. Dynamic structure factor of the Lennard-Jones fluid near its triple point. The points are molecular-dynamics results and the curves show results calculated from (9.4.26) with a two-exponential approximation to $n_{1l}(k,t)$. The unit of time is $\tau = (m\sigma^2/48\varepsilon)^{1/2}$. After Levesque *et al.*[7]

the transverse-current memory function (9.3.20), an excellent fit is obtained, as Figure 9.5 shows, for which $\gamma(k)$ tends to its thermodynamic value as $k \to 0$. The good agreement obtained with a single exponential is to some extent fortuitous, the omission of the long-time part of the viscous contribution to the memory function being offset by an increase in the size of the thermal contribution.

9.5 MODE-COUPLING THEORY I. THE VELOCITY AUTOCORRELATION FUNCTION

The applications of the projection-operator formalism studied thus far are largely phenomenological in character in the sense that a simple functional form has generally been assumed to describe the decay of the various memory functions. Such descriptions can be looked upon as interpolation schemes between the short-time behaviour of correlation functions, which is introduced via frequency sum rules, and the hydrodynamic regime, which governs the choice of dynamical variables to be included in the vector **A**. A more ambitious programme would be to derive expressions for the memory functions from first principles, starting from the formally exact definitions of Section 9.1. A possible route towards such a microscopic theory is provided by the mode-coupling approach, which we have already used in Section 8.7 to investigate the slow decay of the velocity autocorrelation function at long times. In this section we show how mode-coupling concepts can be applied to the calculation of time-correlation functions and their associated memory functions within the framework of the projection-operator formalism. The basic idea behind mode-coupling theory is that the fluctuation (or "excitation") of a given dynamical variable decays predominantly into pairs of hydrodynamic modes associated with conserved single-particle or collective dynamical variables. The possible "decay channels" of a fluctuation

are determined by "selection rules" based, for example, on time-reversal symmetry or on physical considerations. If a further, decoupling approximation is made, time-correlation functions are expressible as sums of products of the correlation functions of conserved variables.

To illustrate the method, we first use the projection-operator formalism to rederive the asymptotic form (8.7.15) of the velocity autocorrelation function. Let u_{ix} be the x-component of the velocity of a tagged particle i. In the notation of Section 9.1 the velocity autocorrelation function has the from

$$Z(t) = \big(u_{ix}, \exp(i\mathcal{L}t)u_{ix}\big) \tag{9.5.1}$$

From the discussion in Section 8.7 we can expect the tagged-particle velocity to be strongly coupled to the longitudinal and transverse components of the collective particle current, while the form of (8.7.8) suggests that we take the tagged-particle density $\rho_{\mathbf{k}'i}$ and the current $\mathbf{j}_{-\mathbf{k}''}$ to be the modes into which fluctuations in u_{ix} decay. Translational invariance implies that the only products of Fourier components whose inner product with the tagged-particle velocity are non-zero are those for which $\mathbf{k}' = \mathbf{k}''$. The first approximation of the mode-coupling treatment therefore consists in replacing the full evolution operator $\exp(i\mathcal{L}t)$ by its projection onto the subspace of the product variables $\rho_{\mathbf{k}i}\mathbf{j}_{-\mathbf{k}}$, i.e.

$$\exp(i\mathcal{L}t) \approx \mathcal{P}\exp(i\mathcal{L}t)\mathcal{P} \tag{9.5.2}$$

The projection operator $\mathcal{P}$ is defined, as in (9.1.1), by its action on a dynamical variable B:

$$\mathcal{P}B = \sum_{\mathbf{k}}\sum_{\alpha}\big(\rho_{\mathbf{k}i}\, j^{\alpha}_{-\mathbf{k}}, B\big)\big(\rho_{\mathbf{k}i}\, j^{\alpha}_{-\mathbf{k}}, \rho_{\mathbf{k}i}\, j^{\alpha}_{-\mathbf{k}}\big)^{-1}\rho_{\mathbf{k}i}\, j^{\alpha}_{-\mathbf{k}} \tag{9.5.3}$$

where the sum on α runs over all cartesian components. Thus

$$\begin{aligned}\exp(i\mathcal{L}t)\mathcal{P}u_{ix} = \sum_{\mathbf{k}'}\sum_{\beta}&\big(\rho_{\mathbf{k}'i}\, j^{\beta}_{-\mathbf{k}'}, u_{ix}\big)\big(\rho_{\mathbf{k}'i}\, j^{\beta}_{-\mathbf{k}'}, \rho_{\mathbf{k}'i}\, j^{\beta}_{-\mathbf{k}'}\big)^{-1}\\ &\times \exp(i\mathcal{L}t)\rho_{\mathbf{k}'i}\, j^{\beta}_{-\mathbf{k}'}\end{aligned} \tag{9.5.4}$$

and

$$\begin{aligned}Z(t) &\approx \big(u_{ix}, \mathcal{P}\exp(i\mathcal{L}t)\mathcal{P}u_{ix}\big)\\ &= \sum_{\mathbf{k},\mathbf{k}'}\sum_{\alpha}\sum_{\beta}\big(\rho_{\mathbf{k}'i}\, j^{\beta}_{-\mathbf{k}'}, u_{ix}\big)\big(\rho_{\mathbf{k}'i}\, j^{\beta}_{-\mathbf{k}'}, \rho_{\mathbf{k}'i}\, j^{\beta}_{-\mathbf{k}'}\big)^{-1}\\ &\quad\times\big(\rho_{\mathbf{k}i}\, j^{\alpha}_{-\mathbf{k}}, \exp(i\mathcal{L}t)\rho_{\mathbf{k}'i}\, j^{\beta}_{-\mathbf{k}'}\big)\\ &\quad\times\big(\rho_{\mathbf{k}i}\, j^{\alpha}_{-\mathbf{k}}, \rho_{\mathbf{k}i}\, j^{\alpha}_{-\mathbf{k}}\big)^{-1}\big(u_{ix}, \rho_{\mathbf{k}i}\, j^{\alpha}_{-\mathbf{k}}\big)\end{aligned} \tag{9.5.5}$$

In this expression the time-correlation functions of the product variables are bracketed by two time-independent "vertices", each of which has the same value. For example, since

$\langle \rho_{\mathbf{k}i} j^{\alpha}_{-\mathbf{k}} \rho_{-\mathbf{k}i} j^{\alpha}_{\mathbf{k}} \rangle = N(k_{\mathrm{B}}T/m)$ and $\langle u_{ix} \rho_{-\mathbf{k}i} j^{\alpha}_{\mathbf{k}} \rangle = (k_{\mathrm{B}}T/m)\delta_{\alpha x}$, it follows that

$$\left(\rho_{\mathbf{k}i} j^{\alpha}_{-\mathbf{k}}, \rho_{\mathbf{k}i} j^{\alpha}_{-\mathbf{k}}\right)^{-1} \left(u_{ix}, \rho_{\mathbf{k}i} j^{\alpha}_{-\mathbf{k}}\right) = \frac{1}{N}\delta_{\alpha x} \tag{9.5.6}$$

The time-correlation functions appearing on the right-hand side of (9.5.5) are of an unusual type, since they involve four, rather than two, dynamical variables. A second approximation usually made is to assume that the two modes appearing in the product variables propagate independently of each other. This means that the four-variable functions factorise into products of two-variable functions. In the present case:

$$\begin{aligned} \left(\rho_{\mathbf{k}i} j^{\alpha}_{-\mathbf{k}}, \exp(i\mathcal{L}t)\rho_{\mathbf{k}'i} j^{\beta}_{-\mathbf{k}'}\right) &\approx \left(\rho_{\mathbf{k}i}, \exp(i\mathcal{L}t)\rho_{\mathbf{k}'i}\right)\left(j^{\alpha}_{-\mathbf{k}}, \exp(i\mathcal{L}t) j^{\beta}_{-\mathbf{k}'}\right)\delta_{\mathbf{k},\mathbf{k}'} \\ &\equiv \left\langle \rho_{\mathbf{k}i}(t)\rho_{-\mathbf{k}i}\right\rangle \left\langle j^{\beta}_{-\mathbf{k}}(t) j^{\alpha}_{\mathbf{k}}\right\rangle \end{aligned} \tag{9.5.7}$$

and use of (9.5.6) and (9.5.7) reduces (9.5.5) to the simpler form given by

$$Z(t) = \frac{1}{N^2} \sum_{\mathbf{k}} \left\langle \rho_{\mathbf{k}i}(t)\rho_{-\mathbf{k}i}\right\rangle \left\langle j^{x}_{\mathbf{k}}(t) j^{x}_{-\mathbf{k}}\right\rangle \tag{9.5.8}$$

The first factor in the sum over wavevectors is the self intermediate scattering function $F_{\mathrm{s}}(k,t)$ and the second is a current correlation function; the latter can be decomposed into its longitudinal and transverse parts in the manner of (7.4.24). On switching from a sum to an integral and replacing the current correlation function by its average over a sphere, (9.5.8) becomes

$$Z(t) = \frac{1}{3\rho}(2\pi)^{-3} \int F_{\mathrm{s}}(k,t) \frac{1}{k^2}\left[C_l(k,t) + 2C_t(k,t)\right] \mathrm{d}\mathbf{k} \tag{9.5.9}$$

If the time-correlation functions on the right-hand side of (9.5.9) are replaced by the hydrodynamic expressions, (9.5.9) leads back to (8.7.14), which is valid for long times. At short times, however, (9.5.9) breaks down: as $t \to 0$, $Z(t)$ diverges, since $F_{\mathrm{s}}(k, t=0) = 1$ and $C_l(k, t=0) = C_t(k, t=0) = k^2(k_{\mathrm{B}}T/m)$. To overcome this difficulty a cut-off at large wavenumbers must be introduced in the integration over $\mathbf{k}$. Such a cut-off occurs naturally in the so-called velocity-field approach,[13] in which a result very similar to (9.5.9) is obtained on the basis of a microscopic expression for the local velocity of the tagged particle. This expression involves a "form factor" $f(r)$, which in the simplest model used is represented by a unit step-function that vanishes for distances greater than the particle "radius" a and has the effect of making the velocity field constant over the range $r \leqslant a$. Replacement of the Fourier components of the velocity field by their projections along the particle current leads to an expression of the form

$$Z(t) = \tfrac{1}{3}(2\pi)^{-3} \int \hat{f}(k) F_{\mathrm{s}}(k,t) \frac{1}{k^2}\left[C_l(k,t) + 2C_t(k,t)\right] \mathrm{d}\mathbf{k} \tag{9.5.10}$$

where $\hat{f}(k=0) = 1/\rho$ and $\lim_{k\to\infty} \hat{f}(k) = 0$. This result reduces to that obtained by the mode-coupling approach in the long-wavelength limit, but the behaviour at short times is much improved compared with (9.5.9). In particular, the zero-time value is now correct:

$$Z(0) = (2\pi)^{-3} \int \hat{f}(k) \frac{k_B T}{m} \, d\mathbf{k} = \frac{k_B T}{m} f(r=0) = \frac{k_B T}{m} \tag{9.5.11}$$

Equation (9.5.10) does not represent a complete theory, since its evaluation requires a knowledge of the intermediate scattering function and the two current-correlation functions. For numerical purposes, however, use can be made of the viscoelastic approximations for $C_l(k,t)$ and $C_t(k,t)$ and the gaussian approximation (8.2.15) for $F_s(k,t)$. As Figure 9.6 shows, results obtained in this way for the velocity autocorrelation function and corresponding power spectrum of liquid rubidium are in good agreement with results obtained by molecular dynamics. The pronounced, low-frequency peak in the power spectrum arises from the coupling to the transverse current and the shoulder at higher frequencies comes from the coupling to the longitudinal current.

Another method whereby the short-time behaviour of the mode-coupling approximation can be improved is to include the exact, low-order frequency moments of $Z(\omega)$ in a systematic way by working in the continued-fraction representation.[14] Truncation of (9.1.37) at second order gives

$$\tilde{Z}(z) = \cfrac{1}{-iz + \cfrac{\Omega_0^2}{-iz + \tilde{N}_2(z)}} \tag{9.5.12}$$

where Ω_0 is the Einstein frequency (7.2.13) and $\tilde{N}_2(z) \equiv \Delta_2^2 \tilde{M}_2(z)$. The Laplace transform of $\tilde{N}_2(z)$ is related to the autocorrelation function of the second-order random force $R_2 = \mathcal{Q}_2(i\mathcal{L})^2 u_{ix} = \mathcal{Q}_1(i\mathcal{L})^2 u_{ix}$ by

$$\begin{aligned} N_2(t) &= \big(R_2, \exp(i\mathcal{Q}_2\mathcal{L}\mathcal{Q}_2 t) R_2\big)(R_1, R_1)^{-1} \\ &= \frac{m}{\Omega_0^2 k_B T} \big(\mathcal{Q}_1\mathcal{L}^2 u_{ix}, \exp(i\mathcal{Q}_2\mathcal{L}\mathcal{Q}_2 t)\mathcal{Q}_1\mathcal{L}^2 u_{ix}\big) \end{aligned} \tag{9.5.13}$$

The operator $\mathcal{Q}_1 = 1 - \mathcal{P}_1$ projects onto the subspace orthogonal to u_{ix} while $\mathcal{Q}_2 = \mathcal{Q}_1 - \mathcal{P}_2$ projects onto the subspace orthogonal to both u_{ix} and the acceleration $\dot{u}_{ix} = i\mathcal{L}u_{ix}$. The fact that $(i\mathcal{L})^2 u_{ix}$ is automatically orthogonal to $(i\mathcal{L})u_{ix}$ makes it possible to replace $\mathcal{Q}_2$ by $\mathcal{Q}_1$ in the definition of R_2.

If the product variables $\rho_{\mathbf{k}i}\mathbf{j}_{-\mathbf{k}}$ are again chosen as the basis set, use of the approximation (9.5.2) allows (9.5.13) to be rewritten as

$$\begin{aligned} N_2(t) \approx \frac{m}{\Omega_0^2 k_B T} \sum_{\mathbf{k},\mathbf{k}'} \sum_{\alpha} \sum_{\beta} &\big(\rho_{\mathbf{k}'i} j^{\beta}_{-\mathbf{k}'}, \mathcal{Q}_1\mathcal{L}^2 u_{ix}\big)\big(\rho_{\mathbf{k}'i} j^{\beta}_{-\mathbf{k}'}, \rho_{\mathbf{k}'i} j^{\beta}_{-\mathbf{k}'}\big)^{-1} \\ &\times \big(\rho_{\mathbf{k}i} j^{\alpha}_{-\mathbf{k}}, \exp(i\mathcal{Q}_2\mathcal{L}\mathcal{Q}_2 t)\rho_{\mathbf{k}'i} j^{\beta}_{-\mathbf{k}'}\big) \\ &\times \big(\rho_{\mathbf{k}i} j^{\alpha}_{-\mathbf{k}}, \rho_{\mathbf{k}i} j^{\alpha}_{-\mathbf{k}}\big)^{-1}\big(\mathcal{Q}_1\mathcal{L}^2 u_{ix}, \rho_{\mathbf{k}i} j^{\alpha}_{-\mathbf{k}}\big) \end{aligned} \tag{9.5.14}$$

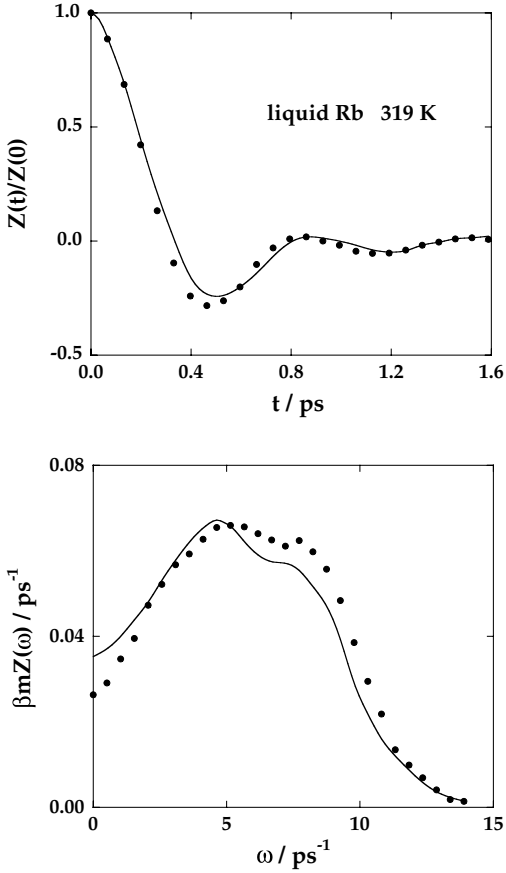

FIG. 9.6. Normalised velocity autocorrelation function (above) and the corresponding power spectrum (below) for a model of liquid rubidium. The points are molecular-dynamics results and the curves are calculated from the velocity-field approximation (9.5.10). After Gaskell and Miller.[13]

If we again assume that the variables $\rho_{\mathbf{k}i}$ and $\mathbf{j}^{\alpha}_{\mathbf{k}}$ evolve in time independently of each other, and make the further approximation of replacing the projected operator $\mathcal{Q}_2\mathcal{L}\mathcal{Q}_2$ by the full Liouville operator $\mathcal{L}$ in the propagator governing the time evolution of the factorised correlation functions, (9.5.14) becomes

$$\begin{aligned} N_2(t) \approx \frac{m}{\Omega_0^2 k_{\mathrm{B}} T} \sum_{\mathbf{k},\mathbf{k}'} \sum_{\alpha} \sum_{\beta} \big(\rho_{\mathbf{k}'i}\, j^{\beta}_{-\mathbf{k}'},\, \mathcal{Q}_1\mathcal{L}^2 u_{ix}\big)\big(\rho_{\mathbf{k}'i}\, j^{\beta}_{-\mathbf{k}'},\, \rho_{\mathbf{k}'i}\, j^{\beta}_{-\mathbf{k}'}\big)^{-1} \\ \times \big(\rho_{\mathbf{k}i},\, \rho_{\mathbf{k}'i}(t)\big)\big(j^{\alpha}_{-\mathbf{k}},\, j^{\beta}_{-\mathbf{k}'}(t)\big)\delta_{\mathbf{k}\mathbf{k}'} \\ \times \big(\rho_{\mathbf{k}i}\, j^{\alpha}_{-\mathbf{k}},\, \rho_{\mathbf{k}i}\, j^{\alpha}_{-\mathbf{k}}\big)^{-1}\big(\mathcal{Q}_1\mathcal{L}^2 u_{ix},\, \rho_{\mathbf{k}i}\, j^{\alpha}_{-\mathbf{k}}\big) \end{aligned} \tag{9.5.15}$$

The time-correlation functions appearing here are the same as in (9.5.7), but the time-independent vertices have a more complicated form; a detailed calculation shows that

$$\left(\mathcal{Q}_1\mathcal{L}^2 u_{i\alpha},\, \rho_{\mathbf{k}i}\, j^{\beta}_{-\mathbf{k}}\right) = -\frac{\Omega_0^2 k_{\mathrm{B}}T}{m}\mathcal{V}_{\alpha\beta}(k) \tag{9.5.16}$$

where

$$\mathcal{V}_{\alpha\beta}(k) = \frac{\rho}{\Omega_0^2 m}\int \exp(-i\mathbf{k}\cdot\mathbf{r})g(r)\nabla_\alpha\nabla_\beta v(r)\,\mathrm{d}\mathbf{r} \tag{9.5.17}$$

is a normalised "vertex function". Then, proceeding as before by switching from a sum over wavevectors to an integral, we find that

$$N_2(t) = N_{2l}(t) + 2N_{2t}(t) \tag{9.5.18}$$

$$N_{2l,t}(t) = \frac{\Omega_0^2 m}{3\rho k_{\mathrm{B}}T}(2\pi)^{-3}\int \mathcal{V}_{l,t}^2(k)F_{\mathrm{s}}(k,t)\frac{1}{k^2}C_{l,t}(k,t)\,\mathrm{d}\mathbf{k} \tag{9.5.19}$$

where $\mathcal{V}_{l,t}$ are the longitudinal and transverse components of the vertex tensor, defined in a manner analogous to (7.4.24).

There is striking similarity between the structure of (9.5.19) and that of the mode-coupling expression (9.5.9) obtained earlier for $Z(t)$ except that (9.5.19) contains the vertex factors $\mathcal{V}_{l,t}$. Inclusion of these factors ensures that the integral over wavevectors converges for all t; they therefore play a similar role to that of the form factor $\hat{f}(k)$ in the velocity-field approach, but have the advantage of being defined unambiguously through (9.5.17). The theory is also self-consistent, since the correlation functions required as input may be obtained by a mode-coupling calculation of the same type. Numerically, however, the results are less satisfactory than those pictured in Figure 9.6.

9.6 MODE-COUPLING THEORY II. THE KINETIC GLASS TRANSITION

The mode-coupling ideas introduced in Section 9.5 were first used by Kawasaki[15] to study the "critical slowing down" of density fluctuations near the liquid–gas critical point. Here we describe the application of the same general approach[16] to the not dissimilar phenomena associated with the kinetic glass transition of a fragile glass former, already discussed in a qualitative way in Section 8.8. The theory shows that the structural arrest and associated dynamical anomalies that appear in the supercooled liquid at a well-defined temperature (on cooling) or density (on compression) are a direct consequence of a non-linear, feedback mechanism, the source of which is the fact that the memory function of the density autocorrelation function $F(k,t)$ may be expressed, at least approximately, in terms of $F(k,t)$ itself. Although real glass-forming liquids are usually multi-component in nature, we limit the discussion to one-component systems; the generalisation to mixtures is straightforward.

We saw in Section 9.4 that the decay of density fluctuations in a simple liquid above its triple point is well described within the memory-function formalism by choosing as components of the dynamical vector $\mathbf{A}$ the three variables $\rho_{\mathbf{k}}$ (particle density), $j_{\mathbf{k}} \equiv \mathbf{k} \cdot \mathbf{j}_{\mathbf{k}}/k$ (longitudinal particle current) and $T_{\mathbf{k}}$ (a microscopic temperature variable). It turns out, however, that temperature fluctuations are not important for the description of structural arrest and for present purposes the variable $T_{\mathbf{k}}$ can therefore be omitted. To simplify the resulting equations we first introduce a normalised density autocorrelation function

$$\phi(k,t) = F(k,t)/S(k) \tag{9.6.1}$$

with $\phi(k, t=0) = 1$. Then, by following steps similar to those used to derive the memory-function equation (9.4.16), we arrive at an expression for the Laplace transform of $\phi(k,t)$ in the form

$$\tilde{\phi}(k,z) = \frac{1}{-iz + \dfrac{\Omega_k^2}{-iz + \widetilde{M}(k,z)}} \tag{9.6.2}$$

where $\Omega_k^2 = v_T^2 k^2/S(k)$ and $v_T = (k_{\mathrm{B}}T/m)^{1/2}$ is the thermal velocity. The structure of this result is identical with that in (9.4.16) and the function $\widetilde{M}(k,z)$, like $\widetilde{N}_l(k,z)$ in (9.4.16), is again the memory function of the longitudinal current, but the two choices made for the vector $\mathbf{A}$ means that the explicit form of the memory function is different in the two cases. In the two-variable description the random-force vector has only one component, given by

$$K_{\mathbf{k}} = \mathcal{Q}(i\mathcal{L}j_{\mathbf{k}}) \tag{9.6.3}$$

and the corresponding memory function is

$$M(k,t) = \frac{1}{Nv_T^2}\big(K_{\mathbf{k}},\, R_{\mathbf{k}}(t)\big) \tag{9.6.4}$$

with $R_{\mathbf{k}}(t) = \exp(i\mathcal{Q}\mathcal{L}\mathcal{Q}t)K_{\mathbf{k}}$, where the operator $\mathcal{Q} = 1 - \mathcal{P}$ projects an arbitrary dynamical variable onto the subspace orthogonal to the variables $\rho_{\mathbf{k}}$ and $j_{\mathbf{k}}$. The time dependence of $\phi(k,t)$ is obtained from (9.6.2) via an inverse Laplace transform:

$$\ddot{\phi}(k,t) + \Omega_k^2\phi(k,t) + \int_0^t M(k,t-t')\dot{\phi}(k,t')\,\mathrm{d}t' = 0 \tag{9.6.5}$$

which can be recognised as the equation of motion of a harmonic oscillator of frequency Ω_k, damped by a time-retarded, frictional force.

The theoretical task is to derive an expression for the memory function that accounts for the structural slowing-down near the transition temperature T_{C}; to achieve this, we follow the original arguments of Götze and collaborators.[17] The random force $K_{\mathbf{k}}$ is by construction orthogonal to the slow variable $\rho_{\mathbf{k}}$ and the simplest slow variables having a non-zero correlation with $K_{\mathbf{k}}$ are the pair products

$$A_{\mathbf{p},\mathbf{q}} = \rho_{\mathbf{p}}\rho_{\mathbf{q}} \tag{9.6.6}$$

Hence the first approximation, one of typical mode-coupling type, is to replace the random force $K_{\mathbf{k}}$ in (9.6.3) by its projection onto the subspace spanned by all pair products, i.e.

$$K_{\mathbf{k}} \approx \sum_{\mathbf{p},\mathbf{q}} \sum_{\mathbf{p}',\mathbf{q}'} (A_{\mathbf{p}',\mathbf{q}'}, K_{\mathbf{k}})(A_{\mathbf{p},\mathbf{q}}, A_{\mathbf{p}',\mathbf{q}'})^{-1} A_{\mathbf{p},\mathbf{q}} \tag{9.6.7}$$

Substitution of (9.6.7) and the corresponding expression for $R_{\mathbf{k}}(t)$ in (9.6.4) gives

$$\begin{aligned} M(k,t) = \frac{1}{N v_T^2} &\sum_{\mathbf{p},\mathbf{q}} \sum_{\mathbf{p}',\mathbf{q}'} (A_{\mathbf{p}',\mathbf{q}'}, K_{\mathbf{k}})(A_{\mathbf{p},\mathbf{q}}, A_{\mathbf{p}',\mathbf{q}'})^{-1} \\ &\times \sum_{\mathbf{p}'',\mathbf{q}''} \sum_{\mathbf{p}''',\mathbf{q}'''} (A_{\mathbf{p}''',\mathbf{q}'''}, K_{\mathbf{k}})(A_{\mathbf{p}'',\mathbf{q}''}, A_{\mathbf{p}''',\mathbf{q}'''})^{-1} \\ &\times \big(A_{\mathbf{p},\mathbf{q}}, \exp(i\mathcal{Q}\mathcal{L}\mathcal{Q}t) A_{\mathbf{p}'',\mathbf{q}''}\big) \end{aligned} \tag{9.6.8}$$

The next step is to factorise the static and dynamic four-point correlation functions in (9.6.8) into products of two-point functions, and simultaneously to replace the propagator of the projected dynamics by the full propagator. Thus

$$\begin{aligned} \big(A_{\mathbf{p},\mathbf{q}}, \exp(i\mathcal{Q}\mathcal{L}\mathcal{Q}t) A_{\mathbf{p}'',\mathbf{q}''}\big) &= \big(\rho_{\mathbf{p}}\rho_{\mathbf{q}}, \exp(i\mathcal{Q}\mathcal{L}\mathcal{Q}t)\rho_{\mathbf{p}''}\rho_{\mathbf{q}''}\big) \\ &\approx \big(\rho_{\mathbf{p}}, \exp(i\mathcal{L}t)\rho_{\mathbf{p}''}\big)\big(\rho_{\mathbf{q}}, \exp(i\mathcal{L}t)\rho_{\mathbf{q}''}\big) \\ &= \delta_{\mathbf{p},\mathbf{p}''}\delta_{\mathbf{q},\mathbf{q}''} N^2 S(p) S(q) \phi(p,t)\phi(q,t) \end{aligned} \tag{9.6.9}$$

while for $t = 0$:

$$\begin{aligned} (A_{\mathbf{p},\mathbf{q}}, A_{\mathbf{p}',\mathbf{q}'}) &= \delta_{\mathbf{p},\mathbf{p}'}\delta_{\mathbf{q},\mathbf{q}'} N^2 S(p) S(q) \\ (A_{\mathbf{p},\mathbf{q}}, A_{\mathbf{p}',\mathbf{q}'})^{-1} &= \frac{\delta_{\mathbf{p},\mathbf{p}'}\delta_{\mathbf{q},\mathbf{q}'}}{N^2 S(p) S(q)} \end{aligned} \tag{9.6.10}$$

The three-point static correlation functions that appear in the terms involving $K_{\mathbf{k}}$ in (9.6.8) can be eliminated with a help of a generalisation of the Yvon equality (7.2.11), i.e.

$$\langle \dot{A} B^* \rangle = \big\langle (i\mathcal{L}A) B^* \big\rangle \equiv -\big\langle \{\mathcal{H}, A\}, B^* \big\rangle = k_{\mathrm{B}} T \big\langle \{A, B^*\} \big\rangle \tag{9.6.11}$$

the proof of which now requires a double integration by parts. We also make use of the Ornstein–Zernike relation in the form $S(k) = 1/(1 - \rho\hat{c}(k))$ and the convolution approximation (4.2.10). Then, for example:

$$(\rho_{\mathbf{p}',\mathbf{q}'}, i\mathcal{L} j_{\mathbf{k}}) = -i v_T^2 N \delta_{\mathbf{k},\mathbf{p}'+\mathbf{q}'} \big[\mathbf{k}\cdot\mathbf{p}' S(q') + \mathbf{k}\cdot\mathbf{q}' S(p')\big]/k \tag{9.6.12}$$

The final result of these manipulations is

$$M(k,t) = \frac{v_T^2 \rho^2}{2Nk^2} \sum_{\mathbf{p},\mathbf{q}} \delta_{\mathbf{k},\mathbf{p}+\mathbf{q}} S(p) S(q) \big[\hat{c}(p)\mathbf{k}\cdot\mathbf{p} + \hat{c}(q)\mathbf{k}\cdot\mathbf{q}\big]^2 \phi(p,t)\phi(q,t) \tag{9.6.13}$$

The factor $\frac{1}{2}$ on the right-hand side arises from the fact that all double sums over pairs of wavevectors must be ordered in such a way that each product variable $A_{\mathbf{p},\mathbf{q}}$ appears only once.

The appearance of the product $\phi(p,t)\phi(q,t)$ in (9.6.13) means that the memory function decays on the same time-scale as the correlation function. This represents only the long-time contribution to the total memory function and cannot describe the behaviour at short times, which is dominated by nearly instantaneous, binary collisions. To describe the effect of collisions it is assumed that the short-time contribution $M^{(0)}(k,t)$ can be represented by a δ-function, i.e.

$$M^{(0)}(k,t) = \nu(k)\delta(t) \tag{9.6.14}$$

The complete memory function is therefore written as

$$M(k,t) = \nu(k)\delta(t) + \Omega_k^2 m(k,t) \tag{9.6.15}$$

Comparison with (9.6.13) shows that

$$m(k,t) = \frac{1}{2V}\sum_{\mathbf{p},\mathbf{q}} \delta_{\mathbf{k},\mathbf{p}+\mathbf{q}} \mathcal{V}(\mathbf{k},\mathbf{p},\mathbf{q})\phi(p,t)\phi(q,t) \tag{9.6.16}$$

where the vertex function $\mathcal{V}$ is

$$\mathcal{V}(\mathbf{k},\mathbf{p},\mathbf{q}) = \frac{\rho S(k)S(p)S(q)}{k^4}\left[\hat{c}(p)\mathbf{k}\cdot\mathbf{p} + \hat{c}(q)\mathbf{k}\cdot\mathbf{q}\right]^2 \tag{9.6.17}$$

The non-linear, integro-differential equation (9.6.5) may then be rewritten as

$$\ddot{\phi}(k,t) + \Omega_k^2\phi(k,t) + \nu(k)\dot{\phi}(k,t) + \Omega_k^2\int_0^\infty m(k,t-t')\dot{\phi}(k,t')\,\mathrm{d}t' = 0 \tag{9.6.18}$$

The coupled equations (9.6.16) and (9.6.18) form a closed, self-consistent set; the only input required for their solution is the static structure factor of the supercooled liquid, which determines the value of the vertex function via (9.6.17). The feedback mechanism is provided by the quadratic dependence of the memory function on $\phi(k,t)$, with the density and temperature dependence of the effect coming from the vertex function. Numerical solution of the coupled equations reveals the existence of a sharp crossover from ergodic to non-ergodic behaviour of $\phi(k,t)$ at a well-defined temperature (at constant density) or density (at constant temperature). The predicted correlation function can also be used as input to a similar set of equations for the self correlation function $F_\mathrm{s}(k,t)$, where the memory function now involves the product $\phi(k,t)F_\mathrm{s}(k,t)$.

In the case of hard spheres the theory outlined above predicts a kinetic glass transition at a packing fraction $\eta_\mathrm{C} \approx 0.516$ when the Percus–Yevick approximation for the structure factor is used. At the critical packing fraction the order parameter[18] $f_k = \lim_{t\to\infty}\phi(k,t)$ changes discontinuously from zero to a wavenumber-dependent value $0 < f_k \leqslant 1$. That this transition is a direct consequence of the non-linearity of the equation of motion (9.6.18)

can be demonstrated with the help of some further approximations.[17,19] The largest contribution to the vertex function comes from the region $k \approx k_{\max}$ of the main peak in the structure factor. It is therefore not unreasonable to ignore the sum over wavevectors by putting $S(k) \approx 1 + a\delta(k - k_{\max})$, where a is the area under the main peak. With this assumption, (9.6.18) becomes an equation for the single correlation function $\phi(k_{\max}, t) \equiv \phi(t)$, which we write as

$$\ddot{\phi}(t) + \Omega^2\phi(t) + \nu\dot{\phi}(t) + \lambda\Omega^2 \int_0^\infty \big[\phi(t - t')\big]^2 \dot{\phi}(t')\,\mathrm{d}t' = 0 \tag{9.6.19}$$

where $\Omega \equiv \Omega_{k_{\max}}$, ν can be interpreted as a collision frequency and λ, which replaces the complicated vertex function, acts as a "control parameter", a role played by inverse temperature or density in the more complete theory. By taking the Laplace transform of (9.6.19) we recover (9.6.2) in the form

$$\tilde{\phi}(z) = \cfrac{1}{-iz + \cfrac{\Omega^2}{-iz + \nu + \Omega^2\tilde{m}(z)}} \tag{9.6.20}$$

with

$$\tilde{m}(z) = \lambda \int_0^\infty \big[\phi(t)\big]^2 \exp(izt)\,\mathrm{d}t \tag{9.6.21}$$

Equation (9.6.20) can be rearranged to give

$$\frac{\tilde{\phi}(z)}{1 + iz\tilde{\phi}(z)} = \frac{1}{\Omega^2}\big[-iz + \nu + \Omega^2\tilde{m}(z)\big] \tag{9.6.22}$$

Let $\lim_{t\to\infty} \phi(t) = f$, where the order parameter f is now independent of k. Then

$$\lim_{z\to 0} \tilde{\phi}(z) = \frac{f}{-iz} \tag{9.6.23}$$

and hence, from substitution in (9.6.22):

$$\lim_{z\to 0} \tilde{m}(z) = \frac{f}{-iz(1 - f)} \tag{9.6.24}$$

In the non-ergodic or structurally arrested phase, where $f > 0$, the power spectrum $\phi(\omega)$ will contain a fully elastic component, $f\delta(\omega)$; experimentally this would correspond to scattering from the frozen structure.

Equation (9.2.21) shows that

$$\lim_{z\to 0} \tilde{m}(z) = \frac{\lambda f^2}{-iz} \tag{9.6.25}$$

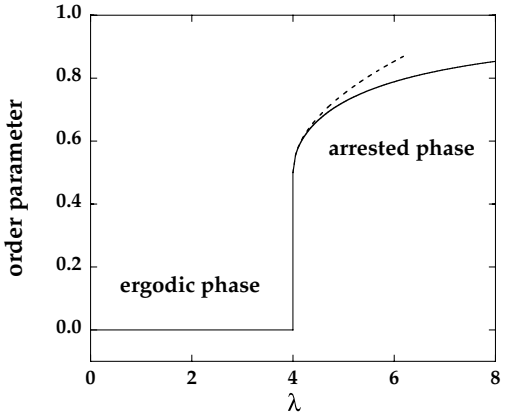

FIG. 9.7. Predictions of mode-coupling theory for the dependence on λ of the order parameter f. The full curve is the result obtained from the equation of motion (9.6.19) and the dashes show the approximate solution (9.6.27).

Identification of (9.6.25) with (9.6.24) leads to a simple equation for the order parameter:

$$\frac{f}{1-f} = \lambda f^2 \tag{9.6.26}$$

the solutions to which are

$$f = 0, \qquad f = \tfrac{1}{2}\left[1 \pm (1 - 4/\lambda)^{1/2}\right] \tag{9.6.27}$$

Since f must be real, the only acceptable solution for $\lambda < 4$ is $f = 0$, corresponding to the ergodic phase. This remains a solution at larger values of λ, but at the critical value, $\lambda_C = 4$, there is a bifurcation to the non-ergodic solution, $f = \frac{1}{2}[1 + (1 - 4/\lambda)^{1/2}]$; for $\lambda = 4$, $f = \frac{1}{2}$. The root $f = \frac{1}{2}[1 - (1 - 4/\lambda)^{1/2}]$ is not acceptable, since it implies that the system would revert to ergodic behaviour in the limit $\lambda \to \infty$. Let $\lambda = 4(1 + \sigma\varepsilon)$, where $\sigma = -1$ and $+1$ in the ergodic and arrested phases, respectively. The quantity $\varepsilon = (\lambda - \lambda_C)/\sigma\lambda_C$ is a positive number that measures the distance from the transition. Substitution in (9.6.27) shows that for $\sigma = +1$, f has a square-root cusp as $\varepsilon \to 0$:

$$\lim_{\varepsilon \to 0} f = \tfrac{1}{2}\left(1 + \varepsilon^{1/2}\right) \tag{9.6.28}$$

The dependence of f on λ calculated from (9.6.27) and (9.6.28) is sketched in Figure 9.7.

Equation (9.6.28) describes the infinite-time behaviour of the correlation function in the arrested phase for $\lambda \approx \lambda_C$. To extend this result to finite times, we look for a solution to (9.6.19) of the form

$$\phi(t) = \tfrac{1}{2} + \varepsilon^{1/2} g_\varepsilon(\tau) \tag{9.6.29}$$

where $\tau = \varepsilon^s t$ is a scaled time and $g_\varepsilon(\tau)$ is a scaling function. The quantity s (> 0) is a scaling exponent, which is determined later by requiring $\phi(t)$ to be independent of ε in the

short-time limit. This restriction on ϕ follows from the fact that the short-time behaviour is controlled by the collision frequency ν, not by the mode-coupling contribution to the memory function. The Laplace transform of (9.6.29) is

$$\tilde{\phi}(z) = \varepsilon^{-s}\left(\frac{1}{-2i\zeta} + \varepsilon^{1/2}\tilde{g}_\varepsilon(\zeta)\right) \tag{9.6.30}$$

where $\zeta \equiv \varepsilon^{-s}z$. If we substitute (9.6.29) in (9.6.21) (with $\lambda = 4(1+\sigma\varepsilon)$) and (9.6.30) in (9.6.22), combine the two results and let $\varepsilon \to 0$, we obtain an equation for the scaling function at the critical point ($\varepsilon = 0$):

$$-8i\zeta\left[\tilde{g}_0(\zeta)\right]^2 - 4\int_0^\infty \left[g_0(\tau)\right]^2 \exp(i\zeta\tau)\,\mathrm{d}\tau = \frac{\sigma}{-i\zeta} \tag{9.6.31}$$

To derive this result it must be assumed that $\varepsilon^{1/2}\tilde{g}_0(\zeta)$ vanishes with ε; the solution obtained below is consistent with that assumption.

The β-relaxation regime corresponds to scaled times $\tau \ll 1$ (or $\zeta \gg 1$). We look for a power-law solution for $g_0(\tau)$ such that

$$g_0(\tau) = a_0\tau^{-a}, \quad \tau \to 0 \tag{9.6.32}$$

with a Laplace transform given by

$$\tilde{g}_0(\zeta) = a_0\Gamma(1-a)(-i\zeta)^{a-1}, \quad \zeta \to \infty \tag{9.6.33}$$

where $\Gamma(x)$ is the gamma function. Substitution in (9.6.31) gives

$$(-i\zeta)^{2a-1}4a_0^2\left[2\Gamma^2(1-a) - \Gamma(1-2a)\right] = 0 \tag{9.6.34}$$

i.e. $2\Gamma^2(1-a) = \Gamma(1-2a)$, the positive solution to which is $a \approx 0.395$. When written in terms of the original time variable t, combination of (9.6.29) and (9.6.32) shows that

$$\phi(t) = \tfrac{1}{2} + a_0\varepsilon^{-as+1/2}t^{-a} \tag{9.6.35}$$

Since $\phi(t)$ must be independent of ε in the limit $t \to 0$, it follows that $s = 1/2a \approx 1.265$. Thus the correlation function decays as

$$\phi(t) = \tfrac{1}{2} + a_0t^{-a} \tag{9.6.36}$$

The result expressed by (9.6.36) is independent of σ. It therefore describes both the decay of $\phi(t)$ towards its non-zero, asymptotic value in the arrested phase and the first relaxation process in the ergodic phase, where the power-law behaviour will persist so long as $\tau \ll 1$. Times $\tau \gg 1$ corresponds to α-relaxation in the ergodic phase. A scaling analysis similar to the previous one starts from the ansatz

$$g_0(\tau) = -b_0\tau^b, \quad \tau \to \infty \tag{9.6.37}$$

and leads to the exponent relation

$$2\Gamma^2(1+b) - \Gamma(1+2b) = 0 \tag{9.6.38}$$

The only acceptable solution to this equation is $b = 1$. Thus

$$\phi(t) = \tfrac{1}{2} - b_0\varepsilon^{1/2}\tau, \quad 1 \ll \tau \ll 1/b_0\varepsilon^{1/2} \tag{9.6.39}$$

The upper limit on τ in (9.6.39) appears because $|\varepsilon^{1/2}g_0(\tau)|$ must be less than unity for the asymptotic analysis to be valid. For yet longer times, a purely exponential decay is predicted, in contrast to the stretched-exponential decay seen both experimentally and in simulations (see Section 8.8). To reproduce the observed behaviour the simplified model represented by (9.6.19), in which $m(t)$ behaves as $[\phi(t)]^2$, must be generalised[16] to include more control parameters and other powers of $\phi(t)$.

The scaling predictions of mode-coupling theory have been tested against experimental data and the results of simulations,[20] and generally good agreement is found at temperatures just above T_C. However, the distinction between ergodic and strictly non-ergodic phases that appears in the original version of the theory is unrealistic. At sufficiently long times, thermally activated processes of the type evident, for example, in Figure 8.8 will eventually cause ergodicity to be restored. Such effects can be accommodated within the theory by inclusion of the coupling of fluctuations in the microscopic density with those in particle current.[21] The "ideal" transition is then suppressed and the correlation function is found to decay to zero even below T_C, though only after a period of near-complete structural arrest that rapidly lengthens as the temperature is lowered.[22]

NOTES AND REFERENCES

1. Zwanzig, R., *In* "Lectures in Theoretical Physics", vol. III (W.E. Britton, B.W. Downs and J. Downs, eds). Wiley Interscience, New York, 1961.
2. (a) Mori, H., *Prog. Theor. Phys.* **33**, 423 (1965). (b) Mori, H., *Prog. Theor. Phys.* **34**, 399 (1965).
3. Lovesey, S.W., *J. Phys. C* **6**, 1856 (1973).
4. See, e.g., de Jong, P.H.K., Verkerk, P. and de Graaf, L.A., *J. Phys.: Condens. Matter* **6**, 8391 (1994).
5. Balucani, U., Torcini, A., Stangl, A. and Morkel, C., *J. Non-Cryst. Solids* **299–303**, 205 (1996).
6. Levesque, D. and Verlet, L., *Phys. Rev. A* **2**, 2514 (1970).
7. Levesque, D., Verlet, L. and Kürkijarvi, J., *Phys. Rev. A* **7**, 1690 (1973).
8. See, e.g., Kambayashi, S. and Kahl, G., *Phys. Rev. A* **46**, 3255 (1992).
9. Lovesey, S.W., *J. Phys. C* **4**, 3057 (1971).
10. Rahman, A., *In* "Statistical Mechanics: New Concepts, New Problems, New Applications" (S.A. Rice, K.F. Freed and J.C. Light, eds). University of Chicago Press, Chicago, 1972.
11. Copley, J.R.D. and Lovesey, S.W., *Rep. Prog. Phys.* **38**, 461 (1975).
12. (a) Scopigno, T., Balucani, U., Ruocco, G. and Sette, F., *Phys. Rev.* **85**, 4076 (2000). (b) Scopigno, T., Balucani, U., Ruocco, G. and Sette, F., *J. Non-Cryst. Solids* **312–314**, 121 (2002).
13. Gaskell, T. and Miller, S., *J. Phys. C* **11**, 3749 (1978).
14. Bosse, J., Götze, W. and Zippelius, A., *Phys Rev. A* **18**, 1214 (1978).
15. Kawasaki, K., *Ann. Phys. N.Y.* **61**, 1 (1970).
16. (a) Götze, W. and Sjögren, L., *Rep. Prog. Phys.* **55**, 241 (1992). (b) Götze, W., *In* "Liquids, Freezing and the Glass Transition: Les Houches, Session LI" (J.P. Hansen, D. Levesque and J. Zinn-Justin, eds). Elsevier, Amsterdam, 1991. (c) Das, S.P., *Rev. Mod. Phys.* **76**, 785 (2004).

17. Bengtzelius, U., Götze, W. and Sjölander, A., *J. Phys. C* **17**, 5915 (1984).
18. The terms non-ergodicity parameter or Edwards–Anderson parameter are also used, the latter by analogy with a related problem in spin glasses: Edwards, S.F. and Anderson, P.W., *J. Phys. F* **5**, 965 (1975).
19. Leutheusser, E., *Phys. Rev. A* **29**, 2765 (1984).
20. For a review, see Götze, W., *J. Phys. Condens. Matter* **11**, A1 (1999).
21. (a) Das, S.P. and Mazenko, G.F., *Phys. Rev. A* **34**, 2265 (1986). (b) Götze, W. and Sjögren, L., *Z. Phys. B* **65**, 415 (1987).
22. For later developments in the theory of slow relaxations and the kinetic glass transition, see "Nonequilibrium Dynamics and Slow Relaxations in Condensed Matter" (J.L. Barrat, J. Kurchan, M. Feigelman and J. Dalibard, eds). Springer, Berlin, 2003.

CHAPTER 10

Ionic Liquids

10.1 CLASSES AND MODELS OF IONIC LIQUIDS

We have been concerned so far almost exclusively with fluids in which the range of the interparticle forces is of the order of a few atomic radii. This chapter is devoted to systems in which the particles carry an electric charge. Ionic liquids have certain properties that are absent in fluids composed of neutral particles and many of their distinguishing features are associated in some way with the slow decay of the Coulomb potential. Our attention will be focused on three types of system: molten salts, ionic solutions and liquid metals. *Molten salts* are in many respects the simplest class of ionic liquids. We shall consider in detail only the case in which there is a single cation and a single anion species, of which the alkali halides are the best understood examples. Molten salts are characterised by large cohesive energies and high temperatures, and by ionic conductivities of the order of 1 Ω^{-1} cm^{-1}. There exist also certain crystalline salts that have conductivities comparable with those of the molten phase. These are the so-called "fast-ion" conductors, or "solid electrolytes", in which one of the ionic species becomes liquid-like in behaviour above a certain temperature.[1] *Ionic solutions* are liquids consisting of a solvent formed from neutral, polar molecules and a solute that dissociates into positive and negative ions. They vary widely in complexity. In the classic *electrolyte solutions* the cations and anions are of comparable size and absolute charge, whereas macromolecular ionic solutions contain both macroions (charged polymer chains, micelles, charged colloidal particles, etc.) and microscopic counterions. Despite their complexity, some systems of the latter type, including charged colloidal suspensions, can be treated quantitatively by standard methods of liquid-state theory. Finally, *liquid metals* are similar in composition to molten salts, the anion of the salt being replaced by electrons from the valence or conduction bands of the metal. The analogy is a superficial one, however, because the small mass of the electron leads to a pronounced asymmetry between the two charge-carrying species. Whereas the behaviour of the ions can be discussed within the framework of classical statistical mechanics, the electrons form a degenerate Fermi gas for which a quantum-mechanical treatment is required. The presence of "free" electrons is also the origin of the very high electrical conductivies of liquid metals, which are typically three to four orders of magnitude larger than those of molten salts. "Simple" metals are those in which the electronic valence states are well separated in energy from the tightly bound, core states; they include the alkali metals, magnesium, zinc, mercury, gallium and aluminium.

The systems we have listed vary widely in character but they have two important features in common: first, that of overall, macroscopic charge neutrality and, secondly, the presence of mobile charge carriers. The condition of overall charge neutrality imposes a constraint on the relative concentrations of the ions. If the fluid contains $\rho_\nu = N_\nu / V$ ions per unit volume of species ν and if the charge carried by ions of that species is $q_\nu = z_\nu e$, where e is the elementary charge, overall charge neutrality requires that

$$\sum_\nu z_\nu \rho_\nu = 0 \tag{10.1.1}$$

We shall see in the next section that a tendency towards charge neutrality exists even at the local, microscopic level. This effect gives rise in turn to the phenomenon of *screening*. Introduction of an external charge into an ionic fluid causes a rearrangement, or polarisation, of the surrounding charge density of a nature such that the net electrostatic potential due to the external charge and the "polarisation cloud" decays much faster than the bare Coulomb potential. In fact, as we shall show later, the potential decays exponentially. Since it is permissible to regard any ion in the fluid as an "external" charge, it follows that the screening mechanism determines the long-range behaviour of the ionic distribution functions. Screening also requires that the distribution functions satisfy a number of important sum rules. In ionic liquids of high density, such as molten salts, there is a competition between packing effects and screening; this leads to a *charge ordering* of the ions, which manifests itself as an alternation in sign of the charge carried by successive coordination shells around a central ion.

The presence of mobile charge carriers plays an important role in determining the dynamical properties of ionic liquids. It leads most obviously to new kinds of transport, of which electrical conduction is the most familiar example. In addition, the interplay between Maxwell's equations and the equations of hydrodynamics causes the long-wavelength charge fluctuations to relax in a manner qualitatively different from that of concentration fluctuations in mixtures of uncharged particles. Under conditions achievable, in particular, in molten salts, fluctuations in charge may give rise to propagating, high-frequency, collective modes. These excitations are similar in character to the optic modes of ionic crystals and are also closely related to the charge oscillations found in plasmas.

Theories of ionic liquids rely heavily on the use of simple hamiltonian models that retain only the essential features of the ionic interactions. One simplifying approximation commonly made is to ignore the polarisability of the ions and represent the interactions by a *rigid-ion model*. The total potential energy is then assumed to be pairwise-additive and written as the sum of short-range (S) and coulombic (C) terms in the form

$$V_N(\mathbf{r}^N) = V_N^{\mathrm{S}}(\mathbf{r}^N) + V_N^{\mathrm{C}}(\mathbf{r}^N) = V_N^{\mathrm{S}}(\mathbf{r}^N) + \sum_{i=1}^{N} \sum_{j>i}^{N} \frac{z_i z_j e^2}{\varepsilon |\mathbf{r}_j - \mathbf{r}_i|} \tag{10.1.2}$$

where N is the total number of ions and ε is the dielectric constant of the medium in which the ions are immersed. It is often convenient to replace the Coulomb term in (10.1.2) by a sum in reciprocal space. Let $\rho_{\mathbf{k}}^Z$ be a Fourier component of the microscopic charge density,

given by

$$\rho_{\mathbf{k}}^{Z} = \sum_{\nu} z_{\nu} \rho_{\mathbf{k}}^{\nu} \tag{10.1.3}$$

where $\rho_{\mathbf{k}}^{\nu}$ is a Fourier component of the microscopic number density of species ν. Then the total Coulomb energy of a periodic system of volume V is

$$V_N^{\mathrm{C}}(\mathbf{r}^N) = \frac{1}{2V} \sum_{\mathbf{k}} \hat{v}(k) \left(\rho_{\mathbf{k}}^{Z} \rho_{-\mathbf{k}}^{Z} - \sum_{i=1}^{N} z_i^2 \right) \tag{10.1.4}$$

where the sum on $\mathbf{k}$ runs over wavevectors compatible with the assumed periodic boundary conditions and the (negative) second term inside brackets cancels the infinite self-energy of the ions. The function $\hat{v}(k)$ is the Fourier transform of the Coulomb potential between two elementary charges, i.e.

$$\hat{v}(k) = 4\pi e^2 / k^2 \tag{10.1.5}$$

The same expression was used earlier in the derivation of the Debye–Hückel result (4.6.26); the k^{-2} singularity in the limit $k \to 0$ is an important characteristic of Coulomb systems. In the thermodynamic limit the sum over wavevectors in (10.1.4) becomes an integral over $\mathbf{k}$ divided by $(2\pi)^3$; the equivalence of the two expressions for V_N^{C} in (10.1.2) and (10.1.4) is then an immediate consequence of elementary properties of the Fourier transform.

If electrical neutrality is to be achieved, an ionic fluid must contain at least two species of opposite charge. The simplest representation of such a system is obtained by replacing one of the species by a uniformly smeared-out, structureless background, the total charge of which must cancel that of the discrete ions. When the discrete ions are identical point charges, the resulting model (already discussed in Section 4.6) is called the *one-component plasma* or OCP.[2] The total potential energy of an OCP in which the ions carry a charge ze is given by the sum over $\mathbf{k}$ in (10.1.4), with $\rho_{\mathbf{k}}^{Z} = z\rho_{\mathbf{k}}$, except that the presence of the neutralising background means that the term for $\mathbf{k} = 0$ must be omitted. The OCP has certain unphysical features. For example, mass and charge fluctuations are proportional to each other and the system therefore has zero resistivity, because conservation of total momentum is equivalent to conservation of the microscopic electric current. Nevertheless, as the prototypical ionic fluid, the OCP plays a conceptual role similar to that filled by the hard-sphere model in the theory of simple, insulating liquids. It provides, in particular, a useful starting point for the study of liquid metals, where the mobile species corresponds to the metal ions and the background represents the conduction electrons.

To illustrate the usefulness of the OCP in the qualitative discussion of the properties of ionic liquids we return briefly to the question of the high-frequency, charge-fluctuation modes mentioned earlier. The characteristic frequency of the longitudinal mode is the plasma frequency, ω_{p}. In the case of the OCP an expression for ω_{p} can be obtained by a simple argument based on a δ-function representation of the dynamic structure factor. Use of such a model is justified by the fact that conservation of momentum of the ions means that there is no damping of charge fluctuations in the long-wavelength limit. We therefore assume that $S(k, \omega)$ consists of a pair of δ-functions located at frequencies $\pm\omega_k$,

and identify the plasma frequency as $\omega_p = \lim_{k\to 0}\omega_k$. If the spectrum is to satisfy the sum rules (7.4.23) and (7.4.30), ω_k must be such that

$$\omega_k^2 = \frac{\omega_0^2}{S(k)} = \frac{k_B T}{mS(k)}k^2 \tag{10.1.6}$$

The long-wavelength limit of $S(k)$ can be estimated within the random-phase approximation of Section 5.5. If we choose the ideal gas as reference system and make the substitution $\hat{c}(k) = -\beta z^2 \hat{v}(k)$, (5.5.25) becomes

$$S(k) = \frac{1}{1+\beta\rho z^2\hat{v}(k)} = \frac{1}{1+4\pi\beta\rho z^2 e^2/k^2} \sim \frac{k^2}{k_D^2}, \quad k \to 0 \tag{10.1.7}$$

where k_D is the Debye wavenumber defined by (4.6.23); as we shall see later, (10.1.7) is exact for the OCP. If we now substitute for $S(k)$ in (10.1.6), we find that

$$\omega_p^2 = \lim_{k\to 0}\omega_k^2 = \frac{4\pi\rho z^2 e^2}{m} \tag{10.1.8}$$

The frequency of the propagating mode therefore remains non-zero even in the long-wavelength limit; this is a characteristic feature of an optic-type excitation. The fact that ω_p is non-zero is a direct consequence of the k^{-2} singularity in $\hat{v}(k)$, since it is this singularity that determines the small-k behaviour of $S(k)$. Note also that the plasma frequency is independent of temperature.

If the fluid is genuinely two-component in character, a short-range repulsion is essential if the system is to be stable against the collapse of oppositely charged pairs. Within a model, stability is most easily achieved by imposing a hard-sphere repulsion between ions, a choice of interaction that defines the *primitive model* of electrolytes and molten salts. The primitive model has been widely adopted in studies of the osmotic properties of ionic solutions, the solvent being replaced by a continuum of dielectric constant ε that acts to reduce the Coulomb interaction between ions; the *restricted* version of the model is one in which all ions have the same diameter, d, and the same absolute valency, z.

The restricted primitive model with $\varepsilon = 1$ provides the simplest example of a rigid-ion model of a molten salt. Alternatively, the short-range interactions in the salt can be modelled by soft-core repulsions characterised by a single length parameter σ. For example, the short-range contribution to the pair potential can be written as

$$v_{\nu\mu}^S(r) = \frac{z^2e^2}{n\sigma}\left(\frac{\sigma}{r}\right)^n \tag{10.1.9}$$

for all pairs ν, μ; the parameter σ is the separation at which the cation–anion potential has its minimum value. Equation (10.1.9), together with the coulombic term, defines what we shall call the "simple molten salt". This provides a fair representation of the ionic interactions in the molten alkali halides, particularly of salts in which the positive and negative ions are of approximately equal size. The values of n appropriate to the alkali

halides are in the range $n = 8$ to 10; in the limit $n \to \infty$, the simple molten salt reduces to the restricted primitive model. If the two ionic species have equal masses, the hamiltonian of the system is fully symmetric under charge conjugation, meaning that cations and anions play identical roles.

The examples given in later sections of this chapter draw heavily on calculations for the restricted primitive model and the simple molten salt, but a number of more realistic models appropriate to molten salts have also been extensively studied both theoretically and by simulation. The best known of these are the rigid-ion potentials derived for salts of the alkali-halide family[3] in which the short-range interaction between a given ion pair is written as the sum of an exponential repulsion and attractive terms arising from dipole–dipole and dipole–quadrupole dispersion forces. If the ions are highly polarisable, however, as is often the case for the anion, the effect of induction forces cannot be ignored. A variety of schemes have therefore been devised that allow the incorporation of ionic polarisation into molecular-dynamics simulations of molten salts. Much of the early work on polarisable systems was based on the "shell model" of lattice dynamics, in which the total charge of the ion is divided between a core and a massless shell. The shell is bound to the core by a harmonic potential and polarisation of the ion corresponds to a bodily shift of the shell relative to the core; the shells, being of zero mass, are assumed to adjust themselves instantaneously in such a way as to minimise the total potential energy. Some interesting results have been obtained in this way, but the model has a number of unsatisfactory features. For example, the parameters characterising a particular ion species are not transferable from one salt to another. A different approach has subsequently been developed[4] in which the dipole moments are treated as additional degrees of freedom within an "extended lagrangian" scheme; this method resembles closely one devised earlier for the treatment of many-body polarisation effects in polar fluids.[5]

10.2 SCREENING AND CHARGE ORDERING

The microscopic structure of an n-component ionic fluid can be discussed in terms of $\frac{1}{2}n(n+1)$ partial structure factors $S_{\nu\mu}(k)$ with $\nu,\ \mu = 1$ to n, but it is certain linear combinations of these functions that are of most physical relevance. If

$$\rho_{\mathbf{k}}^{N} = \sum_{\nu} \rho_{\mathbf{k}}^{\nu} \tag{10.2.1}$$

is a Fourier component of the microscopic number density, and if the components of the charge density are defined as in (10.1.3), fluctuations in the densities are described by three static structure factors of the form

$$S_{NN}(k) = \frac{1}{N}\langle \rho_{\mathbf{k}}^{N} \rho_{-\mathbf{k}}^{N} \rangle = \sum_{\nu}\sum_{\mu} S_{\nu\mu}(k) \tag{10.2.2a}$$

$$S_{NZ}(k) = \frac{1}{N}\langle \rho_{\mathbf{k}}^{N} \rho_{-\mathbf{k}}^{Z} \rangle = \sum_{\nu}\sum_{\mu} z_{\mu} S_{\nu\mu}(k) \tag{10.2.2b}$$

$$S_{ZZ}(k) = \frac{1}{N}\langle \rho^Z_{\mathbf{k}} \rho^Z_{-\mathbf{k}} \rangle = \sum_\nu \sum_\mu z_\nu z_\mu S_{\nu\mu}(k) \tag{10.2.2c}$$

Of these three functions, the number–number structure factor $S_{NN}(k)$ is the closest in significance to the single structure factor of a one-component fluid.

Let $\delta\phi_\mu(\mathbf{r})$ be a weak, external potential that couples to the microscopic number density of species μ. We saw in Section 3.6 that the change induced in a Fourier component of the single-particle density of species ν is

$$\delta\hat{\rho}^{(1)}_\nu(\mathbf{k}) = \chi_{\nu\mu}(k)\delta\hat{\phi}_\mu(\mathbf{k}) \tag{10.2.3}$$

where the static response function $\chi_{\nu\mu}(k)$ is related to the corresponding partial structure factor by

$$\chi_{\nu\mu}(k) = -\beta\rho S_{\nu\mu}(k) \tag{10.2.4}$$

The problem of greatest interest here concerns the response of the fluid to a weak field produced by an external charge density with Fourier components $e\delta\hat{\rho}^{\text{ext}}(\mathbf{k})$; to simplify the discussion we consider a system of rigid ions *in vacuo* ($\varepsilon = 1$). The electric potential due to the external charge density is obtained from the **k**-space version of Poisson's equation, i.e.

$$\delta\hat{\phi}^{\text{ext}}(\mathbf{k}) = \frac{4\pi e}{k^2}\delta\hat{\rho}^{\text{ext}}(\mathbf{k}) \tag{10.2.5}$$

The electric potential couples directly to the microscopic charge density of the fluid, giving rise to a mean induced charge density $\delta\hat{\rho}_Z(\mathbf{k})$. The latter is proportional to $e\delta\hat{\phi}^{\text{ext}}(\mathbf{k})$, the constant of proportionality being, by definition, the charge-density response function, $\chi_{ZZ}(k)$. Thus

$$\delta\hat{\rho}_Z(\mathbf{k}) = \sum_\nu z_\nu \delta\hat{\rho}^{(1)}_\nu(\mathbf{k}) = \chi_{ZZ}(k)e\delta\hat{\phi}^{\text{ext}}(\mathbf{k}) \tag{10.2.6}$$

If we put $\delta\hat{\phi}_\mu(\mathbf{k}) = z_\mu e\delta\hat{\phi}^{\text{ext}}(\mathbf{k})$ in (10.2.3) and then substitute for $\delta\hat{\rho}^{(1)}_\nu(\mathbf{k})$ in (10.2.6), we find that the response function can be identified as

$$\chi_{ZZ}(k) = \sum_\nu \sum_\mu z_\nu z_\mu \chi_{\nu\mu}(k) \tag{10.2.7}$$

and combination of (10.2.2c), (10.2.4) and (10.2.7) leads to the charge-response version of the fluctuation–dissipation theorem:

$$\chi_{ZZ}(k) = -\beta\rho S_{ZZ}(k) \tag{10.2.8}$$

The electrostrictive behaviour of the fluid, i.e. the number-density response to an external electric potential, is characterised by a cross response function $\chi_{NZ}(k)$ through an expression analogous to (10.2.6):

$$\delta\hat{\rho}_N(\mathbf{k}) = \sum_\nu \delta\hat{\rho}^{(1)}_\nu(\mathbf{k}) = \chi_{NZ}(k)e\delta\hat{\phi}^{\text{ext}}(\mathbf{k}) \tag{10.2.9}$$

The charge response to the external potential can equally well be described in terms of a longitudinal dielectric function $\varepsilon(k)$; this is simply a k-dependent generalisation of the macroscopic dielectric constant of elementary electrostatics. If **E** is the electric field and **D** is the electric displacement, $\varepsilon(k)$ is given by

$$\frac{1}{\varepsilon(k)} = \frac{\mathbf{k}\cdot\widehat{\mathbf{E}}(k)}{\mathbf{k}\cdot\widehat{\mathbf{D}}(k)} = 1 + \frac{\delta\hat{\rho}_Z(\mathbf{k})}{\delta\hat{\rho}^{\text{ext}}(\mathbf{k})} \tag{10.2.10}$$

where Maxwell's equations have been used to relate **E** and **D**, respectively, to the total and external charge densities. Equations (10.2.5), (10.2.6) and (10.2.10) can now be combined to yield the fundamental relation between the dielectric and charge-response functions:

$$\frac{1}{\varepsilon(k)} = 1 + \frac{4\pi e^2}{k^2}\chi_{ZZ}(k) \tag{10.2.11}$$

The definition (10.2.2c) shows that $S_{ZZ}(k)$ can never be negative. Equations (10.2.8) and (10.2.11) therefore imply that $1/\varepsilon(k) \leqslant 1$ for all k.

It is known experimentally that an external charge distribution is completely screened by a conducting fluid. In other words, the total charge density vanishes in the long-wavelength limit, or

$$\lim_{\mathbf{k}\to 0}\left[\delta\hat{\rho}^{\text{ext}}(\mathbf{k}) + \delta\hat{\rho}_Z(\mathbf{k})\right] = 0 \tag{10.2.12}$$

If this result is to be consistent with (10.2.10), it follows that

$$\lim_{k\to 0}\varepsilon(k) = \infty \tag{10.2.13}$$

In combination with (10.2.8) and (10.2.11), the assumption of *perfect screening* contained in (10.2.13) implies that the charge structure factor at long wavelengths behaves as

$$\lim_{k\to 0}\frac{k_{\text{D}}^2}{k^2}S_{ZZ}(k) = \sum_\nu x_\nu z_\nu^2 \tag{10.2.14}$$

where $x_\nu = \rho_\nu/\rho$ and k_{D}, the Debye wavenumber, is given by a generalisation of (4.6.23):

$$k_{\text{D}}^2 = \frac{4\pi\beta\rho e^2}{\varepsilon}\sum_\nu x_\nu z_\nu^2 \tag{10.2.15}$$

The quantity $\Lambda_{\text{D}} = 1/k_{\text{D}}$ is the Debye screening length, familiar from ionic-solution theory; in a dilute electrolyte it is the distance beyond which the electric potential due to an ion is completely screened by the local, induced charge distribution. From comparison of (10.2.14) with the compressibility equation (3.6.11) we see that large-scale (long-wavelength) charge fluctuations are strongly inhibited in comparison with the number-density fluctuations of a neutral fluid. It has been proved rigorously[6] that the fluctuation in the total charge Q_V contained in a volume V, i.e. $(\langle Q_V^2\rangle - \langle Q_V\rangle^2)$, is proportional only

to the surface area bounding the volume. By contrast, (2.4.23) shows that the fluctuation in the number of particles within V is proportional to V itself.

Equation (10.2.14) leads directly to two important relations between the partial pair distribution functions of an ionic fluid, known as the Stillinger–Lovett sum rules.[7] We see from (3.6.15) and (10.2.2c) that the charge structure factor is related to the partial pair correlation functions $h_{\nu\mu}(r)$ by

$$S_{ZZ}(k) = \sum_{\nu}\sum_{\mu} z_\nu z_\mu \left(x_\nu \delta_{\nu\mu} + 4\pi\rho x_\nu x_\mu \int_0^\infty \frac{\sin kr}{kr} h_{\nu\mu}(r) r^2 \, \mathrm{d}r \right) \tag{10.2.16}$$

If the functions $h_{\nu\mu}(r)$ decay sufficiently rapidly at large r, the Fourier integrals in (10.2.16) may be expanded to order k^2. The two sum rules are then obtained by equating terms of zeroth and second order in k in (10.2.14) and (10.2.16) and exploiting the condition of overall charge neutrality expressed by (10.1.1). The results derived in this way are

$$\begin{aligned} \rho \sum_{\nu} x_\nu z_\nu \sum_{\mu} \int x_\mu z_\mu g_{\nu\mu}(r) \, \mathrm{d}\mathbf{r} &= -\sum_{\nu} x_\nu z_\nu^2 \\ \rho \sum_{\nu} x_\nu z_\nu \sum_{\mu} \int x_\mu z_\mu g_{\nu\mu}(r) r^2 \, \mathrm{d}\mathbf{r} &= -6\Lambda_{\mathrm{D}}^2 \sum_{\nu} x_\nu z_\nu^2 \end{aligned} \tag{10.2.17}$$

The assumption concerning the large-r behaviour of the correlation functions is equivalent to a "clustering" hypothesis for the particle densities. An n-particle density $\rho^{(n)}(\mathbf{r}^n)$ is said to have a clustering property if, for all $m < n$, it reduces to the product $\rho^{(m)}(\mathbf{r}^m)\rho^{(n-m)}(\mathbf{r}^{(n-m)})$ faster than a prescribed inverse power of the distance between the centres of mass of the clusters $(\mathbf{r}_1, \ldots, \mathbf{r}_m)$ and $(\mathbf{r}_{m+1}, \ldots, \mathbf{r}_n)$ as the clusters become infinitely separated. If the clustering hypothesis is used, the Stillinger–Lovett sum rules can be derived from the YBG hierarchy of Section 4.2 without making any assumption about the small-k behaviour of $S_{ZZ}(k)$. The derivation is therefore not dependent on the perfect-screening condition (10.2.13); perfect screening appears instead as a consequence of the sum rules.

The first of the Stillinger–Lovett rules is just a linear combination of local electroneutrality conditions of the form

$$\rho \sum_{\mu} \int x_\mu z_\mu g_{\nu\mu}(r) \, \mathrm{d}\mathbf{r} = -z_\nu \tag{10.2.18}$$

The physical meaning of (10.2.18) is that the total charge around a given ion must exactly cancel the charge of the ion. This is the first of a series of sum rules satisfied by the multipole moments of the charge distribution in the vicinity of a given number of fixed ions.[8] The sum rules can again be derived from the YBG hierarchy if appropriate clustering assumptions are made. In particular, if correlations are assumed to decay exponentially, it can be shown that the charge distribution around any number of fixed ions has no multipole moment of any order. The local electroneutrality condition may be re-expressed in

terms of the long-wavelength limits of the partial structure factors. In the case of a two-component system, (10.2.18) becomes $z_1^2 S_{11}(0) = -z_1 z_2 S_{12}(0) = z_2^2 S_{22}(0)$ or, because the fluid is electrically neutral overall:

$$x_2^2 S_{11}(0) = x_1 x_2 S_{12}(0) = x_1^2 S_{22}(0) \tag{10.2.19}$$

No such property holds for the partial structure factors of a mixture of neutral fluids.

The $k \to 0$ limits of the partial structure factors of a binary ionic fluid are related to the isothermal compressibility via the Kirkwood–Buff formula (3.6.17). The conditions imposed by charge neutrality mean, however, that direct substitution of (10.2.19) in (3.6.17) leads to an indeterminate result. To avoid this problem we invert the system of linear equations represented by (10.2.2) and rewrite (3.6.17) in terms of $S_{NN}(k)$, $S_{NZ}(k)$ and $S_{ZZ}(k)$ in the form

$$\rho k_{\mathrm{B}} T \chi_T = \lim_{k \to 0} \frac{S_{NN}(k) S_{ZZ}(k) - S_{NZ}^2(k)}{S_{ZZ}(k)} \tag{10.2.20}$$

The small-k limits of the three structure factors in (10.2.20) can be deduced from the asymptotic behaviour of the partial direct correlation functions $c_{\nu\mu}(r)$. At large r we may expect these functions to decay as $c_{\nu\mu}(r) \sim -\beta z_\nu z_\mu e^2/r$. It is therefore natural to separate $c_{\nu\mu}(r)$ into short-range and coulombic parts; in $\mathbf{k}$-space $\hat{c}_{\nu\mu}(k)$ becomes

$$\hat{c}_{\nu\mu}(k) = \hat{c}_{\nu\mu}^{\mathrm{S}}(k) - \frac{4\pi\beta z_\nu z_\mu e^2}{k^2} \tag{10.2.21}$$

where $\hat{c}_{\nu\mu}^{\mathrm{S}}(k)$ is a regular function in the limit $k \to 0$. Substitution of (10.2.21) in the Ornstein–Zernike relation (3.6.12) leads, after some straightforward algebra and use of (10.1.1) and (10.2.2), to the required results: at small k, $S_{NN}(k) \sim k^0$, $S_{NZ}(k) \sim k^2$ and $S_{ZZ}(k) \sim k^2$; the last result agrees with (10.2.14). Thus (10.2.20) reduces to the simpler expression

$$\rho k_{\mathrm{B}} T \chi_T = \lim_{k \to 0} S_{NN}(k) \tag{10.2.22}$$

while (3.6.16) becomes

$$\frac{1}{\rho k_{\mathrm{B}} T \chi_T} = 1 - \rho \lim_{k \to 0} \sum_\nu \sum_\mu x_\nu x_\mu \hat{c}_{\nu\mu}^{\mathrm{S}}(k) \tag{10.2.23}$$

Because fluctuations in concentration correspond to fluctuations in charge density, and because such fluctuations are suppressed at long wavelengths, all reference to the two-component nature of the fluid has vanished from (10.2.22), which therefore resembles the corresponding result for a one-component system of uncharged particles.

The coefficients of the terms of order k^4 in the small-k expansions of $S_{ZZ}(k)$ and $S_{NZ}(k)$ and those of order k^2 in the expansion of $S_{NN}(k)$ can be determined by macroscopic arguments based on linearised hydrodynamics or thermodynamic fluctuation theory. We give here the corresponding calculation for the OCP, where the problem is simplified by the fact

that fluctuations in particle number are equivalent to fluctuations in charge. In the absence of any flow the force per unit volume due to the electric field must exactly balance the force due to the pressure gradient. Thus

$$ze\rho\mathbf{E}(\mathbf{r}) = \nabla P(\mathbf{r}) \tag{10.2.24}$$

where $ze\rho$ is the mean charge density of the mobile ions and the field $\mathbf{E}(\mathbf{r})$ is related to the sum of external and induced charge densities by Poisson's equation:

$$\nabla \cdot \mathbf{E}(\mathbf{r}) = 4\pi e\left[\delta\rho^{\text{ext}}(\mathbf{r}) + \delta\rho_Z(\mathbf{r})\right] \tag{10.2.25}$$

If the system is in local thermodynamic equilibrium, the pressure change in an isothermal process is

$$\delta P(\mathbf{r}) \equiv P(\mathbf{r}) - P = \left(\frac{\partial P}{\partial \rho}\right)_T \delta\rho(\mathbf{r}) = \frac{1}{z\rho\chi_T}\,\delta\rho_Z(\mathbf{r}) \tag{10.2.26}$$

Equations (10.2.24) to (10.2.26) may now be combined to give a differential equation for $\delta\rho_Z(\mathbf{r})$ of the form

$$\frac{1}{k_s^2}\nabla^2\delta\rho_Z(\mathbf{r}) - \delta\rho_Z(\mathbf{r}) = \delta\rho^{\text{ext}}(\mathbf{r}) \tag{10.2.27}$$

where

$$k_s^2 = 4\pi z^2 e^2 \rho^2 \chi_T = k_D^2 \frac{\chi_T}{\chi_T^{\text{id}}} \tag{10.2.28}$$

The solution to (10.2.27), obtained by taking Fourier transforms, is

$$\delta\hat{\rho}_Z(\mathbf{k}) = -\frac{\delta\hat{\rho}^{\text{ext}}(\mathbf{k})}{1 + k^2/k_s^2} \tag{10.2.29}$$

Comparison of (10.2.29) with (10.2.10) shows that the long-wavelength limit of $\varepsilon(k)$ is

$$\lim_{k\to 0} \varepsilon(k) = 1 + k_s^2/k^2 \tag{10.2.30}$$

which clearly satisfies the perfect-screening condition (10.2.13). The corresponding long-wavelength expression for $S_{ZZ}(k)$ $(= z^2 S(k))$, derived from (10.2.8) and (10.2.11), is

$$\lim_{k\to 0} S_{ZZ}(k) = \frac{z^2 k^2/k_D^2}{1 + k^2/k_s^2} \tag{10.2.31}$$

in agreement with (10.1.7). Equations (10.2.30) and (10.2.31) also apply to mixtures of oppositely charged ions with $z_1 = -z_2 = z$, except that k_s is differently defined.[9]

The Fourier components of the total electrostatic potential $\delta\phi(\mathbf{r})$ are related to the components of the total charge density by the analogue of (10.2.5). In the long-wavelength

limit it follows from (10.2.10) and (10.2.30) that

$$\delta\hat{\phi}(\mathbf{k}) = \frac{4\pi e}{k^2}\left[\delta\hat{\rho}^{\text{ext}}(\mathbf{k}) + \delta\hat{\rho}_Z(\mathbf{k})\right]$$
$$= \frac{4\pi e}{k^2\varepsilon(k)}\delta\hat{\rho}^{\text{ext}}(\mathbf{k}) = \frac{4\pi e}{k^2 + k_s^2}\delta\hat{\rho}^{\text{ext}}(\mathbf{k}) \tag{10.2.32}$$

If an ion of species ν in the fluid is regarded as an "external" charge placed at the origin, the "external" charge density is $e\delta\rho^{\text{ext}}(\mathbf{r}) = z_\nu e\delta(\mathbf{r})$, and (10.2.32) shows that the effective potential due to the ion decays as

$$\phi_\nu(r) = \frac{z_\nu e}{r}\exp(-k_s r) \tag{10.2.33}$$

The quantity $\phi_\nu(r)$ $(= \delta\phi(r))$ is the potential of mean force for ions of species ν. In the case of the OCP, k_s is given by (10.2.28); this becomes equal to the Debye wavenumber in the weak-coupling limit ($\rho \to 0$ or $T \to \infty$), where χ_T may be replaced by its ideal-gas value, $\chi_T^{\text{id}} = \beta\rho$. With these simplifications, (10.2.33) reduces to the Debye–Hückel result (4.6.25). In the strong-coupling regime the compressibility of the OCP becomes negative, k_s takes on imaginary values, and the potential of mean force develops the oscillations characteristic of systems with short-range order.

Oscillations of the charge density around a given ion are also a feature of two-component ionic fluids, where they arise as a result of competition between hard-core packing and local charge neutrality. In the case of the restricted primitive model a simple argument[7(a)] based on the sum rules (10.2.17) shows that the radial charge distribution function $[g_{11}(r) - g_{12}(r)]$ (or $[g_{22}(r) - g_{12}(r)]$) must change sign as a function of r if $k_D d \geqslant \sqrt{6}$. Charge ordering of this type is a very strong effect in molten salts and oscillations in the charge density around a central ion extend over many ionic radii. Computer simulations of a variety of monovalent salts show that the pair distribution functions for ions of like sign, $g_{11}(r)$ and $g_{22}(r)$, are very similar in form and that the oscillations in these two functions are almost exactly out of phase with those in the much more sharply peaked, cation–anion distribution function $g_{12}(r)$. Thus the radial charge distribution functions around either a cation or anion are essentially the same and strongly oscillatory. The similarity between $g_{11}(r)$ and $g_{22}(r)$ gives support to the use of the simple molten salt defined by (10.1.9) as a model of the alkali halides. Some molecular-dynamics results for such a model (with $n = 9$) are shown in Figure 10.1. The regular alternation of concentric shells of oppositely charged ions is clearly visible in the pair distribution functions plotted in part (a) of the figure. In **k**-space the effects of charge ordering reflect themselves in the very sharp main peak in the charge–charge structure factor $S_{ZZ}(k)$ (the Fourier transform of $[g_{11}(r) + g_{22}(r) - 2g_{12}(r)]$), shown in part (b); by contrast, $S_{NN}(k)$ (the transform of $[g_{11}(r) + g_{22}(r) + 2g_{12}(r)]$) is a relatively structureless function. The symmetry of the model means that charge and number fluctuations are completely decoupled; thus $S_{NZ}(k)$ is zero at all k. In the general case, the fluctuations are strictly independent only in the long-wavelength limit, since $S_{NZ}(k) \sim k^2$ as $k \to 0$.

The main structural features exhibited by the simple molten salt are also seen in computer simulations of more realistic rigid-ion models of the alkali halides. The results are

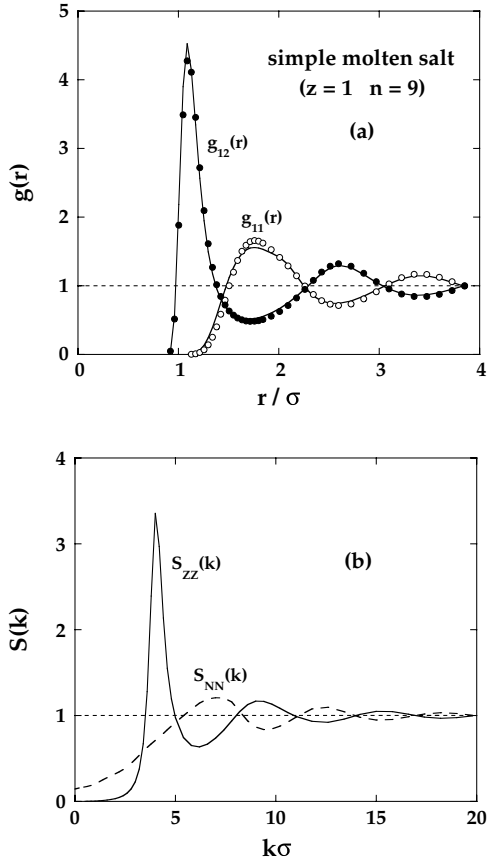

FIG. 10.1. Charge ordering in the simple molten salt[10] in a thermodynamic state corresponding roughly to that of molten sodium chloride at $T \approx 1270$ K. (a) Distribution functions for cation–anion and cation–cation (or anion–anion) pairs. The points show the results of molecular-dynamics calculations and the curves are calculated from the HNC approximation (see Section 10.3). (b) Molecular-dynamics results for the static charge–charge and number–number structure factors.

consistent with those obtained by neutron-scattering experiments, which rely on the use of isotopic substitution to separate the contributions of the partial structure factors $S_{\nu\mu}(k)$ to the measured cross-section. Similar experiments have been carried out for the alkaline-earth halides and are again in good general agreement with those obtained in simulations based on rigid-ion models. Because the absolute charges of the two ionic species are now different, the marked similarity seen in the alkali halides between $g_{11}(r)$ and $g_{22}(r)$ is lost.

10.3 INTEGRAL-EQUATION THEORIES

The techniques introduced in Chapters 3 to 5 provide a number of possible routes to the calculation of thermodynamic and structural properties of simple ionic liquids. Versions of

the optimised cluster theory of Section 5.5 and other, closely related methods have proved particularly successful in describing the thermodynamic behaviour of dilute systems. In this section, however, we focus on the integral-equation approach, in which the emphasis is placed on the calculation of the pair distribution functions. Much of the published work in this field is concerned with the alkali halides, either in the molten phase or in solution, though there has also been considerable interest in the properties of 2 : 1 and 2 : 2 electrolyte solutions, the structure of which is characterised by a high degree of ionic association. The physical conditions are, of course, very different in the molten-salt and electrolyte regimes. If we adopt the primitive model of Section 10.1, the thermodynamic state is conveniently characterised by the reduced density $\rho^* = Nd^3/V$, where N is the total number of ions and $d = \frac{1}{2}(d_{11} + d_{22})$ is the mean ionic diameter, and a reduced Coulomb coupling parameter, or inverse temperature, defined as

$$\beta^* = \frac{|z_1 z_2| e^2}{\varepsilon k_B T d} \tag{10.3.1}$$

Near the melting point of an alkali halide, $\rho^* \approx 0.4$ and $\beta^* \approx 65$, while for a 1 M aqueous solution of the same salt at room temperature, $\rho^* \approx 0.01$ and $\beta^* \approx 3$. We must therefore expect the nature of the interionic correlations to be very different in the two cases. The liquid–vapour phase diagram of a molten alkali halide is qualitatively similar to that, say, of a rare gas, but the reduced critical densities of the salts are only about one-third of those of typical insulating liquids.

The value of different theoretical approaches can be illustrated by limiting attention initially to systems of charged hard spheres and, in particular, to the restricted primitive model, with $z_1 = -z_2 = 1$. A convenient starting point for the discussion is the mean spherical approximation (MSA) introduced in Section 4.5, since in this case the MSA has a completely analytic solution.[11] The MSA for equisized hard spheres of diameter d is

$$g_{\nu\mu} = 0, \quad r < d; \qquad c_{\nu\mu}(r) = -\frac{\beta z_\nu z_\mu e^2}{\varepsilon r}, \quad r > d \tag{10.3.2}$$

which must be used in conjunction with the Ornstein–Zernike relation for equimolar binary mixtures; this is obtained as a special case of (3.6.12), with $x_1 = x_2 = \frac{1}{2}$. The symmetry of the restricted primitive model allows the Ornstein–Zernike relation to be rewritten as two independent equations for the linear combinations

$$h_S(r) = \tfrac{1}{2}\big[h_{11}(r) + h_{12}(r)\big], \qquad h_D(r) = h_{11}(r) - h_{12}(r) \tag{10.3.3}$$

and the corresponding direct correlation functions $c_S(r)$ and $c_D(r)$; $h_S(r)$ is a number-density correlation function and $h_D(r)$ describes the correlation in charge density. When written in terms of the new functions the MSA becomes

$$h_S(r) = -1, \quad r < d; \qquad c_S(r) = 0, \quad r > d \tag{10.3.4a}$$

$$h_D(r) = 0, \quad r < d; \qquad c_D(r) = -\frac{2\beta e^2}{\varepsilon r}, \quad r > d \tag{10.3.4b}$$

The closure relation (10.3.4a) is just the Percus–Yevick approximation for hard spheres, for which the solution is known (see Section 4.4). The solution to (10.3.4b) and the associated Ornstein–Zernike relation between $h_D(r)$ and $c_D(r)$ can also be obtained in closed form by incorporating the sum rules (10.2.17) into generalised versions of the methods used to solve the PY equation for hard spheres. The result for $c_D(r)$ inside the hard core is

$$c_D(r) = -\frac{2\beta e^2}{\varepsilon d}(2 - Br/d)B \tag{10.3.5}$$

with $B = [\xi + 1 - (1 + 2\xi)^{1/2}]/\xi$, where $\xi^2 = k_D^2 d^2 = 4\pi\rho^*\beta^*$ and k_D is the Debye wavenumber defined by (10.2.15). The excess internal energy has a very simple form:

$$\frac{U^{ex}}{N} = -\frac{e^2}{\varepsilon d}B \tag{10.3.6}$$

and is a function of the single coupling constant ξ and not separately of ρ^* and β^*. In the high-temperature or low-density (or concentration) limit, i.e. for $\xi \ll 1$, the MSA internal energy reduces to the Debye–Hückel result:

$$\frac{U_{DH}^{ex}}{N} = -\frac{e^2}{2\varepsilon d}\xi = -\frac{k_B T}{8\pi\rho}k_D^3 \tag{10.3.7}$$

The limiting law (10.3.7) is valid when ion-size effects are negligible; it corresponds to the case when the direct correlation functions $c_{\nu\mu}(r)$ are replaced by their asymptotic forms (10.3.2) for all r. The virial pressure in the MSA is the sum of a hard-sphere contact term and the contribution of the Coulomb forces, i.e.

$$\frac{\beta P^v}{\rho} = 1 + \frac{2\pi\rho^*}{3}g_S(d) + \frac{\beta U^{ex}}{3N} \tag{10.3.8}$$

Alternatively, the pressure can be calculated by first integrating (10.3.6) to give the free energy and then differentiating with respect to density. The comparison made in Figure 10.2 for the case of a 1 : 1 electrolyte shows that the results for the excess internal energy are in good agreement with those of Monte Carlo calculations, but there is a serious inconsistency between the pressures calculated by the two different routes. In the molten-salt regime the results, not surprisingly, are much less satisfactory.[13]

Although the MSA is a good starting point for the calculation of thermodynamic properties of the restricted primitive model, it is less reliable in predicting the correlation functions. If the density and temperature are such that $\xi \gg 1$, use of the MSA leads to distribution functions $g_{11}(r)$ (or $g_{22}(r)$) that become negative at separations close to contact. The situation is improved if, at small r, the direct correlation functions $c_S(r)$ and $c_D(r)$ are allowed to deviate from their asymptotic forms.[14] In the "generalised" MSA or GMSA the deviations are expressed in terms of Yukawa functions and the closure relations for $c_S(r)$ and $c_D(r)$ in (10.3.4) are replaced by

$$c_S(r) = \frac{A_1}{r}\exp\big[-t_1(r - d)\big], \quad r > d$$

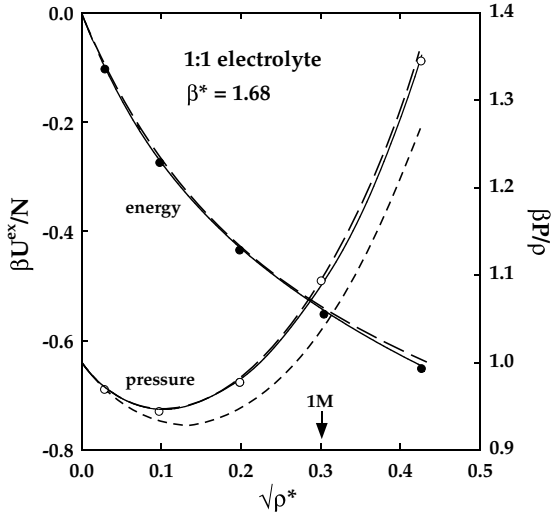

FIG. 10.2. Thermodynamic properties of the restricted primitive model of a 1 : 1 electrolyte. The points show the results of Monte Carlo simulations and the curves are calculated from the MSA and the HNC approximation. Energy: dashes, MSA; full curve, HNC. Pressure: long and short dashes, MSA via the energy and virial equations, respectively; full curve, HNC via the virial (or energy) equation. The value of β^* corresponds to an aqueous solution of ions of diameter 4.25 Å at $T = 298$ K; the arrow marks the value of $\sqrt{\rho^*}$ corresponding to a 1 M solution. After Rasaiah *et al.*[12]

$$c_{\mathrm{D}}(r) = -\frac{2\beta e^2}{\varepsilon r} - \frac{A_2}{r}\exp\bigl[-t_2(r-d)\bigr], \quad r > d \tag{10.3.9}$$

The parameters A_1, t_1, A_2 and t_2 are related through a set of algebraic equations to the internal energy, compressibility, virial pressure and contact value of $g_{\mathrm{D}}(r)$, and can be fitted to those quantities if the necessary data are available from an independent source. Where that is possible, the resulting pair distribution functions represent a significant improvement over the MSA, but in this form the theory is not self-contained.

The main appeal of theories such as the MSA or GMSA in the calculation of the pair distribution functions is the fact that they can be solved analytically in closed or nearly closed form, but their applicability is limited, at least in their conventional forms, to systems of charged hard spheres. These "primitive" models display certain structural features that are artefacts of the hard-sphere interaction. In particular, for values of ρ^* and β^* appropriate to molten salts, the main peak in the distribution functions for ions of like charge, i.e. $g_{++}(r)$ or $g_{--}(r)$, shows a marked splitting not seen experimentally. The splitting disappears when the short-range repulsion is softened, but different theoretical methods are then required. Of the integral-equation theories described in Chapter 4 the HNC approximation is far better suited to ionic systems than its PY counterpart. Equation (4.4.3) shows that the PY approximation cannot account for the exponential screening of the pair correlations at large separations, since within that approximation the pair distribution function decays as the pair potential. The HNC equation does describe the long-range correlations correctly

and there is also a close connection between HNC theory and the traditional form of the Debye–Hückel approach. When generalised to a system of more than one component, the exact relation (4.6.13) becomes

$$\ln\left[h_{\nu\mu}(r)+1\right] = -\beta v_{\nu\mu}(r) + d_{\nu\mu}(r) + h_{\nu\mu}(r) - c_{\nu\mu}(r) \tag{10.3.10}$$

and the HNC approximation corresponds to setting $d_{\nu\mu}(r) = 0$ for all pairs ν, μ. As Figure 10.2 illustrates, the thermodynamic results obtained in this way for a 1 : 1 electrolyte agree very well with those calculated by the Monte Carlo method. The degree of thermodynamic consistency in the theory is high; even at the highest concentration studied, pressures calculated via the compressibility and virial (or energy) routes differ by less than 1%. Good results are also obtained for the thermodynamic properties of the restricted primitive model of a 2 : 2 electrolyte, where the superiority of the HNC approximation over the MSA becomes more evident.[15] On the other hand, over a range of low to moderate concentrations the calculated like-ion distribution function of the 2 : 2 system has a pronounced peak at $r \approx 2d$, a feature that persists even when the hard-sphere term in the pair potential is replaced by an inverse-power repulsion.[16] No similar peak is seen in simulations of the same potential models, as the examples shown in Figure 10.3 illustrate; instead, the distribution function increases monotonically towards its limiting value at large r. Conversely, the HNC calculations significantly underestimate the height (of order 100) of the peak in the unlike-ion distribution function, the strength of which provides a measure of the degree of ion pairing in the system. These defects in the theory are linked to the difference in form of the bridge functions for like and unlike pairs. The results of simulations[16,17] show that the function $d_{++}(r)$ (or $d_{--}(r)$) is negative at all separations, and therefore resembles the bridge function of the Lennard-Jones fluid (see Figure 4.6), but $d_{+-}(r)$ is everywhere positive. Thus the HNC approximation acts in such a way as to weaken both the effective repulsion between ions of like charge and the effective attraction between those of unlike charge, with differing consequences for the calculated distribution functions.[18] At high concentrations the bridge functions maintain their difference in sign but their magnitude is greatly reduced. The error involved in neglecting them is therefore small and the spurious peak in the like-ion distribution function becomes progressively less pronounced.

The HNC approximation is also successful in reproducing the pair structure under state conditions typical of molten salts, as shown by the results for the simple molten salt plotted in Figure 10.1. The deficiencies in the approximation are evident only in the small-k region of $S_{NN}(k)$; the error there means that the calculated compressibility is about twice as large as that obtained by simulation. A systematic study of the alkali halides has confirmed that HNC theory is able to reproduce quantitatively all the main features of the pair distribution functions of more realistic potential models; still better results are obtained by including the contributions from the bridge diagrams in a semiempirical way[19] or by enforcing thermodynamic self-consistency through the hybrid, HMSA scheme[20] mentioned in Section 4.7.

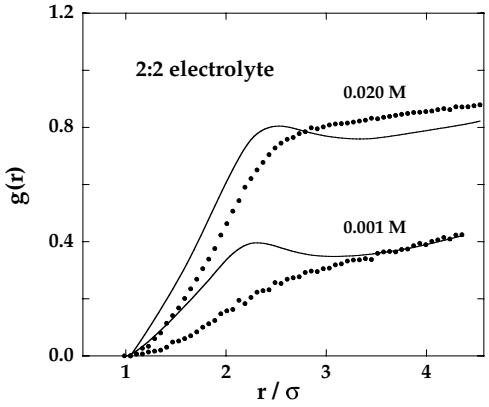

FIG. 10.3. Pair distribution function for like-charged ions in a 2:2 electrolyte solution under state conditions corresponding to an aqueous solution at $T = 298$ K. Short-range repulsions are represented by a soft-sphere (r^{-9}) potential and σ is the separation at which the cation–anion potential is a minimum. The points show the results of molecular-dynamics simulations and the curves are calculated from the HNC approximation. The spurious peak in the HNC results is less pronounced at the higher concentration and disappears for concentrations greater than about 0.06 M. After Duh and Haymet.[16]

10.4 FREQUENCY-DEPENDENT ELECTRIC RESPONSE

We have seen in earlier sections of this chapter that the static properties of ionic liquids are strongly affected by the long-range nature of the Coulomb potential or, equivalently, the k^{-2} singularity in its Fourier transform. We now turn to the question of how the same factors influence the dynamical correlations. The discussion here is limited to two-component systems of ions *in vacuo*, the case of liquid metals being deferred until Section 10.9. The phenomena of greatest interest are those linked to charge fluctuations; these generate a local electric field that acts as a restoring force on the local charge density. At low frequencies the charge density responds in a diffusive manner, but at high frequencies there is a reactive behaviour, which gives rise to a propagating mode of the type briefly discussed in Section 10.1.

The linear combinations of microscopic partial densities that arise naturally in a discussion of the collective dynamics are the mass (M) and charge (Z) densities, defined in terms of Fourier components as

$$\rho_{\mathbf{k}}^{M}(t) = \sum_{\nu} m_\nu \rho_{\mathbf{k}}^{\nu}(t), \qquad \rho_{\mathbf{k}}^{Z}(t) = \sum_{\nu} z_\nu \rho_{\mathbf{k}}^{\nu}(t) \tag{10.4.1}$$

where m_ν is the mass of an ion of species ν. With each fluctuating density we may associate a current. Thus

$$\mathbf{j}_{\mathbf{k}}^{M}(t) = \sum_{\nu} m_\nu \mathbf{j}_{\mathbf{k}}^{\nu}(t), \qquad \mathbf{j}_{\mathbf{k}}^{Z}(t) = \sum_{\nu} z_\nu \mathbf{j}_{\mathbf{k}}^{\nu}(t) \tag{10.4.2}$$

where the partial currents $\mathbf{j}_{\mathbf{k}}^{\nu}$ are given by an expression identical to (7.4.7) except that the sum on i is restricted to ions of a given species. Each current can be divided into

longitudinal (l) and transverse (t) parts in the manner of (7.4.25); the longitudinal currents satisfy equations of continuity analogous to (7.4.4). The mass current is related to the stress tensor $\boldsymbol{\Pi}_{\mathbf{k}}$ by

$$\frac{\partial}{\partial t}\mathbf{j}_{\mathbf{k}}^{M}(t) + i\mathbf{k}\cdot\boldsymbol{\Pi}_{\mathbf{k}} = 0 \tag{10.4.3}$$

where the components of $\boldsymbol{\Pi}_{\mathbf{k}}$ are given by a two-component generalisation of (8.4.14). Equation (10.4.3) shows that the time derivative of $\mathbf{j}_{\mathbf{k}}^{M}(t)$ vanishes as $k \to 0$. The mass current is therefore a conserved variable in the sense of Section 7.1, but the charge current is not. Although the total momentum of the ions is conserved, there is a continuous exchange of momentum between the two species; this momentum exchange is the source of the electrical resistivity of the fluid.

The mass and charge densities can be used to construct three, independent, time-correlation functions $F_{AB}(k,t)$ (with $A, B = M$ or Z), the definitions of which are similar to that of the intermediate scattering function (7.4.20). The initial values of the correlation functions are equal to the static structure factors in (10.2.2), but with number N replaced by mass M, and their Fourier transforms with respect to t are the corresponding dynamic structure factors. A function of particular interest for our purposes is the charge–charge dynamic structure factor, defined as

$$S_{ZZ}(k,\omega) = \frac{1}{2\pi N}\int_{-\infty}^{\infty}\left\langle \rho_{\mathbf{k}}^{Z}(t)\rho_{-\mathbf{k}}^{Z}\right\rangle \exp(i\omega t)\,\mathrm{d}t \tag{10.4.4}$$

Finally, three longitudinal and three transverse current correlation functions can be defined through straightforward generalisations of (7.4.25):

$$C_{AB,l}(k,t) = \frac{k^2}{N}\left\langle j_{\mathbf{k}}^{Az}(t)\, j_{-\mathbf{k}}^{Bz}\right\rangle \tag{10.4.5a}$$

$$C_{AB,t}(k,t) = \frac{k^2}{N}\left\langle j_{\mathbf{k}}^{Ax}(t)\, j_{-\mathbf{k}}^{Bx}\right\rangle \tag{10.4.5b}$$

where, as usual, the z-axis is chosen parallel to $\mathbf{k}$. Each $C_{AB,l}(k,t)$ is related to the corresponding $F_{AB}(k,t)$ by an analogue of (7.4.26).

We next consider how the response of the system to an external electric field can be described in terms of the correlation functions introduced above. This requires a generalisation to frequency-dependent perturbations of the result in (10.2.6). As an extension of the linear-response relation (7.6.26), we find that the mean induced charge density is

$$\delta\hat{\rho}_Z(\mathbf{k},t) = \left\langle \rho_{\mathbf{k}}^{Z}(t)\right\rangle = \chi_{ZZ}(k,\omega)e\phi_{\mathbf{k}}^{\mathrm{ext}}\exp(-i\omega t) \tag{10.4.6}$$

The imaginary part of the complex dynamic susceptibility $\chi_{ZZ}(k,\omega)$ is related to the dynamic structure factor $S_{ZZ}(k,\omega)$ through a trivial modification of the fluctuation–dissipation theorem (7.6.28), i.e.

$$S_{ZZ}(k,\omega) = -\frac{k_{\mathrm{B}}T}{\pi\rho\omega}\chi_{ZZ}''(k,\omega) \tag{10.4.7}$$

and the susceptibility can also be expressed in terms of the complex dielectric function $\varepsilon(k,\omega)$ by a frequency-dependent generalisation of (10.2.11):

$$\frac{1}{\varepsilon(k,\omega)} = 1 + \frac{4\pi e^2}{k^2}\chi_{ZZ}(k,\omega) \tag{10.4.8}$$

The functions $\chi_{ZZ}(k,\omega)$ and $1/\varepsilon(k,\omega)$ measure the linear response of a fluid of charged particles to an external electric field. The external field polarises the fluid and the local, internal field (the Maxwell field) is the sum of the field due to the external charge distribution and that due to the induced charge density. The local field is, of course, the field experienced by the ions. The response of the system to the local electric potential is described by a screened response function $\chi^{\rm sc}_{ZZ}(k,\omega)$, defined through the expression

$$\delta\hat{\rho}_Z(\mathbf{k},t) = \chi^{\rm sc}_{ZZ}(k,\omega)e\left[\phi^{\rm ext}_{\mathbf{k}}\exp(-i\omega t) + \delta\hat{\phi}^{\rm ind}(\mathbf{k},\omega)\right] \tag{10.4.9}$$

where the induced electric potential $\delta\hat{\phi}^{\rm ind}(\mathbf{k},\omega)$ is related to the induced charge density by Poisson's equation (cf. (10.2.5)):

$$\delta\hat{\phi}^{\rm ind}(\mathbf{k},\omega) = \frac{4\pi e}{k^2}\delta\hat{\rho}_Z(\mathbf{k},\omega) \tag{10.4.10}$$

Comparison of (10.4.9) with (10.4.6) shows that the relation between the external and screened susceptibilities is

$$\chi_{ZZ}(k,\omega) = \frac{\chi^{\rm sc}_{ZZ}(k,\omega)}{1 - \dfrac{4\pi e^2}{k^2}\chi^{\rm sc}_{ZZ}(k,\omega)} \tag{10.4.11}$$

and hence, from (10.4.8), that

$$\varepsilon(k,\omega) = 1 - \frac{4\pi e^2}{k^2}\chi^{\rm sc}_{ZZ}(k,\omega) \tag{10.4.12}$$

The response function $\chi_{ZZ}(k,\omega)$ satisfies the Kramers–Kronig relations (7.6.37) and (7.6.38), which are merely consequences of causality. The same is not necessarily true of the screened function $\chi^{\rm sc}_{ZZ}(k,\omega)$, which determines the response of the system to the local field. Since the local field depends on the material properties of the system, it cannot be controlled at will in an experiment.

The electric response of an ionic fluid can also be discussed in terms of the induced electric current. Let $\mathbf{E}(\mathbf{k},\omega)$ be a Fourier component of the local electric field. Ohm's Law in its most general form states that the induced electric current $\mathbf{J}^Z$ is linearly related to the field, i.e.

$$\mathbf{J}^Z(\mathbf{k},\omega) = \boldsymbol{\sigma}(\mathbf{k},\omega)\cdot\mathbf{E}(\mathbf{k},\omega) \tag{10.4.13}$$

The quantity $\boldsymbol{\sigma}$ is the conductivity tensor, which can be divided into longitudinal and transverse parts in the form

$$\boldsymbol{\sigma}(\mathbf{k},\omega) = \frac{\mathbf{kk}}{k^2}\sigma_l(\mathbf{k},\omega) + \left(\boldsymbol{I} - \frac{\mathbf{kk}}{k^2}\right)\sigma_t(\mathbf{k},\omega) \tag{10.4.14}$$

where σ_l and σ_t are scalars. The longitudinal and transverse projections of the induced current are related, respectively, to the longitudinal (or irrotational) and transverse (or divergence-free) components of the local electric field. Thus

$$\mathbf{J}_l^Z(\mathbf{k},\omega) = \sigma_l(\mathbf{k},\omega)\mathbf{E}_l(\mathbf{k},\omega), \qquad \mathbf{J}_t^Z(\mathbf{k},\omega) = \sigma_t(\mathbf{k},\omega)\mathbf{E}_t(\mathbf{k},\omega) \tag{10.4.15}$$

Since $\mathbf{E} = -\nabla\delta\phi$, it follows that the component $\mathbf{E}_l(\mathbf{k},\omega)$ of the local field is related to the total electric potential by the expression

$$\mathbf{E}_l(\mathbf{k},\omega) = -i\mathbf{k}\delta\hat{\phi}(\mathbf{k},\omega) = -i\mathbf{k}\left[\phi_{\mathbf{k}}^{\text{ext}}\exp(-i\omega t) + \delta\hat{\phi}^{\text{ind}}(\mathbf{k},\omega)\right] \tag{10.4.16}$$

Equations (7.4.4), (10.4.9), (10.4.12), (10.4.15) and (10.4.16) can now be combined to yield the fundamental relation between the dielectric function and the conductivity tensor:

$$\varepsilon(k,\omega) = 1 + \frac{4\pi i}{\omega}\sigma_l(k,\omega) \tag{10.4.17}$$

Note that $\sigma_l(k,\omega)$ is a screened response function in the same sense as $\chi_{ZZ}^{\text{sc}}(k,\omega)$, since it measures a response to the internal field.

Linear-response theory was used in Section 7.7 to derive a microscopic expression for the frequency-dependent electrical conductivity; this "external" conductivity measures the response of a fluid to a uniform ($\mathbf{k} = 0$) applied electric field. A uniform field corresponds to a situation in which the boundaries of the system are removed to infinity, thereby avoiding the appearance of a surface polarisation. The electric response to an inhomogeneous ($\mathbf{k}$-dependent) applied field is measured by a wavenumber-dependent external conductivity that can be related to the time-autocorrelation function of the fluctuating charge current $\mathbf{j}_{\mathbf{k}}^Z(t)$. In the case of the longitudinal component the required generalisation of (7.7.10) is simply

$$\sigma_l^{\text{ext}}(k,\omega) = \frac{\beta e^2}{V}\int_0^\infty \left\langle j_{\mathbf{k}}^{Zz}(t)\, j_{-\mathbf{k}}^{Zz}\right\rangle \exp(i\omega t)\,\mathrm{d}t \tag{10.4.18}$$

However, the macroscopic electrical conductivity σ given by the low-frequency limit of (7.7.10) is not the same as the $k,\ \omega \to 0$ limit of $\sigma_l^{\text{ext}}(k,\omega)$. Indeed, it follows from the continuity equation (see (7.4.4)) that the integral in (10.4.18) can be re-expressed as

$$\begin{aligned}\int_0^\infty \left\langle j_{\mathbf{k}}^{Zz}(t)\, j_{-\mathbf{k}}^{Zz}\right\rangle \exp(i\omega t)\,\mathrm{d}t &= \frac{1}{k^2}\int_0^\infty \left\langle \dot{\rho}_{\mathbf{k}}^{Z}(t)\,\dot{\rho}_{-\mathbf{k}}^{Z}\right\rangle \exp(i\omega t)\,\mathrm{d}t \\ &= \frac{-i\omega N S_{ZZ}(k) + \omega^2 N\widetilde{F}_{ZZ}(k,\omega)}{k^2}\end{aligned} \tag{10.4.19}$$

Written in this form it is easy to see that the integral vanishes as $k,\ \omega \to 0$, since $S_{ZZ}(k) \sim k^2$ for small k. (Note that $\widetilde{F}_{ZZ}(k,\omega)$ is the Laplace transform of $F_{ZZ}(k,t)$, which is bounded above by $S_{ZZ}(k)$: see (7.1.14).) On the other hand, the rotational invariance of an isotropic fluid implies that the macroscopic longitudinal and transverse conductivities must be the same, i.e. $\sigma_l^{\text{ext}}(0,\omega) = \sigma_t^{\text{ext}}(0,\omega) = \sigma(\omega)$. Hence σ may be defined in terms of the transverse charge–current autocorrelation function; the transverse current is not related to the charge density by a continuity equation and is therefore unaffected by the small-k divergence of the longitudinal electric field. Thus

$$\begin{aligned}\sigma &= \lim_{\omega\to 0}\lim_{k\to 0}\frac{\beta e^2}{V}\int_0^\infty \left\langle j_{\mathbf{k}}^{Zx}(t)\, j_{-\mathbf{k}}^{Zx}\right\rangle \exp(i\omega t)\,\mathrm{d}t \\ &= \lim_{\omega\to 0}\lim_{k\to 0}\frac{\beta\rho e^2}{k^2}\widetilde{C}_{ZZ,t}(k,\omega) \end{aligned} \tag{10.4.20}$$

The differing behaviour of the longitudinal and transverse charge–current autocorrelation functions is also evident from the sum rules for the corresponding spectra. The short-time expansions of $C_{ZZ,l}(k,t)$ and $C_{ZZ,t}(k,t)$ can be written in a form similar to (7.4.31) and (7.4.36), namely

$$C_{ZZ,l}(k,t) = \omega_0^2\left(1 - \omega_{1l}^2\frac{t^2}{2!} + \cdots\right) \tag{10.4.21a}$$

$$C_{ZZ,t}(k,t) = \omega_0^2\left(1 - \omega_{1t}^2\frac{t^2}{2!} + \cdots\right) \tag{10.4.21b}$$

where, in the case when $z_1 = -z_2 = z$:

$$\omega_0^2 = z^2k^2\left(\frac{k_{\mathrm{B}}T}{2M}\right) \tag{10.4.22}$$

with $M = m_1m_2/(m_1+m_2)$. The frequency moments ω_{1l}^2 and ω_{1t}^2 are the charge–current analogues of the quantities defined in Section 7.4. If the interionic potentials are separated into their coulombic and short-range parts, the derivation of (7.4.35) and (7.4.38) can be suitably generalised.[21] The resulting expressions are lengthy, but reduce in the limit $k \to 0$ to the simpler forms given by

$$\lim_{k\to 0}\omega_{1l}^2(k) = \tfrac{2}{3}\omega_{\mathrm{p}}^2 + \frac{\rho}{6M}\int \nabla^2 v_{12}^{\mathrm{S}}(r)\, g_{12}(r)\,\mathrm{d}\mathbf{r} \tag{10.4.23a}$$

$$\lim_{k\to 0}\omega_{1t}^2(k) = -\tfrac{1}{3}\omega_{\mathrm{p}}^2 + \frac{\rho}{6M}\int \nabla^2 v_{12}^{\mathrm{S}}(r)\, g_{12}(r)\,\mathrm{d}\mathbf{r} \tag{10.4.23b}$$

where $v_{12}^{\mathrm{S}}(r)$ is the short-range part of the cation–anion potential and ω_{p} is the plasma frequency (10.1.8), generalised to the two-component case:

$$\omega_{\mathrm{p}}^2 = \sum_{\nu} \frac{4\pi\rho_\nu z_\nu^2 e^2}{m_\nu} \tag{10.4.24}$$

Thus, in contrast to the results obtained in Section 7.4, the characteristic frequencies of the charge–current fluctuations remain non-zero as $k \to 0$. In addition, the longitudinal and transverse frequencies at $\mathbf{k} = 0$ are split according to the rule

$$\omega_{1l}^2(0) - \omega_{1t}^2(0) = \omega_{\mathrm{p}}^2 \tag{10.4.25}$$

This result is of the same form as the well-known relation between the longitudinal and transverse optic frequencies of ionic crystals. The behaviour of $\omega_{1l}(k)$ and $\omega_{1t}(k)$ at finite wavelengths is also similar to that of the corresponding phonon dispersion curves for the crystal: initially, $\omega_{1l}(k)$ falls rapidly with increasing k, but the curve of $\omega_{1t}(k)$ is almost flat. In the case of the alkali halides, $\omega_{1l}(0)$ is typically 20–30% larger than ω_{p}.

The nature of the collective modes associated with fluctuations in mass, charge and temperature in a molten salt can be analysed by methods described in Chapters 8 and 9. By analogy with the phonon spectra of ionic crystals, the collective modes are expected to be of acoustic and optic character, corresponding to low-frequency sound waves and high-frequency "plasma" oscillations. The different fluctuations are, in general, strongly coupled, and the associated memory functions have a complicated structure. A considerable simplification occurs when the anions and cations differ only in the sign of their electrical charge. Under such conditions, charge fluctuations are completely decoupled from fluctuations in mass and temperature at all frequencies and all wavenumbers. The same is true for any molten salt in the long-wavelength limit, thereby making it possible to calculate the spectrum of charge fluctuations at long wavelengths by the following, simple, macroscopic argument.[9] The Laplace transform of the continuity equation for the induced charge density is

$$-i\omega\delta\tilde{\rho}_Z(\mathbf{k},\omega) = \delta\hat{\rho}_Z(\mathbf{k},t=0) + i\mathbf{k}\cdot\mathbf{J}^Z(\mathbf{k},\omega) \tag{10.4.26}$$

while Poisson's equation may be written as

$$-i\mathbf{k}\cdot\mathbf{E}(\mathbf{k},\omega) = 4\pi\delta\tilde{\rho}_Z(\mathbf{k},\omega) \tag{10.4.27}$$

These two expressions can be combined with the longitudinal projection of Ohm's Law to give

$$\delta\tilde{\rho}_Z(\mathbf{k},\omega) = \frac{\delta\hat{\rho}_Z(\mathbf{k},t=0)}{-i\omega + 4\pi\sigma_l(k,\omega)} \tag{10.4.28}$$

If we multiply (10.4.28) through by $\delta\hat{\rho}_Z(-\mathbf{k},t=0)$ and take the thermal average, we find that

$$\widetilde{F}_{ZZ}(k,\omega) = \frac{S_{ZZ}(k)}{-i\omega + 4\pi\sigma_l(k,\omega)} \tag{10.4.29}$$

In the limit $k \to 0$, $\sigma_l(k, \omega)$ can be replaced by $\sigma(\omega)$. This gives an important result:

$$\lim_{k\to 0} \frac{\widetilde{F}_{ZZ}(k,\omega)}{S_{ZZ}(k)} = \frac{1}{-i\omega + 4\pi\sigma(\omega)} \tag{10.4.30}$$

Comparison with (7.3.23) shows that the frequency-dependent, complex conductivity is the memory function for the long-wavelength limit of the charge-density autocorrelation function. The spectrum of charge-density fluctuations may therefore be expressed in terms of the real (σ') and imaginary (σ'') parts of $\sigma(\omega)$ in the form

$$\lim_{k\to 0} \frac{S_{ZZ}(k,\omega)}{S_{ZZ}(k)} = \frac{1}{\pi} \frac{4\pi\sigma'(\omega)}{[\omega - 4\pi\sigma''(\omega)]^2 + [4\pi\sigma'(\omega)]^2} \tag{10.4.31}$$

In the low-frequency limit, $\sigma'(\omega) \to \sigma$, $\sigma''(\omega) \to 0$, and (10.4.31) reduces to

$$S_{ZZ}(k,\omega) \sim \frac{1}{\pi} \frac{4\pi\sigma(k/k_{\mathrm{D}})^2}{\omega^2 + (4\pi\sigma)^2}, \quad k, \omega \to 0 \tag{10.4.32}$$

Charge fluctuations in the low-frequency, long-wavelength regime are therefore of a non-propagating type. The same is true of concentration fluctuations in a mixture of uncharged particles, but the two cases differ in a significant way. If the coupling to other hydrodynamic variables is weak, a Fourier component of a fluctuation in the local concentration $c(\mathbf{r}, t)$ in a non-ionic, binary mixture decays in approximately the same way as a component of the density of tagged particles in a one-component system (see (8.2.5)), i.e.

$$c_{\mathbf{k}}(t) \approx c_{\mathbf{k}} \exp\left(-Dk^2 t\right) \tag{10.4.33}$$

where D is the interdiffusion coefficient.[22] The spectrum of concentration fluctuations therefore has approximately the same functional form as the self dynamic structure factor (8.2.9):

$$\begin{aligned} S_{cc}(k,\omega) &= \frac{1}{2\pi} \int_{-\infty}^{\infty} \left\langle c_{\mathbf{k}}(t) c_{-\mathbf{k}} \right\rangle \exp(i\omega t)\, \mathrm{d}t \\ &\approx \frac{\langle |c_{\mathbf{k}}|^2 \rangle}{\pi} \frac{Dk^2}{\omega^2 + (Dk^2)^2} \end{aligned} \tag{10.4.34}$$

Equation (10.4.34) represents a lorentzian curve centred at $\omega = 0$ and having a width that varies as k^2, whereas the width of the charge-fluctuation spectrum (10.4.32) remains non-zero even in the long-wavelength limit. The source of this difference in behaviour is the fact that in the coulombic case the "restoring force" is proportional to the charge-density fluctuation, while in the neutral system it is proportional to the laplacian of the concentration fluctuation.

Although the hydrodynamic analysis yields the correct low-frequency behaviour, the possibility that a propagating charge-density oscillation could occur at higher frequencies has to be investigated within the framework either of generalised hydrodynamics or of the

memory-function formalism. In particular, the memory-function representations developed in Sections 9.3 and 9.4 lend themselves easily to a unified treatment of transverse and longitudinal charge fluctuations. Here, however, we consider only the more interesting question of the nature of the longitudinal fluctuations. We also restrict the discussion to long wavelengths and to the case when $z_1 = -z_2 = z$, and use the fact that

$$\lim_{k\to 0} \frac{\omega_0^2}{S_{ZZ}(k)} = \omega_\mathrm{p}^2 \tag{10.4.35}$$

which follows from the long-wavelength relation (10.2.14) and the definitions (10.4.22) and (10.4.24). When adapted to the problem of the longitudinal charge current, the memory-function equation (9.4.7) becomes

$$\widetilde{C}_{ZZ,l}(k,\omega) = \frac{\omega_0^2}{-i\omega + \dfrac{\omega_\mathrm{p}^2}{-i\omega} + \widetilde{N}_l(k,\omega)} \tag{10.4.36}$$

Use of (10.4.19) shows that the corresponding expression for the charge-density autocorrelation function is given in terms of Laplace transforms by

$$\widetilde{F}_{ZZ}(k,\omega) = \frac{S_{ZZ}(k)}{-i\omega + \dfrac{\omega_\mathrm{p}^2}{-i\omega + \widetilde{N}_l(k,\omega)}} \tag{10.4.37}$$

The high-frequency behaviour can now be studied in an approximate way by assuming that the memory function $N_l(k,t)$ decays exponentially with a relaxation time equal τ_l. This is the characteristic approximation of the viscoelastic model introduced in Chapter 9, and leads, for small k, to

$$\widetilde{N}_l(k,\omega) = \frac{\omega_{1l}^2 - \omega_\mathrm{p}^2}{-i\omega + 1/\tau_l} \tag{10.4.38}$$

A simple calculation then shows that if $\omega\tau_l \gg 1$, the charge–charge dynamic structure factor (proportional to $\mathrm{Re}\,\widetilde{F}_{ZZ}(k,\omega)$) has peaks at $\omega = 0$ and $\omega = \pm\omega_{1l}$; those at $\pm\omega_{1l}$ correspond to charge fluctuations that propagate at a frequency comparable with the plasma frequency, but modified by the short-range interactions between ions. The calculation is a crude one, limited as it is to high frequencies and long wavelengths, but it provides a fair description of the dispersion of the propagating mode observed in simulations (see below in Figure 10.5).

10.5 MICROSCOPIC DYNAMICS IN MOLTEN SALTS

Much of our current understanding of the microscopic dynamics in strongly coupled ionic systems comes from molecular-dynamics simulations. In this section we give some examples, taken from studies of monovalent molten salts, that illustrate the richness of the observed single-particle and collective behaviour.

Single-particle motion is conveniently discussed in terms of the velocity autocorrelation functions $Z_\nu(t)$ and self-diffusion coefficients D_ν of the two ionic species; D_ν is related to $Z_\nu(t)$ in the manner of (7.2.7). For mixtures of neutral particles in which cross correlations of velocity of the type $\langle \mathbf{u}_i(t) \cdot \mathbf{u}_j \rangle$ $(i \neq j)$ are negligible, the two self-diffusion coefficients are related to the interdiffusion coefficient D by the expression

$$D \approx \mathcal{F} \frac{x_1 x_2}{N k_B T} (x_2 D_1 + x_1 D_2) \tag{10.5.1}$$

where $\mathcal{F} = (\partial^2 G / \partial x_1^2)_{P,T}$ is a purely thermodynamic quantity.[22] If, in addition, the mixture is nearly ideal, which is a good approximation for mixtures of simple liquids, $\mathcal{F} \approx N k_B T / x_1 x_2$, and (10.5.1) becomes

$$D \approx x_2 D_1 + x_1 D_2 \tag{10.5.2}$$

In an ionic liquid interdiffusion is equivalent to electrical conduction. We have shown in Section 7.7 that the static electrical conductivity σ is proportional to the time integral of the electric-current autocorrelation function $J(t)$, defined as

$$J(t) = \langle \mathbf{j}^Z(t) \cdot \mathbf{j}^Z \rangle = \sum_{i=1}^{N} \sum_{j=1}^{N} \langle z_i \mathbf{u}_i(t) \cdot z_j \mathbf{u}_j \rangle \tag{10.5.3}$$

If the self-correlation terms $(i = j)$ in (10.5.3) are separated from the cross terms $(i \neq j)$, integration over time and use of (7.7.10) shows that

$$\sigma = \beta e^2 \rho \left(x_1 z_1^2 D_1 + x_2 z_2^2 D_2 \right) (1 - \Delta) \tag{10.5.4}$$

Equation (10.5.4), with $\Delta = 0$, is called the Nernst–Einstein relation; the value of the deviation factor Δ is a measure of the importance of cross-correlations. If $\Delta = 0$, (10.5.4) becomes the ionic equivalent of the approximate relation (10.5.2). In practice, at least for the alkali halides, Δ is significantly different from zero and always positive. The importance of cross correlations in monovalent salts is illustrated in Figure 10.4, where molecular-dynamics results for the velocity and electric-current autocorrelation functions of the simple molten salt are plotted. The symmetry of the model means that the velocity autocorrelation functions of cations and anions are identical; if cross-correlations of velocities were negligible, the normalised curves of $Z(t)$ and $J(t)$ would also be the same. At short times, however, there are substantial differences between the two functions, and the calculated Nernst–Einstein deviation factor for the case shown is $\Delta = 0.19$. The positive value of Δ corresponds physically to the fact that motion in the same direction by a pair of oppositely charged ions contributes to self-diffusion but not to electrical conduction. The numerical result agrees well with experimental data: the mean value of Δ for eight alkali-halide salts is 0.26. The observed deviations from the Nernst–Einstein relation therefore have a natural explanation in terms of positive correlations between the velocities of nearest-neighbour ions that persist for times which, for a real molten salt, would be of order 10^{-12} s. Such

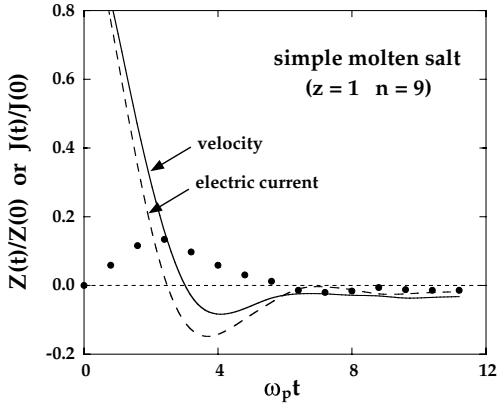

FIG. 10.4. Normalised velocity and electric-current autocorrelation functions of the simple molten salt[10] under the state conditions described in the caption to Figure 10.1. Full curve: $Z(t)/Z(0)$; dashes: $J(t)/J(0)$. The points show the difference between the two functions.

correlations are of a nature that physical intuition would lead one to expect, but it is not necessary to assume the existence of well-defined ion pairs.

The velocity autocorrelation function shown in Figure 10.4 has a negative plateau similar to that seen in argon-like liquids. Both the shape of $Z(t)$ and the value of the diffusion coefficient are reasonably well reproduced by a mode-coupling calculation[23] of the type discussed in Section 9.5. The mode-coupling results for the electric-current autocorrelation function are much less satisfactory and the theoretical value for the case illustrated in the figure is about 30% too small. These discrepancies have been attributed to the neglect of temperature fluctuations in the mode-coupling calculations.

Molecular-dynamics results on self diffusion are also available for rigid-ion models of the alkali halides in which allowance is made for the differences in mass and size of the two ions. Where the mass difference is large, the velocity autocorrelation function of the lighter ion is strongly oscillatory. This effect is the result of a "rattling" motion of the ion in the relatively long-lived cage formed by its heavier neighbours and is particularly marked in the case of the very light Li^+ ion. The calculated diffusion coefficients are in general smaller than the experimental values, sometimes significantly so, but the agreement with experiment is substantially improved when allowance is made for polarisation of the ions.[24] In a rigid-ion model, local charge neutrality around a diffusing ion can be maintained only by bodily displacement of its neighbours; when the ions are polarisable, an additional screening mechanism is present that does not entail movement of the ion cores. The net result is that the cage effect is smaller for polarisable ions; this leads to an increased damping of oscillations in the velocity-autocorrelation function and a consequent increase in the diffusion coefficient.

The wavenumber-dependent collective motions in molten salts have also been studied by molecular dynamics. The simple molten salt is particularly well-suited to theoretical investigation of the collective modes,[10] because the fluctuations in mass and charge densities are strictly independent at all wavelengths (see Section 10.4). The main objects of interest are the optic-type modes associated with charge fluctuations, since these are specific to ionic

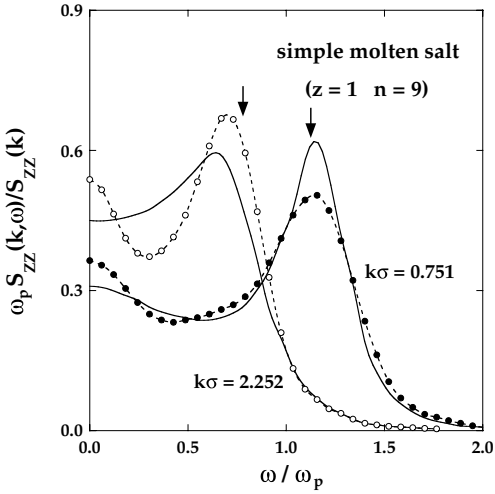

FIG. 10.5. Charge–charge dynamic structure factor of the simple molten salt[10] at two values of k under the state conditions described in the caption to Figure 10.1. The points show the results of molecular-dynamics calculations, the dashes are guides to the eye and the curves are calculated from a single-relaxation time approximation for the memory function $N_l(k,t)$, with the relaxation time determined by a least-squares fit to the simulated spectra. The arrows mark the value of $\omega_{1l}(k)$.

fluids. The results of the simulations show that the charge-density autocorrelation function $F_{ZZ}(k,t)$ is strongly oscillatory at wavelengths up to about twice the mean interionic spacing. These oscillations give rise to a "plasmon" peak in the dynamic structure factor $S_{ZZ}(k,\omega)$, as shown in Figure 10.5. The frequency ω_k at which the optic peak is seen is in the region of the plasma frequency ω_p, but its dispersion is strongly negative and described reasonably well by the relation $\omega_k \approx \omega_{1l}(k)$, as suggested by the rough calculation made in the previous section. The peak eventually disappears at a value of k close to the position of the main peak in the charge–charge structure factor $S_{ZZ}(k)$. More surprising is the fact that at small wavenumbers the optic peak initially sharpens as k increases, i.e. the damping of the plasmon mode becomes weaker. This behaviour is in striking contrast to that of the sound-wave mode; in molten salts, as in systems of neutral particles, the sound-wave damping increases rapidly with k.

The main features of the charge-fluctuation spectrum of the simple molten salt are also seen in simulations of more realistic rigid-ion models; the effect of including polarisation is to broaden the optic peak and shift it to lower frequencies.[25] It can be seen from Figure 10.5 that in the case of the simple molten salt the single-relaxation time, viscoelastic approximation cannot account for the detailed shape of the spectrum. At least two relaxation times are required, and other calculations have confirmed that the memory function for the longitudinal charge–current correlation function consists of a rapidly decaying term and a long-time, quasi-exponential tail; it therefore has a structure similar to that required to describe the density fluctuations in argon-like liquids (see Section 9.4). A fair description of the spectra of mass and charge fluctuations in the simple molten salt has been obtained by mode-coupling methods along the general lines of Section 9.5. In particular, a mode-

coupling calculation[26] has shown that the width of the plasmon peak should decrease with increasing k in a certain wavenumber range, in qualitative agreement with the unexpected behaviour observed in the simulations.

Several attempts have been made to detect a collective, plasmon-like excitation in molten salts by inelastic neutron scattering. If b_1 and b_2 are the coherent neutron scattering lengths of the two ionic species, and if $z_1 = -z_2$, a straightforward extension of the derivation given for a one-component fluid in Section 7.5 shows that the coherent, inelastic cross-section for a monovalent salt can be written in the form

$$\frac{\mathrm{d}^2\sigma}{\mathrm{d}\Omega\,\mathrm{d}\omega} \propto (b_1+b_2)^2 S_{NN}(k,\omega) + 2\left(b_1^2 - b_2^2\right) S_{NZ}(k,\omega) + (b_1-b_2)^2 S_{ZZ}(k,\omega) \tag{10.5.5}$$

Thus a single experiment yields only a linear combination of the three dynamic structure factors (number–number, number–charge and charge–charge). Moreover, the contribution made by the charge-fluctuation component is very low at small wavenumbers, since $S_{ZZ}(k)$ (the integral of $S_{ZZ}(k,\omega)$) is proportional to k^2 in the limit $k \to 0$. Only when the scattering lengths are such that $b_1 \approx -b_2$ does the component $S_{ZZ}(k,\omega)$ dominate, and this situation is not easily achievable with readily available isotopes. The most convincing experimental evidence obtained so far for the existence of a plasmon mode in ionic liquids comes from the analysis of infrared reflectivity data for molten lithium fluoride.[27] The resulting spectrum, which corresponds effectively to $S_{ZZ}(k,\omega)$ at zero wavenumber, displays a well-defined plasmon-like response, at a frequency somewhat above ω_p, which is well separated from a central, diffusive peak.

The autocorrelation functions of the transverse components of the mass and charge currents have been calculated in molecular-dynamics simulations of a number of model systems. The frequency of the transverse optic mode lies roughly an amount ω_p below that of its longitudinal counterpart, as suggested by the sum rule (10.4.25), and is relatively insensitive to wavenumber. As in the case of the longitudinal modes, an accurate memory-function fit of the transverse-current spectra requires the introduction of two relaxation times that are very different in value.[25]

10.6 THE ELECTRIC DOUBLE LAYER

So far in this chapter the emphasis has been placed on the bulk properties of ionic liquids. In this section and the one that follows we discuss some of the new phenomena that arise in the vicinity of a charged surface, and show how the resulting inhomogeneities can be described within the framework of the density-functional theory developed in Chapters 3 and 6.

When colloidal particles or macromolecules are dissolved in a highly polar solvent such as water, they will normally release counterions into the solvent, leaving behind a "polyion" carrying a surface charge of opposite sign. The solvent will in general be an electrolyte solution, and itself is therefore a source of both counterions and coions, coions being those of like charge to that of the polyion. Counterions are attracted by the surface charge, but

the effect is counterbalanced by the tendency for ions to spread into the bulk solution in order to maximise the entropy. These competing effects lead to the formation of an electric double layer at the charged surface, to which both coions and counterions contribute. In the discussion that follows we restrict ourselves to the situation in which only two ionic species are present, with charges $z_\nu e$, $\nu = +$ or $-$. The inhomogeneous solution in the vicinity of the charged surface is assumed to be in chemical equilibrium with a bulk solution (or reservoir) of the same ions at chemical potentials, μ_ν. The surface charge is the source of an external field acting on the ions and the solution of the electrostatic problem involves boundary conditions on the local electrostatic field.

Within a confined dielectric medium of permittivity ε, the electrostatic potential at $\mathbf{r}'$ due to a unit point charge at $\mathbf{r}$ is given by the Green's function $\mathcal{G}(\mathbf{r}, \mathbf{r}')$ that satisfies Poisson's equation:

$$\nabla^2 \mathcal{G}(\mathbf{r}, \mathbf{r}') = -\frac{4\pi}{\varepsilon}\delta(\mathbf{r}' - \mathbf{r}) \tag{10.6.1}$$

for given boundary conditions at any interfaces.[28] If there are no boundaries, the Green's function is the usual Coulomb potential, $\mathcal{G}(\mathbf{r}, \mathbf{r}') = \mathcal{G}(\mathbf{r}' - \mathbf{r}) = 1/\varepsilon|\mathbf{r}' - \mathbf{r}|$; when boundaries are present, the solution can be obtained by the method of images, at least for sufficiently simple geometries.[29] Let $\rho_Z(\mathbf{r})$ be the local charge density of the fluid, defined as[30]

$$\rho_Z(\mathbf{r}) = \sum_\nu z_\nu \rho_\nu^{(1)}(\mathbf{r}) \tag{10.6.2}$$

where $\rho_\nu^{(1)}(\mathbf{r})$ is the single-particle density of species ν. The local electrostatic potential $\Phi^{\mathrm{C}}(\mathbf{r})$ that satisfies Poisson's equation:

$$\nabla^2 \Phi^{\mathrm{C}}(\mathbf{r}) = -\frac{4\pi e}{\varepsilon}\rho_Z(\mathbf{r}) \tag{10.6.3}$$

subject to any boundary conditions, is

$$\Phi^{\mathrm{C}}(\mathbf{r}) = \int \mathcal{G}(\mathbf{r}, \mathbf{r}') e \rho_Z(\mathbf{r}')\, \mathrm{d}\mathbf{r}' \tag{10.6.4}$$

The electrostatic energy of the system is then given by

$$U^{\mathrm{C}} = \tfrac{1}{2} e \int \Phi^{\mathrm{C}}(\mathbf{r}) \rho_Z(\mathbf{r})\, \mathrm{d}\mathbf{r} = \tfrac{1}{2} e^2 \iint \rho_Z(\mathbf{r}) \mathcal{G}(\mathbf{r}, \mathbf{r}') \rho_Z(\mathbf{r}')\, \mathrm{d}\mathbf{r}\, \mathrm{d}\mathbf{r}' \tag{10.6.5}$$

where the integral extends over the region occupied by the fluid. From now on, however, we shall restrict ourselves to the situation in which there are no dielectric discontinuities and the permittivity is the same throughout space. Lifting this restriction introduces only technical complications.

The grand, potential functional of the fluid is

$$\Omega\big[\rho_+^{(1)}, \rho_-^{(1)}\big] = \mathcal{F}\big[\rho_+^{(1)}, \rho_-^{(1)}\big] - \sum_\nu \int \big[\mu_\nu - \phi_\nu(\mathbf{r})\big] \rho_\nu^{(1)}(\mathbf{r})\, \mathrm{d}\mathbf{r} \tag{10.6.6}$$

where $\phi_\nu(\mathbf{r})$ is the total external potential acting on ions of species ν, which may have both coulombic and non-coulombic components. The intrinsic free-energy functional $\mathcal{F}$ can be split, as usual, into ideal and excess parts:

$$\mathcal{F}\big[\rho_+^{(1)}, \rho_-^{(1)}\big] = \sum_\nu \mathcal{F}_\nu^{\mathrm{id}}\big[\rho_\nu^{(1)}\big] + \mathcal{F}^{\mathrm{ex}}\big[\rho_+^{(1)}, \rho_-^{(1)}\big] \tag{10.6.7}$$

where the ideal contributions are defined as in (3.1.22) and the excess contribution is given by a two-component generalisation of (3.5.23). If the reference state, corresponding to $\lambda = 0$ in (3.5.23), is taken as one in which the chemical potentials are the same as those of the bulk solution, then

$$\begin{aligned}\mathcal{F}^{\mathrm{ex}}&\big[\rho_+^{(1)}, \rho_-^{(1)}\big] \\ &= F^{\mathrm{ex}}(n_+, n_-) + \sum_\nu \mu_\nu^{\mathrm{ex}} \int \Delta\rho_\nu^{(1)}(\mathbf{r})\,\mathrm{d}\mathbf{r} \\ &\quad - k_{\mathrm{B}}T \sum_\nu \sum_\mu \int_0^1 \mathrm{d}\lambda\,(1-\lambda) \iint \Delta\rho_\nu^{(1)}(\mathbf{r}) c_{\nu\mu}(\mathbf{r}, \mathbf{r}'; \lambda) \Delta\rho_\mu^{(1)}(\mathbf{r}')\,\mathrm{d}\mathbf{r}\,\mathrm{d}\mathbf{r}'\end{aligned} \tag{10.6.8}$$

where n_+, n_- are the number densities in the bulk.

The direct correlation functions in (10.6.8) may be decomposed in the form

$$c_{\nu\mu}(\mathbf{r}, \mathbf{r}') = c_{\nu\mu}^{\mathrm{S}}(\mathbf{r}, \mathbf{r}') - z_\nu z_\mu l_{\mathrm{B}}/|\mathbf{r}' - \mathbf{r}| \tag{10.6.9}$$

where $l_{\mathrm{B}} = e^2/\varepsilon k_{\mathrm{B}}T$ is called the Bjerrum length. The second term on the right-hand side is the asymptotic value of the function; the first term therefore represents the short-range correlations. If we now substitute for $c_{\nu\mu}(\mathbf{r}, \mathbf{r}')$ in (10.6.8), the excess free-energy functional separates into a mean-field, purely coulombic part, $\mathcal{F}^{\mathrm{C}}$, and a correlation term, $\mathcal{F}^{\mathrm{corr}}$. The mean-field part is given by (10.6.5), with $\mathcal{G}(\mathbf{r}, \mathbf{r}')$ taking its coulombic form, and the correlation term is formally identical to (10.6.8), but with the direct correlation functions replaced by their short-range parts. Thus

$$\mathcal{F}^{\mathrm{ex}} = \mathcal{F}^{\mathrm{C}} + \mathcal{F}^{\mathrm{corr}}, \quad \mathcal{F}^{\mathrm{C}} = \tfrac{1}{2}e^2 \iint \frac{\rho_Z(\mathbf{r})\rho_Z(\mathbf{r}')}{\varepsilon|\mathbf{r}' - \mathbf{r}|}\,\mathrm{d}\mathbf{r}\,\mathrm{d}\mathbf{r}' \tag{10.6.10}$$

A particularly simple approximation is to set $\mathcal{F}^{\mathrm{corr}} = 0$, implying that the fluid behaves as an ideal gas in which each ion experiences only the average electrostatic potential due to other ions and the charges at any interfaces. The density profile $\rho_\nu^{(1)}(\mathbf{r})$ derived from the variational principle (3.4.3) is then

$$\rho_\nu^{(1)}(\mathbf{r}) = \xi_\nu \exp\big(-\beta\big[\phi_\nu(\mathbf{r}) + z_\nu e\Phi^{\mathrm{C}}(\mathbf{r})\big]\big) \tag{10.6.11}$$

where the electrostatic potential $\Phi^{\mathrm{C}}(\mathbf{r})$ is given by (10.6.4) and $\xi_\nu = \exp(\beta\mu_\nu)/\Lambda_\nu^3$ is the activity of species ν, which in the mean-field approximation is equal to the bulk density n_ν.

If the external potentials have a coulombic component, arising from an external charge density $\rho_Z^{\text{ext}}(\mathbf{r})$, (10.6.11) may be rewritten as

$$\rho_\nu^{(1)}(\mathbf{r}) = n_\nu \exp\bigl(-\beta\bigl[\phi_\nu^{\text{S}}(\mathbf{r}) + z_\nu e\Phi(\mathbf{r})\bigr]\bigr) \tag{10.6.12}$$

where $\phi_\nu^{\text{S}}(\mathbf{r})$ is the short-range, non-coulombic contribution to $\phi_\nu(\mathbf{r})$ and $\Phi(\mathbf{r})$ is the total electrostatic potential, which is related to the total charge density by

$$\nabla^2\Phi(\mathbf{r}) = -\frac{4\pi e}{\varepsilon}\bigl[\rho_Z^{\text{ext}}(\mathbf{r}) + \rho_Z(\mathbf{r})\bigr] \tag{10.6.13}$$

The coupled equations (10.6.11) (or (10.6.12)) and (10.6.3) (or (10.6.13)) are the equations of Poisson–Boltzmann theory.

As a first application of the theory we take the case of an electric double layer near an inpenetrable, planar wall at $z = 0$. The wall separates the ionic solution for $z > 0$ from a dielectric medium of the same permittivity for $z < 0$; the density profiles now depend only on z. The wall carries a surface charge density σ and overall charge neutrality requires that

$$\int_0^\infty e\rho_Z(z)\,\mathrm{d}z = -\sigma \tag{10.6.14}$$

If we assume that the absolute charges of the two ionic species are equal, it follows that $n_+ = n_- = \frac{1}{2}n_0$, and combination of (10.6.2), (10.6.12) and (10.6.13) gives

$$\frac{\mathrm{d}^2\Phi(z)}{\mathrm{d}z^2} = \frac{4\pi e n_0}{\varepsilon}\sinh\bigl[\beta e\Phi(z)\bigr], \quad z > 0 \tag{10.6.15}$$

with the constraint, valid for point ions, that $\rho_\nu^{(1)}(z) = 0$ for $z < 0$. Equation (10.6.15) is the Poisson–Boltzmann equation; it must be solved subject to two boundary conditions:

$$\lim_{z\to 0}\frac{\mathrm{d}\Phi(z)}{\mathrm{d}z} = 0, \qquad \left.\frac{\mathrm{d}\Phi(z)}{\mathrm{d}z}\right|_{z=0} = -\frac{4\pi\sigma}{\varepsilon} \tag{10.6.16}$$

The local number density of microions is $\rho_N(z) = \rho_+^{(1)}(z) + \rho_-^{(1)}(z)$, the gradient of which is easily obtained from (10.6.2), (10.6.12) and (10.6.13):

$$\frac{\mathrm{d}\rho_N(z)}{\mathrm{d}z} = -\beta\frac{\mathrm{d}\Phi(z)}{\mathrm{d}z}e\rho_Z(z) = \frac{\beta\varepsilon}{4\pi}\frac{\mathrm{d}\Phi(z)}{\mathrm{d}z}\frac{\mathrm{d}^2\Phi(z)}{\mathrm{d}z^2} = \frac{\beta\varepsilon}{8\pi}\frac{\mathrm{d}}{\mathrm{d}z}\left(\frac{\mathrm{d}\Phi(z)}{\mathrm{d}z}\right)^2 \tag{10.6.17}$$

Integration of both sides of (10.6.17) from z to infinity yields a relation between the local number density and the local electric field $E(z) = -\mathrm{d}\Phi(z)/\mathrm{d}z$:

$$k_{\text{B}}T\bigl[\rho_N(z) - n_0\bigr] = \frac{\varepsilon}{8\pi}\bigl[E(z)\bigr]^2 \tag{10.6.18}$$

Since the microions behave as an ideal gas, the left-hand side of (10.6.18) is the difference in local osmotic pressure $P(z) = k_B T \rho_N(z)$ between a point z and a point in the bulk, where $\rho_N(z) = n_0$; the right-hand side is the electrostatic pressure,[28] which vanishes in the bulk. Differentiation of (10.6.18) with respect to z and use of Poisson's equation leads to the condition necessary for hydrostatic equilibrium, i.e.

$$\frac{\mathrm{d}P(z)}{\mathrm{d}z} = eE(z)\rho_Z(z) = f(z) \tag{10.6.19}$$

where $f(z)$ is the local force per unit volume acting on the solution. By evaluating (10.6.18) at $z = 0$ and making use of the second of the boundary conditions (10.6.16), we obtain an expression for the enhancement of the microion density at contact over its bulk value:

$$k_B T \rho_N(0) = k_B T n_0 + \frac{\varepsilon[E(0)]^2}{8\pi} = k_B T n_0 + \frac{2\pi\sigma^2}{\varepsilon} \tag{10.6.20}$$

This result is a special case of the contact theorem for ionic systems:[31]

$$k_B T \rho_N(0) = P + \frac{2\pi\sigma^2}{\varepsilon} \tag{10.6.21}$$

where P is the bulk osmotic pressure, which for an ideal solution is equal to $k_B T n_0$. Equation (10.6.21) is a generalisation of (6.5.3b), which applies to uncharged systems. As the surface charge increases, the contact density will eventually become sufficiently large that the role of ion–ion correlations can no longer be ignored. The correlation term in the free-energy functional (10.6.10) must then be included in some approximate form,[32] such as a weighted-density approximation of the type discussed in Section 6.2.

Equation (10.6.15) can be solved analytically. The dimensionless potential $\Phi^*(z) = e\Phi(z)/k_B T$ satisfies the equation

$$\frac{\mathrm{d}^2\Phi^*(z)}{\mathrm{d}z^2} = k_D^2 \sinh \Phi^*(z) \tag{10.6.22}$$

where k_D is the Debye wavenumber (10.2.15). The solution to (10.6.22) is

$$\Phi^*(z) = 4\tanh^{-1}\left[g \exp(-k_D z)\right] \tag{10.6.23}$$

where g is related to the dimensionless surface potential $\Phi^*(0)$ by

$$g = \tanh \tfrac{1}{4}\Phi^*(0) \tag{10.6.24}$$

The density profiles follow from (10.6.11):

$$\rho_{\pm}^{(1)}(z) = \tfrac{1}{2} n_0 \left(\frac{1 \mp g \exp(-k_D z)}{1 \pm g \exp(-k_D z)} \right)^2 \tag{10.6.25}$$

At distances $z \approx k_{\mathrm{D}}^{-1}$ or larger, the density profiles approach their bulk values exponentially, so the thickness of the double layer is of the order of Λ_{D}, the Debye screening length.

We next consider the question of what the effective interaction is between charged surfaces separated by an inhomogeneous ionic solution. The simplest geometry is that of two infinite, parallel, uniformly charged planes placed at $z = \pm\frac{1}{2}L$. If the two surface charge densities are the same, there is a plane of symmetry at $z = 0$ where the local electric field must vanish. The ionic fluid is assumed to be in chemical equilibrium with a reservoir of non-interacting, monovalent microions, which fixes the chemical potentials of the two species at their ideal values, $\mu_\nu = k_{\mathrm{B}}T \ln(\Lambda_\nu^3 n_\nu)$. The mirror symmetry means that it is necessary to solve the Poisson–Boltzmann equation only in the interval $-\frac{1}{2}L \leqslant z \leqslant 0$, with the boundary conditions

$$\left.\frac{\mathrm{d}\Phi(z)}{\mathrm{d}z}\right|_{z=-L/2} = -\frac{4\pi\sigma}{\varepsilon}, \qquad \left.\frac{\mathrm{d}\Phi(z)}{\mathrm{d}z}\right|_{z=0} = 0 \tag{10.6.26}$$

For this problem, apart from the somewhat academic case when the solution contains only counterions, the solution to the non-linear differential equation (10.6.15) must be obtained numerically. If the surface charge σ is sufficiently low, however, it is justifiable to linearise (10.6.22) by setting $\sinh\Phi^*(z) \approx \Phi^*(z)$. The resulting linear equation is easily solved to give

$$\Phi(z) = \frac{\Phi_0}{\sinh(k_{\mathrm{D}}L/2)}\cosh(k_{\mathrm{D}}z) \tag{10.6.27}$$

with $\Phi_0 = 4\pi\sigma/\varepsilon k_{\mathrm{D}}$.

The normal component $P_{\mathrm{N}}(z)$ of the stress tensor determines the force per unit area on a test surface placed at z within the fluid. In mechanical equilibrium, P_{N} must be constant throughout the interval between the planes, i.e.

$$\frac{\mathrm{d}P_{\mathrm{N}}(z)}{\mathrm{d}z} = 0, \quad -\tfrac{1}{2}L < z < \tfrac{1}{2}L \tag{10.6.28}$$

The quantity $P_{\mathrm{N}}(z)$ is the sum of the osmotic pressure of the ions, $P(z) = k_{\mathrm{B}}T\rho_N(z)$, and an electrostatic contribution, which is related to Maxwell's electrostatic stress tensor:[28]

$$P_{\mathrm{N}} = P(z) - \frac{\varepsilon}{8\pi}\left(\frac{\mathrm{d}\Phi(z)}{\mathrm{d}z}\right)^2 = k_{\mathrm{B}}T\rho_N(z) - \frac{\varepsilon}{8\pi}\big[E(z)\big]^2 \tag{10.6.29}$$

Taken together, (10.6.28) and (10.6.29) lead back to the equilibrium condition (10.6.19). The pressure difference

$$\Delta P = P_{\mathrm{N}}(L) - P_{\mathrm{N}}(\infty) \tag{10.6.30}$$

is the force per unit area that must be applied to the charged planes in order to maintain them at a separation L; it can therefore be identified with the solvation force f_{S} introduced in Section 6.1. Since the local electrical field is zero at $z = 0$, it follows from (10.6.29) that

$$f_{\mathrm{S}} \equiv \Delta P = k_{\mathrm{B}}T\big[\rho_N(0) - n_0\big] \tag{10.6.31}$$

Combination of (10.6.27), (10.6.31) and the linearised version of (10.6.12) shows that to lowest, non-vanishing order in $\Phi(z=0)$:

$$f_{\mathrm{S}}(L) = \tfrac{1}{2}k_{\mathrm{B}}Tn_0\big[\beta e\Phi(0)\big]^2 = \frac{2\pi\sigma^2}{\varepsilon}\frac{1}{\sinh^2(k_{\mathrm{D}}L/2)}$$
$$\approx \frac{8\pi\sigma^2}{\varepsilon}\exp(-k_{\mathrm{D}}L) \tag{10.6.32}$$

Thus the effective interaction between the charged plates is always repulsive. The same conclusion is reached within non-linear Poisson–Boltzmann theory. However, when correlations between ions are taken into account, the force between the planes may become attractive at small separations.[33] Such correlations are particularly strong in the case of divalent (or polyvalent) counterions, as illustrated by the results of Monte Carlo calculations shown in Figure 10.6.

Attraction between two like-charged surfaces can be accounted for within density-functional theory only if the correlation term in the excess free-energy functional is adequately approximated. If the ions are modelled as charged hard spheres, the correlations between ions arise both from hard-core effects and from short-range, coulombic interactions. This suggests that $\mathcal{F}^{\mathrm{ex}}$ can be usefully rewritten as

$$\mathcal{F}^{\mathrm{ex}}\big[\rho_+^{(1)}, \rho_-^{(1)}\big]$$
$$= \tfrac{1}{2}\int e\rho_Z(\mathbf{r})\Phi(\mathbf{r})\,\mathrm{d}\mathbf{r} + \mathcal{F}^{\mathrm{HS}}\big[\rho_+^{(1)}, \rho_-^{(1)}\big]$$
$$- k_{\mathrm{B}}T\sum_{\nu}\sum_{\mu}\int_0^1 \mathrm{d}\lambda(1-\lambda)\iint \Delta\rho_\nu^{(1)}(\mathbf{r})\Delta c_{\nu\mu}(\mathbf{r},\mathbf{r}';\lambda)\Delta\rho_\mu^{(1)}(\mathbf{r}')\,\mathrm{d}\mathbf{r}\,\mathrm{d}\mathbf{r}' \tag{10.6.33}$$

The first term on the right-hand side of (10.6.33) is the mean-field, purely coulombic contribution; the second is the excess free-energy functional for a binary hard-sphere mixture, corresponding to uncharged ions; and the last term contains the "residual" direct correlation functions, defined as

$$\Delta c_{\nu\mu}(\mathbf{r},\mathbf{r}';\lambda) = c_{\nu\mu}(\mathbf{r},\mathbf{r}';\lambda) + \frac{z_\nu z_\mu \lambda l_{\mathrm{B}}}{|\mathbf{r}-\mathbf{r}'|} - c_{\nu\mu}^{\mathrm{HS}}(\mathbf{r},\mathbf{r}';\lambda) \tag{10.6.34}$$

and represents the remaining correlations.[34] The hard-sphere direct correlation functions $c_{\nu\mu}^{\mathrm{HS}}(\mathbf{r}'\mathbf{r}')$ are those compatible with the assumed form of the functional $\mathcal{F}^{\mathrm{HS}}$, for which a weighted-density approximation can be used, and the residual direct correlation functions can be replaced by those of the bulk solution obtained, for example, from the solution of the MSA given in Section 10.3. Figure 10.6 makes a comparison between the results obtained in this way and those of Poisson–Boltzmann theory for restricted primitive models of both 1 : 1 and 2 : 2 electrolyte solutions. In the case of the 1 : 1 solution, where the force is everywhere repulsive, the two theories give similar results. In the divalent system, however, the inclusion of correlations gives rise to a strongly attractive force at small separations, with a minimum at $L \approx 2d$; the results are in good agreement with those obtained by

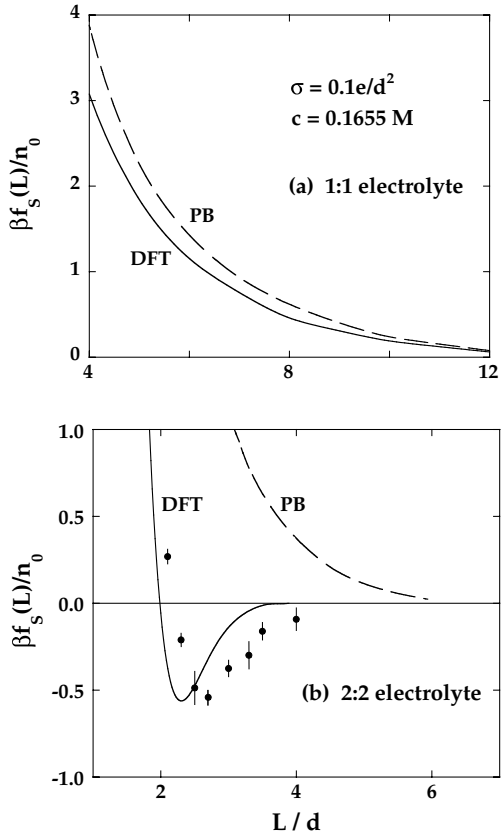

FIG. 10.6. Electric double-layer force between charged plates in restricted primitive models of (a) 1 : 1 and (b) 2 : 2 electrolyte solutions as a function of the plate separation L. The state conditions correspond in each case to an aqueous solution of ions of diameter $d = 4.2$ Å at 298 K. The curves are calculated from the Poisson–Boltzmann approximation (PB) or from density-functional theory (DFT) and the points are the results of Monte Carlo simulations.[33(b)] See text for details. After Tang *et al.*[34]

simulation for the same system. Poisson–Boltzmann theory, by contrast, again predicts that the force should be repulsive for all L. Ion correlations may also lead to charge inversion or "overscreening" of the surface charge: the total charge of the double layer, integrated over a few ionic diameters, can be of opposite sign to that of the planes. Similar results have been reached on the basis of numerical solution of the so-called anisotropic HNC equation, which represents an extension of bulk HNC theory to inhomogeneous situations.[35]

10.7 EFFECTIVE INTERACTIONS BETWEEN COLLOIDAL PARTICLES

We now show how the methods developed in the previous section can be used to calculate the effective interaction between large polyions in solution. The example we choose

is that of a dispersion of spherical, colloidal particles in a polar solvent of dielectric constant ε. The radius R of a particle, which we treat as a hard sphere, would be typically tens or even hundreds of nanometres, and the particle would carry a charge Ze ($|Z| \gg 1$), with the consequent formation of an electric double layer at the surface. We again adopt a primitive-model description of the solvent, with both coions and counterions being represented as charged hard spheres of diameter d ($\ll R$), and assume that the dispersion is in equilibrium with a salt reservoir, which fixes the chemical potentials μ_+, μ_- of the microions. The three-component system can be described within the so-called semi-grand canonical ensemble, characterised by the variables N_0, μ_+, μ_-, V and T, in which the number of polyions, N_0, is fixed but the numbers of microions are allowed to fluctuate. If we denote the coordinates of the polyions and microions by $\{\mathbf{R}_i\}$ and $\{\mathbf{r}_j\}$, respectively, the total potential energy of the system may be written in a shorthand form in which subscripts 0 and M refer, respectively, to polyions and microions:

$$V\big(\{\mathbf{R}_i\},\{\mathbf{r}_j\}\big) = V_{00}\big(\{\mathbf{R}_i\}\big) + V_{0\mathrm{M}}\big(\{\mathbf{R}_i\},\{\mathbf{r}_j\}\big) + V_{\mathrm{MM}}\big(\{\mathbf{r}_j\}\big) \tag{10.7.1}$$

where V_{00}, $V_{0\mathrm{M}}$ and V_{MM} are all sums of pair potentials of primitive-model form.

The large difference, both in size and charge, between polyions and microions renders the conventional integral-equation approaches impractical. A coarse-graining strategy is needed whereby the degrees of freedom of the microions are averaged out, so reducing the problem to that of an effective, one-component system of polyions dressed by their electric double layers. The reduction is achieved by writing the partition function of the semi-grand canonical system in the form

$$Q_{N_0} = \frac{1}{N_0!\Lambda_0^{3N_0}} \int \exp(-\beta V_{00})\,\Xi_{\mathrm{M}}\big(\mu_+,\mu_-,V,T;\{\mathbf{R}_i\}\big)\,\mathrm{d}\mathbf{R}^{N_0} \tag{10.7.2}$$

where

$$\Xi_{\mathrm{M}} = \sum_{N_+=0}^{\infty}\sum_{N_-=0}^{\infty} \frac{\xi_+^{N_+}\xi_-^{N_-}}{N_+!N_-!} \iint \exp\big[-\beta(V_{0\mathrm{M}}+V_{\mathrm{MM}})\big]\,\mathrm{d}\mathbf{r}^{N_+}\,\mathrm{d}\mathbf{r}^{N_-} \tag{10.7.3}$$

is the grand partition function of the microions in the external potential $\phi_\nu(\mathbf{r})$ of the polyions in a configuration $\{\mathbf{R}_i\}$:

$$\phi_\nu(\mathbf{r}) = \sum_{i=1}^{N_0} v_{0\nu}\big(|\mathbf{r}-\mathbf{R}_i|\big) \tag{10.7.4}$$

and ξ_+, ξ_- are the activities of the microions. Equation (10.7.2) can be re-expressed as

$$Q_{N_0} = \frac{1}{N_0!\Lambda_0^{3N_0}} \int \exp\big(-\beta V_{\mathrm{eff}}\big(\{\mathbf{R}_i\}\big)\big)\,\mathrm{d}\mathbf{R}^{N_0} \tag{10.7.5}$$

in which the effective interaction between the dressed polyions is

$$V_{\rm eff}\big(\{\mathbf{R}_i\}\big) = V_{00}\big(\{\mathbf{R}_i\}\big) + \Omega_{\rm M}\big(\mu_+, \mu_-, V, T; \{\mathbf{R}_i\}\big) \tag{10.7.6}$$

where $\Omega_{\rm M} = -k_{\rm B}T \ln \Xi_{\rm M}$ is the grand potential of the microions. The first term on the right-hand side of (10.7.6) arises from the direct interaction between polyions, while the second is a state-dependent, microion-induced interaction, which depends parametrically on the coordinates $\{\mathbf{R}_i\}$. Whereas the direct interaction is pairwise additive, the effective interaction is not; the effective interaction also includes a "volume" term, which is independent of the polyion coordinates.

The grand potential $\Omega_{\rm M}$ can be evaluated by the methods of density-functional theory. If we limit ourselves to a mean-field approach, we can take over the grand-potential functional defined by (10.6.6), (10.7.7) and (10.6.10) (with $\mathcal{F}^{\rm corr} = 0$). The solution of the resulting Euler–Lagrange equations for the local densities $\rho_\nu^{(1)}(\mathbf{r})$ in the multi-centre external potential (10.7.4) poses a formidable task. Numerical results may be obtained through a form of molecular-dynamics calculation in which the Fourier components of the local densities are treated as dynamical variables,[36] a scheme inspired by the Car–Parrinello method for simulating systems of classical ions and quantum mechanical, valence electrons.[37] However, further progress can be made analytically if the inhomogeneities induced by the polyions are assumed to be weak. In that case it is justifiable to expand the ideal free-energy functional (3.1.22) to second order in the deviation $\Delta\rho_\nu^{(1)}(\mathbf{r})$ of the local density from its bulk value, i.e.

$$\Delta\rho_\nu^{(1)}(\mathbf{r}) = \rho_\nu^{(1)}(\mathbf{r}) - n_\nu \tag{10.7.7}$$

The intrinsic free-energy functional of the microions is then

$$\mathcal{F}\big[\rho_+^{(1)}, \rho_-^{(1)}\big] = \sum_\nu \Bigg(F^{\rm id}(n_\nu) + k_{\rm B}T \ln\big(\Lambda_\nu^3 n_\nu\big) \int \Delta\rho_\nu^{(1)}(\mathbf{r})\, {\rm d}\mathbf{r} + \frac{k_{\rm B}T}{2n_\nu} \int \big[\Delta\rho_\nu^{(1)}\mathbf{r}\big]^2 {\rm d}\mathbf{r} \Bigg) + \tfrac{1}{2} \int e\rho_Z(\mathbf{r}) \Phi^{\rm C}(\mathbf{r})\, {\rm d}\mathbf{r} \tag{10.7.8}$$

where the electrostatic potential $\Phi^{\rm C}(\mathbf{r})$ satisfies Poisson's equation (10.6.3). Substitution of (10.7.8) in (10.6.6), replacement of the chemical potentials μ_ν by their ideal values and use of the variational principle (3.4.3) gives

$$\frac{\Delta\rho_\nu^{(1)}(\mathbf{r})}{n_\nu} + z_\nu \Phi^{\rm C}(\mathbf{r}) = -\beta\phi_\nu(\mathbf{r}), \quad \nu = +, - \tag{10.7.9}$$

These two equations are coupled through the terms in $\Phi^{\rm C}$. If we were to suppose for the moment that the polyions are point particles, i.e. that $R = 0$, the coulombic contribution to $\phi_\nu(\mathbf{r})$ would be everywhere equal to $z_\nu e \Phi^{\rm ext}(\mathbf{r})$, where $\Phi^{\rm ext}(\mathbf{r})$ is the "external" electrostatic potential acting on the microions.[38] If there were no boundaries, the total electrostatic

potential within the fluid would then be

$$\Phi(\mathbf{r}) = \Phi^{\mathrm{C}}(\mathbf{r}) + \Phi^{\mathrm{ext}}(\mathbf{r}) = e\int \frac{\rho_Z(\mathbf{r}') + Z\rho^{\mathrm{ext}}(\mathbf{r}')}{\varepsilon|\mathbf{r}-\mathbf{r}'|}\,\mathrm{d}\mathbf{r}' \tag{10.7.10}$$

where $\rho^{\mathrm{ext}}(\mathbf{r}) = \sum_i \delta(\mathbf{r}-\mathbf{R}_i)$ is the microscopic density of the polyions. Equation (10.7.9) now becomes

$$\Delta\rho_\nu^{(1)}(\mathbf{r}) = -\frac{n_\nu z_\nu e^2}{k_{\mathrm{B}}T}\int \frac{\rho_Z(\mathbf{r}') + Z\rho^{\mathrm{ext}}(\mathbf{r}')}{\varepsilon|\mathbf{r}-\mathbf{r}'|}\,\mathrm{d}\mathbf{r}' \tag{10.7.11}$$

To simplify the problem, we consider only the salt-free case, where all microions are counterions. The coupled equations (10.7.11) then reduce to a single integral equation from which the subscript ν can be dropped and the charge density $\rho_Z(\mathbf{r})$ replaced by $z\rho^{(1)}(\mathbf{r})$. On taking Fourier transforms of both sides of (10.7.11), applying the convolution theorem and incorporating the result in (10.1.5), we find that the Fourier transform of $\Delta\rho^{(1)}(\mathbf{r})$ is

$$\hat{\rho}^{(1)}(\mathbf{k}) = \frac{Zk_{\mathrm{D}}^2}{k^2+k_{\mathrm{D}}^2}\sum_{i=1}^{N_0}\exp(-i\mathbf{k}\cdot\mathbf{R}_i) \tag{10.7.12}$$

where $k_{\mathrm{D}}^2 = 4\pi n z^2 e^2/\varepsilon k_{\mathrm{B}}T$ is the square of the Debye wavenumber associated with the counterions. Inverse Fourier transformation of (10.7.12) leads to a counterion density profile given by

$$\rho^{(1)}(\mathbf{r}) = \sum_{i=1}^{N_0}\frac{Zk_{\mathrm{D}}^2}{4\pi}\frac{\exp(-k_{\mathrm{D}}|\mathbf{r}-\mathbf{R}_i|)}{|\mathbf{r}-\mathbf{R}_i|} \equiv \sum_{i=1}^{N_0}\rho_i^{(1)}(\mathbf{r}) \tag{10.7.13}$$

The total profile is therefore a superposition of profiles associated with each of the polyions. The radius of the polyions is now reintroduced by imposing the constraint that $\rho_i^{(1)}(\mathbf{r})$ must be zero whenever $|\mathbf{r}-\mathbf{R}_i| < R$. Charge neutrality means that $\rho_i^{(1)}(\mathbf{r})$ must be normalised such that

$$\int_{|\mathbf{r}-\mathbf{R}_i|>R}\rho_i^{(1)}(\mathbf{r})\,\mathrm{d}\mathbf{r} = |Z/z| \tag{10.7.14}$$

and for the profile defined by (10.7.13) this requirement would be met if the polyion charge Ze were replaced by a renormalised charge $Z'e$, where

$$Z' = Z\frac{\exp(k_{\mathrm{D}}R)}{1+k_{\mathrm{D}}R} \tag{10.7.15}$$

The normalisation in (10.7.14) implicitly assumes that the colloid concentration is low and hence that the electric double-layers associated with neighbouring polyions have, on average, little overlap. From Poisson's equation it is evident that the total electrostatic

potential may similarly be written as a superposition of N_0 screened potentials:

$$\Phi(\mathbf{r}) = \sum_{i=1}^{N_0} \frac{Z'e}{\varepsilon} \frac{\exp(-k_{\mathrm{D}}|\mathbf{r}-\mathbf{R}_i|)}{|\mathbf{r}-\mathbf{R}_i|} \equiv \sum_{i=1}^{N_0} \Phi_i(\mathbf{r}) \tag{10.7.16}$$

If the density profile (10.7.13) and the potential (10.7.16) are substituted in the free-energy functional (10.7.8), we find that the effective interaction energy (10.7.6) is of the form

$$V_{\mathrm{eff}}\big(\{\mathbf{R}_i\}\big) = V_0 + \sum_{i=1}^{N} \sum_{j>i}^{N} v_{\mathrm{eff}}\big(|\mathbf{R}_i - \mathbf{R}_j|\big) \tag{10.7.17}$$

where the effective pair potential $v_{\mathrm{eff}}(R)$ provides the electrostatic contribution to the well-known Derjaguin–Landau–Verwey–Overbeek (DLVO) potential:[39]

$$\begin{aligned} v_{\mathrm{eff}}\big(|\mathbf{R}_i - \mathbf{R}_j|\big) &= \int \Phi_i(\mathbf{r}) \rho_j^{(1)}(\mathbf{r})\, \mathrm{d}\mathbf{r} \\ &= \frac{Z'^2 e^2}{\varepsilon} \frac{\exp(-k_{\mathrm{D}}|\mathbf{R}_i - \mathbf{R}_j|)}{|\mathbf{R}_i - \mathbf{R}_j|} \end{aligned} \tag{10.7.18}$$

The pairwise additivity is a consequence of the quadratic form of the approximate functional (10.7.8).

The effective interaction energy (10.7.17) contains a structure-independent term, V_0. This term has no effect on the forces acting between the polyions, but it has a significant influence on the phase diagram.[40] It includes, among other contributions, the self-energy of the double layers associated with individual polyions. The DLVO potential is a function of density and temperature through its dependence on the Debye wavenumber; its form remains the same even in the presence of coions, provided the contributions of all microions are included in the definition of k_{D} and in V_0. It is strictly repulsive, thereby stabilising the colloidal suspension against irreversible aggregation (flocculation) induced by the strong van der Waals attractive forces between particles. However, if the salt concentration is sufficiently low, the structure-independent term can drive a phase transition into colloid-rich and colloid-poor dispersions, even in the absence of attractive forces.

The quadratic functional is inadequate for highly-charged polyions. The strong electrostatic attraction exerted by the polyions on the counterions leads to a substantial fraction of the latter becoming tightly bound to the colloid surface; this reduces[41] the magnitude of the bare polyion charge to an effective value $|Z_{\mathrm{eff}}|e$. The remaining counterions therefore experience a much weaker external potential, so the diffuse part of the double layer can still be described within the quadratic approximation. Direct measurement of the effective pair potential between charged colloidal particles shows that (10.7.18) provides a good representation of the data when Z_{eff} is suitably chosen, as the results shown in Figure 10.7 illustrate. The strong, coulombic correlations between microions that arise in the presence of divalent or trivalent counterions lead to a short-range attraction between like-charged polyions, similar to that calculated for planar surfaces in Section 10.6.

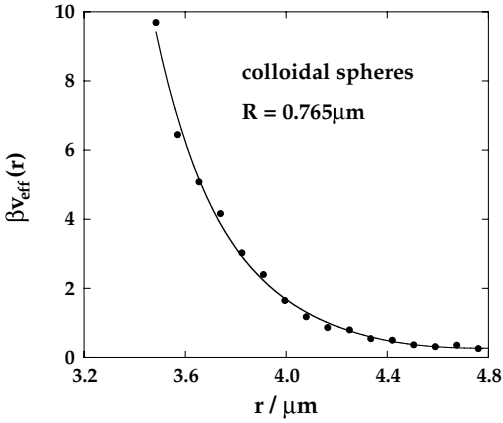

FIG. 10.7. Effective pair potential between polystyrene sulphate spheres of radius 0.765 ± 0.01 μm dispersed in water. The points are experimental results and the curve is calculated from (10.7.18) for an effective charge $|Z_{\text{eff}}| = 22\,793$. After Crocker and Grier.[42]

10.8 LIQUID METALS: ELECTRONS AND IONS

Pure liquid metals are two-component fluids consisting of N_{i} positive ions and $N_{\text{e}} = zN_{\text{i}}$ conduction electrons, where z is the ionic valency. The ionic core radius is usually only a small fraction of the mean interionic spacing, with the result that the ion cores occupy less than 10% of the total volume of the metal. In the "nearly free electron" picture the conduction electrons are assumed to move more or less freely through the liquid, interacting only rarely with the ions; the mean-free path of the electrons is typically ten to a hundred times larger than the separation of neighbouring ions. In the crudest approximation, interactions are neglected altogether, and the electrons are treated as an ideal Fermi gas characterised by the energy ε_{F} of the highest occupied (Fermi) level, i.e. $\varepsilon_{\text{F}} = \hbar^2 k_{\text{F}}^2/2m_{\text{e}} = \hbar^2(3\pi^2\rho_{\text{e}})^{2/3}/2m_{\text{e}}$, where k_{F} is the Fermi wavenumber, ρ_{e} is the number density of conduction electrons and m_{e} is the electron mass. The Fermi temperature, $T_{\text{F}} = \varepsilon_{\text{F}}/k_{\text{B}}$, is always some two orders of magnitude higher than the melting temperature. It is therefore a good approximation to assume that the electron gas is completely degenerate under normal liquid–metal conditions.

The simplest model that takes account of electron–ion interactions is the "jellium" model of Wigner. This is the quantum-mechanical analogue of the one-component plasma (OCP) discussed in Section 10.1. It treats the conduction electrons as an interacting Coulomb gas moving in the uniform background provided by the positively charged ions, with a hamiltonian $\mathcal{H} = K_{N_{\text{e}}} + V_{N_{\text{e}}}$, where $K_{N_{\text{e}}}$ is the kinetic-energy operator and the potential energy $V_{N_{\text{e}}}$ is the sum of electron–electron, electron–background and background–background terms. In a **k**-space representation, $V_{N_{\text{e}}}$ is given as a special case of (10.1.4) by

$$V_{N_{\text{e}}} = \frac{1}{2V}{\sum_{\mathbf{k}}}' \hat{v}_{\text{ee}}(k)\left(\rho^{\text{e}}_{\mathbf{k}}\rho^{\text{e}}_{-\mathbf{k}} - N_{\text{e}}\right) \tag{10.8.1}$$

where $\rho^{\mathrm{e}}_{\mathbf{k}}$ is a Fourier component of the microscopic electron density, $\hat{v}_{\mathrm{ee}}(k) = 4\pi e^2/k^2$ is the Fourier transform of the electron–electron potential and the prime on the summation means that the contribution for $\mathbf{k} = 0$ is omitted because of cancellation by the background. The ground-state energy has been calculated by methods of quantum-mechanical many-body theory;[43] it is the sum of kinetic, exchange and correlation terms and is expressible as a function of the single, dimensionless parameter $r_{\mathrm{S}} = a_{\mathrm{e}}/a_0$, where $a_{\mathrm{e}} = (3/4\pi\rho_{\mathrm{e}})^{1/3}$ is the "electron-sphere" radius and a_0 is the Bohr radius. The minimum energy, corresponding to zero pressure, occurs at $r_{\mathrm{S}} \approx 4.2$. This result is independent of the chemical nature of the system, but is in fair agreement with experimental results for the alkali metals, which range from 3.30 (for Li) to 5.78 (for Cs).

In a more realistic model the hamiltonian of a liquid metal is written as the sum of a purely electronic term $\mathcal{H}_{\mathrm{e}}$, a purely ionic term $\mathcal{H}_{\mathrm{i}}$ and an electron–ion interaction V_{ei}. The Coulomb repulsion between ions is in general sufficiently strong to prevent any short-range forces coming into play, while dispersion forces are weak because the ion cores are only weakly polarisable. It is therefore a good approximation to set the ion–ion interaction $v_{\mathrm{ii}}(R)$ equal to z^2e^2/R for all R. The electron–electron interaction $v_{\mathrm{ee}}(r)$ is purely coulombic and the electron–ion potential v_{ei} is also coulombic outside the ion core; we shall see below that inside the core, v_{ei} can be replaced by a weak "pseudopotential". We proceed[44] by adding to and subtracting from the hamiltonian the two contributions that would arise if the electrons were replaced by a uniform background of charge density $-e\rho_{\mathrm{e}}$. The terms involved are the ion–background interaction V_{ib} and the background self-energy V_{bb}, given by

$$V_{\mathrm{ib}} = -\rho_{\mathrm{e}} \sum_{j=1}^{N_{\mathrm{i}}} \int \frac{ze^2}{|\mathbf{R}_j - \mathbf{r}|}\,\mathrm{d}\mathbf{r}, \qquad V_{\mathrm{bb}} = \tfrac{1}{2}\rho_{\mathrm{e}}^2 \iint \frac{e^2}{|\mathbf{r} - \mathbf{r}'|}\,\mathrm{d}\mathbf{r}\,\mathrm{d}\mathbf{r}' \tag{10.8.2}$$

where $\mathbf{R}_j$ denotes the coordinates of ion j. The hamiltonian can then be written as

$$\mathcal{H} = \mathcal{H}'_{\mathrm{e}} + \mathcal{H}'_{\mathrm{i}} + V'_{\mathrm{ei}} \tag{10.8.3}$$

with

$$\mathcal{H}'_{\mathrm{e}} = \mathcal{H}_{\mathrm{e}} - V_{\mathrm{bb}}, \qquad \mathcal{H}'_{\mathrm{i}} = \mathcal{H}_{\mathrm{i}} + V_{\mathrm{ib}} + V_{\mathrm{bb}}, \qquad V'_{\mathrm{ei}} = V_{\mathrm{ei}} - V_{\mathrm{ib}} \tag{10.8.4}$$

In $\mathbf{k}$-space:

$$\begin{aligned}
\mathcal{H}'_{\mathrm{e}} &= K_{\mathrm{e}} + \frac{1}{2V}{\sum_{\mathbf{k}}}' \frac{4\pi e^2}{k^2}\left(\rho^{\mathrm{e}}_{\mathbf{k}}\rho^{\mathrm{e}}_{-\mathbf{k}} - N_{\mathrm{e}}\right) \\
\mathcal{H}'_{\mathrm{i}} &= K_{\mathrm{i}} + \frac{1}{2V}{\sum_{\mathbf{k}}}' \frac{4\pi z^2e^2}{k^2}\left(\rho^{\mathrm{i}}_{\mathbf{k}}\rho^{\mathrm{i}}_{-\mathbf{k}} - N_{\mathrm{i}}\right) \\
V'_{\mathrm{ei}} &= U_0 + \frac{1}{V}{\sum_{\mathbf{k}}}' \hat{v}_{\mathrm{ei}}(k)\rho^{\mathrm{i}}_{\mathbf{k}}\rho^{\mathrm{e}}_{-\mathbf{k}}
\end{aligned} \tag{10.8.5}$$

where K_i is the kinetic energy of the ions and

$$U_0 = \frac{1}{V}\lim_{k\to 0}\left(\hat{v}_{ei}(k) + \frac{4\pi z e^2}{k^2}\right)\rho^i_{\mathbf{k}}\rho^e_{-\mathbf{k}} = N_i\rho_e\int\left(v_{ei}(r) + \frac{ze^2}{r}\right)d\mathbf{r} \tag{10.8.6}$$

The term $\mathcal{H}'_e$ is the jellium hamiltonian and $\mathcal{H}'_i$ is the hamiltonian of an OCP of positive ions in a uniform background. In this formulation of the problem a liquid metal emerges as a "mixture" of a classical OCP and a quantum-mechanical jellium, the two components being coupled together through the term V'_{ei}.

Inside the ion core the interaction of the conduction electrons with the ion is determined by details of the charge distribution of the core electrons. The true electron–ion interaction is therefore a complicated, non-local function for $r < r_C$, where r_C is the ion-core radius. In addition, the potential has a singularity at $r = 0$. Despite these difficulties it is possible to treat the electron–ion coupling by perturbation theory if the interaction is recast in pseudopotential form. The procedure adopted in practice is to parametrise an assumed functional form for the pseudopotential by fitting to experimental results for quantities that are sensitive to electron–ion collisions. A particularly simple and widely adopted pseudopotential $v^*_{ei}(r)$ consists in taking

$$\begin{aligned} v^*_{ei}(r) &= 0, \qquad r < r_C, \\ &= -ze^2/r, \quad r > r_C \end{aligned} \tag{10.8.7}$$

This is called the "empty-core" pseudopotential;[45] values of the parameter r_C can be derived from transport and Fermi-surface data and lie close to generally accepted values for the ionic radii of simple metals.

If the pseudopotential is weak, the electron–ion term in (10.8.5) can be treated as a perturbation, the reference system being a superposition of a classical OCP and a degenerate, interacting electron gas. To lowest order in perturbation theory, the structure of each component of the reference system is unaffected by the presence of the other. In this approximation, assuming the two fluids to be homogeneous:

$$\langle\rho^i_{\mathbf{k}}\rho^e_{-\mathbf{k}}\rangle = \langle\rho^i_{\mathbf{k}}\rangle\langle\rho^e_{-\mathbf{k}}\rangle = 0, \quad \mathbf{k}\neq 0 \tag{10.8.8}$$

Hence, on averaging the perturbation V'_{ei}, only the structure-independent term survives. The internal energy of the metal is then the sum of three terms: the energy of the degenerate electron gas, given by the jellium model; the internal energy of the classical OCP, which is known from Monte Carlo calculations[46] as a function of the dimensionless coupling constant $\Gamma = z^2e^2/a_i k_B T$, where $a_i = (3/4\pi\rho_i)^{1/3}$; and the quantity U_0, which can be calculated from (10.8.6) and (10.8.7). When combined, these results allow the calculation of the internal energy and equation of state as functions of the density parameter r_S for values of Γ and r_C appropriate to a particular metal. Figure 10.8 shows the equation of state obtained in this way for four alkali metals along isotherms corresponding to the experimental melting temperatures. Given the crudeness of the model, the agreement between theory and experiment for the zero-pressure value of r_S is surprisingly good.

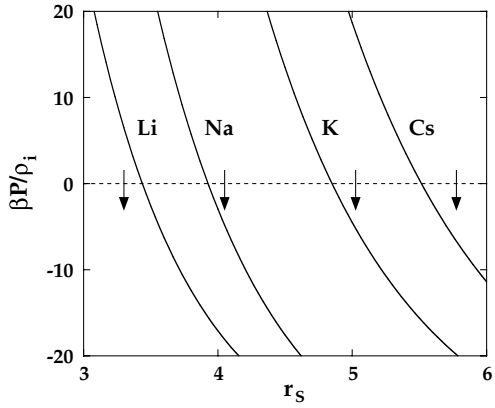

FIG. 10.8. Equation of state of four alkali metals along isotherms corresponding to the experimental melting temperatures (Li, 452 K; Na, 371 K; K, 337 K; Cs, 303 K). The curves are calculated from the first-order perturbation theory described in the text and the arrows mark the experimental values of r_S at atmospheric pressure.

A more accurate calculation has to take account of the influence of the ionic component on the structure of the electron gas and vice versa. To do so, we must go to second order in perturbation theory. We also use an adiabatic approximation: the electrons are assumed to adjust themselves instantaneously to the much slower changes in the ionic coordinates. Thus the problem to be considered is that of an inhomogeneous, interacting electron gas in the external field produced by a given ionic charge distribution; because the electron–ion pseudopotential is assumed to be weak, the influence of the external field can be treated by linear-response theory. The polarisation of the electron gas by the ionic charge distribution leads to a screening of the external field and hence, as we shall see, to a new, effective interaction between the ions. Although different in detail, the calculation is similar in spirit to that of the effective interaction between colloidal particles in solution, described in the previous section.

The partition function corresponding to the hamiltonian (10.8.3) is

$$Q_{N_\mathrm{i}N_\mathrm{e}} = \frac{1}{N_\mathrm{i}!h^{3N_\mathrm{i}}} \iint \exp(-\beta\mathcal{H}'_\mathrm{i}) \operatorname{Tr}_\mathrm{e} \exp\bigl[-\beta(\mathcal{H}'_\mathrm{e} + V'_\mathrm{ei})\bigr] \mathrm{d}\mathbf{R}^{N_\mathrm{i}} \, \mathrm{d}\mathbf{P}^{N_\mathrm{i}} \tag{10.8.9}$$

where $\mathbf{P}^{N_\mathrm{i}} \equiv \{\mathbf{P}_j\}$ represents the momenta of the ions. The trace is taken over a complete set of quantum states of the electron gas in the field due to a fixed ionic configuration; the free energy F'_e of the inhomogeneous electron gas is a function of the ionic coordinates $\{\mathbf{R}_j\}$ and given by

$$F'_\mathrm{e}\bigl(\{\mathbf{R}_j\}\bigr) = -k_\mathrm{B}T \ln\bigl(\operatorname{Tr}_\mathrm{e} \exp\bigl[-\beta(\mathcal{H}'_\mathrm{e} + V'_\mathrm{ei})\bigr]\bigr) \tag{10.8.10}$$

If the homogeneous electron gas is taken as the reference system, and $V'_{\rm ei}$ is again treated as a perturbation, $F'_{\rm e}$ is obtained from the coupling-parameter formula (5.2.5) as[47]

$$F'_{\rm e} = F_{\rm e} + \int_0^1 \langle V'_{\rm ei}\rangle_\lambda \, {\rm d}\lambda \tag{10.8.11}$$

where $F_{\rm e}$ is the free energy of the reference system and the subscript λ shows that the average is to be taken over an ensemble characterised by the hamiltonian $\mathcal{H}'_{\rm e} + \lambda V'_{\rm ei}$. From (10.8.5), with $\hat{v}_{\rm ei}(k)$ replaced by $\hat{v}^*_{\rm ei}(k)$, we find that for a fixed ionic configuration:

$$\langle V'_{\rm ei}\rangle_\lambda = U_0 + \frac{1}{V}{\sum_{\mathbf{k}}}' \hat{v}^*_{\rm ei}(k)\rho^{\rm i}_{\mathbf{k}}\langle\rho^{\rm e}_{-\mathbf{k}}\rangle_\lambda \tag{10.8.12}$$

The result of first-order perturbation theory corresponds to setting $\lambda = 0$. But $\langle\rho^{\rm e}_{-\mathbf{k}}\rangle_0$ is zero because the reference system is homogeneous; the second term on the right-hand side of (10.8.12) therefore disappears and we are led back to our earlier result. To obtain the second-order term it is sufficient to calculate the components of the induced electron density to first order in $\lambda V'_{\rm ei}$. If $\chi_{\rm e}(k)$ is the static electron-density response function, the induced density is

$$\langle\rho^{\rm e}_{-\mathbf{k}}\rangle_\lambda = \chi_{\rm e}(k)\lambda\hat{v}^*_{\rm ei}(k)\rho^{\rm i}_{-\mathbf{k}} \tag{10.8.13}$$

If we now substitute for $\langle V'_{\rm ei}\rangle$ in (10.8.11) and integrate over λ, we find that the free energy of the electron gas is given to second order in the electron–ion coupling by

$$F'_{\rm e} = F_{\rm e} + U_0 + \frac{1}{2V}{\sum_{\mathbf{k}}}' \chi_{\rm e}(k)\big[\hat{v}^*_{\rm ei}(k)\big]^2\rho^{\rm i}_{\mathbf{k}}\rho^{\rm i}_{-\mathbf{k}} \tag{10.8.14}$$

On comparing this result with (10.8.9) and (10.8.10) we see that the system can be regarded as a one-component fluid for which the total interaction energy is

$$V_{N_{\rm i}}\big(\{\mathbf{R}_j\}\big) = V_0 + \frac{1}{2V}{\sum_{\mathbf{k}}}' \big(\hat{v}_{\rm ii}(k) + \chi_{\rm e}(k)\big[\hat{v}^*_{\rm ei}(k)\big]^2\big)\big(\rho^{\rm i}_{\mathbf{k}}\rho^{\rm i}_{-\mathbf{k}} - N_{\rm i}\big) \tag{10.8.15}$$

where

$$V_0 = U_0 + F_{\rm e} + \tfrac{1}{2}\rho_{\rm i}{\sum_{\mathbf{k}}}' \chi_{\rm e}(k)\big[\hat{v}^*_{\rm ei}(k)\big]^2 \tag{10.8.16}$$

is independent of the structure of the liquid. Since T is normally much less than $T_{\rm F}$, $F_{\rm e}$ can be replaced by the ground-state energy of the interacting electron gas (the jellium model).

The total interaction energy may now be rewritten in a form that involves a sum of pair interactions:

$$V_{N_{\rm i}} = V_0 + \sum_{j=1}^{N_{\rm i}}\sum_{j'>j}^{N_{\rm i}} v^{\rm eff}_{\rm ii}\big(|\mathbf{R}_{j'} - \mathbf{R}_j|\big) \tag{10.8.17}$$

The effective ion–ion potential $v_{\rm ii}^{\rm eff}(R)$ is the Fourier transform of the sum of the bare ion–ion interaction $v_{\rm ii}(R)$ and an electron-induced term $v'_{\rm ii}(R)$ or, in **k**-space:

$$\hat{v}_{\rm ii}^{\rm eff}(k) = \hat{v}_{\rm ii}(k) + \hat{v}'_{\rm ii}(k) = \frac{4\pi z^2 e^2}{k^2} + \left[\hat{v}^*_{\rm ei}(k)\right]^2 \chi_{\rm e}(k)$$
$$= \frac{4\pi z^2 e^2}{k^2} + \frac{[\hat{v}^*_{\rm ei}(k)]^2}{(4\pi e^2/k^2)}\left(\frac{1}{\varepsilon_{\rm e}(k)} - 1\right) \tag{10.8.18}$$

where $\varepsilon_{\rm e}(k)$, the dielectric function of the electron gas, is related to the susceptibility $\chi_{\rm e}(k)$ in the manner of (10.2.11).[43] In the long-wavelength limit, $\varepsilon_{\rm e}(k)$ behaves as

$$\lim_{k\to 0} \varepsilon_{\rm e}(k) = 1 + k_{\rm e}^2/k^2 \tag{10.8.19}$$

with

$$k_{\rm e}^2 = k_{\rm TF}^2 \frac{\chi_{T\rm e}}{\chi_{T\rm e}^{\rm id}} \tag{10.8.20}$$

where $\chi_{T\rm e}$ and $\chi_{T\rm e}^{\rm id}$ are the isothermal compressibilities, respectively, of the interacting and non-interacting electron gas, and $k_{\rm TF} = 2(k_{\rm F}/\pi a_0)^{1/2}$ is the Thomas–Fermi wavenumber. Equation (10.8.19) is the electronic counterpart of the relation (10.2.30) satisfied by the classical OCP and $k_{\rm e}$ is the analogue of the ionic screening wavenumber $k_{\rm s}$. In the same limit, $\hat{v}^*_{\rm ei}(k) \to 4\pi z e^2/k^2$. It follows that the effective interaction $\hat{v}_{\rm ii}^{\rm eff}(k)$ is a regular function in the limit $k \to 0$, the k^{-2} singularity in the bare potential $\hat{v}_{\rm ii}(k)$ being cancelled by the same singularity in $\hat{v}'_{\rm ii}(k)$. In other words, the bare ion–ion potential $v_{\rm ii}(R)$ is completely screened by the polarisation of the electron gas, and the effective potential $v_{\rm ii}^{\rm eff}(R)$ is therefore a short-range function. A typical effective potential for an alkali metal has a soft repulsive core, an attractive well with a depth (in temperature units) of a few hundred kelvin and a weakly oscillatory tail.[48] An example of a calculated effective potential for liquid potassium is shown in Figure 1.4.

The results of the second-order calculation can be summarised by saying that we have reduced the liquid–metal problem to one of calculating the classical partition function of a fluid of $N_{\rm i}$ pseudoatoms in which the particles interact through a short-range effective potential $v_{\rm ii}^{\rm eff}(R)$. After integration over momenta, the partition function becomes

$$Q_{N_{\rm i}} = \frac{\exp(-\beta V_0)}{N_{\rm i}! \Lambda_{\rm i}^{3N_{\rm i}}} \int \exp\left(-\beta V_{N_{\rm i}}^{\rm eff}\right) {\rm d}\mathbf{R}^{N_{\rm i}} \tag{10.8.21}$$

where $V_{N_{\rm i}}^{\rm eff}$ is the sum of the pairwise-additive effective interactions for a given ionic configuration and $\Lambda_{\rm i}$ is the de Broglie thermal wavelength of the ions. Equation (10.8.21) differs from the usual partition function of a monatomic fluid in two important ways: first, in the appearance of a large, structure-independent energy V_0; and, secondly, in the fact that both V_0 and the pair potential from which $V_{N_{\rm i}}^{\rm eff}$ is derived are functions of density by virtue of the density dependence of the properties of the electron gas. The reduction of

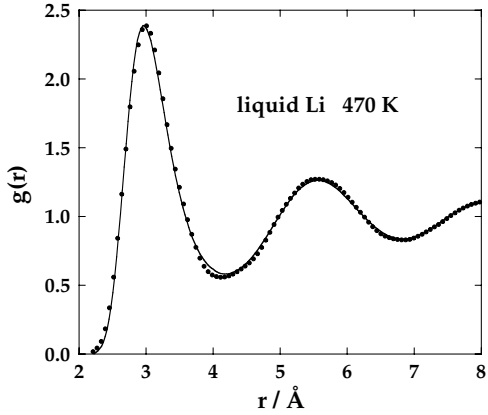

FIG. 10.9. Pair distribution function of liquid lithium near the normal melting. temperature. The curve shows results obtained by molecular-dynamics calculations for an effective ion–ion potential and the points are the results of neutron-scattering measurements. After Salmon *et al.*[50]

the problem to the form described by (10.8.21) means that the theoretical methods developed for the calculation of static properties of simple classical liquids can also be applied to liquid metals. Special care is needed only when evaluating volume derivatives of the free energy, because the density dependence of the effective interaction gives rise to extra terms. Computer simulations have shown that effective ion–ion potentials can account quantitatively for many of the observed properties of simple liquid metals. From Figure 10.9, for example, we see that the pair distribution function obtained in this way for liquid lithium[49] is in excellent agreement with that derived from neutron-diffraction data.

10.9 IONIC DYNAMICS IN LIQUID METALS

The microscopic dynamics of the ions in liquid metals do not differ in any fundamental way from the corresponding motions in simple, insulating liquids such as the rare gases. This is not surprising, since the pair potentials for metallic pseudoatoms and rare-gas atoms are qualitatively similar. For the same reason, experimental and theoretical methods that have been used successfully to study and describe the dynamics of argon-like liquids have, for the most part, met with comparable success in their application to simple liquid metals. However, as comparison of Figures 1.3 and 1.4 shows, the interactions in, say, potassium and argon do differ considerably in detail, and this gives rise to quantitative differences in the dynamical behaviour of the two types of system. For example, as we have seen in earlier chapters, experiments and simulations have combined to show that propagating collective modes of both transverse and longitudinal character persist over ranges of wavelength relative to the particle diameters that are considerably wider in liquid metals than in argon-like liquids.[51]

A different insight into the dynamics can be obtained through the representation of a liquid metal as an ion–electron plasma along the lines followed for static properties in

Section 10.8. In this picture of the liquid, the ionic and electronic components are only weakly coupled through the electron–ion pseudopotential, and each component may be regarded as an external perturbation on the other. Let $\phi_\nu(\mathbf{k},\omega)$ be an external potential that acts on component ν, where $\nu = 1$ for the ions and 2 for the electrons. Within linear-response theory the Fourier components of the induced densities are related to the external potentials by a matrix of density-response functions:

$$\left\langle \rho^\nu_{\mathbf{k}}(\omega)\right\rangle = \sum_\mu \chi_{\nu\mu}(k,\omega)\phi_\mu(\mathbf{k},\omega) \tag{10.9.1}$$

The response to the internal field is described by a similar matrix of screened response functions, $\chi^{\mathrm{sc}}_{\nu\mu}$. Written in matrix form the response is

$$\left\langle \boldsymbol{\rho}_{\mathbf{k}}(\omega)\right\rangle = \boldsymbol{\chi}^{\mathrm{sc}}(k,\omega)\cdot\left[\boldsymbol{\phi}(\mathbf{k},\omega) + \hat{\boldsymbol{v}}(k)\cdot\left\langle \boldsymbol{\rho}_{\mathbf{k}}(\omega)\right\rangle\right] \tag{10.9.2}$$

where $\hat{\boldsymbol{v}}(k)$ is the matrix of bare potentials $\hat{v}_{\nu\mu}(k)$ and the second term in square brackets is the "polarisation potential". Elimination of $\langle\rho^\nu_{\mathbf{k}}(\omega)\rangle$ between (10.9.1) and (10.9.2) leads to a matrix generalisation of the relation (10.4.11) between the external and screened response functions:

$$\boldsymbol{\chi}(k,\omega) = \boldsymbol{\chi}^{\mathrm{sc}}(k,\omega) + \boldsymbol{\chi}^{\mathrm{sc}}(k,\omega)\cdot\hat{\boldsymbol{v}}(k)\cdot\boldsymbol{\chi}(k,\omega) \tag{10.9.3}$$

or, in terms of elements of the inverse matrices:

$$\left[\boldsymbol{\chi}(k,\omega)\right]^{-1}_{\nu\mu} = \left[\boldsymbol{\chi}^{\mathrm{sc}}(k,\omega)\right]^{-1}_{\nu\mu} - \hat{v}_{\nu\mu}(k) \tag{10.9.4}$$

To lowest order in the ion–electron coupling the two species respond to the internal field as two, independent, one-component plasmas. The off-diagonal elements of $\boldsymbol{\chi}^{\mathrm{sc}}$ are then zero, and the diagonal elements $\chi^{\mathrm{sc}}_{\nu\nu}(k,\omega)$ are the screened response functions of the classical OCP ($\nu = 1$) and the degenerate electron gas in a uniform background (jellium) ($\nu = 2$). It follows, given (10.4.11) and (10.4.12), that

$$\begin{aligned}\left[\boldsymbol{\chi}^{\mathrm{sc}}(k,\omega)\right]^{-1}_{11} &= 1/\chi_{\mathrm{OCP}}(k,\omega) + \hat{v}_{11}(k)\\ \left[\boldsymbol{\chi}^{\mathrm{sc}}(k,\omega)\right]^{-1}_{22} &= \frac{\hat{v}_{22}(k)}{1-\varepsilon_{\mathrm{e}}(k,\omega)}\end{aligned} \tag{10.9.5}$$

and the external susceptibility of the ions is obtained from (10.9.4) as

$$\chi_{11}(k,\omega) = \frac{\chi_{\mathrm{OCP}}(k,\omega)}{1-\hat{v}(k,\omega)\chi_{\mathrm{OCP}}(k,\omega)} \tag{10.9.6}$$

where $\hat{v}(k,\omega)$ describes the dynamical screening of the ion–ion interaction by the electrons:

$$\hat{v}(k,\omega) = \frac{k^2[\hat{v}_{12}(k)]^2}{4\pi e^2}\left(\frac{1}{\varepsilon_{\mathrm{e}}(k,\omega)} - 1\right) \tag{10.9.7}$$

The frequency scale of the electronic motion is much higher than any frequency associated with the ions. It is therefore reasonable to make an adiabatic approximation in which $\hat{v}(k,\omega)$ is replaced by $\hat{v}(k,0)$. The characteristic frequencies of the longitudinal modes of the screened ionic plasma are given by the roots of the denominator in (10.9.6) or, in the adiabatic approximation, by the solution to the equation

$$1 - \hat{v}(k,0)\chi_{\mathrm{OCP}}(k,\omega) = 0 \tag{10.9.8}$$

In the limit $k \to 0$, the ratio $\widetilde{F}_{\mathrm{OCP}}(k,\omega)/S_{\mathrm{OCP}}(k)$ is related to the frequency-dependent electrical conductivity by (10.4.30). Thus, from (7.6.21):[52]

$$\begin{aligned}\lim_{k\to 0}\chi_{\mathrm{OCP}}(k,\omega) &= -\beta\rho_{\mathrm{i}}\lim_{k\to 0}\lim_{\varepsilon\to 0}\left[S_{\mathrm{OCP}}(k) + i(\omega+i\varepsilon)\widetilde{F}_{\mathrm{OCP}}(k,\omega+i\varepsilon)\right] \\ &= -\beta\rho_{\mathrm{i}}\lim_{k\to 0}S_{\mathrm{OCP}}(k)\lim_{\varepsilon\to 0}\frac{4\pi\sigma(\omega+i\varepsilon)}{-i(\omega+i\varepsilon)+4\pi\sigma(\omega+i\varepsilon)}\end{aligned} \tag{10.9.9}$$

The long-wavelength limit of $S_{\mathrm{OCP}}(k)$ is given by (10.2.31) and the complex conductivity $\sigma(\omega+i\varepsilon)$ can be expressed, via (7.7.10), in the form

$$\sigma(\omega+i\varepsilon) = \frac{\beta}{V}\int_0^\infty J(t)\exp\left[i(\omega+i\varepsilon)t\right]\mathrm{d}t \tag{10.9.10}$$

where $J(t)$ is the charge–current autocorrelation function. In the OCP the proportionality of mass and charge means that the conservation of total linear momentum is equivalent to the conservation of charge current, i.e. the resistivity is zero. Hence

$$J(t) = J(0) = \frac{N_{\mathrm{i}}z^2e^2k_{\mathrm{B}}T}{m_{\mathrm{i}}} \tag{10.9.11}$$

and, from (10.9.10):

$$\sigma(\omega+i\varepsilon) = \frac{i\omega_{\mathrm{pi}}^2}{4\pi(\omega+i\varepsilon)} \tag{10.9.12}$$

where $\omega_{\mathrm{pi}}^2 = 4\pi\rho_{\mathrm{i}}z^2e^2/m_{\mathrm{i}}$ is the square of the ionic plasma frequency. Substitution of (10.9.12) in (10.9.9) shows that

$$\lim_{k\to 0}\frac{\chi_{\mathrm{OCP}}(k,\omega)}{S_{\mathrm{OCP}}(k)} = \frac{\beta\rho_{\mathrm{i}}\omega_{\mathrm{pi}}^2}{\omega^2-\omega_{\mathrm{pi}}^2} \tag{10.9.13}$$

At small k, $\varepsilon_{\mathrm{e}}(k,0) \approx k_{\mathrm{e}}^2/k^2$, from (10.8.19), and $\hat{v}_{12}(k)$, in the empty-core model, behaves as

$$\hat{v}_{12}(k) = \frac{4\pi z^2e^2\cos kr_{\mathrm{c}}}{k^2} \approx \frac{4\pi ze^2}{k^2}\left(1-\tfrac{1}{2}k^2r_{\mathrm{c}}^2\right) \tag{10.9.14}$$

so that

$$\lim_{k\to 0}\hat{v}(k,0)=\frac{4\pi z^2e^2}{k^2}\left(1-k^2r_c^2\right)\left(\frac{k^2}{k_e^2}-1\right) \tag{10.9.15}$$

When the results are brought together we find that to order k^2 the solution to (10.9.8) leads to a dispersion relation characteristic of a propagating sound wave, i.e.

$$\omega=\omega_{pi}\left(k_e^{-2}+k_s^{-2}+r_c^2\right)^{1/2}k=ck \tag{10.9.16}$$

where k_s is the ionic screening wavenumber defined by (10.2.28) and c is the speed of sound. Thus the effect of electron screening is to convert the plasmon mode at frequency ω_{pi} into a sound wave of a frequency that vanishes linearly with k. A more detailed analysis shows that c can be identified with the isothermal speed of sound, but this differs little from the adiabatic value, since the ratio of specific heats is close to unity for liquid metals.

NOTES AND REFERENCES

1. Gillan, M.J., *In* "Ionic Solids at High Temperatures" (A.M. Stoneham, ed.). World Scientific, Singapore, 1989.
2. For a review of the properties of the OCP, see Baus, M. and Hansen, J.P., *Phys. Rep.* **59**, 1 (1980).
3. Tosi, M.P. and Fumi, F.G., *J. Phys. Chem. Solids* **25**, 45 (1964).
4. Wilson, M. and Madden, P.A., *J. Phys. Condens. Matter* **5**, 2687 (1993).
5. Sprik, M. and Klein, M.L., *J. Chem. Phys.* **89**, 7558 (1988).
6. Martin, P.A. and Yalcin, T., *J. Stat. Phys.* **31**, 691 (1983).
7. (a) Stillinger, F.H. and Lovett, R., *J. Chem. Phys.* **48**, 3858 (1968). (b) Stillinger, F.H. and Lovett, R., *J. Chem. Phys.* **49**, 1991 (1968).
8. Blum, L., Gruber, C., Lebowitz, J.L. and Martin, P.A., *Phys. Rev. Lett.* **48**, 1769 (1982).
9. Giaquinta, P.V., Parrinello, M. and Tosi, M.P., *Phys. Chem. Liq.* **5**, 305 (1976).
10. Hansen, J.P. and McDonald, I.R., *Phys. Rev. A* **11**, 2111 (1975).
11. Waisman, E. and Lebowitz, J.L., *J. Chem. Phys.* **56**, 3086 and 3091 (1972).
12. Rasaiah, J.C., Card, D.N. and Valleau, J.P., *J. Chem. Phys.* **56**, 248 (1972).
13. Larsen, B., *J. Chem. Phys.* **65**, 3431 (1976).
14. (a) Høye, J.S., Stell, G. and Waisman, E., *Mol. Phys.* **32**, 209 (1976). (b) Høye, J.S. and Stell, G., *J. Chem. Phys.* **67**, 524 (1977).
15. Valleau, J.P., Cohen, L.K. and Card, D.N., *J. Chem. Phys.* **5942** (1980).
16. See, e.g., Duh, D.-M. and Haymet, A.J., *J. Chem. Phys.* **97**, 7716 (1992).
17. Bresme, F., Lomba, E., Weis, J.J. and Abascal, J.L.F., *Phys. Rev. E* **51**, 289 (1995).
18. See the discussion surrounding (4.7.2).
19. Ballone, P., Pastore, G. and Tosi, M.P., *J. Chem. Phys.* **81**, 3174 (1984).
20. Zerah, G. and Hansen, J.P., *J. Chem. Phys.* **84**, 2336 (1986).
21. Abramo, M.C., Parrinello, M. and Tosi, M.P., *J. Non-Metals* **2**, 67 (1973).
22. Cohen, C., Sutherland, J.W.H. and Deutch, J.M., *Phys. Chem. Liq.* **2**, 213 (1971).
23. (a) Sjögren, L. and Yoshida, F., *J. Chem. Phys.* **77**, 3703 (1982). (b) Munakata, T. and Bosse, J., *Phys. Rev. A* **27**, 455 (1983).
24. See, e.g., Morgan, B. and Madden, P.A., *J. Chem. Phys.* **120**, 1402 (2004).
25. See, e.g., Madden, P.A. and O'Sullivan, K.F., *J. Chem. Phys.* **95**, 1980 (1991).
26. Bosse, J. and Munakata, T., *Phys. Rev. A* **25**, 2763 (1982).
27. Giaquinta, P.V., Parrinello, M. and Tosi, M.P., *Physica A* **92**, 185 (1978). The Raman spectra of molten salts can also be analysed in terms of fluctuations in mass and charge densities: see ref. 24.

28. Jackson, J.D., “Classical Electrodynamics”, 3rd edn. John Wiley, New York, 1999.
29. Stillinger, F.H., *J. Chem. Phys.* **35**, 1584 (1961). See also Allen, R.J., Hansen, J.P. and Melchionna, S., *Phys. Chem. Chem. Phys.* **3**, 4177 (2001).
30. This definition is already implicit in (10.2.6).
31. Henderson, D. and Blum, L., *J. Chem. Phys.* **69**, 5441 (1978).
32. For a review of approximations beyond Poisson–Boltzmann theory, see Hansen, J.P. and Löwen, H., *Ann. Rev. Phys. Chem.* **51**, 209 (2000).
33. (a) Guldbrand, L., Jönsson, B., Wennerström, H. and Linse, P., *J. Chem. Phys.* **80**, 2221 (1984). (b) Valleau, J.P., Ivkov, R. and Torrie, G.M., *J. Chem. Phys.* **95**, 520 (1991).
34. Tang, Z., Scriven, L.E. and Davis, H.T., *J. Chem. Phys.* **97**, 9258 (1992).
35. (a) Kjellander, R., Åkesson, T., Jönsson, B. and Marčelia, S., *J. Chem. Phys.* **97**, 1424 (1992). (b) Greberg, H. and Kjellander, R., *J. Chem. Phys.* **108**, 2940 (1998).
36. Löwen, H., Hansen, J.P. and Madden, P.A., *J. Chem. Phys.* **98**, 3275 (1993).
37. Car, R. and Parrinello, M., *Phys. Rev. Lett.* **55**, 247 (1985).
38. We ignore any non-coulombic component of the external potential.
39. Verwey, E.J.W. and Overbeek, J.T.G., “Theory of Stability of Lyophobic Colloids”. Elsevier, Amsterdam, 1948.
40. (a) van Roij, R., Dijkstra, M. and Hansen, J.P., *Phys. Rev. E* **59**, 2010 (1999). (b) van Roij, R. and Evans, R., *J. Phys. Condens. Matter* **11**, 1004 (1999).
41. (a) Belloni, L., *Colloids Surf. A* **140**, 227 (1998). (b) Bocquet, L., Trizac, E. and Aubouy, M., *J. Chem. Phys.* **117**, 8138 (2002).
42. Crocker, J.C. and Grier, D.G., *Phys. Rev. Lett.* **73**, 352 (1994).
43. Pines, D. and Nozières, P., “The Theory of Quantum Liquids”. W.A. Benjamin, New York, 1966.
44. Ashcroft, N.W. and Stroud, D., *Sol. State Phys.* **33**, 1 (1978).
45. Ashcroft, N.W., *J. Phys. C* **1**, 232 (1966).
46. (a) Hansen, J.P., *Phys. Rev. A* **8**, 3096 (1973). (b) Slattery, W.L., Doolen, G.D. and DeWitt, H.E., *Phys. Rev. A* **21**, 2087 (1980).
47. Note that the prime has different meanings in (5.2.5) and (10.8.11).
48. The oscillatory behaviour at large separations is linked to a logarithmic singularity in the dielectric function. See Faber, T.E., “An Introduction to the Theory of Liquid Metals”. Cambridge University Press, Cambridge, 1972, p. 28.
49. The potential used in the simulations was derived from an empty-core pseudo-potential with a core radius obtained by fitting to the height of the first peak in the experimental structure factor: Anento, N., Canales, M. and Gonzàlez, L.E., unpublished results. See also Canales, M., Gonzàlez, L.E. and Pàdro, J.A., *Phys Rev. E* **50**, 3656 (1994).
50. Salmon, P.S., Petri, I., de Jong, P.H.K., Verkerk, P., Fischer, H.E. and Howells, W.S., *J. Phys. Condens. Matter* **16**, 195 (2004).
51. For a review of experimental results on liquid metals, see Scopigno, T., Ruocco, G. and Sette, F., *Rev. Mod. Phys.* **77**, 881 (2005).
52. The origin of the minus sign in (10.9.9) is explained in Section 7.6.

CHAPTER 11

Molecular Liquids

The earlier parts of the book have dealt almost exclusively with atomic systems. In this chapter we consider some of the new problems that arise when the theory is broadened to include molecular fluids.

11.1 THE MOLECULAR PAIR DISTRIBUTION FUNCTION

The description of the structure of a homogeneous molecular fluid in terms of particle densities and distribution functions can be developed along lines similar to those followed in the atomic case. The main added complication is the fact that the phase-space probability density for particles with rotational degrees of freedom is not immediately factorisable into kinetic and configurational parts. This problem is very well treated in the book by Gray and Gubbins[1] and we shall not dwell on it here. The final expressions for the molecular distribution functions resemble closely those obtained for atomic fluids, except that all quantities are now functions of the molecular orientations.

In this chapter we shall be concerned almost exclusively with pair correlations. We therefore take as our starting point a suitably generalised form of the definition (2.5.13) of the pair density in a uniform fluid. Let $\mathbf{R}_i$ be the translational coordinates of molecule i and let $\boldsymbol{\Omega}_i$ be the orientation of i in a laboratory-fixed frame of reference. If the molecule is linear, $\boldsymbol{\Omega}_i \equiv (\theta_i, \phi_i)$, where θ_i, ϕ_i are the usual polar angles; if it is non-linear, $\boldsymbol{\Omega}_i \equiv (\theta_i, \phi_i, \chi_i)$, where θ_i, ϕ_i, χ_i are the Euler angles. Then the molecular pair density is defined as

$$\rho^{(2)}(\mathbf{R}, \mathbf{R}', \boldsymbol{\Omega}, \boldsymbol{\Omega}') = \left\langle \sum_{i=1}^{N} \sum_{j \neq i}^{N} \delta(\mathbf{R} - \mathbf{R}_i)\delta(\mathbf{R}' - \mathbf{R}_j)\delta(\boldsymbol{\Omega} - \boldsymbol{\Omega}_i)\delta(\boldsymbol{\Omega}' - \boldsymbol{\Omega}_j) \right\rangle \quad (11.1.1)$$

and the molecular pair distribution function as

$$g(\mathbf{R}_{12}, \boldsymbol{\Omega}_1, \boldsymbol{\Omega}_2) = (\Omega/\rho)^2 \rho^{(2)}(\mathbf{R}_{12}, \boldsymbol{\Omega}_1, \boldsymbol{\Omega}_2) \quad (11.1.2)$$

where $\Omega \equiv \int \mathrm{d}\boldsymbol{\Omega}_i$. The definition of Ω means that

$$\Omega = \iint \mathrm{d}(\cos\theta_i)\, \mathrm{d}\phi_i = 4\pi, \quad \text{if linear} \quad (11.1.3a)$$

$$\Omega = \iiint \mathrm{d}(\cos\theta_i)\,\mathrm{d}\phi_i\,\mathrm{d}\chi_i = 8\pi^2, \quad \text{if non-linear} \tag{11.1.3b}$$

The coordinates $\mathbf{R}_i$ are often taken to be those of the molecular centre of mass or some other point of high symmetry in the molecule, but the choice of molecular "centre" is entirely arbitrary. To simplify the notation it is convenient to use the symbol $i \equiv (\mathbf{R}_i, \boldsymbol{\Omega}_i)$ to denote both the coordinates of the molecular centre and the orientation of molecule i. Thus the molecular pair distribution function will often be written simply as $g(1,2)$ and the molecular pair correlation function as $h(1,2) = g(1,2) - 1$. The functions $e(1,2) = \exp[-\beta v(1,2)]$, $f(1,2) = e(1,2) - 1$ and $y(1,2) = g(1,2)/e(1,2)$ have the same significance as in the atomic case, but are now functions of the orientations $\boldsymbol{\Omega}_1$, $\boldsymbol{\Omega}_2$. Finally, the molecular direct correlation function $c(1,2)$ is related to $h(1,2)$ by a generalisation of the Ornstein–Zernike relation (3.5.12):

$$h(1,2) = c(1,2) + \frac{\rho}{\Omega}\int c(1,3)h(3,2)\,\mathrm{d}3 \tag{11.1.4}$$

Integration of the pair distribution function over the variables $\boldsymbol{\Omega}_1$, $\boldsymbol{\Omega}_2$ yields a function $g_\mathrm{c}(R)$ (with $R \equiv |\mathbf{R}_{12}|$) that describes the radial distribution of molecular centres:

$$g_\mathrm{c}(R) = \frac{1}{\Omega^2}\iint g(\mathbf{R}, \boldsymbol{\Omega}_1, \boldsymbol{\Omega}_2)\,\mathrm{d}\boldsymbol{\Omega}_1\,\mathrm{d}\boldsymbol{\Omega}_2 \equiv \big\langle g(1,2)\big\rangle_{\boldsymbol{\Omega}_1\boldsymbol{\Omega}_2} \tag{11.1.5}$$

Here and elsewhere in this chapter we use angular brackets with subscripts $\boldsymbol{\Omega}_1 \cdots$ to denote an unweighted average over the angles $\boldsymbol{\Omega}_1 \cdots$, i.e.

$$\langle \cdots \rangle_{\boldsymbol{\Omega}_1} \equiv \frac{1}{\Omega}\int \cdots \mathrm{d}\boldsymbol{\Omega}_1 \tag{11.1.6}$$

With this convention the Ornstein–Zernike relation (11.1.4) may be re-expressed as

$$h(1,2) = c(1,2) + \rho\int \big\langle c(1,3)h(3,2)\big\rangle_{\boldsymbol{\Omega}_3}\,\mathrm{d}\mathbf{R}_3 \tag{11.1.7}$$

If $g(1,2)$ is multiplied by some function of the orientations $\boldsymbol{\Omega}_1$, $\boldsymbol{\Omega}_2$ and then integrated over all coordinates of the pair 1 and 2, the result is a quantity that measures the importance of angular correlations of a specific type. Let us suppose that molecule i has an axis of symmetry and let $\mathbf{u}_i$ be a unit vector along that axis. A set of angular order parameters that are of interest both theoretically and experimentally are those defined as

$$\begin{aligned} G_l &= \rho\int \big\langle P_l(\mathbf{u}_1\cdot\mathbf{u}_2)g(\mathbf{R}_{12}, \boldsymbol{\Omega}_1, \boldsymbol{\Omega}_2)\big\rangle_{\boldsymbol{\Omega}_1\boldsymbol{\Omega}_2}\,\mathrm{d}\mathbf{R}_{12} \\ &= \big\langle (N-1)P_l(\mathbf{u}_1\cdot\mathbf{u}_2)\big\rangle \end{aligned} \tag{11.1.8}$$

where $P_l(\cdots)$ denotes a Legendre polynomial. The value of the first-rank order parameter G_1 determines the dielectric constant of a polar fluid, as we show in Section 11.5, while

G_2 is related to a number of measurable quantities, including the integrated intensity of the spectrum observed in depolarised light-scattering experiments.

When the total potential energy of the fluid is a sum of pair terms the internal energy and equation of state can both be written as integrals over $g(1,2)$. The excess internal energy, for example, is given by

$$\begin{aligned}\frac{U^{\mathrm{ex}}}{N} &= \frac{\rho}{2\Omega^2}\iiint v(1,2)g(1,2)\,\mathrm{d}\mathbf{R}_{12}\,\mathrm{d}\boldsymbol{\Omega}_1\,\mathrm{d}\boldsymbol{\Omega}_2 \\ &= 2\pi\rho\int_0^\infty \big\langle v(1,2)g(1,2)\big\rangle_{\boldsymbol{\Omega}_1\boldsymbol{\Omega}_2} R_{12}^2\,\mathrm{d}R_{12} \end{aligned} \tag{11.1.9}$$

which is the molecular analogue of (2.5.20) The corresponding result for the pressure is a generalisation of (2.5.22):

$$\frac{\beta P}{\rho} = 1 - \frac{2\pi\beta\rho}{3}\int_0^\infty \big\langle v'(1,2)g(1,2)\big\rangle_{\boldsymbol{\Omega}_1\boldsymbol{\Omega}_2} R_{12}^3\,\mathrm{d}R_{12} \tag{11.1.10}$$

where the prime denotes differentiation with respect to R_{12} with $\boldsymbol{\Omega}_1$, $\boldsymbol{\Omega}_2$ held constant. Irrespective of whether or not the potential energy is pairwise additive, an argument similar to that leading to (2.6.12) shows that the isothermal compressibility is given by

$$\rho k_{\mathrm{B}} T\chi_T = 1 + \rho\int \big\langle g(1,2)-1\big\rangle_{\boldsymbol{\Omega}_1\boldsymbol{\Omega}_2}\,\mathrm{d}\mathbf{R}_{12} = 1 + \rho\int \big[g_{\mathrm{c}}(R)-1\big]\,\mathrm{d}\mathbf{R} \tag{11.1.11}$$

This result is of particular interest insofar as all reference to angular coordinates has disappeared.

Equations (11.1.9), (11.1.10) and (11.1.11) are identical to their atomic counterparts except for the fact that the pair functions (or products of pair functions) in the integrands are replaced by their unweighted angular averages. Their significance, however, is largely formal. The many-dimensional character of the molecular pair distribution function means that, in general, these results do not represent practical routes to the calculation of thermodynamic properties. The shape of $g(1,2)$ is difficult even to visualise and if progress is to be made the basic problem must be cast in simpler form. Two different approaches have been widely used. In one, which we review in the next section, $g(1,2)$ (or $h(1,2)$) is expanded in a series of suitably chosen, angle-dependent basis functions; in the other, which we discuss in Section 11.3, the fluid structure is described in terms of *site–site distribution functions*. Use of site–site distribution functions is particularly appropriate when the intermolecular potential is cast in site–site form, as in (1.2.6).

11.2 EXPANSIONS OF THE PAIR DISTRIBUTION FUNCTION

The pair distribution function for molecules of arbitrary symmetry can be expanded in terms of the Wigner rotation matrices or generalised spherical harmonics.[2] The general formalism has not been widely used, however, and the discussion that follows is limited

to linear molecules. In this case the natural expansion functions are the usual spherical harmonics, which we denote by $Y_{lm}(\theta, \phi)$.[3] Let $\boldsymbol{\Omega}_1$, $\boldsymbol{\Omega}_2$ be the orientations of molecules 1, 2 in a system of polar coordinates in which the z-axis lies along the vector $\mathbf{R}_{12} = \mathbf{R}_2 - \mathbf{R}_1$ (the "intermolecular" frame). Then $g(1,2)$ may be written as

$$g(1,2) = 4\pi \sum_{l_1} \sum_{l_2} \sum_{m} g_{l_1 l_2 m}(R) Y_{l_1 m}(\boldsymbol{\Omega}_1) Y_{l_2 \bar{m}}(\boldsymbol{\Omega}_2) \tag{11.2.1}$$

where $R \equiv |\mathbf{R}_{12}|$ and $\bar{m} \equiv -m$. The sum on m runs from $-l$ to l, where l is the lesser of l_1 and l_2; the indices m of the two harmonics are equal (apart from sign) by virtue of the cylindrical symmetry with respect to the axis $\mathbf{R}_{12}$. Important properties of the spherical harmonics include the fact that they are normalised and orthogonal:

$$\int Y^*_{lm}(\boldsymbol{\Omega}) Y_{l'm'}(\boldsymbol{\Omega}) \, \mathrm{d}\boldsymbol{\Omega} = \delta_{ll'} \delta_{mm'} \tag{11.2.2}$$

and that $Y_{l\bar{m}}(\boldsymbol{\Omega}) = (-1)^m Y^*_{lm}(\boldsymbol{\Omega})$.

If (11.2.1) is multiplied through by $Y^*_{l_1 \bar{m}}(\boldsymbol{\Omega}_1) Y^*_{l_2 m}(\boldsymbol{\Omega}_2)$ and integrated over angles, it follows from the properties just quoted that

$$\begin{aligned} g_{l_1 l_2 m}(R) &= \frac{1}{4\pi} \iint Y_{l_1 \bar{m}}(\boldsymbol{\Omega}_1) Y_{l_2 m}(\boldsymbol{\Omega}_2) g(1,2) \, \mathrm{d}\boldsymbol{\Omega}_1 \, \mathrm{d}\boldsymbol{\Omega}_2 \\ &= 4\pi \left\langle Y_{l_1 \bar{m}}(\boldsymbol{\Omega}_1) Y_{l_2 m}(\boldsymbol{\Omega}_2) g(1,2) \right\rangle_{\boldsymbol{\Omega}_1 \boldsymbol{\Omega}_2} \end{aligned} \tag{11.2.3}$$

The expansion coefficients $g_{l_1 l_2 m}(R)$ are called the "projections" of $g(1,2)$ onto the corresponding angular functions and are easily calculated by computer simulation. Certain projections of $g(1,2)$ are closely related to quantities introduced in Section 11.1. Given that $Y_{00}(\boldsymbol{\Omega}) = (1/4\pi)^{1/2}$, we see that $g_{000}(R)$ is identical to the centres distribution function $g_c(R)$; this is the reason for the inclusion of the factor 4π in (11.2.1). Moreover, the order parameters defined by (11.1.8) can be re-expressed as

$$G_l = \frac{\rho}{2l+1} \sum_m (-1)^m \int g_{llm}(R) \, \mathrm{d}\mathbf{R} \tag{11.2.4}$$

This result is a consequence of the addition theorem for spherical harmonics, i.e.

$$P_l(\cos \gamma_{12}) = \frac{4\pi}{2l+1} \sum_m Y^*_{lm}(\boldsymbol{\Omega}_1) Y_{lm}(\boldsymbol{\Omega}_2) \tag{11.2.5}$$

where γ_{12} is the angle between two vectors with orientations $\boldsymbol{\Omega}_1$ and $\boldsymbol{\Omega}_2$.

An expansion similar to (11.2.1) can be made of any scalar function of the variables $\mathbf{R}_{12}$, $\boldsymbol{\Omega}_1$ and $\boldsymbol{\Omega}_2$, including both the intermolecular potential $v(1,2)$ and its derivative with respect to R_{12}. The corresponding expansion coefficients $v_{l_1 l_2 m}(R)$ and $v'_{l_1 l_2 m}(R)$ can be calculated numerically for any pair potential and in some cases are expressible in analytical

form. If we introduce the expansions of $g(1,2)$ and $v(1,2)$ into (11.1.9) and integrate over angles, the energy equation becomes

$$\frac{U^{\text{ex}}}{N} = 2\pi\rho \sum_{l_1}\sum_{l_2}\sum_{m} \int_0^\infty v_{l_1 l_2 m}(R) g_{l_1 l_2 m}(R) R^2 \, \mathrm{d}R \tag{11.2.6}$$

The pressure equation (11.1.10) can be similarly rewritten in terms of the coefficients $v'_{l_1 l_2 m}(R)$ and $g_{l_1 l_2 m}(R)$. The multidimensional integrals appearing on the right-hand sides of (11.1.9) and (11.1.10) are thereby transformed into infinite sums of one-dimensional integrals. In general, however, the new expressions do not represent an improvement in the computational sense. The evidence from Monte Carlo calculations for systems of diatomic molecules is that on the whole the rate of convergence of the sums is poor and becomes rapidly worse as the elongation of the molecule increases.[4]

A different expansion of $g(1,2)$ is obtained if the orientations $\boldsymbol{\Omega}_1$, $\boldsymbol{\Omega}_2$ are referred to a laboratory-fixed frame of reference (the "laboratory" frame). Let $\boldsymbol{\Omega}_R$ be the orientation of the vector $\mathbf{R}_{12}$ in the laboratory frame. Then $g(1,2)$ may be expanded in the form

$$\begin{aligned} g(1,2) = &\sum_{l_1}\sum_{l_2}\sum_{l} g(l_1 l_2 l;\, R) \sum_{m_1}\sum_{m_2}\sum_{m} C(l_1 l_2 l;\; m_1 m_2 m) \\ &\times Y_{l_1 m_1}(\boldsymbol{\Omega}_1) Y_{l_2 m_2}(\boldsymbol{\Omega}_2) Y^*_{lm}(\boldsymbol{\Omega}_R) \end{aligned} \tag{11.2.7}$$

where $C(\cdots)$ is a Clebsch–Gordan coefficient. The coefficients $g(l_1 l_2 l;\; R)$ are linear combinations of the coefficients in (11.2.1) and the two expansions are equivalent if the z-axis of the laboratory frame is taken parallel to $\mathbf{R}_{12}$. The relation between the two sets of coefficients is

$$g(l_1 l_2 l;\; R) = \left(\frac{64\pi^3}{2l+1}\right)^{1/2} \sum_{m} C(l_1 l_2 l;\; m\bar{m}0) g_{l_1 l_2 m}(R) \tag{11.2.8}$$

with, as a special case, $g(000;\; R) = (4\pi)^{3/2} g_{000}(R)$. Equation (11.2.7) is sometimes written in the abbreviated form

$$g(1,2) = \sum_{l_1}\sum_{l_2}\sum_{l} g(l_1 l_2 l;\; R) \Phi^{l_1 l_2 l}(\boldsymbol{\Omega}_1, \boldsymbol{\Omega}_2, \boldsymbol{\Omega}_R) \tag{11.2.9}$$

where $\Phi^{l_1 l_2 l}$ is a "rotational invariant".

Use of (11.2.7) in preference to (11.2.1) does not help in resolving the problem of slow convergence in expansions such as (11.2.6), but it does have some advantages, particularly in the manipulation of Fourier transforms. We shall use the notation $\hat{g}(1,2) \equiv \hat{g}(\mathbf{k}, \boldsymbol{\Omega}_1, \boldsymbol{\Omega}_2)$ to denote a Fourier transform with respect to $\mathbf{R}_{12}$, i.e.

$$\hat{g}(\mathbf{k}, \boldsymbol{\Omega}_1, \boldsymbol{\Omega}_2) = \int g(\mathbf{R}_{12}, \boldsymbol{\Omega}_1, \boldsymbol{\Omega}_2) \exp(-i\mathbf{k}\cdot\mathbf{R}_{12}) \, \mathrm{d}\mathbf{R}_{12} \tag{11.2.10}$$

Then $\hat{g}(1,2)$ can be written in terms of laboratory-frame harmonics as

$$\hat{g}(1,2) = \sum_{l_1}\sum_{l_2}\sum_{l} g(l_1 l_2 l;\ k) \sum_{m_1}\sum_{m_2}\sum_{m} C(l_1 l_2 l;\ m_1 m_2 m) \times Y_{l_1 m_1}(\boldsymbol{\Omega}_1) Y_{l_2 m_2}(\boldsymbol{\Omega}_2) Y^*_{lm}(\boldsymbol{\Omega}_k) \tag{11.2.11}$$

where $\boldsymbol{\Omega}_k$ is the orientation of $\mathbf{k}$ in the laboratory frame. The reason that this expansion and the corresponding expansions of $\hat{h}(1,2)$ and $\hat{c}(1,2)$ are so useful is the fact that the coefficients $g(l_1 l_2 l;\ k)$ and $g(l_1 l_2 l;\ R)$ are related by a generalised Fourier or Hankel transform, i.e.

$$g(l_1 l_2 l;\ k) = 4\pi i^l \int_0^\infty j_l(kR) g(l_1 l_2 l;\ R) R^2\, \mathrm{d}R \tag{11.2.12}$$

where $j_l(\cdots)$ is the spherical Bessel function of order l. No equivalent simplification is found in the case of the intermolecular-frame expansion. We shall not give a general proof of (11.2.12), since in this book we are concerned only with $l = 0$ and $l = 2$. The case when $l = 0$ corresponds to the usual Fourier transform of a spherically symmetric function; the case when $l = 2$ is considered in detail in Section 11.4.

Expansions of $g(1,2)$ and other pair functions along the lines of (11.2.1) and (11.2.7) have been applied most successfully in the theory of polar fluids, as we shall see in Sections 11.5 and 11.6.

11.3 SITE–SITE DISTRIBUTION FUNCTIONS

When an interaction-site model is used to represent the intermolecular potential the natural way to describe the structure of the fluid is in terms of site–site distribution functions. If the coordinates of site α on molecule i are denoted by $\mathbf{r}_{i\alpha}$ and those of site β on molecule j ($j \neq i$) by $\mathbf{r}_{j\beta}$, then the site–site pair distribution function $g_{\alpha\beta}(r)$ is defined in a manner similar to (2.5.15):

$$\begin{aligned} \rho g_{\alpha\beta}(r) &= \left\langle \frac{1}{N} \sum_{i=1}^{N} \sum_{j\neq i}^{N} \delta(\mathbf{r} + \mathbf{r}_{2\beta} - \mathbf{r}_{1\alpha}) \right\rangle \\ &= \left\langle (N-1)\delta(\mathbf{r} + \mathbf{r}_{2\beta} - \mathbf{r}_{1\alpha}) \right\rangle \end{aligned} \tag{11.3.1}$$

The corresponding site–site pair correlation function is defined as $h_{\alpha\beta}(r) = g_{\alpha\beta}(r) - 1$. The site–site distribution functions are, of course, of interest in a wider context than that of interaction-site models. For any real molecular fluid the most important site–site distribution functions are those that describe the distribution of atomic sites.

The definition (11.3.1) can be used to relate the site–site distribution functions to the molecular pair distribution function $g(1,2)$. Let $\boldsymbol{\ell}_{i\alpha}$ be the vector displacement of site α in molecule i from the molecular centre $\mathbf{R}_i$, i.e.

$$\boldsymbol{\ell}_{i\alpha} = \mathbf{r}_{i\alpha} - \mathbf{R}_i \tag{11.3.2}$$

Then $g_{\alpha\beta}(r)$ is given by the integral of $g(1,2)$ over all coordinates, subject to the constraint that the vector separation of sites α, β is equal to $\mathbf{r}$:

$$\begin{aligned} g_{\alpha\beta}(\mathbf{r}) &= \frac{1}{\Omega^2}\iiiint \mathrm{d}\mathbf{R}_1\,\mathrm{d}\mathbf{R}_2\,\mathrm{d}\boldsymbol{\Omega}_1\,\mathrm{d}\boldsymbol{\Omega}_2\,g(1,2) \\ &\quad\times\delta\big[\mathbf{R}_1+\boldsymbol{\ell}_{1\alpha}(\boldsymbol{\Omega}_1)\big]\delta\big[\mathbf{R}_2+\boldsymbol{\ell}_{2\beta}(\boldsymbol{\Omega}_2)-\mathbf{r}\big] \\ &= \frac{1}{\Omega^2}\iiint \mathrm{d}\mathbf{R}_{12}\,\mathrm{d}\boldsymbol{\Omega}_1\,\mathrm{d}\boldsymbol{\Omega}_2\,g(1,2) \\ &\quad\times\delta\big[\mathbf{R}_{12}+\boldsymbol{\ell}_{2\beta}(\boldsymbol{\Omega}_2)-\boldsymbol{\ell}_{1\alpha}(\boldsymbol{\Omega}_1)-\mathbf{r}\big] \end{aligned} \tag{11.3.3}$$

It follows from (11.3.3) that the Fourier transform of $g_{\alpha\beta}(\mathbf{r})$ with respect to $\mathbf{r}$ is

$$\begin{aligned} \hat{g}_{\alpha\beta}(\mathbf{k}) &= \frac{1}{\Omega^2}\iiiint \mathrm{d}\mathbf{R}_{12}\,\mathrm{d}\boldsymbol{\Omega}_1\,\mathrm{d}\boldsymbol{\Omega}_2\,g(1,2) \\ &\quad\times\delta\big[\mathbf{R}_{12}+\boldsymbol{\ell}_{2\beta}(\boldsymbol{\Omega}_2)-\boldsymbol{\ell}_{1\alpha}(\boldsymbol{\Omega}_1)-\mathbf{r}\big]\exp(-i\mathbf{k}\cdot\mathbf{r})\,\mathrm{d}\mathbf{r} \\ &= \frac{1}{\Omega^2}\iiint \mathrm{d}\mathbf{R}_{12}\,\mathrm{d}\boldsymbol{\Omega}_1\,\mathrm{d}\boldsymbol{\Omega}_2\,g(1,2)\exp(-i\mathbf{k}\cdot\mathbf{R}_{12}) \\ &\quad\times\exp\big[-i\mathbf{k}\cdot\boldsymbol{\ell}_{2\beta}(\boldsymbol{\Omega}_2)\big]\exp\big[i\mathbf{k}\cdot\boldsymbol{\ell}_{1\alpha}(\boldsymbol{\Omega}_1)\big] \\ &= \big\langle\hat{g}(1,2)\exp\big[-i\mathbf{k}\cdot\boldsymbol{\ell}_{2\beta}(\boldsymbol{\Omega}_2)\big]\exp\big[i\mathbf{k}\cdot\boldsymbol{\ell}_{1\alpha}(\boldsymbol{\Omega}_1)\big]\big\rangle_{\boldsymbol{\Omega}_1\boldsymbol{\Omega}_2} \end{aligned} \tag{11.3.4}$$

where $\hat{g}(1,2)$ is defined by (11.2.10). There is an analogous expression for $\hat{h}_{\alpha\beta}(\mathbf{k})$ in terms of $h(1,2)$.

The site–site distribution functions have a simple physical interpretation. They are also directly related to the structure factors measured in x-ray and neutron-scattering experiments. On the other hand, the integrations in (11.3.3) involve an irretrievable loss of information, and $g(1,2)$ cannot be reconstructed exactly from any finite set of site–site distribution functions.

Many of the quantities that are expressible as integrals over $g(1,2)$ can also be written in terms of site–site distribution functions. For example, if the intermolecular potential is of the interaction-site form and the site–site potentials are spherically symmetric, the excess internal energy is given by

$$\frac{U^{\mathrm{ex}}}{N} = 2\pi\rho\sum_{\alpha}\sum_{\beta}\int_0^{\infty} v_{\alpha\beta}(r)g_{\alpha\beta}(r)r^2\,\mathrm{d}r \tag{11.3.5}$$

Equation (11.3.5) is a straightforward generalisation of (2.5.20) and can be derived by the same intuitive approach discussed in connection with the earlier result. The generalisation of the virial equation (2.5.22) is more complicated and knowledge of $g_{\alpha\beta}(r)$ for all α, β is not sufficient to determine the pressure. The equation of state can, however, be determined by integration of the compressibility equation (11.1.11). Because the choice of molecular

centre is arbitrary, and need not be the same for each molecule, (11.1.11) can be written as

$$\rho k_{\mathrm{B}} T \chi_T = 1 + \rho \int \left[g_{\alpha\beta}(r) - 1 \right] \mathrm{d}\mathbf{r} = 1 + \rho \hat{h}_{\alpha\beta}(0) \tag{11.3.6}$$

where α, β refer to any pair of sites. Finally, the angular correlation parameters G_l defined by (11.1.8) can be expressed[5] as integrals over combinations of the functions $h_{\alpha\beta}(r)$. In the case of a heteronuclear but non-polar molecule with atomic sites α and β the result for G_1 is[6]

$$G_1 = -\frac{\rho}{2L^2} \int_0^\infty r^2 \Delta h(r) \, \mathrm{d}\mathbf{r} \tag{11.3.7}$$

where L is the bondlength and

$$\Delta h(r) = h_{\alpha\alpha}(r) + h_{\beta\beta}(r) - 2h_{\alpha\beta}(r) \tag{11.3.8}$$

If $\hat{h}_{\alpha\beta}(k)$ is expanded in powers of k in the form

$$\hat{h}_{\alpha\beta}(k) = 4\pi \int_0^\infty h_{\alpha\beta}(r) \frac{\sin kr}{kr} r^2 \, \mathrm{d}r = \hat{h}_{\alpha\beta}(0) + h^{(2)}_{\alpha\beta} k^2 + \cdots \tag{11.3.9}$$

we find that G_1 is proportional to the coefficient of k^2 in the small-k expansion of $\Delta\hat{h}(k)$:

$$G_1 = \frac{3\rho}{L^2} \Delta h^{(2)} \tag{11.3.10}$$

Similarly, G_l for $l > 1$ can be written in terms of the higher-order coefficients $\Delta h^{(n)}$. The example given is somewhat artificial, since any real heteronuclear molecule will have a dipole moment; in that case (11.3.7) is no longer correct. Nonetheless, it serves to illustrate the general form of the results, and we shall see in Section 11.5 how (11.3.7) can be recovered from the expression appropriate to polar molecules. If the molecule is homonuclear, all site–site distribution functions are the same and G_1 vanishes, as it must do on grounds of symmetry.

Information on the atom–atom distribution functions of real molecules is gained experimentally from the analysis of radiation-scattering experiments. Consider first the case of a homonuclear diatomic. Let $\mathbf{u}_i$ be a unit vector along the internuclear axis of molecule i. Then the coordinates of atoms α, β relative to the centre of mass $\mathbf{R}_i$ are

$$\mathbf{r}_{i\alpha} = \mathbf{R}_i + \tfrac{1}{2}\mathbf{u}_i L, \qquad \mathbf{r}_{i\beta} = \mathbf{R}_i - \tfrac{1}{2}\mathbf{u}_i L \tag{11.3.11}$$

We define the Fourier components of the atomic density as

$$\rho_{\mathbf{k}} = \sum_{i=1}^{N} \left[\exp(-i\mathbf{k} \cdot \mathbf{r}_{i\alpha}) + \exp(-i\mathbf{k} \cdot \mathbf{r}_{i\beta}) \right] \tag{11.3.12}$$

and the molecular structure factor as

$$S(k) = \left\langle \frac{1}{4N} \rho_{\mathbf{k}} \rho_{-\mathbf{k}} \right\rangle \tag{11.3.13}$$

where N is the number of molecules. The factor $\frac{1}{4}$ is included in order to make the definition of $S(k)$ reduce to that of an atomic fluid in the limit $L \to 0$. The statistical average in (11.3.13) may be rewritten in terms of either the atomic or molecular pair distribution functions. In the first case, by exploiting the fact that atoms α, β in each molecule play equivalent roles, we can write

$$\left\langle \frac{1}{4N} \rho_{\mathbf{k}} \rho_{-\mathbf{k}} \right\rangle = \frac{1}{2} + \frac{1}{2N} \sum_{i=1}^{N} \left\langle \cos(\mathbf{k} \cdot \mathbf{u}_i L) \right\rangle_{\boldsymbol{\Omega}_i} + \left\langle \frac{1}{4N} \sum_{i=1}^{N} \sum_{j \neq i}^{N} \exp\left[-i\mathbf{k} \cdot (\mathbf{r}_{j\beta} - \mathbf{r}_{i\alpha}) \right] \right\rangle \tag{11.3.14}$$

The second term on the right-hand side involves only an average over angles and the third term can be related to any of the four identical distribution functions $g_{\alpha\beta}(r)$ via the definition (11.3.1). Thus

$$S(k) = S_{\text{intra}}(k) + S_{\text{inter}}(k) \tag{11.3.15}$$

The first term on the right-hand side of (11.3.15) is the intramolecular contribution:

$$S_{\text{intra}}(k) = \tfrac{1}{2}\left(1 + \langle \cos \mathbf{k} \cdot \mathbf{u}_i L \rangle_{\boldsymbol{\Omega}_i}\right) = \tfrac{1}{2}\left[1 + j_0(kL)\right] \tag{11.3.16}$$

where $j_0(x) = x^{-1} \sin x$. The intermolecular part is given by

$$S_{\text{inter}}(k) = \rho \int h_{\alpha\beta}(r) \exp(-i\mathbf{k} \cdot \mathbf{r}) \, \mathrm{d}\mathbf{r} = S_{\alpha\beta}(k) - 1 \tag{11.3.17}$$

where $S_{\alpha\beta}(k)$ is the atomic structure factor and a physically unimportant term in $\delta(\mathbf{k})$ has been omitted. The total intensity of scattered radiation at a given value of k is proportional to the structure factor (11.3.15); this can be inverted to yield the atomic pair distribution function if the intramolecular part is first removed.[7]

In order to relate $S(k)$ to the molecular pair distribution function we start from the definition (11.3.13) and proceed as follows:

$$\begin{aligned} S(k) &= \left\langle \frac{1}{4N} \rho_{\mathbf{k}} \rho_{-\mathbf{k}} \right\rangle \\ &= \left\langle \frac{1}{N} \sum_{i=1}^{N} \sum_{j=1}^{N} \exp(-i\mathbf{k} \cdot \mathbf{R}_{ij}) \cos\left(\tfrac{1}{2}\mathbf{k} \cdot \mathbf{u}_i L\right) \cos\left(\tfrac{1}{2}\mathbf{k} \cdot \mathbf{u}_j L\right) \right\rangle \\ &= \tfrac{1}{2}\left[1 + j_0(kL)\right] \end{aligned}$$

$$+\left\langle \frac{1}{N}\sum_{i=1}^{N}\sum_{j\neq i}^{N}\exp(-i\mathbf{k}\cdot\mathbf{R}_{ij})\cos\left(\tfrac{1}{2}\mathbf{k}\cdot\mathbf{u}_i L\right)\cos\left(\tfrac{1}{2}\mathbf{k}\cdot\mathbf{u}_j L\right)\right\rangle$$

$$= S_{\text{intra}}(k) + \frac{\rho}{\Omega^2}\iiint \left[g(1,2)-1\right]\exp(-i\mathbf{k}\cdot\mathbf{R}_{12})$$

$$\times \cos\left(\tfrac{1}{2}\mathbf{k}\cdot\mathbf{u}_1 L\right)\cos\left(\tfrac{1}{2}\mathbf{k}\cdot\mathbf{u}_2 L\right)\mathrm{d}\mathbf{R}_{12}\,\mathrm{d}\boldsymbol{\Omega}_1\,\mathrm{d}\boldsymbol{\Omega}_2 \tag{11.3.18}$$

Equation (11.3.18) is an exact relation between $S(k)$ and $g(1,2)$. Comparison with (11.3.4) shows that the second term on the right-hand side is $\hat{h}_{\alpha\beta}(k)$; this can also be deduced from inspection of Eqns (11.3.15) to (11.3.17). A more tractable expression is obtained by replacing $g(1,2)$ by it spherical-harmonic expansion (11.2.1). The structure factor can then be written as

$$S(k) = S_{\text{intra}}(k) + f(k)\left[S_{\text{c}}(k)-1\right] + S_{\text{aniso}}(k) \tag{11.3.19}$$

where

$$f(k) = \left\langle \cos\left(\tfrac{1}{2}\mathbf{k}\cdot\mathbf{u}_1 L\right)\cos\left(\tfrac{1}{2}\mathbf{k}\cdot\mathbf{u}_2 L\right)\right\rangle_{\boldsymbol{\Omega}_1\boldsymbol{\Omega}_2} = \left[j_0\left(\tfrac{1}{2}kL\right)\right]^2 \tag{11.3.20}$$

and $S_{\text{c}}(k)$ is the Fourier transform of the centres distribution function $g_{\text{c}}(r)$. The term $S_{\text{aniso}}(k)$ in (11.3.19) represents the contribution to $S(k)$ from the angle-dependent terms in $g(1,2)$, i.e. from all spherical harmonics beyond $(l_1, l_2, m) = (0,0,0)$. If the intermolecular potential is only weakly anisotropic, $S_{\text{aniso}}(k)$ will be small. In those circumstances it follows from (11.3.15), (11.3.17) and (11.3.19) that

$$S_{\alpha\beta}(k) \approx 1 + f(k)\left[S_{\text{c}}(k)-1\right] \tag{11.3.21}$$

Equation (11.3.21) is called the "free-rotation" approximation. This can be expected to work well only when the intermolecular potential is very weakly anisotropic, as in the case of liquid nitrogen, for example. At the same time, even in the absence of strong orientational correlations, the modulating role of the function $f(k)$ means that the intermolecular contribution to $S(k)$ will differ from the structure factor of an atomic fluid. This is evident in Figure 11.1, which shows the results of x-ray scattering experiments on liquid nitrogen. Although the function $S_{\text{c}}(k)$ cannot usually be determined experimentally,[9] the evidence from computer simulations[10] is that for small molecules it has a strongly oscillatory character and can be well fitted by the structure factor of an atomic system. By contrast, as comparison of Figures 3.2 (or 5.1) and 11.1 reveals, the first peak in the molecular structure factor is significantly weaker and the later oscillations are more strongly damped than in the case of a typical atomic fluid. Note also that beyond the first peak the behaviour of the molecular structure factor is dominated by the intramolecular term. The free-rotation approximation becomes exact in the limit $k \to 0$ because the cosine terms in (11.3.18) all approach unity. Thus

$$\rho k_{\text{B}} T \chi_T = \lim_{k\to 0} S(k) = 1 + \rho\int \left[g_{\text{c}}(R)-1\right]\mathrm{d}\mathbf{R} \tag{11.3.22}$$

which is the same result as in (11.1.11).

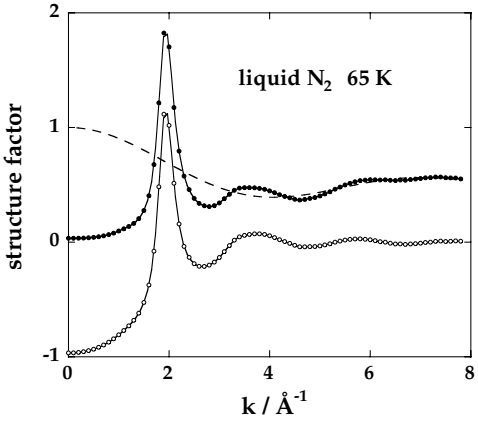

FIG. 11.1. Results obtained by x-ray scattering for the structure factor of liquid nitrogen near its triple point. Filled circles: $S(k)$; open circles: $S_{\text{inter}}(k)$; dashes: $S_{\text{intra}}(k)$. After Narten *et al.*[8]

For heteronuclear molecules there is normally little value in defining a structure factor through a formula analogous to (11.3.13). It is more useful instead to focus attention on those combinations of atomic structure factors that are experimentally accessible. In the case of neutron scattering the measured structure factor can again be written in the form of (11.3.15), but now

$$\left(\sum_\alpha b_\alpha\right)^2 S^{\text{N}}_{\text{intra}}(k) = \sum_\alpha b_\alpha^2 + \sum_\alpha \sum_{\beta\neq\alpha} b_\alpha b_\beta j_0(kL_{\alpha\beta}) \tag{11.3.23a}$$

$$\begin{aligned}\left(\sum_\alpha b_\alpha\right)^2 S^{\text{N}}_{\text{inter}}(k) &= \rho \sum_\alpha \sum_\beta b_\alpha b_\beta \int \big[g_{\alpha\beta}(r) - 1\big] \exp(-i\mathbf{k}\cdot\mathbf{r})\, \mathrm{d}\mathbf{r} \\ &= \sum_\alpha \sum_\beta b_\alpha b_\beta \big[S_{\alpha\beta}(k) - 1\big]\end{aligned} \tag{11.3.23b}$$

where the sums run over all nuclei in the molecule, b_α is the coherent neutron scattering length of nucleus α and $L_{\alpha\beta}$ is the separation of nuclei α, β. These expressions reduce to (11.3.16) and (11.3.17) for a diatomic molecule with $b_\alpha = b_\beta$. After removal of the intramolecular term, Fourier transformation yields a weighted sum of atomic pair distribution functions of the form

$$g^{\text{N}}(r) = \sum_\alpha \sum_\beta b_\alpha b_\beta g_{\alpha\beta}(r) \Big/ \left(\sum_\alpha b_\alpha\right)^2 \tag{11.3.24}$$

Isotopic substitution makes it possible to vary the weights with which the different $g_{\alpha\beta}(r)$ contribute to $g^{\text{N}}(r)$ and hence, in favourable cases, to determine some or all of the individual atom–atom distribution functions.

Formulae similar to (11.3.23) apply also to x-ray scattering, the only difference being that the nuclear scattering lengths are replaced by the atomic form factors (see Section 4.1). Since the form factors are functions of k, the weighted distribution function $g^{\mathrm{X}}(r)$ obtained by Fourier transformation of the measured structure factor $S^{\mathrm{X}}(k)$ is not a linear combination of the functions $g_{\alpha\beta}(r)$, but for large atoms the error introduced by ignoring this fact is small.

In Figure 11.2 we show some results obtained by x-ray scattering for the carbon–carbon distribution function $g_{\mathrm{CC}}(r)$ in liquid ethylene near its triple point. Although ethylene is a polyatomic molecule, $g_{\mathrm{CC}}(r)$ resembles the pair distribution function for diatomics, as seen in both simulations and experiments. The main peak is appreciably weaker than in argon-like liquids and there is a pronounced shoulder on the large-r side. Both these features are consequences of the interference between inter- and intramolecular correlations. Simple geometry suggests that shoulders might be seen at combinations of distances such that $r_{\alpha\gamma} \approx |\sigma_{\alpha\beta} \pm L_{\beta\gamma}|$, where σ is an atomic diameter and $L_{\beta\gamma}$ is a bondlength, but they are often so smooth as to be undetectable. In the case of fused-hard sphere models of the intermolecular potential the shoulders appear as cusps in the site–site distribution functions, i.e. as discontinuities in the derivative of $g_{\alpha\beta}(r)$ with respect to r. The shoulder seen in Figure 11.2 is associated with "T-shaped" configurations of the type pictured in Figure 11.3.

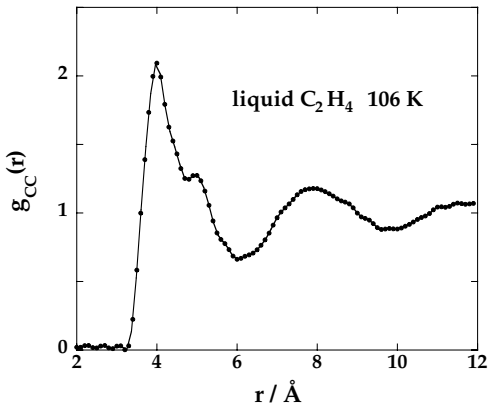

FIG. 11.2. Results obtained by x-ray scattering for the carbon–carbon distribution function in liquid ethylene. After Narten and Habenschuss.[11]

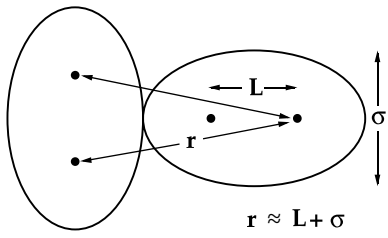

FIG. 11.3. The T-shaped configuration for a pair of homonuclear diatomics.

This particular feature is enhanced for molecules having a large quadrupole moment, such as bromine,[12] since the quadrupolar interaction strongly favours the T-configuration.

11.4 CORRELATION-FUNCTION EXPANSIONS FOR SIMPLE POLAR FLUIDS

In the simplest models of a polar fluid the intermolecular potential can be written as the sum of a small number of spherical-harmonic components. The prospects for success of theories are therefore greater than in situations where the potential contains an infinite number of harmonics and the series expansions are only slowly convergent, as is true, for example, in the case of Lennard-Jones diatomics.[4] In this section we discuss some of the general questions that arise in attempts to treat polar fluids in this way.

Consider a polar fluid for which the intermolecular potential is the same as in (1.2.4), but which we rewrite here as

$$v(1,2) = v_0(R) - \frac{\mu^2}{R^3} D(1,2) \tag{11.4.1}$$

with

$$D(1,2) = 3(\mathbf{u}_1 \cdot \mathbf{s})(\mathbf{u}_2 \cdot \mathbf{s}) - \mathbf{u}_1 \cdot \mathbf{u}_2 \tag{11.4.2}$$

where $R \equiv |\mathbf{R}_{12}|$, $\mathbf{s}$ is a unit vector in the direction of $\mathbf{R}_{12}$, $\mathbf{u}_i$ is a unit vector parallel to the dipole moment of molecule i, $v_0(R)$ is assumed to be spherically symmetric and the angle-dependent terms represent the ideal dipole–dipole interaction. It was first shown by Wertheim[13] and subsequently elaborated by others[14] that an adequate description of the static properties of such a fluid can be obtained by working with a basis set consisting of only three functions: $S(1,2) = 1$, $\Delta(1,2) = \mathbf{u}_1 \cdot \mathbf{u}_2$ and $D(1,2)$, defined above. The solution for $h(1,2)$ is therefore assumed to be of the form

$$h(1,2) = h_S(R) + h_\Delta(R)\Delta(1,2) + h_D(R)D(1,2) \tag{11.4.3}$$

On multiplying through (11.4.3) successively by S, Δ and D and integrating over angles we find that the projections $h_S(R)$, $h_\Delta(R)$ and $h_D(R)$ are given by

$$h_S(R) = \langle h(1,2) \rangle_{\Omega_1 \Omega_2} \tag{11.4.4}$$

$$h_\Delta(R) = 3\langle h(1,2)\Delta(1,2) \rangle_{\Omega_1 \Omega_2} \tag{11.4.5}$$

$$h_D(R) = \tfrac{3}{2}\langle h(1,2)D(1,2) \rangle_{\Omega_1 \Omega_2} \tag{11.4.6}$$

Equation (11.4.3) is equivalent to an expansion in laboratory-frame harmonics, since the functions Δ and D are the same, respectively, as the rotational invariants Φ^{110} and Φ^{112} introduced in (11.2.9).

The direct correlation function $c(1,2)$ can be treated in similar fashion to $h(1,2)$. We therefore write

$$c(1,2) = c_S(R) + c_\Delta(R)\Delta(1,2) + c_D(R)D(1,2) \tag{11.4.7}$$

and introduce both (11.4.3) and (11.4.7) into the molecular Ornstein–Zernike relation (11.1.4). After taking Fourier transforms we find that

$$\hat{h}(1,2) = \hat{c}(1,2) + \rho\langle \hat{c}(1,3)\hat{h}(3,2)\rangle_{\boldsymbol{\Omega}_3} \tag{11.4.8}$$

where, for example:

$$\hat{h}(1,2) = \hat{h}_S(k) + \hat{h}_\Delta(k)\Delta(1,2) + \int h_D(R)D(1,2)\exp(-i\mathbf{k}\cdot\mathbf{R})\,\mathrm{d}\mathbf{R} \tag{11.4.9}$$

The term in D can be transformed by taking the direction of $\mathbf{k}$ as the z-axis and making the substitution $\mathbf{s} = (\sin\theta\cos\phi, \sin\theta\sin\phi, \cos\theta)$. Two integrations by parts show that

$$\begin{aligned}\int_{-1}^{1}\int_{0}^{2\pi} &(\mathbf{u}_1\cdot\mathbf{s})(\mathbf{u}_2\cdot\mathbf{s})\exp(-i\mathbf{k}\cdot\mathbf{R}\cos\theta)\,\mathrm{d}\phi\,\mathrm{d}(\cos\theta)\\ &= -4\pi R^2\big(3u_{1z}u_{2z}j_2(kR) - \mathbf{u}_1\cdot\mathbf{u}_2\big[j_0(kR) + j_2(kR)\big]\big)\end{aligned} \tag{11.4.10}$$

where $j_2(x) = 3x^{-3}\sin x - 3x^{-2}\cos x - x^{-1}\sin x$. Thus

$$\int h_D(R)D(1,2)\exp(-i\mathbf{k}\cdot\mathbf{R})\,\mathrm{d}\mathbf{R} = D_k(1,2)\bar{h}_D(k) \tag{11.4.11}$$

with

$$D_k(1,2) = 3u_{1z}u_{2z} - \mathbf{u}_1\cdot\mathbf{u}_2 = \frac{3(\mathbf{u}_1\cdot\mathbf{k})(\mathbf{u}_2\cdot\mathbf{k})}{k^2} - \mathbf{u}_1\cdot\mathbf{u}_2 \tag{11.4.12}$$

and the Hankel transform $\bar{h}_D(k)$ is

$$\bar{h}_D(k) = -4\pi\int_0^\infty j_2(kR)h_D(R)R^2\,\mathrm{d}R \tag{11.4.13}$$

Equation (11.4.11) is a particular case of the general result (11.2.12); the transform of $c_D(R)D(1,2)$ is handled in the same way.

In order to summarise the effect of the angular integrations in (11.4.8), we define the angular convolution of two functions A, B as

$$A * B = B * A = \frac{1}{\Omega}\int A(1,3)B(3,2)\,\mathrm{d}\boldsymbol{\Omega}_3 \equiv \langle A(1,3)B(3,2)\rangle_{\boldsymbol{\Omega}_3} \tag{11.4.14}$$

For the functions of interest here the "multiplication" rules shown in Table 11.1 are easily established. We see from the table that the functions S, Δ and D_k form a closed set under

TABLE 11.1. *Rules for the evaluation of angular convolutions of the functions S, Δ and D_k*

	S	Δ	D_k
S	S	0	0
Δ	0	$\Delta/3$	$D_k/3$
D_k	0	$D_k/3$	$(D_k+2\Delta)/3$

the operation (11.4.14) in the sense that convolution of any two functions yields only a function in the same set (or zero). The practical significance of this result is the fact that if $h(1,2)$ is assumed to be of the form (11.4.3), then $c(1,2)$ is necessarily given by (11.4.7), and vice versa. A closure of the Ornstein–Zernike relation is still required. However, if this does not generate any new harmonics, (11.4.3) and (11.4.7) together form a self-consistent approximation, to which a solution can be found either analytically (as in the MSA, Section 11.6) or numerically.

At large R, $c(1,2)$ behaves as $-\beta v(1,2)$. Hence $c_D(R)$ must be long ranged, decaying asymptotically as R^{-3}. It turns out, as we shall see in Section 11.5, that $h_D(R)$ also decays as R^{-3}, the strength of the long-range part being related to the dielectric constant of the fluid, but the other projections of $h(1,2)$ and $c(1,2)$ are all short ranged. The slow decay of $h_D(R)$ and $c_D(R)$ creates difficulties in numerical calculations. It is therefore convenient to introduce two short-range, auxiliary functions $h_D^0(R)$ and $c_D^0(R)$. These are defined in terms, respectively, of $h_D(R)$ and $c_D(R)$ in such a way as to remove the long-range parts. Thus

$$h_D^0(R) = h_D(R) - 3\int_R^\infty \frac{h_D(R')}{R'}\,\mathrm{d}R' \tag{11.4.15}$$

with an analogous definition of $c_D^0(R)$; we see from (11.4.15) that $h_D^0(R)$ vanishes for R in the range where $h_D(R)$ has reached its asymptotic value. The inverse of (11.4.15) is

$$h_D(R) = h_D^0(R) - \frac{3}{R^3}\int_0^R h_D^0(R')R'^2\,\mathrm{d}R' \tag{11.4.16}$$

which can be checked by first differentiating (11.4.16) with respect to R and then integrating from R to $R=\infty$ (where both $h_D(R)$ and $h_D^0(R)$ are zero); this leads back to (11.4.15). Equation (11.4.16) shows that $h_D(R)$ behaves asymptotically as

$$\lim_{R\to\infty} h_D(R) = -\frac{3}{4\pi R^3}\lim_{k\to 0}\hat{h}_D^0(k) \tag{11.4.17}$$

The short-range functions $h_D^0(R)$ and $c_D^0(R)$ play an important part in the analytical solution of the MSA for dipolar hard spheres.

We have seen that use of the approximation (11.4.3) has some attractive mathematical features. The solution is of physical interest, however, only because the projections $h_S(R)$, $h_\Delta(R)$ and $h_D(R)$ contain between them all the information needed to calculate both the thermodynamic and static dielectric properties of the fluid. We postpone discussion of the

difficult problem of dielectric behaviour until the next section, but expressions for thermodynamic properties are easily derived. If $v_0(R)$ in (11.4.1) is the hard-sphere potential, the excess internal energy is determined solely by the dipole–dipole interaction and (11.1.9) becomes

$$\frac{U^{\mathrm{ex}}}{N} = -2\pi\rho \int_0^\infty \frac{\mu^2}{R_{12}} \langle D(1,2) g(1,2) \rangle_{\boldsymbol{\Omega}_1 \boldsymbol{\Omega}_2} \, \mathrm{d}R_{12}$$
$$= -\frac{4\pi\mu^2\rho}{3} \int_0^\infty \frac{h_D(R)}{R} \, \mathrm{d}R \tag{11.4.18}$$

where we have used the definition (11.4.6) and the fact that the angle average of $D(1,2)$ is zero. If $v_0(R)$ is the Lennard-Jones potential or some other spherically symmetric but continuous interaction, there will be a further contribution to U^{ex} that can be expressed as

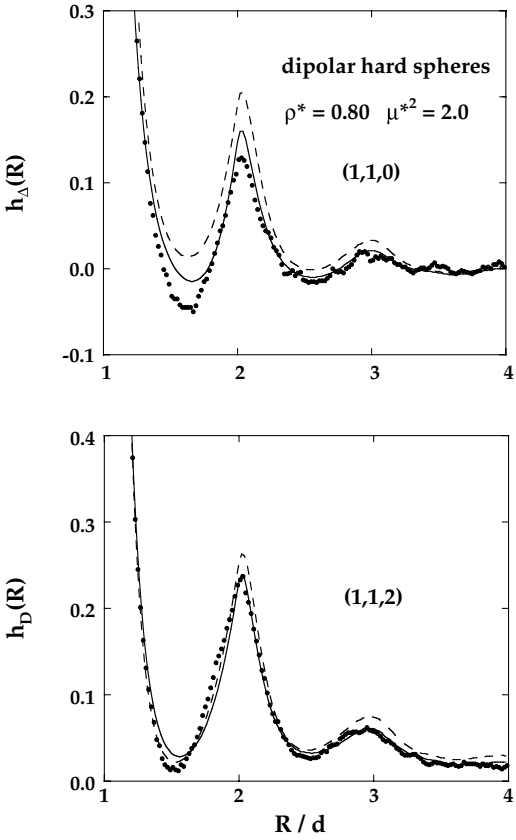

FIG. 11.4. Projections of $h(1,2)$ for a fluid of dipolar hard spheres at $\rho d^3 = 0.80$, $\beta\mu^2/d^3 = 2.0$. The points are Monte Carlo results and the curves are calculated from the LHNC (dashes) and RHNC (continuous lines) approximations discussed in Section 11.6. After Fries and Patey.[15]

an integral over $h_S(R)$. Similarly, (11.1.10) can be used to relate the equation of state to the projections $h_S(R)$ and $h_D(R)$. Thermodynamic properties are therefore not explicitly dependent on $h_\Delta(R)$.

Examples of $h_\Delta(R)$ and $h_D(R)$ for the dipolar hard-sphere fluid are shown in Figure 11.4. For the state point concerned, corresponding to a static dielectric constant ε of approximately 30, the curves retain a pronounced oscillatory character over a range of three to four molecular diameters. The structure in $h_\Delta(R)$ and $h_D(R)$ disappears as the dipole moment is reduced, but $h_S(R)$ (not shown) is much less sensitive to the value of ε and bears a strong resemblance to the pair correlation function of a fluid of non-polar hard spheres. The structure seen in the Δ and D projections is also depressed by addition of a quadrupole moment, as we discuss again in Section 11.6.

11.5 THE STATIC DIELECTRIC CONSTANT

Our goal in this section is to obtain molecular expressions for the static dielectric constant. We show, in particular, that ε is related to the long-wavelength behaviour of each of the functions $\hat{h}_\Delta(k)$ and $\bar{h}_D(k)$ introduced in the previous section.[16] By suitably combining the two results it is also possible to express ε in terms of site–site distribution functions.[17]

Consider a sample of dielectric material (a polar fluid) placed in an external electric field. Let $\mathbf{E}(\mathbf{R}, t)$ be the field at time t at a point $\mathbf{R}$ inside the sample (the Maxwell field), let $\mathbf{P}(\mathbf{R}, t)$ be the polarisation induced in the sample and let $\mathbf{E}^0(\mathbf{R}, t)$ be the field that would exist at the same point if the sample were removed (the external field). The polarisation is related to the Maxwell field by

$$\mathbf{P}(\mathbf{R}, t) = \int \mathrm{d}\mathbf{R}' \int_{-\infty}^{t} \boldsymbol{\chi}(\mathbf{R} - \mathbf{R}', t - t') \cdot \mathbf{E}(\mathbf{R}', t') \, \mathrm{d}t' \tag{11.5.1}$$

where the tensor $\boldsymbol{\chi}(\mathbf{R}, t)$ is an after-effect function of the type introduced in Section 7.6. A Fourier–Laplace transform of (11.5.1) (with z on the real axis) gives

$$\widehat{\mathbf{P}}(\mathbf{k}, \omega) = \boldsymbol{\chi}(\mathbf{k}, \omega) \cdot \widehat{\mathbf{E}}(\mathbf{k}, \omega) \tag{11.5.2}$$

where the susceptibility $\boldsymbol{\chi}(\mathbf{k}, \omega)$ is related to the dielectric permittivity $\boldsymbol{\varepsilon}(\mathbf{k}, \omega)$ by

$$\boldsymbol{\chi}(\mathbf{k}, \omega) = \frac{1}{4\pi}\big[\boldsymbol{\varepsilon}(\mathbf{k}, \omega) - \boldsymbol{I}\big] \tag{11.5.3}$$

The polarisation is also related to the external field via a second susceptibility, $\boldsymbol{\chi}^0(\mathbf{k}, \omega)$:

$$\widehat{\mathbf{P}}(\mathbf{k}, \omega) = \boldsymbol{\chi}^0(\mathbf{k}, \omega) \cdot \widehat{\mathbf{E}}^0(\mathbf{k}, \omega) \tag{11.5.4}$$

The external field and Maxwell field will not, in general, be the same, because the polarisation of the sample makes a contribution to the Maxwell field. The relation between the

two fields, and hence also that between $\boldsymbol{\chi}$ and $\boldsymbol{\chi}^0$, is dependent on sample geometry. We shall assume that the system is infinite, in which case the relation between $\mathbf{E}$ and $\mathbf{E}^0$ is

$$\mathbf{E}(\mathbf{R}, t) = \mathbf{E}^0(\mathbf{R}, t) + \int \boldsymbol{T}(\mathbf{R} - \mathbf{R}') \cdot \mathbf{P}(\mathbf{R}', t)\, \mathrm{d}\mathbf{R}' \tag{11.5.5}$$

where $\boldsymbol{T}(\mathbf{R})$ is the dipole–dipole interaction tensor defined by (1.2.5). Integrals involving the dipole–dipole tensor must be handled with care, since $\boldsymbol{T}(\mathbf{R})$ has a singularity at the origin; the usual procedure is to cut off the integrand inside a sphere of radius σ centred on the origin and take the limit $\sigma \to 0$ after integration.[18] The transform of (11.5.5) is then given by

$$\widehat{\mathbf{E}}(\mathbf{k}, \omega) = \widehat{\mathbf{E}}^0(\mathbf{k}, \omega) - \frac{4\pi}{k^2}\mathbf{k}\mathbf{k} \cdot \widehat{\mathbf{P}}(\mathbf{k}, \omega) \tag{11.5.6}$$

The relationship between the two susceptibilities follows immediately from consideration of (11.5.2), (11.5.4) and (11.5.6):[19]

$$\boldsymbol{\chi}^0(\mathbf{k}, \omega) = \left[\boldsymbol{I} + \left(4\pi/k^2\right)\mathbf{k}\mathbf{k} \cdot \boldsymbol{\chi}(\mathbf{k}, \omega)\right]^{-1} \cdot \boldsymbol{\chi}(\mathbf{k}, \omega) \tag{11.5.7}$$

It is an experimental fact that the dielectric permittivity is an intensive property of the fluid, having a value that for given $\mathbf{k}$ and ω is independent of sample size and shape. The same is therefore true of the susceptibility $\boldsymbol{\chi}(\mathbf{k}, \omega)$, since the two quantities are trivially linked by (11.5.3). It follows, provided the system is isotropic, that both $\boldsymbol{\varepsilon}$ and $\boldsymbol{\chi}$ must be independent of the direction of $\mathbf{k}$. Thus, in the limit $\mathbf{k} \to 0$:

$$\lim_{\mathbf{k}\to 0} \boldsymbol{\varepsilon}(\mathbf{k}, \omega) = \varepsilon(\omega)\boldsymbol{I}, \qquad \lim_{\mathbf{k}\to 0} \boldsymbol{\chi}(\mathbf{k}, \omega) = \chi(\omega)\boldsymbol{I} \tag{11.5.8}$$

where $\varepsilon(\omega)$ and $\chi(\omega)$ are scalars. On the other hand, the longitudinal (parallel to $\mathbf{k}$) and transverse (perpendicular to $\mathbf{k}$) components of $\boldsymbol{\chi}^0(\mathbf{k}, \omega)$ must behave differently in the long-wavelength limit; this is inevitable, given that the relation between $\boldsymbol{\chi}^{(0)}$ and $\boldsymbol{\varepsilon}$ is shape dependent. Taking the z-axis along the direction of $\mathbf{k}$, we find from (11.5.3), (11.5.7) and (11.5.8) that

$$4\pi \lim_{\mathbf{k}\to 0} \chi^0_{\alpha\alpha}(\mathbf{k}, \omega) = \varepsilon(\omega) - 1, \quad \alpha = x, y \tag{11.5.9a}$$

$$4\pi \lim_{\mathbf{k}\to 0} \chi^0_{zz}(\mathbf{k}, \omega) = \frac{\varepsilon(\omega) - 1}{\varepsilon(\omega)} \tag{11.5.9b}$$

and

$$4\pi \lim_{\mathbf{k}\to 0} \operatorname{Tr} \boldsymbol{\chi}^0(\mathbf{k}, \omega) = \frac{[\varepsilon(\omega) - 1][2\varepsilon(\omega) + 1]}{\varepsilon(\omega)} \tag{11.5.10}$$

The statistical-mechanical problem is to obtain expressions for the components of $\boldsymbol{\chi}^0$ in terms of microscopic variables. The microscopic expression for the polarisation induced

by the external field is

$$\mathbf{P}(\mathbf{R},t)=\big\langle\mathbf{M}(\mathbf{R},t)\big\rangle_{\mathbf{E}^0}=\left\langle\mu\sum_{i=1}^{N}\mathbf{u}_i(t)\delta\big[\mathbf{R}-\mathbf{R}_i(t)\big]\right\rangle_{\mathbf{E}^0} \tag{11.5.11}$$

where $\mathbf{M}(\mathbf{R},t)$ is the dipole-moment density, $\langle\cdots\rangle_{\mathbf{E}^0}$ denotes a statistical average in the presence of the external field and the other symbols have the same meaning as in earlier sections of this chapter. The susceptibility $\boldsymbol{\chi}^0$ can now be calculated by the methods of linear-response theory described in Section 7.6. (Note that $\boldsymbol{\chi}$ cannot be treated in the same way as $\boldsymbol{\chi}^0$, because the Maxwell field is not an "external" field in the required sense.) As an application of the general result given by (7.6.21) we find that

$$\boldsymbol{\chi}^0(\mathbf{k},\omega)=\frac{\beta}{V}\left(\langle\mathbf{M}_{\mathbf{k}}\mathbf{M}_{-\mathbf{k}}\rangle+i\omega\int_0^\infty\big\langle\mathbf{M}_{\mathbf{k}}(t)\mathbf{M}_{-\mathbf{k}}\big\rangle\exp(i\omega t)\,\mathrm{d}t\right) \tag{11.5.12}$$

where the statistical averages are now computed in the absence of the field, $\mathbf{M}_{\mathbf{k}}\equiv\mathbf{M}_{\mathbf{k}}(t=0)$ and

$$\mathbf{M}_{\mathbf{k}}(t)=\mu\sum_{i=1}^{N}\mathbf{u}_i(t)\exp\big[-i\mathbf{k}\cdot\mathbf{R}_i(t)\big] \tag{11.5.13}$$

If we take the limit $\omega\to0$, (11.5.12) reduces to

$$\chi^0_{\alpha\alpha}(\mathbf{k},0)=\frac{\beta}{V}\big\langle M^\alpha_{\mathbf{k}}M^\alpha_{-\mathbf{k}}\big\rangle,\quad\alpha=x,y,z \tag{11.5.14}$$

By combining this result with (11.5.10) we find that

$$\frac{(\varepsilon-1)(2\varepsilon+1)}{9\varepsilon}=g_{\mathrm{K}}y \tag{11.5.15}$$

where $\varepsilon\equiv\varepsilon(0)$ is the static dielectric constant, y is a molecular parameter defined as

$$y=\frac{4\pi\mu^2\rho}{9k_{\mathrm{B}}T} \tag{11.5.16}$$

and g_{K}, the Kirkwood "g-factor", is given by

$$g_{\mathrm{K}}=\big\langle|\mathbf{M}|^2\big\rangle/N\mu^2 \tag{11.5.17}$$

where $\mathbf{M}\equiv\mathbf{M}_{\mathbf{k}=0}$ is the total dipole moment of the sample. Equation (11.5.17) can be rewritten, with the help of (11.4.5), as

$$\begin{aligned}g_{\mathrm{K}}&=1+\big\langle(N-1)\mathbf{u}_1\cdot\mathbf{u}_2\big\rangle\\&=1+\frac{4\pi\rho}{3}\int_0^\infty h_\Delta(R)R^2\,\mathrm{d}R=1+\tfrac{1}{3}\rho\hat{h}_\Delta(0)\end{aligned} \tag{11.5.18}$$

where $h_\Delta(R)$ is the function appropriate to an infinite system.

Equation (11.5.15) is the first of two key results of this section. It was originally derived by Kirkwood[20] via a calculation of the fluctuation in total dipole moment of a spherical region surrounded by a dielectric continuum and is commonly referred to as the Kirkwood formula. By setting $g_K = 1$ we obtain the result known as the Onsager equation; this amounts to ignoring the short-range angular correlations represented by the function $h_\Delta(R)$. The Kirkwood formula could have been obtained by working throughout in the $\omega = 0$ limit, but the frequency-dependent results are needed for the discussion of dielectric relaxation in Section 11.11.

The next task is to relate ε to the function $h_D(R)$. To do this we must consider separately the longitudinal and transverse components of $\boldsymbol{\chi}^0$. For the longitudinal component we find from (11.5.13) and (11.5.14) that

$$\begin{aligned}\chi^0_{zz}(\mathbf{k},0) &= \frac{\beta}{V}\langle M^z_{\mathbf{k}} M^z_{-\mathbf{k}}\rangle \\ &= \tfrac{1}{3}\mu^2\rho\beta + \mu^2\rho\beta\big\langle (N-1)u_{1z}u_{2z}\exp(-i\mathbf{k}\cdot\mathbf{R}_{12})\big\rangle \\ &= \tfrac{1}{3}\mu^2\rho\beta \\ &\quad + \frac{\mu^2\rho^2\beta}{\Omega^2}\iiint \frac{(\mathbf{k}\cdot\mathbf{u}_1)(\mathbf{k}\cdot\mathbf{u}_2)}{k^2}h(1,2) \\ &\quad \times \exp(-i\mathbf{k}\cdot\mathbf{R}_{12})\,\mathrm{d}\mathbf{R}_{12}\,\mathrm{d}\boldsymbol{\Omega}_1\,\mathrm{d}\boldsymbol{\Omega}_2 \\ &= \tfrac{1}{3}\mu^2\rho\beta + \mu^2\rho^2\beta\big\langle k^{-2}(\mathbf{k}\cdot\mathbf{u}_1)(\mathbf{k}\cdot\mathbf{u}_2)\hat{h}(1,2)\big\rangle_{\boldsymbol{\Omega}_1\boldsymbol{\Omega}_2} \end{aligned} \tag{11.5.19}$$

We now substitute for $\hat{h}(1,2)$ from (11.4.9) and evaluate the angular averages with the help of the following, easily proved results (here $\mathbf{n}$ is a unit vector of fixed orientation):

$$\big\langle (\mathbf{n}\cdot\mathbf{u}_1)(\mathbf{n}\cdot\mathbf{u}_2)(\mathbf{u}_1\cdot\mathbf{u}_2)\big\rangle_{\boldsymbol{\Omega}_1\boldsymbol{\Omega}_2} = \big\langle (\mathbf{n}\cdot\mathbf{u}_1)^2(\mathbf{n}\cdot\mathbf{u}_2)^2\big\rangle_{\boldsymbol{\Omega}_1\boldsymbol{\Omega}_2} = \tfrac{1}{9} \tag{11.5.20}$$

A simple calculation shows that

$$\lim_{\mathbf{k}\to 0}\chi^0_{zz}(\mathbf{k},0) = \tfrac{1}{3}\mu^2\rho\beta\big[1 + \tfrac{1}{3}\rho\hat{h}_\Delta(0) + \tfrac{2}{3}\rho\bar{h}_D(0)\big] \tag{11.5.21}$$

Although we have used the approximation (11.4.9), (11.5.21) is an exact result, since the terms ignored in (11.4.9) make no contribution to the angular average in (11.5.19).

The transverse component can be treated in a similar way. It is possible, however, to take a short-cut, since we are interested only in the $\mathbf{k} \to 0$ limit. Equations (11.5.10), (11.5.15) and (11.5.18) show that the trace of the tensor $\boldsymbol{\chi}^0(\mathbf{k},\omega)$ in the long-wavelength, low-frequency limit is

$$\lim_{\mathbf{k}\to 0}\operatorname{Tr}\boldsymbol{\chi}^0(\mathbf{k},0) = \mu^2\rho\beta\big[1 + \tfrac{1}{3}\hat{h}_\Delta(0)\big] \tag{11.5.22}$$

As the two transverse components are equivalent, we find from (11.5.21) and (11.5.22) that

$$\lim_{\mathbf{k}\to 0}\chi^0_{xx}(\mathbf{k},0) = \tfrac{1}{3}\mu^2\rho\beta\big[1 + \tfrac{1}{3}\rho\hat{h}_\Delta(0) - \tfrac{1}{3}\rho\bar{h}_D(0)\big] \tag{11.5.23}$$

Use of (11.5.9) leads to the second main result:

$$\frac{(\varepsilon-1)^2}{\varepsilon} = 4\pi \lim_{\mathbf{k}\to 0}\left[\chi^0_{xx}(\mathbf{k},0) - \chi^0_{zz}(\mathbf{k},0)\right] = -3y\rho\bar{h}_D(0) \tag{11.5.24}$$

It can be shown[21] that the Hankel transform in (11.5.24) is also the Fourier transform of the short-range function $h^0_D(R)$ defined by (11.4.15), i.e. $\bar{h}_D(k) = \hat{h}^0_D(k)$. Equations (11.4.17) and (11.5.24) may therefore be combined to give

$$\lim_{R\to\infty} h_D(R) = \frac{(\varepsilon-1)^2}{4\pi y\rho\varepsilon}\frac{1}{R^3} \tag{11.5.25}$$

The calculation establishes both that $h(1,2)$ is long ranged and that the long range of the correlations is responsible for the difference in behaviour of the longitudinal and transverse components of the susceptibility $\boldsymbol{\chi}^{(0)}(\mathbf{k},0)$.

The expansion of $h(1,2)$ in terms of the functions S, $\Delta(1,2)$ and $D(1,2)$ is particularly well suited to treating the type of potential model described by (11.4.1), but its range of applicability is wider than this. It can be used, in particular, to discuss the dielectric properties of linear, interaction-site molecules. Consider a diatomic molecule of bondlength L with charges $\pm q$ located on atoms α, β and a dipole moment $\mu = qL$. If ℓ_α is the distance of atom α from the molecular centre, (11.3.4) shows that the Fourier transform of any of the atomic pair correlation functions may be written as

$$\hat{h}_{\alpha\beta}(k) = \left\langle \hat{h}(1,2)\exp(-i\mathbf{k}\cdot\mathbf{u}_1\ell_\alpha)\exp(i\mathbf{k}\cdot\mathbf{u}_2\ell_\beta)\right\rangle_{\boldsymbol{\Omega}_1\boldsymbol{\Omega}_2} \tag{11.5.26}$$

with $\ell_\alpha + \ell_\beta = L$. The plane-wave functions can be replaced by their Rayleigh expansions:[22]

$$\exp(-i\mathbf{k}\cdot\mathbf{r}) = \sum_{n=0}^{\infty}(2n+1)i^n j_n(kr)P_n(\mathbf{k}\cdot\mathbf{r}/kr) \tag{11.5.27}$$

but since our concern is only with the behaviour of $\hat{h}_{\alpha\beta}(k)$ to order k^2, it is necessary to retain only the contributions from $n=0$ and $n=1$. If, in addition, we substitute for $\hat{h}(1,2)$ from (11.4.9), (11.5.26) becomes

$$\begin{aligned}\hat{h}_{\alpha\beta}(k) = \big\langle \big(&\hat{h}_S(k) + \hat{h}_\Delta(k)\mathbf{u}_1\cdot\mathbf{u}_2 + \bar{h}_D(k)\left[3k^{-2}(\mathbf{k}\cdot\mathbf{u}_1)(\mathbf{k}\cdot\mathbf{u}_2) - \mathbf{u}_1\cdot\mathbf{u}_2\right]\big)\\ &\times\left[j_0(-k\ell_\alpha) + 3ij_1(-k\ell_\alpha)\mathbf{k}\cdot\mathbf{u}_1/k\right]\\ &\times\left[j_0(k\ell_\beta) + 3ij_1(k\ell_\beta)\mathbf{k}\cdot\mathbf{u}_2/k\right]\big\rangle_{\boldsymbol{\Omega}_1\boldsymbol{\Omega}_2}\end{aligned} \tag{11.5.28}$$

where $j_1(x) = x^{-2}\sin x - x^{-1}\cos x$.

The terms in (11.5.28) that survive the integration over angles are those of the type shown in (11.5.20). On multiplying out, integrating with the help of (11.5.20) and collecting terms we find that

$$\hat{h}_{\alpha\beta}(k) = \hat{h}_S(k)j_0(-k\ell_\alpha)j_0(k\ell_\beta) - \left[\hat{h}_\Delta(k) + 2\bar{h}_D(k)\right]j_1(-k\ell_\alpha)j_1(k\ell_\beta) \tag{11.5.29}$$

The functions $\hat{h}_{\alpha\alpha}(k)$, $\hat{h}_{\beta\alpha}(k)$ and $\hat{h}_{\beta\beta}(k)$ can be expressed in a similar way. If we now expand the Bessel functions to order k^2, the result obtained for the Fourier transform of the function $\Delta h(r)$ in (11.3.8) is

$$\Delta\hat{h}(k) = \frac{k^2L^2}{9}\left[\hat{h}_\Delta(0) + 2\bar{h}_D(0)\right] + \mathcal{O}(k^4) \tag{11.5.30}$$

or, from (11.5.9b) and (11.5.21):

$$\Delta h^{(2)} = \frac{L^2}{9\rho}\left(\frac{\varepsilon - 1}{y\varepsilon} - 3\right) \tag{11.5.31}$$

where $\Delta h^{(2)}$ is the coefficient introduced in (11.3.10). Equation (11.5.31) expresses the dielectric constant as a combination of integrals involving only the site–site distribution functions and may be rewritten as

$$\sum_\alpha \sum_\beta q_\alpha q_\beta h^{(2)}_{\alpha\beta} = \frac{\mu^2}{9\rho}\left(\frac{\varepsilon - 1}{y\varepsilon} - 3\right) \tag{11.5.32}$$

where q_α is the charge on site α. The result in this form is not limited to diatomics: it applies to any interaction-site molecule.[23]

It is clear from (11.5.18) that $\hat{h}_\Delta(0)$ is related to the angular correlation parameter (11.3.10) by $G_1 = \frac{1}{3}\rho\hat{h}_\Delta(0)$. This is true whether or not the molecule has a dipole moment, but the analysis that leads to (11.3.10) is valid only in the non-polar case. The difference between polar and non-polar molecules lies in the long-range function $h_D(R)$. The significance of $h_D(R)$ can be seen in the fact that whereas $\hat{h}_\Delta(0)$ contributes equally to the longitudinal and transverse components of the long-wavelength susceptibility $\boldsymbol{\chi}(\mathbf{k}, 0)$, $\bar{h}_D(0)$ does not. The effect of long-range correlations can therefore be suppressed by setting $\bar{h}_D(0) = 0$ in (11.5.30), which then reduces to (11.3.10).

11.6 INTEGRAL-EQUATION APPROXIMATIONS FOR DIPOLAR HARD SPHERES

The expansion of $h(1, 2)$ or $c(1, 2)$ in terms of S, $\Delta(1, 2)$ and $D(1, 2)$ was first exploited by Wertheim[13] in obtaining the analytic solution to the MSA (mean spherical approximation) for dipolar hard spheres. Although the MSA is not a quantitatively satisfactory theory, Wertheim's methods have had a considerable influence on later work on simple models of polar fluids.

The groundwork for the solution has already been laid in Section 11.4. The next stage in the calculation consists in substituting for $\hat{h}(1, 2)$ and $\hat{c}(1, 2)$ in the Ornstein–Zernike relation (11.4.8), integrating over angles with the help of Table 11.1, and equating coefficients of S, Δ and D_k on the two sides of the equation. The terms in S separate from those in Δ

and D_k to give

$$\hat{h}_S(k) = \hat{c}_S(k) + \rho\hat{c}_S(k)\hat{h}_S(k) \tag{11.6.1a}$$

$$\hat{h}_\Delta(k) = \hat{c}_\Delta(k) + \tfrac{1}{3}\rho\big[\hat{c}_\Delta(k)\hat{h}_\Delta(k) + 2\bar{c}_D(k)\bar{h}_D(k)\big] \tag{11.6.1b}$$

$$\bar{h}_D(k) = \bar{c}_D(k) + \tfrac{1}{3}\rho\big[\bar{c}_D(k)\bar{h}_D(k) + \bar{c}_D(k)\hat{h}_\Delta(k) + \hat{c}_\Delta(k)\bar{h}_D(k)\big] \tag{11.6.1c}$$

The Hankel transforms in these equations are the Fourier transforms of the short-range functions $h_D^0(R)$ and $c_D^0(R)$; this fact has already been used in the derivation of (11.5.25). The inverse Fourier transforms of $\hat{h}_S(k)$, $\hat{h}_\Delta(k)$ and $\bar{h}_D(k)$ can therefore all be written in terms of spatial convolution integrals (denoted by the symbol $\otimes$):

$$h_S(R) = c_S(R) + \rho c_S \otimes h_S \tag{11.6.2a}$$

$$h_\Delta(R) = c_\Delta(R) + \tfrac{1}{3}\rho\big(c_\Delta \otimes h_\Delta + 2c_D^0 \otimes h_D^0\big) \tag{11.6.2b}$$

$$h_D(R) = c_D(R) + \tfrac{1}{3}\rho\big(c_D^0 \otimes h_D^0 + c_D^0 \otimes h_\Delta + c_\Delta \otimes h_D^0\big) \tag{11.6.2c}$$

These equations are to be solved subject to the MSA closure relations (4.5.2). For dipolar hard spheres, (4.5.2) becomes

$$h(1,2) = -1, \quad R < d; \qquad c(1,2) = \frac{\beta\mu^2 D(1,2)}{R^3}, \quad R > d \tag{11.6.3}$$

or, equivalently:

$$\begin{aligned} h_S(R) &= -1, \quad R < d; \qquad & h_\Delta(R) = h_D(R) &= 0, \quad R < d \\ c_D(R) &= \frac{\beta\mu^2}{R^3}, \quad R > d; \qquad & c_S(R) = c_\Delta(R) &= 0, \quad R > d \end{aligned} \tag{11.6.4}$$

It is clear from (11.6.2a) and (11.6.4) that within the MSA the functions $h_S(R)$ and $c_S(R)$ are simply the solution to the PY equation for non-polar hard spheres: the dipolar interaction has no effect on the distribution of molecular centres. The closure relations involving the projections $h_D(R)$ and $c_D(R)$ can also be written as

$$h_D^0(R) = -3K, \quad R < d; \qquad c_D^0(R) = 0, \quad R > d \tag{11.6.5}$$

where K is the dimensionless parameter defined as

$$K = \int_d^\infty \frac{h_D(R)}{R}\,\mathrm{d}R \tag{11.6.6}$$

We now look for a linear combination of functions that causes (11.6.2b) and (11.6.2c) to become decoupled. Direct substitution shows that this is achieved by taking

$$\begin{aligned} h_+(R) &= \frac{1}{3K}\big[h_D^0(R) + \tfrac{1}{2}h_\Delta(R)\big] \\ h_-(R) &= \frac{1}{3K}\big[h_D^0(R) - h_\Delta(R)\big] \end{aligned} \tag{11.6.7}$$

with analogous expressions for $c_+(R)$ and $c_-(R)$. The new functions satisfy the equations

$$\begin{aligned} h_+(R) &= c_+(R) + 2K\rho c_+ \otimes h_+ \\ h_-(R) &= c_-(R) - K\rho c_- \otimes h_- \end{aligned} \tag{11.6.8}$$

Equations (11.6.8) are to be solved subject to the closure relations $h_+(R) = h_-(R) = -1$, $R < d$ (this is why the factor $1/3K$ is included in (11.6.7)) and $c_+(R) = c_-(R) = 0$, $R > d$.

The original problem has now been greatly simplified. The effect of decoupling the different projections, first in (11.6.2) and then in (11.6.8), means that the Ornstein–Zernike relation has been reduced to three independent equations, namely (11.6.2a) and (11.6.8). These equations, with their corresponding closure relations, are just the Percus–Yevick approximation for hard spheres at densities equal, respectively, to ρ, $2K\rho$ and $-K\rho$. The fact that one solution is required at a negative density poses no special difficulty.

To complete the analytical solution it is necessary to relate the quantity K to hard-sphere properties. Given the analogue of (11.4.16) for $c_D(R)$, the closure relation (11.6.5) requires that

$$c_D(R) = -\frac{3}{R^3}\int_0^d c_D^0(R')R'^2\,\mathrm{d}R', \quad R > d \tag{11.6.9}$$

Because $c_D^0(R)$ vanishes for $R > d$, comparison of (11.6.4) with (11.6.9) shows that

$$\beta\mu^2 = -3\int_0^d c_D^0(R)R^2\,\mathrm{d}R = -\frac{3}{4\pi}\bar{c}_D(0) \tag{11.6.10}$$

The function $c_D^0(R)$ may be written as

$$\begin{aligned} c_D^0(R) &= K\big[c_+(R) + c_-(R)\big] \\ &= K\big[2c_{\mathrm{PY}}(R;\,2K\rho) + c_{\mathrm{PY}}(R;\,-K\rho)\big] \end{aligned} \tag{11.6.11}$$

where $c_{\mathrm{PY}}(R;\,\rho)$ is the PY hard-sphere direct correlation function at a density ρ. Let $Q(\eta) = \beta(\partial P/\partial\rho)_T$ be the PY approximation to the inverse compressibility of the hard-sphere fluid at a packing fraction η. Integrals over $c_{\mathrm{PY}}(R;\,\rho)$ can be related to $Q(\eta)$ via the general expression (3.8.8) and the approximate result (4.4.12). A short calculation shows that

$$Q(\eta) = 1 - 4\pi\rho\int_0^d c_{\mathrm{PY}}(R;\,\rho)R^2\,\mathrm{d}R = \frac{(1+2\eta)^2}{(1-\eta)^4} \tag{11.6.12}$$

On combining the last three equations we find that

$$\beta\mu^2 = -3K\int_0^d \left[2c_{\mathrm{PY}}(R;\,2K\rho) + c_{\mathrm{PY}}(R;\,-K\rho)\right]R^2\,\mathrm{d}R$$
$$= \frac{3}{4\pi\rho}\left[Q(2K\eta) - Q(-K\eta)\right] \tag{11.6.13}$$

or

$$3y = Q(2K\eta) - Q(-K\eta) \tag{11.6.14}$$

where y is the parameter defined by (11.5.16). Equations (11.6.12) and (11.6.14) determine K implicitly for given choices of y and η; as y varies from 0 to ∞, $K\eta$ varies from 0 to $\frac{1}{2}$.

As an alternative to (11.6.12) we can write

$$\frac{1}{Q(\eta)} = 1 + 4\pi\rho\int_0^\infty h_{\mathrm{PY}}(R;\,\rho)R^2\,\mathrm{d}R \tag{11.6.15}$$

whence, from (11.6.7):

$$\rho\hat{h}_{\Delta}(0) = 8\pi\rho K\int_0^\infty \left[h_+(R) - h_-(R)\right]R^2\,\mathrm{d}R$$
$$= 8\pi\rho K\int_0^\infty \left[h_{\mathrm{PY}}(R;\,2K\rho) - h_{\mathrm{PY}}(R;\,-K\rho)\right]R^2\,\mathrm{d}R$$
$$= \frac{1}{Q(2K\eta)} + \frac{2}{Q(-K\eta)} - 3 \tag{11.6.16}$$

Taken together, (11.5.15), (11.6.14) and (11.6.16) lead to a remarkably simple expression for the dielectric constant:

$$\varepsilon = \frac{Q(2K\eta)}{Q(-K\eta)} \tag{11.6.17}$$

The same result is obtained if (11.5.24) is used instead of (11.5.15).

Although the method of solution is very elegant, comparison with the results of Monte Carlo calculations shows that the MSA does not provide a quantitatively acceptable description of the properties of the dipolar hard-sphere fluid. As is evident from comparison of (11.6.14) with (11.6.17), the dielectric constant in the MSA is dependent only on the parameter y and not separately on the two independent parameters $\rho^* = \rho d^3$ and $\mu^{*2} = \beta\mu^2/d^3$ required to specify the thermodynamic state of the system. When both these variables are large (for liquid water, $\mu^{*2} \approx 3$), use of the MSA gives values of ε that are much too small, as shown by the results in Figure 11.5.

The analytical solution to the MSA has also been found for dipolar hard-sphere mixtures[25] and for dipolar hard spheres with a Yukawa tail.[26] The numerical results obtained for dipolar mixtures show again that the MSA seriously underestimates the dielectric constant. Addition of a Yukawa term to the pair potential leads to changes in thermodynamic properties, but the dielectric constant remains the same.

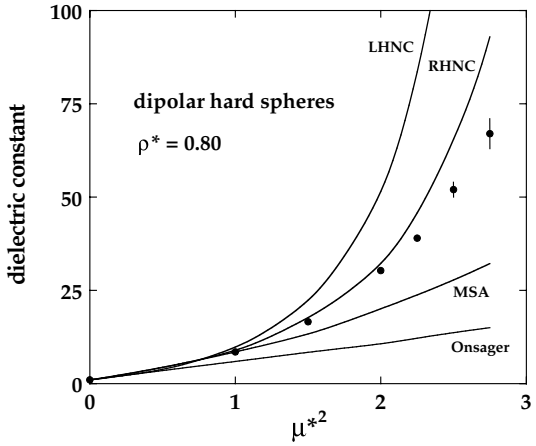

FIG. 11.5. Dielectric constant of the dipolar hard-sphere fluid at $\rho d^3 = 0.80$ as a function of $\mu^{*2} = \beta\mu^2/d^3$, showing a comparison between Monte Carlo results[24] (points) and the predictions of theories discussed in the text (curves). After Stell *et al.*[14]

Of the developments inspired by Wertheim's work on the MSA the simplest to implement is the "linearised HNC" or LHNC approximation of Patey and coworkers.[27] The LHNC approximation is equivalent to one proposed earlier by Wertheim himself and called by him the "single-superchain" approximation.[28] In the case of dipolar hard spheres the LHNC approximation resembles the MSA in basing itself on expansions of $h(1,2)$ and $c(1,2)$ limited to the terms in S, $\Delta(1,2)$ and $D(1,2)$, but improves on it by employing a closure relation that is applicable to other simple models of polar liquids, such as the Stockmayer fluid. As the name suggests, the LHNC closure corresponds to a linearisation of the HNC approximation, which in its general form is

$$c(1,2) = h(1,2) - \ln g(1,2) - \beta v(1,2) \tag{11.6.18}$$

The LHNC closure is obtained by substituting for $h(1,2)$ and $c(1,2)$ from (11.4.3) and (11.4.7) and linearising with respect to the functions Δ and D. The result is

$$\begin{aligned} c(1,2) = {} & h_S(R) - \ln g_S(R) - \beta v_0(R) + h_\Delta(R)\big[1 - 1/g_S(R)\big]\Delta(1,2) \\ & + \big(h_D(R)\big[1 - 1/g_S(R)\big] + \beta\mu^2/R^3\big)D(1,2) \end{aligned} \tag{11.6.19}$$

where $g_S(R) = h_S(R) + 1$. When $v_0(R)$ is the hard-sphere potential, (11.6.19) reduces to the MSA closure if the substitution $g_S(R) = 1$ for $R > d$ is made; the MSA may therefore be regarded as the low-density limit of the LHNC approximation.

The linearisation involved in (11.6.19) means that the closure relation involves only the harmonics S, Δ and D. This is consistent with the assumed form of $h(1,2)$ and $c(1,2)$ and the results in (11.6.2) remain valid. In other words, the relation between $h_S(R)$ and $c_S(R)$ remains independent of the other projections, and the results for these two functions are just the solutions to the HNC equation for the potential $v_0(R)$. In contrast to the MSA,

however, the projections on Δ and D are influenced by the projections on S through the appearance of $g_S(R)$ in the closure relations for $c_\Delta(R)$ and $c_D(R)$.

The method of solution of the LHNC equations for the problem of dipolar hard spheres parallels that used for the MSA up to the point at which the linear combinations (11.6.7) are introduced. In the LHNC approximation the functions $h_+(R)$, $c_+(R)$ remain coupled to $h_-(R)$, $c_-(R)$ through the closure relations; the solution must therefore be completed numerically. Some results for the projections $h_\Delta(R)$ and $h_D(R)$ are compared with those obtained by the Monte Carlo method in Figure 11.4. The general agreement between theory and simulation is fair and improves markedly as the value of the parameter μ^* is reduced. However, in contrast to the MSA, the calculated values of the dielectric constant are now everywhere too large, as is evident from Figure 11.5, and the discrepancy between theory and simulation increases rapidly with μ^*. The LHNC approximation has also been applied to systems of quadrupolar hard spheres and to fluids of hard spheres carrying both dipoles and quadrupoles.[27(b,d)] The calculations are more complicated than in the purely dipolar case because the pair potentials contain additional harmonics and still more are generated by the angular convolutions in the Ornstein–Zernike relation. The results for the mixed, dipolar–quadrupolar system are of particular interest for the light they throw on the way in which the quadrupolar interaction modifies the dipolar correlations in the fluid. The effect on the projection $h_\Delta(R)$ is particularly striking. In the purely dipolar case, when both ρ^* and μ^* are large, $h_\Delta(R)$ is positive nearly everywhere, and significantly different from zero out to values of R corresponding to ten or more molecular diameters. Since ε is determined by the integral of $R^2 h_\Delta(R)$ over all R (see (11.5.18)), these effects combine to give very large values for the dielectric constant. The addition of even a small quadrupole moment leads to a marked falling off in both the magnitude and range of $h_\Delta(R)$; ε therefore decreases rapidly as the quadrupole moment is increased. This could have been anticipated from the discussion in Section 11.3, since Δ is zero for the ideal T-shaped configurations favoured by the quadrupolar interaction.

The LHNC approximation for dipolar hard spheres resembles the MSA to the extent that the function $g_S(R)$ is the pair distribution function of the underlying hard-sphere system, and is therefore independent of the strength of the dipole–dipole interaction. This unrealistic feature disappears when the expansion of the HNC closure relation is taken to second order, since $h_S(R)$ and $c_S(R)$ can no longer be decoupled from the other projections. In other respects, the results are not always an improvement on those of the linearised version, and the theory becomes computationally more awkward to implement. Rather than pursuing the expansion to higher orders, it seems preferable to return to the full HNC closure (11.6.18) or its "reference" (RHNC) modification.[15,29] The molecular generalisation of the RHNC closure (4.7.1) is

$$\ln g(1,2) = -\beta\big[v(1,2) - k_\mathrm{B}T d_0(1,2)\big] + h(1,2) - c(1,2) \tag{11.6.20}$$

where $d_0(1,2)$ is the bridge function of some anisotropic reference system. In the case of dipolar hard spheres, however, hard spheres are the obvious choice of reference system. Because the closure relation couples together all harmonic components of $h(1,2)$ and $c(1,2)$, the results obtained depend on the number of harmonics retained when expanding the pair functions, but essentially complete convergence is achieved with a basis set of easily manageable size. Some results for $h_\Delta(R)$ and $h_D(R)$ are shown in Figure 11.4. The theoretical

curves lie systematically below those given by the LHNC approximation; the dielectric constant is therefore much reduced and the agreement with simulations correspondingly improved, as Figure 11.5 confirms.

It is known experimentally that the Kirkwood g-factors of many non-associating polar liquids are close to unity, and the very large discrepancies seen in Figure 11.5 between the Monte Carlo results and the predictions of the Onsager approximation (for which $g_K = 1$) show that the dipolar hard-sphere model gives dielectric constants that are unrealistically large.[30] The role played by quadrupolar forces provides a possible explanation of the experimental facts, but a more realistic model of a polar fluid must also make allowance for the inevitable anisotropy in the short-range, repulsive forces. The simplest such model consists of a hard, homonuclear diatomic with a dipole moment superimposed at the mid-point between the two spheres. Within the RHNC approximation the natural choice of reference system is now the underlying hard-dumbbell fluid, the bridge function of which can be calculated from the molecular version of the PY approximation.[31] The same general approach can be used for heteronuclear molecules having either soft or hard cores. Some good results have been achieved in this way, though a strong empirical element is often involved both in the choice of reference system and in the form of closure relation used to calculate the corresponding bridge function.[32]

11.7 INTERACTION-SITE DIAGRAMS

The diagrammatic expansions of $c(1,2)$, $h(1,2)$ and $y(1,2)$ given in Chapters 3 and 4 are also applicable to molecular fluids if certain minor changes in interpretation are made. First, the circles in a "molecular" diagram are associated with both the translational and orientational coordinates of a molecule and the black circles imply integrations over both sets of coordinates. Secondly, black circles carry a weight factor equal to $1/\Omega$, where Ω is defined by (11.1.3). As an illustration of these rules, the diagram

which appears at order ρ in the ρ-circle, f-bond expansion of $h(1,2)$ (see (4.6.2)) now represents the integral

$$\frac{\rho}{\Omega}\iint f(\mathbf{R}_{13}, \boldsymbol{\Omega}_1, \boldsymbol{\Omega}_3) f(\mathbf{R}_{23}, \boldsymbol{\Omega}_2, \boldsymbol{\Omega}_3)\, \mathrm{d}\mathbf{R}_3\, \mathrm{d}\boldsymbol{\Omega}_3$$

and is therefore much more complicated to evaluate than in the atomic case.

The diagrammatic expansion of $h(1,2)$ is not immediately useful in cases where the focus of interest is the set of site–site distribution functions $h_{\alpha\beta}(r)$ rather than $h(1,2)$. Ladanyi and Chandler[33] have shown how the diagrammatic approach can be adapted to the needs of such a situation and this section is devoted to a brief review of their results.

We give only a simplified treatment, restricting the detailed discussion to the case of rigid, diatomic (or two-site) molecules. The generalisation to larger numbers of interaction sites is straightforward, but requires a more complex notation.

The first step is to rewrite the molecular Mayer function $f(1,2)$ as a product of interaction-site Mayer functions $f_{\alpha\beta}(r)$:

$$\begin{aligned} f(1,2) = \exp\bigl[-\beta v(1,2)\bigr] - 1 &= \exp\biggl(-\beta \sum_{\alpha}\sum_{\beta} v_{\alpha\beta}\bigl(|\mathbf{r}_{2\beta} - \mathbf{r}_{1\alpha}|\bigr)\biggr) - 1 \\ &= -1 + \prod_{\alpha,\beta}\bigl[f_{\alpha\beta}\bigl(|\mathbf{r}_{2\beta} - \mathbf{r}_{1\alpha}|\bigr) + 1\bigr] \end{aligned} \tag{11.7.1}$$

The subscripts α, β run over all interaction sites in the molecule; if there are two sites per molecule, the right-hand side of (11.7.1) consists of 15 separate terms. Equation (11.7.1) can be used to rewrite the integrals occurring in the density expansion of $h(1,2)$. As the simplest possible example, consider the low-density limit of $h(1,2)$, namely $\lim_{\rho\to 0} h(1,2) = f(1,2)$. The corresponding approximation to, say, $h_{\alpha\alpha}(\mathbf{r},\mathbf{r}')$ is

$$\lim_{\rho\to 0} h_{\alpha\alpha}(\mathbf{r},\mathbf{r}') = \iint f(1,2)\delta(\mathbf{r}_{1\alpha} - \mathbf{r})\delta(\mathbf{r}_{2\alpha} - \mathbf{r}')\,\mathrm{d}1\,\mathrm{d}2 \tag{11.7.2}$$

When $f(1,2)$ is replaced by (11.7.1), (11.7.2) becomes

$$\begin{aligned} \lim_{\rho\to 0} h_{\alpha\alpha}(\mathbf{r},\mathbf{r}') = f_{\alpha\alpha}\bigl(|\mathbf{r}' - \mathbf{r}|\bigr) &+ \bigl[1 + f_{\alpha\alpha}\bigl(|\mathbf{r}' - \mathbf{r}|\bigr)\bigr] \\ &\times \iint \bigl[f_{\alpha\beta}\bigl(|\mathbf{r}_{2\beta} - \mathbf{r}_{1\alpha}|\bigr) + \text{six other terms}\bigr] \\ &\times \delta(\mathbf{r}_{1\alpha} - \mathbf{r})\delta(\mathbf{r}_{2\alpha} - \mathbf{r}')\,\mathrm{d}1\,\mathrm{d}2 \end{aligned} \tag{11.7.3}$$

The integrals appearing on the right-hand side of (11.7.3) can be re-expressed in terms of an intramolecular site–site distribution function $s_{\alpha\beta}(\mathbf{x}-\mathbf{y})$ defined as

$$\begin{aligned} s_{\alpha\beta}(\mathbf{x}-\mathbf{y}) &= (1-\delta_{\alpha\beta}) \int \delta(\mathbf{R}_1 + \mathbf{u}_1\ell_\alpha - \mathbf{x})\delta(\mathbf{R}_1 - \mathbf{u}_1\ell_\beta - \mathbf{y})\,\mathrm{d}1 \\ &= (1-\delta_{\alpha\beta})\bigl\langle \delta(\mathbf{x}-\mathbf{y}-\mathbf{u}_1 L)\bigr\rangle_{\boldsymbol{\Omega}_1} \\ &= \frac{(1-\delta_{\alpha\beta})}{4\pi L^2}\delta\bigl(|\mathbf{x}-\mathbf{y}| - L\bigr) \end{aligned} \tag{11.7.4}$$

where ℓ_α, ℓ_β and $\mathbf{u}_1$ have the same meaning as in (11.5.26) and $L = \ell_\alpha + \ell_\beta$. The function $s_{\alpha\beta}(\mathbf{r})$ is the probability density for finding site β of a molecule at a position $\mathbf{r}$, given that site α of the same molecule is at the origin. The definition (11.7.4) satisfies the obvious conditions that the interpretation as an intramolecular distribution function requires, i.e.

$s_{\alpha\beta}(\mathbf{r}) = s_{\beta\alpha}(\mathbf{r})$, $\mathbf{s}_{\alpha\alpha}(\mathbf{r}) = 0$ and $\int s_{\alpha\beta}(\mathbf{r})\,\mathrm{d}\mathbf{r} = 1$, $\alpha \neq \beta$. The integral shown explicitly in (11.7.3) can now be transformed as follows:

$$\begin{aligned}
&\iint \delta(\mathbf{r}_{1\alpha} - \mathbf{r})\delta(\mathbf{r}_{2\alpha} - \mathbf{r}')\, f_{\alpha\beta}\big(|\mathbf{r}_{2\beta} - \mathbf{r}_{1\alpha}|\big)\,\mathrm{d}1\,\mathrm{d}2 \\
&\quad = \int \mathrm{d}\mathbf{x} \iint \delta(\mathbf{r}_{1\alpha} - \mathbf{r})\delta(\mathbf{r}_{2\alpha} - \mathbf{r}')\, f_{\alpha\beta}(\mathbf{r}_{1\alpha} - \mathbf{x})\delta(\mathbf{r}_{2\beta} - \mathbf{x})\,\mathrm{d}1\,\mathrm{d}2 \\
&\quad = \int \mathrm{d}1\,\delta(\mathbf{r}_{1\alpha} - \mathbf{r}) \int \mathrm{d}\mathbf{x}\, f_{\alpha\beta}(\mathbf{r}_{1\alpha} - \mathbf{x}) \int \mathrm{d}2\,\delta(\mathbf{r}_{2\alpha} - \mathbf{r}')\delta(\mathbf{r}_{2\beta} - \mathbf{x}) \\
&\quad = \int f_{\alpha\beta}\big(|\mathbf{r} - \mathbf{x}|\big) s_{\alpha\beta}(\mathbf{x} - \mathbf{r}')\,\mathrm{d}\mathbf{x} \qquad (11.7.5)
\end{aligned}$$

All other integrals in (11.7.3) may be treated in the same way and each can then be represented by an *interaction-site diagram*. The circles (white or black) of an interaction-site diagram are associated with the coordinates of interaction sites and the bonds, in the two-site case, represent components of the 2×2 matrices $\boldsymbol{f}$ and $\boldsymbol{s}$ formed by the functions $\{f_{\alpha\beta}\}$ and $\{s_{\alpha\beta}\}$, respectively. The symmetry number and value of an interaction-site diagram are defined as in the atomic case (see Section 3.7), except that black circles imply a summation over all sites in the molecule in addition to integration over site coordinates. For example, if we denote an $\boldsymbol{f}$-bond by a solid line and an $\boldsymbol{s}$-bond by a broken line, the diagrammatic representation of the sum of integrals in (11.7.3) is

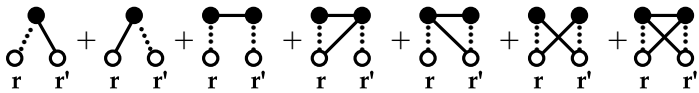

The diagrams shown all have a symmetry number of one. They are of zeroth order in density, since they arise from a molecular diagram – their "molecular origin" – that represents the low-density limit of $h(1, 2)$. Thus all circles, white or black, are 1-circles. The order in density of any interaction-site diagram in the expansion of a site–site pair correlation function is equal to the number of black circles in its molecular origin, which in turn is equal to the number of black circles in the interaction-site diagram minus the number of $\boldsymbol{s}$-bonds.

The procedure outlined above can be applied to each of the integrals appearing in the density expansion of $h(1, 2)$. This yields an expansion of any of the functions $h_{\alpha\beta}(\mathbf{r})$ in terms of interaction-site diagrams. As the example (11.7.3) demonstrates, each molecular diagram is replaced by a large number of interaction-site diagrams, but the interaction-site diagrams are mathematically simpler objects because all reference to orientational coordinates has disappeared. (Note that the black circles no longer carry the weight factor Ω^{-1} associated with the black circles of a molecular diagram.)

The topology of allowed interaction-site diagrams is restricted in certain ways. Diagrams must be simple and connected; white circles must not be connected by an $\boldsymbol{s}$-bond (because different white circles always refer to different molecules); all black circles must be intersected by at least one $\boldsymbol{f}$-bond (otherwise they contribute nothing to the intermolecular

correlations); no circle may be intersected by more than one $\boldsymbol{s}$-bond (for reasons to be explained below); and diagrams must be free of articulation circles and articulation $\boldsymbol{s}$-bonds, i.e. $\boldsymbol{s}$-bonds whose removal causes the diagram to separate into two or more components of which at least one contains no white circle. The last restriction is imposed because any such diagram would have as its molecular origin a diagram containing one or more articulation circles; as we showed in Chapters 3 and 4, the expansions of the pair functions of interest here consist entirely of irreducible diagrams.

Given the restrictions listed above, the site–site pair correlation functions may be characterised as follows:

$$h_{\alpha\beta}(\mathbf{r}_{1\alpha}, \mathbf{r}_{2\beta}) = \big[\text{all interaction-site diagrams consisting of two white 1-circles labelled } 1\alpha \text{ and } 2\beta\text{, black 1-circles, } \boldsymbol{f}\text{-bonds and } \boldsymbol{s}\text{-bonds, each diagram to be multiplied by } \rho^n\text{, where } n \text{ is the number of black circles minus the number of } \boldsymbol{s}\text{-bonds}\big] \tag{11.7.6}$$

The generalisation of this result to molecules with more than two interaction sites requires the introduction of three-body and higher-order intramolecular distribution functions. It remains true, however, that no circle may be intersected by more than one $\boldsymbol{s}$-bond or, indeed, by more than one intramolecular bond of any order. Consider the diagram shown in (a) below. For a two-site molecule such a diagram is physically meaningless, because one site is bonded to two others. But it is also not an allowed diagram even for a three-site (or larger) molecule, because the three black circles would then be linked, as in (b), by a single bond or "face", representing a three-body intramolecular distribution function.

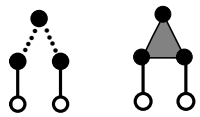

(a) (b)

The diagrammatic formalism can be extended to flexible molecules, but in that case the intramolecular distribution functions become statistically averaged quantities.

11.8 INTERACTION-SITE MODELS: THE RISM EQUATIONS

We saw in Section 11.3 that the static structure factors measured in neutron and x-ray scattering experiments on molecular liquids are weighted sums of atomic pair distribution functions. In this section we describe an integral-equation theory that has been widely used in the interpretation of diffraction experiments and, more generally, in the calculation of site–site distribution functions for interaction-site potential models: this is the "reference interaction-site model" or RISM approximation of Andersen and Chandler.[34] The theory

has been applied with particular success in calculations for model fluids composed of hard molecules. From experience with atomic systems we can expect the structure of simple molecular liquids to be dominated by the strongly repulsive part of the pair potential, and an obvious way represent to the short-range repulsions is through an interaction-site model consisting of fused hard spheres.

The key ingredient of the RISM approximation is an Ornstein–Zernike-like relation between the site–site pair correlation functions $h_{\alpha\beta}(r)$ and a set of direct correlation functions $c_{\alpha\beta}(r)$. In the atomic case the meaning of the Ornstein–Zernike relation is that the total correlation between particles 1 and 2 is the sum of all possible paths of direct correlations that propagate via intermediate particles 3, 4, ... etc. The same, intuitive idea can be applied to site-site correlations, but allowance must now be made for the fact that correlations also propagate via the intramolecular distribution functions. Hence, whereas in an atomic fluid $h(1,2)$ is given diagrammatically by the sum of all simple chains consisting of c-bonds, $h_{\alpha\beta}(r)$ consists of all simple chains formed from $\boldsymbol{c}$-bonds and $\boldsymbol{s}$-bonds. We make this idea precise by writing $h_{\alpha\beta}(r)$ as a sum of interaction-site diagrams in the form

$h_{\alpha\beta}(\mathbf{r}_{1\alpha}, \mathbf{r}_{2\beta}) =$ [all interaction-site chain diagrams consisting of two white terminal 1-circles labelled 1α and 2β, black 1-circles, at least one $\boldsymbol{c}$-bond, and $\boldsymbol{s}$-bonds, each diagram to be multiplied by ρ^{n-1}, where n is the number of $\boldsymbol{c}$-bonds]

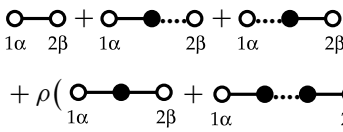

(11.8.1)

where a full line denotes a $\boldsymbol{c}$-bond and a broken line denotes an $\boldsymbol{s}$-bond. We recall that within the diagrammatic formalism a black circle implies a summation over all sites in the molecule. Thus, for example, the value of the third diagram on the right-hand side of (11.8.1) is

$$\sum_{\gamma} \int s_{\alpha\gamma}(\mathbf{r}_{1\gamma} - \mathbf{r}_{1\alpha}) c_{\gamma\beta}\big(|\mathbf{r}_{2\beta} - \mathbf{r}_{1\gamma}|\big)\, \mathrm{d}\mathbf{r}_{1\gamma}$$

The term for which $\alpha = \gamma$ contributes nothing to the sum because the intramolecular distribution function is zero when the two sites are the same.

We now have to sum the chain diagrams in (11.8.1). To do so, we use the same techniques as in Section 5.5, because the diagrams have the same topology as those in the diagrammatic expansion (5.5.16) of the renormalised potential $C(1,2)$. We define a matrix of functions $\boldsymbol{\omega}(r)$ by

$$\omega_{\alpha\beta}\big(|\mathbf{r}_{1\beta} - \mathbf{r}_{1\alpha}|\big) = \delta_{\alpha\beta}\delta(\mathbf{r}) + s_{\alpha\beta}(\mathbf{r}) \tag{11.8.2}$$

and represent $\omega_{\alpha\beta}(|\mathbf{r}_{1\beta} - \mathbf{r}_{1\alpha}|)$ by the hypervertex

Then the sum of all chain diagrams with n $\boldsymbol{c}$-bonds becomes a single diagram consisting of $(n+1)$ $\boldsymbol{\omega}$-hypervertices and n $\boldsymbol{c}$-bonds. For example:

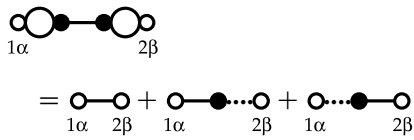

$$= \sum_{\gamma}\sum_{\delta} \iint \omega_{\alpha\gamma}\big(|\mathbf{r}_{1\alpha} - \mathbf{r}_{1\gamma}|\big) c_{\gamma\delta}\big(|\mathbf{r}_{1\gamma} - \mathbf{r}_{2\delta}|\big) \omega_{\delta\beta}\big(|\mathbf{r}_{2\delta} - \mathbf{r}_{2\beta}|\big)\, \mathrm{d}\mathbf{r}_{1\gamma}\, \mathrm{d}\mathbf{r}_{2\delta} \tag{11.8.3}$$

A hypervertex corresponds to a single molecule and incorporates all the intramolecular constraints represented by the $\boldsymbol{s}$-bonds. The Fourier transform of (11.8.3) is the $\alpha\beta$-component of the matrix $\hat{\boldsymbol{\omega}}(k) \cdot \hat{\boldsymbol{c}}(k) \cdot \hat{\boldsymbol{\omega}}(k)$, i.e.

$$\sum_{\gamma}\sum_{\delta} \hat{\omega}_{\alpha\gamma}(k)\hat{c}_{\gamma\delta}(k)\hat{\omega}_{\delta\beta}(k) = (\hat{\boldsymbol{\omega}}\hat{\boldsymbol{c}}\hat{\boldsymbol{\omega}})_{\alpha\beta} \tag{11.8.4}$$

The components of the matrix $\hat{\boldsymbol{\omega}}(k)$ are

$$\hat{\omega}_{\alpha\beta}(k) = \delta_{\alpha\beta} + (1 - \delta_{\alpha\beta}) j_0(kL_{\alpha\beta}) \tag{11.8.5}$$

where $L_{\alpha\beta}$ is the intramolecular separation of sites α, β. Similarly, the Fourier transform of the sum of all chain diagrams containing precisely n $\boldsymbol{c}$-bonds is $\rho^{n-1}((\hat{\boldsymbol{\omega}}\hat{\boldsymbol{c}})^n\hat{\boldsymbol{\omega}})_{\alpha\beta}$ (cf. (5.5.22)), and $\hat{h}_{\alpha\beta}(k)$ is the sum of a geometric series (cf. (5.5.23)). The matrix $\hat{\boldsymbol{h}}(k)$ is therefore given by

$$\hat{\boldsymbol{h}}(k) = \hat{\boldsymbol{\omega}}(k) \cdot \hat{\boldsymbol{c}}(k) \cdot \big[\boldsymbol{I} - \rho\hat{\boldsymbol{\omega}}(k) \cdot \hat{\boldsymbol{c}}(k)\big]^{-1} \cdot \hat{\boldsymbol{\omega}}(k) \tag{11.8.6a}$$

or

$$\hat{\boldsymbol{h}}(k) = \hat{\boldsymbol{\omega}}(k) \cdot \hat{\boldsymbol{c}}(k) \cdot \hat{\boldsymbol{\omega}}(k) + \rho\hat{\boldsymbol{\omega}}(k) \cdot \hat{\boldsymbol{c}}(k) \cdot \hat{\boldsymbol{h}}(k) \tag{11.8.6b}$$

Equation (11.8.6) is the Ornstein–Zernike-like relation. It can be derived in other ways than the one we have described, but the diagrammatic method[35] has a strong intuitive appeal. We shall refer to it as the RISM-OZ relation, though we shall see later that its status differs from that of the molecular Ornstein–Zernike relation (11.1.4). If $\boldsymbol{\omega}$ is the identity matrix and ρ is appropriately reinterpreted, it reduces to the Ornstein–Zernike relation for a mixture of atomic fluids.

If the RISM-OZ relation is to be useful, it must be combined with some approximate closure relation. For systems of fused hard spheres the obvious choice is a generalisation of the PY approximation for atomic hard spheres, i.e.

$$h_{\alpha\beta}(r) = -1, \quad r < d_{\alpha\beta}; \qquad c_{\alpha\beta}(r) = 0, \quad r > d_{\alpha\beta} \tag{11.8.7}$$

where $d_{\alpha\beta}$ is the $\alpha - \beta$ hard-sphere diameter. When the site–site potentials are continuous, generalisations of either the PY or HNC approximations can be used. A number of schemes have been devised for numerical solution of the resulting system of equations and calculations have been made for a wide variety of molecular liquids. Figure 11.6 shows the results of RISM calculations based on the PY closure relation for the atomic pair distribution function of a two-site Lennard-Jones model of liquid chlorine. There are some differences in detail, but all the main features seen in molecular-dynamics calculations for the same potential model are well reproduced. Note that the shoulder in the ethylene results of Figure 11.2 appears here as a well-defined subsidiary peak.

The agreement between theory and simulation seen in Figure 11.6 is typical of that achieved for other small, rigid molecules. More surprisingly, a version of the theory[37] known as "polymer" RISM or PRISM has also been applied successfully in studies of the structure of realistic models of polymer melts. Consider a chain molecule consisting of n identical monomers in a linear sequence, each represented by a single interaction site. Then, if the sites are assumed to be geometrically equivalent, the pair functions $h_{\alpha\beta}(r)$ and $c_{\alpha\beta}(r)$ are the same for all α, β and the matrix relation (11.8.6b) reduces to a single, scalar equation:

$$\hat{h}(k) = \widehat{\Omega}(k)\hat{c}(k)\widehat{\Omega}(k) + n\rho\widehat{\Omega}(k)\hat{c}(k)\hat{h}(k) \tag{11.8.8}$$

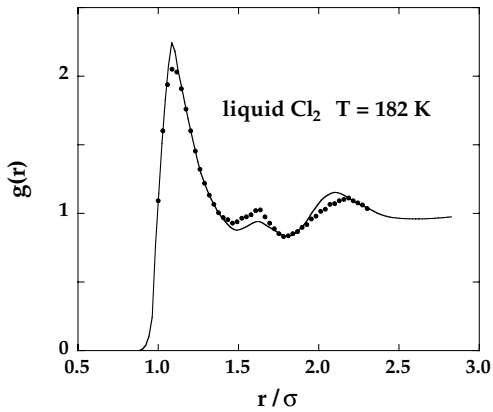

FIG. 11.6. Atom–atom distribution function for a Lennard-Jones diatomic model of liquid chlorine. The points show the results of a molecular-dynamics simulation and the curve is calculated from the RISM approximation with PY closure. After Monson.[36]

where

$$\widehat{\Omega}(k) = \frac{1}{n} \sum_{\alpha} \sum_{\beta} \hat{\omega}_{\alpha\beta}(k) \tag{11.8.9}$$

is the single-chain (or intramolecular) structure factor. This reduction in form is exact for ring polymers, but it is also a good approximation for chains if end-effects can be ignored. In either case it represents a huge simplification of the original problem, even for values of n as small as 10.

When combined with a suitable closure relation, (11.8.8) can be solved numerically to yield the site–site correlation function $h(r)$, provided the single-chain structure factor is known. In principle, intramolecular and intermolecular correlations should be calculated in a self-consistent way.[38] This complication can be avoided by treating the chains as "ideal", meaning that their average conformation is determined only by the connectivity constraints along the chain. The excluded-volume interactions between sites far apart in chemical sequence are assumed to be screened by interactions with surrounding chains.[39] For highly simplified models, such as the freely jointed chain, $\widehat{\Omega}(k)$ can be calculated analytically; for more elaborate models, it can be determined from a single-chain simulation in which the interactions are truncated at some cut-off point along the chain.

11.9 ANGULAR CORRELATIONS AND THE RISM FORMALISM

Although successful in many applications, the RISM formalism suffers from a number of defects. First, it does not lend itself readily to a calculation of the equation of state and the results obtained are thermodynamically inconsistent in the sense of Section 4.4. Secondly, calculated structural properties show an unphysical dependence on the presence of "auxiliary" sites, which are sites that label a point in the molecule but contribute nothing to the intermolecular potential. Thirdly, and most unexpectedly, trivial and incorrect results are obtained for certain quantities descriptive of angular correlations in the fluid.[40] As an example, we show below that the order parameter G_1 defined by (11.1.8) is identically zero for any asymmetric but non-polar diatomic. The only assumption made is that the site–site potentials are short ranged.

We note first that all elements of the matrix $\hat{\boldsymbol{\omega}}(k)$ defined by (11.8.5) are unity when $k = 0$. If we define a matrix $\boldsymbol{Q}$ as

$$\boldsymbol{Q} = \boldsymbol{I} - n^{-1}\hat{\boldsymbol{\omega}}(0) = \begin{pmatrix} \frac{1}{2} & -\frac{1}{2} \\ -\frac{1}{2} & \frac{1}{2} \end{pmatrix} \tag{11.9.1}$$

where n is the number of sites (here equal to two), then

$$\boldsymbol{Q} \cdot \hat{\boldsymbol{\omega}}(0) = \hat{\boldsymbol{\omega}}(0) \cdot \boldsymbol{Q} = 0 \tag{11.9.2}$$

Next we write the RISM-OZ relation (11.8.6b) in the form

$$\hat{\boldsymbol{h}}(k) = \hat{\boldsymbol{\omega}}(k) \cdot \boldsymbol{X}(k) \tag{11.9.3}$$

where

$$\boldsymbol{X}(k) = \hat{\boldsymbol{c}}(k) \cdot \left[\hat{\boldsymbol{\omega}}(k) + \rho\hat{\boldsymbol{h}}(k)\right] \tag{11.9.4}$$

Expanding $\hat{\boldsymbol{\omega}}(k)$ in powers of k, we find to order k^2 that

$$\hat{\boldsymbol{h}}(k) = \left[\hat{\boldsymbol{\omega}}(0) + k^2\boldsymbol{\omega}^{(2)} + \cdots\right] \cdot \boldsymbol{X}(k) \tag{11.9.5}$$

If multiplied on the left by $\boldsymbol{Q}$, (11.9.5) reduces, by virtue of the property (11.9.2), to

$$\boldsymbol{Q} \cdot \hat{\boldsymbol{h}}(k) = \boldsymbol{Q} \cdot \left[k^2\boldsymbol{\omega}^{(2)} + \cdots\right] \cdot \boldsymbol{X}(k) \tag{11.9.6}$$

We now suppose that $\hat{\boldsymbol{h}}(k)$ and $\hat{\boldsymbol{c}}(k)$ (and hence also $\boldsymbol{X}(k)$) have small-k expansions at least up to order k^2. This is plausible, since the site–site potentials are assumed to be short ranged. Then

$$\boldsymbol{Q} \cdot \left[\hat{\boldsymbol{h}}(0) + k^2\boldsymbol{h}^{(2)} + \cdots\right] = \boldsymbol{Q} \cdot \left[k^2\boldsymbol{\omega}^{(2)} + \cdots\right] \cdot \left[\boldsymbol{X}(0) + k^2\boldsymbol{X}^{(2)} + \cdots\right] \tag{11.9.7}$$

and by equating coefficients of k^2 we find that

$$\boldsymbol{Q} \cdot \boldsymbol{h}^{(2)} = \boldsymbol{Q} \cdot \boldsymbol{\omega}^{(2)} \cdot \boldsymbol{X}(0) \tag{11.9.8}$$

We have seen in Section 11.3 that all elements of $\hat{\boldsymbol{h}}(0)$ are the same and related to the compressibility by (11.3.6). Thus $\boldsymbol{X}(0)$ may be written as

$$\boldsymbol{X}(0) = \left[1 + \rho\hat{h}_0(0)\right]\hat{\boldsymbol{c}}(0) \cdot \hat{\boldsymbol{\omega}}(0) \tag{11.9.9}$$

where $\hat{h}_0(0)$ (a scalar) is any element of $\hat{\boldsymbol{h}}(0)$. Inserting (11.9.9) in (11.9.8), multiplying on the right by $\boldsymbol{Q}$, and using again the property (11.9.2), we find that

$$\boldsymbol{Q} \cdot \boldsymbol{h}^{(2)} \cdot \boldsymbol{Q} = 0 \tag{11.9.10}$$

But every element of the matrix $\boldsymbol{Q} \cdot \boldsymbol{h}^{(2)} \cdot \boldsymbol{Q}$ is proportional to $\Delta h^{(2)}$, where $\Delta h(r)$ is defined by (11.3.8). Thus $\Delta h^{(2)} = 0$ and hence, from (11.3.10), $G_1 = 0$. As we pointed out in Section 11.3, this result is obvious on symmetry grounds for a homonuclear molecule, but in the general case it will be true (unless accidentally) only in the ideal-gas limit. Similarly, by considering terms of order k^4 in (11.9.7), it can be that $G_2 = 0$ for an asymmetric, linear, triatomic molecule.

If the molecule is polar, with the interaction sites carrying point charges, the problem becomes more complicated. When expanding $\hat{\boldsymbol{c}}(k)$, allowance must be made for a term in k^{-2}, corresponding to an r^{-1} decay of the site–site potential. This term must be treated separately, but it is then possible to show that for any interaction-site molecule

$$\rho \sum_{\alpha} \sum_{\beta} q_\alpha q_\beta h_{\alpha\beta}^{(2)} = -\frac{y\mu^2}{1+3y} \tag{11.9.11}$$

where q_α is the charge carried by site α. Comparison of (11.9.11) with the exact result (11.5.32) shows that within the RISM approximation

$$\varepsilon = 1 + 3y \tag{11.9.12}$$

which is a well-known result for the dielectric constant of an ideal gas of polar molecules.

The results in (11.9.10) and (11.9.12) are consequences solely of the RISM-OZ relation (11.8.6). They are independent of the choice of closure relation except insofar as the latter must be consistent with the assumed small-k behaviour of $\hat{\boldsymbol{h}}(k)$ and $\hat{\boldsymbol{c}}(k)$. It follows that the RISM-OZ relation, when combined with a conventional closure approximation, cannot describe correctly certain long-wavelength properties of molecular systems, of which G_1, G_2 and ε are important examples.

Attempts to develop a more satisfactory theory have developed along two different lines. The first relies on treating the RISM-OZ relation as providing the definition of the site–site direct correlation functions. So far as the calculation of angular order parameters is concerned, it then appears necessary to abandon the assumption that $c_{\alpha\beta}(r)$ is a short-range function, even when the corresponding site–site potential is short ranged. For example,[41] a non-zero value of G_1 for a symmetric diatomic is obtained if $c_{\alpha\beta}(r)$ is assumed to decay as r^{-1}. In such circumstances the concept of "direct correlation" no longer has a clear physical meaning. In the alternative approach the view is taken that the RISM-OZ relation, though plausible, does not provide an adequate basis for a complete theory of interaction-site models of molecular liquids. Accordingly, it is there rather than in the closure relation that improvement must be sought.[42] The argument is based on the difference in diagrammatic structure between the RISM-OZ relation and the molecular Ornstein–Zernike relation (11.1.4). In the latter case the indirect correlation function $b(1,2) = h(1,2) - c(1,2)$ is given, as in (4.6.1), by the sum of all simple chain diagrams containing two or more c-bonds. In any such diagram, every black circle is a nodal circle, and $c(1,2)$ consists of the subset of diagrams in the ρ-circle, f-bond expansion of $h(1,2)$ that are free of nodal circles. By analogy, it might be supposed that the $\boldsymbol{c}$-bonds in (11.8.1) represent the subset of diagrams in the expansion of $h_{\alpha\beta}(r)$ that are free of nodal circles. This is not the case. For example, the diagram

which appears at zeroth order in the density expansion of $h_{\alpha\beta}(r)$ is a diagram without nodal circles. If this is substituted into the second and third diagrams on the right-hand side of (11.8.1), it yields, respectively, diagrams (a) and (b) below:

(a) (b)

Diagram (a) is a diagram in the exact expansion of $h_{\alpha\beta}(r)$, but (b) is not. In fact, (b) is not even an allowed diagram, because two $\boldsymbol{s}$-bonds intersect the same black circle. Chandler

and coworkers[42] have shown how this problem can be overcome through the introduction of another Ornstein–Zernike-like relation that reduces to (11.8.6) in the limit $\rho \to 0$ but in which the direct correlation functions correspond to well-defined subsets of diagrams in $\boldsymbol{h}$. Calculations based on the new relation lead to non-trivial results for the angular order parameters and dielectric constant when approximate closures of conventional type are employed. However, the theory has not been widely applied, and so far as the description of short-range order is concerned it is not clear that the method represents an improvement on the original formulation.[43]

11.10 ASSOCIATING LIQUIDS

Although hydrogen-bonded liquids and other associating fluids are not normally classed as "simple", our understanding of the link between the macroscopic properties of such systems and their behaviour at the microscopic level has improved greatly in recent years. This is a development to which both experiment and simulation have made major contributions. For understandable reasons, much of the effort has been focused on studies of water. The particular geometry of the water molecule gives rise to structural features in the liquid that are not seen for other small, hydrogen-bonded species, and the macroscopic properties of water display a number of anomalies that are directly attributable to hydrogen bonding, of which the best known is the fact that the density at atmospheric pressures passes through a maximum at a temperature of 4 °C. One of the most important advances on the experimental front has been the resolution of significant differences that had previously existed between the results of x-ray and neutron-scattering measurements of the structure of liquid water. X-ray scattering is sensitive primarily to the oxygen–oxygen correlations,[44] while neutron scattering is the main source of information on correlations involving hydrogen atoms.[45] Figure 11.7 shows the results obtained by x-ray scattering for the distribution function of oxygen atoms in water at room temperature, contrasting these with the results for liquid argon already shown in Chapter 2. To assist comparison, the horizontal axis is scaled so as to bring the two main peaks into coincidence. Clearly the structure is very different in the two liquids. Two features in particular stand out. First, the area under the main peak is significantly smaller for water than it is for argon, leading to a large reduction in the nearest-neighbour coordination number defined in Section 2.5, from approximately 12 for argon to about four for water. Secondly, the oscillations in the two curves are out of phase. The second peak for water is displaced inwards with respect to that for argon and appears at a distance $r/r_{\max} = 1.61 \pm 0.01$, which is very close to the value found for the ratio of the second-neighbour separation to that of first neighbours in the ideal ice structure, i.e. $2\sqrt{(2/3)} \approx 1.63$. Both the value of the coordination number and the position of the second peak in the oxygen–oxygen distribution function provide clear evidence that the molecules in liquid water form a hydrogen-bonded network which represents a strained version of the tetrahedral ordering found in ice.

A similar picture to that outlined above emerges from the many simulations of water that have been carried out.[48] Such calculations provide a level of detail that cannot be matched experimentally concerning the number, energies and lifetimes of the hydrogen bonds formed by individual molecules. A very large number of empirical intermolecular

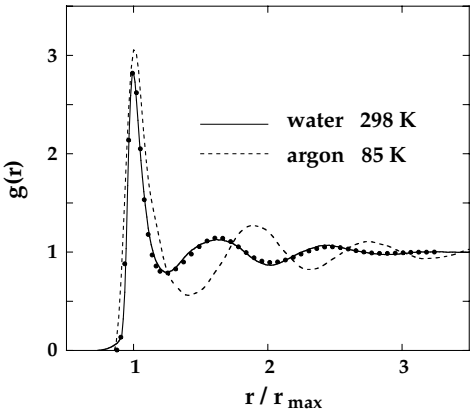

FIG. 11.7. Experimental results for the pair distribution function for oxygen atoms in water at room temperature (from x-ray scattering[44]) and for liquid argon near its triple point (from neutron scattering[46]). The points are the results for $g_{OO}(r)$ obtained by Monte Carlo calculations[47] for an interaction-site model of water. The quantity r_{max} is the separation at which the corresponding experimental curve has its main peak: 2.74 Å for water and 3.68 Å for argon.

potentials have been designed for use in simulations, which differ from each other mainly in the way in which the electrostatic interaction between molecules is described. The majority are based on rigid charge distributions represented by three or more point charges, though a number of polarisable models have also been developed, and the best of these empirical potentials give results in impressive agreement with experiment for a wide range of properties. An example of what can be achieved is illustrated by the Monte Carlo results shown in Figure 11.7. These were obtained with a model[47] (TIP5P) consisting of a Lennard-Jones interaction centred on the oxygen atom and four rigid charges, one on each hydrogen site and two at sites chosen to represent the lone-pair electrons. The same model is also successful in reproducing the density anomaly at 4 °C, while a predecessor (TIP4P) has been shown to capture all the main features of the experimental phase diagram.[49]

A number of standard, integral-equation approximations have been used in calculations for models of specific hydrogen-bonded liquids, including water,[50] but progress has also been achieved in the development of a general approach to the theory of associating fluids.[51–53] One of the most successful of these theories is that of Wertheim, which in its commonly used form has the character of a thermodynamic perturbation theory.[53(b)] The theory is designed for application to a class of highly simplified models in which the associating species are treated as particles with repulsive cores in which a number of attractive interaction sites are embedded; it is at these sites that association occurs. In the examples discussed below the particles are taken to be hard spheres of diameter d and the association sites are represented by off-centre, square-well potentials with a well-depth ε_A. Because hard spheres cannot overlap, the square-well potential can always be made sufficiently short ranged that the formation of more than one bond at any given site is forbidden, as in the example shown in Figure 11.8. A model with one association site describes a dimerising fluid; with two sites, illustrated in the figure, the spheres can form chains and rings;

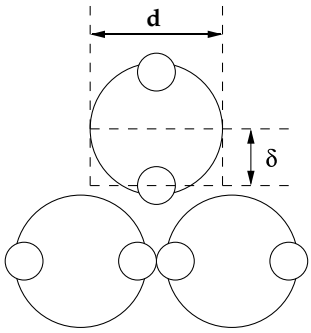

FIG. 11.8. A simple interaction-site model of an associating liquid. The large circles represent hard spheres and the small circles represent square-well interaction sites displaced from the centre of the hard sphere by a distance δ. The range of the square-well potential is sufficiently short to ensure that multiple bonding at any association site is forbidden, since that would require hard spheres to overlap.

with three sites, chain branching and network formation become possible; and a sphere with four, tetrahedrally disposed sites serves as a crude model of a water molecule.

If the attractive interactions between particles are sufficiently strong to promote association, we cannot expect a conventional perturbation calculation to succeed. In Wertheim's approach this difficulty is circumvented by treating different association aggregates as distinct species, each described by a separate single-particle density within a "multi-density" formalism. The theory leads ultimately to an expression for the free energy in terms of the densities of particles in different bonding states. As a specific example, consider the case of a system of hard spheres with a single association site. Since only dimer formation is allowed, the total number density of spheres can be written as

$$\rho = \rho_{\mathrm{M}} + 2\rho_{\mathrm{D}} \tag{11.10.1}$$

where ρ_{M} and ρ_{D} are the number densities of monomers and dimers, respectively. Diagrammatic arguments along the general lines of those pursued in Section 3.8 can then be used to show that

$$\rho = \rho_{\mathrm{M}} + \rho_{\mathrm{M}}^2 \int g_{\mathrm{MM}}(1,2)\, f_{\mathrm{A}}(1,2)\, \mathrm{d}2 \tag{11.10.2}$$

where $g_{\mathrm{MM}}(1,2)$ is the pair distribution function of the free monomers and $f_{\mathrm{A}}(1,2)$ is the Mayer function for the association potential.

The starting point in the derivation of (11.10.2) is the activity expansion of $\ln \Xi$ provided by (3.8.3). By decomposing the Mayer function for the full pair potential in the form

$$f(1,2) = f_0(1,2) + \Phi(1,2), \quad \Phi(1,2) = e_0(1,2)\, f_{\mathrm{A}}(1,2) \tag{11.10.3}$$

where $e_0(1,2)$ and $f_0(1,2)$ are, respectively, the Boltzmann factor and Mayer function for the hard-sphere potential, the right-hand side of (3.8.3) can be written a sum of diagrams consisting of z^*-circles, f_0-bond and Φ-bonds. The assumption that multiple bonding at a

single site is blocked by steric effects means that many of the diagrams either vanish or are cancelled by other diagrams; this greatly simplifies the subsequent analysis. The diagrammatic representation of the total single-particle density $\rho^{(1)}(1)$ is again obtained from the prescription given by (3.8.4), i.e. as the sum of all topologically distinct diagrams obtained from $\ln \Xi$ by whitening a black circle and labelling it 1. Now, however, the diagrams that contribute to $\rho^{(1)}(1)$ can be divided into two classes:

$$\rho^{(1)}(1) = \rho_{\mathrm{M}}^{(1)}(1) + \rho_{\mathrm{A}}^{(1)}(1) \tag{11.10.4}$$

where $\rho_{\mathrm{M}}^{(1)}(1)$ is the density of unassociated spheres (monomers) and $\rho_{\mathrm{A}}^{(1)}(1)$ is the density of spheres that form part of an associated aggregate, which in the present case can only be a dimer; the class of monomer diagrams consists of those diagrams in which the white circle is not intersected by a Φ-bond. The last step in the derivation involves a topological reduction in which the z^*-circles in the z^*-expansion of $\ln \Xi$ are replaced by $\rho^{(1)}$ or $\rho_{\mathrm{M}}^{(1)}$-circles, which in turn leads to expressions for the free energy and pressure as functionals of the two densities. The monomer density is not a free parameter; it is determined self-consistently by a relation between $\rho^{(1)}(1)$ and $\rho_{\mathrm{M}}^{(1)}(1)$, which in the homogeneous limit reduces to (11.10.2).

The full calculation is too lengthy to reproduce here, but the brief sketch we have given is enough to show that the derivation of the expression that relates ρ and ρ_{M} does not rely on the assumption that the association potential is in some sense weak. However, for the purposes of evaluating the integral in (11.10.2), the characteristic approximation of first-order perturbation theory can now be made, whereby the unknown function $g_{\mathrm{MM}}(1,2)$ in (11.10.2) is replaced by the pair distribution function of the underlying hard-sphere system, $g_0(1,2)$. Thus

$$\rho \approx \rho_{\mathrm{M}} + \rho_{\mathrm{M}}^2 \int g_0(1,2)\, f_{\mathrm{A}}(1,2)\, \mathrm{d}2 \equiv \rho_{\mathrm{M}} + \rho_{\mathrm{M}}^2 D(\rho, T) \tag{11.10.5}$$

It can then be shown that the change in free energy due to dimerisation, F^{A}, is given, to the same order in perturbation theory, by a very simple formula:

$$\frac{\beta F^{\mathrm{A}}}{N} = \frac{\beta F}{N} - \frac{\beta F_0}{N} = \ln x + \tfrac{1}{2}(1-x) \tag{11.10.6}$$

where F_0 is the free energy of the reference system and $x = \rho_{\mathrm{M}}/\rho$ is the fraction of spheres that remain unassociated. The value of x is given by the positive root of the equation obtained by dividing (11.10.5) though by ρ:

$$x^2 \rho D(\rho, T) + x - 1 = 0 \tag{11.10.7}$$

Since the association potential is very short ranged, the integral $D(\rho, T)$ can be adequately approximated in the form

$$D(\rho, T) \approx g_0(d) \int f_{\mathrm{A}}(1,2)\, \mathrm{d}2 \equiv g_0(d) D'(T) \tag{11.10.8}$$

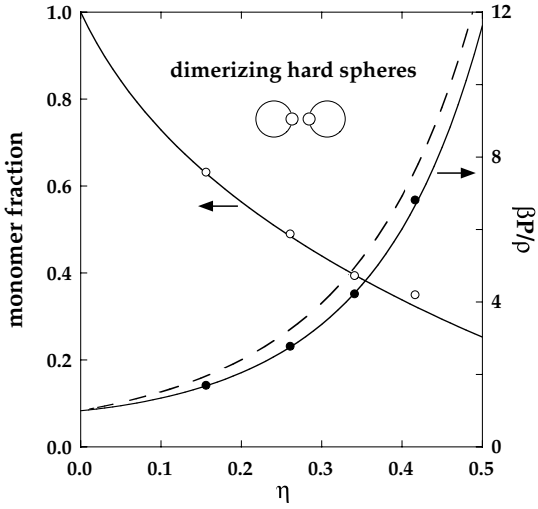

FIG. 11.9. Equilibrium composition and equation of state of a dimerising hard-sphere fluid at a reduced inverse temperature $\varepsilon_A/k_BT = 7$, where ε_A is the depth of the square-well potential. The points are the results of Monte Carlo calculations and the full curves are obtained by perturbation theory. The broken curve shows the Carnahan–Starling equation of state for the hard-sphere reference system. After Jackson *et al.*[54]

where $g_0(d)$ is the value of the hard-sphere distribution function at contact. Once the free energy is known, other thermodynamic properties can be obtained by differentiation. Figure 11.9 shows results obtained for the equilibrium composition and equation of state as a function of the hard-sphere packing fraction at a temperature such that $\varepsilon_A/k_BT = 7$. The agreement between theory and simulation is very good.

The final results of the theory and, in particular, the self-consistency of (11.10.5) and (11.10.6), can be made plausible by considering the simplest possible case, that of a dimerising ideal gas.[55] In the low-density limit, (11.10.5) reduces to[56]

$$\rho = \rho_M + \rho_M^2 \int e_0(1,2)\, f_A(1,2)\, d2 \equiv \rho_M + \rho_M^2 \Delta(T) \tag{11.10.9}$$

The role of the association potential is limited to that of dimer formation and the free energy of the partly associated system is that of a ideal gas composed of monomers and dimers. At equilibrium, the chemical potential of a sphere must be the same in its monomer and dimer states and therefore equal to $k_BT \ln \rho_M \Lambda^3$, and the pressure is $k_BT(\rho_M + \rho_D)$. A short calculation shows that the free energy $F = N\mu - PV$ of the associated system relative to that of the ideal monomeric gas is

$$\frac{\beta F^A}{V} = \rho \ln \frac{\rho_M}{\rho} + \tfrac{1}{2}(\rho - \rho_M) \tag{11.10.10}$$

which is equivalent to (11.10.6). At equilibrium, F^A must be a minimum with respect to variations in ρ_M at constant ρ, subject to the constraint imposed by (11.10.9). If we replace

the second term on the right-hand side of (11.10.10) by $(\rho - \rho_M) - \frac{1}{2}\rho_M^2 \Delta(T)$, we find that

$$\frac{\beta}{V}\frac{\partial F^A}{\partial \rho_M} = \frac{\rho}{\rho_M} - 1 - \rho_M \Delta(T) \tag{11.10.11}$$

which vanishes when (11.10.9) is satisfied. Equations (11.10.9) and (11.10.10) are therefore mutually consistent.

An important feature of Wertheim's approach is that it leads naturally to a theory of polymerisation.[57] This extension of the theory is easily illustrated, in a non-rigorous way, for the case of dimer formation. The degree of dimerisation approaches unity as the depth of the square-well potential is increased to values appropriate to a covalent bond and the Mayer function $f_A(1,2)$ becomes correspondingly large. Equation (11.10.7) implies that as the limit of complete dimerisation is approached, the monomer fraction must vanish as $x \to 1/[\rho D(\rho, T)]^{1/2}$. If we adopt the approximation (11.10.8), we find that the free energy of association in the limit $\rho \to 2\rho_D$ is

$$\frac{\beta F^A}{N} \approx -\tfrac{1}{2}\ln \rho D'(T) + \tfrac{1}{2} \tag{11.10.12}$$

implying that the equation of state of the fully dimerised system, i.e. a fluid of hard diatomics, is

$$\beta(P - P_0) = -\beta\frac{\partial F^A}{\partial V} = -\tfrac{1}{2}\rho\left(1 + \rho g_0(d)\frac{\partial \ln g_0(d)}{\partial \rho}\right) \tag{11.10.13}$$

where P_0 is the pressure of the hard-sphere fluid. If the Carnahan–Starling equation of state is used for P_0, the contact value $g_0(d)$ is given by

$$g_0(d) = \frac{\left(1 - \frac{1}{2}\eta\right)}{(1-\eta)^3} \tag{11.10.14}$$

and (11.10.13) (with $\rho = 2\rho_D$) becomes

$$\frac{\beta P}{\rho_D} = \frac{2(1 + \eta + \eta^2 - \eta^3)}{(1-\eta)^3} - \frac{\left(1 + \eta - \frac{1}{2}\eta^2\right)}{(1-\eta)\left(1 - \frac{1}{2}\eta\right)} \tag{11.10.15}$$

Equation (11.10.15) proves to be remarkably accurate. It yields results that agree with those of simulations of systems of tangent hard spheres to within 0.15% over the full density range.[57(a)]

Wertheim's theory and its extensions provide the basis for the general approach called "statistical associating fluid theory" or SAFT, within which equations of state have been developed for a wide range of complex fluids of importance in chemical engineering.[58]

11.11 REORIENTATIONAL TIME-CORRELATION FUNCTIONS

The description of the dynamical properties of molecular liquids differs most obviously from that used for atomic systems through the appearance of a class of reorientational time-correlation functions. We end this chapter by briefly considering some of the properties of these functions, limiting ourselves mainly to the case of linear molecules. We consider first the simpler problem of the single-molecule functions, leaving until later the question of collective reorientational properties.

Reorientation of a linear molecule can be described in a compact way through the introduction of a family of time-correlation functions defined as

$$C^{(l)}(t) = \left\langle P_l\left[\mathbf{u}_i(t)\cdot\mathbf{u}_i\right]\right\rangle \tag{11.11.1}$$

where, as before, $\mathbf{u}_i$ is a unit vector parallel to the internuclear axis of molecule i and $P_l(\cdots)$ is again a Legendre polynomial. The functions $C^{(l)}(t)$ are time-dependent generalisations of the angular order parameters G_l of Section 11.1. Apart from their application to linear molecules, they are also the most important functions for the description of the reorientational motion of spherical-top molecules, i.e. those in which all three principal moments of inertia are the same (CCl_4, SF_6, etc.), and of the reorientation of the main symmetry axis of symmetric-top molecules, i.e. those in which two of the principal moments of inertia are equal (NH_3, CH_3I, etc.). The $l = 1$ and $l = 2$ functions are related to the spectral bandshapes measured in infrared absorption ($l = 1$) and Raman or depolarised light scattering ($l = 2$) experiments. Information on the correlation functions can be obtained by Fourier transformation of the experimental spectra, but the interpretation of the results is complicated by a number of factors, including uncertainty about the contributions to the spectra from vibrational relaxation and collision-induced effects or, in the case of depolarised light scattering, the importance of angular correlations of the type described by the order parameter G_2.

Figure 11.10 shows some typical results for the $l = 2$ function, derived from spectroscopic measurements on carbon dioxide in two very different thermodynamic states and, in the inset, liquid acetonitrile. Under liquid-state conditions the function is approximately exponential in form, except at short times, but at low densities oscillations appear; infrared-absorption experiments on polar molecules give qualitatively similar results for the $l = 1$ function. The oscillations seen at low densities can be understood by considering the behaviour of the correlation functions in the ideal-gas limit. Let $\boldsymbol{\omega} = \mathbf{u}\times\dot{\mathbf{u}}$ be the angular velocity of a linear molecule of moment of inertia I. In the absence of any interactions the angular velocity is a constant of the motion, and in a time t the molecule will rotate through an angle $\omega t = \cos^{-1}\mathbf{u}(t)\cdot\mathbf{u}(0)$, where $\omega \equiv |\boldsymbol{\omega}|$. The probability that a molecule will rotate through such an angle is therefore determined by the probability that its angular velocity lies in the range $\omega \to \omega + \mathrm{d}\omega$. Thus the correlation function $C^{(l)}(t)$ is the value of $P_l(\cos\omega t)$ averaged over a Maxwell–Boltzmann distribution of angular velocities and appropriately normalised, i.e.

$$C^{(l)}(t) = \frac{I}{k_\mathrm{B}T}\int_0^\infty P_l(\cos\omega t)\exp\left(-\tfrac{1}{2}\beta I\omega^2\right)\omega\,\mathrm{d}\omega \tag{11.11.2}$$

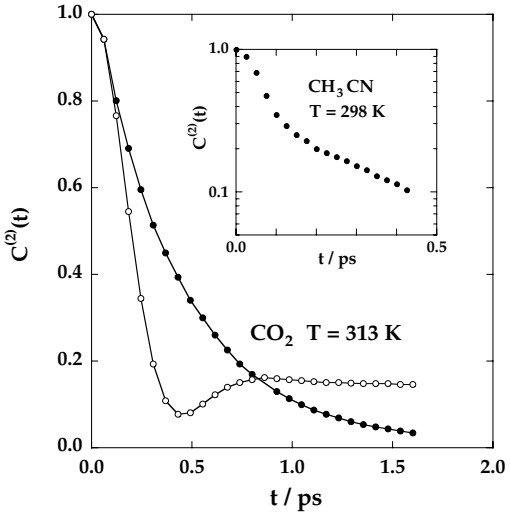

FIG. 11.10. The $l = 2$ reorientational correlation function derived from experiments on liquid and gaseous carbon dioxide (main figure) and liquid acetonitrile (inset, plotted on a logarithmic scale). Open and closed circles in the main figure show the results for $\rho/\rho_c = 0.09$ and $\rho/\rho_c = 2.35$, respectively, where ρ_c is the critical density. After Versmold[59] and Bien *et al.*[60]

These functions are oscillatory and tend to zero as $t \to \infty$ only for odd l. They are commonly called the "free-rotor" correlation functions and the oscillations seen in gas-phase experimental results are the remnants of free-rotor behaviour. Similar results are obtained for the free-rotor functions of non-linear molecules; the principle of the calculation is the same, but the final expressions have a more complicated form.[61]

The short-time expansion of the Legendre polynomial in (11.11.2) begins as

$$P_l(\cos\omega t) = 1 - \tfrac{1}{4}l(l+1)\omega^2 t^2 + \cdots \tag{11.11.3}$$

If we expand the correlation function in powers of t:

$$C^{(l)}(t) = 1 - M_2^{(l)}\frac{t^2}{2!} + \cdots \tag{11.11.4}$$

a simple integration shows that

$$M_2^{(l)} = l(l+1)\frac{k_B T}{I} \tag{11.11.5}$$

At sufficiently short times a molecule rotates freely. Hence, although (11.11.5) has been derived only in the free-rotor limit, it is also valid for interacting molecules; there is an analogy here with the short-time behaviour of the mean-square translational displacement. From the general properties of time-correlation functions discussed in Section 7.1 it follows that the coefficient $M_2^{(l)}$ is the second moment of the power spectrum of $C^{(l)}(t)$. The

mean-square width of the experimental bandshape is therefore independent of the molecular interactions. The fourth moment, however, contains a contribution proportional to the mean-square torque acting on the molecule.

The quasi-exponential behaviour of the correlation functions at high densities can be explained by invoking an approximation similar in spirit to the Langevin equation (7.3.21). We begin by writing a memory-function equation for $C^{(l)}(t)$ and taking the Laplace transform to give

$$\widetilde{C}^{(l)}(\omega) = \frac{1}{-i\omega + \widetilde{N}^{(l)}(\omega)} \tag{11.11.6}$$

From (11.11.5) it follows that the memory function $N^{(l)}(t)$ behaves as

$$N^{(l)}(t) = l(l+1)\left(\frac{k_{\mathrm{B}}T}{I}\right)n^{(l)}(t) \tag{11.11.7}$$

with $n^{(l)}(0) = 1$. We now suppose that reorientation occurs as the result of a succession of small, uncorrelated steps. This is the Debye approximation or "small-step-diffusion" model. In memory-function language the Debye approximation is equivalent to the assumption that $\widetilde{N}^{(l)}(\omega)$ is independent of frequency. To preserve the l-dependence contained in the exact result (11.11.7) we approximate the memory function in the form $\widetilde{N}^{(l)} \approx l(l+1)D_R$, where D_R (a frequency) is a "rotational-diffusion coefficient". Then

$$C^{(l)}(t) = \exp\bigl[-l(l+1)D_R t\bigr] \tag{11.11.8}$$

In this approximation the correlation functions decay exponentially at all times and for all values of l, and the entire family of functions is characterised by the single parameter D_R; for small molecules under triple-point conditions, D_R is typically of order $10^{11}\,\mathrm{s}^{-1}$. The characteristic decay times for different values of l are related by the simple rule

$$\frac{\tau_l}{\tau_{l+1}} = \frac{l+2}{l} \tag{11.11.9}$$

The correlation times derived from infrared and Raman measurements should therefore be in the ratio $\tau_1/\tau_2 = 3$. This is approximately true of many liquids and also of correlation times obtained by simulation.[62]

A weakness of the Debye approximation is its neglect of the fact that molecules rotate freely at short times. It therefore cannot account for the quadratic time dependence of the reorientational correlation functions at small t. A more complete theory must also describe correctly the details of the transition to the long-time, quasi-exponential behaviour. In the case of acetonitrile, for example, the transition region is characterised by a marked change in slope of the curve of $\ln C^{(2)}(t)$ versus t. The behaviour in the different time regimes can be described in a unified way by relating the form of the reorientational correlation functions to that of the angular-velocity autocorrelation function $C_\omega(t)$.[63] By analogy with (7.2.6) and (7.2.7) we define the rotational-diffusion coefficient of a linear

molecule as

$$D_R = \frac{k_B T}{I} \lim_{t\to\infty} \int_0^t \left(1 - \frac{s}{t}\right) C_\omega(s)\,\mathrm{d}s \tag{11.11.10}$$

where

$$C_\omega(t) = \frac{\langle \boldsymbol{\omega}_i(t)\cdot\boldsymbol{\omega}_i\rangle}{\langle|\boldsymbol{\omega}_i|^2\rangle} = \frac{I}{2k_B T}\langle \boldsymbol{\omega}_i(t)\cdot\boldsymbol{\omega}_i\rangle \tag{11.11.11}$$

Then substitution of (11.11.10) in (11.11.8) gives an expression for $C^{(l)}(t)$ in terms of $C_\omega(t)$:

$$\ln C^{(l)}(t) = -l(l+1)\left(\frac{k_B T}{I}\right)\int_0^t (t-s)C_\omega(s)\,\mathrm{d}s \tag{11.11.12}$$

The main merit of this approximation is the fact that it contains the correct short-time behaviour yet goes over to the Debye model at long times. Let τ_ω be the integral correlation time for the angular velocity, i.e.

$$\tau_\omega = \int_0^\infty C_\omega(t)\,\mathrm{d}t \tag{11.11.13}$$

At times $t \ll \tau_\omega$, $C_\omega(t) \approx 1$ and (11.11.12) becomes

$$\ln C^{(l)}(t) \approx -l(l+1)\left(\frac{k_B T}{I}\right)\frac{t^2}{2} \tag{11.11.14}$$

in agreement with the exact result (11.11.5). In the opposite limit, $t \gg \tau_\omega$, (11.11.12) becomes

$$\ln C^{(l)}(t) \approx -l(l+1)\left(\frac{k_B T}{I}\right)\tau_\omega t \tag{11.11.15}$$

which is equivalent to the Debye approximation (11.11.8) with the identification $D_R = (k_B T/I)\tau_\omega$. Finally, the behaviour at intermediate times can be related to the shape of the function $C_\omega(t)$. Differentiating (11.11.12) twice with respect to t we find that

$$\frac{\mathrm{d}^2 \ln C^{(l)}(t)}{\mathrm{d}t^2} = -l(l+1)\left(\frac{k_B T}{I}\right)C_\omega(t) \tag{11.11.16}$$

The angular-velocity autocorrelation function is not measurable experimentally, but molecular-dynamics calculations show that for liquids such as acetonitrile, in which the intermolecular torques are strong, it decays rapidly at short times and then becomes negative.[62] The change in sign occurs because the direction of the angular-velocity vector is on average soon reversed; the behaviour is similar to that seen in the linear-velocity autocorrelation function at high densities and low temperatures (see Figure 7.1). Equation (11.11.16) shows that a change in sign of $C_\omega(t)$ corresponds to a point of inflexion in $\ln C^{(l)}(t)$ of the type visible in Figure 11.10, which in turn is a common feature of the reorientational correlation functions of high-torque fluids.

A variety of theoretical schemes have been devised to treat those cases in which the Debye model is inadequate. Many of these are expressible in terms of simple approximations for the relevant memory functions, but none has proved to be satisfactory either for any large group of molecules or for any particular molecule over a wide range of density and temperature. The failure to develop an adequate theory is striking in view of the apparent simplicity in structure of the correlation functions themselves.

We have focused until now on the reorientational motion of single molecules. There are, in addition, a number of collective reorientational correlation functions that are of experimental significance and are also many-particle generalisations of single-particle functions. It is therefore of interest to establish an approximate relation between the corresponding collective and single-particle functions and, in particular, between the two correlation times, since this allows a connection to be made between the results of very different experiments. We take as an example the collective motions that determine the frequency-dependent dielectric behaviour of a polar fluid,[16] as described by the complex dielectric permittivity $\varepsilon(\omega)$ introduced in Section 11.5. The quantities of interest in the study of dielectric relaxation are the correlation functions and associated power spectra of the longitudinal (l) and transverse (t) components of the dipole-moment density (11.5.13), i.e.

$$C_l(k,t) = \frac{\langle M^z_{\mathbf{k}}(t) M^z_{-\mathbf{k}} \rangle}{\langle |M^z_{\mathbf{k}}|^2 \rangle}, \qquad C_t(k,t) = \frac{\langle M^x_{\mathbf{k}}(t) M^x_{-\mathbf{k}} \rangle}{\langle |M^x_{\mathbf{k}}|^2 \rangle} \tag{11.11.17}$$

where we have followed the usual convention that $\mathbf{k}$ is parallel to the z-axis. The functions $C_l(k,t)$ and $C_t(k,t)$ are collective analogues, generalised to non-zero k, of the single-molecule function $C^{(1)}(t)$. It follows from (11.5.9) and (11.5.12) that the long-wavelength limits of the Laplace transforms $\widetilde{C}_l(k,\omega)$ and $\widetilde{C}_t(k,\omega)$ are related to $\varepsilon(\omega)$ by

$$\begin{aligned} \frac{4\pi\beta}{V} \lim_{\mathbf{k}\to 0} \langle |M^z_{\mathbf{k}}|^2 \rangle \big[1 + i\omega \widetilde{C}_l(k,\omega)\big] &= \frac{\varepsilon(\omega) - 1}{\varepsilon(\omega)} \\ \frac{4\pi\beta}{V} \lim_{\mathbf{k}\to 0} \langle |M^x_{\mathbf{k}}|^2 \rangle \big[1 + i\omega \widetilde{C}_t(k,\omega)\big] &= \varepsilon(\omega) - 1 \end{aligned} \tag{11.11.18}$$

We begin by writing memory-function equations for $C_l(k,t)$ and $C_t(k,t)$ in the form

$$\widetilde{C}_l(k,\omega) = \frac{1}{-i\omega + \widetilde{N}_l(k\cdot\omega)}, \qquad \widetilde{C}_t(k,\omega) = \frac{1}{-i\omega + \widetilde{N}_t(k\cdot\omega)} \tag{11.11.19}$$

The initial values of the memory functions $N_l(k,t)$ and $N_t(k,t)$ in the limit $k \to 0$ can be deduced from the general property (9.1.29) and the limiting behaviour described by (11.11.18), taken for $\omega = 0$:

$$\begin{aligned} \lim_{\mathbf{k}\to 0} N_l(k, t=0) &= \lim_{\mathbf{k}\to 0} \frac{\langle |\dot{M}^z_{\mathbf{k}}|^2 \rangle}{\langle |M^z_{\mathbf{k}}|^2 \rangle} = \frac{4\pi\beta\varepsilon}{3V(\varepsilon - 1)} \langle |\dot{\mathbf{M}}|^2 \rangle \\ \lim_{\mathbf{k}\to 0} N_t(k, t=0) &= \lim_{\mathbf{k}\to 0} \frac{\langle |\dot{M}^x_{\mathbf{k}}|^2 \rangle}{\langle |M^x_{\mathbf{k}}|^2 \rangle} = \frac{4\pi\beta}{3V(\varepsilon - 1)} \langle |\dot{\mathbf{M}}|^2 \rangle \end{aligned} \tag{11.11.20}$$

where $\varepsilon \equiv \varepsilon(0)$ and $\dot{\mathbf{M}} \equiv \dot{\mathbf{M}}_{\mathbf{k}\to 0}$. In deriving these results we have exploited the fact that the different components of $\langle|\dot{\mathbf{M}}_{\mathbf{k}}|^2\rangle$ (unlike those of $\langle|\mathbf{M}_{\mathbf{k}}|^2\rangle$) are equivalent and, in particular, that $\lim_{\mathbf{k}\to 0}\langle|\dot{M}^{\alpha}_{\mathbf{k}}|^2\rangle = \frac{1}{3}\langle|\dot{\mathbf{M}}|^2\rangle$, where $\alpha = x$, y or z.

The form of (11.11.20) makes it convenient to write the memory functions at long wavelengths as

$$\lim_{\mathbf{k}\to 0}\widetilde{N}_l(k,\omega) = \frac{\varepsilon\widetilde{R}_l(\omega)}{\varepsilon - 1}, \qquad \lim_{\mathbf{k}\to 0}\widetilde{N}_t(k,\omega) = \frac{\widetilde{R}_t(\omega)}{\varepsilon - 1} \tag{11.11.21}$$

It is clear from comparison of (11.11.20) with (11.11.21) that $R_l(t=0) = R_t(t=0) = (4\pi\beta/3V)\langle|\dot{\mathbf{M}}|^2\rangle$. More generally, if the two parts of (11.11.18) are to be consistent with each other in the sense of giving the same result for $\varepsilon(\omega)$, some straightforward algebra shows that $R_l(t)$ and $R_t(t)$ must be the same for all t. Thus

$$R_l(t) = R_t(t) = R(t), \quad \text{say} \tag{11.11.22}$$

This has the immediate consequence that in the long-wavelength limit the correlation times for the longitudinal and transverse functions differ by a factor ε, i.e. $\lim_{\mathbf{k}\to 0}\widetilde{C}_l(k,0)/\widetilde{C}_t(k,0) = \varepsilon^{-1}$ or

$$\lim_{\mathbf{k}\to 0}\int_0^{\infty} C_l(k,t)\,\mathrm{d}t = \frac{1}{\varepsilon}\lim_{\mathbf{k}\to 0}\int_0^{\infty} C_t(k,t)\,\mathrm{d}t \tag{11.11.23}$$

The diffusion approximation analogous to (11.11.8) now corresponds to setting

$$R(t) = R(0)\delta(t) = \frac{4\pi\beta}{3V}\langle|\dot{\mathbf{M}}|^2\rangle\delta(t) \tag{11.11.24}$$

so that both $\widetilde{N}_l(k,\omega)$ and $\widetilde{N}_t(k,\omega)$ are assumed to be independent of frequency in the limit $\mathbf{k}\to 0$. If we define a characteristic time τ_{D} as

$$\tau_{\mathrm{D}} = \frac{3V}{4\pi\beta}\frac{\varepsilon - 1}{\langle|\dot{\mathbf{M}}|^2\rangle} \tag{11.11.25}$$

it follows from (11.11.19) and (11.11.21) that

$$\lim_{\mathbf{k}\to 0} C_l(k,t) = \exp(-\varepsilon t/\tau_{\mathrm{D}}), \qquad \lim_{\mathbf{k}\to 0} C_t(k,t) = \exp(-t/\tau_{\mathrm{D}}) \tag{11.11.26}$$

which represents a special case of the general result in (11.11.23). Simulations of strongly polar fluids confirm that the longitudinal and transverse correlation functions at small $\mathbf{k}$ do decay on very different timescales and that the ratio of correlation times is approximately equal to the value of ε derived from fluctuations in the mean-square dipole moment of the sample.[64] The transverse function is also approximately exponential in form with a decay time only weakly dependent on $\mathbf{k}$, in qualitative agreement with (11.11.26), but the longitudinal function has oscillations at large t; to describe these oscillations it is necessary

to allow for some frequency dependence of the memory function. The approximation for $\varepsilon(\omega)$ corresponding to (11.11.26) is

$$\frac{\varepsilon(\omega)-1}{\varepsilon(0)-1}=\frac{1}{1-i\omega\tau_{\mathrm{D}}} \tag{11.11.27}$$

This is an expression much used in the analysis of experimental data on $\varepsilon(\omega)$, in which context τ_{D} is invariably called the Debye relaxation time. A feature of the approximation is the fact that the curve, or Cole–Cole plot, of the real versus imaginary part of $\varepsilon(\omega)$ is a semicircle with a maximum at a frequency such that $\omega\tau_{\mathrm{D}}=1$. Many real liquids have Cole–Cole plots that are approximately semicircular. Because of its neglect of short-time, inertial effects, the diffusion approximation is least satisfactory at high frequencies, where the deviations from (11.11.27) are mostly to be found. However, as in the case of the single-molecule problem, it has proved difficult to develop an alternative theory having a wide range of applicability.

One goal of dielectric-relaxation theory is to relate the decay times that characterise the collective functions (11.11.17) and the single-molecule correlation function $C^{(1)}(t)$. The necessary link can be established by postulating some relationship between the memory functions $R(t)$ and $N^{(1)}(t)$. A simple but useful result is obtained by supposing that the two memory functions have the same time dependence, but also have their correct initial values. It follows from (9.1.29) that

$$N^{(1)}(0)=\left\langle|\dot{\mathbf{u}}_i|^2\right\rangle=\frac{\langle|\dot{\mathbf{M}}|^2\rangle}{N\mu^2}=\frac{R(0)}{3y} \tag{11.11.28}$$

where y is the molecular parameter defined by (11.5.16). If, for simplicity, we adopt the diffusion model, we find immediately from the definition (11.11.25) that

$$\tau_{\mathrm{D}}=\left(\frac{\varepsilon-1}{3y}\right)\tau_1 \tag{11.11.29}$$

or, after substitution from the Kirkwood formula (11.5.15):

$$\tau_{\mathrm{D}}=\left(\frac{3\varepsilon g_K}{2\varepsilon+1}\right)\tau_1 \tag{11.11.30}$$

This expression relates the dielectric relaxation time to the correlation time measured by infrared spectroscopy in a form determined solely by static dielectric properties of the fluid.

NOTES AND REFERENCES

1. Gray, C.G. and Gubbins, K.E., "Theory of Molecular Fluids". Clarendon Press, Oxford, 1984, p. 151.
2. Steele, W.A., *J. Chem. Phys.* **39**, 3197 (1963).
3. For a discussion of the properties of the spherical harmonics and their use in liquid-state theory, see ref. 1, particularly Appendix A.

4. See, e.g., Streett, W.B. and Tildesley, D.J., *Proc. Roy. Soc. A* **355**, 239 (1977).
5. The general procedure is described by Høye, J.S. and Stell, G., *J. Chem. Phys.* **66**, 795 (1977).
6. Sullivan, D.E. and Gray, C.G., *Mol. Phys.* **42**, 443 (1981).
7. A correction for the effects of nuclear vibration is also usually made.
8. Narten, A.H., Johnson, E. and Habenschuss, A., *J. Chem. Phys.* **73**, 1248 (1980).
9. X-ray scattering from methane is a special case. See Habenschuss, A., Johnson, E. and Narten, A.H., *J. Chem. Phys.* **74**, 5234 (1981).
10. Weis, J.J. and Levesque, D., *Phys. Rev. A* **13**, 450 (1976).
11. Narten, A.H. and Habenschuss, A., *J. Chem. Phys.* **75**, 3072 (1981).
12. (a) Narten, A.H., Agrawal, R. and Sandler, S.I., *Mol. Phys.* **35**, 1077 (1978). (b) Agrawal, R., Sandler, S.I. and Narten, A.H., *Mol. Phys.* **35**, 1087 (1978).
13. Wertheim, M.S., *J. Chem. Phys.* **55**, 4291 (1971).
14. See, e.g., Stell, G., Patey, G.N. and Høye, J.S., *Adv. Chem. Phys.* **48**, 183 (1981).
15. Fries, P.H. and Patey, G.N., *J. Chem. Phys.* **82**, 429 (1985).
16. We follow in outline the arguments of Madden, P.A. and Kivelson, D., *Adv. Chem. Phys.* **56**, 467 (1984).
17. (a) Høye, J.S. and Stell, G., *J. Chem. Phys.* **65**, 18 (1976). (b) Chandler, D., *J. Chem. Phys.* **67**, 1113 (1977).
18. Ramshaw, J.D., *J. Chem. Phys.* **70**, 1577 (1979).
19. Note the similarity with the relation (10.4.11) between the external and screened susceptibilities of charged fluids.
20. Kirkwood, J.G., *J. Chem. Phys.* **7**, 911 (1939).
21. Høye, J.S., Lebowitz, J.L. and Stell, G., *J. Chem. Phys.* **61**, 3253 (1974).
22. See ref. 1, p. 527.
23. The same result follows directly from the Stillinger–Lovett sum rules (10.2.17). See Martin, P.A., *Rev. Mod. Phys.* **60**, 1075 (1988).
24. Weis, J.J., unpublished results.
25. Cummings, P.T. and Blum, L., *J. Chem. Phys.* **85**, 6658 (1986).
26. Henderson, D., Boda, D., Szalai, I. and Chan, K.Y., *J. Chem. Phys.* **110**, 7348 (1999).
27. (a) Patey, G.N., *Mol. Phys.* **34**, 427 (1977). (b) Patey, G.N., *Mol. Phys.* **35**, 1413 (1978). (c) Patey, G.N., Levesque, D. and Weis, J.J., *Mol. Phys.* **38**, 219 (1979). (d) Patey, G.N., Levesque, D. and Weis, J.J., *Mol. Phys.* **38**, 1635 (1979).
28. Wertheim, M.S., *Mol. Phys.* **26**, 1425 (1973).
29. Lee, L.Y., Fries, P.H. and Patey, G.N., *Mol. Phys.* **55**, 751 (1985).
30. The dipolar hard-sphere model has other unsatisfactory features. See Teixeira, P.I.C., Tavares, J.M. and Telo da Gama, M.M., *J. Phys. Condens. Matter* **12**, R4111 (2000).
31. (a) Lado, F., *Mol. Phys.* **47**, 283 (1982). (b) Lado, F., Lombardero, M., Enciso, E., Abascal, J.L.F. and Lago, S., *J. Chem Phys.* **85**, 2916 (1986). (c) Lomba, E., Lombardero, M. and Abascal, J.L.F., *J. Chem. Phys.* **91**, 2581 (1989).
32. See, e.g., Lombardero, M., Martin, C., Lomba, E. and Lado, F., *J. Chem. Phys.* **104**, 6710 (1996).
33. Ladanyi, B.M. and Chandler, D., *J. Chem. Phys.* **62**, 4308 (1975).
34. Andersen, H.C. and Chandler, D., *J. Chem. Phys.* **53**, 547 (1970).
35. Chandler, D., *Mol. Phys.* **31**, 1213 (1976).
36. Monson, P.A., *Mol. Phys.* **47**, 435 (1982).
37. Schweizer, K.S. and Curro, J.G., *Phys. Rev. Lett.* **58**, 246 (1987). For a review, see Schweizer, K.S. and Curro, J.G., *Adv. Chem. Phys.* **98**, 1 (1997). The same formalism can be used for systems other than polymers: see Harnau, L. and Hansen, J.P., *J. Chem. Phys.* **116**, 9051 (2002).
38. Schweizer, K.S., Honnell, K.G. and Curro, J.G., *J. Chem. Phys.* **96**, 3211 (1992).
39. Rubinstein, M. and Colby, R.H., "Polymer Physics". Oxford University Press, Oxford, 2003. Note that the assumption of ideality is made solely for the purpose of computing the single-chain structure factor.
40. This remarkable fact was first pointed out by Chandler, D., *Faraday Disc. Chem. Soc*. **66**, 74 (1978) and later expanded upon by Sullivan and Gray, ref. 6. The derivation given in the text follows the method of Sullivan and Gray. See also Morriss, G.P. and Perram, J.W., *Mol. Phys.* **43**, 669 (1981).
41. Cummings, P.T. and Stell, G., *Mol. Phys.* **46**, 383 (1982). For later work on closure of the RISM-OZ relation, see, e.g., Raineri, F.O. and Stell, G., *J. Phys. Chem. B* **105**, 11880 (2001).

42. (a) Chandler, D., Silbey, R. and Ladanyi, B.M., *Mol. Phys.* **46**, 1335 (1982). (b) Chandler, D., Joslin, C.G. and Deutch, J.M., *Mol. Phys.* **47**, 871 (1982). (c) Chandler, D. and Richardson, D.M., *J. Phys. Chem.* **87**, 2060 (1983). See also Rossky, P.J. and Chiles, R.A., *Mol. Phys.* **51**, 661 (1984).
43. See, e.g., Reddy, G., Lawrence, C.P., Skinner, J.L. and Yethiraj, A., *J. Chem. Phys.* **119**, 13012 (2003).
44. Sorensen, J.M., Hura, G., Glaeser, R.M. and Head-Gordon, T., *J. Chem. Phys.* **113**, 9149 (2000).
45. Soper, A.K., *Chem. Phys.* **258**, 121 (2000).
46. Yarnell, J.L., Katz, M.J., Wenzel, R.G. and Koenig, S.H., *Phys. Rev. A* **7**, 2130 (1973).
47. Mahoney, M.W. and Jorgensen, W.L., *J. Chem. Phys.* **112**, 8910 (2000). TIP5P is one of a series of "transferable intermolecular potentials" devised for the simulation of water in different environments.
48. For a review, see Guillot, B., *J. Mol. Liq.* **101**, 219 (2002).
49. Sanz, E., Vega, C., Abascal, J.L.F. and MacDowell, L.G., *Phys. Rev. Lett.* **92**, 255701 (2004).
50. See, e.g., ref. 45 and Lombardero, M., Martin, C., Jorge, S., Lado, F. and Lomba, E., *J. Chem. Phys.* **110**, 1148 (1999).
51. (a) Andersen, H.C., *J. Chem. Phys.* **59**, 4714 (1973). (b) Andersen, H.C., *J. Chem. Phys.* **61**, 4985 (1974).
52. Cummings, P.T. and Stell, G., *Mol. Phys.* **51**, 253 (1984).
53. (a) Wertheim, M.S., *J. Stat. Phys.* **35**, 19 (1984). (b) Wertheim, M.S., *J. Stat. Phys.* **35**, 35 (1984).
54. Jackson, G., Chapman, W.G. and Gubbins, K.E., *Mol. Phys.* **65**, 1 (1988).
55. Galindo, A., Burton, S.J., Jackson, G., Visco, D.P. and Kofke, D.A., *Mol. Phys.* **100**, 2241 (2002).
56. Equation (11.10.9) can also be derived from the virial expansion via a calculation of the equilibrium constant for the dimerisation process. See Hill, T.L., "Introduction to Statistical Thermodynamics". Addison-Wesley, Reading, 1960, Sect. 15.3.
57. (a) Wertheim, M.S., *J. Chem. Phys.* **85**, 2929 (1986). (b) Wertheim, M.S., *J. Chem. Phys.* **87**, 7323 (1987). (c) Chapman, W.G., Jackson, G. and Gubbins, K.E., *Mol. Phys.* **65**, 1057 (1988).
58. For a review, see Müller, E.A. and Gubbins, K.E., *Ind. Eng. Chem. Res.* **40**, 2193 (2001).
59. Versmold, H., *Mol. Phys.* **43**, 383 (1981).
60. Bien, T., Possiel, M., Döge, G., Yarwood, J. and Arnold, K.E., *Chem. Phys.* **56**, 203 (1981).
61. St Pierre, A.G. and Steele, W.A., *Mol. Phys.* **43**, 123 (1981).
62. See, e.g., Madden, P.A. and Tildesley, D.J., *Mol. Phys.* **48**, 129 (1983).
63. Lynden-Bell, R.M. and McDonald, I.R., *Mol. Phys.* **43**, 1429 (1981).
64. Pollock, E.L. and Alder, B.J., *Phys. Rev. Lett.* **46**, 950 (1981).

Appendix A

FLUCTUATIONS

It is shown in Chapter 2 that certain thermodynamic properties are expressible in terms of fluctuations in the microscopic variables of a system. Here we examine the question of fluctuations from a purely thermodynamic point of view.

Consider a subsystem of macroscopic dimensions that forms part of a much larger thermodynamic system. The subsystem is assumed to be in thermal, mechanical and chemical equilibrium with the rest of the system which, being much larger, plays the role of a reservoir. The thermodynamic properties of the subsystem fluctuate around the average values characteristic of the total system, and the mean-square deviations from the average values can be derived systematically from the thermodynamic theory of fluctuations.

We assume that the total system is isolated from its surroundings. Then the probability p that a fluctuation will occur is

$$p \propto \exp(\Delta S_{\mathrm{t}}/k_{\mathrm{B}}) \tag{A.1}$$

where ΔS_{t} is the entropy change of the total system due to the fluctuation. Because S_{t} is a maximum at equilibrium, ΔS_{t} (< 0) will be a quadratic function of the thermodynamic variables, higher-order terms in the expansion of S_{t} around its maximum value being negligible for large systems. Let P, T and μ be the average pressure, temperature and chemical potential, respectively, of the reservoir. Then, given that the energy, volume and number of particles of the total system remain constant, the entropy change ΔS_{t} is

$$\Delta S_{\mathrm{t}} = \Delta S + (-\Delta U - P\Delta V + \mu\Delta N)/T \tag{A.2}$$

where ΔS, ΔU, ΔV and ΔN are the changes in thermodynamic variables of the subsystem and the second term on the right-hand side represents the entropy change of the reservoir. Since the fluctuations are very small, it is permissible to replace ΔU by an expansion in powers of ΔS, ΔV and ΔN truncated at second order, i.e.

$$\Delta U \approx T\Delta S - P\Delta V + \mu\Delta N + \tfrac{1}{2}(\Delta T\Delta S - \Delta P\Delta V + \Delta\mu\Delta N) \tag{A.3}$$

Then

$$p \propto \exp\left[-\tfrac{1}{2}\beta(\Delta T\Delta S - \Delta P\Delta V + \Delta\mu\Delta N)\right] \tag{A.4}$$

The subsystem can be defined either by the fraction of volume it occupies in the total system or by the number of particles it contains. In the second case, $\Delta N = 0$, and of

the four remaining variables (P, V, T and S) only two are independent. If T and V are chosen as independent variables, and ΔS and ΔP are expressed in terms of ΔT and ΔV, (A.4) becomes

$$p \propto \exp\left(-\frac{\beta C_V}{2T}(\Delta T)^2 + \frac{\beta}{2}\left(\frac{\partial P}{\partial V}\right)_{N,T}(\Delta V)^2\right) \tag{A.5}$$

The probability that a fluctuation will occur is therefore a gaussian function of the deviations ΔT and ΔV. Equation (A.5) shows that the system is stable against fluctuations in temperature and volume provided $C_V > 0$ and $(\partial P/\partial V)_{N,T} < 0$. The mean-square fluctuations derived from (A.5) are

$$\left\langle(\Delta T)^2\right\rangle = \frac{k_B T^2}{C_V}, \qquad \left\langle(\Delta V)^2\right\rangle = -k_B T\left(\frac{\partial V}{\partial P}\right)_{N,T} = V k_B T \chi_T \tag{A.6}$$

while $\langle \Delta T \Delta V \rangle = 0$. Fluctuations in temperature are therefore independent of those in volume. Alternatively, choice of S and P as independent variables transforms (A.4) into

$$p \propto \exp\left(-\frac{1}{2k_B C_P}(\Delta S)^2 + \frac{\beta}{2}\left(\frac{\partial V}{\partial P}\right)_{N,S}(\Delta P)^2\right) \tag{A.7}$$

where C_P is the heat capacity at constant pressure. The averages calculated from (A.7) are

$$\left\langle(\Delta S)^2\right\rangle = k_B C_P, \qquad \left\langle(\Delta P)^2\right\rangle = -k_B T\left(\frac{\partial P}{\partial V}\right)_{N,S} = \frac{k_B T}{V \chi_S} \tag{A.8}$$

where $\chi_S = -(1/V)(\partial V/\partial P)_{N,S}$ is the adiabatic compressibility, and $\langle \Delta S \Delta P \rangle = 0$. Fluctuations in entropy are therefore independent of those in pressure.

Finally, if the subsystem is defined as occupying a fixed fraction of the total volume, the mean-square fluctuation in the number of particles in the subsystem can be calculated, with the help of (2.4.22), to be

$$\left\langle(\Delta N)^2\right\rangle = k_B T\left(\frac{\partial N}{\partial \mu}\right)_{V,T} = \rho N k_B T \chi_T \tag{A.9}$$

Equation (A.9) is identical to the statistical mechanical relation relation (2.4.23), while comparison of (A.9) with (A.6) shows that volume fluctuations at constant N are equivalent to number fluctuations at constant V.

Appendix B

TWO THEOREMS IN DENSITY-FUNCTIONAL THEORY

In this appendix we prove two of the key results of density-functional theory, usually called the Hohenberg–Kohn–Mermin theorems. In doing so we use a simplified notation in which

$$\mathrm{Tr}\cdots \equiv \sum_{N=0}^{\infty} \frac{1}{h^{3N}N!} \iint \cdots \mathrm{d}\mathbf{r}^N\, \mathrm{d}\mathbf{p}^N$$

This operation is called the "classical trace", by analogy with the corresponding operation in quantum statistical mechanics. The definition of the grand partition function Ξ and the normalisation of the equilibrium phase-space probability density f_0 can then be expressed in the compact form

$$\Xi = \mathrm{Tr}\exp\bigl[-\beta(\mathcal{H}-N\mu)\bigr], \quad \mathrm{Tr}\, f_0 = 1$$

We first prove the following lemma.

Lemma. *Let f be a normalised phase-space probability density and let $\Omega[f]$ be the functional defined as*

$$\Omega[f] = \mathrm{Tr}\, f(\mathcal{H} - N\mu + k_\mathrm{B}T \ln f) \tag{B.1}$$

Then

$$\Omega[f] \geqslant \Omega[f_0] \tag{B.2}$$

where f_0 is the equilibrium phase-space density.

PROOF. From the definition of f_0 in (2.4.5) it follows that

$$\begin{aligned}\Omega[f_0] &= \mathrm{Tr}\, f_0(\mathcal{H} - N\mu - k_\mathrm{B}T \ln \Xi - \mathcal{H} + N\mu) = -k_\mathrm{B}T \ln \Xi \\ &\equiv \Omega\end{aligned} \tag{B.3}$$

where Ω is the grand potential. Thus

$$\Omega[f] - \Omega[f_0] = k_\mathrm{B}T\bigl[\mathrm{Tr}(f \ln f) - \mathrm{Tr}(f \ln f_0)\bigr] \tag{B.4}$$

The term inside square brackets can be written as

$$\mathrm{Tr}(f \ln f) - \mathrm{Tr}(f \ln f_0) = \mathrm{Tr}\, f_0\big[(f/f_0)\ln(f/f_0) - (f/f_0) + 1\big] \tag{B.5}$$

The right-hand side is always non-negative, since $x \ln x \geqslant x - 1$ for any $x > 0$. The inequality (B.2) is thereby verified.

This result is an example of the Gibbs–Bogoliubov inequalities, which are essentially a consequence of the convexity of the exponential function.

Theorem 1. *For given choices of V_N, T and μ, the intrinsic free-energy functional*

$$\mathcal{F}\big[\rho^{(1)}\big] = \mathrm{Tr}\, f_0(K_N + V_N + k_\mathrm{B}T \ln f_0) \tag{B.6}$$

is a unique functional of the equilibrium single-particle density $\rho^{(1)}(\mathbf{r})$.

PROOF. The equilibrium phase-space probability density f_0 is a functional of $\phi(\mathbf{r})$. The same is therefore true of the single-particle density $\rho^{(1)}(\mathbf{r}) = \mathrm{Tr}(f_0\rho(\mathbf{r}))$, where $\rho(\mathbf{r})$ is the microscopic density. Let us assume that there exists a different external potential, $\phi'(\mathbf{r}) \neq \phi(\mathbf{r})$, that gives rise to the same $\rho^{(1)}(\mathbf{r})$. With the hamiltonian $\mathcal{H}' = K_N + V_N + \Phi'_N$ we may associate an equilibrium phase-space density f'_0 and grand potential Ω'. The inequality (B.2) implies that

$$\begin{aligned}\Omega' = \mathrm{Tr}\, f'_0(\mathcal{H}' - N\mu + k_\mathrm{B}T \ln f'_0) &\leqslant \mathrm{Tr}\, f_0(\mathcal{H}' - N\mu + k_\mathrm{B}T \ln f_0) \\ &= \Omega + \mathrm{Tr}\big[f_0(\Phi'_N - \Phi_N)\big]\end{aligned} \tag{B.7}$$

or

$$\Omega' < \Omega + \int \rho^{(1)}(\mathbf{r})\big[\phi'(\mathbf{r}) - \phi(\mathbf{r})\big]\,\mathrm{d}\mathbf{r} \tag{B.8}$$

If the same argument is carried through with primed and unprimed quantities interchanged, we find that

$$\Omega < \Omega' + \int \rho^{(1)}(\mathbf{r})\big[\phi(\mathbf{r}) - \phi'(\mathbf{r})\big]\,\mathrm{d}\mathbf{r} \tag{B.9}$$

Addition of the two inequalities term by term leads to a contradiction:

$$\Omega + \Omega' < \Omega' + \Omega \tag{B.10}$$

showing that the assumption concerning $\rho^{(1)}(\mathbf{r})$ must be false. We therefore conclude that there is only one external potential that gives rise to a particular single-particle density. Since f_0 is a functional of $\phi(\mathbf{r})$, it follows that it is also a unique functional of $\rho^{(1)}(\mathbf{r})$. This in turn implies that the intrinsic free energy (B.6) is a unique functional of $\rho^{(1)}(\mathbf{r})$ and that its functional form is the same for all external potentials.

Theorem 2. *Let $n(\mathbf{r})$ be some average of the microscopic density. Then the functional*

$$\Omega_\phi[n] = \mathcal{F}[n] + \int n(\mathbf{r})\phi(\mathbf{r})\,\mathrm{d}\mathbf{r} - \mu \int n(\mathbf{r})\,\mathrm{d}\mathbf{r} \tag{B.11}$$

has its minimum value when $n(\mathbf{r})$ coincides with the equilibrium single-particle density $\rho^{(1)}(\mathbf{r})$.

PROOF. Let $n(\mathbf{r})$ be the single-particle density associated with a phase-space probability density f'. The corresponding grand-potential functional is

$$\begin{aligned}\Omega[f'] &= \mathrm{Tr}\, f'(\mathcal{H} - N\mu + k_\mathrm{B}T \ln f') \\ &= \mathcal{F}[n] + \int n(\mathbf{r})\phi(\mathbf{r})\,\mathrm{d}\mathbf{r} - \mu \int n(\mathbf{r})\,\mathrm{d}\mathbf{r} = \Omega_\phi[n]\end{aligned} \tag{B.12}$$

The inequality (B.2) shows that $\Omega[f_0] \leqslant \Omega[f']$. It is also clear that $\Omega_\phi[\rho^{(1)}] = \Omega[f_0] = \Omega$. Thus $\Omega_\phi[\rho^{(1)}] \leqslant \Omega_\phi[n]$: the functional $\Omega_\phi[n]$ is minimised when $n(\mathbf{r}) = \rho^{(1)}(\mathbf{r})$ and its minimum value is equal to the grand potential.

Appendix C

LEMMAS ON DIAGRAMS

We give here proofs of Lemmas 1, 2 and 4 of Section 3.7; the proofs of Lemmas 3 and 5 are similar to those of 2 and 4, respectively, and are therefore omitted.

PROOF OF LEMMA 1. Let $\{g_1, \ldots, g_N\}$ be the set of diagrams in G (N may be infinite). A typical diagram, Γ, in the set H is the star product of n_1 diagrams g_1, n_2 diagrams $g_2, \ldots$, and n_N diagrams g_N, where some of the numbers n_i may be zero; we express this result symbolically by writing

$$\Gamma = (g_1 * *n_1) * (g_2 * *n_2) * \cdots * (g_N * *n_N) \tag{C.1}$$

The value of g_i is by definition $[g_i] = I_i/S_i$, where S_i is the symmetry number, I_i is the integral associated with g_i, and we temporarily adopt the notation $[\cdots]$ to denote the value of a diagram. Then the value of Γ is

$$[\Gamma] = I/S = (1/S)\prod_{i=1}^{N} I_i^{n_i} \tag{C.2}$$

where the symmetry number is

$$S = \prod_{i=1}^{N} n_i! \times \prod_{i=1}^{N} S_i^{n_i} \tag{C.3}$$

The factors $n_i!$ take care of the permutations of the n_i identical diagrams g_i; note that (C.3) is true only for diagrams that are star irreducible. Equation (C.2) can be rewritten as

$$[\Gamma] = \prod_{i=1}^{N} I_i^{n_i} S_i^{-n_i} \Big/ \prod_{i=1}^{N} n_i! = \prod_{i=1}^{N} [g_i]^{n_i} \Big/ \prod_{i=1}^{N} n_i! \tag{C.4}$$

We now sum over all diagrams in H and find that

$$\sum_{\Gamma} [\Gamma] = -1 + \sum_{n_1=0}^{\infty} \cdots \sum_{n_N=0}^{\infty} \prod_{i=1}^{N} \frac{[g_i]^{n_i}}{n_i!} = -1 + \prod_{i=1}^{N} \sum_{n_i=0}^{\infty} \frac{[g_i]^{n_i}}{n_i!}$$

$$= \prod_{i=1}^{N} \exp\bigl([g_i]\bigr) - 1 = \exp\left(\sum_{i=1}^{N} [g_i]\right) - 1 \tag{C.5}$$

We subtract unity in the first line of (C.5) to exclude the case when all $n_i = 0$.

PROOF OF LEMMA 2. If S is the symmetry number and m is the number of black circles of Γ, the number of topologically inequivalent diagrams that are generated by attaching labels $1, \ldots, m$ to the black circles in all possible ways is $\nu = m!/S$. These diagrams we denote by Γ_i. It follows from the definition of a value of a diagram given by (3.7.3) that

$$\Gamma = \frac{1}{m!} \sum_{i=1}^{\nu} \Gamma_i \tag{C.6}$$

We now take the functional derivative of Γ with respect to $\gamma(\mathbf{r})$. Since

$$\frac{\delta\gamma(\mathbf{r}_i)}{\delta\gamma(\mathbf{r})} = \delta(\mathbf{r} - \mathbf{r}_i) \tag{C.7}$$

the differentiation corresponds diagrammatically to replacing successively each black γ-circle in (C.6) by a white 1-circle. In this way, νm diagrams are generated, each containing one white circle and $m - 1$ black circles. These we denote by $\Gamma_i^{(j)}$, where j is the label carried by the whitened circle. Thus

$$\frac{\delta\Gamma}{\delta\gamma(\mathbf{r})} = \frac{1}{m!} \sum_{i=1}^{\nu} \sum_{j=1}^{m} \Gamma_i^{(j)} = \frac{1}{(m-1)!} \sum_{i=1}^{\nu} \Gamma_i^{(1)} \tag{C.8}$$

In the second step we have replaced the sum over j by m times the contribution for $j = 1$; this is permissible, since the value of any $\Gamma_i^{(j)}$ is independent of j for given i.

The ν diagrams $\Gamma_i^{(1)}$ can now be divided into μ groups, chosen according to the topologically distinct diagrams into which each reduces when the labels of the $m - 1$ black circles are removed. If these diagrams are denoted by $\Gamma_1', \ldots, \Gamma_\mu'$, definition (3.7.3) implies that

$$\frac{\delta\Gamma}{\delta\gamma(\mathbf{r})} = \Gamma_1' + \cdots + \Gamma_\mu' \tag{C.9}$$

which is the required result.

PROOF OF LEMMA 4. Let m be the number of black circles in Γ. Any diagram in the set H can be expressed as $h(\Gamma; \{g_i\})$, where $\{g_i\} \equiv \{g_1, \ldots, g_m\}$ is a set of diagrams drawn from G that are attached to the black circles of Γ; some of the g_i may be identical. Two diagrams h obtained from two distinct sets $\{g_i\}$ are not necessarily different. Lemma 4 can

then be written in more compact form as

$$\sum_{\{g_i\}}{}' h(\Gamma;\{g_i\}) = \big[\text{the diagram obtained from } \Gamma \text{ by associating the function } \mathcal{G}(\mathbf{r}) \text{ with each of the black circles}\big] \tag{C.10}$$

The sum in (C.10) is taken over all sets $\{g_i\}$, with the restriction (denoted by the prime) that the diagrams $h(\Gamma;\{g_i\})$ must be topologically distinct.

Let $S(\Gamma)$ be the symmetry number of Γ, and let $S(g_i)$ and $S(\Gamma;\{g_i\})$ be, respectively, the symmetry numbers of the diagrams in G and H; $S(\Gamma)$ is obviously also the symmetry number of the right-hand side of (C.10). According to the definition (3.7.4):

$$h\big(\Gamma;\{g_i\}\big) = h\big(\Gamma';\{g_i'\}\big)\big/S\big(\Gamma;\{g_i\}\big) \tag{C.11}$$

where $h(\Gamma';\{g_i'\})$ is a diagram derived from $h(\Gamma;\{g_i\})$ by labelling its black circles in an arbitrary way. Let $h(\Gamma';\{g_i\})$ be the diagram obtained from $h(\Gamma';\{g_i'\})$ by removing the labels of the black circles of the g_i', but retaining the labels of the black circles of Γ', and let $S^*(\Gamma;\{g_i\})$ be the number of permutations of the m labels of $h(\Gamma';\{g_i\})$ that give rise to topologically equivalent diagrams. For each of the S^* permutations there are $\prod_{i=1}^m S(g_i)$ permutations of the black circles of the g_i that yield diagrams equivalent to $h(\Gamma';\{g_i'\})$. We can therefore write

$$S\big(\Gamma;\{g_i\}\big) = S^*\big(\Gamma;\{g_i\}\big)\prod_{i=1}^{m} S(g_i) \tag{C.12}$$

We now require a relation between $S(\Gamma)$ and $S^*(\Gamma;\{g_i\})$. Note that $S(\Gamma) \geqslant S^*(\Gamma;\{g_i\})$, since the process of decorating the black circles of Γ can never lead to an increase in symmetry number. Let $n(\Gamma;\{g_i\})$ be the number of labellings that give rise to diagrams $h(\Gamma';\{g_i\})$ that are topologically inequivalent, but yield diagrams Γ' (i.e. labelled versions of Γ on its own) that are equivalent. Consider now the set of $S(\Gamma)$ diagrams that are obtained from $h(\Gamma';\{g_i\})$ by making the $S(\Gamma)$ permutations that leave Γ' topologically unaltered. This set can be divided into precisely $n(\Gamma;\{g_i\})$ groups, such that the diagrams in different groups are topologically inequivalent to each other. Each of the $n(\Gamma,\{g_i\})$ groups consists of $S^*(\Gamma;\{g_i\})$ topologically inequivalent diagrams. Thus

$$S(\Gamma) = n\big(\Gamma;\{g_i\}\big)S^*\big(\Gamma;\{g_i\}\big) \tag{C.13}$$

Illustration.

$\Gamma =$ 

$g_1 =$ 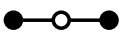

$g_2 = g_3 =$ 

$h(\Gamma; \{g_i\}) =$ 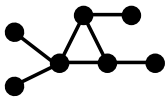

$h(\Gamma; \{g_i\}) =$ 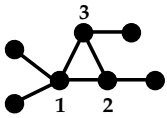

In this example, $S(\Gamma) = 6$; $S^*(\Gamma; g_1, g_2, g_3) = 2$, because labels 2 and 3 can be permuted in $h(\Gamma'; g_1, g_2, g_3)$; and $n(\Gamma; g_1, g_2, g_3) = 3$, because permutation of labels 1 and 2 or 1 and 3 in $h(\Gamma'; g_1, g_2, g_3)$ generates diagrams that are topologically inequivalent.

By combining (C.12) and (C.13) we find that

$$S(\Gamma; \{g_i\}) = S(\Gamma) \prod_{i=1}^{m} S(g_i)/n(\Gamma; \{g_i\}) \tag{C.14}$$

If use is made of (C.11) and (C.14), the left-hand side of (C.10) can be rewritten as

$$\sum_{\{g_i\}}{}' \frac{n(\Gamma; \{g_i\})}{S(\Gamma) \prod_{i=1}^{m} S(g_i)} h(\Gamma'; \{g_i'\}) \tag{C.15}$$

or, from (3.7.4):

$$\sum_{\{g_i\}}{}' \frac{n(\Gamma; \{g_i\})}{S(\Gamma)} h(\Gamma'; \{g_i\}) \tag{C.16}$$

Remembering the significance of $n(\Gamma; \{g_i\})$, we see that (C.16) can also be expressed as

$$\sum_{g_i} \cdots \sum_{g_m} h(\Gamma'; g_1, \ldots, g_m)/S(\Gamma) \tag{C.17}$$

where the m summations are now unrestricted. But (C.17) is just a labelled diagram obtained from Γ' by associating the function $\mathcal{G}(\mathbf{r})$ with each black circle and dividing by the symmetry number $S(\Gamma)$. It follows from (3.7.4) that (C.17) is equal to the right-hand side of (C.10).

Appendix D

SOLUTION OF THE PY EQUATION FOR HARD SPHERES

The PY closure relation for hard spheres is

$$h(r) = -1, \quad r < d \tag{D.1a}$$

$$c(r) = 0, \quad r > d \tag{D.1b}$$

When substituted in the Ornstein–Zernike relation (3.5.12), this approximation yields an integral equation that can be solved in closed form. We follow here the method of Baxter, which is based on a transformation of the Ornstein–Zernike relation via a so-called Wiener–Hopf factorisation of the function $\hat{A}(k)$ defined as

$$\hat{A}(k) = \frac{1}{S(k)} = 1 - \rho\hat{c}(k) = 1 - \frac{4\pi\rho}{k}\int_0^\infty r\sin(kr)c(r)\,\mathrm{d}r \tag{D.2}$$

The three-dimensional Fourier transform of any function f of $r \equiv |\mathbf{r}|$ can be cast in the form

$$\begin{aligned}\hat{f}(k) &= \frac{4\pi}{k}\int_0^\infty r\sin(kr)f(r)\,\mathrm{d}r = 4\pi\int_0^\infty \cos(kr)F(r)\,\mathrm{d}r \\ &= 2\pi\int_{-\infty}^{\infty}\exp(ikr)F(r)\,\mathrm{d}r\end{aligned} \tag{D.3}$$

where

$$F(r) = \int_r^\infty sf(s)\,\mathrm{d}s = F(-r) \tag{D.4}$$

The second equality in (D.4) follows immediately if the convention that $f(r) = f(-r)$ is followed. Substitution of (D.1b), (D.3) and (D.4) in (D.2) leads to

$$\hat{A}(k) = 1 - 4\pi\rho\int_0^d \cos(kr)S(r)\,\mathrm{d}r = \hat{A}(-k) \tag{D.5}$$

where

$$S(r) = \int_r^d tc(t)\,\mathrm{d}t \tag{D.6}$$

Similarly:

$$\hat{h}(k) = 2\pi \int_{-\infty}^{\infty} \exp(ikr) J(r)\, \mathrm{d}r \tag{D.7}$$

with

$$J(r) = \int_{r}^{\infty} sh(s)\, \mathrm{d}s \tag{D.8}$$

Consider now the behaviour of the function $\hat{A}(k)$ in the complex k-plane and set $k = x + iy$. Because $\hat{A}(k)$, as given by (D.5), is a Fourier transform over a finite interval, it is regular throughout the complex plane. It also has no zeros on the real axis ($y = 0$), since it is the inverse of the static structure factor; the latter is a finite quantity at all wavenumbers. Moreover, according to (D.5), $\hat{A}(k)$ tends uniformly to unity as $|x| \to \infty$ in any strip $y_1 < y < y_2$. Thus there exists a strip $|y| \leqslant \varepsilon$ about the real axis within which $\hat{A}(k)$ has no zeros. The function $\ln \hat{A}(k)$ is therefore regular within that strip and tends uniformly to zero as $|x| \to \infty$. Integrating around the strip and applying Cauchy's theorem, we find that for any $k = x + iy$ such that $|y| < \varepsilon$:

$$\ln \hat{A}(k) = \ln \widehat{Q}(k) + \ln \widehat{P}(k) \tag{D.9}$$

where

$$\ln \widehat{Q}(k) = \frac{1}{2\pi i} \int_{-i\varepsilon-\infty}^{-i\varepsilon+\infty} \frac{\ln \hat{A}(k')}{k' - k}\, \mathrm{d}k' \tag{D.10a}$$

$$\ln \widehat{P}(k) = -\frac{1}{2\pi i} \int_{i\varepsilon-\infty}^{i\varepsilon+\infty} \frac{\ln \hat{A}(k')}{k' - k}\, \mathrm{d}k' \tag{D.10b}$$

Since $\hat{A}(k)$ is an even function of k, (D.10) implies that

$$\ln \widehat{P}(k) = \ln \widehat{Q}(-k) \tag{D.11}$$

From (D.10a) we see that $\ln \widehat{Q}(k)$ is regular in the domain $y > -\varepsilon$. It follows from (D.9) and (D.11) that when $|y| < \varepsilon$:

$$\hat{A}(k) = \widehat{Q}(k)\widehat{Q}(-k) \tag{D.12}$$

The function $\widehat{Q}(k)$ is regular and has no zeros in the domain $y > -\varepsilon$, since it is the exponential of a function that is regular in the same domain. Equation (D.12) is the Wiener–Hopf factorisation of $\hat{A}(k)$.

When $|x| \to \infty$ within the strip $|y| < \varepsilon$, it follows from (D.10a) that $\ln \widehat{Q}(k) \sim x^{-1}$ and hence that $\widehat{Q}(k) \sim 1 - \mathcal{O}(x^{-1})$. The function $1 - \widehat{Q}(k)$ is therefore Fourier integrable along the real axis and a function $Q(r)$ can be defined as

$$2\pi\rho Q(r) = \frac{1}{2\pi} \int_{-\infty}^{\infty} \exp(-ikr)\big[1 - \widehat{Q}(k)\big]\, \mathrm{d}k \tag{D.13}$$

Equation (D.10a) shows that if k is real, the complex conjugate of $\widehat{Q}(k)$ is $\widehat{Q}(-k)$, and hence that $Q(r)$ is a real function. The same equation also shows that when $y \geqslant 0$, $\ln \widehat{Q}(k) \to 0$, and therefore $\widehat{Q}(k) \to 1$, as $k \to \infty$. Thus, if $r < 0$, the integration in (D.13) can be closed around the upper half-plane, where $\widehat{Q}(k)$ is regular, to give

$$Q(r) = 0, \quad r < 0 \tag{D.14}$$

The right-hand side of (D.10a) is a different analytic function of k according to whether $y > -\varepsilon$ or $y < -\varepsilon$. The analytic continuation of $\widehat{Q}(k)$ into the lower half-plane is therefore given, not by (D.10a), but by (D.12), i.e.

$$\widehat{Q}(k) = \hat{A}(k)/\widehat{Q}(-k) \tag{D.15}$$

where (D.10a) can be used to evaluate $\widehat{Q}(-k)$. Since $\hat{A}(k)$ is regular everywhere, and $\widehat{Q}(-k)$ is regular and has no zeros for $y < \varepsilon$, we see from (D.15) that $\widehat{Q}(k)$ is also regular for $y < \varepsilon$. Furthermore, since $\widehat{Q}(-k) \to 1$ as $y \to -\infty$, it follows from (D.5) and (D.15) that both $\hat{A}(k)$ and $\widehat{Q}(k)$ grow exponentially as $\exp(ikd) = \exp(ixd)\exp(-yd)$ when y becomes large and negative. Thus, when $r > d$, the integration in (D.13) can be closed around the lower half-plane, giving

$$Q(r) = 0, \quad r > d \tag{D.16}$$

On inversion of the Fourier transform in (D.13), (D.14) and (D.16) together yield

$$\widehat{Q}(k) = 1 - 2\pi\rho \int_0^d \exp(ikr)\, Q(r)\, \mathrm{d}r \tag{D.17}$$

Substitution in (D.12) of the expressions (D.5) for $\hat{A}(k)$ and (D.17) for $\widehat{Q}(k)$, followed by multiplication by $\exp(-ikr)$ and integration with respect to k from $-\infty$ to $+\infty$, shows that

$$S(r) = Q(r) - 2\pi\rho \int_r^d Q(s)\, Q(s-r)\, \mathrm{d}s, \quad 0 < r < d \tag{D.18}$$

Equations (3.5.13), (D.2) and (D.12) imply that

$$\widehat{Q}(k)\big[1 + \rho\hat{h}(k)\big] = 1/\widehat{Q}(k) \tag{D.19}$$

where $\hat{h}(k)$ is given by (D.7). We now multiply both sides of (D.19) by $\exp(-ikr)$ and integrate with respect to k from $-\infty$ to $+\infty$. The contribution from the right-hand side vanishes when $r > 0$, since the integration can then be closed around the lower half-plane, where $\widehat{Q}(k)$ is regular, has no zeros and tends to unity at infinity. On substituting (D.7) and (D.17) into the left-hand side of (D.19) and carrying out the integration, we obtain a relation between $Q(r)$ and $J(r)$ for $r > 0$ of the form

$$-Q(r) + J(r) - 2\pi\rho \int_0^d Q(s)\, J\big(|r-s|\big)\, \mathrm{d}s = 0, \quad r > 0 \tag{D.20}$$

It is clear from (D.6) and (D.18) that $Q(r) \to 0$ as $r \to d$ from below; comparison with (D.16) then shows that $Q(r)$ is continuous at $r = d$.

Equations (D.18) and (D.20) can be expressed in terms of $c(r)$ and $h(r)$, rather than $S(r)$ and $J(r)$, by differentiating them with respect to r. If we use (D.6) and (D.8), and the fact that $Q(d) = 0$, we find after integration by parts that

$$rc(r) = -Q'(r) + 2\pi\rho \int_r^d Q'(s)\,Q(s-r)\,\mathrm{d}s, \quad 0 < r < d \tag{D.21}$$

and

$$rh(r) = -Q'(r) + 2\pi\rho \int_0^d (r-s)h\big(|r-s|\big)\,Q(s)\,\mathrm{d}s, \quad r > 0 \tag{D.22}$$

where $Q'(r) \equiv \mathrm{d}Q(r)/\mathrm{d}r$. Equations (D.21) and (D.22) express $h(r)$ and $c(r)$ in terms of the same function, $Q(r)$, and constitute a reformulation of the Ornstein–Zernike relation that is applicable whenever $c(r)$ vanishes beyond a range d, which is precisely the case with the PY closure. Equation (D.22) is an integral equation for $Q(r)$ that is easy to solve for $0 < r < d$, where $h(r) = -1$ and (D.22) therefore reduces to

$$r = Q'(r) + 2\pi\rho \int_0^d (r-s)\,Q(s)\,\mathrm{d}s, \quad 0 < r < d \tag{D.23}$$

The solution is of the form

$$Q'(r) = ar + b \tag{D.24}$$

with

$$a = 1 - 2\pi\rho \int_0^d Q(s)\,\mathrm{d}s, \qquad b = 2\pi\rho \int_0^d s\,Q(s)\,\mathrm{d}s \tag{D.25}$$

Given the boundary condition $Q(d) = 0$, (D.24) is trivially integrated to yield $Q(r)$. Substitution of the result in (D.25) gives two linear equations, the solutions to which are

$$a = \frac{1+2\eta}{(1-\eta)^2}, \qquad b = \frac{-3d\eta}{2(1-\eta)^2} \tag{D.26}$$

where η is the hard-sphere packing fraction. Thus $Q(r)$ is now a known function of r and $c(r)$ can therefore be calculated from (D.21); this leads to the results displayed in (4.4.10) and (4.4.11). The isothermal compressibility is obtained from (3.8.8), (D.2) and (D.15) as

$$\beta/\rho\chi_T = \hat{A}(0) = \big[\widehat{Q}(0)\big]^2 \tag{D.27}$$

The function $\widehat{Q}(0)$ is easily calculated from (D.17) and the solution for $Q(r)$, leading ultimately to the PY compressibility equation of state (4.4.12).

Appendix E

SCALED-PARTICLE THEORY

Scaled-particle theory is an approximate interpolation scheme that allows the calculation of the work required to create a spherical cavity in a hard-sphere fluid or, equivalently, to insert a solute sphere of the same radius. From this starting point it is possible to derive the equation of state of the fluid. The theory is easily formulated for mixtures, but we restrict the discussion here to the one-component case.

Consider a fluid of N hard spheres of diameter $d = 2R$ at a number density ρ. Let $W(R_0)$ be the reversible work required to create a spherical cavity of radius R_0 centred on a point $\mathbf{r}$ within the fluid. According to the basic principles of thermodynamic fluctuation theory, the probability that such a cavity will appear as the result of spontaneous fluctuations within the system is

$$p_0(R_0) = \exp\bigl[-\beta W(R_0)\bigr] \tag{E.1}$$

This is the same as the probability that there are no spheres whose centres lie within the spherical region of radius $R_0 + R$ around $\mathbf{r}$. That interpretation can be extended to negative values of R_0 in the range $-R \leqslant R_0 \leqslant 0$, in which case the radius of the region of interest is $0 \leqslant R_0 + R \leqslant R$. Since overlap of hard spheres is forbidden, there can be at most one particle in such a region, a situation that occurs with probability

$$p_1(R_0) = \tfrac{4}{3}\pi\rho(R_0 + R)^3 = 1 - p_0(R_0) \tag{E.2}$$

Combination of (E.1) and (E.2) gives

$$W(R_0) = -k_\mathrm{B}T \ln\bigl[1 - (4\pi\rho/3)(R_0 + R)^3\bigr], \quad R_0 \leqslant 0 \tag{E.3}$$

In the opposite limit, that of very large cavities, the reversible work required is given by thermodynamics. If P is the pressure of the fluid and $\Delta V_0 = 4\pi R_0^3/3$ is the volume of the cavity, then $W(R_0)$ is the increase in Helmholtz free energy resulting from a reduction equal to ΔV_0 in the volume accessible to the fluid:

$$W(R_0) = P\,\Delta V_0 = \tfrac{4}{3}\pi P R_0^3, \quad R_0 \gg R \tag{E.4}$$

The assumption now made is that for $R_0 > 0$, $W(R_0)$ is given by a cubic polynomial in R_0, where the term in R_0^3 (the dominant contribution for large cavities) is given by (E.4), i.e.

$$W(R_0) = w_0 + w_1 R_0 + \tfrac{1}{2} w_2 R_0^2 + \tfrac{4}{3}\pi P R_0^3, \quad R_0 \geqslant 0 \tag{E.5}$$

The coefficients w_0, w_1 and w_2 are determined by requiring $W(R_0)$ and its first derivative, as given by (E.3) for $R_0 < 0$ and (E.5) for $R_0 > 0$, to be continuous at $R_0 = 0$. The results obtained in this way are

$$\beta w_0 = -\ln(1-\eta), \qquad \beta w_1 = \frac{4\pi\rho R^2}{1-\eta}$$
$$\beta w_2 = \frac{8\pi\rho R}{1-\eta} + \frac{(4\pi\rho R^2)^2}{(1-\eta)^2} \tag{E.6}$$

where η is the hard-sphere packing fraction.

The excess chemical potential of the fluid is the reversible work required to insert a hard sphere of radius $R_0 = R$. Thus, from (E.5) and (E.6):

$$\begin{aligned}\beta\mu^{\text{ex}} &= \beta W(R_0) \\ &= -\ln(1-\eta) + \frac{6\eta}{1-\eta} + \frac{9\eta^2}{2(1-\eta)^2} + \frac{\beta P\eta}{\rho}\end{aligned} \tag{E.7}$$

Then use of the thermodynamic relation $\partial P/\partial\rho = \rho(\partial\mu/\partial\rho)$ leads to the scaled-particle equation of state in the form

$$\frac{\beta P}{\rho} = \frac{1+\eta+\eta^2}{(1-\eta)^3} \tag{E.8}$$

Equation (E.8) is identical to the Percus–Yevick compressibility equation (4.4.12). The corresponding expression for the excess free energy is

$$\frac{\beta F^{\text{ex}}}{N} = -\ln(1-\eta) + \frac{3\eta}{1-\eta} + \frac{3\eta^2}{2(1-\eta)^2} \tag{E.9}$$

Index